MONASH University

Mitochondrial Function in Diabetic Kidney Disease:

Insights from Targeting Mitochondrial Pore-forming Cell Death Proteins

Runa Sigrid Johanna Lindblom

Bachelor of Science (Honours), University of Melbourne, 2014

Diploma of Languages (Swedish), University of Melbourne, 2014

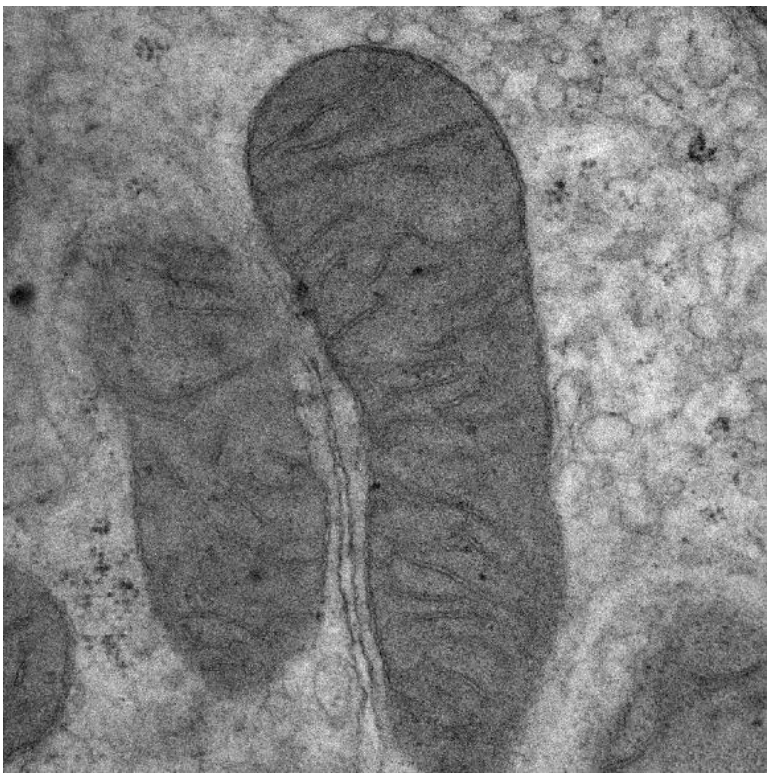

A thesis submitted for the degree of *Doctor of Philosophy* at

Monash University in the year 2019

Faculty of Medicine, Dentistry and Health Science

ABSTRACT

Diabetes is arguably the most important disease of the 21st century. Globally, incidence rates are rising, and with it, the development of diabetes-associated complications, such as diabetic kidney disease (DKD). Diabetes-associated renal injury represents a common morbidity, even in early diabetes, and brings a risk of progression to end stage kidney disease. Clinical interventions currently rely on controlling blood glucose, and blood pressure; however, some patients continue to experience renal decline. New advances are required, both to understand the pathogenesis and to prevent it.

Recently, the importance of maintaining mitochondrial function has been highlighted by their role in cell metabolism, stress response, and cell death outcomes in DKD. The potential for mitochondrial dysfunction to influence DKD progression will be explored in this thesis.

Firstly, mitochondrial function was examined using preclinical mouse models of DKD. Diabetes was confirmed by persistent hyperglycaemia and elevated HbA1c. Renal function was monitored by assessing changes in: urine volume, renal mass, glomerular filtration (creatinine clearance and plasma cystatin C), urinary markers of renal injury (albuminuria, Kim-1), and structural changes (glomerular sclerosis and fibrosis). Analysis of mitochondrial function was performed to investigate the association between dysfunction and DKD progression. The role of mitochondrial pore-forming cell death proteins was then evaluated by utilising several strategies. The time-course progression of mitochondrial function and expression of cell death proteins was examined with an FVB/N model of STZ induced diabetes. Whilst albuminuria was significantly elevated, few structural pathologies were present at 4, 8, 12 and 16 wks of diabetes. Elevations of mitochondrial cell death proteins were present in the 4 wk mice only, however, tubular injury began to develop at 16 wks. Further, mitochondrial function was unaltered in the early progression of DKD.

Next, the contribution of the apoptotic proteins, Bax and Bak, to the progression of DKD were evaluated in a novel mouse model with conditional deletion of of Bax and Bak in the renal proximal tubules only. However, this novel mouse model only developed mild DKD by 24 wks of STZ induced diabetes. No mitochondrial functional changes were evident with mild DKD, and the deletion of Bax and Bak in this model did not elucidate a role for MOMP in the early progression of diabetes.

Finally, the role of the mitochondrial permeability transition pore was evaluated by examining Cyclophilin D. Genetic deletion in an STZ diabetes model revealed that CypD is essential for mitigating DKD severity, as diabetes-associated injury was increased without it. Pharmacological inhibition of the mPTP with the drug, Alisporivir, however revealed no exacerbation of injury nor reduction in DKD markers. However, the use of a mouse model with Type 2 diabetes (db/db mice) demonstrated mitochondrial changes. Surprisingly, a link between CypD and mitochondrial metabolism was elucidated, providing evidience for the importance of functional mitochondrial cell death associated proteins.

Overall, insight from these studies suggest that mitochondrial cell death associated proteins may have inherent physiological functions in the diabetic kidney, and that renal mitochondrial function must involve unique approaches to prevent both mitochondrial and total renal decline.

PUBLICATIONS DURING ENROLLMENT

Lindblom R, Higgins G, Coughlan M, de Haan JB. Targeting Mitochondria and Reactive Oxygen Species-Driven Pathogenesis in Diabetic Nephropathy. Rev Diabet Stud. 2015 Aug 10;12(1-2):134–156.

Tate M, Higgins GC, De Blasio MJ, Lindblom R, Prakoso D, Deo M, et al. The Mitochondria-Targeted Methylglyoxal Sequestering Compound, MitoGamide, Is Cardioprotective in the Diabetic Heart. Cardiovasc Drugs Ther. 2019 Oct 25;

Lindblom RSJ, Higgins GC, Nguyen TV, Arnstein M, Henstridge DC, Granata C, et al. Delineating a role for the Mitochondrial Permeability Transition Pore in Diabetic Kidney Disease by targeting Cyclophilin D. Clin Sci. 2020 Jan 16;

THESIS INCLUDING PUBLISHED WORKS DECLARATION

I hereby declare that this thesis contains no material which has been accepted for the award of any other degree or diploma at any university or equivalent institution and that, to the best of my knowledge and belief, this thesis contains no material previously published or written by another person, except where due reference is made in the text of the thesis.

This thesis includes one (1) original paper published in peer reviewed journals and one (1) submitted publication. The core theme of the thesis is: mitochondrial pore-forming cell death proteins and the intrinsic mitochondrial cell death pathways in the context of diabetic kidney disease. The ideas, development and writing up of all the papers in the thesis were the principal responsibility of myself, the student, working within the Department of Diabetes, at the Monash University Central Clinical School, under the supervision of Associate Professor Melinda Coughlan.

In the specific case of *Chapter 1* and *Chapter 5,* including published works*,* my contribution involved the following:

Thesis Chapter	Publication Title	**Status**	Nature and % of student contribution	Co-author name(s) Nature and % of Co-author's contribution*	Co-author(s), Monash student Y/N*
1	Targeting Mitochondria and Reactive Oxygen Species-Driven Pathogenesis in Diabetic Nephropathy	Published	45%. Researched and written input into manuscript, creation of one figure	1) Gavin Higgins, concept, research and written input into manuscript, creation of one figure 25% 2) Judy deHaan, research and written input into manuscript 10% 3) Melinda Coughlan, research and written input into manuscript 20%	No No No
5	Delineating a role for the Mitochondrial Permeability Transition Pore in Diabetic Kidney Disease by targeting Cyclophilin D	Submitted, returned for revision	65%. Collection of data, data analysis, full written draft and editing, interpretation of results	1) Gavin Higgins Assistance with experimental design, collection of data, and assitance with interpretation of data, editting 8% 2) Tuong-Vi Nguyen Collection of data and assistance with methodology, editting 5%	No No

				3) Maryann Arnstein, Assistance with data collection and analysis 3% 4) Darren Henstridge, Assistance with interpretation of data and methodology, editting 2% 5) Cesare Granata, collection of data, written contribution of one method to methodology 1% 6) Matthew Snelson, Collection of data 1% 7) Vicki Thallas-Bonke Collection of data 1% 8) Mark Cooper, Intellectual input, editting 2% 9) Josephine Forbes Intellectual input, editting 2% 10) Melinda Coughlan, Concept and experimental design, intellectual input, editting 10%	No No No Yes No No No No

I have not renumbered sections of submitted or published papers in order to maintain the distinct presentation of published works within the thesis.

The inclusion of co-authors reflects the fact that the work came from active collaboration between researchers and acknowledges input into team-based research. Additionally, all work within this thesis was conducted within a medical research discipline where experimental work is routinely undertaken in a collaborative manner. The contribution of senior colleagues in the development of research projects, ethics applications, as well as in the development of research protocols, is acknowledged. The research involving the use of animal models would not be possible without the assistance of staff and students from the Glycation, Nutrition and Metabolism laboratory (Coughlan Lab), and technical staff within the Department of Diabetes, and the AMREP Animal Centre. The nature of assistance received extends to the breeding, housing and monitoring animals by trained technical staff. Animal cull procedures, and assays performed on fresh tissue, were conducted with assistance from several colleagues due to the temporal restrictions and technical difficulty involved. At times, assistance with the interpretation of experimental methodology and results was required, and where this was integral to the interpreation of results, this assistance is specified in the acknowlwdgements section, below.

Student name: Runa Sigrid Johanna Lindblom

Student signature: **Date: 1st November 2019**

I hereby certify that the above declaration correctly reflects the nature and extent of the student's and co-authors' contributions to this work. In instances where I am not the responsible author I have consulted with the responsible author to agree on the respective contributions of the authors.

Main Supervisor name: Associate Professor Melinda Coughlan

Main Supervisor signature: **Date: 1st November 2019**

ACKNOWLEDGEMENTS

First and foremost I wish to acknowledge the assistance and support received from my supervisors throughout my PhD. To Associate Professor Melinda Coughlan, whose projects allowed me to explore my interest in mitochondria and cell death. I acknowledge your contribution to the development of the concepts and experimental models that then I took on in my studies. I have enjoyed exploring the outcomes in my research. To Professor Mark Cooper, for your support and rapid review of my writing, particularly in these last few months. And to Dr Gavin Higgins, who patiently explained all the new and difficult concepts I encountered along this journey. I am thankful for your insight and your attention to detail.

In addition I wish to thank my colleagues and friends within the Glycation, Nutrition and Metabolism lab, both past and present. To Tuong-Vi Nguyen, Dr Sih-Min Tan, Maryann Arnstein, Matthew Snelson, Dr Cesare Granata, Adrienne Laskowski, Dr Karly Souris, Vicki Thallas-Bonke, Dr Nicole Kellow and Rachael Clarke . All of you have helped immensely on my research journey with sharing your knowledge of protocols and techniques I have learnt. I thank you for your assistance with animal work and for teaching me how to perform different experimental procedures. I am grateful to have shared the lab with you.

My thanks also extends to all staff within the department of diabetes, and also to platform staff at Monash university. This includes Iska Carmichael and Steven Cody for training and use of the equipment at Monash Micro Imaging. To Georg Ramm for access and use of the Ramaciotti centre for electron microscopy, and to Adam Costin and Joan Clarke for technical assistance, knowledge and training in the preparation of samples for electron microscopy. To Dr Kylie Quinn and the department of Biochemistry and Molecular biology for allowing me to use the Seahorse machine when ours was being repaired.

I also express sincerely my thanks to the specialist medical team, my Surgeon, my GP, and Optometrist, for their part in my meningioma journey. I am grateful to have been under your care through my diagnosis, surgery and recovery. This last year has been the hardest, and I would like to acknowledge all of my colleagues for supporting me during this time. Your patience has been

unyielding, and your advice has been instrumental to the completion of my studies. In particular I would like to thank my supervisors again, for their support and understanding. To Carlos Rosada, Alex Dimitropoulos, and Muthu Mohan, thank you for your support and friendship in the lab, and for helping me when I forgot where everything was. I would also like to acknowledge the Benjamin Padman, who's advice has helped me navigate through the tough times. I also thank Maryann Arnstein and Adrienne Laskowski for assistance with lab work during the last year of my PhD project when health reasons prevented me from working at the top of my game. For this I am very grateful.

Finally I wish to acknowledge the love and support offered to me from my family and friends through this epic journey. Thank you to my mum in particular for helping me in my recovery, and for all your support during this final year. Also to Steve, thank you for your care and persistence that I go for walks in the most beautiful places to help me relax.

I also acknowledge the financial support I received during my PhD. I am thankful to the Baker IDI Bright Sparks award, with a stipend sponsored by the Cybec foundation. Additionally, this project was supported by the Australian research training program (RTP) formerly the Australian Postgraduate Award (APA).

"Leg godt"

- Ole Kirk Christiansen, 1934

TABLE OF CONTENTS

LIST OF FIGURES

LIST OF TABLES

ABBREVIATIONS

Acetyl CoA	Acetyl coenzyme A sodium salt
ACR	Albumin to creatinine ratio
ADP	Adenosine Tri-phosphate
AMREP	Alfred Medical, Research and Education Precinct
ANOVA	Analysis of variance
ANT	ATP/ADP antiporter
Anti-A	Antimycin A
ATP	Adenosine Di-phosphate
Bak, BAK	Bcl-2 homologous antagonist killer
Bax, BAX	Bcl-2 associated X protein
BCA	Bicinchoninic acid
BCL2	B-cell lymphoma 2
BSA	Bovine serum albumin
CI	Complex I
CII	Complex II
CIII	Complex III
CIV	Complex IV
Cat:	Catalogue, or product number
cDNA	cyclical DNA
Col I	Callagen type 1
Col IV	Collagen type 4
CsA	Cyclosporin A (Also Ciclosporine A)
CR_{CL}	creatinine clearance
CVD	Cardiovascular disease
CypD	Cyclophilin D
DAMP	damage-associated molecular patterns
dH_2O	Distilled water
DKD	Diabetic kidney disease
DKO	Double knock out (genetic deletion of two genes)
DNA	Deoxyribonucleic acid
DPX	Dibutylphthalate Polystyrene Xylene
DRP1	Dynamin related protein 1
DTNB	5,5’-Dithiobis(2-nitrobenzoic acid
EDTA	2,2',2'',2'''-(Ethane-1,2-diyldinitrilo)tetraacetic acid
EGTA	Ethylene glycol-bis(2-aminoethylether)-N,N,N′,N′-tetraacetic acid

ELISA	Enzyme-linked immunosorbent assay
ERB	Energised respiratory buffer (Mitochondrial swelling assay)
ESRD	End stage renal disease
EtOH	Ethanol
ETS	Electron transport system (also known as, electron transport chain)
FAO	Fatty acid oxidation
FAS-L	Fas Cell Surface Death Receptor ligand
FCCP	Carbonyl cyanide-4 (trifluoromethoxy) phenylhydrazone
GHb	Glycated haemoglobin
GSI	Glomerular sclerosis index
HbA_{1C}	Haemoglobin A1c
HEPES	4-(2-hydroxyethyl)-1-piperazineethanesulfonic acid)
hr	hour
HRP	Horseradish peroxidase
IDDM	insulin deficient diabetes mellitus
IMM	Inner mitochondrial membrane
kB	Kilo base (of DNA length)
KH_2PO_4	Potassium phosphate
Kim-1	Kidney Injury Molecule, (also hepatitis A virus cellular receptor 1, and T-cell immunoglobulin mucin 1)
KO	Knock out (genetic deletion of gene of interest)
KW:BW	Kidney weight to body weight ratio
KXA	ketamine, xylazine and atropine
MAS	Mitochondrial assay buffer (for Seahorse)
MIB	Mitochondrial isolation buffer
MOMP	Mitochondrial outer membrane pore
MOPS	3-Morpholinopropane-1-sulfonic acid
mPTP	mitochondrial permeability transition pore
mtDNA	mitochondrial deoxyribonucleic acid
NBF	Neutral buffered formalin
NERB	Non-energised respiratory buffer (Mitochondrial swelling assay)
NIDDM	Non-insulin dependent diabetes mellitus

OCR	Oxygen consumption rate
OMM	Outer mitochondrial membrane
Oligo	Oligomycin
PAS	Periodic acid Schiff, histology stain
PBS	Phosphate buffered saline
PCR	Polymerase chain reaction
Ppif	Peptidylprolyl Isomerase F
PTC	(renal) proximal tubule cell
ROS	Reactive oxygen species
ROS/NS	Reactive oxygen and nitrogen species
RAS	Renin angiotensin system
RNA	ribonucleic acid
RCR	Respiratory control ratio
RNA	ribonucleic acid
RTqPCR	Real time quality polymerase chain reaction
SGLT-2	Sodium glucose co-transporter 2
SKO	Single knock out
STZ	Streptozotocin
T1DM	Type 1 diabetes mellitus
T2DM	Type 2 diabetes mellitus
TBS	TRIS buffered saline
TEM	Transmission electron microscopy
TMB	3,3′,5,5′-Tetramethylbenzidine
TRAIL	TNF-related apoptosis-inducing ligand
TRIS	TRIS (hydroxymethyl)aminomethane
TUNEL	DeadEndTM Fluorometric TUNEL System
UCP	Uncoupling protein family
UCP-1	Uncoupling protein 1
UCP-2	Uncoupling protein 2
VDAC2	Voltage-dependent anion-selective channel protein 2

Nomenclature

mouse studies	
db/db	Type 2 diabetic
db/m	heterozygous control, non-diabetic
Ppif -/-	Mouse with global deletion of Ppif gene
Ppif WT/WT	Wildtype control

Wild type	WT
Cre control	Cre +
Bak SKO	Bak -/-
Bax SKO	Bax fl/fl Cre +
Bax DKO	$Bak^{-/-}$ $Bax^{fl/fl}$ Cre^{+} mice

Chapter 1

Chapter 1. Introduction

1.1 History and pathogenesis of diabetes mellitus

1.1.1 Type 1 Diabetes mellitus

Diabetes mellitus was first described as long as 3000 years ago, characterised by the presence of sugar in the urine. Life expectancy was unfortunately short for people with the condition, where affected patients would rapidly develop extreme thirst and muscle wasting. Landmark studies in the late 19th and early 20th century identified the significance of pancreatic disruption and the loss of insulin signalling to the onset of the disease. The subsequent development of insulin therapies resulted in a drastic improvement in life expectancy for diabetic subjects, allowing them to lead a relatively normal life. Today we identify Type 1 diabetes mellitus (T1DM) as an autoimmune instigated disease, where the insulin producing beta cells of the pancreas are targeted, and phagocytised, by a range of autoreactive immune cells, including: neutrophils, dentritic cells, CD4+ and CD8+ T-cells, and B-cells (1–3). Progressively, this immune cell regulated destruction leads to the loss of beta cell mass, which in turn alters systemic glucose regulation. This primarily results from the reduction in circulating insulin levels caused by the loss of beta cells. In euglycaemia, insulin is released from the pancreas, following the ingestion of carbohydrate rich meals, this allows tight regulation of glucose in the plasma. Initial spikes in absorbed glucose are able to be rapidly controlled by insulin; mediating peripheral glucose uptake from the bloodstream into various tissues, as well as the deposition of glucose as glycogen in the liver, muscles, and adipose tissue (4,5). When insulin is absent from this system, such as in T1DM, sustained hyperglycaemia develops. Type 1 diabetes is frequently defined as insulin deficient diabetes mellitus (IDDM). Exogenous insulin supplementation is required for ongoing survival.

1.1.2 Type 2 Diabetes Mellitus

In 1936, the distinction between Type 1 diabetes and Type 2 diabetes mellitus (T2DM) was determined based on insulin sensitivity in diabetic patients (6). The aetiology for insulin resistance in the development of hyperglycaemia, independent of the immune mediated pancreatic dysfunction of T1DM, began to be recognised and designated as T2DM. In the 21st century, T2DM is a common consequence of metabolic syndrome and obesity; primarily regarded as the manifestation

of insulin resistance in peripheral tissue. It is diagnosed by the presence of elevated fasting glucose often in the context of an abnormal oral glucose tolerance test. As T2DM progresses, the development of reduced beta cell mass can occur as the pancreas fails to handle increased insulin demand. Its notoriety as a purely modifiable lifestyle disease, associated with over-eating and lack of exercise, has been mostly dispelled; with contemporary research revealing that a highly complex array of factors influence its aetiology in addition to modifiable ones (7,8). Whist diet and exercise are clear risk factors associated with the development of T2DM in western countries (9,10), genetic data reveal a higher burden within some ethnic populations, indicating a strong genetic component (11–13). Additionally, studies examining the development of insulin resistant diabetes in non-obese people, provide important insights into the range of factors which influence the development of insulin resistance (14,15). This is of particular importance in countries such as India and China, where T2DM is frequently observed in non-obese subjects, with variable phenotypes (16). Non-insulin dependent diabetes mellitus (NIDDM), including insulin resistance as in T2DM, does not initially require exogenous insulin supplementation, and can be responsive to life-style modifications in the early stages of disease.

1.1.3 OTHER TYPES OF DIABETES

The recognition of additional subtypes of diabetes, and diabetes-like conditions, has expanded our understanding of metabolic changes that induce hyperglycaemia. Gestational diabetes is one example, with the incidence rate observed to be increasing, leading to new health initiatives for peri-partum screening (17). Further, the development of gestational diabetes is associated with an increased risk for developing postpartum diabetes (18,19). Beyond systemic glycaemic changes, other metabolic dysfunctions mimicking diabetes have also been observed. This includes tissue specific pathologies in neurological disorders such as insulin resistance during Alzheimer's disease (20). Hyperglycaemia has also been observed alongside the chronic liver dysfunction seen in haemochromatosis and hepatitis, highlighting the importance of hepatic function in glucose homeostasis (21,22). Although no consensus has been reached as to what should constitute type 3 diabetes, many subsets of hyperglycaemia and insulin dysfunction are now recognised. The complexity of diabetes continues to develop as the boundaries between insulin deficient and insulin resistant diabetes are increasingly blurred. It is not uncommon for patients to have multiple subtypes

of diabetes concomitantly, influencing the range of therapeutic interventions available to control the disease (23).

1.1.4 DIABETES AS A CHRONIC DISEASE

Many decades of research have allowed myriad insights into the complexity of human metabolism, yet there is still much more to learn. Although impressive advances are being made into finding a cure, thousands of new diabetes diagnoses are made each year with 1 in 11 people estimated to have some form of diabetes (24). In 2019, diabetes is a burgeoning global health concern as the incidence of both T1DM and T2DM continues to rise. T1DM is estimated to be increasing by 3-6% per year whilst the incidence of T2DM continues to rise at variable rates depending on both global, regional and individual risk factors (25,26). Fortunately, medical advances in patient management now mean that diagnosis is the beginning of a decades long journey living with the disease. This in itself presents challenges, as we recognise the chronic nature of diabetes. Chronic hyperglycaemia is strongly associated with the development of complications, however, other factors within the diabetic milieu also contribute to their development (27,28). Even with excellent glucose control, the development of associated pathology in different organ systems (diabetes complications) is not entirely eliminated (29–31). Whilst improvements have been made, people with diabetes still have reduced life expectancy relative to non-diabetic peers. This relates primarily to these complications, representing a health gap which still needs to be addressed (32,33). Strategies to reduce and prevent the development of diabetic complications are crucial in order to alleviate morbidity and reduce mortality associated with all forms of diabetes.

1.1.5 PREDIABETES AND THE METABOLIC SYNDROME

The development of associated morbidities that precede diabetes itself have also been identified as a significant area of health concern. Indeed, prediabetes and the metabolic syndrome must also be considered when evaluating the burden of elevated blood glucose levels and associated morbidity. Prediabetes is defined as the intermediate stage of rising hyperglycaemia where fasting blood glucose levels fall within the range of 6.1 to 6.9 mmol/L (just below the threshold for diabetes at >7.0mmol/L), alongside dysregulation of insulin sensitivity as measured through oral glucose tolerance testing (34). Prediabetes is largely considered to be a reversible disease, and represents a critical window for implementing dietary and lifestyle interventions to prevent diabetes, however, the insidious and often asymptomatic nature of prediabetes means that patients are often

unaware that they have the condition (35–37). Studies have demonstrated that lifestyle intervention may not prevent the progression to T2DM in all patients (38,39). Other metabolic changes also occur during this stage, including increased glycated haemoglobin, fructosamine, and an elevation in markers of inflammation, albeit with a high level of intra-patient variability (40,41). This highlights the complexities present in defining prediabetes and thus in providing an adequate diagnosis. Whilst a diagnosis of prediabetes does not guarantee progression to T2DM, it still remains as one of the strongest predictors for the development of diabetes (35,37). Indeed, the intermediate elevation in glucose levels and insulin resistance has been associated with an increased risk of cardiovascular complications (42,43). Further, studies such as AusDiab have also demonstrated that many microvascular and macrovascular diabetes complications begin to develop in the prediabetic state (35,44–46).

The metabolic syndrome is also considered a high-risk state for the development of T2DM: which includes the presence of central adiposity, dyslipidemia and hypertension, in addition to hyperglycaemia (47). Risks for the development of CVD and diabetes complications are also elevated with metabolic syndrome and early signs of these co-morbidities are often reported, however, some limitations of metabolic syndrome's predictive power have been noted (47–49). To date large clinical studies, including AusDiab and the Emerging Risk Factors Collaboration, have suggested that glucose levels remain the most important risk factor for assessing associated morbidity (50,51). The ability to delineate the role of glucose from other metabolic changes in T2DM is an important consideration in the identification and management of diabetes related pathologies. Together, prediabetes and the metabolic syndrome can provide a temporal insight into the pathological changes that precede diabetes and the development of diabetes complications associated with chronic hyperglycaemia.

1.2 DIABETES COMPLICATIONS

The chronic physiological changes associated with pancreatic disruption in diabetes, including elevated blood glucose, altered insulin homeostasis, and – in the instance of type 1 diabetes – circulating auto antibodies (amongst others), contribute to the development of a range of sequelae (28). Individual organ systems are susceptible to these changes and manifest as a multitude of complications (***Figure 1.1***). The macrovascular complications, including coronary artery disease and

stroke, are common causes of diabetes-associated mortality (52,53). Several clinical studies have demonstrated the integral link between hyperglycaemia and CVD outcomes, with management of glucose levels able to reduce CVD associated events (54–56). A range of microvascular complications may also manifest in several organ systems and contribute significantly to the development of diabetes-associated morbidity (57). These include retinopathy, neuropathy and nephropathy. Whilst hyperglycaemia directly damages the small vessels, it also induces toxic effects in many other cell populations around the body (58,59). Other co-morbid changes in diabetes, such as blood pressure and insulin signalling changes, can also contribute to the development of associated end organ pathologies (60,61). The field of diabetic complications represents a critical area of research, as the number of people living with the condition continues to rise. Further reductions in the morbidity and mortality will be an important part of improving diabetes care and extending life expectancy into the future. This will be particularly important in poorer and under-resourced areas where the latest interventions may not be available. The ongoing development of diabetes complications requires further research in order to elucidate effective solutions and preventative approaches.

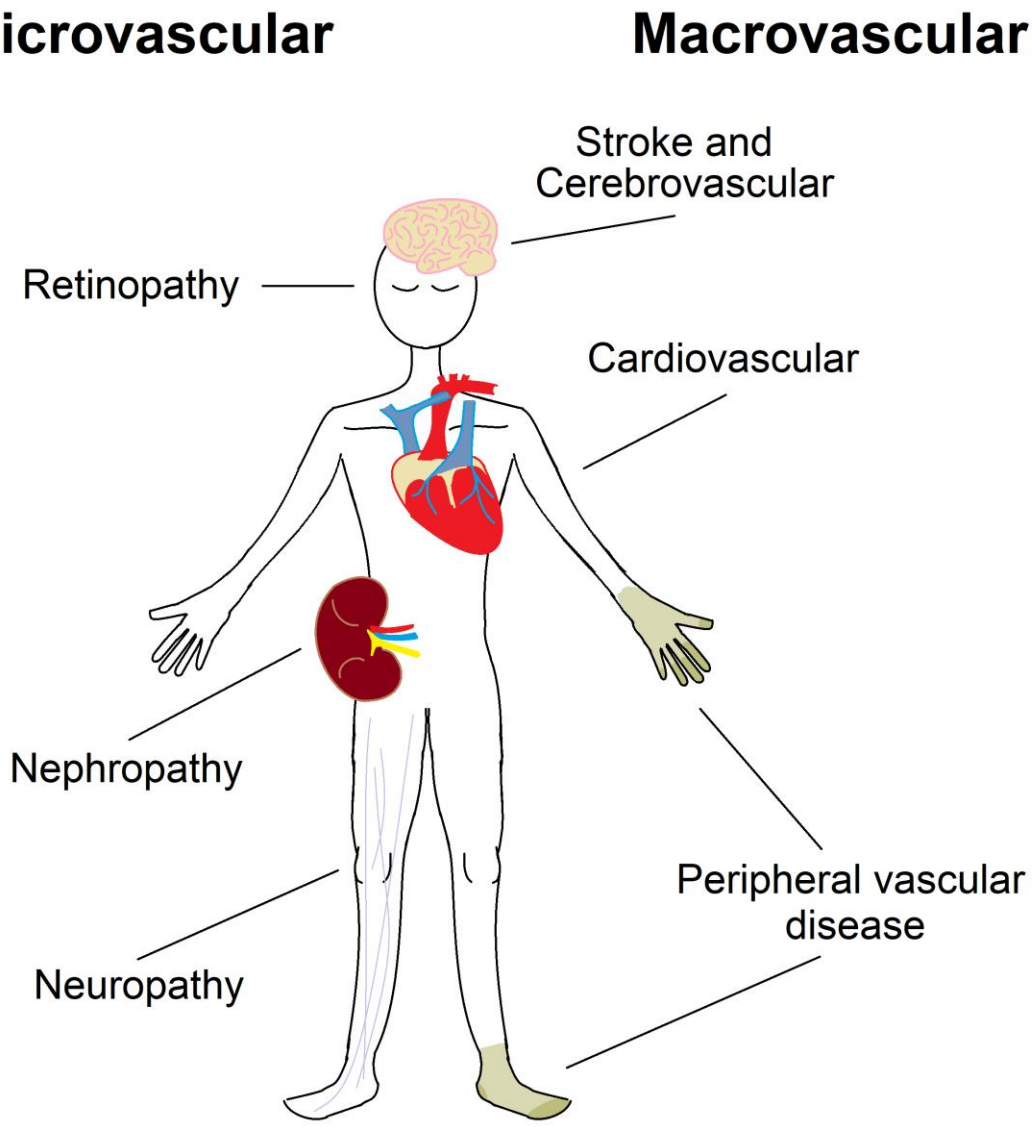

Figure 1.1: The Macrovascular and Microvascular complications of diabetes mellitus

1.3 DIABETIC KIDNEY DISEASE

Globally, renal complications continue to be a major contributor to diabetes associated mortality. In Australia, diabetic kidney disease (DKD), or diabetic nephropathy as it is also known, is estimated to affect more than 250,000 people(62). Currently DKD is the most prevalent cause of end-stage renal disease (ESRD) and accounts for more than 30% of total cases (62,63). There is no cure for ESRD and patients often face lengthy terms of dialysis for survival where no renal transplant is available, or is contraindicated. For indigenous Australians, who are disproportionately affected by ESRD, and patients in parts of Asia and Africa, additional barriers are present with fewer resources available and lengthy travel requirements to receive dialysis treatment (64,65). Current clinical options targeting diabetic nephropathy include rigorous glucose management and the use of renin angiotensin system (RAS) blockers to delay its progression (66). Over the last few years there has been further progress with certain newer glucose lowering classes such as SGLT2 inhibitors and GLP1 agonists conferring some degree of renoprotection in T2DM, although the true benefits remains to be fully determined (67,68). Whilst these approaches have demonstrated benefits, for some patients, this does not slow the progression to ESRD (69). Furthermore, the progression rate of DKD can vary significantly among individuals with no reliable technique available for predicting patient risk for developing ESRD (70). Current therapies are not meeting patient needs, and thus, there is an urgent need to investigate additional therapeutics to halt the progression of renal damage, and to understand the aetiology of diabetic nephropathy.

1.3.1 RENAL STRUCTURE AND FUNCTION

The kidney is a highly heterogeneous organ, which requires complex approaches in the management of diabetes-associated pathologies. Anatomically, the kidney may be separated into three main structures: the renal cortex, where blood is filtered; the medulla, where the urine is collected and concentrated to its final form; and the renal pelvis, where the final urine leaves the kidney via the ureter (***Figure 1.2***). There are five distinct components of the kidney: the glomeruli, tubules, interstitium, blood vessels and nerves; which are all differently affected in the development of DKD. The functional unit of the kidney, known as the nephron, is composed primarily of a single glomerulus and its associated tubule (***Figure 1.3***). The glomerulus is a complex network of capillary loops, surrounded by a basement membrane and podocyte cells (visceral layer), which filter the blood and allow fluid and solutes to pass through. This extravasated fluid, known as ultrafiltrate, is collected

in the Bowman's capsule: a structure surrounding the glomerulus (parietal layer) that forms the beginning of the tubular segment of the nephron. Each tubule begins around a single glomerulus in the kidney cortex and initially descends down towards the medulla (proximal tubule), loops around (Loop of Henle) before retracing its path back up to the cortex (distal tubule), and then redescending down into the medulla once again (collecting ducts). The entire tubular length is responsible for a range of excretion and reabsorption processes involved in the concentration of the final urine, with each section performing highly specialised roles (71). Urine is then passed through the renal pelvis, before being stored in the bladder.

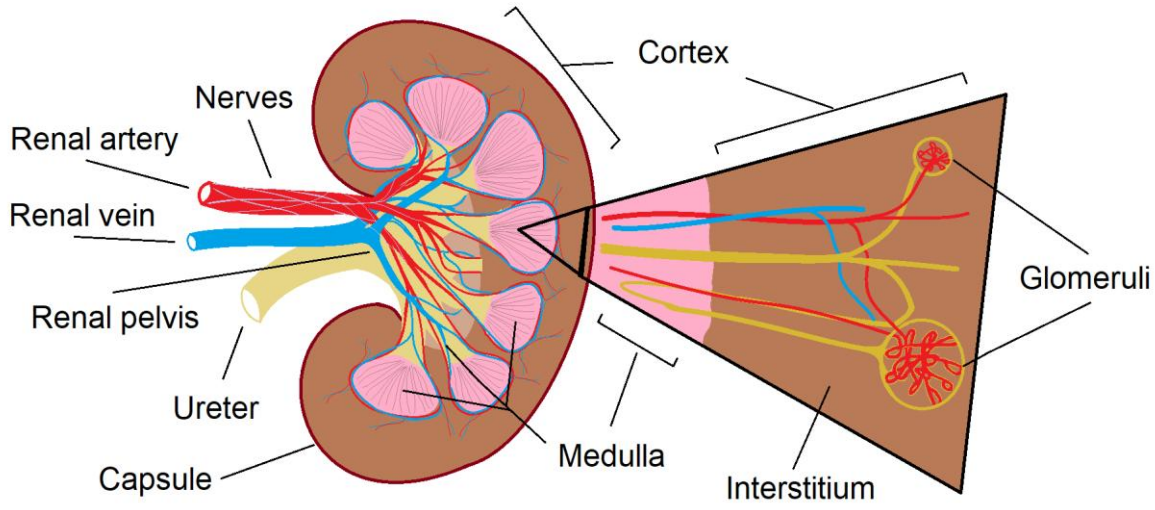

Figure 1.2: The structures of the human kidney

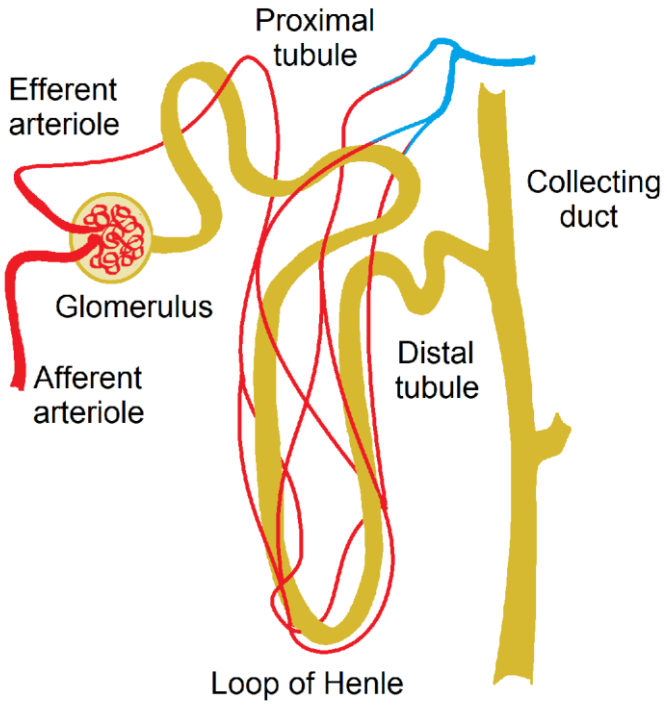

Figure 1.3: The components of the renal nephron

1.3.2 DIABETES ASSOCIATED PATHOLOGICAL CHANGES

In diabetes, a number of pathological changes begin to develop in all of the different structures of the kidney. Elevated glucose is particularly toxic to the endothelial cells of capillaries, such as those in the glomeruli, and endothelial dysfunction is considered one of the major drivers of DKD (72). Glomerulosclerosis is one of the major features associated with renal decline with progressive loss of functional glomeruli used as a clear clinical indicator of renal disease progression. Although renal biopsies are rarely taken, particularly in the early phases of nephropathy, the glomerular damage is assessed indirectly with the use of clinical testing. Measures of renal function (such as creatinine clearance and cystatin C) provide estimates for glomerular filtration rate, which are used to determine the stage of renal disease. Urinary analysis for the presence of albuminuria, a prominent protein in blood plasma that leaks into the ultrafiltrate when glomeruli are damaged, is also important for determining risk of renal failure. The detection of small levels of albumin (30-300mg/day), known as microalbuminuria, is an early sign of renal damage and is frequently also encountered in pre-diabetes (46,73). The progression to macroalbuminuria (>300mg/day) is generally associated with a decline in renal function, however, there are limitations in the predictive ability of this parameter in any individual patient (27,74).

Beyond the glomeruli, many of the other renal structures are also altered in diabetes. Loss of renal mass is one feature of later stage renal disease, along with interstitial fibrosis. Tubular atrophy and dysfunction are also observed. While the extent of the role of tubular pathology in the progression of fibrosis and renal decline remains unclear, recent findings indicate that tubular changes play a larger role than traditionally thought (75,76). There is some evidence to suggest that renal tubulointerstitial damage underpins many of the key changes in the development of renal disease, as the tubules are crucial for the reabsorption of albumin from the ultrafiltrate and preventing loss of the protein as a result of glomerular leakage (75,77).

1.3.3 THE SIGNIFICANCE OF PROXIMAL TUBULAR CELLS IN DKD

The proximal tubules are considered to be particularly susceptible in diabetes due to their role in maintaining plasma sodium, glucose and albumin concentrations by reabsorption (78). Indeed, excess glucose has been shown to mediate proximal tubule cell death via increased oxidative stress (79,80). The proximal tubules are also responsible for the reabsorption of other solutes, ion and proteins from the ultrafiltrate (81). In addition, the proximal tubules also maintain a range of other

important physiological functions. This includes production of hormones involved in the renin-angiotensin-aldosterone system (RAAS) and regulation of blood pressure (82–84). Renal haemodynamics and control of glomerular pressure involve a complex interaction of multiple factors due to the importance of renal function to systemic volume homeostasis. A feedback mechanism exists between the glomeruli and the tubules to locally regulate glomerular flow rate (microcirculation) by constricting or relaxing the afferent arterioles (85). This mechanism, known as tubuloglomerular feedback, underlines the significance of tubular function to the overall health of the kidney and in diabetes-associated changes. Tubular reabsorption rates have been demonstrated to influence the tubuloglomerular feedback loop directly as changes in electrolyte flux through the PTECs subsequently alters the luminal volume of nephrons and thus hydrostatic pressure gradients downstream. Specifically, the role of Na^+ transport across membranes is thought to act as a mechanistic sensor in relaying these feedback signals at the macular densa. In diabetes, the development of hyperfiltration is thought to result from the increase in tubular reabsorption mediated by hyperglycaemia. This includes the elevated concentrations of glucose and sodium ions that are actively transported through the proximal and distal tubules. This may also drive changes in GFR derived from dysfunction within the tubuloglomerular feedback loop (86,87). This is in addition to other processes including vascular factors may also drive changes in GFR (88).

SODIUM AND GLUCOSE REABSORPTION

The proximal tubules are the component of the nephron where excreted sodium ions and glucose may be reabsorbed. The main mechanism by which glucose and sodium is reabsorbed revolves around the sodium-glucose transporter-2 (SGLT-2) which accounts for 80-90% of glucose reabsorption (78). This solute carrier family protein has a very high ATP energy requirement for the transport of Na^+ ions and glucose, which it couples to the action of the Na^+/K^+ ATPase pump. SGLT-2 actively transports Na^+ ions across the basolateral brushborder to maintain intracellular Na^+ concentrations (89). Recent studies have identified this transporter as a therapeutic target for reducing blood glucose in T2DM (90–92). Several pharmacological intervention trials have recently tested the feasibility of SGLT-2 blockade in managing diabetes by preventing the re-uptake of filtered glucose (93–96). This also includes a reduction in diabetes associated hyperfiltration mediated through the blockade of excessive sodium and glucose reuptake (97,98).

SGLT-2 INHIBITION AND RENAL OUTCOMES

Clinical studies have shown promising results for a reduction in cardiovascular events and renal complications with SGLT-2 inhibition, and is a topic that has been reviewed in detail by others (99–101). Briefly, three of the compounds that have been tested in major clinical trials are canagliflozin, dapagliflozin, and empagliflozin. Each of these phlorizin derivatives have been demonstrated to exert a demonstrated reduction in all cause mortality and CVD adverse events. The outcomes from the CREDENCE trial of Canagliflozin revealed a 30% decrease in the relative risk adverse events, including renal outcomes, at the study interim that lead to the early cessation of the trial following ethical guidelines (102). Likewise, the CVD, renal and mortality benefits of Empagliflozin in T2DM have been identified through studies such as the EMPA-REG OUTCOME trial (67,103). Dapagliflozin also demonstrated a reduction in all cause mortality however results were modest in comparison and reported renal functional improvements may be minimal compared with other SGLT-2 inhibitors (104,105). All of these compounds are members of a broad class of glucose-like analogues that competitively bind to SGLT-2, and thus prevent the efficient coupling of Na^+ and glucose import through the apical membrane of renal proximal tubule cells. This effectively prevents the re-uptake of excess luminal glucose that occurs under diabetic conditions. It is likely that each of these three analogues has a slightly different mechanism of action, and these differences are still being investigated.

The promising dynamics of SGLT-2 inhibitors has lead to updated hypotheses for the role of glucose transport and renal cell energetics: particularly within the S1/S2 renal proximal tubule cells which primarily express SGLT-2 (106–108). Whilst the exact mechanisms of the overall systemic benefits are still being elucidated, evidence from several studies and key reviews suggest that this change in energetics stems from the reduced activity of the Na^+/K^+ ATPase pump with reduced uptake of Na^+ through SGLT-2 in addition to elevated intracellular adenosine monophosphate (AMP) and ADP levels (109,110). Mudalier et. al. suggest that the underlying renal and cardiac benefits relate to the switch in cell fuel preference to ketone bodies and suggest that an increase in metabolic efficiency is gained over the usual fuels of glucose and free fatty acids (106). However, the hypothesised improvement in ATP efficiency with ketone bodies remains controversial and has not been confirmed to occur across all metabolic studies (111–113). Regardless, the S1/S2 segments of the PTECs appear to be exempt from ketone switching and instead experience an increase in

gluconeogenesis related to reduced glucose perfusion (114,115). The implications for metabolic alterations with SGLT-2 inhibitors, including potential reductions in mitochondrial function, must be considered in the context of fuel source switching in diabetes (109).

Finally, although there is strong evidence for an improvement in chronic renal outcomes in T2DM the potential for SGLT-2 inhibitors to induce acute renal injury remains under current investigation following advice provided by the Food and Drug Administration of the USA (116). The extent of this risk appears to be unlikely, with recent trials inferring no adverse risk is present in clinical cohorts; and indeed these agents may reduce renal injury (117,118). Currently, SGLT-2 inhibitors are precluded from use in patients with lower eGFR, due to an apparent lack of glucose lowering effects in such individuals. Although the recent CREDENCE trial suggests that even in these subjects, where glucose lowering is not observed, this agent still affords renoprotection (102).

Albumin Reabsorption

Proximal tubules also play a critical role in albumin reabsorption from the ultrafiltrate. In general, albumin is retained in the blood with microalbuminuria developing in early disease states in diabetes. The proximal tubules are able to mediate albumin reabsorption through megalin and cubilin receptors in the apical border (119–121). Interestingly, animal models of diabetic nephropathy can show vastly different outcomes for the development of albuminuria which may reflect the large range of potential factors involved (122). The role of the renal tubules in modulating albuminuria is gaining attention as a target for the prevention of DKD pathology (123,124).

Other metabolic roles

The proximal tubular cells (PTCs) are also the primary site of the final oxidation of Vitamin D 25(OH)D (calcidiol) to its hormonal active form: 1,25(OH)2D (calcitrol) (125). Vitamin 25(OH)D is absorbed through megalin and cubilin receptors by endocytosis in the apical membrane of the PTCs (126). It is then processed at the 1-α-hydroxylase site in mitochondria. Vitamin D has a wide range of important physiological functions; namely calcium homeostasis for muscle function and bone mineralisation. PTCs are also responsible for the reabsorption of calcium ions from the ultrafiltrate (127). Calcium is also important for the tubules themselves as it is crucial for the high load of bioactive mitochondria which require carefully maintained calcium concentrations to produce the required ATP for the continuous active transport processes (128). Interestingly, vitamin D deficiency can be

observed in patients with CKD with one study reporting 40% of patients as Vitamin D deficient in their cohort (129). In patients with CKD caused by diabetes this effect was pronounced with as many as 80% being deficient. Further, in vitro data suggest that key modulators of vitamin D synthesis in the kidney are altered in the diabetic state contributing to senescence and cell death (130). Together the deregulation of both calcium and vitamin D metabolic processes in renal decline and ESRD, contribute to renal osteodystrophy, which is a concern for DKD patients (131).

1.3.4 MITOCHONDRIA IN PTCS

The proximal tubules also contain a dense network of mitochondria, required for the maintenance and function of all these metabolic processes. The mitochondria are central to many diverse biological processes including: energy production (i.e ATP via oxidative phosphorylation and fatty acid synthesis), ion homeostasis (Calcium, Iron, Copper etc.) as well as being key regulators of cell death. Indeed, alterations in mitochondrial biogenesis are suspected to occur in diabetic nephropathy (132). The role of mitochondrial function in the progression of many diseases has been of particular interest in recent times, with the kidney being no exception. The hypothesis that altered mitochondrial function underlies diabetes and its complications is being actively explored. Results from my laboratory, and others, have previously demonstrated a decline in renal mitochondrial function in the settings of diabetes, which is not reversed or attenuated by conventional therapies (133,134). Whether mitochondrial dysfunction is a mediator of pathological change or a consequence of renal disease is one of the key questions being explored. A review examining the advances in targeting mitochondria and the potential therapeutic advantages of improving their function is explored in more detail by contributions from the co-authors in ***Publication 1***. Mitochondrial biology is a complex area of research and their contribution to DKD requires careful elucidation.

SUMMARY

As demonstrated above, the kidney is a heterogeneous organ with diverse roles in maintaining a range of homeostatic functions. All the different components may be affected by diabetes. Although advances are being made in reducing the progression of renal damage associated with hyperglycaemia and other co-morbid effects, many patients still progress to renal failure. New therapeutic targets must continue to be evaluated so that new ways of reducing morbidity and mortality can be found.

THE ROLE OF MITOCHONDRIA IN DIABETIC KIDNEY DISEASE

The significance of mitochondrial health in the development and progression of human disease is a recent advancement with the increased understanding of the importance of these organelles in general cellular processes. Awareness of the evolutionary origins of mitochondria is very important for dissecting the legacy of both energy production and cell death mechanisms. Detailed analysis of mitochondrial function is required to fully grasp the consequences of this specific organelle in the development of DKD.

1.3.5 MITOCHONDRIAL EVOLUTION

Mitochondria power eukaryotic cells with the high energy required to sustain the complexities of multicellular life (135). Originally considered to have arrived in eukaryotes by the resulting endosymbiosis of a non-lethal infection of alphaproteobacteria into a proto-eukaryote cell (likely an Asgard Archaea), mitochondria have persisted ubiquitously due to the large evolutionary advantage they provide (136–139). This advantage is provided by the ability to extract chemical energy from carbohydrate via a step-wise reduction of molecular oxygen (aerobic respiration) within a controlled system (140). The origin of life on earth itself revolves around molecular oxygen and its redox potential to fuel organic processes, along with the abundance of liquid water available on Earth. Mitochondria, much like many prokaryotes, are able to exploit the physical properties of oxygen to allow them to split water molecules and use this energy. The reduction potential of oxygen is crucial as the energy released from atomic bonds is then used to generate complex molecules for other purposes (141,142). The physical properties of oxygen thus enable the high energy extraction from chemical bonds to fuel the generation of important energy storage molecules such as Adenosine Tri-phosphate (ATP) (142). This process generates ATP with around 15 times higher efficiency than that of glycolysis (anaerobic respiration) (141). The ability to store the energy in phosphate bonds allows cells the ability to rapidly perform energy intensive activities with ease. Without mitochondria to provide high quantities of ATP, many of the biological processes we take for granted would not be possible (143).

In addition to energy production, the bacterial origin of mitochondria is also regarded to have provided many other physiological functions imperative to multi-cellular life. Indeed, mitochondria are important regulators of metal ion homeostasis in cells. This includes iron, copper and calcium defects in these systems, having been associated with various disease processes (144–146). They are also

critical in numerous survival sensing mechanisms and provide the ultimate multicellular defence against dysfunctional cells: apoptosis. The accidental symbiosis of prokaryotes inside proto-eukaryote cells, may also have left a legacy in the mechanisms of mitochondrial triggered cell death (147). Under normal circumstances it would be expected that bacterial infection would result in the death of the proto-eukaryotic cell. The ability to evade destruction, and avoid triggering intracellular defence mechanisms, would thus have a survival advantage. Even today bacterial evasion is an important area of immunological research. The legacy of this bacterial origin of mitochondria may be seen in the mitochondrial toxicity observed with broad spectrum antibiotics. A good example is polyamine antibiotics, such as gentamicin, which induce proximal tubular cell injury, in part by directly inducing cytochrome c release and mitochondrial initiated apoptosis (148–150).

1.3.6 MITOCHONDRIAL ORIGINS OF CELL DEATH

Mitochondria interplay the balance between cell survival and cell death in a highly regulated fashion. It is hypothesised that the main cell death and gene integrity sensing proteins arose early in the evolution of Eukaryotes (151). This includes the Bcl-2 family of proteins in mammals, and other related family homologues appearing in other eukaryotes (152). The maintenance of intrinsic, mitochondrial induced, cell death pathways supports the functional importance of healthy mitochondria. Further, mitochondrial fission and fusion proteins are also expected to have arisen in this manner, although the dynamic changes observed in eukaryotes are distinctly different from those traditional prokaryote behaviour. In mammalian cells, mitochondria undergo fission via a process which is guided by the endoplasmic reticulum (153). Mitochondrial fission retains some similarity to bacterial fission, as observed in replicating bacterial populations, with budding of mitochondrial bodies and chromosomal duplication and distribution (154,155). The ability to alter mitochondrial form through dynamic changes is also important for cellular replication. Fragmentation is observed during mitosis to ensure even distribution of mitochondria amongst daughter cells (156). Mitochondrial elongation on the other hand is associated with starvation (eg following autophagy) and resistance to cell death (157,158). Further, the dynamic status of mitochondria has been associated with susceptibility to cell death via interactions between DRP1 and BAX (159–161). A tendency to take on a more fragmented mitochondrial distribution has been observed in renal cells under diabetic conditions, and is thought to be associated with an increased threshold for cell death (162,163). Direct

targeting of the fission/fusion machinery to reverse this dysfunction has been shown to improve renal outcomes in pre-clinical models (164,165).

GENERAL FUNCTIONALITY OF MITOCHONDRIA

Mitochondria were once considered to be homogenous across the various tissues in the body. Recent advances in biology have elucidated that this is not the case, and mitochondria in different organs can have profoundly different form and function. Examples include variation in total content or 'number', shape, turnover, and energy substrate utilisation to name just a few (166). Mitochondrial volume, for example, in cardiac cells is considered to be the highest mass of mitochondria per gram of tissue compared with all tissue types in the human body, as reported previously (167). Other tissues with high levels included kidney, brain and skeletal muscle, while on the lower side of the spectrum were lung, spleen and eye. Shape is expressed by how the mitochondrial volume exists in 3D space. Mitochondria may be the classical depicted elongated sphere shape, however they may fuse and form extensive filamentous networks (168,169). Mitochondria have been observed to continuously undergo active fission and fusion processes (170,171). These processes perform critical functions in regulating function and health by mitochondrial turnover where small fragments are able to be recycled via autophagy (172,173). In addition, highly fragmented populations of mitochondria have been observed in association with changes in metabolic state and disease processes, as well as preceding the onset of apoptosis (168). The idea that a cell contains a certain number of mitochondria is thus erroneous and it is better to consider mitochondria as a dynamic membranous system where the total volume and/or function may change depending on cellular need (174). Key factors that influence the total volume of mitochondria include the availability of energy to both the organ system and to the organism as a whole. This explains, in part, why cardiac mitochondria have the highest volume, as they require sustained energy to contract continuously and pump blood throughout the body. Like-wise renal proximal tubule cells also have a high mitochondrial density due to the extremely high energy requirements of these cells during reabsorption of solutes and proteins. This intensive active transport process results in very high oxygen consumption to fuel the generation of the ATP to perform these actions (175). Under increased pressure load in conditions such as diabetes, this requirement increases the susceptibility of these tissues to hypoxic injury, a phenomenon which has been observed during the development of renal injury (176).

The source of substrates for mitochondrial respiration is also an important consideration. Cellular energy substrate reliance is often uniquely described in mitochondrial biology from isolated mitochondrial preparations, with limited knowledge available concerning the exact variations in *in vivo* biochemistry. A cell may use carbohydrate (pyruvate), or lipid (fatty acid) substrates to fuel mitochondrial respiration in the presence of oxygen, or draw on anaerobic mechanisms, under hypoxia. *In vitro* and *ex vivo* testing has provided some indication of the preferred substrates of different tissue types (177). The mitochondria in the renal tubules predominantly rely on fatty acid oxidation to fuel ATP production, and work at maximum OXPHOS capacity, in order to fulfil their energy intensive processes (178–181). They are also responsible for a number of glucose handling processes that contribute to systemic glucose availability, including reabsorption of glucose from the urinary ultrafiltrate. Additionally, PTCs are also able to undergo gluconeogenesis, as they are able to use glucose-6-phosphatase for de novo glucose synthesis, and thereby contribute significantly to systemic glucose supply during the fasted state (182–184). In addition, glutamate and lactate are important precursors in PTC metabolism and have been demonstrated to be one of the preferred substrates used by these cells (185–187). PTC metabolism has been shown to change under diabetic conditions. Expression of glucose transporters are upregulated, increasing their absorptive capacity (188,189). Curiously, renal gluconeogenic capacity is also upregulated with T2DM (190). It is possible that this increase in cytosolic activity will also impact mitochondrial energy capacity and influence the role of substrate utilisation through multiple pathways. Thus, renal cell metabolism provides an avenue to explore potential therapeutic targets in treating diabetes and its complications. It is uncertain as to what degree of modulation of mitochondrial function will influence overall metabolic functions, or improve renal outcomes for diabetic patients.

TARGETING MITOCHONDRIAL FUNCTION

Mitochondrial function is considered to be important for cellular health due to their capacity for oxidative energy production. The electron transport system (ETS) allows for the careful stepwise extraction of chemical energy stored in carbon based molecules by utilising the redox capacity of oxygen, copper and iron. The ETS is made up of 5 key complexes (denoted I-V) which catalyse the transfer of electrons via redox reactions through a series of small energy transfer steps. This process is highly dependent on the maintenance of a proton gradient across the mitochondrial inner membrane, formed by the redox reactions of Complexes I-IV, which are coupled to the

movement of protons against a concentration gradient. This gradient gives the membrane potential which allows complex V (ATP synthase) to harness the kinetic energy of protons returning to the mitochondrial matrix space. This final step of the process creates a high energy phosphate bond stored in ATP. In an ideal system, oxygen consumption would be coupled perfectly to the production of ATP. In reality, a number of factors allow for the careful modulation of energy storage and energy release to accommodate changes in cellular need (191). One key factor is the family of mitochondrial uncoupling proteins (UCPs), which perforate the inner mitochondrial membrane. This allows for the dissipation of the proton gradient, and a disruption to the crucial driving force of the energy transfer system (192). The expression of UCPs in mitochondria is varied across disease conditions and organ systems. For example UCP-1 is the major uncoupling agent involved in non-shivering thermogenesis in brown fat cells (193,194). Oxygen consumption is thus dissociated from ATP production and instead the chemical energy is released as heat. While thermal energy is one way of using this energy, other mitochondrial uncouplers, such as UCP-2, are not thought to release heat. Rather, they may serve to alter the functional capacity and redox status by modulating the switch between glucose and fatty acid oxidation, and favouring glycolytic processes even in the presence of oxygen (195). This is not dissimilar to the development of the Warburg effect in cancer cells, (aerobic glycolysis) which is a mechanism that protects the cell from the damaging effects of excess free radical oxidation (196). UCP-2 is the main UCP family protein expressed in the kidney and is increased in the kidney the context of diabetes (197). It is hypothesised that the increased expression of UCPs in diabetes may allow for an adaptation to hyperglycaemia by driving the consumption of glucose without storing it in ATP bonds (191).

Finally, it is important to note that the efficiency of complete oxygen reduction to the production of ATP is also highly dependent on a range of factors (198). This includes the availability of reductive metals in the ETS (Fe for complexes I-III and Cu for Complex IV) and the relevant cofactors; as well as the concentrations of substrates at different sites. All participate in the biophysical determination of electron transfer efficiency through the ETS. Interestingly the presence of large antiport carriers such as the ATP/ADP antiporter (ANT), and also other channel proteins (including UCP-2) allow cellular regulation of the ETS in subtle but essential ways. This also includes the ability to modulate proton leak to reduce the production of superoxide (199). Interestingly, ANT is

particularly important in this modulation in *Drosophilia melanogaster* models of heart mitochondria and thermoregulation (200).

ALTERING MITOCHONDRIA CONTENT

The potential for altering mitochondrial parameters to improve disease outcomes is an area of increasing interest. For example, it is generally observed that exercise training can improve the function (efficiency), and also the total content, of mitochondria present in skeletal muscle. In these instances exercise training increases the number of mitochondria within cells to improve total respiration capacity (201,202). Cells also have an inherent mechanism for mitochondrial quality control which allows for the removal of damaged mitochondria (e.g. with mtDNA defects). Autophagy is the process that cells use to turnover (i.e. recycle) damaged or unused components within the cytoplasm. It is a tightly regulated, and highly redundant system, that initiates the encapsulation of cell contents, before fusing with lysosomes for degradation. The term mitophagy is reserved for the specific turnover of mitochondria, which may also be selectively recycled. Physiologically, autophagy can occur in periods of starvation, for example as in caloric restriction diets, and has been demonstrated to reduce mitochondrial volume in an effort to conserve total energy (203). Deficiencies in the turnover process are also observed in some disease states with questions arising on how the regulation of mitophagy is affected during the pathogenesis of many diseases (169,204). There is some evidence that defects in autophagy, and specifically mitophagy, occur in patients with diabetes, and should be a consideration when evaluating mitochondrial health (205,206).

1.3.7 DRIVERS OF MITOCHONDRIAL DYSFUNCTION

Mitochondrial health in systemic wellbeing has recently been highlighted as an area of new interest. Indeed mitochondrial *dysfunction* has been shown to underpin many disease processes, including DKD, highlighting the importance of healthy mitochondria in our day to day physiology. In clinical health, changes to mitochondrial number, shape, and function have been reported in an ever increasing number of human diseases (207,208). The question as to whether this dysfunction drives the aetiology, or is just a consequence of disease conditions, still remains to be elucidated. Key evidence for the support of the former is gathering momentum from an array of sometimes unexpected sources. One compelling reason for why we should be concerned about the health of our mitochondria is perhaps best illustrated by examining the various Mitochondrial

Diseases (or 'Mito'). Underlying genetic defects in Mito disease cause numerous symptoms as a result of the systemic interruption of mitochondrial function. Symptoms may be specific, varied, or non-specific, depending on the underlying triggers. The most debilitating symptoms can include widespread pain (headaches, neuralgia, CNS pain, muscle pain), exercise intolerance, an inability to fast, issues with regulating body temperature, gut issues (eg bloating, pain), cognitive dysfunction, dizziness and balance problems. The most severe types of Mito however are incompatible with life with death occurring *in utero*, or soon after birth. In these instances Mito allows an insight into what can happen when mitochondrial functional defects are inherited.

MITOCHONDRIAL DNA AND DYSFUNCTION

Loss of mitochondrial function can be associated with changes in mtDNA content and sporadic mutations to the mitochondrial chromosome. Fulminant Mitochondrial DNA depletion syndrome is a rare disease that manifests early in those affected leading to death. This highlights the importance of maintaining functional mitochondrial DNA in sustaining life. The effect of small scale loss of healthy mtDNA is less clear. This loss may be associated with aging, and some diseases where mitochondrial damage occurs with changes in mitophagy cycling. Further, mutations in mtDNA may also be related to changes in functional characteristics (Reviewed in further detail in ***Publication 1***) (209). Indeed, the phenotypes of acquired mtDNA mutations may to reflect those of the known inherited mitochondriopathies and is postulated by Forbes and Thorburn 2018, to increase susceptibility to OXPHOS deficits and potentially DKD (86). This is in part inferred from the discovery that acquired mitochondrial mtDNA mutations frequent occur in the general community (210). The acquisition of mitochondrial functional defects through disease processes, and the ability to reverse them is currently being explored in a range of fields including renal medicine.

CAUSES OF MITOCHONDRIAL DYSFUNCTION

Mitochondrial toxicity is a side effect not often considered in the routine administration of drugs. The idea that substances used to treat patients, as well as environmental chemicals, will have a negative effect on mitochondria is a developing area of interest. The possibility that it should be an important consideration is currently an area of interest in certain contexts such as pain disorders and neuropathic syndromes (211,212).

There are many drugs available on the market which have known effects on mitochondrial function including numerous everyday medications used to treat patients with diabetes. These include common antibiotics, and even statins, however, the distribution of effects have been shown to vary among drugs of the same class making this issue an interesting conundrum (213). Additionally, chemotherapeutics drugs are also being shown to affect mitochondrial health and the relation to the development of pain and neuropathies appears to be intricately linked (214). Causes of mitochondrial dysfunction in disease may have multiple conflicting aetiologies, adding complexity to the understanding of therapeutic targets and clinical interventions. The consequences of mitochondrial injury can be severe, due to their fundamental link with the ultimate consequence of disease: cell death. Mitochondria are at the heart of many of the cell death processes available to a cell. Thus the contribution of mitochondrial health to cell death outcomes will be explored.

1.4 CELL DEATH IN DIABETIC NEPHROPATHY

As diabetic renal injury progresses, the development of renal fibrosis and atrophy contributes to a loss of renal function. This may be partially explained by the processes of cell death which occur in response to diabetes associated cellular stress. The ability to slow the progression to ESRD by targeting cell death and sclerosis is an important area for exploring new therapeutic options. Although some mediators of the pathogenesis are relatively well understood, there is still much to be elucidated. Of interest here is the consequence of cellular and mitochondria stress on cell death outcomes. Classically, the two most well known cell death processes are apoptosis and necrosis. Apoptosis is generally regarded as being a tightly controlled process employed to delete cells, without inducing inflammation (regarded as 'immunologically silent'). This includes programmed death that occurs developmentally, but also provides a safeguard against damaged cells accumulating mutations (215). It may be triggered by either internal processes (intrinsic apoptosis) or by external factors (extrinsic apoptosis). Both processes induce signal transductions which converge on the activation of caspases, apoptosome formation, DNA degradation, and the compartmentalisation of cellular contents via membrane "blebbing". The small apoptotic bodies that form are then able to be easily phagocytosed by immune cells. This process relies on the continued production of ATP to fuel the cascade of events and to maintain plasma membrane integrity in order to prevent the release of cellular contents. Necrosis, on the other hand, is considered to be accidental cell death caused by pathological stimuli, resulting in membrane rupture and the expulsion of intracellular contents leading

to the exposure of damage-associated molecular patterns (DAMPs) and other inflammatory markers. It is associated with the induction of inflammatory responses as the body attempts to clear the debris. Necrosis may also occur following unsuccessful apoptosis, where critical steps are blocked, or when ATP is depleted (216,217). Whilst apoptosis and necrosis are two distinct consequences of cellular demise, the dynamics between the induction of one in preference to the other is highly complex, and may involve regulation at the mitochondrial level.

1.4.1 MITOCHONDRIAL CELL DEATH

The role of mitochondria in apoptosis relates to their central role in the initiation of intrinsic cell death pathways. Mitochondria respond to damage within cells and instigate the progression of apoptosis by the formation of distinct pores in their membranes.

THE MITOCHONDRIAL OUTER MEMBRANE PORE

Intrinsic apoptosis is predominantly mediated through mitochondria via the formation of a distinct perforation in the outer mitochondrial membrane (OMM). This is regulated by the activity of the proteins Bax and Bak, which congregate in the OMM and oligomerise into a channel forming pore. The presence of this pore, denoted as the mitochondrial outer membrane pore (MOMP), allows the release of critical ETS proteins and other proteins from the inner membrane space into the cytosol where they interact to induce apoptotic mechanisms (218,219). The most recognised consequence is the loss of cytochrome c from the mitochondrial inner membrane, which then proceeds to activate caspase 3, and 9, with the assistance of other mitochondrial proteins (220,221). A vast number of processes regulate the activation of Bax, which is a cytosolic protein that transiently interacts with the OMM under normal conditions. A complex hierarchy of events occur within the cytosol to both inhibit and to activate the translocation of Bax to the OMM, controlling its ability to participate in forming the MOMP. *See Publication 1 for additional review*. Additionally, mitochondria themselves are able to influence the insertion of Bax via the configuration of its functional homologue Bak, and also through VDAC2, which acts as an anchor for Bax insertion (222,223). The entire process is a careful balance between each protein interaction and other specific conditions, which determines the pro-apoptotic or anti-apoptotic status of a cell. However, Bax and Bak have also been previously demonstrated to participate in the formation of other mitochondrial pore forming processes.

THE MITOCHONDRIAL PERMEABILITY TRANSITION PORE

Whilst Bax and Bak are predominantly regarded as the gatekeepers of the MOMP, a number of secondary roles have also been defined which makes their role in mitochondrial function all the more interesting (224). Most importantly is the delineation of their role in the formation of the outer membrane component of the necrosis associated double membrane pore, the mitochondrial permeability transition pore (mPTP) (225,226). The mPTP is a non-specific pore that transverses both the OMM and the IMM, allowing the passage of solutes and H_2O into the mitochondrial matrix. This increase in permeability results in mitochondrial swelling, inhibition of ETS capacity and is generally considered to precede necrotic type cell death (225,227). Various proteins present in the IMM have been suggested as potential candidates in the formation of the inner membrane conductance channel. These include ATP synthase, ANT, the voltage dependent anion channel (VDAC) and Cyclophilin D (228–230). However, many of these have been re-evaluated as some may be redundantly involved (231–234). Cyclophilin D is one of the few candidates that remains in many of the models, with its direct inhibition being an active therapeutic target in many pathological processes (235,236). While the exact structure of the IMM pore complex remains contentious, evidence for the direct requirement for Bax and/or Bak as the OMM complex is compelling. Studies by others have also demonstrated that Bax plays a critical role in mediating the switch between apoptotic cell death and necrotic-type death (225,237).

1.4.2 TYPES OF CELL DEATH

Recent developments in the cell death field have dramatically expanded our understanding of cell death processes and have led to the identification of many novel forms of regulated and unregulated death pathways (see ***Table 1.1***). This list is by no means exhaustive and, indeed, novel death pathways are frequently being described every year. Whether each type described constitutes a unique form of cell death is an ongoing area of debate. Indeed, several subtypes of apoptosis may simply be reflective of the stimuli with different upstream pathways converging downstream in classically apoptotic forms. This helps to ensure the removal of damaged cells and prevent the accumulation of deleterious mutations, which might lead to oncogenesis. Importantly, the wide availability of cell death mechanisms underlies the significance of evolutionary safeguards in the execution of cell death. Prevention of one type of cell death will likely lead to another being induced if the stimulus is maintained (217). Whilst inhibition of apoptosis is associated

with an increased incidence for the development of neoplasm and cancer, the ability to influence the balance between apoptosis and necrosis may allow for an improvement in renal pathology. For example, there is evidence to suggest that inhibition of necrotic cell death, by inhibition of the mPTP following ischemia, is effective in allowing damaged cells to recover (238,239). This is thought to be achieved by increasing the damage threshold conducive to necrosis, thereby preventing cell loss and preserving overall tissue mass. This example demonstrates the potential for therapeutic targeting of cell death mechanisms to influence disease outcomes.

1.4.3 TARGETING CELL DEATH MECHANISMS IN DKD

The contribution of different types of cell death in DKD needs to be explored in detail in order to enable an assessment of how modulation of cell death pathways may influence DKD outcomes. Higher rates of apoptosis have been observed in the kidneys of patients with diabetic nephropathy and are thought to contribute to the loss of renal mass in the progression of the disease (240,241). Additionally, many apoptotic proteins have been reported to be upregulated in diabetic nephropathy, including TRAIL, FAS-L and decreased Bcl-2/Bax expression ratio (242–245). While the role of apoptosis in diabetic nephropathy is generally well established, (*reviewed further in* **Publication 1**) (209), research into the other mechanisms of cell death require further elucidation. Necrosis has also been demonstrated to be the primary death mechanism that occurs under acute kidney injury conditions, with evidence emerging that this may involve regulated necrotic pathways (e.g necroptosis, ferroptosis) (243,246,247). Whether these pathways remain as drivers of cell loss under diabetic conditions still needs to be determined. A detailed interrogation of the role of different cell death proteins could help elucidate specific targets integral to the loss of renal cell mass under diabetic conditions. It is possible that preventing the loss of renal tissue by interrupting cell death mechanisms may assist in preventing a decline in renal function.

Being able to understanding which pathways are likely to be induced in the development of pathological conditions can provide an insight into the mechanisms of that particular disease. This knowledge may then be harnessed to develop therapeutic targets which preferentially induce more favourable outcomes. The ability to exploit these processes may allow for an improvement in the progression of DKD and is worth exploring in more detail.

PUBLICATION 1

1.4.4 FOREWORD

The following publication expands on the role of cell death in the development of renal complications associated with diabetes. It explores the role and consequences of mitochondria-generated reactive oxygen species and reactive nitrogen species (ROS/NS) in the progression of diabetic kidney disease. As discussed, mitochondrial ROS/NS is a commonly identified feature in the diabetic kidney. Increased ROS/NS has been previously demonstrated to be elevated in both clinical and preclinical studies. The consequences of this mitochondrial ROS/NS can include the loss of cells through intrinsic cell death mechanisms. Mitochondria have varying roles at the centre of cell function. They mediate cell damage responses and ultimately initiate the intrinsic cell death response. This places mitochondrial function at the centre of cell death pathways, as diabetes induced dysfunction may alter the progression of DKD pathology. Publication 1, below, explores the role of mitochondria in sensing and responding to oxidative stress, and also in mediating DNA damage sensing processes to the initiation of apoptosis. It also presents evidence for the role of mitochondrial cell death in the progression of DKD.

This review was compiled along with the three co-authors listed, Dr. Gavin Higgins, who is joint first author. Associate Professor Judy de Haan, and Associate Professor Melinda Coughlan are joint senior authors.

Contribution of co-authors are as follows: Dr Higgins wrote **Section 3:** *Mitochondrial ROS/NS in the pathogenesis of diabetic nephropathy*; designed ***Figure 1***; and assisted in the development of the review's structure. A/Prof de Haan wrote **Section 1:** *Introduction*; and **Section 2:** *Contribution of ROS/NS production to diabetic nephropathy*. A/Prof Coughlan wrote **Section 6:** *Mitochondrial permeability transition as a pathway to renal injury*; and **Section 7**: *Targeting mitochondrial ROS in diabetic nephropathy*.

The following sections were researched and written by myself (R. Lindblom) and edited with assistance from co-authors and the editors of the journal: *Review of Diabetic Studies*. - *Abstract;* **Section 4:** *Consequences of oxidative stress in the diabetic kidney*; **Section 5:** *Modes of cell death during diabetic renal disease*; and designed ***Figure 2***.

Section 8: *concluding remarks and future perspectives* was the combined work of all authors.

The Review of DIABETIC STUDIES

REVIEW

Targeting Mitochondria- and Reactive Oxygen Species-Driven Pathogenesis in Diabetic Nephropathy

Runa Lindblom[1,2,3,4], Gavin Higgins[1,2,4,5], Melinda Coughlan[1,2,3,6,7], and Judy B. de Haan[2,7,8]

[1] *Glycation, Nutrition and Metabolism Laboratory, Baker IDI Heart and Diabetes Institute, Melbourne, Victoria, Australia.* [2] *Diabetic Complications Division, Baker IDI Heart and Diabetes Institute, Melbourne, Victoria, Australia.* [3] *Department of Medicine, Central Clinical School, Monash University, Melbourne, Victoria, Australia.* [4] *Equal contribution by first authors.* [5] *Department of Biochemistry and Molecular Biology, Monash University, Clayton, Victoria, Australia.* [6] *Department of Epidemiology and Preventive Medicine, Monash University, Melbourne, Victoria, Australia.* [7] *Equal contribution by senior authors.* [8] *Oxidative Stress Laboratory, Baker IDI Heart and Diabetes Institute, Melbourne, Victoria, Australia. Address correspondence to: Judy B. de Haan, Head, Oxidative Stress Laboratory, Diabetic Complications Division, Baker IDI Heart and Diabetes Institute, 75 Commercial Road, Melbourne, Victoria 3004, Australia, e-mail: judy.dehaan@bakeridi.edu.au*

Manuscript submitted March 30, 2015; accepted April 15, 2015

■ Abstract

Diabetic kidney disease is one of the major microvascular complications of both type 1 and type 2 diabetes mellitus. Approximately 30% of patients with diabetes experience renal complications. Current clinical therapies can only mitigate the symptoms, and delay the progression to end-stage renal disease, but do not prevent or reverse it. Oxidative stress is an important player in the pathogenesis of diabetic nephropathy. The activity of reactive oxygen and nitrogen species (ROS/NS), which are by-products of the diabetic milieu, has been found to correlate with pathological changes observed in the diabetic kidney. However, many clinical studies have failed to establish antioxidant therapy to be renoprotective. The discovery that increased ROS/NS activity is linked to mitochondrial dysfunction, endoplasmic reticulum stress, inflammation, cellular senescence, and cell death calls for a refined approach to antioxidant therapy. It is becoming clear that mitochondria play a key role in the generation of ROS/NS and their consequences on the cellular pathways involved in apoptotic cell death in the diabetic kidney. Oxidative stress has also been associated with necrosis via induction of mitochondrial permeability transition. This review highlights the importance of mitochondria in regulating redox balance, modulating cellular responses to oxidative stress, and influencing cell death pathways in diabetic kidney disease. ROS/NS-mediated cellular dysfunction corresponds with progressive disease in the diabetic kidney, and consequently represents an important clinical target. Based on this consideration, this review also examines current therapeutic interventions to prevent ROS/NS-derived injury in the diabetic kidney. These interventions, mainly aimed at reducing or preventing mitochondrial-generated oxidative stress, improving mitochondrial antioxidant defense, and maintaining mitochondrial integrity, may deliver alternative approaches to halt or prevent diabetic kidney disease.

Keywords: diabetic nephropathy · reactive oxygen species · apoptosis · necrosis · mitochondrial dysfunction

1. Introduction

Diabetes is recognized as the leading cause of end-stage renal disease (ESRD) in developed countries [1]. Statistics show a steady increase in the global prevalence of type 2 diabetes, with the worldwide obesity epidemic recognized as a major risk factor [2]. With an estimated 7.7% of the world population aged between 20-79 predicted to be diabetic by 2030, microvascular complications such as diabetic nephropathy are expected to contribute to a significant percentage of the worldwide morbidity rate [3]. Furthermore, chronic kidney disease (CKD), which affects ap-

proximately 5-30% of people with type 2 diabetes, is a significant risk factor for the development of cardiovascular disease (CVD) [4, 5]. Indeed, diabetic patients with microalbuminuria are 2-4 times more likely to experience cardiovascular impairments than non-diabetic patients [6], whilst those diabetic patients with overt kidney disease show a 4-8-fold increased risk of cardiovascular disease [7]. Despite the administration of glucose-, lipid-, and blood pressure-lowering drugs, nearly half of all diabetic patients continue on to develop renal and cardiovascular complications. Thus, the search for effective therapies is still a major goal in the treatment of diabetic patients.

Oxidative stress and inflammation, induced by chronic elevations in blood glucose in diabetic patients, are increasingly being recognized as risk factors [8] and significant mechanistic contributors [9-11] inseparably linked with the development of diabetic complications including CKD and ultimately ESRD. There is evidence that reactive oxygen and nitrogen species (ROS/NS) play key roles in the pathogenesis of diabetic nephropathy. This has initiated increased efforts to reduce or prevent the cumulative damage of ROS/NS-induced injury. However, clinical antioxidant trials with primary endpoints of CVD reduction have shown little success, which emphasizes the need for more knowledge about the major sites of ROS/NS production and the processes they are involved in [12-14].

Increased attention is currently paid to the significance of mitochondrial ROS/NS generated in response to elevated glucose level as the major player in the process of cell death. This impacts not only the ability of a cell to function optimally, but ultimately and collectively it dictates how an organ like the diabetic kidney responds to its challenging high-glucose environment. This review will focus on the latest evidence, both clinically and pre-clinically, to evaluate the contribution of ROS/NS to acute kidney failure in diabetes. Therapies that specifically target mitochondrial ROS to prevent cell death will be discussed and newer intervention options around this paradigm will be presented.

2. Contribution of ROS/NS production to diabetic nephropathy

Oxidative stress by definition is due to an overproduction of ROS/NS and/or a deficiency in enzymatic and non-enzymatic antioxidant defense, such that the balance is tipped in favor of ROS/NS accumulation and cell damage. Evidence from preclinical studies supports the role of ROS/NS in-

Abbreviations:

8-OHdG – 8-hydroxy-2'-deoxyguanosine
8-oxodG – 8-oxo-7,8-dihydro-2'-deoxyguanosine
ADP – adenosine diphosphate
AGE – advanced glycation end-product
AIF – apoptosis-inducing factor
aPC – activated protein C
ATM – ataxia telangiectasia mutated
ATP – adenosine triphosphate
ATR – ataxia telangiectasia and Rad3-related
BER – base excision repair
BMF – Bcl-2 modifying factor
CKD – chronic kidney disease
CVD – cardiovascular disease
DIABLO – direct IAP-binding protein with low pI
EMT – endothelial-mesenchymal transition
EndoG – endonuclease G
ER – endoplasmic reticulum
ERK – extracellular signal-regulated kinase
ESRD – end-stage renal disease
ETC – electron transport chain
FADD – FAS-associated protein with death domain
GPx1 – glutathione peroxidase 1
H_2O_2 – hydrogen peroxide
ICR – Institute of Cancer Research
IDH2 – isocitrate dehydrogenase 2
IMS – intermembrane space
MAPK – mitogen-activated protein kinase
MCP-1 – monocyte chemotactic protein 1
MIF – macrophage migration inhibitory factor
MIOX – myo-inositol oxygenase
MOMP – mitochondrial outer membrane permeability
mPTP – mitochondrial permeability transition pore
mtDNA – mitochondrial DNA
MTH1 – mut T homolog 1
MUTYH – mut Y homolog
NADPH – nicotinamide adenine dinucleotide phosphate hydrogen
NF-κB – nuclear factor kappa-light-chain-enhancer of activated B cells
$^{\bullet}NO_2^-$ – nitrogen dioxide
NOX – NADPH-oxidase
NRK – normal rat kidney
$O_2^{\bullet-}$ – superoxide
OGG1 – oxoguanine glycosylase
$OH^{\bullet}$ – hydroxyl radical
$ONOO^-$ – peroxynitrite
OPG – osteoprotegerin
OXPHOS – oxidative phosphorylation
PARP – poly (ADP-ribose) polymerase
PKC – protein kinase C
RAGE – receptor for AGEs
RAS – renin-angiotensin system
ROS/NS - reactive oxygen and nitrogen species
Smac – second mitochondrial-derived activator of caspases
Smad2 – mothers against decapentaplegic homolog 2
SOD2 – superoxide dismutase 2
STZ – streptozotocin
TCA – tricarboxylic acid
TGF – transforming growth factor
TRAIL – tumor necrosis factor-related apoptosis-inducing ligand
VCAM-1 – vascular cell adhesion molecule 1
ZDF – Zucker diabetic fatty

volvement in the pathogenesis of diabetic CKD and ESRD. It has been shown that elevated levels of markers for ROS/NS damage accumulate in diabetic kidneys [15-18] and, under high-glucose conditions mimicking diabetes, in various kidney-derived cultured cells [19, 20]. Data from our laboratory have clearly demonstrated increased oxidative stress and advanced kidney disease in type 1 diabetic mice lacking the major cytosolic and mitochondrial antioxidant enzyme glutathione peroxidase 1 (GPx1) [21]. In particular, our study demonstrated a strong link between increased oxidative stress, enhanced inflammatory response (monocyte chemotactic protein 1 (MCP-1), vascular cell adhesion molecule 1 (VCAM-1)), and increased pro-fibrotic mediators (transforming growth factor (TGF) β, collagens I and III) in the diabetic kidney cortex. Indeed, the ROS/NS, peroxynitrite, has been shown to play a key role in the pathogenesis of the diabetic glomerular lesion [22]. Other preclinical studies with genetic alterations of the major ROS/NS producing enzymes, the NADPH-oxidases (NOX), in particular NOX4, lend further support to the theory of oxidant-mediated diabetic kidney injury [23]. Ablation of NOX4 in a mouse model of type 1 diabetes caused marked protection from both structural and functional kidney damage [9]. Thus, targeting NOX4 with pharmacological inhibitors may offer a viable therapeutic strategy to reduce diabetic kidney injury.

Clinically, type 2 diabetes patients demonstrate elevations of excreted urinary 8-hydroxy-2'-deoxyguanosine (8-OHdG), a marker of oxidative DNA damage, which was positively correlated with the extent of tubulointerstitial kidney injury in these patients [24]. Furthermore, a complementary marker of DNA damage, 8-oxo-7,8-dihydro-2'-deoxyguanosine (8-oxodG), strongly predicted the progression of the disease in type 2 diabetics over a 5-year follow-up period [25].

At the molecular level, ROS/NS, produced as a consequence of elevated glucose levels, affect cell signaling pathways associated with metabolism, cell proliferation, and cell death [26]. Of particular relevance to diabetic kidney disease, a number of studies have shown the involvement of ROS in glucose-mediated activation of the protein kinase C (PKC) pathway in mesangial cells, leading to increased TGF-β levels [27, 28], an important mediator of kidney fibrosis [29, 30]. ROS have also been shown to activate NF-κB signaling in mesangial cells, causing a pro-inflammatory response [31].

Evidence from antioxidant studies has further supported a role for ROS/NS-mediated modulations of cellular signaling. Indeed, our own studies with the antioxidant and GPx1 mimetic ebselen have shown reductions in the activation of p38 MAP kinases (MAPK) and JNK in normal rat kidney (NRK) cells [21], suggesting the involvement of ROS/NS in these pathways linked to diabetic kidney disease. Others have used disparate antioxidants, and found a reduction in TGF-β-stimulated ROS and endothelial-mesenchymal transition (EMT), as well as lower levels of phosphorylated Smad2, p38 MAPK, and extracellular signal-regulated kinase (ERK) in renal tubular epithelial cells [32]. In conclusion, there is sufficient preclinical evidence supporting the role of glucose-stimulated ROS/NS in disrupting the relevant signal transduction cascades and transcription factors involved in cell function and metabolism, leading to glomerular mesangial expansion and tubulointerstitial fibrosis.

3. Mitochondrial ROS/NS in the pathogenesis of diabetic nephropathy

The importance of intact, efficiently functioning mitochondria is imperative to the prevention of kidney damage and renal failure [33, 34]. Mitochondria are involved in many biological processes, such as energy production, calcium homeostasis, and the regulation of cell death pathways, including apoptosis, programmed cell death, and unregulated necrosis [35]. Mitochondria play paradoxical roles in fueling cellular homeostasis through ATP produced by oxidative phosphorylation (OXPHOS), and in initiating cell death via the release of intermembrane space cell death proteins, such as cytochrome *c*, Smac/DIABLO, apoptosis-inducing factor (AIF), and endonuclease G (EndoG). These actions can be linked to an imbalance in redox regulation within the mitochondrial matrix, an association that plays a significant role in diabetic nephropathy. This line of evidence will be further discussed in the next sections.

OXPHOS involves the transfer of electrons across complexes I-IV of the electron transport chain (ETC) to generate a membrane potential ($\Delta\psi_m$) that is essential to establish the proton motive force driving ATP production. While OXPHOS is critical to meet the energy requirements of all eukaryotic cells, this is most evident in proximal and distal tubule cells that depend on ATP to drive Na^+/K^+ antiporters and Ca^{2+} transporters, respectively [36-38]. However, the byproduct of OXPHOS is the production of superoxide ($O_2^{\bullet-}$) that occurs as a result of electrons escaping from complex I and III and reacting with molecular oxygen. In intact

mitochondria, complex I and the Q_1 site of complex III release $O_2^{\bullet-}$ toward the mitochondrial matrix, whilst the Q_0 site of complex III releases $O_2^{\bullet-}$ toward the intermembrane space. [39, 40]. Impairment of complex I can result in an increase in the formation of reactive species and the development of renal damage similar to that seen in diabetic nephropathy, as demonstrated in Ndufs6 knockout mice [41]. Moreover, $O_2^{\bullet-}$ can be converted into other ROS/NS, such as hydrogen peroxide (H_2O_2) and hydroxyl radicals ($OH^{\bullet}$), and can react with nitric oxide to form peroxynitrite ($ONOO^-$) and nitrogen dioxide ($^{\bullet}NO_2^-$) [33]. For proximal tubules, this is thought to be exacerbated under hyperglycemic conditions, where an increase in glucose reabsorption may result in increased glycolysis and OXPHOS, resulting in increased oxidative stress [34]. In addition, methylglyoxal, an α-dicarbonyl byproduct of glycolysis, can induce the formation of advanced glycation end-products (AGEs) that exacerbate ROS production [42].

AGEs accumulate during diabetes. They are associated with an increase in oxidative stress through signaling via the receptor for AGEs (RAGE) [33, 43]. Our group has demonstrated that RAGE-induced cytosolic ROS/NS promotes mitochondrial $O_2^{\bullet-}$ production via activation of complex I of the mitochondrial ETC, triggering mitochondrial permeability transition pore (mPTP) formation and cell death, which can be attenuated in diabetic $RAGE^{-/-}$ mice [44]. Formation of AGEs through methylglyoxal accumulation results in modification of subunits, core protein 1 and cytochrome c_1, of complex III causing $O_2^{\bullet-}$ production, as shown in the cortex of diabetic rat kidneys [45]. Overexpression of glyoxalase I, the enzyme responsible for detoxifying methylglyoxal, has been shown to reduce the expression of complex I, II, and III, while reducing ROS production and apoptosis under hyperglycemic conditions in mouse mesangial cells [46]. In conclusion, existing evidence argues in favor of a significant role for ROS/NS produced as byproducts of the ETC in diabetic nephropathy. Indeed, Brownlee and coworkers proposed the unified hypothesis of diabetic complications where ETC-generated ROS/NS induce diabetic complications [47-49]. Current thinking has expanded on these ideas to speculate that the actions of ETC-generated ROS/NS most likely involve additional pathways and ROS/NS-producing enzymes. These aspects are further discussed below.

The regulation of redox homeostasis within the diabetic milieu has been the subject of two recent studies on diabetic nephropathy. The tubular-specific enzyme myo-inositol oxygenase (MIOX) was identified as a regulator of redox imbalance in the mitochondria under hyperglycemic conditions [50]. These studies showed an increase in MIOX in the renal cortex of streptozotocin (STZ)-induced diabetic ICR (Institute of Cancer Research) outbred male mice. Moreover, an increase in ROS and the incidence of apoptosis associated with increased MIOX expression was observed in the kidney proximal tubule cell line, LLC-PK1 [50]. Likewise, the redox enzyme $p66^{Shc}$, which localizes within mitochondria, has been implicated in the regulation of ROS/NS production and apoptosis during exposure to increased levels of glucose in diabetic nephropathy [51]. This enzyme has been shown to be epigenetically suppressed by the coagulation protease, activated protein C (aPC), in podocytes in diabetic nephropathy [51].

A significant focus of recent research has been on the NADPH oxidases within the renal cortex in the diabetic milieu, particularly NOX4, as discussed above. Block *et al*. demonstrated that NOX4 is upregulated under hyperglycemic conditions within the mitochondrial compartment of the cell [52]. NOX4 has been localized within renal cortex membrane fractions [52]. Since NOX isoenzymes reside within cells and span membranes of cells [53], it is likely that NOX4 spans the inner membrane of mitochondria, and that $O_2^{\bullet-}$ or H_2O_2 are released into the intermembrane space (IMS) of mitochondria. Initially, it had been proposed that NOX4 produces H_2O_2 only [54], but it is also capable of producing $O_2^{\bullet-}$, as shown by Block *et al*. [52].

NOX4 has also been localized in the mitochondrial fraction of kidney glomerular mesangial cells that are known to be primary targets for glucose-mediated oxidative injury [23]. While $NADP^+$/NADPH can traverse the outer mitochondrial membrane, it is impermeable to the inner membrane. NOX4 requires NADPH to become active. The fact that functional $O_2^{\bullet-}$-producing NOX4 has been identified in diabetic mesangial cells suggests that the carboxyl-teminus of NOX4 is positioned in contact with the intermembrane space [52]. Furthermore, NOX4 may indirectly influence the citric acid cycle, which is located within the mitochondrial matrix, through its influence on isocitrate metabolism. This includes the conversion of isocitrate into α-ketoglutarate by isocitrate dehydrogenase 2 (IDH2), which is dependent on $NADP^+$ [55]. Recently, the use of metabolomics has revealed that NOX4 plays a key role in regulating the tricarboxylic acid (TCA) urinary metabolite fumarate in diabetic Akita mice by exerting its ef-

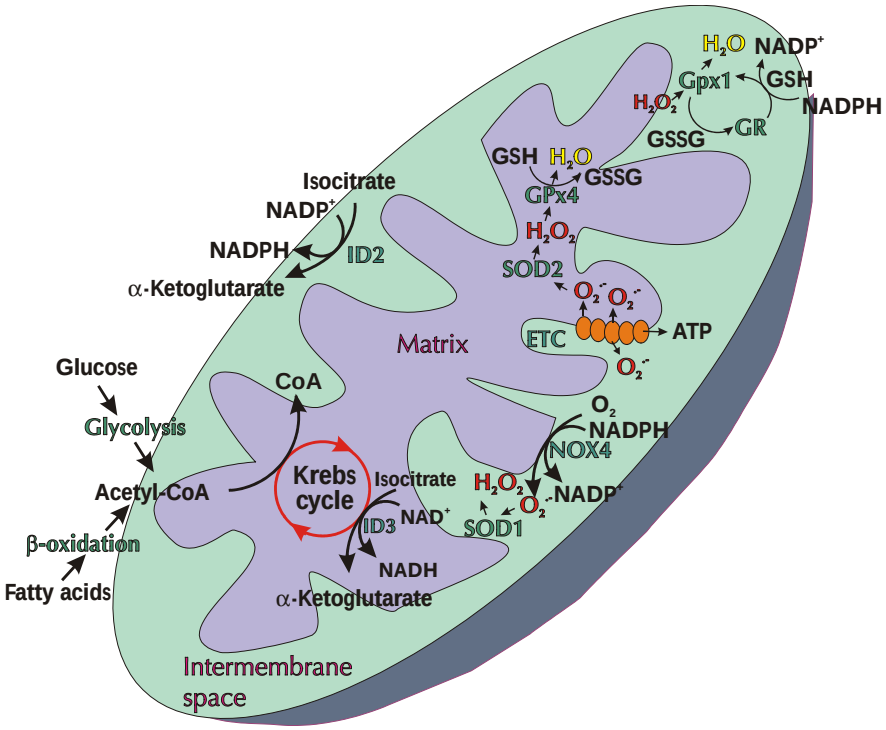

Figure 1. Redox signaling within mitochondria. ROS in the form of superoxide ($O2^{-}$) can be produced via the electron transport chain (ETC) or NOX4 within the inner mitochondrial membrane (IMM). $O_2^{\cdot-}$ is released from complexes I and III of the ETC into the matrix or intermembrane space. $O_2^{\cdot-}$ released from NOX4 or complex III enters the intermembrane space where it is dismutased by SOD1 into hydrogen peroxide (H_2O_2). $O_2^{\cdot-}$ within the matrix is converted into H_2O_2 by SOD2. In turn, H_2O_2 is detoxified into H_2O via GPx1 in the intermembrane space or via GPx4 within the matrix. This delicate balance of ROS within the mitochondria is dependent upon the Krebs (citric acid) cycle, the conversion of $NAD(P)^+$ to NAD(P)H, and *vice versa*. Under diabetic conditions this redox signaling is disrupted, resulting in increased oxidative stress.

fect on the mitochondrial enzyme fumarate hydratase. Importantly, interventions with a NOX1/NOX4 inhibitor restored fumarate hydratase and fumarate levels and reduced albuminuria, glomerular hypertrophy, and mesangial matrix accumulation in these diabetic mice [56]. Nonetheless, it is evident that $O_2^{\bullet-}$ produced by mitochondrial NOX4 cannot have a direct link to deficiencies in the ETC or mitochondrial DNA (mtDNA) integrity that are housed within the inner mitochondrial membrane or matrix respectively, unless converted to membrane permeable molecules such as H_2O_2 or ONOO-, which we have demonstrated to be increased in the diabetic kidney [57].

If NOX4 has any deleterious influence within the mitochondria then it is likely to occur within the IMS. It is also likely that glutathione reductase competes with NOX4 for NADPH to maintain the balance of glutathione used for Gpx1 and Gpx4 within the mitochondria to detoxify H_2O_2 by conversion into H_2O. Indeed, the NOX inhibitor apocynin has been shown to restore the glutathione/glutathione disulfide (GSH/GSSG) ratio in Zucker diabetic fatty (ZDF) rats [58]. Within the IMS, $O_2^{\bullet-}$ produced by NOX4 must be detoxified by SOD1. Otherwise, it exerts damage to the inner and outer mitochondrial membrane [59]. It will be a matter of future research to clarify whether diabetes-induced NOX4 upregulation is sufficient to rupture the outer membrane, initiate the mPTP, or induce mitochondrial outer membrane permeabilization (MOMP), and thereby trigger the redistribution of the IMS cell death proteins. Indeed, it has been demonstrated that NOX4 upregulation mediates TGF-β-induced apoptosis in podocytes, although it was not investigated whether IMS cell death proteins were engaged in this process [60].

Investigations have also focused on deficiencies in the antioxidant network within the mitochondria, including coenzyme Q, SOD2, and GPx4 [34]. The consequence of an imbalance in these ROS generators and antioxidants within the diabetic renal cortex is an elevation in oxidative stress within the mitochondria, which can trigger the intrinsic cell death cascade [61]. **Figure 1** summarizes the key players involved in redox signaling in the mitochondria. Under diabetic conditions, this redox signaling is disrupted, resulting in increased oxidative stress.

Finally, it should be mentioned that results from studies on the occurrence of mitochondrial ROS/NS in diabetes and the amounts produced are inconsistent to some extent. While it is now generally accepted that mitochondria-derived ROS/NS are increased in diabetes, some studies have reported an overall decrease [62, 63]. The discrepancy may result from the cellular heterogeneity and differing metabolic responses of the cells in the kidney [64]. Further research is necessary to clarify this issue.

4. Consequences of oxidative stress in the diabetic kidney

4.1 Nuclear DNA damage

Oxidative stress is known to contribute to a range of harmful intracellular events, including DNA damage within the nucleus. This damage may ultimately cause dysfunction, cell death, and long-term risk of oncogenesis. Generally, oxidative DNA damage, in the form of oxidized bases, occurs as frequently as one million times per day in the human body as a consequence of normal metabolism and other environmental factors [65, 66]. Cells rely on high energy DNA repair mechanisms to clear DNA damage. This includes the recruitment of the base excision repair (BER) protein complex, amongst others, to repair this type of damage [67]. The formation of general DNA repair complexes (e.g. ataxia telangiectasia mutated (ATM), ataxia and rad-related kinase (ATR)) involves the activation of proteins that target gene expression and protein production to respond rapidly to detected damage. Two of the more significant transcription factors are p53 and NF-κB, both of which regulate gene expression.

In cases where the DNA damage level is high, the recruitment of large volumes of repair complexes can result in rapid depletion of available ATP due to elevated energy demand, e.g. by cleavage of the damage-sensing protein poly (ADP-ribose) polymerase (PARP) [68, 69]. This creates the potential for unregulated cell death (i.e. necrosis) as there is insufficient energy for cells to undergo ATP-dependent programmed cell death (apoptosis) [70]. This “switch” in DNA damage-related cell death PARP-1 activation has been observed in canine renal cells [71, 72]. However, if the DNA damage by ROS is sub-lethal, cells can sufficiently repair the damage and even adapt to chronic change [73].

Mitochondria are involved in sensing nuclear DNA damage. They are able to influence cellular responses, including the release of apoptosis-inducing factor (AIF), a protein involved in DNA fragmentation and chromatin condensation during apoptosis [74]. In the pathogenesis of diabetic nephropathy, oxidative stress-related damage to mitochondria contributes to apoptosis and loss of podocytes, which are key events in the progression of the disease [75].

The ability for cells to adapt to increased levels of ROS/NS is a critical component in homeostatic protection. Due to the frequency of oxidative DNA damage across the body, cells have robust mechanisms to identify and repair this damage to prevent cumulative genotoxicity or mutations. BER is one of the mechanisms employed by mammalian cells to repair DNA damage caused by oxidation. [76, 77]. In normal cells, the BER pathway is regulated by 3 main proteins: OGG1, MTH1, and MUTYH that constitute a part of the BER repair complex [78, 79]. When an oxidized deoxyguanosine base (8-oxo-dG) is repaired by BER, the dissected base (8-OHdG) is discharged from the cell and filtered through the kidney [80].

Recent evaluations of DNA breaks induced by oxidative stress showed that they are increased in patients with type 1 and type 2 diabetes, although most studies involved analyses of peripheral lymphocytes [81-83]. The same phenomenon has also been observed in gestational diabetes [84, 85]. Of particular interest is the association with renal complications. The direct effect of high glucose on ROS/NS production and subsequent DNA damage has been assessed in rat models of type 1 diabetes [86]. These studies support the hypothesis that oxidative stress-induced damage occurs in the kidneys of diabetic patients. Clinical investigation into the effects of oxidative stress-induced DNA damage on renal cells is limited, in part because of the need for renal biopsies. However, it is possible to determine indirectly the level of oxidative damage in a patient by analyzing the urinary excretion of oxidized DNA bases in the form of 8-OHdG. This validated method has revealed increased excretion rates in patients with diabetes, corresponding to an increase in generalized oxidative stress-induced DNA damage throughout the body [80].

Interestingly, the occurrence of 8-oxo-dG base damage has been found to coincide with diabetic complications and may be a predictive biomarker for detecting the severity of diabetic complications, including retinopathy and nephropathy [80, 87, 88]. Although a higher excretion rate is correlated with severity of diabetic nephropathy, this critical biomarker can give an idea of systemic DNA damage only (i.e. relative damage in the entire body),

but not the specific incidence in an individual organ. Another limiting factor for the use of 8-OHdG as biomarker for renal damage is that the excretion of 8-OHdG is affected by other compounding factors, including exercise and environmental toxins [89-91]. This limits the clinical implications of these studies as an individual's baseline excretion rate can vary significantly.

4.2 Mitochondrial DNA damage

In addition to the effects of nucleic DNA damage, mtDNA in the diabetic kidney is also susceptible to damage by ROS/NS [18]. The close proximity of mtDNA to the ETC within the mitochondrial matrix makes this type of DNA highly susceptible to damage by ROS/NS produced during OXPHOS. This mechanism is generally considered to account for the increased observation of oxidized mtDNA compared with nuclear DNA damage [92]. Although mtDNA damage is ultimately repaired after a short insult, longer insults lead to persistent damage that could subsequently result in apoptosis [93]. MtDNA damage is also repaired through the BER pathway by the excision of 8-OHdG, although there seems to be some slight differences between the recruited proteins in each organelle. For example, nucleic DNA is repaired primarily by DNA ligase I, whilst mtDNA damage is repaired by DNA ligase III [94].

The role of oxidative stress in DNA damage and mitochondrial dysfunction has already been established in other pathologies such as in neurodegeneration, heart failure, and diabetic retinopathy [95-97]. In a recent clinical study, a link was found between diabetes, damaged mtDNA, and functionally altered mtDNA. Indeed, changes in mtDNA preceded bioenergetic dysfunction, leading the authors to propose that systemic mitochondrial dysfunction initiated by glucose-induced mtDNA damage may be involved in the development of diabetic nephropathy [98].

4.3 Compromised DNA repair mechanisms

Susceptibility to oxidative stress-induced DNA damage has been shown to correlate with certain gene polymorphisms in the BER pathway in type 2 diabetes complications such as distal symmetric polyneuropathy [99, 100]. One study examined changes in the gene expression of the BER complex protein MUTYH, an important protein in the response to cellular stress, following treatment with TGF-β1. The investigators found that expression of the protein in renal proximal tubule cells differs from that in interstitial cells [101]. Furthermore, oxidative DNA damage, as measured by 8-oxoG, was positively associated with renal fibrosis, suggesting that MUTYH mediates tubulointerstitial damage [101]. Other studies have indicated that suppression of MUTYH may actually be protective of renal disease [102, 103]. Importantly, polymorphisms found in these DNA repair pathway genes have also been shown to increase the risk of ESRD progression in a cohort of mixed-cause patients undergoing hemodialysis [102]. It would be interesting to examine this effect in the context of diabetic nephropathy, and earlier in the progression of the disease, to determine whether this correlates with patient risk of progression to ESRD.

Besides BER, additional repair pathways such as homologous recombination and mismatch repair respond to critical DNA damage [104]. When DNA repair fails to proceed adequately, there is a danger of cell death by necrosis due to the high energy requirements of the DNA repair processes [70]. Thus, DNA repair proteins may be inactivated where possible to downregulate their functional activity for the salvation of apoptotic pathways [104]. However, loss of important repair processes, whether mediated by oxidative stress itself or by other factors, is thought to compromise the integrity of mitochondrial and nuclear DNA. Further investigation is required to find out how the repair mechanisms are compromised in diabetic nephropathy.

5. Modes of cell death during diabetic renal disease

Cell death is a natural consequence of oxidative stress when damage exceeds the ability of the cell to respond and repair the insult. The two main types of cell death observed in diabetic nephropathy are apoptosis and necrosis. Apoptosis is a controlled process that is highly dependent on the continued production of ATP to fuel this high-energy process [69]; it is characterized by cell shrinkage, chromatin condensation, and DNA fragmentation [61]. Apoptosis occurs through two types of pathways. One is the death receptor pathway (extrinsic apoptotic pathway) that includes FAS/FAS-ligand; the second is the mitochondrial pathway (intrinsic apoptotic pathway) that requires regulatory proteins such as the Bcl2-related family [105]. Necrosis, by comparison, is considered uncontrolled and catastrophic. In necrotic cell death, ATP production is insufficient to

meet the energy demands of the cell, leading to rupture of cellular contents [106]. This generates a high-level inflammatory response, which is not observed in apoptosis. Each type of cell death has physiological consequences that correspond to the clinical presentation of a disease. Finally, ER stress [107] and cellular senescence within key cell types of the kidney [108] are two additional mechanisms that are now regarded as contributing to cell death processes in diabetic nephropathy.

5.1 Induction of apoptosis

In diabetic nephropathy, pathogenic lesions are characterized by initial hypertrophy followed by a gradual loss of renal mass, sclerosis, and fibrosis. Apoptosis is known to contribute to the later process in both humans and animals [109-111]; it includes the upregulation of cell surface markers which encourages phagocytosis (removal) by resident and circulating immune cells. These surface markers include CD36, CD95 (FAS-ligand), CD74 (MIF-R), OPG, and TRAIL, which are increased in diabetic kidneys [112-115]. FAS-ligand binds to FAS. It has been shown that plasma FAS levels are elevated in diabetes, and that the rate of apoptosis begins early in the development of proteinuria in renal cells [116, 117]. One study in diabetic female rats found that an increase in FAS/FAS-ligand could be attenuated by blockade of the renin-angiotensin system (RAS) [118]. The inner cell membrane portion of the FAS-ligand includes a FAS-associated protein with death domain (FADD). It has been shown that FADD and its dimeric counterpart FADD-DD play an important role in mediating cell death in renal tubule cells in the context of acute renal injury, and that they can mediate early diabetic renal injury [119, 120]. However, it is clear that additional pathways are involved since increased FAS-ligand levels do not directly correlate with apoptosis [116, 117].

Another event that may occur in diabetic nephropathy includes changes in internal pro-apoptotic proteins such as BASP1, Bcl-2 family proteins, and p53 [109]. The Bcl-2 family of proteins are highly conserved in diabetic nephropathy, and are involved in the regulation of both pro-survival and pro-apoptotic signaling. The numerous family members interact downstream of p53 and NF-κB to regulate cell survival. The anti-apoptotic protein Bcl-2 has been shown to play an important role in diabetic nephropathy [121] as it antagonizes the pro-apoptotic Bax and Bak proteins that together control mitochondrial cell death. An increase in the pro-apoptotic Bax relative to the anti-apoptotic Bcl-2 establishes a more pro-apoptotic phenotype; this ratio is a commonly used technique to establish the susceptibility of cells to apoptotic cell death. This change in ratio has been demonstrated in a murine model of type 2 diabetic nephropathy [122]. The increase in the observed pro-apoptotic Bax/Bcl-2 ratio could be reversed through blockade of the RAS pathway in mice overexpressing angiotensinogen in renal proximal tubular cells [123].

In human diabetic nephropathy, the data are limited regarding changes in Bcl-2 and Bax expression. However, it has been identified as a contributing factor in other forms of renal disease [124, 125]. Additionally, other Bcl-2 family members may also be linked with diabetic nephropathy. For example, overexpression of Bcl-2 modifying factor (BMF) is involved in apoptosis in both animal and human studies [126]. BMF is a BH3 only protein (a sub-class of smaller proteins within the Bcl-2 family) that indirectly activates Bax and Bak by inhibiting the related proteins Bid, Noxa, and Bik to promote cell death [127]. Other pathways implicated in diabetic nephropathy include Akt and p38 MAPK [128].

In the diabetic kidney, it is generally considered that ROS/NS-induced apoptosis is associated with specific changes observed in the disease, in particular tubulointerstitial changes [129]. For example, damage by high-glucose-induced ROS/NS has been associated with PKCdelta that regulates the cellular response protein p66Shc [130]. P66Sch mediates high-glucose and ANG II responses to oxidative stress and renal proximal tubule cell (PTC) injury via mitochondrial dysfunction and apoptosis pathways [131]. A recent review on renal tubular apoptosis in diabetic nephropathy reported that high-glucose is one of the major contributors to free radical- and ROS-induced cell death in these cells [61]. Further stressors relating to PTC injury include uric acid transport which is also associated with oxidative stress injury and apoptosis [132].

Prolonged oxidative stress is known to cause adaptive changes in cells. Cells that fail to adapt to the changes die by one of the many cell death pathways available to detect and respond to harmful cellular stress conditions. One pathway by which ROS/NS contributes to cell death is the classical apoptotic cascade engaging the Bcl-2 family proteins [133]. This pathway includes the activation of the Bax protein which translocates to the mitochondria of damaged cells and elicits changes in mitochondrial outer membrane permeability (MOMP) by the formation of the mitochondrial outer membrane pore. The downstream effects in-

clude the release of cytochrome *c* and subsequent caspase-3 cleavage.

Bax is activated by a range of transient protein interactions initiated by ROS/NS damage. However, in silico modeling also proposes a direct activation of Bax via oxidative interactions [134]. Bax is well known as part of the mitochondrial (intrinsic) pathway of apoptosis, although its full repertoire of cellular interactions is not yet understood. It has a clear role in p53-activated apoptosis, but evidence suggests the involvement of Bax in other forms of cell death as well [135, 136]. In apoptotic death, Bax undergoes a conformational change following activation which allows it to associate with mitochondrial membranes and to take part in the formation of the MOMP. In addition to Bax, the related protein Bak is also capable of forming these pores. Bak is a membrane-bound protein, whereas Bax is cytosolic in its inactive state. Studies show that Bax and Bak can oligomerize during MOMP formation [137]. While the precise morphology of this pore is still a matter of debate, it is hypothesized that there are two distinct pore types [138]. Bax expression has been found to be increased in a diabetic STZ rat model and in dbdb mice [122, 139]. However, expression in human renal cells is relatively unexplored in diabetic nephropathy.

Although necrotic cell death has also been observed in diabetic nephropathy [140], the full implications of its contribution to the disease are not yet understood.

5.2 Endoplasmic reticulum stress

Mitochondrial function is closely linked to endoplasmic reticulum (ER) function. ER stress is another important aspect of cellular pathology. It occurs simultaneously with oxidative stress in the context of the diabetic milieu and progression of diabetic complications [107, 141, 142]. In normal conditions, the ER is responsible for regulating protein folding. In situations of high demand or protein damage (as seen in oxidative stress), the unfolded protein response (UPR) is activated to restore ER homeostasis. This is mediated by the proteins XBP1 and IRE1, and allows for transient protection against damage [143, 144]. When the unfolded protein response is overwhelmed ER stress occurs. This is a cytotoxic process involving cellular dysfunction and the activation of proapoptotic factors such as IRE1 [144].

Cells with a high protein production rate are at an increased risk of cellular dysfunction by ER stress. Pancreatic beta-cells are an important example due to the continual production of proinsulin. In type 2 diabetes, this is particularly relevant as the development of insulin resistance and maximum insulin production places the pancreatic cells at an increased risk of ER stress [145, 146]. Additionally, proteinuria and hyperglycemia can directly induce ER stress in renal PTCs *in vitro* [147]. In fact, the upregulation of genes associated with the UPR positively associate with increased severity of diabetic nephropathy, which is regarded as a protective change [147]. ER stress has been shown to mediate renal pathology in diabetic nephropathy and to correspond with disease severity [148, 149]. Examples include albuminuria, which has been shown to cause ER stress by the induction of caspase-12 expression [150]. Furthermore, accumulation of protein in the proximal tubules is known to follow aldosterone administration in rat models (physiological elevated equivalent) and leads to PTC damage if not cleared by autophagy [151].

The ER is primarily responsible for regulating Ca^{2+}. Oxidative stress has been found to alter Ca^{2+} homeostasis [152]. This alteration includes a release of Ca^{2+} from the ER into the cytosol, which in turn affects mitochondria and mitochondrial function [153]. In fact, calcium leakage has been shown to directly cause elevated ROS/NS production in mitochondria via interactions with OXPHOS [154]. Other proteins have been implicated in the reduction of elevated ROS/NS production via oxidative phosphorylation mechanisms in diabetes [155]. However, most of this research has focused on neurodegenerative or skeletal muscle models, not diabetic nephropathy.

In many disease processes, cell death by ER stress occurs via the mitochondrial apoptosis pathway [156]. In type 2 diabetes, ER stress appears to be upregulated and linked with an increase in both apoptosis and necrosis correlating with changes in inflammatory cytokine expression [140]. The translocation of Bax and Bak to the ER membrane may occur during ER stress-mediated apoptosis [157]. Furthermore, caspase-12 cleavage occurs downstream, indicating a pathway of cell death that is potentially independent of the mitochondria in human fibroblast cells [158]. In comparison, the upregulation and accumulation of another pro-apoptotic Bcl-2 family protein, BIM, at the ER membrane is associated with mitochondrial death pathways following caspase-12 activation [159, 160].

Bax/Bak oligomerization at the ER membrane followed by caspase-12 activation has also been demonstrated in mouse models [161]. However,

murine caspase-12 is a homologue of human caspase-4. This variant has also been associated with cell death following ER stress [162]. Additionally, caspase-4 has been observed to mediate PTC death in some types of nephropathy [163], but is yet to be confirmed in diabetic kidney disease. Although human caspase-12 has been analyzed in many studies, its relevance to the general population has been questioned as the full homologue of the gene is only expressed in 2.8% of humans [164].

Additional caspases may be activated downstream of ER stress, including caspase-7 [158] and caspase-8 [165, 166]. It seems that the distribution of Bax to different organelles relates to the type of cell death induced [167]. The structure of the reported ER membrane pore is not yet known, but early results point to changes in membrane permeability [157].

Autophagy is another cell death pathway that has been observed when key components of the mitochondrial apoptotic pathway (i.e. Bax/Bak, caspase-9) are disrupted [165]. Although this aspect is of importance in the field of cancer research and drug resistance, in the context of diabetic nephropathy, it is interesting to consider the implications of altered mitochondrial function in this pathway, particularly as the link between mitochondria and ER relays important signal transfer during cell death [153]. Furthermore, Bcl-2 family proteins, Bax and Bak, have also been linked to this interaction by regulating Ca^{2+} ER homeostasis and efflux to the cytosol [168]. Bcl-2 family proteins play a major role in mediating the response of the ER and mitochondria to oxidative damage. The role of Bax in the progression from ER stress to apoptosis is an interesting area for exploration in diabetic nephropathy, considering the role of Bax in the mitochondria-dependent cell death pathways. Mediation of ER stress could potentially provide a therapeutic target for the prevention of renal disease.

5.3 Cellular senescence

Another potential outcome of oxidative stress is cellular senescence. This is likely to be due to a range of factors, including the inherent growth-inhibition response to DNA mutagenic stimuli. Senescence is a useful state induced by cells to protect from mutagenesis without depleting cell mass by apoptosis. Cells may persist indefinitely in cell cycle arrest. This forms an important physiological function in terminally differentiated tissues such as neurons and adult stem cells, which retain the ability to exit cell cycle arrest.

Senescence of cells can be triggered by oxidative stress. This has been observed in many human cell lines with fibroblasts being particularly susceptible [169-171]. Oxidative stress-induced senescence has also been demonstrated in normal renal cells, and identified as a contributing factor to diabetic nephropathy in animal models and type 2 diabetic patients [169, 172, 173]. The senescent response to oxidative stress can include an increase in mitochondrial mass and mtDNA copy number [174]. Although increased circulatory mtDNA has been detected in patients with type 2 diabetes [98, 175], it may be possible that senescent cells are more susceptible to the effects of ROS and NOS, instead of inducing a protective state. For example, renal podocytes exist as terminally differentiated cells functionally equivalent to senescent cells, but highly susceptible to oxidative stress. There is evidence to suggest that dedifferentiation of these cells occur in diabetes, indicating exit from cell cycle arrest [108] and resulting in podocyte loss. Podocyte loss, as measured by urinary excretion, is associated with early glomerular pathology in diabetic patients [176].

6. Mitochondrial permeability transition as a pathway to renal injury

Since the kidney relies on oxidative phosphorylation (OXPHOS) to provide the bulk requirements of ATP for tubular reabsorption [177], it is not surprising that mitochondrial homeostasis is essential for an optimally functioning kidney. Indeed, in experimental diabetic nephropathy or renal proximal tubule cells exposed to high glucose, mitochondrial ATP content [178] and production [179, 180] are depleted. Mitochondria are able to compensate for decreased cellular ATP production by fusion. This mechanism is an effective adaptive response, as previously observed in other organs [181]. Notably, changes in mitochondrial morphology within renal proximal tubules in both human [182] and animal models of early diabetic nephropathy [183] have long been identified as part of the disease, with mitochondrial enlargement and swelling. Diabetes-induced increases in mitochondria-derived ROS/NS have been shown to provoke the dynamic changes in mitochondrial shape [184]. Another stimulator of change in mitochondrial shape is the induction of mitochondrial permeability transition. This mechanism is independent of the mitochondrial dynamics machinery and oxidative stress, and has been historically detected by electron microscopy imaging showing mitochondrial swelling.

Mitochondrial permeability transition (mPT) is an abrupt increase in inner mitochondrial membrane (IMM) permeability that allows the passage of solutes with molecular masses of less than 1,500 Da. This event is caused by unlocking the mitochondrial permeability transition pore (mPTP), an evolutionary, highly conserved channel [185]. The unlocked pore allows for immediate dissipation of the mitochondrial transmembrane potential and influx of solutes, causing expansion of the matrix and mitochondrial swelling. The loss of the inner mitochondrial membrane potential and the inability to maintain a pH gradient due to proton influx also disrupts mitochondrial ATP synthesis, leading to energy depletion; persistent opening can induce necrotic cell death [186]. Sufficient swelling of the mitochondrial matrix may result in rupture of the outer mitochondrial membrane. This causes cytochrome *c* release with subsequent caspase activation, and results in cellular apoptosis [187]. Opening of the mPTP prevents mitochondria from generating ATP by OXPHOS, and allows reversal of the FoF1 ATP synthase, causing hydrolysis of the ATP produced by glycolysis or any remaining functional mitochondria [178].

The mPTP is composed of multiple macromolecular components which are not yet fully characterized [178, 180, 181]. It was initially thought that mPTP was comprised of the adenine nucleotide translocase (ANT), voltage-dependent anion channel (VDAC), and non-pore forming regulatory component cyclophilin D (CypD), the mitochondrial isoform of the peptidylprolyl cis-trans isomerase cyclophilin chaperone family [188, 189]. The mPTP was thought to be generated as one contiguous pore spanning the intermembrane space [190]. However, gene ablation studies suggested that VDAC and ANT play only a limited role in mPT [191-193]. Also, a significant role for CypD in mPT was established through the development of CypD-deficient mice (*Ppif*$^{-/-}$) whose mitochondria do not undergo syclosporin A (CsA)-sensitive mPT [194]. CypD is considered to regulate mPT by facilitating a calcium-triggered conformational change in the mPTP, converting it into an open state [195]. CypD-deficient mice (*Ppif*$^{-/-}$) are protected from ischemia/reperfusion injury of the heart and focal cerebral ischemia, implicating a role for CypD-dependent mPT opening and subsequent necrotic cell death in end-organ injury [194, 196]. Furthermore, mouse hepatocytes from CypD-deficient mice showed resistance to necrotic cell death induced by ROS and calcium overload [197]. In an updated model of the mPTP, dimers of the F1Fo ATP synthase form the mPTP within the IMM, with CypD binding to the lateral stalk of the FoF1 ATP synthase [198]. Further studies have identified the c-subunit ring of the Fo (i.e. $ab_2c_{10\text{-}14}$, *Escherichia coli* nomenclature) of the FoF1 ATP synthase to form the inner pore of the mPTP [199]. However, this model has not yet been validated.

Mitochondrial permeability transition is induced by mitochondrial sequestration of high levels of calcium, and is sensitized by factors such as decreased ATP levels, inorganic phosphate, and alkaline pH [178]. Hydrogen peroxide and other ROS may lead to induction of mPT [200]. mPT can also induce changes to the mitochondrial respiratory chain, including inhibition of complex I [201] and loss of cytochrome *c* [202]. Both of these conditions contribute to a reduced and decelerated flow of electrons through the respiratory chain, favoring the one-electron reduction of molecular oxygen. Finally, these events result in the generation of superoxide radicals [203, 204]. Loss of cytochrome *c* from the mitochondrial IMS reduces ATP synthesis, and further increases electron leak and ROS generation, setting up a feed-forward cycle of ROS-induced ROS generation [205]. A recent study has found that Bax mediates mPTP opening, which may cause ATP depletion and cellular necrosis [206].

Recently, a role for mPT has been implicated in renal injury in the kidney. Swelling of mitochondria within renal proximal tubules of the kidney has been demonstrated in early experimental diabetic nephropathy [183] and in kidneys from diabetic patients [182]. *Ppif*$^{-/-}$ mice are protected from acute ischemic renal injury [207]. Moreover, in a short-term model of streptozotocin (STZ)-induced diabetes, rats treated with cyclosporin A (CsA), an inhibitor of mPT, were protected against glomerular hypertrophy and extracellular matrix (ECM) accumulation [208]. A previous study has suggested that renal mitochondria from Goto-Kakizaki rats, a model of type 2 diabetes, had enhanced mPT. However, mPT was only measured indirectly by extramitochondrial calcium flux and its amelioration by CsA *in vitro* [209]. Recent studies from our laboratory have suggested that mPT is a candidate for mediating ROS-induced renal damage [179]. However, interruption in physiological mPT and the downstream consequences, including cell death, have not been extensively studied in models of diabetic nephropathy. It is possible that enhanced susceptibility to the mPT contributes to the development of diabetic nephropathy.

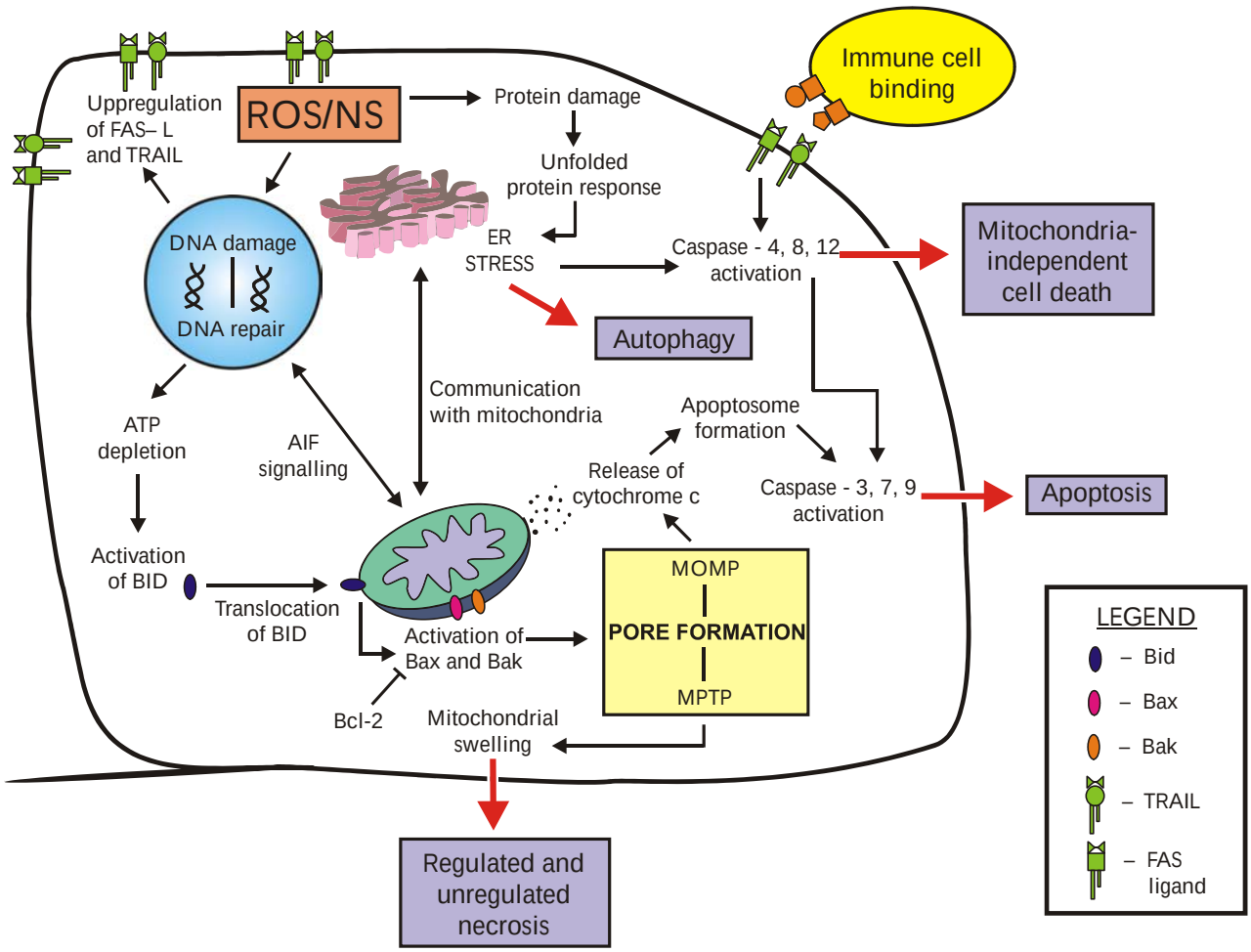

Figure 2. Lethal consequences of ROS/NS. The presence of high levels of ROS/NS can lead to downstream activation of cell death pathways. The type of cell death that occurs depends on the parts of the cell that are damaged. For example, oxidized protein damage can induce ER stress and mediate mitochondrial-independent cell death. However, crosstalk with the mitochondria can induce apoptosis via release of cytochrome *c* if suitable stimuli are present. DNA damage by ROS/NS can induce a range of signaling pathways, including the upregulation of gene expression of the cell surface markers FAS-L and TRAIL. These markers encourage cytotoxic immune cells to bind and activate the extrinsic apoptosis pathway. Furthermore, communication with mitochondria can lead to apoptotic or necrotic cell death if ATP is depleted. Activation of Bax and Bak can cause mitochondrial pore formation and opening, resulting in either mitochondrial swelling and necrosis or apoptosis via cytochrome c release. This process can be blocked by the anti-apoptotic protein BCl-2. The persistence of ROS/NS in diabetes may result in loss of cell mass and subsequent decrease in renal function.

In summary, diabetes-induced oxidative stress is able to stimulate numerous cellular pathways that eventually lead to cell death. Different types of cell death may occur depending on the parts of the cell that are damaged, as illustrated in **Figure 2**. Apoptosis, mostly induced by MOMP formation, mitochondrial shrinkage, and cytochrome c release, activates caspases via intrinsic or extrinsic pathways. Necrosis induced by MPTP formation results in mitochondrial swelling and lysis. As highlighted in this review, evidence for these major cell death pathways can be found in the diabetic kidney.

7. Targeting mitochondrial ROS in diabetic nephropathy

Despite increasing evidence supporting the role of mitochondrial oxidative stress in experimental diabetic nephropathy, the evidence from clinical

trials using antioxidants has not confirmed a beneficial effect. For example in the Heart Outcomes Prevention Evaluation (HOPE) trial, vitamin E treatment for 4.5 years failed to confer benefits in cardiovascular outcomes or nephropathy [13]. Lack of specificity and failure to target the correct sites of ROS production are two reasons often mentioned for the potential failure of vitamin E in the clinic. Therefore, the idea of specifically targeting ROS within ROS-producing organelles such as the mitochondria has been investigated. This strategy aims to increase specificity and to avoid targeting important physiological ROS outside the mitochondria because such ROS may be required for cell signaling. Mitochondria-targeting antioxidants have therefore been suggested as a potential therapeutic strategy [210] for the prevention of cisplatin-induced nephropathy [211], acute kidney injury [212], CKD, and diabetic nephropathy. This strategy may also hold promise for the treatment of cardiovascular diseases [213].

The most effective antioxidants would be those that can cross the outer and inner mitochondrial membrane. Therefore, antioxidants were conjugated with a positively charged triphenylphosphonium cation (TPP^+) to yield compounds such as quinone analogues, mitoquinone (Mito Q), SkQ1 and SkQR1, as well as mitovitamin E, mitophenyltertbutyline, and the SOD mimetic Mito-CP [212]. These antioxidants accumulate within the mitochondrial matrix at concentrations several-fold higher than within the cytosolic compartment due to the high negative membrane potential of the IMM. A study by Chacko *et al*. in type 1 diabetic Ins2-Akita mice showed that oral administration of MitoQ for 12 weeks prevented diabetic kidney damage [214]. Interstitial fibrosis and glomerular damage were significantly reduced in the treated animals. MitoQ also reduced the expression of the pro-fibrotic transcription factors phospho-Smad2 and 3, and prevented the nuclear accumulation of β-catenin, a member of the Wnt pathway that has been implicated in pathological processes such as fibrosis. Similarly, Mito-CP, the SOD mimetic composed of a lipophilic cationic nitroxide conjugated to TPP^+, prevented cisplatin-induced renal injury by effectively limiting oxidative and nitrosative stress, preventing mitochondrial structural damage and tubular injury, attenuating renal inflammation, preventing renal dysfunction, and reducing renal cell death in 6-8 week-old male C57Bl/6J mice [211].

Other strategies to increase the antioxidant defense in the mitochondria include overexpression of hemeoxygenase-1 (HO-1), an antioxidant enzyme that is not normally present in mitochondria [215]. To achieve this, a plasmid containing a mitochondrial permeability sequence was fused to the HO-1 gene sequence and transfected into HEK293 renal epithelial cells. As a result, Mito-HO-1-expressing cells were protected from hypoxia-dependent cell death and loss of mitochondrial membrane potential. However, the treatment was afflicted with long-term limitations due to the negative impact on heme-containing mitochondrial proteins.

Ebselen is a synthetic selenocyteine-containing mimetic of the cytosolic and mitochondrial enzyme glutathione peroxidase-1 (GPx1) [216], In our type 1 diabetic ApoE knockout mouse model, ebselen had renoprotective effects, with reductions in renal inflammation and fibrosis [21, 217]. Ebselen has been shown to cross into the mitochondrial matrix without the need for a leader sequence. It is activated by the intramitochondrial glutathione and thioredoxin systems, making this an extremely attractive therapy for diabetic nephropathy [218]. In summary, these results support the hypothesis that mitochondrially targeted therapies may be beneficial in the treatment of diabetic nephropathy.

An alternative approach has been the development of mitochondrially targeted Szeto-Schiller (SS) tetrapeptides that bind to cardiolipin on the IMM. The SS tetrapeptide/cardiolipin complex protects cardiolipin from peroxidative damage by cytochrome *c*, thus protecting mitochondrial crista and preserving mitochondrial structure and function. Use of the SS-31 peptide, which is known to scavenge ROS and inhibit mPTP opening, protects mitochondrial structure and function. In a rat model of ischemic kidney injury, it accelerated recovery of ATP, reduced apoptosis and necrosis of tubular cells, and abrogated tubular dysfunction [219]. Furthermore, SS-31 peptide decreased ischemia/reperfusion-mediated oxidative stress and the inflammatory response in tubular cells. The SS peptide known as Bendavia (Stealth Peptides, Newton Centre, Massachusetts) has advanced into the clinic as a phase 2a randomized controlled trial (EMBRACE STEMI) to evaluate its safety, tolerability, and efficacy on reperfusion injury in patients after myocardial infarction [220]. A second clinical trial will evaluate the efficacy of Bendavia on renal parameters (estimated glomerular filtration rate (eGFR), renal volume and perfusion, inflammation and urinary osmolarity). This is a promising strategy for the restoration of mito-

chondrial injury, but needs first to be tested preclinically in models of diabetic nephropathy.

The strategy of specifically targeting the mPTP has seen the development of mPTP-opening inhibitors such as cyclosporin A (CsA) or sanglifehrin A [221]. CsA is a well-known immunosuppressant and inhibitor of mPT; it acts via inhibition of peptidyl-prolyl *cis-trans* isomerase (PPIase) activity of cyclophilin D [222, 223]. Clinically, CsA has already shown benefits in reducing human cardiac ischemia/reperfusion injury [224]. However, CsA is nephrotoxic [225], and interacts with the calcineurin pathway, which is activated in diabetic nephropathy [208]. These adverse properties limit its application in the treatment of diabetic nephropathy. Analogues of CsA have been generated, including Debio-025 (Alisporivir). Debio-025 is non-immunosuppressive [226], and unlike CsA, it does not display affinity for calcineurin [227], but it selectively inhibits cyclophilin D, prevents cell death [228, 229], and restores mitochondrial function [230]. To date, Debio-025 has not been tested in experimental models of diabetes.

MitoTempo is a mitochondrially-targeted SOD1. In response to excessive ROS production and calcium overload, it prevents mPTP opening in cultured proximal tubular epithelial cells [231]. Moreover, a recent study targeting glycogen synthase kinase (GSK) 3β through the use of 4-benzyl-2-methyl-1,2,4-thiadiazolidine-3,5-dione (TDZD-8), a highly selective small-molecule inhibitor of GSK3β, has shown promise in protecting podocytes against mPTP opening, ROS production, and apoptosis induced by adriamycin [232].

Other treatments have improved diabetic nephropathy end-points by increasing antioxidant capacity through upregulation of antioxidant response genes using Nrf2 activators such as bardoxolone methyl [233, 234], curcumin [235], sulforaphane [236], cinnamic aldehyde [236], resveratrol [237], and ebselen [21]. Recent studies have shown that metformin, an oral hypoglycemic drug, possesses antioxidant properties, and is effective in lowering end-points of diabetic nephropathy in a rat model [238]. Other studies have investigated the targeting of mitophagy pathways in the hope of restricting the accumulation of fragmented mitochondria in the renal cortex, a process shown to be linked with the development of diabetic nephropathy [34]. Furthermore, some treatments, not necessarily targeted at mitochondria, have included mangiferin, a natural C-glucosyl xanthone and polyhydroxy polyphenol compound that has shown protection against diabetic nephropathy in STZ-induced diabetic Wistar rats via different mechanisms, including inhibition of the PKC, MAPKs (p38, JNK and ERK1/2), NF-κB, and TGF-β1 pathways [239].

Finally, the specific targeting of the main enzymatic source of ROS/NS in the kidney, NOX4, with specific NOX1/NOX4 inhibitors has shown tremendous potential for the treatment of diabetic nephropathy [240], as discussed earlier in section 3. It is unknown whether these inhibitors enter the mitochondria *per se*, but recent evidence suggests that they mediate their inhibitory effect on NOX4, and thus they impact diabetic nephropathy via pathways that include enzymes located within the mitochondria [56]. The existence of disparate NOX inhibitors such as the pan-NOX inhibitors, VAS2870 and VAS3947 [241], await further preclinical analysis with respect to their effectiveness in preventing or reversing diabetic nephropathy. The more specific NOX1/NOX4 inhibitor, GKT137831, which is developed by Genkyotex, has completed phase 1 clinical trials with encouraging results regarding safety and tolerability. A phase 2 clinical study is now planned in diabetic nephropathy patients [242].

8. Concluding remarks and future perspective

Diabetic nephropathy is a leading cause of ESRD. Despite significant advances in the understanding of the cellular mechanisms that are responsible for its initiation and progression, it remains therapeutically elusive. It is clear that blood glucose and blood pressure control are insufficient to prevent its progression, and that new, more effective treatment options are urgently needed. The therapeutic targeting of diabetic kidney mitochondria is a relatively new area that has gained attention due to the involvement of mitochondria in cell death pathways such as apoptosis and necrosis implicated in key cell types such as podocytes.

The involvement of oxidative and nitrosative stress in mediating many of the observed changes has focused attention on antioxidants that specifically target mitochondria. Several approaches have been attempted, as outlined in this review, with a more nuanced approach required to restore redox homeostasis rather than depletion of important oxidants required for signaling. The interwoven involvement of ER stress with oxidative stress means that new targets may be found by closer examination of ER stress-driven pathways.

Preventing the consequences of increased ROS/NS on nuclear and mitochondrial DNA damage via enhanced surveillance by DNA repair

mechanisms may offer an alternative solution. Preventing mPT pore formation is another new area with the potential to regulate renal injury. It is only by careful analysis of the cellular mechanisms governing diabetic renal injury that novel targets will be recognized and verified preclinically prior to translation into the clinic. These approaches promise to pave the way for new, more effective treatment options for diabetic nephropathy.

Acknowledgments: This work has been supported in part by the Victorian Government's OIS Program.

Disclosures: The authors report no conflict of interests.

■ References

1. **Zimmet P, Alberti KG, Shaw J.** Global and societal implications of the diabetes epidemic. *Nature* 2001. 414(6865):782-787.
2. **Spiegel AM, Nabel EG.** NIH research on obesity and type 2 diabetes: providing the scientific evidence base for actions to improve health. *Nat Med* 2006. 12(1):67-69.
3. **Shaw JE, Sicree RA, Zimmet PZ.** Global estimates of the prevalence of diabetes for 2010 and 2030. *Diabetes Res Clin Pract* 2010. 87(1):4-14.
4. **Sarnak MJ, Levey AS, Schoolwerth AC, Coresh J, Culleton B, Hamm LL, McCullough PA, Kasiske BL, Kelepouris E, Klag MJ, et al.** Kidney disease as a risk factor for development of cardiovascular disease: a statement from the American Heart Association Councils on Kidney in Cardiovascular Disease, High Blood Pressure Research, Clinical Cardiology, and Epidemiology and Prevention. *Hypertension* 2003. 42(5):1050-1065.
5. **Schiele F.** Renal dysfunction and coronary disease: a high-risk combination. *J Nephrol* 2009. 22(1):39-45.
6. **Dinneen SF, Gerstein HC.** The association of microalbuminuria and mortality in non-insulin-dependent diabetes mellitus. A systematic overview of the literature. *Arch Intern Med* 1997. 157(13):1413-1418.
7. **Gerstein HC, Mann JF, Yi Q, Zinman B, Dinneen SF, Hoogwerf B, Halle JP, Young J, Rashkow A, Joyce C, et al.** Albuminuria and risk of cardiovascular events, death, and heart failure in diabetic and nondiabetic individuals. *JAMA* 2001. 286(4):421-426.
8. **Mittal M, Siddiqui MR, Tran K, Reddy SP, Malik AB.** Reactive oxygen species in inflammation and tissue injury. *Antioxid Redox Signal* 2014. 20(7):1126-1167.
9. **Jha JC, Gray SP, Barit D, Okabe J, El-Osta A, Namikoshi T, Thallas-Bonke V, Wingler K, Szyndralewiez C, Heitz F, et al.** Genetic targeting or pharmacologic inhibition of NADPH oxidase nox4 provides renoprotection in long-term diabetic nephropathy. *J Am Soc Nephrol* 2014. 25(6):1237-1254.
10. **Tonelli M, Sacks F, Pfeffer M, Jhangri GS, Curhan G, Cholesterol and Recurrent Events (CARE) Trial Investigators.** Biomarkers of inflammation and progression of chronic kidney disease. *Kidney Int* 2005. 68(1):237-245.
11. **Okamura DM, Himmelfarb J.** Tipping the redox balance of oxidative stress in fibrogenic pathways in chronic kidney disease. *Pediatr Nephrol* 2009. 24(12):2309-2319.
12. **McQueen MJ, Lonn E, Gerstein HC, Bosch J, Yusuf S.** The HOPE (Heart Outcomes Prevention Evaluation) Study and its consequences. *Scand J Clin Lab Invest Suppl* 2005. 240:143-156.
13. **Lonn E, Yusuf S, Hoogwerf B, Pogue J, Yi Q, Zinman B, Bosch J, Dagenais G, Mann JF, Gerstein HC.** Effects of vitamin E on cardiovascular and microvascular outcomes in high-risk patients with diabetes: results of the HOPE study and MICRO-HOPE substudy. *Diabetes Care* 2002. 25(11):1919-1927.
14. **Marchioli R, Levantesi G, Macchia A, Marfisi RM, Nicolosi GL, Tavazzi L, Tognoni G, Valagussa F.** Vitamin E increases the risk of developing heart failure after myocardial infarction: Results from the GISSI-Prevenzione trial. *J Cardiovasc Med (Hagerstown)* 2006. 7(5):347-350.
15. **Hakim FA, Pflueger A.** Role of oxidative stress in diabetic kidney disease. *Med Sci Monit* 2010. 16(2):RA37-RA48.
16. **Onozato ML, Tojo A, Goto A, Fujita T, Wilcox CS.** Oxidative stress and nitric oxide synthase in rat diabetic nephropathy: effects of ACEI and ARB. *Kidney Int* 2002. 61(1):186-194.
17. **Chander PN, Gealekman O, Brodsky SV, Elitok S, Tojo A, Crabtree M, Gross SS, Goligorsky MS.** Nephropathy in Zucker diabetic fat rat is associated with oxidative and nitrosative stress: prevention by chronic therapy with a peroxynitrite scavenger ebselen. *J Am Soc Nephrol* 2004. 15(9):2391-2403.
18. **Kakimoto M, Inoguchi T, Sonta T, Yu HY, Imamura M, Etoh T, Hashimoto T, Nawata H.** Accumulation of 8-hydroxy-2'-deoxyguanosine and mitochondrial DNA deletion in kidney of diabetic rats. *Diabetes* 2002. 51(5):1588-1595.
19. **Ha H, Lee HB.** Reactive oxygen species amplify glucose signalling in renal cells cultured under high glucose and in diabetic kidney. *Nephrology (Carlton)* 2005. 10(Suppl):S7-S10.
20. **Lee HB, Yu MR, Yang Y, Jiang Z, Ha H.** Reactive oxygen species-regulated signaling pathways in diabetic nephropathy. *J Am Soc Nephrol* 2003. 14(8 Suppl 3):S241-S245.
21. **Chew P, Yuen DY, Stefanovic N, Pete J, Coughlan MT, Jandeleit-Dahm KA, Thomas MC, Rosenfeldt F, Cooper ME, de Haan JB.** Antiatherosclerotic and renoprotective effects of ebselen in the diabetic apolipoprotein E/GPx1-double knockout mouse. *Diabetes* 2010. 59(12):3198-3207.
22. **Xiao H, Li Y, Qi J, Wang H, Liu K.** Peroxynitrite plays a key role in glomerular lesions in diabetic rats. *J Nephrol* 2009. 22(6):800-808.
23. **Gorin Y, Block K, Hernandez J, Bhandari B, Wagner B, Barnes JL, Abboud HE.** Nox4 NAD(P)H oxidase mediates hypertrophy and fibronectin expression in the diabetic kidney. *J Biol Chem* 2005. 280(47):39616-39626.
24. **Kanauchi M, Nishioka H, Hashimoto T.** Oxidative DNA damage and tubulointerstitial injury in diabetic nephropathy. *Nephron* 2002. 91(2):327-329.
25. **Hinokio Y, Suzuki S, Hirai M, Suzuki C, Suzuki M, Toyota T.** Urinary excretion of 8-oxo-7, 8-dihydro-2'-deoxyguanosine as a predictor of the development of dia-

betic nephropathy. *Diabetologia* 2002. 45(6):877-882.
26. **Evans JL, Goldfine ID, Maddux BA, Grodsky GM.** Oxidative stress and stress-activated signaling pathways: a unifying hypothesis of type 2 diabetes. *Endocr Rev* 2002. 23(5):599-622.
27. **Studer RK, Craven PA, DeRubertis FR.** Antioxidant inhibition of protein kinase C-signaled increases in transforming growth factor-beta in mesangial cells. *Metabolism* 1997. 46(8):918-925.
28. **Ha H, Lee HB.** Reactive oxygen species as glucose signaling molecules in mesangial cells cultured under high glucose. *Kidney Int Suppl* 2000. 77:S19-S25.
29. **Border WA, Noble NA.** TGF-beta in kidney fibrosis: a target for gene therapy. *Kidney Int* 1997. 51(5):1388-1396.
30. **Yamamoto T, Noble NA, Miller DE, Border WA.** Sustained expression of TGF-beta 1 underlies development of progressive kidney fibrosis. *Kidney Int* 1994. 45(3):916-927.
31. **Ha H, Yu MR, Choi YJ, Kitamura M, Lee HB.** Role of high glucose-induced nuclear factor-kappaB activation in monocyte chemoattractant protein-1 expression by mesangial cells. *J Am Soc Nephrol* 2002. 13(4):894-902.
32. **Rhyu DY, Yang Y, Ha H, Lee GT, Song JS, Uh ST, Lee HB.** Role of reactive oxygen species in TGF-beta1-induced mitogen-activated protein kinase activation and epithelial-mesenchymal transition in renal tubular epithelial cells. *J Am Soc Nephrol* 2005. 16(3):667-675.
33. **Forbes JM, Coughlan MT, Cooper ME.** Oxidative stress as a major culprit in kidney disease in diabetes. *Diabetes* 2008. 57(6):1446-1454.
34. **Higgins GC, Coughlan MT.** Mitochondrial dysfunction and mitophagy: the beginning and end to diabetic nephropathy? *Br J Pharmacol* 2014. 171(8):1917-1942.
35. **Dorn GW 2nd.** Molecular mechanisms that differentiate apoptosis from programmed necrosis. *Toxicol Pathol* 2013. 41(2):227-234.
36. **Kyte J.** Immunoferritin determination of the distribution of (Na+ + K+) ATPase over the plasma membranes of renal convoluted tubules. II. Proximal segment. *J Cell Biol* 1976. 68(2):304-318.
37. **Kyte J.** Immunoferritin determination of the distribution of (Na+ + K+) ATPase over the plasma membranes of renal convoluted tubules. I. Distal segment. *J Cell Biol* 1976. 68(2):287-303.
38. **Agus ZS, Chiu PJ, Goldberg M.** Regulation of urinary calcium excretion in the rat. *Am J Physiol* 1977. 232(6):F545-F549.
39. **Chen Q, Vazquez EJ, Moghaddas S, Hoppel CL, Lesnefsky EJ.** Production of reactive oxygen species by mitochondria: central role of complex III. *J Biol Chem* 2003. 278(38):36027-36031.
40. **St-Pierre J, Buckingham JA, Roebuck SJ, Brand MD.** Topology of superoxide production from different sites in the mitochondrial electron transport chain. *J Biol Chem* 2002. 277(47):44784-44790.
41. **Forbes JM, Ke BX, Nguyen TV, Henstridge DC, Penfold SA, Laskowski A, Sourris KC, Groschner LN, Cooper ME, Thorburn DR, Coughlan MT.** Deficiency in mitochondrial complex I activity due to Ndufs6 gene trap insertion induces renal disease. *Antioxid Redox Signal* 2013. 19(4):331-343.
42. **Maessen DE, Stehouwer CD, Schalkwijk CG.** The role of methylglyoxal and the glyoxalase system in diabetes and other age-related diseases. *Clin Sci (Lond)* 2015. 128(12):839-861.
43. **Gugliucci A, Menini T.** The axis AGE-RAGE-soluble RAGE and oxidative stress in chronic kidney disease. *Adv Exp Med Biol* 2014. 824:191-208.
44. **Coughlan MT, Thorburn DR, Penfold SA, Laskowski A, Harcourt BE, Sourris KC, Tan AL, Fukami K, Thallas-Bonke V, Nawroth PP, et al.** RAGE-induced cytosolic ROS promote mitochondrial superoxide generation in diabetes. *J Am Soc Nephrol* 2009. 20(4):742-752.
45. **Rosca MG, Mustata TG, Kinter MT, Ozdemir AM, Kern TS, Szweda LI, Brownlee M, Monnier VM, Weiss MF.** Glycation of mitochondrial proteins from diabetic rat kidney is associated with excess superoxide formation. *Am J Physiol Renal Physiol* 2005. 289(2):F420-F430.
46. **Kim KM, Kim YS, Jung DH, Lee J, Kim JS.** Increased glyoxalase I levels inhibit accumulation of oxidative stress and an advanced glycation end product in mouse mesangial cells cultured in high glucose. *Exp Cell Res* 2012. 318(2):152-159.
47. **Brownlee M.** Biochemistry and molecular cell biology of diabetic complications. *Nature* 2001. 414(6865):813-820.
48. **Nishikawa T, Edelstein D, Du XL, Yamagishi S, Matsumura T, Kaneda Y, Yorek MA, Beebe D, Oates PJ, Hammes HP, et al.** Normalizing mitochondrial superoxide production blocks three pathways of hyperglycaemic damage. *Nature* 2000. 404(6779):787-790.
49. **Kiritoshi S, Nishikawa T, Sonoda K, Kukidome D, Senokuchi T, Matsuo T, Matsumura T, Tokunaga H, Brownlee M, Araki E.** Reactive oxygen species from mitochondria induce cyclooxygenase-2 gene expression in human mesangial cells: potential role in diabetic nephropathy. *Diabetes* 2003. 52(10):2570-2577.
50. **Zhan M, Usman IM, Sun L, Kanwar YS.** Disruption of renal tubular mitochondrial quality control by Myo-inositol oxygenase in diabetic kidney disease. *J Am Soc Nephrol* 2015. 26(6):1304-1321.
51. **Bock F, Shahzad K, Wang H, Stoyanov S, Wolter J, Dong W, Pelicci PG, Kashif M, Ranjan S, Schmidt S, et al.** Activated protein C ameliorates diabetic nephropathy by epigenetically inhibiting the redox enzyme p66Shc. *Proc Natl Acad Sci U S A* 2013. 110(2):648-653.
52. **Block K, Gorin Y, Abboud HE.** Subcellular localization of Nox4 and regulation in diabetes. *Proc Natl Acad Sci U S A* 2009. 106(34):14385-14390.
53. **Drummond GR, Selemidis S, Griendling KK, Sobey CG.** Combating oxidative stress in vascular disease: NADPH oxidases as therapeutic targets. *Nat Rev Drug Discov* 2011. 10(6):453-471.
54. **Dikalov SI, Dikalova AE, Bikineyeva AT, Schmidt HH, Harrison DG, Griendling KK.** Distinct roles of Nox1 and Nox4 in basal and angiotensin II-stimulated superoxide and hydrogen peroxide production. *Free Radic Biol Med* 2008. 45(9):1340-1351.
55. **Jo SH, Son MK, Koh HJ, Lee SM, Song IH, Kim YO, Lee YS, Jeong KS, Kim WB, Park JW, et al.** Control of mitochondrial redox balance and cellular defense against oxidative damage by mitochondrial NADP+-dependent isocitrate dehydrogenase. *J Biol Chem* 2001. 276(19):16168-16176.
56. **You YH, Quach T, Saito R, Pham J, Sharma K.** Metabolomics reveals a key role for fumarate in mediating the effects of NADPH oxidase 4 in diabetic kidney disease. *J Am*

Soc Nephrol 2015. In press.
57. **Coughlan MT, Thallas-Bonke V, Pete J, Long DM, Gasser A, Tong DC, Arnstein M, Thorpe SR, Cooper ME, Forbes JM.** Combination therapy with the advanced glycation end product cross-link breaker, alagebrium, and angiotensin converting enzyme inhibitors in diabetes: synergy or redundancy? *Endocrinology* 2007. 148(2):886-895.
58. **Winiarska K, Focht D, Sierakowski B, Lewandowski K, Orlowska M, Usarek M.** NADPH oxidase inhibitor, apocynin, improves renal glutathione status in Zucker diabetic fatty rats: a comparison with melatonin. *Chem Biol Interact* 2014. 218:12-19.
59. **Weisiger RA, Fridovich I.** Mitochondrial superoxide simutase. Site of synthesis and intramitochondrial localization. *J Biol Chem* 1973. 248(13):4793-4796.
60. **Das R, Xu S, Quan X, Nguyen TT, Kong ID, Chung CH, Lee EY, Cha SK, Park KS.** Upregulation of mitochondrial Nox4 mediates TGF-beta-induced apoptosis in cultured mouse podocytes. *Am J Physiol Renal Physiol* 2014. 306(2):F155-F167.
61. **Habib SL.** Diabetes and renal tubular cell apoptosis. *World J Diabetes* 2013. 4(2):27-30.
62. **Towler DA.** Mitochondrial ROS deficiency and diabetic complications: AMP(K)-lifying the adaptation to hyperglycemia. *J Clin Invest* 2013. 123(11):4573-4576.
63. **Dugan LL, You YH, Ali SS, Diamond-Stanic M, Miyamoto S, DeCleves AE, Andreyev A, Quach T, Ly S, Shekhtman G, et al.** AMPK dysregulation promotes diabetes-related reduction of superoxide and mitochondrial function. *J Clin Invest* 2013. 123(11):4888-4899.
64. **Nishikawa T, Brownlee M, Araki E.** Mitochondrial reactive oxygen species in the pathogenesis of early diabetic nephropathy. *J Diabetes Invest* 2015. 6(2):137-139.
65. **Saul RL, Ames BN.** Background levels of DNA damage in the population. *Basic Life Sci* 1986. 38:529-535.
66. **Ames BN, Shigenaga MK.** Oxidants are a major contributor to aging. *Ann N Y Acad Sci* 1992. 663:85-96.
67. **Dizdaroglu M.** Base-excision repair of oxidative DNA damage by DNA glycosylases. *Mutat Res* 2005. 591(1-2):45-59.
68. **Feldenberg LR, Thevananther S, del Rio M, de Leon M, Devarajan P.** Partial ATP depletion induces Fas- and caspase-mediated apoptosis in MDCK cells. *Am J Physiol* 1999. 276(6 Pt 2):F837-F846.
69. **Eguchi Y, Srinivasan A, Tomaselli KJ, Shimizu S, Tsujimoto Y.** ATP-dependent Steps in Apoptotic Signal Transduction. *Cancer Res* 1999. 59(9):2174-2181.
70. **Leist M, Single B, Castoldi AF, Kuhnle S, Nicotera P.** Intracellular adenosine triphosphate (ATP) concentration: a switch in the decision between apoptosis and necrosis. *J Exp Med* 1997. 185(8):1481-1486.
71. **Koh DW, Dawson TM, Dawson VL.** Mediation of cell death by poly(ADP-ribose) polymerase-1. *Pharmacol Res* 2005. 52(1):5-14.
72. **Hassa PO.** The molecular "Jekyll and Hyde" duality of PARP1 in cell death and cell survival. *Front Biosci (Landmark Ed)* 2009. 14:72-111.
73. **Laval J.** Role of DNA repair enzymes in the cellular resistance to oxidative stress. *Pathol Biol (Paris)* 1996. 44(1):14-24.
74. **Hong SJ, Dawson TM, Dawson VL.** Nuclear and mitochondrial conversations in cell death: PARP-1 and AIF signaling. *Trends Pharmacol Sci* 2004. 25(5):259-264.
75. **Susztak K, Raff AC, Schiffer M, Bottinger EP.** Glucose-induced reactive oxygen species cause apoptosis of podocytes and podocyte depletion at the onset of diabetic nephropathy. *Diabetes* 2006. 55(1):225-233.
76. **Prakash A, Doublie S.** Base Excision Repair in the Mitochondria. *J Cell Biochem* 2015. In press.
77. **Bohr VA, Stevnsner T, de Souza-Pinto NC.** Mitochondrial DNA repair of oxidative damage in mammalian cells. *Gene* 2002. 286(1):127-134.
78. **Campalans A, Moritz E, Kortulewski T, Biard D, Epe B, Radicella JP.** Interaction with OGG1 is required for efficient recruitment of XRCC1 to base excision repair and maintenance of genetic stability after exposure to oxidative stress. *Mol Cell Biol* 2015. 35(9):1648-1658.
79. **Nakabeppu Y, Tsuchimoto D, Ichinoe A, Ohno M, Ide Y, Hirano S, Yoshimura D, Tominaga Y, Furuichi M, Sakumi K.** Biological significance of the defense mechanisms against oxidative damage in nucleic acids caused by reactive oxygen species: from mitochondria to nuclei. *Ann N Y Acad Sci* 2004. 1011:101-111.
80. **Wu LL, Chiou CC, Chang PY, Wu JT.** Urinary 8-OHdG: a marker of oxidative stress to DNA and a risk factor for cancer, atherosclerosis and diabetics. *Clin Chim Acta* 2004. 339(1-2):1-9.
81. **Giovannini C, Piaggi S, Federico G, Scarpato R.** High levels of gamma-H2AX foci and cell membrane oxidation in adolescents with type 1 diabetes. *Mutat Res* 2014. 770:128-135.
82. **Prasad M, Bronson SC, Warrier T, Badarinath A, Rai S, Baid K, Sitaraman S, George A, Moses A, Saraswathy R, et al.** Evaluation of DNA damage in Type 2 diabetes mellitus patients with and without peripheral neuropathy: A study in South Indian population. *J Nat Sci Biol Med* 2015. 6(1):80-84.
83. **Cinkilic N, Kiyici S, Celikler S, Vatan O, Oz Gul O, Tuncel E, Bilaloglu R.** Evaluation of chromosome aberrations, sister chromatid exchange and micronuclei in patients with type-1 diabetes mellitus. *Mutat Res* 2009. 676(1-2):1-4.
84. **Gelaleti RB, Damasceno DC, Lima PH, Salvadori DM, Calderon Ide M, Peracoli JC, Rudge MV.** Oxidative DNA damage in diabetic and mild gestational hyperglycemic pregnant women. *Diabetol Metab Syndr* 2015. 7:1.
85. **Gelaleti RB, Damasceno DC, Salvadori DM, Marcondes JP, Lima PH, Morceli G, Calderon IM, Rudge MV.** IRS-1 gene polymorphism and DNA damage in pregnant women with diabetes or mild gestational hyperglycemia. *Diabetol Metab Syndr* 2015. 7:30.
86. **Simone S, Gorin Y, Velagapudi C, Abboud HE, Habib SL.** Mechanism of oxidative DNA damage in diabetes : tuberin inactivation and downregulation of DNA repair enzyme 8-oxo-7,8-dihydro-2'-deoxyguanosine-DNA glycosylase. *Diabetes* 2008. 57(10):2626-2636.
87. **Xu GW, Yao QH, Weng QF, Su BL, Zhang X, Xiong JH.** Study of urinary 8-hydroxydeoxyguanosine as a biomarker of oxidative DNA damage in diabetic nephropathy patients. *J Pharm Biomed Anal* 2004. 36(1):101-104.
88. **Dong QY, Cui Y, Chen L, Song J, Sun L.** Urinary 8-hydroxydeoxyguanosine levels in diabetic retinopathy patients. *Eur J Ophthalmol* 2008. 18(1):94-98.
89. **Valavanidis A, Vlachogianni T, Fiotakis C.** 8-hydroxy-2'-deoxyguanosine (8-OHdG): A critical biomarker of oxidative stress and carcinogenesis. *J Environ Sci Health C Environ Carcinog Ecotoxicol Rev* 2009. 27(2):120-139.

90. **Orhan H, van Holland B, Krab B, Moeken J, Vermeulen NP, Hollander P, Meerman JH.** Evaluation of a multi-parameter biomarker set for oxidative damage in man: increased urinary excretion of lipid, protein and DNA oxidation products after one hour of exercise. *Free Radic Res* 2004. 38(12):1269-1279.
91. **Lai CH, Liou SH, Lin HC, Shih TS, Tsai PJ, Chen JS, Yang T, Jaakkola JJ, Strickland PT.** Exposure to traffic exhausts and oxidative DNA damage. *Occup Environ Med* 2005. 62(4):216-222.
92. **Bohr VA, Dianov GL.** Oxidative DNA damage processing in nuclear and mitochondrial DNA. *Biochimie* 1999. 81(1-2):155-160.
93. **Yakes FM, Van Houten B.** Mitochondrial DNA damage is more extensive and persists longer than nuclear DNA damage in human cells following oxidative stress. *Proc Natl Acad Sci U S A* 1997. 94(2):514-519.
94. **Gao Y, Katyal S, Lee Y, Zhao J, Rehg JE, Russell HR, McKinnon PJ.** DNA ligase III is critical for mtDNA integrity but not Xrcc1-mediated nuclear DNA repair. *Nature* 2011. 471(7337):240-244.
95. **de Souza-Pinto NC, Wilson DM, Stevnsner TV, Bohr VA.** Mitochondrial DNA, base excision repair and neurodegeneration. *DNA Repair* 2008. 7(7):1098-1109.
96. **Suematsu N, Tsutsui H, Wen J, Kang D, Ikeuchi M, Ide T, Hayashidani S, Shiomi T, Kubota T, Hamasaki N, Takeshita A.** Oxidative stress mediates tumor necrosis factor-alpha-induced mitochondrial DNA damage and dysfunction in cardiac myocytes. *Circulation* 2003. 107(10):1418-1423.
97. **Madsen-Bouterse SA, Mohammad G, Kanwar M, Kowluru RA.** Role of mitochondrial DNA damage in the development of diabetic retinopathy, and the metabolic memory phenomenon associated with its progression. *Antioxid Redox Signal* 2010. 13(6):797-805.
98. **Czajkaa AS, Gnudib L, Parsadea CK, Jonesa P, Reidc F, Malika AN.** Altered mitochondrial function, mitochondrial DNA and reduced metabolic flexibility in patients with diabetic nephropathy. *EBioMedicine* 2015. 2(6):499-512.
99. **Merecz A, Markiewicz L, Sliwinska A, Kosmalski M, Kasznicki J, Drzewoski J, Majsterek I.** Analysis of oxidative DNA damage and its repair in Polish patients with diabetes mellitus type 2: Role in pathogenesis of diabetic neuropathy. *Adv Med Sci* 2015. 60(2):220-230.
100. **Kasznicki J, Kosmalski M, Sliwinska A, Mrowicka M, Stanczyk M, Majsterek I, Drzewoski J.** Evaluation of oxidative stress markers in pathogenesis of diabetic neuropathy. *Mol Biol Rep* 2012. 39(9):8669-8678.
101. **Lu J, Li X, Zhang M, Chen Z, Wang Y, Zeng C, Liu Z, Chen H.** Regulation of MUTYH, a DNA repair enzyme, in renal proximal tubular epithelial cells. *Oxid Med Cell Longev* 2014. In press.
102. **Cai Z, Chen H, Tao J, Guo W, Liu X, Zheng B, Sun W, Wang Y.** Association of Base Excision Repair Gene Polymorphisms with ESRD Risk in a Chinese Population. *Oxid Med Cell Longev* 2012. 2012:10.
103. **Cai Z, Guo W, Chen H, Tao J, Cao L, Sun W, Wang Y.** Base excision repair gene polymorphisms are associated with inflammation in patients undergoing chronic hemodialysis. *Biochem Biophys Res Commun* 2012. 424(3):611-615.
104. **Bernstein C, Bernstein H, Payne CM, Garewal H.** DNA repair/pro-apoptotic dual-role proteins in five major DNA repair pathways: fail-safe protection against carcinogenesis. *Mutat Res* 2002. 511(2):145-178.
105. **Ashkenazi A, Dixit VM.** Apoptosis control by death and decoy receptors. *Curr Opin Cell Biol* 1999. 11(2):255-260.
106. **Eguchi Y, Shimizu S, Tsujimoto Y.** Intracellular ATP Levels Determine Cell Death Fate by Apoptosis or Necrosis. *Cancer Res* 1997. 57(10):1835-1840.
107. **Malhotra JD, Kaufman RJ.** Endoplasmic reticulum stress and oxidative stress: a vicious cycle or a double-edged sword? *Antioxid Redox Signal* 2007. 9(12):2277-2293.
108. **Herman-Edelstein M, Thomas MC, Thallas-Bonke V, Saleem M, Cooper ME, Kantharidis P.** Dedifferentiation of immortalized human podocytes in response to transforming growth Factor-beta: a model for diabetic podocytopathy. *Diabetes* 2011. 60(6):1779-1788.
109. **Sanchez-Nino MD, Sanz AB, Lorz C, Gnirke A, Rastaldi MP, Nair V, Egido J, Ruiz-Ortega M, Kretzler M, Ortiz A.** BASP1 promotes apoptosis in diabetic nephropathy. *J Am Soc Nephrol* 2010. 21(4):610-621.
110. **Kumar D, Robertson S, Burns KD.** Evidence of apoptosis in human diabetic kidney. *Mol Cell Biochem* 2004. 259(1-2):67-70.
111. **Kumar D, Zimpelmann J, Robertson S, Burns KD.** Tubular and interstitial cell apoptosis in the streptozotocin-diabetic rat kidney. *Nephron Exp Nephrol* 2004. 96(3):E77-E88.
112. **Susztak K, Ciccone E, McCue P, Sharma K, Böttinger EP.** Multiple metabolic hits converge on CD36 as novel mediator of tubular epithelial apoptosis in diabetic nephropathy. *Plos Med* 2005. 2(2):e45.
113. **Lorz C, Benito-Martín A, Boucherot A, Ucero AC, Rastaldi MP, Henger A, Armelloni S, Santamaría B, Berthier CC, Kretzler M, et al.** The death ligand TRAIL in diabetic nephropathy. *J Am Soc Nephrol* 2008. 19(5):904-914.
114. **Sanchez-Nino MD, Benito-Martin A, Ortiz A.** New paradigms in cell death in human diabetic nephropathy. *Kidney Int* 2010. 78(8):737-744.
115. **Chang YH, Lin KD, He SR, Hsieh MC, Hsiao JY, Shin SJ.** Serum osteoprotegerin and tumor necrosis factor related apoptosis inducing-ligand (TRAIL) are elevated in type 2 diabetic patients with albuminuria and serum osteoprotegerin is independently associated with the severity of diabetic nephropathy. *Metabolism* 2011. 60(8):1064-1069.
116. **Verzola D, Gandolfo MT, Ferrario F, Rastaldi MP, Villaggio B, Gianiorio F, Giannoni M, Rimoldi L, Lauria F, Miji M, et al.** Apoptosis in the kidneys of patients with type II diabetic nephropathy. *Kidney Int* 2007. 72(10):1262-1272.
117. **Baba K, Minatoguchi S, Sano H, Kagawa T, Murata I, Takemura G, Hirano T, Ohashi H, Takemura M, Fujiwara T, Fujiwara H.** Involvement of apoptosis in patients with diabetic nephropathy: A study on plasma soluble Fas levels and pathological findings. *Nephrology (Carlton)* 2004. 9(2):94-99.
118. **Kelly DJ, Stein-Oakley A, Zhang Y, Wassef L, Maguire J, Koji T, Thomson N, Wilkinson-Berka JL, Gilbert RE.** Fas-induced apoptosis is a feature of progressive diabetic nephropathy in transgenic (mRen-2)27 rats: attenuation with renin-angiotensin blockade. *Nephrology (Carlton)* 2004. 9(1):7-13.
119. **Justo P, Sanz AB, Lorz C, Egido J, Ortiz A.** Lethal activity of FADD death domain in renal tubular epithelial cells. *Kidney Int* 2006. 69(12):2205-2211.

120. **Erkan E, De Leon M, Devarajan P.** Albumin overload induces apoptosis in LLC-PK(1) cells. *Am J Physiol Renal Physiol* 2001. 280(6):F1107-F1114.
121. **Cipollone F, Chiarelli F, Iezzi A, Fazia ML, Cuccurullo C, Pini B, De Cesare D, Torello M, Tumini S, Cuccurullo F, Mezzetti A.** Relationship between reduced BCL-2 expression in circulating mononuclear cells and early nephropathy in type 1 diabetes. *Int J Immunopathol Pharmacol* 2005. 18(4):625-635.
122. **Ortiz A, Ziyadeh FN, Neilson EG.** Expression of apoptosis-regulatory genes in renal proximal tubular epithelial cells exposed to high ambient glucose and in diabetic kidneys. *J Investig Medi* 1997. 45(2):50-56.
123. **Liu F, Brezniceanu ML, Wei CC, Chenier I, Sachetelli S, Zhang SL, Filep JG, Ingelfinger JR, Chan JS.** Overexpression of angiotensinogen increases tubular apoptosis in diabetes. *J Am Soc Nephrol* 2008. 19(2):269-280.
124. **Qiu LQ, Sinniah R, I-Hong Hsu S.** Downregulation of Bcl-2 by podocytes is associated with progressive glomerular injury and clinical indices of poor renal prognosis in human IgA nephropathy. *J Am Soc Nephrol* 2004. 15(1):79-90.
125. **Goumenos DS, Tsamandas AC, Kalliakmani P, Tsakas S, Sotsiou F, Bonikos DS, Vlachojannis JG.** Expression of apoptosis-related proteins bcl-2 and bax along with transforming growth factor (TGF-beta1) in the kidney of patients with glomerulonephritides. *Ren Fail* 2004. 26(4):361-367.
126. **Lau GJ, Godin N, Maachi H, Lo CS, Wu SJ, Zhu JX, Brezniceanu ML, Chenier I, Fragasso-Marquis J, Lattouf JB, et al.** Bcl-2-modifying factor induces renal proximal tubular cell apoptosis in diabetic mice. *Diabetes* 2012. 61(2):474-484.
127. **Gerecova G, Kopanicova J, Jaka P, Behalova L, Juhasova B, Bhatia-Kissova I, Forte M, Polcic P, Mentel M.** BH3-only proteins Noxa, Bik, Bmf, and Bid activate Bax and Bak indirectly when studied in yeast model. *FEMS Yeast Res* 2013. 13(8):747-754.
128. **Rane MJ, Song Y, Jin S, Barati MT, Wu R, Kausar H, Tan Y, Wang Y, Zhou G, Klein JB, et al.** Interplay between Akt and p38 MAPK pathways in the regulation of renal tubular cell apoptosis associated with diabetic nephropathy. *Am J Physiol Renal Physiol* 2010. 298(1):F49-F61.
129. **Wagener FA, Dekker D, Berden JH, Scharstuhl A, van der Vlag J.** The role of reactive oxygen species in apoptosis of the diabetic kidney. *Apoptosis* 2009. 14(12):1451-1458.
130. **Song P, Yang S, Xiao L, Xu X, Tang C, Yang Y, Ma M, Zhu J, Liu F, Sun L.** PKCdelta promotes high glucose induced renal tubular oxidative damage via regulating activation and translocation of p66Shc. *Oxid Med Cell Longev* 2014. 2014:746531.
131. **Sun L, Xiao L, Nie J, Liu FY, Ling GH, Zhu XJ, Tang WB, Chen WC, Xia YC, Zhan M, et al.** p66Shc mediates high-glucose and angiotensin II-induced oxidative stress renal tubular injury via mitochondrial-dependent apoptotic pathway. *Am J Physiol Renal Physiol* 2010. 299(5):F1014-F1025.
132. **Verzola D, Ratto E, Villaggio B, Parodi EL, Pontremoli R, Garibotto G, Viazzi F.** Uric acid promotes apoptosis in human proximal tubule cells by oxidative stress and the activation of NADPH oxidase NOX 4. *Plos One* 2014. 9(12):e115210.
133. **Susnow N, Zeng L, Margineantu D, Hockenbery DM.** Bcl-2 family proteins as regulators of oxidative stress. *Semin Cancer Biol* 2009. 19(1):42-49.
134. **D'Alessio M, De Nicola M, Coppola S, Gualandi G, Pugliese L, Cerella C, Cristofanon S, Civitareale P, Ciriolo MR, Bergamaschi A, et al.** Oxidative Bax dimerization promotes its translocation to mitochondria independently of apoptosis. *Faseb J* 2005. 19(11):1504-1506.
135. **Karch J, Molkentin JD.** Regulated necrotic cell death: the passive aggressive side of Bax and Bak. *Circ Res* 2015. 116(11):1800-1809.
136. **Whelan RS, Konstantinidis K, Wei AC, Chen Y, Reyna DE, Jha S, Yang Y, Calvert JW, Lindsten T, Thompson CB, et al.** Bax regulates primary necrosis through mitochondrial dynamics. *Proc Natl Acad Sci U S A* 2012. 109(17):6566-6571.
137. **Dewson G, Kluck RM.** Mechanisms by which Bak and Bax permeabilise mitochondria during apoptosis. *J Cell Sci* 2009. 122(16):2801-2808.
138. **Lin SH, Perera MN, Nguyen T, Datskovskiy D, Miles M, Colombini M.** Bax forms two types of channels, one of which is voltage-gated. *Biophys J* 2011. 101(9):2163-2169.
139. **Chen Y, Gui D, Chen J, He D, Luo Y, Wang N.** Down-regulation of PERK-ATF4-CHOP pathway by Astragaloside IV is associated with the inhibition of endoplasmic reticulum stress-induced podocyte apoptosis in diabetic rats. *Cell Physiol Biochem* 2014. 33(6):1975-1987.
140. **Baban B, Liu JY, Mozaffari MS.** Endoplasmic reticulum stress response and inflammatory cytokines in type 2 diabetic nephropathy: Role of indoleamine 2,3-dioxygenase and programmed death-1. *Exp Mol Pathol* 2013. 94(2):343-351.
141. **Brosius FC, Kaufman RJ.** Is the ER stressed out in diabetic kidney disease? *J Am Soc Nephrol* 2008. 19(11):2040-2042.
142. **Forbes JM, Coughlan MT, Cooper ME.** Oxidative stress as a major culprit in kidney disease in diabetes. *Diabetes* 2008. 57(6):1446-1454.
143. **Lee AH, Iwakoshi NN, Glimcher LH.** XBP-1 Regulates a Subset of Endoplasmic Reticulum Resident Chaperone Genes in the Unfolded Protein Response. *Mol Cell Biol* 2003. 23(21):7448-7459.
144. **Chen Y, Brandizzi F.** IRE1: ER stress sensor and cell fate executor. *Trends Cell Biol* 2013. 23(11):547-555.
145. **Fonseca SG, Gromada J, Urano F.** Endoplasmic reticulum stress and pancreatic beta-cell death. *Trends Endocrinol Metab* 2011. 22(7):266-274.
146. **Laybutt DR, Preston AM, Akerfeldt MC, Kench JG, Busch AK, Biankin AV, Biden TJ.** Endoplasmic reticulum stress contributes to beta cell apoptosis in type 2 diabetes. *Diabetologia* 2007. 50(4):752-763.
147. **Lindenmeyer MT, Rastaldi MP, Ikehata M, Neusser MA, Kretzler M, Cohen CD, Schlöndorff D.** Proteinuria and hyperglycemia induce endoplasmic reticulum stress. *J Am Soc Nephrol* 2008. 19(11):2225-2236.
148. **Zhuang A, Forbes JM.** Stress in the kidney is the road to pERdition: is endoplasmic reticulum stress a pathogenic mediator of diabetic nephropathy? *J Endocrinol* 2014. 222(3):R97-R111.
149. **Inagi R.** Endoplasmic reticulum stress as a progression factor for kidney injury. *Curr Opin Pharmacol* 2010. 10(2):156-165.
150. **Brezniceanu ML, Lau CJ, Godin N, Chenier I, Duclos A, Ethier J, Filep JG, Ingelfinger JR, Zhang SL, Chan JS.** Reactive oxygen species promote caspase-12 ex-

pression and tubular apoptosis in diabetic nephropathy. *J Am Soc Nephrol* 2010. 21(6):943-954.
151. **Cheema MU, Damkier HH, Nielsen J, Poulsen ET, Enghild JJ, Fenton RA, Praetorius J.** Distal renal tubules are deficient in aggresome formation and autophagy upon aldosterone administration. *Plos One* 2014. 9(7):e101258.
152. **Feissner RF, Skalska J, Gaum WE, Sheu SS.** Crosstalk signaling between mitochondrial Ca(2+) and ROS. *Front Biosci (Landmark Ed)* 2009. 14:1197-1218.
153. **Grimm S.** The ER–mitochondria interface: The social network of cell death. *Biochim Biophys Acta* 2012. 1823(2):327-334.
154. **Brookes PS, Yoon Y, Robotham JL, Anders MW, Sheu SS.** Calcium, ATP, and ROS: a mitochondrial love-hate triangle. *Am J Physiol Cell Physiol* 2004. 287(4):C817-C833.
155. **Pospisilik JA, Knauf C, Joza N, Benit P, Orthofer M, Cani PD, Ebersberger I, Nakashima T, Sarao R, Neely G, et al.** Targeted deletion of AIF decreases mitochondrial oxidative phosphorylation and protects from obesity and diabetes. *Cell* 2007. 131(3):476-491.
156. **Sano R, Reed JC.** ER stress-induced cell death mechanisms. *Biochim Biophys Acta* 2013. 1833(12):3460-3470.
157. **Wang X, Olberding KE, White C, Li C.** Bcl-2 proteins regulate ER membrane permeability to luminal proteins during ER stress-induced apoptosis. *Cell Death Differ* 2011. 18(1):38-47.
158. **Zong WX, Li C, Hatzivassiliou G, Lindsten T, Yu QC, Yuan J, Thompson CB.** Bax and Bak can localize to the endoplasmic reticulum to initiate apoptosis. *J Cell Biol* 2003. 162(1):59-69.
159. **Kennedy D, Mnich K, Samali A.** Heat shock preconditioning protects against ER stress-induced apoptosis through the regulation of the BH3-only protein BIM. *FEBS Open Bio* 2014. 4:813-821.
160. **Morishima N, Nakanishi K, Tsuchiya K, Shibata T, Seiwa E.** Translocation of Bim to the endoplasmic reticulum (ER) mediates ER stress signaling for activation of caspase-12 during ER stress-induced apoptosis. *J Biol Chem* 2004. 279(48):50375-50381.
161. **Lin ML, Chen SS, Huang RY, Lu YC, Liao YR, Reddy MV, Lee CC, Wu TS.** Suppression of PI3K/Akt signaling by synthetic bichalcone analog TSWU-CD4 induces ER stress- and Bax/Bak-mediated apoptosis of cancer cells. *Apoptosis* 2014. 19(11):1637-1653.
162. **Matsuzaki S, Hiratsuka T, Kuwahara R, Katayama T, Tohyama M.** Caspase-4 is partially cleaved by calpain via the impairment of Ca2+ homeostasis under the ER stress. *Neurochem Int* 2010. 56(2):352-356.
163. **Sansanwal P, Kambham N, Sarwal MM.** Caspase-4 may play a role in loss of proximal tubules and renal injury in nephropathic cystinosis. *Pediatr Nephrol* 2010. 25(1):105-109.
164. **Sanchez-Nino MD, Sanz AB, Ortiz A.** Caspase-12 and Diabetic Nephropathy: From Mice to Men? *J Am Soc Nephrol* 2010. 21(6):886-888.
165. **Deegan S, Saveljeva S, Logue SE, Pakos-Zebrucka K, Gupta S, Vandenabeele P, Bertrand MJ, Samali A.** Deficiency in the mitochondrial apoptotic pathway reveals the toxic potential of autophagy under ER stress conditions. *Autophagy* 2014. 10(11):1921-1936.
166. **Ueda M, Li S, Itoh M, Hayakawa-Yano Y, Wang MX, Hayakawa M, Hasebe-Matsubara R, Ohta K, Ohta E, Mizuno A, et al.** Polyglutamine expansion disturbs the endoplasmic reticulum formation, leading to caspase-7 activation through Bax. *Biochem Biophys Res Commun* 2014. 443(4):1232-1238.
167. **Gill MB, Bockhorst K, Narayana P, Perez-Polo JR.** Bax shuttling after neonatal hypoxia-ischemia: hyperoxia effects. *J Neurosci Res* 2008. 86(16):3584-3604.
168. **Bonneau B, Prudent J, Popgeorgiev N, Gillet G.** Non-apoptotic roles of Bcl-2 family: the calcium connection. *Biochim Biophys Acta* 2013. 1833(7):1755-1765.
169. **Small DM, Bennett NC, Roy S, Gabrielli BG, Johnson DW, Gobe GC.** Oxidative stress and cell senescence combine to cause maximal renal tubular epithelial cell dysfunction and loss in an in vitro model of kidney disease. *Nephron Exp Nephrol* 2012. 122(3-4):123-130.
170. **Frippiat C, Chen QM, Zdanov S, Magalhaes JP, Remacle J, Toussaint O.** Subcytotoxic H2O2 stress triggers a release of transforming growth factor-beta1, which induces biomarkers of cellular senescence of human diploid fibroblasts. *J Biol Chem* 2001. 276(4):2531-2537.
171. **de Haan JB, Bladier C, Lotfi-Miri M, Taylor J, Hutchinson P, Crack PJ, Hertzog P, Kola I.** Fibroblasts derived from Gpx1 knockout mice display senescent-like features and are susceptible to H2O2-mediated cell death. *Free Radic Biol Med* 2004. 36(1):53-64.
172. **Zhu K, Kakehi T, Matsumoto M, Iwata K, Ibi M, Ohshima Y, Zhang J, Liu J, Wen X, Taye A, et al.** NADPH oxidase NOX1 is involved in activation of protein kinase C and premature senescence in early stage diabetic kidney. *Free Radic Biol Med* 2015. 83:21-30.
173. **Verzola D, Gandolfo MT, Gaetani G, Ferraris A, Mangerini R, Ferrario F, Villaggio B, Gianiorio F, Tosetti F, Weiss U, et al.** Accelerated senescence in the kidneys of patients with type 2 diabetic nephropathy. *Am J Physiol Renal Physiol* 2008. 295(5):F1563-F1573.
174. **Lee HC, Yin PH, Lu CY, Chi CW, Wei YH.** Increase of mitochondria and mitochondrial DNA in response to oxidative stress in human cells. *Biochem J* 2000. 348(Pt 2):425-432.
175. **Malik AN, Shahni R, Iqbal MM.** Increased peripheral blood mitochondrial DNA in type 2 diabetic patients with nephropathy. *Diabetes Res Clin Pract* 2009. 86(2):E22-E24.
176. **Nakamura T, Ushiyama C, Suzuki S, Hara M, Shimada N, Ebihara I, Koide H.** Urinary excretion of podocytes in patients with diabetic nephropathy. *Nephrol Dial Transplant* 2000. 15(9):1379-1383.
177. **Soltoff SP.** ATP and the regulation of renal cell function. *Annu Rev Physiol* 1986. 48:9-31.
178. **Halestrap AP.** What is the mitochondrial permeability transition pore? *J Mol Cell Cardiol* 2009. 46(6):821-831.
179. **Halestrap AP, Pasdois P.** The role of the mitochondrial permeability transition pore in heart disease. *Biochim Biophys Acta* 2009. 1787(11):1402-1415.
180. **Bernardi P.** The mitochondrial permeability transition pore: a mystery solved? *Front Physiol* 2013. 4:95.
181. **Karch J, Molkentin JD.** Identifying the components of the elusive mitochondrial permeability transition pore. *Proc Natl Acad Sci U S A* 2014. 111(29):10396-10397.
182. **Takebayashi S, Kaneda K.** Mitochondrial derangement: possible initiator of microalbuminuria in NIDDM. *J Diabet Complications* 1991. 5(2-3):104-106.
183. **Kaneda K, Iwao J, Sakata N, Takebayashi S.** Correlation between mitochondrial enlargement in renal proximal

tubules and microalbuminuria in rats with early streptozotocin-induced diabetes. *Acta Pathol Jpn* 1992. 42(12):855-860.
184. **Yu T, Robotham JL, Yoon Y.** Increased production of reactive oxygen species in hyperglycemic conditions requires dynamic change of mitochondrial morphology. *Proc Natl Acad Sci U S A* 2006. 103(8):2653-2658.
185. **Zoratti M, Szabo I.** The mitochondrial permeability transition. *Biochim Biophys Acta* 1995. 1241(2):139-176.
186. **Crompton M.** The mitochondrial permeability transition pore and its role in cell death. *Biochem J* 1999. 341(Pt 2):233-249.
187. **Halestrap AP.** Calcium, mitochondria and reperfusion injury: a pore way to die. *Biochem Soc Trans* 2006. 34(Pt 2):232-237.
188. **Armstrong JS.** The role of the mitochondrial permeability transition in cell death. *Mitochondrion* 2006. 6(5):225-234.
189. **Zorov DB, Juhaszova M, Yaniv Y, Nuss HB, Wang S, Sollott SJ.** Regulation and pharmacology of the mitochondrial permeability transition pore. *Cardiovasc Res* 2009. 83(2):213-225.
190. **Baines CP.** The molecular composition of the mitochondrial permeability transition pore. *J Mol Cell Cardiol* 2009. 46(6):850-857.
191. **Baines CP, Kaiser RA, Sheiko T, Craigen WJ, Molkentin JD.** Voltage-dependent anion channels are dispensable for mitochondrial-dependent cell death. *Nat Cell Biol* 2007. 9(5):550-555.
192. **Kokoszka JE, Waymire KG, Levy SE, Sligh JE, Cai J, Jones DP, MacGregor GR, Wallace DC.** The ADP/ATP translocator is not essential for the mitochondrial permeability transition pore. *Nature* 2004. 427(6973):461-465.
193. **Krauskopf A, Eriksson O, Craigen WJ, Forte MA, Bernardi P.** Properties of the permeability transition in VDAC1(-/-) mitochondria. *Biochim Biophys Acta* 2006. 1757(5-6):590-595.
194. **Schinzel AC, Takeuchi O, Huang Z, Fisher JK, Zhou Z, Rubens J, Hetz C, Danial NN, Moskowitz MA, Korsmeyer SJ.** Cyclophilin D is a component of mitochondrial permeability transition and mediates neuronal cell death after focal cerebral ischemia. *Proc Natl Acad Sci U S A* 2005. 102(34):12005-12010.
195. **Woodfield K, Ruck A, Brdiczka D, Halestrap AP.** Direct demonstration of a specific interaction between cyclophilin-D and the adenine nucleotide translocase confirms their role in the mitochondrial permeability transition. *Biochem J* 1998. 336(Pt 2):287-290.
196. **Baines CP, Kaiser RA, Purcell NH, Blair NS, Osinska H, Hambleton MA, Brunskill EW, Sayen MR, Gottlieb RA, Dorn GW, et al.** Loss of cyclophilin D reveals a critical role for mitochondrial permeability transition in cell death. *Nature* 2005. 434(7033):658-662.
197. **Nakagawa T, Shimizu S, Watanabe T, Yamaguchi O, Otsu K, Yamagata H, Inohara H, Kubo T, Tsujimoto Y.** Cyclophilin D-dependent mitochondrial permeability transition regulates some necrotic but not apoptotic cell death. *Nature* 2005. 434(7033):652-658.
198. **Giorgio V, von Stockum S, Antoniel M, Fabbro A, Fogolari F, Forte M, Glick GD, Petronilli V, Zoratti M, Szabo I, et al.** Dimers of mitochondrial ATP synthase form the permeability transition pore. *Proc Natl Acad Sci U S A* 2013. 110(15):5887-5892.
199. **Alavian KN, Beutner G, Lazrove E, Sacchetti S, Park HA, Licznerski P, Li H, Nabili P, Hockensmith K, Graham M, et al.** An uncoupling channel within the c-subunit ring of the F1FO ATP synthase is the mitochondrial permeability transition pore. *Proc Natl Acad Sci U S A* 2014. 111(29):10580-10585.
200. **Takeyama N, Miki S, Hirakawa A, Tanaka T.** Role of the mitochondrial permeability transition and cytochrome C release in hydrogen peroxide-induced apoptosis. *Exp Cell Res* 2002. 274(1):16-24.
201. **Batandier C, Leverve X, Fontaine E.** Opening of the mitochondrial permeability transition pore induces reactive oxygen species production at the level of the respiratory chain complex I. *J Biol Chem* 2004. 279(17):17197-17204.
202. **Scorrano L, Ashiya M, Buttle K, Weiler S, Oakes SA, Mannella CA, Korsmeyer SJ.** A distinct pathway remodels mitochondrial cristae and mobilizes cytochrome c during apoptosis. *Dev Cell* 2002. 2(1):55-67.
203. **Boveris A, Oshino N, Chance B.** The cellular production of hydrogen peroxide. *Biochem J* 1972. 128(3):617-630.
204. **Turrens JF.** Mitochondrial formation of reactive oxygen species. *J Physiol* 2003. 552(Pt 2):335-344.
205. **Zorov DB, Juhaszova M, Sollott SJ.** Mitochondrial ROS-induced ROS release: an update and review. *Biochim Biophys Acta* 2006. 1757(5-6):509-517.
206. **Whelan RS, Konstantinidis K, Wei AC, Chen Y, Reyna DE, Jha S, Yang Y, Calvert JW, Lindsten T, Thompson CB, et al.** Bax regulates primary necrosis through mitochondrial dynamics. *Proc Natl Acad Sci U S A* 2012. 109(17):6566-6571.
207. **Devalaraja-Narashimha K, Diener AM, Padanilam BJ.** Cyclophilin D gene ablation protects mice from ischemic renal injury. *Am J Physiol Renal Physiol* 2009. 297(3):F749-F759.
208. **Gooch JL, Barnes JL, Garcia S, Abboud HE.** Calcineurin is activated in diabetes and is required for glomerular hypertrophy and ECM accumulation. *Am J Physiol Renal Physiol* 2003. 284(1):F144-F154.
209. **Oliveira PJ, Esteves TC, Seica R, Moreno AJ, Santos MS.** Calcium-dependent mitochondrial permeability transition is augmented in the kidney of Goto-Kakizaki diabetic rat. *Diabetes Metab Res Rev* 2004. 20(2):131-136.
210. **Smith RA, Porteous CM, Gane AM, Murphy MP.** Delivery of bioactive molecules to mitochondria in vivo. *Proc Natl Acad Sci U S A* 2003. 100(9):5407-5412.
211. **Mukhopadhyay P, Horvath B, Zsengeller Z, Zielonka J, Tanchian G, Holovac E, Kechrid M, Patel V, Stillman IE, Parikh SM, et al.** Mitochondrial-targeted antioxidants represent a promising approach for prevention of cisplatin-induced nephropathy. *Free Radic Biol Med* 2012. 52(2):497-506.
212. **Tabara LC, Poveda J, Martin-Cleary C, Selgas R, Ortiz A, Sanchez-Nino MD.** Mitochondria-targeted therapies for acute kidney injury. *Expert Rev Mol Med* 2014. 16:e13.
213. **Subramanian S, Kalyanaraman B, Migrino RQ.** Mitochondrially targeted antioxidants for the treatment of cardiovascular diseases. *Recent Pat Cardiovasc Drug Discov* 2010. 5(1):54-65.
214. **Chacko BK, Reily C, Srivastava A, Johnson MS, Ye Y, Ulasova E, Agarwal A, Zinn KR, Murphy MP, Kalyanaraman B, Darley-Usmar V.** Prevention of diabetic nephropathy in Ins2(+/)(-)(AkitaJ) mice by the mitochondria-targeted therapy MitoQ. *Biochem J* 2010. 432(1):9-

19.

215. **Bolisetty S, Traylor A, Zarjou A, Johnson MS, Benavides GA, Ricart K, Boddu R, Moore RD, Landar A, Barnes S, et al.** Mitochondria-targeted heme oxygenase-1 decreases oxidative stress in renal epithelial cells. *Am J Physiol Renal Physiol* 2013. 305(3):F255-F264.
216. **Nakamura Y, Feng Q, Kumagai T, Torikai K, Ohigashi H, Osawa T, Noguchi N, Niki E, Uchida K.** Ebselen, a glutathione peroxidase mimetic seleno-organic compound, as a multifunctional antioxidant. Implication for inflammation-associated carcinogenesis. *J Biol Chem* 2002. 277(4):2687-2694.
217. **Tan SM, Sharma A, Yuen DY, Stefanovic N, Krippner G, Mugesh G, Chai Z, de Haan JB.** The modified selenenyl amide, M-hydroxy ebselen, attenuates diabetic nephropathy and diabetes-associated atherosclerosis in ApoE/GPx1 double knockout mice. *Plos One* 2013. 8(7):e69193.
218. **Filipovska A, Kelso GF, Brown SE, Beer SM, Smith RA, Murphy MP.** Synthesis and characterization of a triphenylphosphonium-conjugated peroxidase mimetic. Insights into the interaction of ebselen with mitochondria. *J Biol Chem* 2005. 280(25):24113-24126.
219. **Szeto HH, Liu S, Soong Y, Wu D, Darrah SF, Cheng FY, Zhao Z, Ganger M, Tow CY, Seshan SV.** Mitochondria-targeted peptide accelerates ATP recovery and reduces ischemic kidney injury. *J Am Soc Nephrol* 2011. 22(6):1041-1052.
220. **Chakrabarti AK, Feeney K, Abueg C, Brown DA, Czyz E, Tendera M, Janosi A, Giugliano RP, Kloner RA, Weaver WD, et al.** Rationale and design of the EMBRACE STEMI study: a phase 2a, randomized, double-blind, placebo-controlled trial to evaluate the safety, tolerability and efficacy of intravenous Bendavia on reperfusion injury in patients treated with standard therapy including primary percutaneous coronary intervention and stenting for ST-segment elevation myocardial infarction. *Am Heart J* 2013. 165(4):509-514.
221. **Javadov S, Karmazyn M, Escobales N.** Mitochondrial permeability transition pore opening as a promising therapeutic target in cardiac diseases. *J Pharmacol Exp Ther* 2009. 330(3):670-678.
222. **Halestrap AP, Davidson AM.** Inhibition of Ca2(+)-induced large-amplitude swelling of liver and heart mitochondria by cyclosporin is probably caused by the inhibitor binding to mitochondrial-matrix peptidyl-prolyl cis-trans isomerase and preventing it interacting with the adenine nucleotide translocase. *Biochem J* 1990. 268(1):153-160.
223. **Tanveer A, Virji S, Andreeva L, Totty NF, Hsuan JJ, Ward JM, Crompton M.** Involvement of cyclophilin D in the activation of a mitochondrial pore by Ca2+ and oxidant stress. *Eur J Biochem* 1996. 238(1):166-172.
224. **Piot C, Croisille P, Staat P, Thibault H, Rioufol G, Mewton N, Elbelghiti R, Cung TT, Bonnefoy E, Angoulvant D, et al.** Effect of cyclosporine on reperfusion injury in acute myocardial infarction. *N Engl J Med* 2008. 359(5):473-481.
225. **Li C, Lim SW, Sun BK, Yang CW.** Chronic cyclosporine nephrotoxicity: new insights and preventive strategies. *Yonsei Med J* 2004. 45(6):1004-1016.
226. **Ptak RG, Gallay PA, Jochmans D, Halestrap AP, Ruegg UT, Pallansch LA, Bobardt MD, de Bethune MP, Neyts J, De Clercq E, et al.** Inhibition of human immunodeficiency virus type 1 replication in human cells by Debio-025, a novel cyclophilin binding agent. *Antimicrob Agents Chemother* 2008. 52(4):1302-1317.
227. **Tiepolo T, Angelin A, Palma E, Sabatelli P, Merlini L, Nicolosi L, Finetti F, Braghetta P, Vuagniaux G, Dumont JM, et al.** The cyclophilin inhibitor Debio 025 normalizes mitochondrial function, muscle apoptosis and ultrastructural defects in Col6a1(-/-) myopathic mice. *Br J Pharmacol* 2009. 157(6):1045-1052.
228. **Angelin A, Tiepolo T, Sabatelli P, Grumati P, Bergamin N, Golfieri C, Mattioli E, Gualandi F, Ferlini A, Merlini L, et al.** Mitochondrial dysfunction in the pathogenesis of Ullrich congenital muscular dystrophy and prospective therapy with cyclosporins. *Proc Natl Acad Sci U S A* 2007. 104(3):991-996.
229. **Tiepolo T, Angelin A, Palma E, Sabatelli P, Merlini L, Nicolosi L, Finetti F, Braghetta P, Vuagniaux G, Dumont JM, et al.** The cyclophilin inhibitor Debio 025 normalizes mitochondrial function, muscle apoptosis and ultrastructural defects in Col6a1-/- myopathic mice. *Br J Pharmacol* 2009. 157(6):1045-1052.
230. **Quarato G, D'Aprile A, Gavillet B, Vuagniaux G, Moradpour D, Capitanio N, Piccoli C.** The cyclophilin inhibitor alisporivir prevents hepatitis C virus-mediated mitochondrial dysfunction. *Hepatology* 2012. 55(5):1333-1343.
231. **Liang HL, Sedlic F, Bosnjak Z, Nilakantan V.** SOD1 and MitoTEMPO partially prevent mitochondrial permeability transition pore opening, necrosis, and mitochondrial apoptosis after ATP depletion recovery. *Free Radic Biol Med* 2010. 49(10):1550-1560.
232. **Wang Z, Bao H, Ge Y, Zhuang S, Peng A, Gong R.** Pharmacological targeting of GSK3beta confers protection against podocytopathy and proteinuria by desensitizing mitochondrial permeability transition. *Br J Pharmacol* 2015. 172(3):895-909.
233. **de Zeeuw D, Audhya P, Bakris GL, Chin M, Christ-Schmidt H, Goldsberry A, Houser M, Krauth M, Lambers Heerspink HJ, McMurray JJ, et al.** Bardoxolone methyl in type 2 diabetes and stage 4 chronic kidney disease. *N Engl J Med* 2013. 369(26):2492-2503.
234. **Tan SM, Sharma A, Stefanovic N, Yuen DY, Karagiannis TC, Meyer C, Ward KW, Cooper ME, de Haan JB.** Derivative of bardoxolone methyl, dh404, in an inverse dose-dependent manner lessens diabetes-associated atherosclerosis and improves diabetic kidney disease. *Diabetes* 2014. 63(9):3091-3103.
235. **Trujillo J, Chirino YI, Molina-Jijon E, Anderica-Romero AC, Tapia E, Pedraza-Chaverri J.** Renoprotective effect of the antioxidant curcumin: Recent findings. *Redox Biol* 2013. 1:448-456.
236. **Jiang T, Huang Z, Lin Y, Zhang Z, Fang D, Zhang DD.** The protective role of Nrf2 in streptozotocin-induced diabetic nephropathy. *Diabetes* 2010. 59(4):850-860.
237. **Xu Y, Nie L, Yin YG, Tang JL, Zhou JY, Li DD, Zhou SW.** Resveratrol protects against hyperglycemia-induced oxidative damage to mitochondria by activating SIRT1 in rat mesangial cells. *Toxicol Appl Pharmacol* 2012. 259(3):395-401.
238. **Alhaider AA, Korashy HM, Sayed-Ahmed MM, Mobark M, Kfoury H, Mansour MA.** Metformin attenuates streptozotocin-induced diabetic nephropathy in rats through modulation of oxidative stress genes expression. *Chem Biol Interact* 2011. 192(3):233-242.

239. **Pal PB, Sinha K, Sil PC.** Mangiferin attenuates diabetic nephropathy by inhibiting oxidative stress mediated signaling cascade, TNFalpha related and mitochondrial dependent apoptotic pathways in streptozotocin-induced diabetic rats. *Plos One* 2014. 9(9):e107220.
240. **Sedeek M, Gutsol A, Montezano AC, Burger D, Nguyen Dinh Cat A, Kennedy CR, Burns KD, Cooper ME, Jandeleit-Dahm K, Page P, et al.** Renoprotective effects of a novel Nox1/4 inhibitor in a mouse model of Type 2 diabetes. *Clin Sci (Lond)* 2013. 124(3):191-202.
241. **ten Freyhaus H, Huntgeburth M, Wingler K, Schnitker J, Baumer AT, Vantler M, Bekhite MM, Wartenberg M, Sauer H, Rosenkranz S.** Novel Nox inhibitor VAS2870 attenuates PDGF-dependent smooth muscle cell chemotaxis, but not proliferation. *Cardiovasc Res* 2006. 71(2):331-341.
242. **Lv M, Chen Z, Hu G, Li Q.** Therapeutic strategies of diabetic nephropathy: recent progress and future perspectives. *Drug Discov Today* 2015. 20(3):332-346.

1.5 RATIONALE FOR THIS THESIS

1.5.1 HYPOTHESIS

Mitochondrial dysfunction and cell death are important areas in which to explore potential novel therapeutics to interrupt the progression of chronic kidney disease in diabetes. It is hypothesised that renal cell death mechanisms play an important role in deciding cell fate in the diabetic kidney, and that elucidating these mechanisms will allow a greater understanding of the pathogenesis of DKD. Further, mitochondrial dysfunction may influence which cell death pathways are induced. Finally, the ability to target these cell death pathways may provide new therapeutic targets, to improve mitochondrial function and ultimately kidney function.

1.5.2 AIMS

The primary aim of this thesis is to investigate the role of cell death processes in the development of mitochondrial dysfunction in diabetic kidney disease, by investigating the contribution of mitochondrial pore forming cell death proteins. To address this, the following specific aims are:

- To investigate the development of mitochondrial dysfunction, in the development of diabetes-associated renal injury, using different mouse models of DKD

- To investigate the contribution of the two mitochondrial outer membrane pore forming proteins: Bax and Bak, to the development and progression of DKD

- To investigate the role of the mitochondrial permeability transition pore, via targeting of the key pore opening protein Cyclophilin D, in the development and progression of DKD

Chapter 2

Chapter 2. Materials and Methods

Overview

This thesis aims to explore the role of mitochondrial function in the progression of diabetic kidney disease, by examining the importance of the mitochondrial cell death pathways. To address these research aims, the primary experimental analyses will be performed using rodent models of diabetic kidney disease. Mouse models allow for the preclinical assessment of biochemical processes by controlling for genotype, environmental conditions, etc. and by allowing the controlled induction of disease processes. The ability to generate genetic knock out studies also provides an opportunity to investigate the isolated role of specific proteins within a biological system. Four different mouse models will be used to explore renal mitochondrial function in the context of diabetes. Specific details of each of the four models are explained in detail within each experimental chapter (Chapter 3-5). These models include chemically induced Type 1 diabetes (using streptozotocin), and also a genetic model of Type 2 diabetes (the *db/db* mouse). All four mouse models will begin by exploring the development of diabetes phenotypes by monitoring changes in blood glucose, body weight, organ weights and metabolic changes. The development of diabetes-associated renal injury will be explored by examining changes in renal pathology. Glomerular and tubular markers available in tissue histology, and blood and urine samples will be compared to non-diabetic and treatment relevant control groups. An assessment of mitochondrial health will be performed via functional analyses. Details of the techniques and procedures used to explore these research aims are described below.

2.1 MATERIALS

2.1.1 LIST OF CHEMICALS

Routine chemicals were purchased from the following companies:

Astral Scientific (Tarren Point, NSW, Australia)

TRIS (hydroxymethyl)aminomethane, ultra pure (Cat: BIO3094T); Sodium chloride, ACS grade (Cat:BIOSB0476-5KG); KH_2PO_4 Potassium phosphate monobasic anhydrous, ACS grade (Cat: BIOPB0445)

Amresco (Solon, OH USA)

Sucrose, Ultra pure, RNase & Dnase free, (Cat:0335-5KG); KCl Potassium chloride (Cat: 0395); K_2HPO_4 Potassium phosphate dibasic anhydrous, ACS grade (Cat: 0705-500G); MOPS [3-N-Morpholino)Propane Sulfunic acid], ultra pure grade (Cat: 0670); EDTA Disodium salt dihydrous, biotechnology grade (Cat: 0105);

Sigma-Aldrich (St Louis, MO USA)

$MgCl_2.6H_2O$ Magnesium chloride hexahydrate, BioUltra >99% (Cat: 63068); HEPES, minimum 99.5% (Cat:H3375); D-Mannitol, >98% (M4125); Na_2HPO_4 Sodium Phosphate dibasic, (Cat: 795410); TWEEN® 20 (Cat:1379), Bovine Serum Albumin, heat shock fraction, protease free, pH 7, 98% , for ELISAs (Cat: A3294); EGTA Ethyleneglycol-bis(β-aminoethyl)-N,N,N',N'-tetraacetic Acid (Cat: E8145)

VWR Chemicals (BDH AnalaR) (Aukland, New Zealand)

Calcium chloride (Cat: 10070.4Y);

Specific chemicals used for mitochondrial assays were purchased from Sigma-Aldrich (St Louis, MO, USA):

Bovine serum albumin, fatty-acid free, heat shock fraction 98% pH 7 (Cat: A9647); Cyclosporin A (Cat: 30024); Oligomycin (Cat: 049876); Antimycin-A, FCCP; Rotenone (Cat: R8875); Adenosine 5'-diphosphate sodium salt, ADP (Cat: A2754); Oxaloacetic acid, OAA (Cat: 04126); 5,5'-Dithiobis(2-nitrobenzoic acid), DTNB (Cat: D8130); L-Glutamic acid monosodium salt hydrate (Cat: G1626); L-Malic acid (Cat: 112577); Sodium succinate dibasic hexahydrate (Cat: S2378); Acetyl coenzyme A sodium salt (Cat: A2056);

Jackson ImmunoResearch Inc (West Grove, PA, USA)

Bovine serum albumin, IgG-Free, Protease-Free - for western blotting

2.1.2 ROUTINE BUFFERS

Phosphate buffered saline (PBS)

137 mM NaCl, 12 mM Phosphate, and 2.7 mM KCl, - pH 7.4

TRIS buffered saline (TBS)

50 mM TRIS and 150 mM sodium chloride, - pH 7.2

Mitochondrial isolation buffer (MIB)

70mM Sucrose; 210mM D-Mannitol; 5mM HEPES; 1mM EGTA; 0.5% (w/v) Bovine Serum Albumin (fatty-acid free, 98%) - pH7.2

Mitochondrial assay buffer (MAS)

70mM Sucrose; 220mM D-Mannitol; 10mM KH_2PO4; 5mM $MgCl_2.6H_2O$; 2mM HEPES; 1mM EGTA; 0.2% (w/v) Bovine Serum Albumin (fatty-acid free, 98%) - pH 7.2

Non-energised respiratory buffer (NERB)

210 mM Manitol, 70mM Sucrose, 5mM HEPES in dH_2O - pH 7.5 (with NaOH)

Energised respiratory buffer (ERB)

210 mM Manitol, 70 mM Sucrose, 5 mM HEPES, 5 mM Glutamate, 5 mM Malate, 50mM TRIS in dH_2O - pH 7.5 (with NaOH))

Western blot Transfer buffer

- 200 ml methanol.
- 80 ml Tris-Glycine (x10)
- 720 ml of dH2O

2.1.3 LIST OF EQUIPMENT

Routine equipment used includes:

Neolus Hypodermic needles and syringes (Terumo Pharmaceutical Solutions, Leuven, Belgium)

Oral gavage needles, Disposable AFN 20g x 1.5", 1.9mm Flex PTFE (Cadence Science Inc, Cranston, RI, USA; Cat: 9920)

Homogenisers

10mL Glass/PTFE, Potter-Elvehjem homogeniser (DWK Life Sciences LLC, Millville, NJ, USA)

Polytron PT 2100 homogeniser (Kinematica, Luzern, Switzerland)

Centrifuges

Bench Centrifuge 5415 D (blood spinning, 6000rpm = 3300 rcf) (Eppendorf,, Hamburg Germany)

Bench Centrifuge with cooling 5427 R (Eppendorf, Hamburg, Germany)

Allegra X-12R Centrifuge, with plate spinners (Beckman Coulter, Brea, CA, USA)

Microscopes

FSX-100 Upright, fluorescence microscope (Olympus, Shinjuku, Japan)

BX-43 Upright microscope (Olympus, Shinjuku, Japan)

Eclipse Ci, upright, brightfield microscope (Nikon Instruments Inc, Melville, NY, USA)

Plate readers

EnSpire™ multilabel plate reader (PerkinElmer, Waltham, MA, USA)

FLUOstar ® OMEGA (BMG Labtech, Mornington, VIC, Australia)

SPECTROstar ® OMEGA (BMG Labtech, Mornington, VIC, Australia)

Specialised equipment

XFe 96-well Seahorse Bioanalyzer (Agilent, Santa Clara, CA, USA)

EchoMRI (EchoMRI™, Houston, TX, USA).

Comprehensive laboratory animal monitoring system (CLAMS) (Columbus Instruments, Columbus, Ohio, USA)

2.2 ANIMAL STUDIES AND CULL PROCEDURES

2.2.1 ETHICS APPROVAL AND ANIMAL HOUSING

All animals used in this study were approved for use by the Alfred Medial, Research and Education Precinct (AMREP) animal ethics committee, and the National Health and Medical Research Council of Australia. All procedures were performed according the ethical guidelines outlined in the Australian code of conduct for ethical research involving animals. All mice were bred in-house from colony stock. Mice allocated to the studies, under the appropriate ethics applications, were housed at the AMREP animal precinct, at an ambient temperature of 22°C, with a 12hr light/dark cycle. Mice were fed standard rodent chow (Specialty Feeds, Perth, WA, Australia) ad libetum, with access to fresh drinking water. Measurements of body weight, and blood glucose testing from tail vein samples, were taken weekly for the duration of each study. All mice were checked daily for signs of distress and illness. Any mouse identified as unwell received supportive care, and if deemed necessary, were culled before endpoint in accordance with ethical procedures. At endpoint, mice were anaesthetised with a lethal overdose of pentobarbitone (Euthatal; sigma-Aldrich, Castle Hill, Australia) or KXA (ketamine 80 kg/mg, xylazine 30 mg/kg and atropine 1.2 mg/kg,), administered by intra-peritoneal injection. Once unresponsiveness was confirmed, cardiac puncture and exsanguination was performed. Organs were then collected, weighed, and processed depending on the needs of each study. A range of mouse models, mouse strains and techniques were performed for each study. Further details pertaining to each section of these studies are available with the additional methods sections in chapters 3, 4 and 5.

2.2.2 GENOTYPING

All genotyping was contracted to the services of TransnetYX (Memphis, TN, USA). At 3-4 weeks of age, all mouse pups had a small section of the tail dissected, and sent for genotyping by PCR using customised, validated primers for each gene.

2.2.3 STZ INDUCED DIABETES

Three strains of mice were selected for the study of Type 1 diabetes in this thesis. The *FVB/N* M298 mice from the Alfred Precinct Animal Centre breeding colony for chapter 3; a mixed

background model with a specific genetic double knock out described in detail in chapter 4, section 4.1.3; and C57BL/6 mice purchased from the Jackson Laboratory in chapter 5. To induce insulin deficient diabetes, mice of 6-7 weeks of age were treated with a 55mg/kg per day dose of Streptozotocin (Sigma-Aldrich, St Louis, MO, USA), in 0.05M sodium citrate pH 4.5, or vehicle control, by intra-peritoneal injection, for five consecutive days. STZ is selectively toxic to pancreatic β-cells, and results in insulin deficient diabetes with insulitis when administered by this low dose routine (248,249). Plasma glucose concentrations were then determined weekly to confirm diabetes development and mice that did not meet these criteria were excluded from the study (>15 mmol/l glucose, observed in >98% of mice). None of the animals with diabetes required supplemental insulin to maintain body weight or to prevent ketosis. Any mouse which did lose more than 10% of its body weight was culled early according to ethical guidelines. All studies used male mouse pups only. Male mice have better survival following the use of STZ toxin to induce insulin deficient diabetes. Further, male mice develop more robust hyperglycaemia and more pronounced diabetes- associated renal injury(250).

STRAIN SELECTION FOR STZ STUDIES

All mouse strains used required suitable susceptibility to the development of prolonged, sustained hyperglycaemia following the above STZ treatment protocol. Specific mouse strains for treatment with STZ were selected based on key characteristics required within each study and the requirement for the development of DKD associated pathology. The AMDCC guidelines for mouse models of diabetic nephropathy stipulate a range of pathological features which should ideally be present within an animal model of DKD. This includes (1) 50% reduction in GFR, (2) 10 fold increase in albuminuria; and (3) pathology of kidneys, i.e. mesangial expansion, hyalinosis, glomerular basement membrane thickening and tubular fibrosis (251). However, no mouse model available to date can effectively capture all of these features.

In chapter 3, FVB/N mice are known to be susceptible to STZ treatment and demonstrate: haemodynamic changes associated with prolonged hyperglycaemia, elevated GFR, marked polyuria and demonstrated tubular pathology (122,250). Although they have been reported to have minimal glomerular damage, this study is concerned with the changes in mitochondrial function within the tubules. Chapter 4 involves the investigation of a novel mouse strain, and so renal outcomes were not known prior to commencement; however, the background strains 129/S and DBA and C57BL/6 type

mice all experience some degree of renal injury as per the AMDCC criteria (122,250,251). In chapter 5, the C57BL/6 background strain was selected primarily due to the availability of the specific genetic knockout model for purchase through the Jackson Laboratory.

2.2.4 ORGAN MEASUREMENTS

Kidneys were rapidly dissected, de-capsulated, and then weighed immediately following confirmation of death. No perfusion procedures were performed. The right kidney was bisected, with one-half sections fixed in 10% (v/v) neutral buffered formalin for the purpose of paraffin embedding. The remaining half was used to collect renal cortical tissue and were snap-frozen in liquid nitrogen, and stored at -80°C. Whole hearts were excised and rinsed of blood in sodium chloride solution (0.9% solution, Baxter International Inc, Deerfield, IL, USA). All pericardial fat and major vessels removed for total heart weight. Left ventricles were then dissected with removal of auricles, atria and right ventricle with fine sharp-point scissors. The whole liver was excised and weighed.

2.3 DIABETES ANALYSIS

2.3.1 METABOLIC CAGING

To routinely assess renal function, 24hr urine was collected from each mouse using a specially designed cage system denoted as a 'metabolic cage' (Iffa Credo, L'Arbresele, France). Water and food intake were also measured across the 24hr period. Mice were singly housed in metabolic cages for 24 hours at designated time points for each study. Generally, baseline (Week 0), Midpoint, and Endpoint (1 week before cull). Urine samples, collected at the end of the 24hr period, were stored at -80°C for subsequent analysis. Additionally, 100µL of whole blood from the submandibular vein was collected into at the conclusion of the caging period. Blood was collected with a 25G needle (Terimo Pharmaceutical Solutions, Leuven, Belgium).

2.3.2 WEEKLY BLOOD GLUCOSE MONITORING

All mice allocated to each study were assessed for blood glucose levels once for each consecutive week of study. Blood glucose was measured using a glucometer (Accutrend;

Boehringer Manheim Biochemica, Manheim, Germany) with disposable test strip (Accu-Chek® Performa, Roche Diagnostics, Forrenstrasse, Switzerland; Cat. No. 06454038).

2.3.3 PLASMA ASSESSMENT

Sodium citrate treated whole blood was centrifuged at 3300rcf for 6 minutes in a 5415 D Eppendorf centrifuge. Plasma was separated and stored at -80°C for subsequent analysis.

2.3.4 PLASMA GLUCOSE

Glucose concentrations were assayed using a glucose colorimetric assay kit (Cayman, Ann Arbor, MI, USA; Cat. 10009582) on non-fasted plasma samples and performed according to the manufacturer's instructions, and using kit supplied 96-well plates. Reagents provided by the kit (Sodium buffered saline, pH 7.2) were diluted in molecular grade water.

Plasma samples were diluted 1:50 with the supplied reagent diluent as indicated from previous optimisation steps. Samples were then incubated for 10 minutes at room temp, before being assayed for absorbance at 500nm in a SPECTROStar nano plate reader (BMG Labtech, Mornington, VIC, Australia). Linear regression of blank corrected data, interpolated from the standard curve was performed using MARS Data Analysis Software (BMG Labtech, Mornington, VIC, Australia).

2.3.5 GLYCATED HAEMOGLOBIN

An assessment of glycated haemoglobin (HbA_{1C}) was performed once, at the end of the study to assess long-term glycaemic control. Glycated haemoglobin (GHb) was determined by turbidimetric inhibition immunoassay using a Cobas b 101 POC system (Roche Diagnostics, Basel, Switzerland) in lysates of erythrocytes separated from whole blood. Assay detection range is limited to between 4 and 14% HbA_{1C} with values outside this range designated as HIGH (>14%) or LOW (<4%). For HbA_{1C} reference ranges for mouse strains used in the following studies see **Appendix 2.2.**

ASSESSMENT OF RENAL FUNCTION

2.3.1 PROTEIN CONCENTRATION DETERMINATION

Protein concentration in all protocols was determined using the Bicinchoninic acid method (Pierce-Thermo Fisher Scientific, Melbourne, Australia). This includes all protein samples derived from whole tissue homogenates, mitochondrial isolation preparations and assay buffers used for background corrections, etc. Protein homogenates were diluted, as required, in dH_2O. All samples were assayed in duplicate. Standards were prepared according to the kit instructions, and samples interpolated from blank corrected absorbance at 560nm. Additionally, values were corrected for background protein concentration of buffers used where appropriate. (e.g Bovine serum albumin in isolated mitochondrial preparations).

2.3.2 CYSTATIN C ELISA

Plasma cystatin C was measured using a commercially available ELISA kit (Duoset anti-mouse Cystatin C - R&D Systems Inc., Minneapolis MN, USA), according to the manufacturer's instructions. Plasma samples collected from metabolic caging blood samples were diluted 1:1200 in reagent diluent (PBS + 1% BSA, 99% quality). Samples and standards were incubated in 96-well clear NUNC maxisorp plates that were pre-coated overnight at room temperature with capture antibody. Samples were washed off with PBS + 0.05% Tween x3 then incubated with capture antibody for 1 hr and washed again x3. HRP was added and incubated for 1 hr, then washed x3 followed by chromogen development with TMB for 30 minutes. Reactions were stopped with 1M H_2SO_4 and absorbance was read at 420nm in a spectrophotometer. Blank corrected values were interpolated from the standard curve.

2.3.3 URINARY ALBUMIN ELISA

The 24hr urinary albumin excretion was determined using a mouse-specific sandwich ELISA (Bethyl Laboratories, Montgomery, TX, USA) according to the manufacturer's instructions. Briefly, urine samples collected during metabolic caging were diluted 1:1000 in the provided reaction buffer, as optimised. Dilute urine samples were incubated in duplicate in 96-well Nunc maxisorp plates, pre-coated with capture antibody, for 1hr at room temperature. Plates were washed x3 with PBS+0.5% Tween, then incubated with the detection antibody (1 hr at room temperature), washed again, and followed with HRP for a further 1 hr. Colour was developed with TMB chromogen for 30

minutes, and the reaction was stopped with 1M H_2SO_4. Absorbance was read at 420nm and blank corrected to the 0µL, and interpolated from the standard curve. Values were then corrected to 24 hr urine volume.

2.3.4 CREATININE

Creatinine clearance was assessed with a commercially available kit for the Cobas Integra 400 Plus computerised analyser (Roche diagnostics, Basel, Switzerland). Plasma and urine samples collected at the endpoint metabolic caging were prepared into specialised Cobas cups (Roche diagnostics, Basel, Switzerland) with the use of the Creatinine Plus 2 reagent cassette (for Cobas Intergra 400 Plus, Roche diagnostics, Cat: 03263991190)

2.3.5 KIM-1

Urinary content of Kidney Injury Molecule (KIM)-1 was measured using a commercially available sandwich ELISA (USCN Life Sciences, Wuhan, China) according to the kit protocol. Briefly, urine samples collected during metabolic caging were diluted in the provided reaction buffer, according to a pre-optimised dilution value, and incubated in duplicate in 96-well Nunc maxisorp plates, pre-coated with capture antibody, for 2hrs at room temperature. Plates were washed x3 with PBS+0.5% Tween, then incubated with the detection antibody (1hr at room temperature), washed again, and followed with HRP for a further 1hr. Colour was developed with TMB chromogen for 30 minutes, and the reaction was stopped with 1M H_2SO_4. Absorbance was read at 420nm and blank corrected to the 0µL Kim-1 standard control. Results were then corrected to 24hr total urine volume.

2.4 HISTOLOGICAL ASSESSMENT OF RENAL INJURY

Kidney samples used for histological analysis were fixed in 10% Neutral buffered formalin and were embedded in paraffin by the external services of Gribble Veterinary Pathology (Melbourne, VIC, Australia). Parafin blocks were sectioned onto silanated glass specimen slides using a rotary microtome (Leica, Wetzlar, Germany), and baked at 37°C for 48hrs. Slides were dewaxed by processing through baths of Xylene (x2), absolute ethanol (x3), and running water, for 3 minutes each step, and finally brought into distilled water. (Note: slides were stored in TBS overnight if required).

2.4.1 PERIODIC ACID SCHIFF STAINING

Sections of 3µm renal tissue were dewaxed as above. Briefly, slides were stained in Schiffs reagent (8%w/v pararosaniline acetate in 1M HCl with 1% w/v sodium metabisulphite) for 20 minutes, washed in running water for 15 minutes, then briefly (~30 secs) counterstained with Mayer's Haematoxilin and washed again in running water. Blueing in Scott's Tap water was performed before final rinsing, and dehydration through graded ethanol (95% EtOH x3, absolute EtOH x 2) and Xylene (x2). Slides were mounted with DPX medium (Sigma-Aldrich, Cat: 06522).

GLOMERULOSCLEROSIS INDEX

Glomerulosclerosis index (GSI) was assessed in 3 µm paraffin embedded periodic acid Schiff (PAS) stained sections by a semi-quantitative method using the following weighted formula, as previously described (252).

$$GSI = \frac{(N_1 \times 1) + (N_2 \times 2) + (N_3 \times 3) + (N_4 \times 4)}{\text{Total number of glomeruli}}$$

Twenty glomeruli from each mouse were scored based on the following classification of sclerosis severity and PAS intensity: (**1**): <25%; (**2**): >25%, to <50%; (**3**): >50% to <75%; (**4**): <75%. Images were taken at x400 magnification using the BX-43 microscope (Olympus, Shinjuku, Japan) for the *db/db* mouse study in Chapter 5, study 2; or the Eclipse Ci brightfield (Nikon Instruments Inc, Melville, NY, USA) for all other studies.

TUBULAR DAMAGE SCORING

Areas of renal cortex at x200 magnification were scored in PAS stained images for tubular dilation. The following scale was used to categorise each image: 0=normal (<10%), 1=minimal (10–25%), 2=mild (25–50%), 3=moderate (45–75%), 4: severe (>75%). Data were then averaged across all ~20 images at 200x magnification per mouse. Tubular casts were also scored for each mouse and averaged per field.

GLYCOGEN SCORING

Glycogen content of PAS stained renal cortex was assessed by manual quantitation of renal tubular cells with glycogen inclusions. Glycogen is evident as intense fuchsia staining bodies. Number of whole tubules with predominant intra-cellular glycogen inclusions were scored per field for 20 images at 200x magnification. Additionally, the number of nuclei with glycogen inclusions were also scored and averaged per field within the same set of PAS staining images.

2.4.2 COLLAGEN IV IMMUNOSTAINING

Sections of 10% Neutral buffered formalin fixed renal cortex, embedded in paraffin wax, were cut to 4 µm, and processed as above. Tissue sections were then digested with pepsin (porcine gastric mucosa P 6887, Sigma-Aldrich, St Louis, MO, USA), washed in TBS and blocked in 0.5% skim milk powder, and incubated with goat polyclonal collagen IV antibody (Southern Biotech, Birmingham, AL, USA) (253) diluted in normal horse serum. Vector Avidin/Biotin (Maravai LifeSciences; SP - 2001) blocking was then performed followed by incubation with Vector Biot Horse anti-goat 1/500 secondary antibodies (Maravai LifeSciences; BA – 9500) and Vector ABC reagent (Maravai LifeSciences; Cat: PK – 6100 Elite). Slides were developed with DAB (Sigma-Aldrich, St Louis, MO USA; Cat: D5905) and then counter stained with Haematoxylin and blued in Scotts tap water. Finally, slides were and mounted with DPX (Sigma-Aldrich, St Louis, MO, USA; Cat: 06522). A minimum of 20 glomeruli were imaged using a Nikon Eclipse Ci Brightfield microscope at x400 magnification. ImageJ software was then used to quantitate % glomerular collagen IV deposition using the following protocol:

1.Open image

2. Set colour threshold to area of staining. Toggle controls to get “orange/red” colour region only for brown staining. Grab the highest saturation points and high brightness to enable selection coverage of staining only eg:

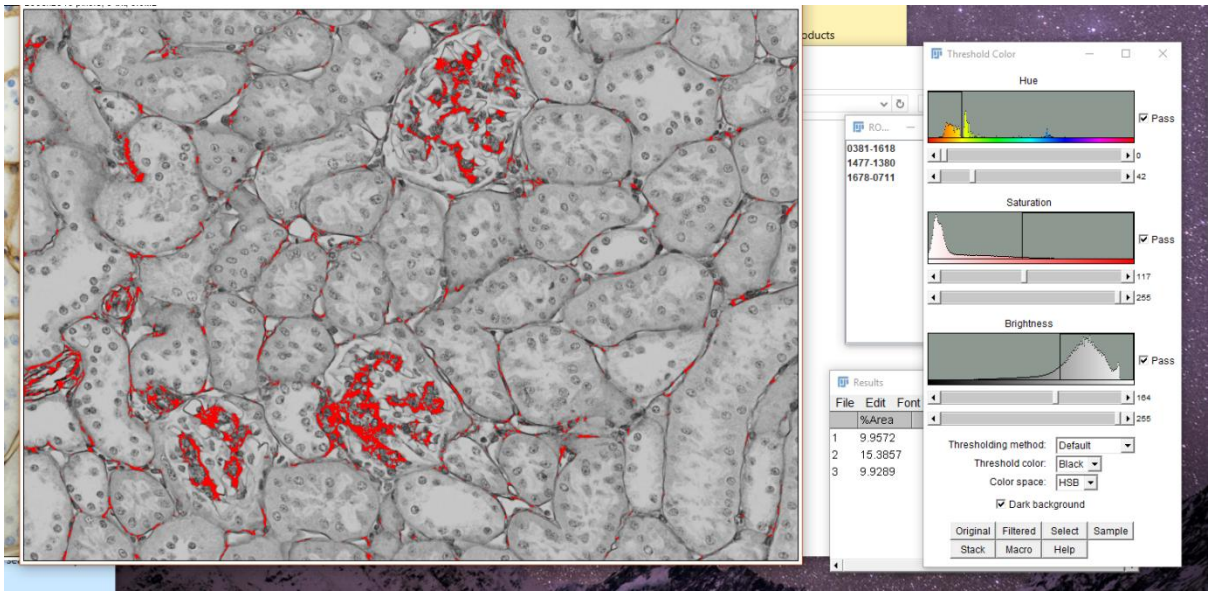

Make threshold colour is set to black.

3. Convert image to 8bit

4. Set threshold. Set each bar to zero so only selection region is highlighted.

5. Set measurements. Area Fraction only, and limit to threshold

6. Circle each glom and add to ROI manager. Then measure. Measurements give % area of gloms which are positive for staining.

Mean and Standard deviation for each treatment group was then calculated.

2.4.3 TUNEL STAIN

One method for detecting cells undergoing apoptosis in vivo utilises a fluorometric labelling system to detect fragmented Nuclear DNA known as "TdT-mediated d-UTP Nick-Ended Labelling" or TUNEL. A "DeadEndTM Fluorometric TUNEL System" staining kit (Promega, Maddison, WI, USA; Cat: G3250) was used to assess the number of apoptotic cells in 10% NBF fixed paraffin sections. Sections of mouse kidney (dissected in the coronal plane) were freshly cut at 4µm with a rotary microtome (Leica, Wetzlar, Germany) and prepared according to the manufacturer's instructions. Slides were fixed in 4% paraformaldehyde and then permeabilised with 0.2% Triton X-100. Wash steps were completed using PBS as prepared in section 2.1.2. A positive control sample was prepared at this step by digesting a section from a non-diabetic mouse with DNAse 1 (Thermo Fisher Scientific; Cat: EN0521), and processed in separate equipment to prevent cross contamination. Slides were then incubated with rTdT buffer with mixed nucleotides as per the kit instructions using supplied reagents for 1hr at 37°C before terminating the reaction. A negative control sample was prepared with a second section of kidney (from the same mouse as the positive control) by skipping this step. Nuclei were then counter stained with DAPI (Sigma Aldrich, St Louis, MO, USA; Cat: D9542) and slides were mounted with VECTASHIELD® anti-fade (Maravai Lifesciences, San Diego, CA, USA ; Cat: H-1000). All slides were prepared together on the same day, and imaged consecutively on the following day using an FSX100 inverted fluorescent microscope (Olympus Australia Pty Ltd, Notting Hill, VIC, Australia). To ensure fast acquisition of all slides, 3x3 stitched images (x170 magnification) were acquired using the automatic acquisition function, giving an area of 1.512 x 1.147 mm, per image, for analysis. Three areas of renal cortex were imaged per slide using the "next field" option available in the software package to reduce operator bias between imaged areas. Fluorescent positive cells were then counted 'per slide' and totals averaged for each treatment group.

2.4.4 BLINDING OF SAMPLES

In order to reduce bias in image scoring, all animals were allocated a unique identifier number (UIN) that did not contain any information about group or treatment. All samples were imaged in random order and scored according to this UIN. Upon completion of data collection, samples were unblinded (en mass) in a spreadsheet, and separated from the UIN. Data were then automatically sorted into treatment groups and extracted to a new spreadsheet for final data analysis. In this manner UIN and information about each animal was kept separate.

2.5 GENE EXPRESSION ANALYSIS

2.5.1 RNA EXTRACTION

RNA was isolated from ~10mg kidney cortex (20-30mg) using 1mL TRIzol Reagent (Life Technologies, Gran Island, NY USA). Samples were homogenized with a 1:1 mix of 1mm and 2mm zirconium oxide beads in a "Bullet Blender" (Next Advance, Averill Park, NY USA). Samples were centrifuged at 13,000 RCF using 1:49 Chloroform:isoamyl alcohol to separate the aqueous phase, which was then precipitated over night at -20°C in isopropanol. RNA was then washed in absolute ethanol and suspended in RNAse free water. RNA concentration was determined with a QIAxpert UV/VIS spectrophotometer (Qiagen, Hilden, Germany).

2.5.2 cDNA SYNTHESIS

Contaminating DNA was removed after treatment with DNA-free DNAse according to the manufacturer's specifications (Ambion Inc, Austin, USA). DNA-free RNA was reverse transcribed into cDNA using the Superscript First Strand Synthesis System according to the manufacturer's specifications (Life Technologies BRL, Grand Island, NY). The following reagents were used:

Deoxyribonuclease (DNAse) (Thermo Fisher Scientific; Cat: 2238G) in DNAse buffer (Thermo Fisher Scientific; Cat: 8167G).

DNAse inactivation reagent (Thermo Fisher Scientific; Cat: 8174G).

First-strand buffer (Thermo Fisher Scientific; Cat: Y02321)

dNTP (Thermo Fisher Scientific; dATP R0142, dCTP R0152, dGTP R0162, dTTP R0172)

DTT (Invitrogen; Cat: Y00147); RNase inhibitor (20 U/µL New england biolabs, Ipswich, MA, USA; Cat: M0314L), M-MuLV reverse transcriptase (200U/µL, Thermo Fisher Scientific; Cat: 28025-021).

2.5.3 RTqPCR PROCEDURE

Real-time PCR was performed using SYBR green PCR mix (Applied Biosystems, primer concentration of 500 nM) or Taqman PCR kit (18S rRNA TaqMan Control Reagent kit, ABI Prism 7500; Perkin-Elmer) using a 7500 Fast Real-time PCR System (Applied Biosystem, VIC, Australia), and normalized relative to 18S ribosomal RNA. Reactions were completed in a volume of 6µL of primer/probe mix, with 1µL of cDNA, per well in a MicroAmp™ Optical 384-Well Reaction Plate

(Thermo Fisher Scientific, Waltham, MA, USA; Cat: 4309849) and performed using the QuantStudio 5 Real-Time PCR system (Thermo Fisher Scientific, Waltham, MA, USA). After an initial denaturation step at 95°C for 20 seconds, 50 thermo-cycles of denaturation (95°C, 1 second), annealing and extension (60°C, 20 seconds) were performed All values are presented as fold change normalised to endogenous 18S rRNA, and fold-change relative to biological control groups using the $2^{-\Delta\Delta Ct}$ method.

2.5.4 PRIMER LIST

For a list of primers used within this thesis, see Appendix 2.1.

2.6 MITOCHONDRIAL ANALYSIS

2.6.1 MITOCHONDRIAL ISOLATION

Freshly collected kidney cortex was minced on ice and placed into 1mL of ice-cold Mitochondrial Isolation Buffer (MIB, see above) followed by 6-8 careful piston plunges in a Potter-Elvehjem homogenizer in an ice-bath. Lysate was then collected and any remaining tissue homogenised with an additional 1mL MIB for 2-3 more plunges. The supernatant underwent differential centrifugation at 4°C. Briefly, ~2mL total supernatant was centrifuged for 5 minutes at 800g. Supernatant was then centrifuged at 8000g x10 minutes. Mitochondrial pellet was washed in 500µL MIB and centrifuged again at 8000g x10mins. Final pellet was resuspended in 115µL MIB and stored on ice. Total protein was determined by the Bicinchoninic acid method (Pierce-Thermo Fisher Scientific, Melbourne, Australia). Samples were left to stand for 30 minutes on ice before use. Prior to aliquoting for each experimental assay, samples were resuspended by gently flicking and tapping the tubes. All experimental protocols were performed within 6 hrs of isolation.

2.6.2 SEAHORSE BIOANALYZER

Mitochondria were resuspended in Mitochondrial Assay Buffer (MAS, see above) at the required dilutions, and 25µL of mitochondrial suspension were loaded per well into a XFe96well Seahorse Bioanalyzer plate (Seahorse Bioscience, Agilent, Santa Clara, CA, USA). A minimum of 5 replicate wells per mouse were prepared. Plates were gently rocked 2-3 times, to evenly disperse mitochondria, before centrifugation at 2000*g* for 20 minutes at 4°C. Pre-warmed (37°C) substrates in MAS buffer were then added to each well to bring the total volume to 200uL. For complex I respiration 10µg of mitochondria was loaded per well to a final concentration of 10mM Glutamate and

10mM Malate. For complex II 10mM succinate with 5µM rotenone. Plates were then immediately loaded into the XFe96 Seahorse machine. Basal respiration with substrates was measured twice for 3 minutes each, followed by subsequent injections the following compounds to a final concentration of: A) 0.5mM ADP (State 3o), B) 2.5µg/uL Oligomycin (State 4), C) 1µM FCCP (State 3u), and D) 4µM Antimycin-A. Each injection was allowed to mix for 30 seconds, before reading dynamic OCR for 3 minutes (Basal, Oligomycin, FCCP, Anti-A) or 5 minutes (ADP) (***Figure 2.1***).

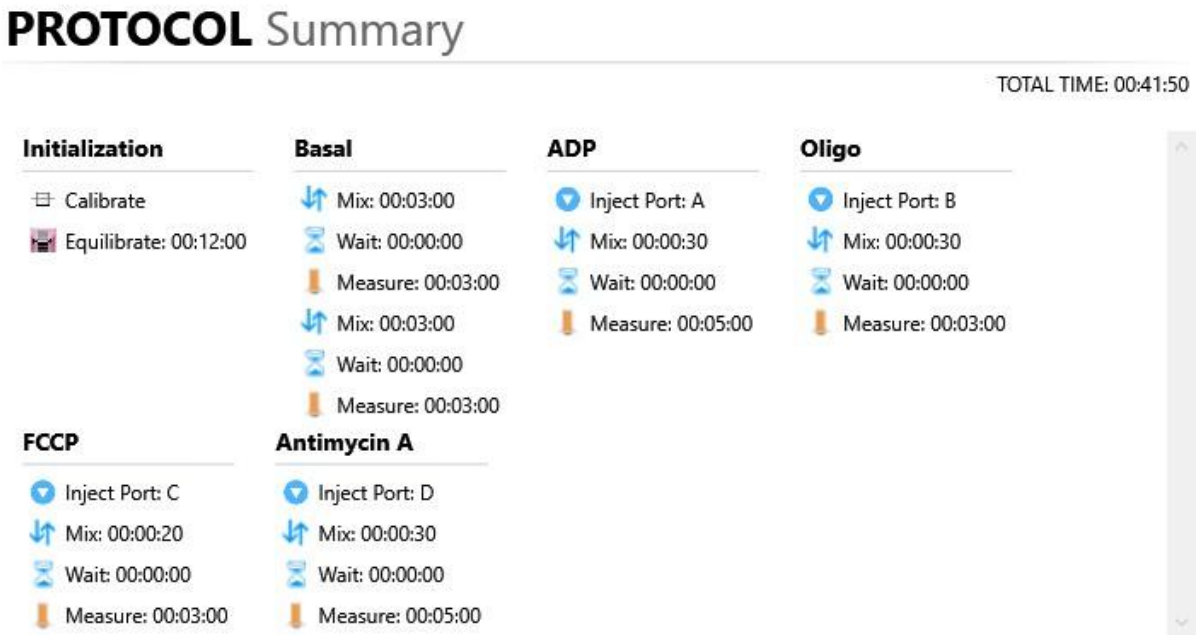

Figure 2.1 Seahorse Bioanalyzer protocol for the mitochondrial stress test.

Data were analysed per individual mouse with each injection point assessed for successful response via pre-defined criteria. Injection measurements were excluded where oxygen consumption was reduced to 0 pmoles/min, or where the compounds did not perform as expected for that individual replicate (e.g., no response to Oligomycin). The average value of remaining replicates was used. Individual animals were excluded where ADP injection did not increase OCR. Values for each reading were then used to calculate the following information: ATP production (ADP minus oligomycin OCR); Respiratory control ratio (ADP max OCR to Oligomycin ratio); Proton leak (Oligomycin minus Antimycin A). All values for OCR were compared as raw data, and as baseline corrected values (% change from basal OCR).

2.6.3 MITOCHONDRIAL SWELLING BY CALCIUM CHALLENGE

Mitochondrial swelling was assessed by measuring the change in absorbance of 540nm light scattering through diluted isolated mitochondria. Mitochondrial concentration was first determined using the BCA method above (section 2.4.1). 100µg of mitochondria in 110µL Energised Respiratory Buffer, was aliquoted per well into a 96-well plate (Sarstedt, Nümbrecht, Germany; Cat: 82.1581.210). After background absorbance was measured, 10µL of 10µM CsA or NERB (buffer control) was added to 2 replicates per sample, and incubated for 5 minutes. Immediately before loading the plate into the plate reader, 5µL of 500mM Calcium plus K_2HPO_4, or ERB, was added to begin the calcium challenge. Change in absorbance was followed for 30 minutes at 540nm with a reading every 1 minute, with short shaking cycle prior to each read, using the EnSpire plate reader (Perkin Elmer, Waltham, MA, USA). Data were averaged between the two technical replicates and then corrected to initial absorbance in order to determine the change in absorbance at 540nm. Individual results per mouse were then used to calculate the average curve for each group.

2.6.4 AMPLEX RED H_2O_2

Hydrogen peroxide (HRP) production in renal cortical mitochondrial preparations was measured by fluorescence using the Amplex® Red reagent (10-acetyl-3,7-dihydroxyphenoxazine) (Molecular Probes - Invitrogen, Carlsbad CA, USA). Briefly, isolated mitochondria were diluted 1:200 and assayed in Krebs Ringer Phosphate Glucose buffer (145mM NaCl, 4.86mM KCl, 0.54mM $CaCl_2$, 1.22mM $MgSO_4$, 5.5mM glucose, 5.7mM sodium phosphate - pH 7.35). A standard curve of H_2O_2 reaction was prepared in the reaction buffer ranging from 0 to 10µM. 50µL of samples or standards were loaded into individual wells, in duplicate, in a black 96-well plate. 50µL of Amplex red/HRP solution was then added and the reaction was incubated for 30 minutes in the dark, before reading the blank-corrected fluorescence at 590nm, with optical correction at 530nm. Optical gain was corrected to the highest standard for every individual plate, as recommended in the manufacturer's protocol. In addition to the standard protocol, hydrogen peroxide production was also assessed in the presence of: 10mM glutamate and 10mM malate for complex I; and 10mM succinate for complex II, with 5µM rotenone (a complex I inhibitor). Results were then normalised to the no substrates group to determine effects of complex I and II stimulation. Results were then corrected to total mitochondrial protein concentration for each sample.

2.6.5 CITRATE SYNTHASE

To determine the quality of mitochondrial preparations and as a measure of mitochondrial function, Citrate Synthase activity was measured using the following protocol as adapted from Srere et al 1968 (254).

Frozen samples of isolated mitochondria were lysed by x3 freezer/thaw cycles on dry ice. 5µL mitochondrial preparation was diluted 1:20 into to 95µL of cold TRIS buffer (100mM TRIS, pH 8.3). 10µL of dilute mitochondria was added in duplicate to a clear 96 well plate (NUNC Maxisorp, Thermo Scientific, Waltham, MA, USA). 225µL of reaction buffer (100mM TRIS buffer, 1mM DTNB, 3mM Acetyl CoA, 10% Triton X) was aliquoted per well and absorbance followed for 5 minutes at 412nm to obtain background enzymatic reaction. 20µL of 7.5mM Oxaolacetate (OAA) was then added per well and change in absorbance measured over 10 minutes to obtain citrate synthase activity. The linear portion of each reaction curve was then estimated for the same time duration across all wells using Graphpad Prism V. 8.0. Any R^2 value below 0.97 was excluded. Background calculated slope was subtracted from OAA stimulated reaction slope. The formula was then used to calculate Citrate Synthase activity per well. Average of duplicates was calculated and used to normalise data.

$$\text{CsA } (\mu\text{M/ml/min}) = \frac{(\Delta_{412})/\text{min} \times V(\text{ml}) \times \text{dil}}{\varepsilon^{mM} \times L(\text{cm}) \times V_{enz}(\text{ml})}$$

Δ_{412} **–** change in absorbance

dil - the dilution factor of the original sample

V(ml) – the reaction volume:

· for assay in 96-well plate = 0.255 ml

$\mathbf{V_{enz}}$ (ml) – the volume of the enzyme sample in ml

$\boldsymbol{\varepsilon^{mM}}$ (mM^{-1} cm^{-1}) – the extinction coefficient of DTNB at 412 nm is 13.6.

L(cm) – path length

2.7 STATISTICS

All statistical computations were performed using GraphPad Prism version 7.0 (GraphPad Software, San Diego, California, USA). Values of experimental groups are given as mean, with error bars showing SD, unless otherwise stated. Outliers were only excluded where a valid biological or technical issue indicated exclusion. Two-way ANOVA was performed with unweighted means for each variable. Normal distribution was confirmed by Shapiro-Wilk normality test. Where data did not follow a normal distribution data were log transformed using Log(y), and tested again. Bonferroni post-hoc test was used to determine statistical significance and correct for multiple comparisons between each factor. Bonferroni post hoc test comparing simple effects to compare differences was used where F-test results for a specific factor are found to be significant ($P<0.05$).. Differences were considered to be statistically significant where alpha was less than 0.05. Additionally, significance in graphs is indicated as: Diabetic versus non-diabetic: *$P<0.05$, **$P<0.01$,***$P<0.001$, ****$P<0.0001$; Intervention versus non-intervention: † $P<0.05$. Where required a Two-way ANOVA with repeated measures was performed on data representing different time points with § $P<0.05$

Chapter 3

Chapter 3. Mitochondrial dysfunction in the early progression of a Murine model of STZ induced diabetes

3.1 OUTLINE

This study aims to evaluate the progression of mitochondrial function in the context of diabetic renal injury in STZ treated mice. A time-course progression was established using cohorts of mice culled at 4, 8, 12 and 16 weeks post STZ treatment. The renal phenotypes of these diabetic mice were evaluated through routine analyses (metabolic caging, urinary albumin excretion, creatinine clearance, ACR, plasma cystatin C, glomerulosclerosis index, urinary Kim-1). Additionally, a brief assessment of tubular injury was performed along with an analysis of apoptotic nuclei via TUNEL fluorometric analysis of renal tissue. Mitochondrial function was assessed in freshly isolated mitochondrial samples extracted from the renal cortex of each mouse (Seahorse BioScience 'mitostress test', mitochondrial swelling assay). Finally, some gene expression studies (RTqPCR) were performed to evaluate changes in mitochondrial dynamics and cell death pathways.

3.2 INTRODUCTION

Diabetic kidney injury is one of the microvascular complications associated with chronic hyperglycaemia. Within the diabetic milieu other pathophysiological changes also contribute to the onset of renal injury, including changes to insulin signalling, blood pressure, and also immunological changes (255–257). It remains unclear as to why some diabetic patients will progress more rapidly towards renal decline than others. Unknown biochemical and metabolic processes may play key roles in disease susceptibility, thereby emphasising the importance of exploring new pathways for therapeutic strategies. It is hypothesised that early interventions may play a key role in maintaining glomerular function and decreasing morbidity associated with renal disease (258,259). This is pertinent with the projected increase in diagnoses of diabetes worldwide, and the requirement for new, effective therapies that can preserve renal function (260–262). Many pre-diabetic patients already show signs of early nephropathy (microalbuminuria), indicating that the kidney is susceptible to damage even before people have been diagnosed with diabetes (46,73). For patients with Type 1 diabetes, who will live with the disease for decades, preventing the onset of albuminuria is a desirable clinical target. To advance this area of medical research we require a detailed understanding of the

basic processes underlying normal renal physiology and biochemistry, and the changes that occur in the pathogenesis of diabetic kidney disease (DKD).

Mitochondrial dysfunction is a frequent pathological observation in the development of overt nephropathy (263,264). It is still unclear whether these changes underlie the aetiology or if they are sequelae to the diabetic milieu; however, an underlying genetic susceptibility involving mitochondrial genes confers increased risk of nephropathy (265,266). Mitochondrial dysfunction has been observed in multiple rodent models of DKD at different time points along the trajectory of disease development (267–269). Changes in mitochondrial substrate utilisation under diabetic conditions, including lipid oxidation, are associated with elevated ROS production (180,270–272). Additionally, ATP production is dependent on mitochondrial membrane potential, and Complex V of the Electron Transport System can consume ATP through reverse electron transport where a negative proton motive force develops across the inner mitochondrial membrane (273). This makes cell types with high metabolic activity, such as renal proximal tubule cells, vulnerable as a rapid decline in ATP levels may lead to apoptosis (274). Thus, it is important to monitor mitochondrial health as any changes may also affect the progression of renal injury.

To gain an understanding of the changes in mitochondrial function which occur with chronic DKD an observational time-course study was undertaken. Here, the use of 4 week time intervals following the induction of insulin deficient (Type 1) diabetes, using Streptozotocin (STZ), in *FVB/N* mice were used to observe early mitochondrial changes in the development of DKD. This time-course model was selected to assist in determining whether the co-incident mitochondrial dysfunction previously observed in DKD progression has a temporal association with the onset of the disease.

It is important to understand the dynamics of mitochondrial functional changes in early diabetes in order to evaluate the impact of intervention studies on mitochondrial parameters.

3.3 RATIONALE

3.3.1 HYPOTHESIS

That changes in mitochondrial function will be evident in the early progression of diabetic kidney disease, and represent a key driver of the metabolic changes associated with DKD pathology.

3.3.2 AIMS

- To assess mitochondrial functional changes in the early progression of DKD

and

- To briefly examine the status of cell death proteins in DKD

3.4 MATERIALS & METHODS

3.4.1 MOUSE STUDIES AND CULL PROCEDURE

FVB/N M298 mice were obtained at 4 weeks of age from the Alfred Animal Centre breeding colony. All mice were bred an housed as per the Australian code of conduct for the use of laboratory animals as per Chapter 2, section 2.2.1. All procedures received prior approval through the Alfred Medical Precinct Animal Ethics committee under Animal Ethics number: E/1535/2015/B.

Six week old male mice were treated with 55mg/kg per day Streptozotocin for 5 consecutive days to induce pancreatic β-cell dysfunction and the development of insulin deficient (Type 1) diabetes, as described in Chapter 2, section 2.2.4. A total of 15 mice were allocated to each group to be followed for 4wks, 8wks, 12wks or 16wks post STZ treatment. Litters of mouse pups were divided randomly, and equally as best as possible between control and diabetic groups. For each batch a minimum of 50% were allocated to receive streptozotocin treatment. Control mice received the vehicle control buffer of sodium citrate buffer.

When mice reached endpoint, they were culled by injection with KXA (ketamine 80 kg/mg, xylazine 30 mg/kg and atropine 1.2 mg/kg), followed by cardiac exsanguination. Heart tissue was rapidly excised and weighed, followed by dissection of both whole kidneys. Capsules were discarded and kidneys were weighed. The right kidney was dissected along the lateral pole. The whole renal cortex was dissected from one half and snap frozen in plastic cryotubes in liquid nitrogen and stored at -80°C. The other half was bisected further with one quarter fixed in 10% NBF for 24hrs before

being embedded in paraffin wax. The whole cortex of the left kidney was rapidly dissected into ice cold mitochondrial isolation buffer for the purpose of mitochondrial isolation (Chapter 2, section 2.7.1). Additionally, tibia length was obtained after protein digestion of the left hind leg to obtain kidney to tibia length ratios.

3.4.2 Assessment of diabetes and renal injury

Diabetes was monitored throughout the study as described in Chapter 2, section 2.3 via metabolic caging, blood glucose monitoring, and HbA1c. Renal functional analysis included evaluation of albuminuria, creatinine clearance, urinary Kim-1 excretion, and plasma cystatin C as described in Chapter 2, section 2.4. Renal pathology was assessed by an evaluation of changes in glomerulosclerosis index score as described in Chapter 2, section 2.5. Additionally, an analysis of apoptosis-associated DNA damage was performed by TUNEL analysis Chapter 2, section 2.5.3.

3.4.3 Mitochondrial functional analysis

Mitochondria were isolated from the kidney as described in Chapter 2, section 2.7.1. Analysis of mitochondrial oxygen consumption was performed using the Seahorse Bioanalyzer as outlined in section 2.7.2. Mitochondrial swelling was measured as per section 2.7.3. Additionally, a subset of liver mitochondria were isolated from 2 CIT control and 2 STZ diabetic mice, using the same method presented in section 2.7.1, to allow a comparison of the response of the kidney mitochondria.

3.4.4 Gene expression studies

The gene expression profile of several genes were evaluated using Real-Time qPCR as described in Chapter 2, section 2.6.

3.5 RESULTS

3.5.1 ASSESSMENT OF DIABETES

BODY WEIGHT AND GLUCOSE MONITORING

Throughout the study, all mice were monitored bi-weekly for body weight and random spot blood glucose testing. This was to ensure animals remained sufficiently diabetic and did not develop ketoacidosis (as confirmed by positive ketone test of spot urine). Any animal which did not maintain blood glucose levels above 20mmol/L for more than 2 measurements was marked for exclusion (***Table 3.1***). One mouse was excluded due to illness. Final values for body weight and blood glucose are presented in ***Table 3.2***. Body weight increased slightly from 4wks through to 16wks however no significant difference was evident between CIT control and STZ diabetic mice. Results for random spot glucose at endpoint was significantly elevated as expected. These data were then confirmed using $HbA1_C$ measurement to assess chronic glucose exposure. HbA1c of non-diabetic mice was expected to be at the lower end of the range, at around 20.0mmol/mol (***Table 3.2***). Results reveal the final mice included in this study had developed hyperglycaemia associated with insulin deficient diabetes.

Table 3.1 Total number of mice included in the study

	4 weeks		8 weeks		12 weeks		16 weeks	
Treatment	CIT	STZ	CIT	STZ	CIT	STZ	CIT	STZ
Total allocated	10	12	9	12	9	15	11	15
Excluded due to illness	0	0	0	0	0	1	0	0
Excluded due to poor diabetes development	0	2	0	2	0	6	0	4
Final used for analysis	10	10	9	10	9	8	11	11

Note: CIT = control; STZ = diabetic.

Table 3.2 Body weight and blood glucose values at endpoint.

	4 weeks		8 weeks		12 weeks		16 weeks	
Treatment	CIT	STZ	CIT	STZ	CIT	STZ	CIT	STZ
n =	10	10	9	10	9	8	11	11
Body weight (g)	27.4 ± 1.6	26.2 ± 1.4	26.3 ± 1.7	26.4 ± 2.9	32.6 ± 4.0	31.1 ± 3.4	31.2 ± 3.4	30.1 ± 2.2
Blood glucose (mmol/l)	12.5 ± 1.2	32.1 (0.9)	11.8 ± 0.7	31.4 (1.7)	11.8 ± 1.2	28.0 (5.0)	10.9 ± 1.8	29.0 (4.0)
HbA1c (mmol/mol)	20.3 (0.7)	58.6 ±12.9	21.6 (1.0)	62.8 ±12.5	20.0† (0.0)	49.7 ±9.5	21.7 (2.5)	73.6 ±12.2

Note: Blood glucose was measured at endpoint using a glucometer with a maximum range of 34mmol/L. HbA_{1C} data were also limited to a detection range of 20mmol/mol and 134mmol/mol. Table shows mean ±SD. Values in parenthesis indicate SD of samples where the range limits the actual mean and SD. For HbA_{1C} reference ranges see ***Appendix 2.2****.*

† for 12wk CIT group only n=3 HbA1C results were available, all were at the lowest detection value of 20mmol/mol.

METABOLIC CAGING

One week prior to end point all animals underwent metabolic caging. Animals were placed in cages for 24hrs with food and water intake, as well as urine volume, measured (***Table 3.3***). No statistically significant difference was observed comparing time points for each measurement. Food and water intake were increased in STZ treated animals compared to CIT controls for each individual time point. This increase in water consumption coincides with the development of polyuria as demonstrated by the significantly elevated 24hr urine production.

Table 3.3 24hr metabolic caging revealed diabetic animals had increased food and water intake, and polyuria.

	4 weeks		8 weeks		12 weeks		16 weeks	
Treatment	CIT	STZ	CIT	STZ	CIT	STZ	CIT	STZ
n =	10	9	9	10	9	8	11	11
Food intake (g)	3.6 ± 0.5	5.3 ± 0.6 **	4.0 ± 0.8	5.7 ± 1.4 **	2.9 ± 1.2	5.1 ± 1.0 ***	3.2 ± 1.2	5.1 ± 1.2 ***
Water intake (mL)	3.4 ± 2.2	14.2 ± 7.2 **	3.9 ± 2.3	16.6 ± 9.7 ***	3.1 ± 2.1	14.9 ± 9.3 **	2.1 ± 1.5	15.2 ± 10.3 ****
Urinary output (ml/day)	0.7 ± 0.3	13.30 ± 7.0 ****	0.3 ± 0.3	13.6 ± 9.2 ****	0.7 ± 0.5	11.7 ± 8.5 **	0.7 ± 0.4	12.2 ± 8.8 ****

*Table shows mean ±SD. Data analysed by Two-way ANOVA with Bonferoni post hoc test comparing CIT vs STZ. *p<0.05, **p<0.01, ***p<0.001, ****p<0.0001. No significant difference was found between time points.*

3.5.2 Assessment of Diabetic Kidney Disease

Renal Hypertrophy

Left and right kidneys were weighed immediately after decapsulation. Diabetic animals had an increase in kidney weight compared with CIT controls at each time point (***Table 3.4***). This was statistically significant for all time points with the exception of the 12wk STZ mice, where left kidney mass did not reach significance (*P*=0.071). Total kidney weight was then normalised to body weight (***Figure 3.1A***) and also tibia length (***Figure 3.1B***) to account for variation in animal size which may influence renal mass. Tibia length data followed a similar trend to the K:BW ratio. Renal hypertrophy was evident across all diabetic groups, indicating that it develops early in the progression of DKD and is sustained to at least 16 weeks duration.

Table 3.4 Kidney weight was increased in STZ diabetic animals.

	4 weeks		8 weeks		12 weeks		16 weeks	
Treatment	CIT	STZ	CIT	STZ	CIT	STZ	CIT	STZ
n =	10	9	9	10	9	7[†]	11	11
Left Kidney (mg)	166 ± 11	229 ± 22 ****	183 ± 24	233 ± 26 ****	206 ± 24	234 ± 27 p=0.07	192 ± 18	257 ± 31 ****
Right Kidney (mg)	170 ± 11	229 ± 23 ****	182 ± 12	228 ± 34 ***	200 ± 17	236 ± 30 *	202 ± 20	260 ± 41 ****

Data shown as mean ± SD. Two-way ANOVA with Bonferroni Post hoc test demonstrated a significant increase in kidney weights at most time points. Note: [†] Some measurements were unavailable; so lower than expected n are presented.

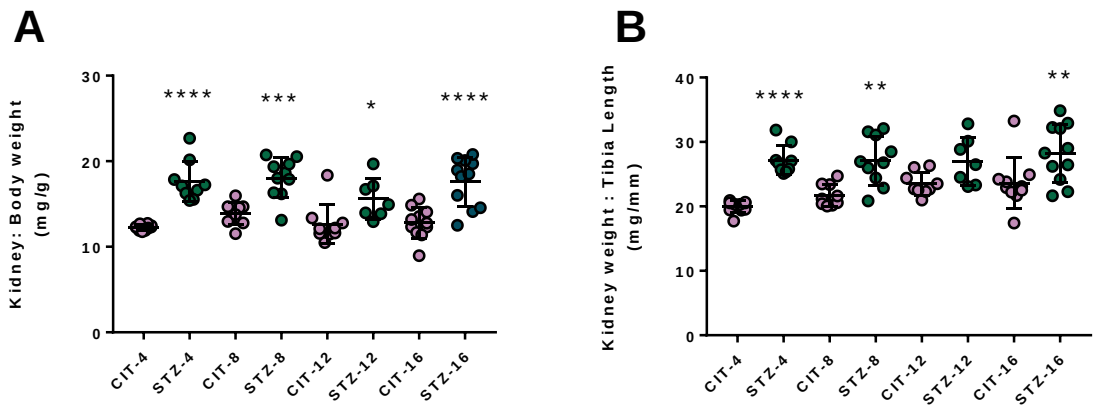

*Figure 3.1: Renal Hypertrophy developed in STZ treated animals as early as 4 weeks of diabetes. Kidney weight in mg was normalised to (A) Body weight (g); or (B) Tibia Length (mm) for each individual animal. Graphs show Mean ±SD. Two-way ANOVA was performed with Bonferroni post hoc test. *P<0.05, **P<0.01, ***P<0.001, ****P<0.0001.*

ALBUMIN EXCRETION

Renal functional parameters were then evaluated, including testing for the presence of urinary albumin excretion. 24hr urine collected during metabolic caging was used to determine urinary albumin excretion by quantitative ELISA. Aliquots were diluted 1:1000 and interpolated values were normalised to total 24hr volume (***Figure 3.2A***). As data were not normally distributed, all values were log transformed prior to statistical analysis (***Figure 3.2B***). Normality of transformed data distribution was confirmed with the Shapiro-Wilk normality test. Two-way ANOVA confirmed a significant increase in urinary albumin excretion in STZ treated mice at all time points, confirming onset of diabetic albuminuria as an early pathological change.

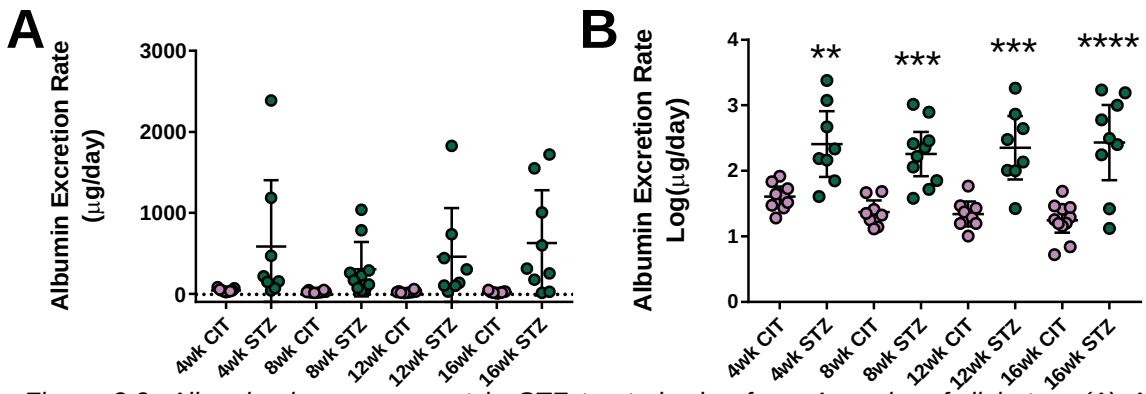

*Figure 3.2: Albuminuria was present in STZ treated mice from 4 weeks of diabetes. (A) Albumin excretion rate assessed by quantitative ELISA in 24hr urine samples. (B) Log transformed data used for statistical testing. Graphs show mean and 95% CI. Two-way ANOVA with Bonferroni post hoc test comparing CIT vs STZ. **P<0.01, ***P<0.001, ****P<0.0001.*

CREATININE CLEARANCE

Creatinine clearance was calculated from urine and plasma samples to estimate glomerular filtration rate. Values were corrected to body surface area using the Meeh equation (***Figure 3.3***). As data were not normally distributed values were log transformed before performing a Two-way ANOVA with Bonferroni post hoc test. No difference was found in the clearance rate of creatinine between CIT control and STZ diabetic mice at any time-point.

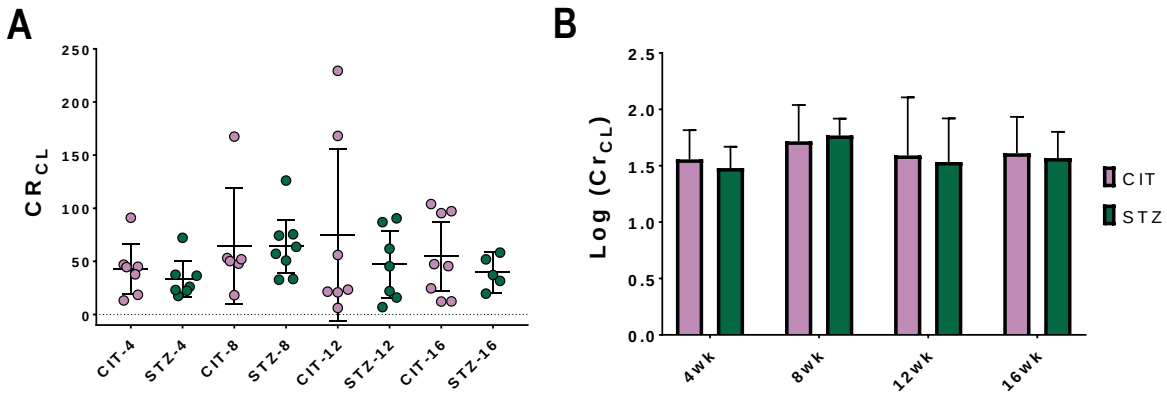

Figure 3.3 Creatinine clearance (CR_{CL}) was unchanged with duration of diabetes. *Values for creatinine concentration were assessed in urine and plasma samples taken at 1 week before endpoint. Correction for body surface area (m^2) was performed using the Meeh equation. (**A**) CRCL for individual mice with error bars showing Mean ±95%CI; (**B**) Log (CR_{CL}). No difference was found by Two-way ANOVA.*

ACR

Albumin (µg/mL) to creatinine (mg/mL) ratio (ACR) was calculated from the results of the albumin ELISA and the urinary creatinine data for each individual mouse. Means of group data reveal an increase in ACR in most diabetic mice compared with CIT controls (***Figure 3.4A***). Data were not normally distributed, thus each value was logarithmically transformed and retested using the Shapiro-Wilk normality test. Normal distribution was thus confirmed and Two-way ANOVA was performed with Bonferroni post hoc test for multiple comparisons (***Figure 3.4B***). This increase was statistically significant at all time points.

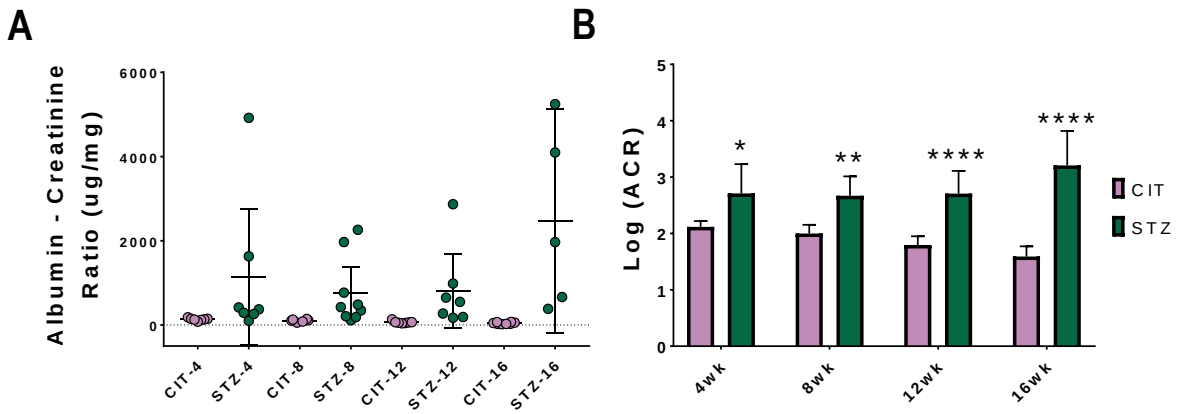

Figure 3.4 Albumin to Creatinine Ratio was increased with STZ at all time points*. (A) Urine Albumin to Creatinine ratio (ACR) for each mouse with error bars showing Mean ±95%CI. (B) Log transformed data for statistical analysis. Two-way ANOVA with Bonferroni post hoc test was performed. *P<0.05, **P<0.01, ***P<0.001, ****P<0.0001. n= 5-10 per group.*

CYSTATIN C

Plasma cystatin C was analysed as a surrogate marker of glomerular filtration. A subset of 7-8 samples per group were tested. A trend towards a decrease in plasma levels was present between all groups, however statistical significance was only reached for the 8 week group comparing CIT vs STZ. No difference between time points was observed.

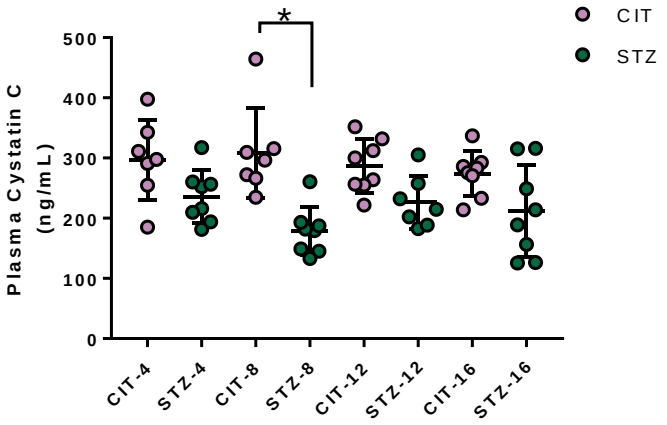

Figure 3.5 Plasma cystatin C in the early progression of DKD. *Plasma from blood collected at endpoint were analysed by ELISA for changes in cystatin C. Graph shows mean ±SD. Two-way ANOVA with Bonferroni post hoc test was performed comparing CIT vs STZ. *P<0.05, **P<0.01, ***P<0.001, ****P<0.0001 n=7-8 per group*

GSI

Glomerular injury was assessed by histological scoring of mesangial expansion using 3µm Periodic Acid Schiff stained sections of paraffin-embedded renal cortex. Weighted scores revealed no mesangial expansion in the glomeruli of *FVB/N* STZ treated mice at any time point (***Figure 3.6***).

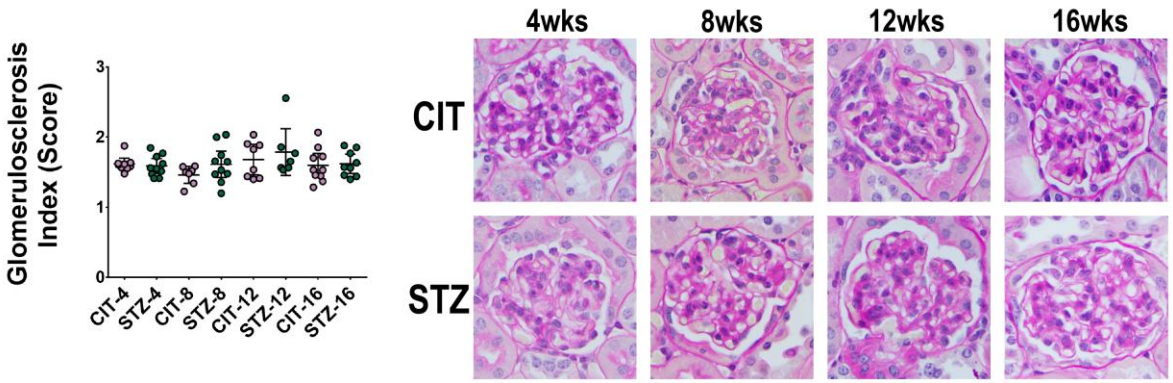

Figure 3.6: STZ treated mice did not develop mesangial expansion by 16 wks. *Glomerulosclerosis assessed by weighted average of histological score for mesangial expansion. 3µm sections of renal cortex stained with Periodic Acid Shiff. Images (x400 magnification) are representative of graphical results. Two-way ANOVA with Bonferroni post hoc test where *P<0.05, **P<0.01, ***P<0.001, ****P<0.0001.n=8-12 per group.*

KIM-1

Tubular injury can be assessed by evaluating protein markers in the urine. Kim-1 is one such protein which can indicate tubular damage and was assessed by quantitative ELISA on 24hr urine samples. KIM-1 was mostly undetected in CIT mice, with STZ diabetic mice having significantly elevated KIM-1 levels (***Figure 3.6***). All time points were statistically significant (P<0.05) with the exception of the 12 week group (P=0.064). This group only had n=3 samples available for analysis which may explain the result, as 2 out of 3 mice had elevated Kim-1.

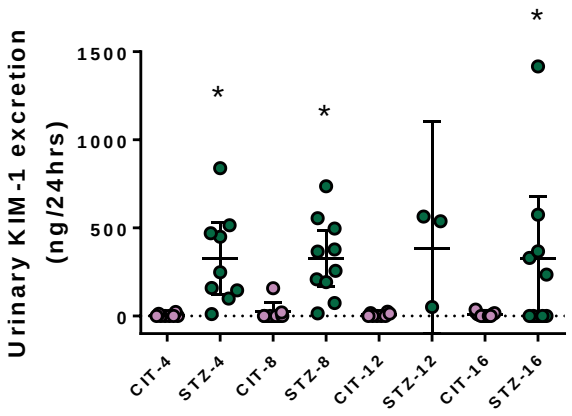

*Figure 3.7: Kidney Injury Molecule 1 (Kim-1) was detected in the urine of STZ diabetic mice. Quantitative ELISA on 24hr urine samples. Graph shows mean and SD. Data analysed using Two-way ANOVA with Bonferroni post hoc test where *P<0.05.*

TUBULAR DAMAGE

The total number of whole damaged tubules (displaying significant eosinophilic deposition and abnormal morphology) were counted across 20 fields at x400 magnification. The average number per treatment group revealed that the number of damaged tubules was significantly increased at 16wks (***Figure 3.7A***). Examples of damaged tubules are provided in ***Figure 3.7B*****.** Some mice showed a tendency to increase at earlier time-points, however the difference was not statistically significant.

Another marker of injury in the kidney includes the production of tubular casts. These proteinacious deposits can be assessed in PAS-stained sections as they stain magenta. In this study only a few casts were observed mostly with progressing DKD, indicating that casts were not a

common pathological feature up to 16wks of STZ diabetes in *FVB/N* mice. Specifically, casts were present in one mouse at 8 weeks of STZ, two at 12wks and two at 16 wks, and one control mouse at 16 weeks (***Figure 3.8***).

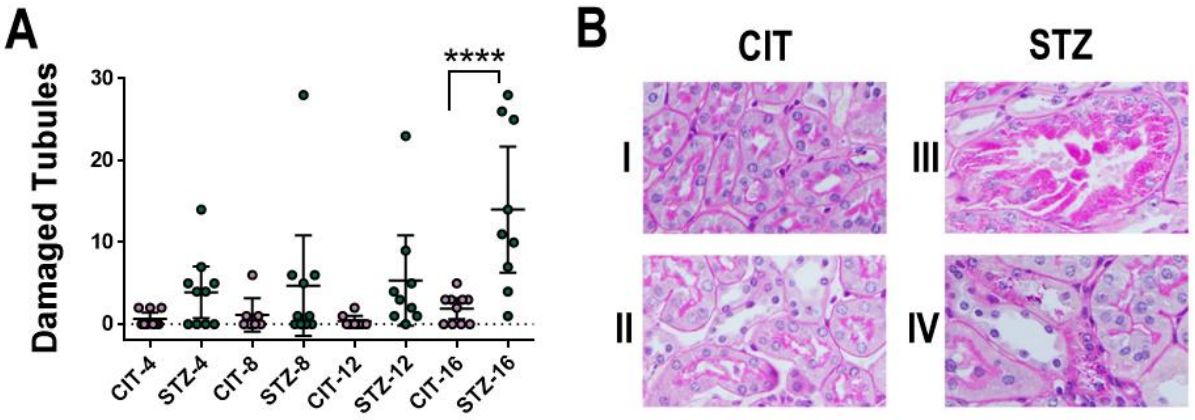

*Figure 3.8: Tubular injury was observed in the renal cortex of STZ diabetic mice. (A) Total number of damaged tubules scored per mouse, assessed by PAS staining in renal cortex. Twenty images of renal cortex at x400 magnification were scored for each mouse. Data points are meanvalues of individual mice, with error bars showing Mean ±SD for each treatment group. (B) Tubular damage present in 16wk mice (n=2 representative images) comparing CIT controls (I and II) with STZ diabetic (III and IV). Two-way ANOVA with Bonferroni post hoc test where ****P<0.0001. n=6-10 per group.*

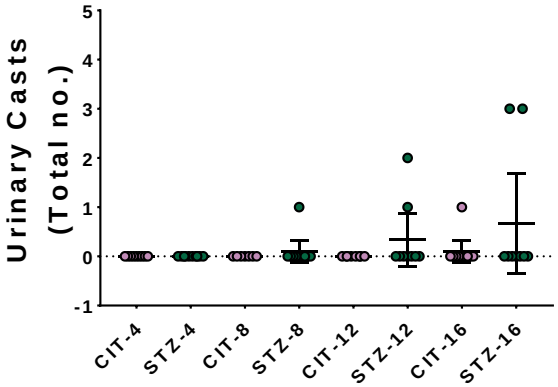

Figure 3.9: Number of Urinary Casts scored per mouse. *Total number of tubules with protein casts counted across 20 image fields. Each point is the total for one mouse. Error bars show mean ±SD.*

TERMINAL DUTP NICK END LABELLING (TUNEL) STAIN

To further investigate the tubular damage observed above, a 3'in situ end labelling of fragmented DNA with biotinylated deoxyuridine-triphosphate (TUNEL) stain was performed (***Figure***

3.9). TUNEL staining can identify DNA fragmentation damage, and serves as an indirect marker of apoptosis. Negative control samples (no TdT incubation) reveal high auto-fluorescence in the green channel was present in the renal cortex, however, the positive control (DNAse 1 digested tissue) demonstrates that nuclei with damaged DNA are able to be clearly identified (***Figure 3.9B***). Results for mean number of TUNEL positive nuclei per group demonstrated a trend towards an increase in STZ mice at 4wks and 8wks only. Mean values for these STZ groups were double that of CIT controls; (**CIT**: 4wks 2.7 ±1.5; 8wks 3.3 ±1.8; 12wks 3.9 ±2.8; 16wks 5.3 ±3.5; **STZ**: 4wks 5.5 ±3.4; 8wks 7.4 ±4.6; 12wks 3.6 ±0.9; 16wks 5.8 ±4.0). However, the differences between groups were not statistically significant. It was also noted that damaged nuclei were predominantly located in non-tubular structures (e.g. glomeruli, intersitium). *A negative, posturised version of Figure 3.10 is presented in Appendix 3.1.*

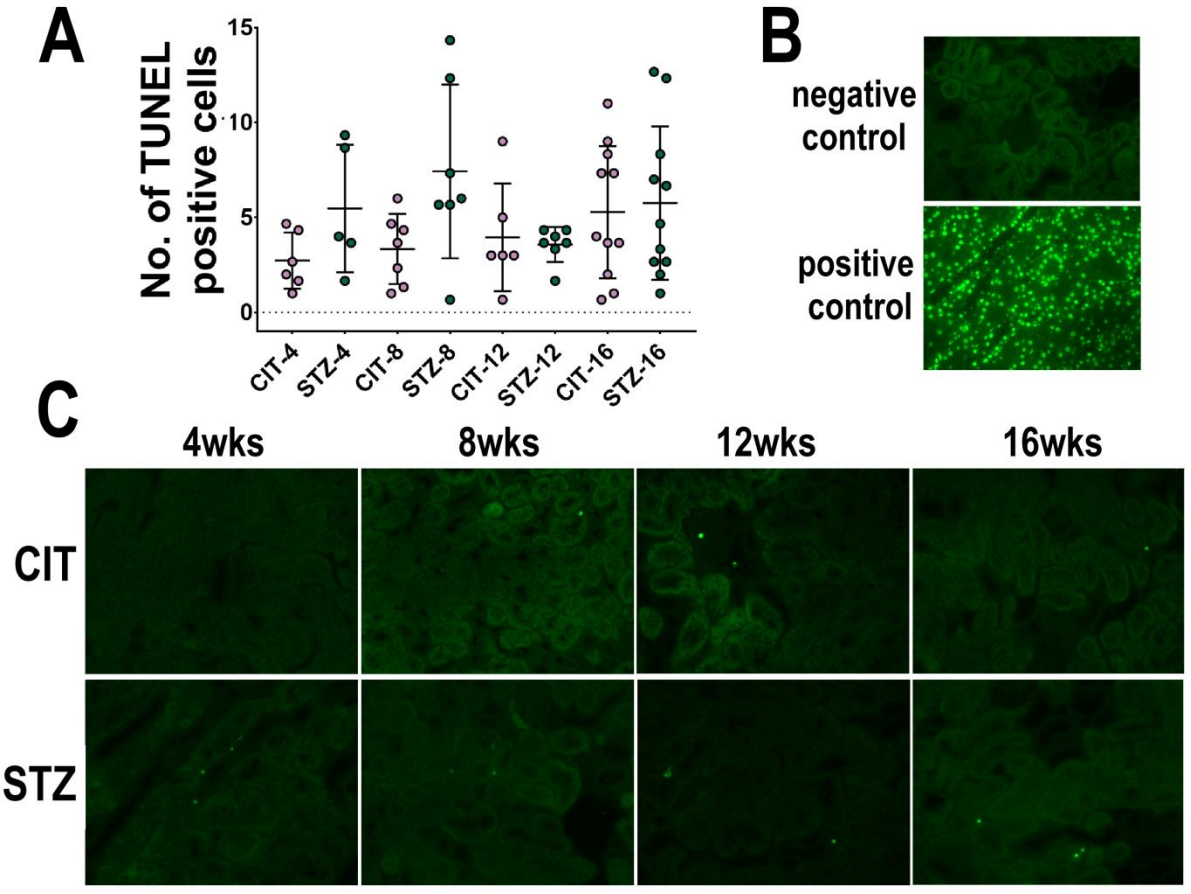

Figure 3.10: Analysis of TUNEL positive cells in STZ diabetic mice. *Sections of renal cortex were stained for TdT-mediated d-UTP Nick-Ended Labelling to assess DNA strand breakage associated with apoptosis. (A) Total number of TUNEL positive cells for 3 images (x170 magnification) were counted for n=5 controls and all diabetic animals per group. Each point is the mean result for individual mice. Error bars show mean ±SD for each group; (B) Staining positive and negative controls; (C) Representative images. All images are 511 x 384µm.*

3.5.3 ASSESSMENT OF MITOCHONDRIAL FUNCTION

OXYGEN CONSUMPTION RATE

Mitochondrial respiration was assessed in isolated mitochondrial samples using the Seahorse Bioanalyzer "Mitochondrial stress test" and expressed per µg of total protein (***Figure 3.10***). OCR of mitochondria were assessed at baseline, followed by the addition of ADP to stimulate respiration, Oligomycin to inhibit complex IV, FCCP to induce maximal uncoupled electron transfer, and finally Antimycin A to inhibit complex III activity. Results for both the 4wk and at 16wk STZ diabetic mice values for complex I respiration, (stimulated with glutamate and malate), were identical to their time-point controls (***Figure 3.10A***). The 8wk STZ mice trended towards a slightly higher OCR across all injected compounds; however this difference did not persist when data was normalised to basal respiration, which helps account for intra-assay variation (***Figure 3.10B***). All other values were unchanged following normalisation to basal respiration (***3.10B***). The Mitochondrial stress test results also allow the calculation of the following information: Respiratory control ratio; ADP linked respiration; Spare respiratory capacity; and Proton leak (***Figure 3.10C***). Once again, there was no difference between CIT control and STZ mice. However, some variation was present between time-points, with the 16wk mice showing higher RCR (***Figure 3.10C i***), and ADP-linked respiration (***Figure. 3.10C ii***) compared with both 4wk and 8wk groups. Spare capacity (***Figure 3.10C iii***), was also lower in the 16wk than the earlier time points, indicating that uncoupling with FCCP was unable to induce greater OCR than that observed with ADP alone. There was also a trend toward an increase in Proton leak with longer duration of diabetes (***Figure 3.10C iv***). Complex I respiration was then compared with complex II respiration using succinate and rotenone (a complex I inhibitor) to determine the capacity of electron transport through each complex (***Figure 3.10D***). OCR mediated through CII was increased in all mice relative to CI rates. An assessment of complex II to complex I respiration ratio revealed a statistically significant decrease in 8wk and 16wk mice compared with 4wk mice for all groups (except CIT 4wk vs 8wk, p=0.066). †

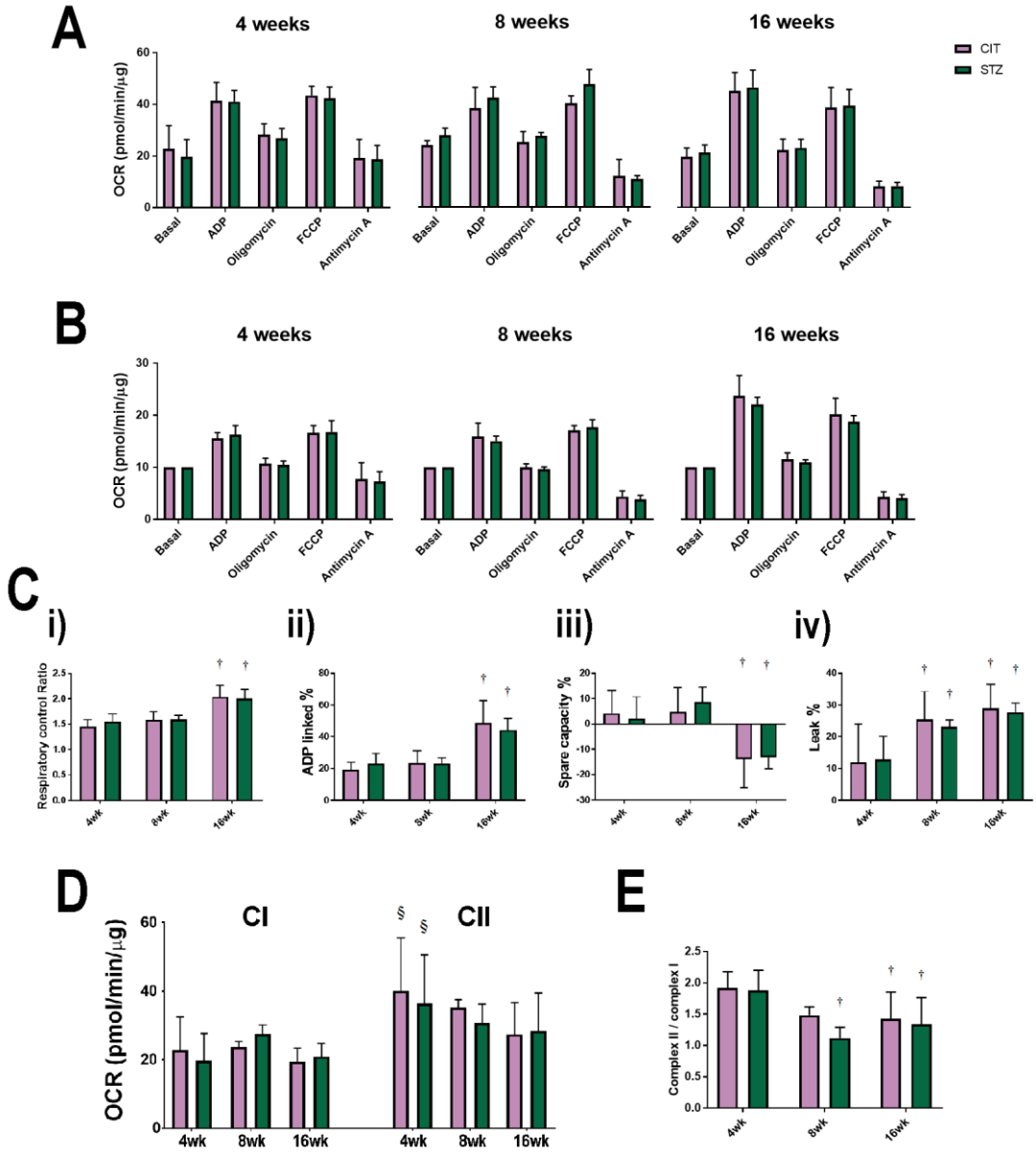

Figure 3.11 Mitochondrial respiration was unchanged with duration of diabetes. *Respiration was tested in isolated mitochondria using the 96 well XFe Seahorse Bioanalyzer. No difference was found between complex I stimulated respiration between CIT controls and STZ diabetic mic for: (**A**) Oxygen Consumption Rate (OCR) per µg isolated mitochondria; (**B**) OCR normalised to Basal respiration; (**C**) Calculated values i) Respiratory control ratio - ADP divided by Oligomycin; ii) ADP minus Basal respiration; iii) ADP minus FCCP; iv) Basal minus Antimycin-A. A comparison of complex I and complex II respiration was evaluated for (**D**) basal OCR; and (E) Ratio of complex II to complex I respiration. Data are mean ±SD for n=3-11 per group. Two-way ANOVA with Bonferroni post hoc test where † P<0.05, between time-points compared to 4wk group. § P<0.05 CI vs CII at each time-point.*

MITOCHONDRIAL SWELLING

Mitochondrial response to calcium induced challenge was observed by assessing the change in absorbance at 540nm for 10 minutes. Isolated mitochondria from individual mice were treated with calcium (Ca^{2+}) or calcium plus CsA (a mPTP inhibitor). Additionally, untreated mitochondria (no Ca^{2+}) were also assessed as an intra assay control. Results reveal that the addition of calcium ions triggered a rapid swelling response in both CIT control and STZ diabetic samples (***Figure 3.12***). No significant difference between CIT and STZ mice for the rate of mitochondrial swelling response was found. A tendency towards an increase in swelling response was observed for the STZ diabetic mice in the 16 week. Cyclosporine A (CsA) was able to inhibit this swelling response during the 10 minute observation period.

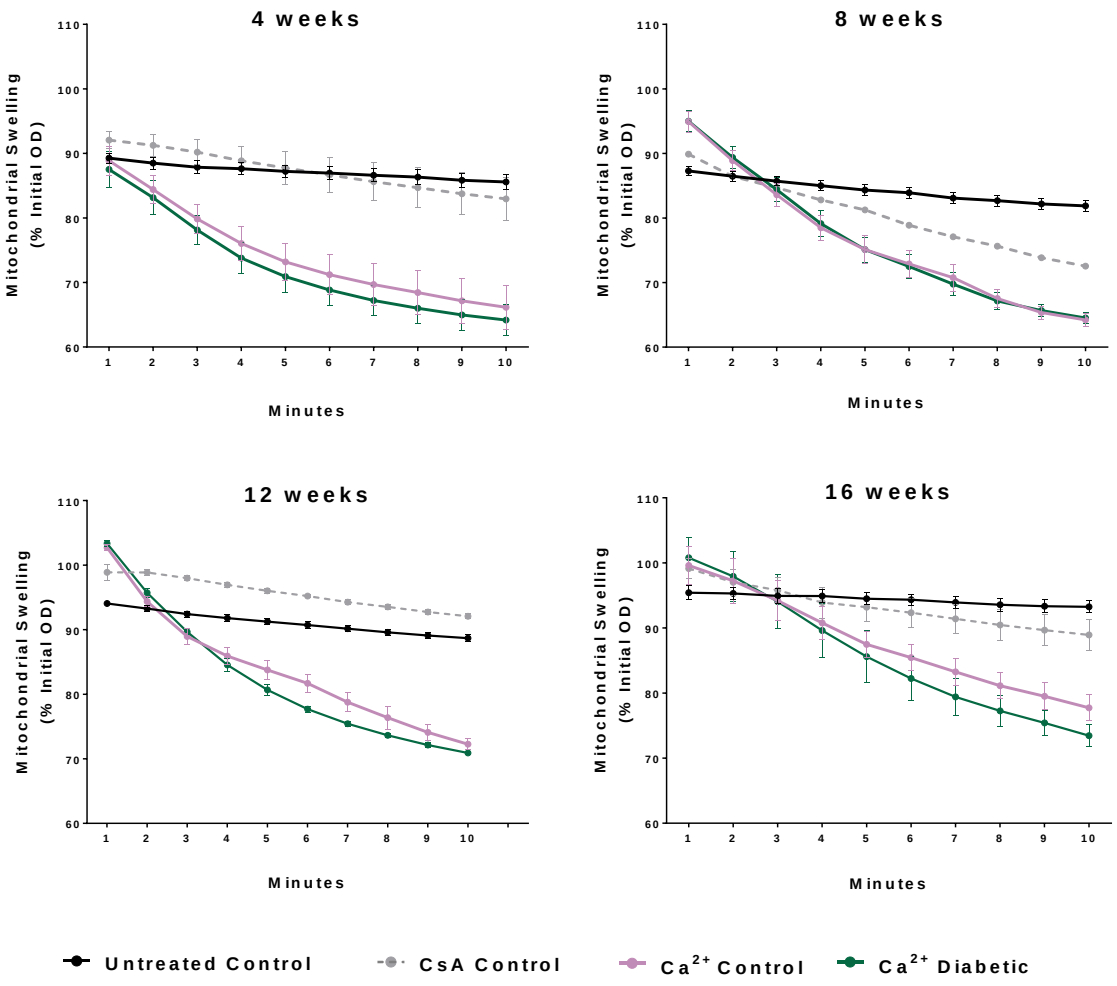

Figure 3.12: Mitochondrial swelling response at 4, 8, 12 and 16 weeks of STZ induced diabetes. 100µg of isolated mitochondria from the renal cortex was assayed for light scattering at 540nm (Untreated). Addition of free calcium ions induce mitochondrial swelling (Ca2+) which may be inhibited by Cyclosporine A (CsA). The change in absorbance is shown relative to initial optical density (OD). Each curve represents the mean and SEM of n=6-11 mice per group.

SWELLING TEST IN IIVER

As renal mitochondria seemed to undergo immediate swelling in response to calcium stimulus, a comparison with liver mitochondria was performed in a subset of 16 week mice (*n*=2 per group). Liver mitochondria were extracted on the same day, using the same method, as the kidney samples and run in tandem with the corresponding kidney mitochondria. Results revealed that liver mitochondria did not undergo rapid swelling in response to Calcium stimulation (***Figure 3.12***). Indeed, liver mitochondria of one citrate control mouse did not swell until 27 minutes after calcium addition, and the second did not swell at all during the 30 minute observation period. For the diabetic samples, the liver mitochondria did not undergo swelling until the 27 minute point in the first sample and 8 minutes in the second. This result is in contrast to the corresponding kidney mitochondrial samples which all underwent rapid swelling after the addition of calcium.

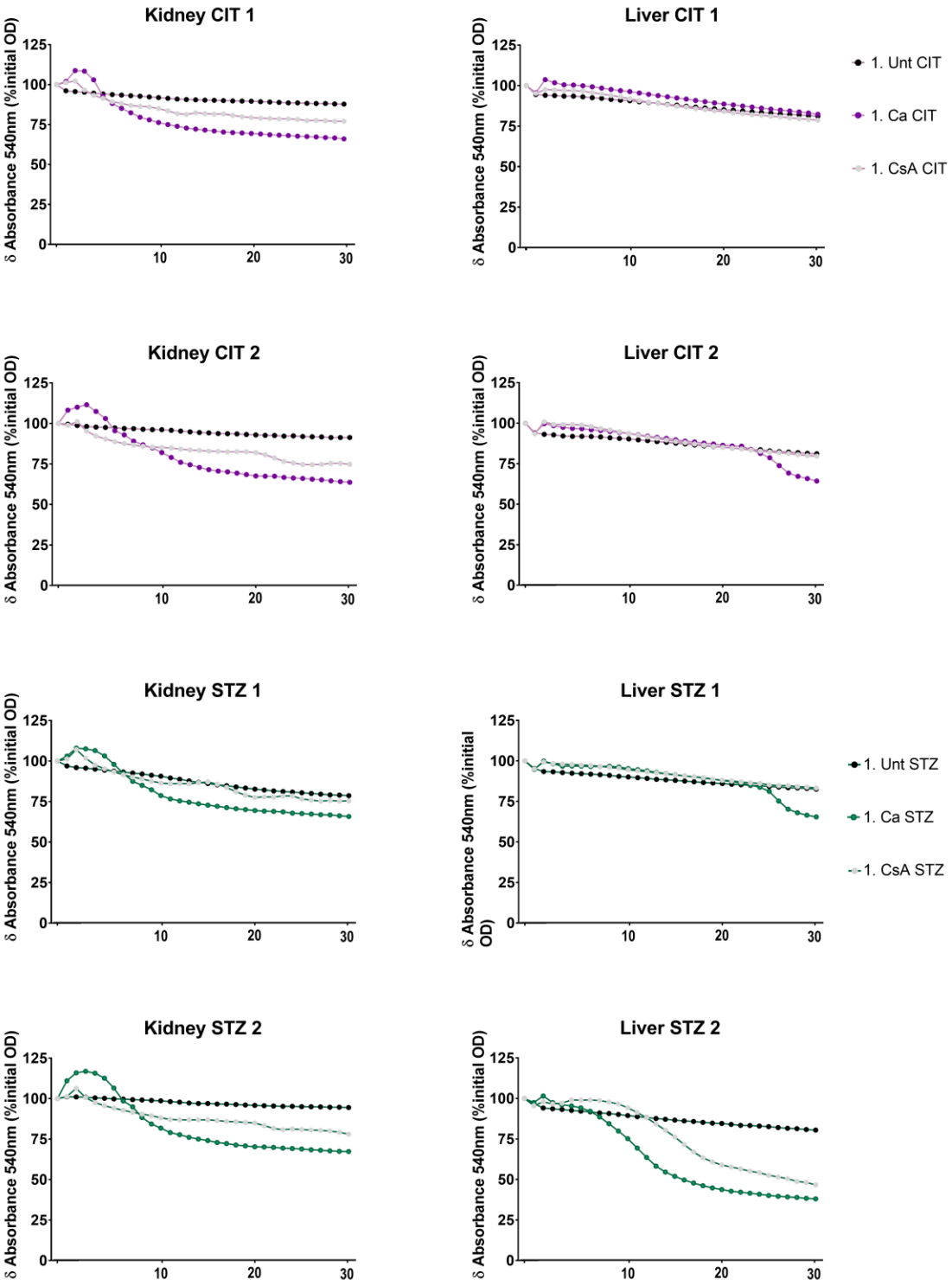

Figure 3.13 Mitochondrial swelling response to calcium challenge was different in the kidney compared to the liver. Kidney and Liver mitochondria were isolated from the same animal and run in tandem to assess response to calcium challenge. Swelling response was measured by observing a change in absorbance at 540nm.

3.5.4 RTQPCR

Gene expression changes were assessed for a range of mitochondrial and cell death associated genes. $2^{-\Delta\Delta Ct}$ was calculated for each sample, by first calculating fold change relative to the endogenous control gene: 18S; followed by a comparison with treatment controls. Both the fold change relative to the 4wk CIT group mean (i) and to the corresponding CIT time-point mean (ii) were calculated to allow a comparison of variation across time points as well as any differences between CIT control and STZ diabetic mice. For the purpose of statistical testing all fold change values were log transformed before performing Two-way ANOVA with Bonferroni post hoc test. Most genes tested showed no significant change between CIT control and STZ diabetic animals at any time point indicating that STZ diabetes did not affect their expression profiles.

Two genes regulating mitochondrial elongation, *Mief1* (***Figure 3.13A***) and *Mief2* (***Figure 3.13B***), demonstrated some minor trends toward an increase in early diabetes; however, there was no statistically significant difference. Mitophagy related genes *Pink1* (***Figure 3.13C***) and *Usp30* (***Figure 3.13D***) were unchanged with diabetes. For both Manganese superoxide dismutase-2 (*Sod2*) (***Figure 3.13E***) and Apoptosis Inducing Factor (*Aif*) (***Figure 3.13F***), which modulate redox reactions at the ETS, some individual diabetic animals showed increased expression, particularly for earlier time points, however group means were not statistically significant.

Mitochondrial ETS genes showed some variation in expression with diabetes. ATP synthase subunit F1alpha was significantly increased at 4 weeks of STZ diabetes (***Figure 3.14A***). Although it trended toward an increase at other time points, this was not statistically significant. No significant changes were observed for either NAD(P)H Quinone Oxidoreductase 1 (*Nqo1*) (***Figure 3.14B***) or Acyl-CoA oxidase 1 (*Acox1*) (***Figure 3.14C***), although the 12 wk STZ group appeared to be slightly increased. *Ppif* gene expression was significantly increased at 4 weeks only (***Figure 3.14E***).

Cell death associated *Casp 3* showed no change (***Figure 3.15A***), however *Caspase 9* trended toward an increase in expression (p=0.078) at 4 weeks (***Figure 3.15B***). *Caspase 8* was also unchanged, however data were quite variable (***Figure 3.15C***). *Bcl-2* family proteins are known to activate caspase activity downstream of their role in intrinsic cell death. No change in *Bcl-2* expression was noted (***Figure 3.15D***), however the *Bak1* gene was significantly raised in 4 week STZ mice; a decreasing trend followed with increased diabetes duration (***Figure 3.15E***). *Bax* was also

significantly increased for the 4 week STZ group, and trended towards an increase for the other time points (***Figure 3.15F***).

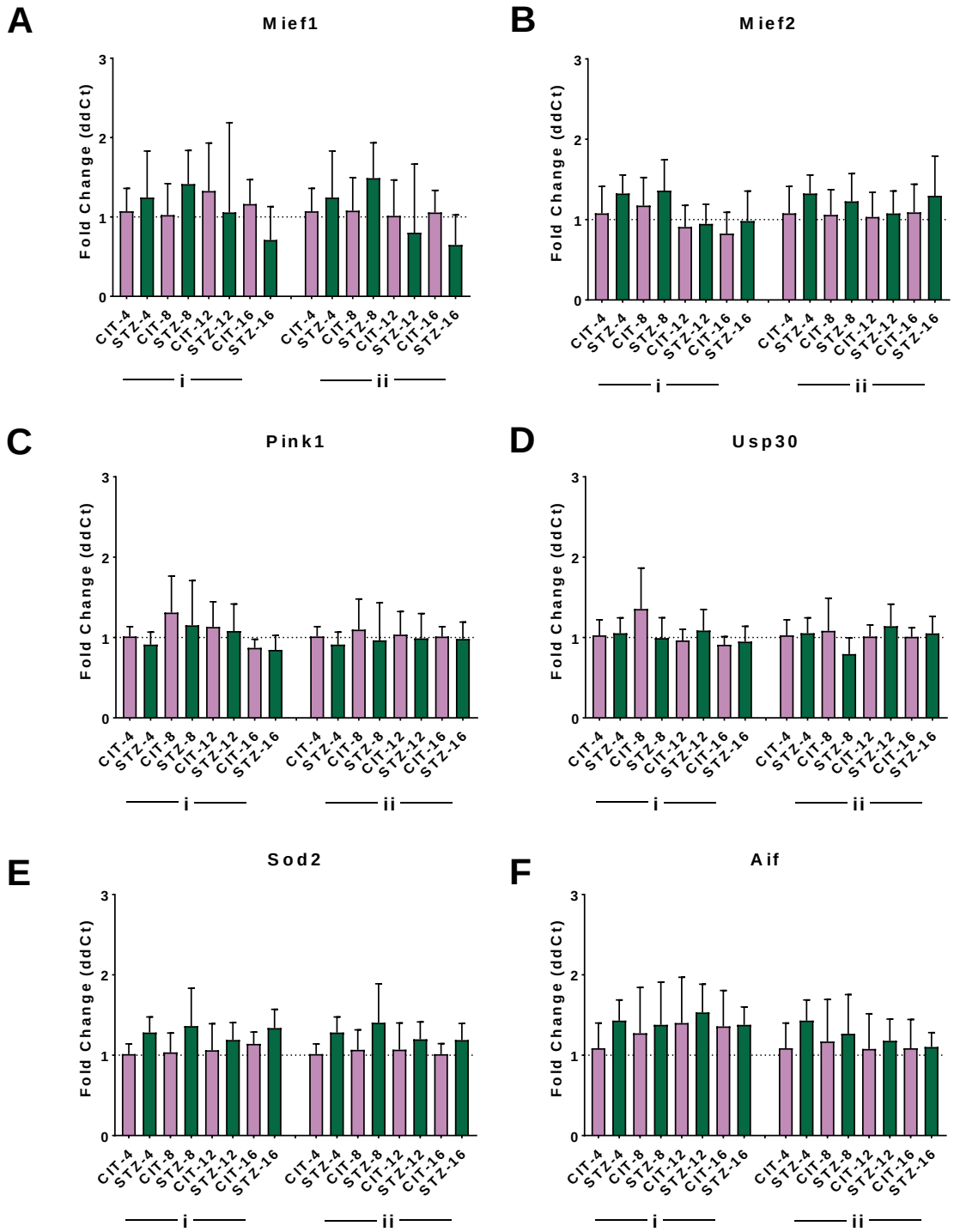

*Figure 3.14 RTqPCR results for mitochondrial morphology genes. (A) Mitochondrial elongation factor-1 (Mief1); (B) Mitochondrial elongation factor-2 (Mief2); (C) Pink1; (D) Usp30; (E) Manganese superoxide dismutase-2 (SOD2); (F) Apoptosis Inducing Factor (AIF). All values are fold change relative to i) CIT-4 control group; ii) Each corresponding Time-point control group. Data are mean ±SD. Differences were analysed by Two-way ANOVA with Bonferroni post hoc test on Log transformed data. *P=0.05. n=7-11 per group.*

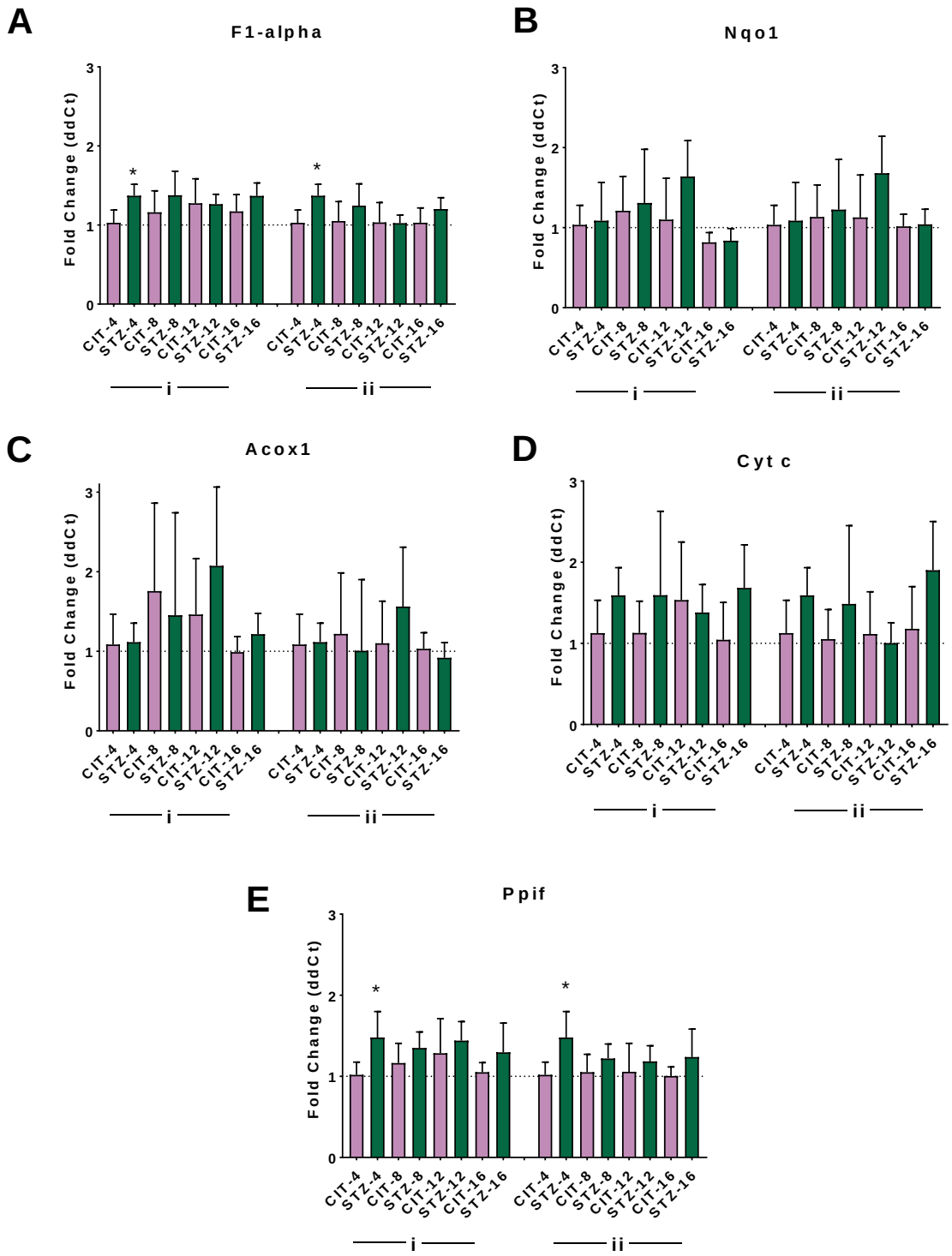

*Figure 3.15 RTqPCR for Mitochondrial Electron Transport System gene expression. (A) ATP synthase, F1-alpha unit; (B) NAD(P)H Quinone Oxidoreductase 1 (Nqo1); (C) Acyl-CoA oxidase 1 (Acox1); (D) Cytochrome c (Cyt c); and the ETS associated gene (D) Ppif. All values are fold change relative to i) CIT-4 control group; ii) Each corresponding Time-point control group. Data are mean ±SD. Differences were analysed by Two-way ANOVA with Bonferroni post hoc test on Log transformed data. *p=0.05. n=7-11 per group.*

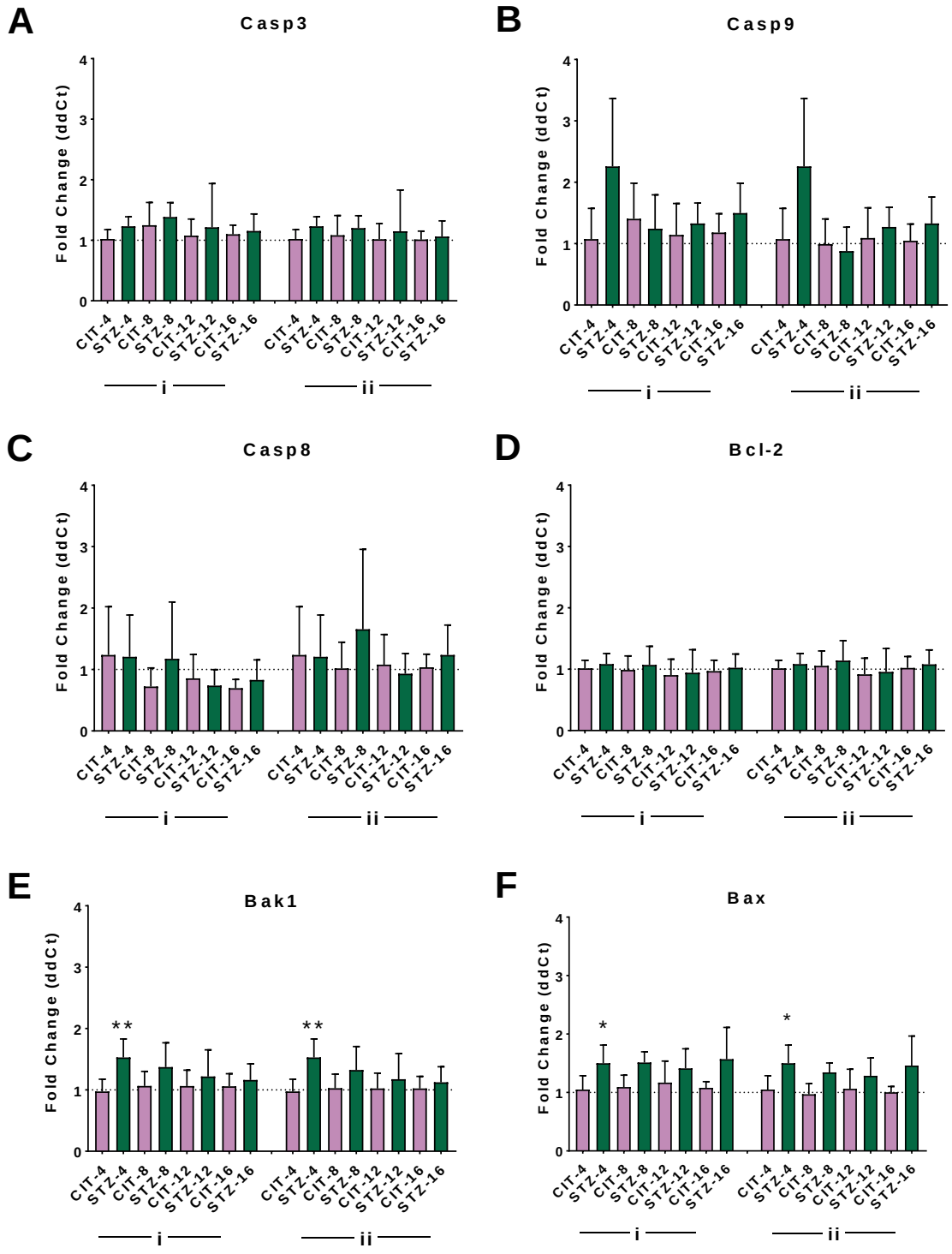

Figure 3.16: RTqPCR for apoptosis related genes. *(A) Caspase 3; (B) Caspase 9; (C) Caspase 8; (D) Bcl-2; (E) Bak1; (F) Bax. All values are fold change relative to i) CIT-4 control group; ii) Each corresponding Time-point control group. Data are mean ±SD. Differences were analysed by Two-way ANOVA with Bonferroni post hoc test on Log transformed data. *p=0.05. n=7-11 per group.*

3.6 DISCUSSION

As expected Streptozotocin treated mice developed overt hyperglycaemia with early renal damage. This was reflected by the development of renal hypertrophy, polyuria, and albuminuria. These data were consistent across the four time-points indicating that these changes occur early and are persistent with diabetes progression. There were no changes in Creatinine clearance however, suggesting that a decline in glomerular filtration rate did not occur. This is consistent with data from both mouse models and mathematical modelling of diabetes which suggest that hyperfiltration precedes renal decline and is mediated through an increase in hyperglycaemic-associated tubular absorption (275,276). Whilst cystatin C trended towards a decrease with STZ diabetes across all time points, data do not indicate any temporal associated decline in glomerular filtration occurred by 16 weeks. Glomerulosclerosis did not develop in this *FVB/N* model of diabetes. Indeed, *FVB/N* mice are considered to have predominately haemodynamic changes, such as high albuminuria, with mild structural changes following STZ treatment (122). Urinary markers of tubular injury were observed as early as 4 wks post STZ treatment and generally persisted through to 16 wks. The level of renal damage appeared to worsen at the 16-week time-point for some markers, for example, with the appearance of tubular specific damage and urinary casts in the later progression.

Analysis of apoptosis-related DNA damage via a TUNEL stain revealed that there was a slight increase in apoptotic cells in the early progression of disease. Although this result did not show a statistically significant difference, the magnitude was still equivalent to a doubling of apoptotic cells, a magnitude of which has been previously observed in human diabetic kidney disease (80,240). In the present study, however, these apoptotic cells were not confined to the proximal tubular epithelial cell regions and thus did not coincide with the pattern of tubular injury described from the PAS image analysis. It is likely that the TUNEL stain analysis on the total renal cortex has also counted apoptotic podocytes for example, which are also known to undergo apoptosis in response to hyperglycaemia (277). These data may suggest that other mechanisms of cell death predominate in the tubules under diabetic conditions. Indeed, other models of cell death are considered to occur in renal injury including necroptosis and ferroptosis which have both been observed to occur following acute renal injury (246). Additionally, the synchronised loss of whole tubules following acute injury may also influence the ability to detect cell death in vivo via a static temporal assessment.

Assessment of mitochondrial function by oxygen consumption rate through complex I and II revealed no difference between control and diabetic mice at any of the tested time points. Unfortunately, no data were able to be collected for the 12 week group. As no differences were present between the remaining time points, these data are unlikely to change this conclusion. This result suggests that mitochondrial function is unchanged in early DKD and does not support the hypothesis of mitochondrial decline being an early event in DKD. However, it is possible that any mitochondrial functional decline is simply not detectable by OCR analysis as performed here, in the early stages of diabetic kidney injury. Indeed, defects in other processes, including complexes III, have also been observed to occur and may drive dysfunction in mitochondrial metabolism (278,279). Mitochondrial swelling data also revealed no apparent differences associated with diabetes duration, although they may suggest that a decline will develop beyond 16 weeks, as has been demonstrated to occur in a rat model of DKD, something which should be explored in future (267). Interestingly however, the results for the liver mitochondria suggest that renal mitochondria have unique behaviours. Indeed, different populations of mitochondria from different organs routinely demonstrate divergent responses to stress (270,280,281). As such, the renal mitochondria may have a different ability to respond to the stressors associated with diabetes. Indeed, renal mitochondria have been observed to be metabolically unique, for example, the predominate metabolic substrates used by proximal tubule cells are produced via beta-oxidation of fatty acids, and the citric acid cycle, via aerobic respiration (282). Additionally, inhibition of fatty acid oxidation has been associated with an increase in renal damage via ATP depletion (283). Indeed, studies have demonstrated that renal proximal tubules cells (PTCs) do not metabolise glucose to lactate, unlike cells of the renal medulla (282,284). However, PTCs may utilize free lactate from the renal ultrafiltrate (186). In diabetes, the increased oxidation of substrates has been demonstrated to induce hypoxia and may create a dependence on anaerobic substrate metabolism (176,285). One mechanism for mitochondrial regulated protection from damaging ROS has been found to be mediated through upregulation of Uncoupling protein-2 (286). This suggests that an observable change in oxygen consumption rate would be unlikely without significant mitochondrial dysfunction; as some adaptation through this uncoupling mechanism is possible. This phenomenon is worth exploring in future studies of renal mitochondria.

Finally, to gain an insight into the molecular mechanisms underlying mitochondrial change and adaptation to early diabetes an analysis of gene expression of several key proteins was explored. Overall, gene expression changes in mitochondrial and cell death proteins were minor, indicating that diabetes was not associated with any significant alteration to these pathways. Reviews by others examining cell death proteins in the progression of DKD reveal a complexity of changes occur in DKD (243). Available data from RNAseq studies have identified that some cell death proteins are upregulated in early DKD, however changes in cell death pathways are observed to associate with advancing disease (242,287). Pathways associated with mitochondrial dysfunction however have been observed to be upregulated in early DKD and also may correlate with lesion severity (287,288) In general the literature suggests that mitochondrial dysfunction is a key mediator of diabetic kidney disease (86,289). The findings presented within the chapter do not support mitochondrial dysfunction as preceding the development of DKD instead suggest that the early progression of diabetes is not associated with overt mitochondrial dysfunction.

Interestingly, the gene expression data may suggest an induction in cell death pathway genes that is present at 4 weeks of STZ but is resolved by 16 weeks following STZ treatment. This is indicated by the increase in *Bak1*, *Bax* and *Ppif*. It is possible that this small change is associated with the nephrotoxic action of STZ itself, as it is taken up by GLUT-2 receptors present in both kidney and the pancreas (290,291). However, it is unexpected to see these effects persist 4 weeks after STZ treatment. Indeed, the avoidance of STZ related toxicity relies on the low-dose regimen used in this study, however the effects of STZ per se with a co-incident background of hyperglycemia are difficult to distinguish and are thus still being investigated. This may indicate that STZ is unsuitable for early diabetic renal analysis as diabetes associated renal injury may not be distinguishable from the effects of STZ at 4 weeks. As these initially detected changes appeared to have disappeared at the 16 week time-point, these results demonstrate that STZ is more suited to studies exploring chronic kidney disease.

3.7 CONCLUSIONS

The development of early diabetic kidney disease was evident in this *FVB/N* mouse model of Streptozotocin-induced, insulin deficient (Type 1) diabetes, with the development of high albuminuria and renal hypertrophy. Tubular injury was observed to develop progressively over this time-course study; however, this injury did not directly correlated with apoptotic DNA fragmentation. Consequently, a decline in mitochondrial function, as determined by oxygen consumption rate of isolated mitochondria, was not detected between 4 and 16 weeks following STZ treatment. These results suggest that mitochondrial functional may decline later in the progression of diabetic kidney disease.

3.8 SUMMARY

This study evaluated the diabetes-associated changes in the early progression of renal injury using a mouse model of Streptozotocin induced diabetes. Although evidence of renal injury was observed, mitochondrial functional parameters were unchanged in early diabetes.

3.9 FUTURE DIRECTIONS

Following the results of the current study, the next step will be to examine the development of renal injury in more chronic models of STZ-induced diabetic kidney disease. As such, future mouse models will explore the progression of disease at a more advanced duration of diabetes. Additionally, the role of cell death proteins identified as upregulated in the RTqPCR data, *Bax*, *Bak* and *Ppif*, will be explored. The following chapter will explore the contribution of two key apoptotic proteins: Bax and Bak, to the progression of DKD. As evidence for apoptosis was restricted it is worth exploring whether deletion of these two proteins will influence disease progression. Primarily Chapter 4 will explore whether the loss of the two key mitochondrial outer membrane pore proteins, will influence mitochondrial function and cell death outcomes in the progression of DKD. Additionally, the identification of renal tubular injury in this model of STZ diabetes provides the impetus to consider studies where the proximal tubule is specifically targeted. The role of *Ppif* and the mitochondrial permeability transition pore will be explored in Chapter 5.

Chapter 4

Chapter 4. Characterisation of renal function in a novel mouse model with conditional deletion of Bax and Bak in the proximal tubules

4.1 Introduction

4.1.1 Mitochondrial health and the intrinsic apoptotic pathway

The link between mitochondrial health and mitochondrial-driven cell death has the potential to explain at least some of the consequences of mitochondrial dysfunction on the progression of DKD. Mitochondrial dysfunction can manifest as changes in electron transport efficiency, increases in damaging reactive oxygen species (ROS), defects in fatty acid oxidation (FAO), and other changes (180,292,293). Where pathological insults are irreparably detrimental, these changes lead to downstream activation of cellular stress responses, that ultimately result in cell death. Indeed, aberrant mitochondrial ROS production can lead to cellular injury and cell death and has been observed to underlie certain neurodegenerative diseases and cardiac disorders (294–296). Indeed, many new therapeutic strategies to prevent ischemic injury in the kidney and in other tissues focus on protecting mitochondria from irreversible damage (297,298). Whilst mitochondrial dysfunction is clearly associated with cell death, the implications of mitochondrial health to the initiation of these pathways is still being elucidated. Factors controlling intrinsic apoptosis at the level of the mitochondrion should thus be evaluated for their potential modifying effects in the context of disease.

4.1.2 Intrinsic apoptosis and the BCL-2 family proteins

Central to the intrinsic apoptotic cascade are the BCL-2 family proteins. This family covers a hierarchy of highly conserved proteins with various roles in sensing and responding to cellular stress signals, thus orchestrating the balance between cell survival and death. BCL-2 itself is a pro-survival protein associated with promoting the survival of damaged cells to reduce deleterious loss of tissue mass. Whilst this has its benefits, the necessity of strict regulation of BCL-2 is demonstrated by its association as a proto-oncogene, whereby its over activation promotes the survival of mutated cells (299). However, under normal conditions the upregulation of BCL-2 is associated with increased survival and resilience to cellular stress (300). The ratio of anti-apoptotic

BCL-2 expression to that of the pro-apoptotic protein BAX is a commonly used indicator to determine the susceptibility of a population of cells to undergo apoptosis. Indeed BCL-2 actively binds to BAX to prevent its role in apoptosis (301). BAX, and its functional homologue, BAK, are two proteins with a joint role in effecting the intrinsic cell death cascade by forming the mitochondrial outer membrane pore (MOMP). BAX is a cytosolic protein that displays transient affinity with mitochondrial membranes in its inactive state. BAK, on the other hand, is anchored to the outer mitochondrial membrane (OMM) by VDAC2 and displays a transient cytosolic phase (302). Upon activation, BAX undergoes a conformational change, which enables it to translocate to the OMM, whilst activated BAK is released from VDAC2. Both BAX and BAK are then able to oligomerise to form the MOMP. The formation of this pore is consistent with the release of cytochrome *c* and downstream caspase cleavage; leading to the formation of the apoptosome (303,304). The activation of both BAX and BAK is tightly regulated by an intricate signalling cascade that includes other BCL-2 family proteins, such as BH3-only proteins (305,306). In most cell types BAX and BAK are functionally redundant with studies showing the absence of either is insufficient to prevent MOMP formation (225,307,308). Dual deletion of BAX and BAK is required and KO studies in mouse embryonic fibroblast (MEF) cells *in vitro* have demonstrated a decreased susceptibility to induce apoptosis and initiate the apoptotic cascade (309). Further, elevated BAX can be correlated with a heightened sensitivity to cell death, and has been demonstrated to occur in murine models of diabetic nephropathy (241,310).

The relationship between the activity of BAX and BAK and the functionality of mitochondria is also evident in mouse models with dual deletion of Bax/Bak. Previous studies have demonstrated that changes in mitochondrial function and morphology occur in their absence (224,309). High glucose is also associated with a decrease in cell survival that may be mediated through intrinsic apoptotic pathways and the BCL-2 family of proteins (311,312). Indeed, the elevation of glucose derived ROS observed in diabetes has been associated with increases in both death receptor and mitochondrial mediated apoptosis (313). The ability to differentiate the role of mitochondrial induced cell death from receptor-mediated death would increase the understanding of therapeutic windows available to target these processes and alleviate pathological outcomes in DKD.

4.1.3 BAX AND BAK IN MURINE MODELS OF DKD

As with human BAX and BAK, murine Bax and Bak are also considered functionally redundant proteins. Deletion of Bax or Bak individually has limited impact on MOMP formation in most murine tissues. Whilst some scenarios have been shown to activate one in preference to the other, single knockout models of either gene alone demonstrate few abnormalities (314). One example includes the requirement of Bak in the development of epididymal tissue in male mice (315). Global deletion of both Bak and Bax is associated with a high incidence of embryonic lethality, and also interference with developmental programmed death in multiple tissues (308). Mouse pups that do survive to birth are characterised as having stunted growth and poor survival, rendering traditional global knock out models unsuitable for *in vivo* preclinical studies of Bax/Bak deletion. Importantly, however, this same study indicated that kidney development was normal in the double knockout mice that did survive postnatally (308). However, studies examining the effects of loss of both Bax and Bak require selective gene knock down strategies in order to investigate the physiological effects of their absence.

Cre-lox gene technology is one such strategy which may be used to generate a conditional knock out model (316). In this system, the gene of interest is tagged with a "floxed" cassette (called a LoxP site) on either side of the specific protein coding regions of the gene. This cassette is then able to harness the activity of the Cre-recombinase enzyme, which binds to the LoxP sites and excises the intra-spanning region of DNA by catalytic ligation. Conditional deletion is thus achieved by the targeted insertion of the Cre-recombinase transgene, within a second target gene, thus allowing conditional expression in a restricted cell type or tissue as required. Both the target gene and the transgene are transcribed concurrently.

In diabetic kidney disease, pathological changes arise in many of the heterogeneous cell populations. Whilst finding a "kidney specific" marker with minimal off-target effects is difficult, different portions of the kidney may be targeted individually. This allows for the elucidation of both the roles of specific proteins, and the contribution of the different parts of the kidney to the development of DKD. As the renal proximal tubule cells contain a very high quantity of mitochondria, a PTC specific protein was selected to evaluate the role of Bax and Bak in mitochondrial dysfunction in DKD.

The sodium-glucose cotransporter, Sglt2, is a solute carrier involved in the reabsorption of glucose and sodium across the apical brush-border of the PTCs. It is exclusively expressed in the S1

and S2 (most proximal portion) of the renal tubules (78,317). Whilst some evidence suggests that it may have limited expression in other tissues (Reviewed in detail by Chen et al., 2010) there has not been conclusive evidence to support the expression of Sglt2 protein in extra-renal tissues in mice (318,319). Sglt2-Cre promoted mouse models have been successfully utilised by others to examine a range of renal associated pathologies (320,321). Here, Sglt2-Cre mice (The Jackson Laboratory: ME, USA), were selected for use as the conditional promoter in this study. They were cross-bred with the Bak1 global negative (KO) mouse model which also expresses floxed Bax (a kind gift from Isabelle Rubera and Michel Tauc, Nice, France), to generate a proximal tubular specific deletion of Bax. This renal PTC targeted deletion enables an evaluation of the roles of Bax and Bak in DKD by examining the physiological effects in the absence of these two proteins.

4.2 RATIONALE

HYPOTHESIS

It is hypothesised that the key cell death proteins Bax and Bak are mediators in the pathogenesis of diabetic nephropathy due to their critical role in interfacing with the mitochondrial intrinsic cell death pathway.

AIMS

-To investigate whether the cell death proteins Bax and Bak mediate mitochondrial function and cell death of renal proximal tubule cells during the development of diabetic kidney disease.

and:

- To investigate the contribution of Bax and Bak to mitochondrial changes reported in diabetic kidney disease

4.3 MATERIALS AND METHODS

4.3.1 EXPLORATION OF CELL DEATH PROTEINS REPORTED IN HUMAN PTCS

The protein expression of a range of cell death proteins was evaluated from the Human Protein Atlas, to confirm the expression of key mitochondrial cell death proteins, and other death associated proteins, in the renal tubules. Data were compared with reported expression in glomeruli, and heart muscle. Protein names were queried through the publically available database at: https://www.proteinatlas.org/humanproteome/tissue. Results for tissue expression of protein were collated where antibody expression was available in normal tissue only. The Human Protein Atlas reports tissue protein expression as either high, moderate, low, or undetected.

4.3.2 GENERATION OF THE CONDITIONAL DKO MOUSE MODEL

Five generations of strategic breeding were required to generate the Bak $^{-/-}$ Bax $^{fl/fl}$ Sglt2-Cre $^{+}$ colony. Sglt2-Cre mice with DBA/2 x C57BL/6 background (Tg(Slc5a2-cre)1Tauc; a kind gift from Isabell Rubera and Michel Tauc, Nice, France), were cross-bred with Bak1 $^{-/-}$/Bax $^{fl/fl}$ mouse strain with mixed 129x1/SvJ x 129S1/Sv background (B6;129-*Bax*^{tm2Sjk} *Bak1*^{tm1Thsn}/J; The Jackson Laboratory: ME, USA). The first three generations were randomly inter-bred to allow heterozygous mixing of background strains. Of these, specific genotypes were then selected to begin breeding the required genotypes for the purpose of the study.

Genotyping of individual mice were undertaken by TransnetYX, Inc (Cordova TN, USA). Validated primer sets for the presence or absence of Bak1, Floxed Bax, WT Bax, and Sglt2-Cre were performed on tail samples of all mouse pups collected at 3-4 weeks of age. These data were used to ensure that only mice of the correct genotype were allocated to the study. At 6-7 weeks of age diabetes was induced in male mice as per the protocol in Chapter 2, section 2.2.4. Only homozygous mice for each of the required genes were allocated to the experimental study. However, Cre-recombinase was reported as either positive or negative. The following genetic groups were used (***Table 4.1***):

Table 4.1: Genotypes of groups used for 24 week experimental study

Group	genotype	Bak1	Bax WT	Bax floxed	Cre
WT control	Bak $^{+/+}$ Bax $^{+/+}$ Sglt2-Cre $^{-}$	+/+	+/+	-/-	-ve
Cre control	Bak $^{+/+}$ Bax $^{+/+}$ Sglt2-Cre $^{+}$	+/+	+/+	-/-	+ve
Bak Single KO	Bak $^{-/-}$ Bax $^{+/+}$ Sglt2-Cre $^{-}$	-/-	+/+	-/-	-ve
Bax Single KO	Bak $^{+/+}$ Bax $^{fl/fl}$ Sglt2-Cre $^{+}$	+/+	-/-	+/+	+ve
Bax/Bak DKO	Bak $^{-/-}$ Bax $^{fl/fl}$ Sglt2-Cre $^{+}$	-/-	-/-	+/+	+ve
Notes: WT - Wild type; KO - Knock out; DKO - Double Knock out; +/+ homozygous positive; -/- homozygous negative, +ve: expresses Cre-recombinase; -ve :no Cre-recombinase					

WESTERN BLOTTING

Small pieces of renal cortex, cardiac left ventricle, and liver, (previously LN_2 snap frozen and stored at -80°C) were homogenised in lysis (RIPA) buffer using 1-2 mm zirconium oxide beads in a "bullet blender" (Next Advance, Averill Park, NY USA). 45µg of protein homogenate was then mixed with 1µL reducing agent (Novex, Life Technologies, Carlsbad, CA, USA; Cat: B0007), and 2.5µL LDS sample buffer (Novex, Life Technologies, Carlsbad, CA, USA; Cat: B0009), and denatured at 70°C for 10 minutes. Samples were loaded into Bolt™ 10% Bis-Tris western blotting gels (Thermo Fisher Scientific, Scoresby, VIC, AU; Cat: NW00100BOX), in 1x MOPS buffer (Thermo Fisher, Scoresby, VIC, AU; Cat: NP0001) and run at 165V for 30 minutes. Transfer to PVDF membranes was performed using a sandwich cassette submerged in transfer buffer (see Materials section 2.1.2) for 1hr at 100 volts. Membranes were then blocked with 5% BSA in TBS for 12hrs at 4°C, followed by incubation with a 1:1000 dilution of mouse anti-Bax, and rabbit anti-Bak antibodies (BD Pharmingen, San Diego, CA, USA) in 0.5% BSA + 0.2% Tween, for 1 hour at room temp. Blots were rinsed with TBS x3, and incubated with 1:10,000 dilute IRDye-680RD goat anti-rabbit (LI-COR, Lincoln, NE, USA; 926-68071) and IRDye-800CW donkey anti-mouse (LI-COR, Lincoln, NE, USA; Cat: 926-32212) secondary antibodies in 0.5% BSA + 0.2% Tween, for 1hr at room temperature. Blots were imaged using an Odyssey CLx imager (LI-COR, Lincoln, NE, USA) and analysed using Image Studio software (LI-COR, Lincoln, NE, USA). Blots were then re-probed for Beta-actin (Abcam, Cambridge, UK; Cat: ab16039) as loading control.

GENE SEQUENCING

DNA was extracted using the REDExtract-N-Amp^{TM} Tissue PCR kit following the manufacturer's instructions (Sigma-Aldrich, St Louis, MO, USA), from whole renal cortices of six experimental mice at 30 weeks of age with mixed genotypes. PCR amplification was optimised for DNA concentration and amplified with an annealing temperature of 57°C, for 40 cycles, using primers specific to the Bax gene:

Primers
Forward: 5'- ATGTTGCGGGGCACCCACGTGAGGG -3'

Reverse: 3' - TCTGATCAGCTCGGGCACTTTAGTG - 5'
complementary: 5'- CACTAAAGTGCCCGAGCTGATCAGA -3'

Electrophoresis was then performed on the PCR products. DNA bands were visualised using the ChemiDoc (Bio-rad, Hercules, CA, USA). Specific bands were then dissected under UV light, and collected into eppendorf tubes. DNA was then separated from the gel using the QIAquick® Gel extraction kit (Qiagen, Hilden, Germany; Cat: 28704) following the manufacturer's instructions. DNA was then sent for sequencing at the Micromon sequencing platform at Monash University (Clayton, AU). Nucleotide base calling was analysed using FinchTV v1.4.0 (Geospiza, Inc.; Seattle, WA, USA; http://www.geospiza.com). Nucleotide base sequence reads were then aligned to the mouse reference genome using the NCBI BLAST sequence alignment tool (NCBI, U.S National Library of Medicine; https://blast.ncbi.nlm.nih.gov/Blast.cgi).

4.3.3 ASSESSMENT OF DIABETES STATUS

Diabetes assessment and monitoring were performed as per the protocols outlined in Chapter 2, section 2.3.

4.3.4 ASSESSMENT OF RENAL FUNCTION

Renal functional parameters were assessed by comparing data obtained from: Metabolic caging, urinary albumin excretion, kidney to body weight ratio, plasma cystatin C, and urinary Kim-1 excretion. These protocols are described in detail in Chapter 2, section 2.3 and 2.4.

4.3.5 HISTOLOGY

Renal samples were processed as per the protocol in Chapter 2, section 2.5. PAS staining was performed on renal sections (*n*=10-12 mice per group) as per the protocol in section 2.5.1.

All images were blinded prior to imaging and scoring as per the protocol in Chapter 2, section 2.5.3.

Glomerulosclerosis index, tubular injury and glycogen deposition were assessed as per the protocols in section 2.5.1.

4.3.6 MITOCHONDRIAL FUNCTIONAL ANALYSIS

Mitochondria were isolated from the renal cortex of the left kidney of experimental animals, as per the protocol in Chapter 2, section 2.7.1. Functional analysis using a Seahorse Bioanalyzer (Seahorse Bioscience, Agilent, Santa Clara, CA, USA), was performed as per the protocol in section 2.7.2. Assessment of mitochondrial swelling was performed according to the protocol in section 2.7.3.

4.3.7 STATISTICS

Two-way ANOVA was performed for all statistical testing. The two Factors were considered to be: diabetes status, and genotype. Post hoc tests for multiple comparisons were selected based on a pre-determined set of comparisons of biological interest. Bonferroni post hoc test was used to test the interaction of diabetes status by only comparing genotype pairs of citrate (CIT) control vs STZ diabetic mice (5 comparisons). The factor "genotype" consisted of five groups: WT, Cre^{+} , $Bak^{-/-}$, $Bax^{fl/fl}$ Cre^{+}, and $Bak^{-/-}$ $Bax^{fl/fl}$ Cre^{+}. Genotype groups were nested into 2 families based on diabetes status (CIT, and STZ) with comparisons of all genotypes within each family (10 comparisons). This strategy was used to reduce type I and type II errors, by excluding biologically redundant comparisons. Results of Post hoc multiple comparisons tests are reported as: **P*<0.05, ***P*<0.01, ****P*<0.001, *****P*<0.0001.

Additional note on statistics: Due to the large number of family wise comparisons undertaken in this study, the importance of each *P*-value will not be considered independently, rather, trends between independent experimental outcomes will be regarded as evidence of a real effect. This strategy is employed to reduce the false discovery rate of differences between all of the genetic groups.

4.4 RESULTS

4.4.1 EVALUATION OF CELL DEATH PROTEINS PRESENT IN THE HUMAN KIDNEY

To confirm that the strategies of targeting cell death mechanisms in the mouse model are comparable to the human kidney an exploration of the specific proteins observed to be expressed was performed using the data available from the Human Protein Atlas. A list of commonly associated cell death proteins were queried through the database for expression level in both the Renal Glomeruli, and the Tubules [Sic, non-specific]. Data were also collated for heart tissue, due to the energetic similarities between renal and cardiac tissue, and the high mitochondrial content in both organs. Results revealed that Bax, Bak, and most other Bcl-2 family proteins, were expressed in the renal tubules. Further, Bcl-2 family proteins, and most of the Caspase family proteins, were highly expressed in renal tubules and generally higher than that observed in either glomeruli or cardiac tissue. These data confirm that an investigation into the role of these proteins and cell death pathways in the diabetic kidney will be biologically relevant.

4.4.2 CHARACTERISATION OF THE BAK/BAX/SGLT2 CRE GENETIC MODEL

To enable a detailed understanding of the role of Bax and Bak in DKD, a novel, proximal tubule specific, double knock out mouse model was developed. A colony of mixed background mice was generated by crossing two mouse stains:

Bak1 KO/Bax $^{fl/fl}$ (mixed 129 background) x Sglt2-Cre (DBA/2; C57BL/6 background)

Mice were bred to include heterozygous expression of wild type Bax$^{+/+}$, wild type Bak$^{+/+}$, wild type Sglt2 (Cre negative), and modified the genes: Bax $^{fl/fl}$, Bak $^{-/-}$, and Sglt2 promoted Cre recombinase (Cre $^{+}$) expressing mice. The mice were interbred for 3 generations to produce heterozygous mice, before strategic breeding pairs were established to generate experimental animals with the required genotypes. To characterise this genetic model of (non-STZ treated) Bax and Bak deletion, tissue from 12 animals, with variable expression of the above genes, were collected.

As the Bak $^{-/-}$ Bax $^{fl/fl}$ Sglt-2 $^{+/+}$ Cre $^{+}$ mouse is a novel mouse strain, an analysis of gene and protein expression was performed to confirm that the model was successfully generated. First, the global deletion of Bak1 was confirmed by western blot. Tissue from liver, heart and kidney were

tested for Bak protein expression in six mice with various genotypes. Results for each mouse were consistent with reported genotypes, as expected. Representative results comparing a mouse with WT expression (**A**: Bak $^{+/-}$ Bax$^{+/+}$ Sglt-2 $^{+/+}$ Cre $^{-}$) to a Bax/Bak double knock out (DKO) mouse (**B**: Bak $^{-/-}$ Bax $^{fl/fl}$ Sglt2 $^{+/+}$ Cre^{+}) are presented in ***Figure 4.1***. Here, Bak protein was detected in all tissues for the WT expressing mouse, but not in the DKO mouse, confirming that Bak1 deletion had occurred.

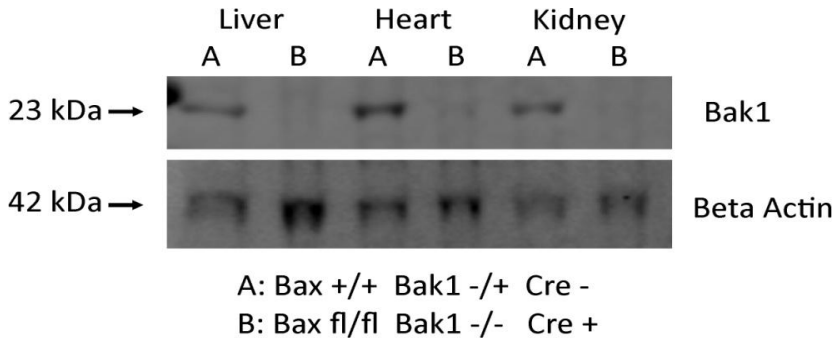

Figure 4.1 Western blot for Bak1 protein expression. *Bak1 deletion was confirmed by western blot comparing: (**A**) a mouse expressing WT proteins (with heterozygous Bak1), to (**B**) the Bax/Bak DKO mouse. Bak1 expression was present in the Bak$^{+/-}$ mouse, but absent from the Bak$^{-/-}$ mouse in all tissue examined. Data are representative of n=6 mice analysed over 3 independent blots.*

Next, the expression of WT Bax protein was determined. To do so, a number of techniques were employed, due to the complexity of the Cre conditional deletion of Bax in the renal tissue. Initial analysis examined whether the presence of the floxed tags allowed normal Bax protein to be expressed. As the genetic knock out is conditional on the expression of Sglt2, tissue from liver, heart and renal cortex were compared. Representative results for three of these mice are presented in ***Figure 4.2***. All three are of the Bax $^{fl/fl}$ genotype, with either positive (Bax KO) or negative (Bax WT) Cre expression. Expression of normal Bax protein was confirmed to be present in the renal cortex of Bax $^{fl/fl}$ Cre^{+} mice as indicated by western blot. However, an additional protein band was present across all samples at ~23kDa, which may represent an additional splice variant of the Bax protein. Exploration of splice variants is beyond the scope of this study. These data demonstrate that the presence of the floxed cassette still allowed normal expression of the Bax protein.

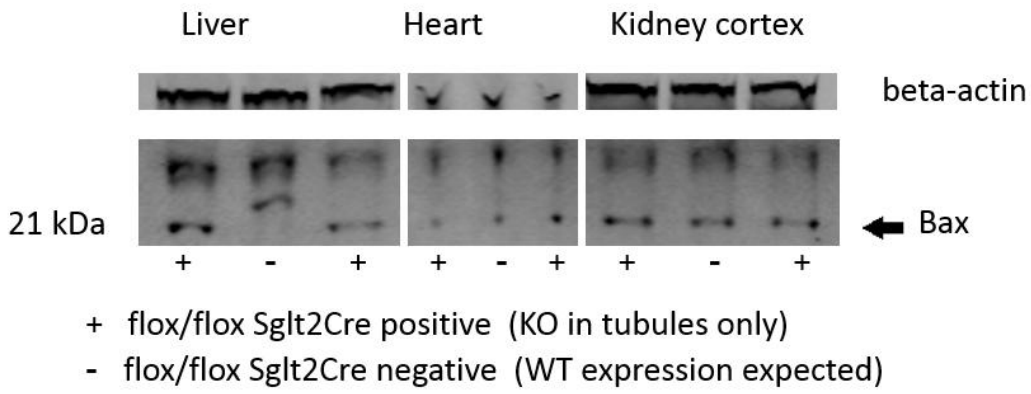

Figure 4.2 Western blot for Bax protein expression. *Bax protein expression was analysed and found to be expressed in liver, heart and whole kidney cortex extracts. This indicates that the Cre – Lox system did not interfere with the normal expression of the protein. Although the proximal tubules are present in the whole kidney cortex the presence in other cell types masks any absence here.*

(Full blot presented in Appendix 4.1)

The kidney is a heterogeneous organ with many different cell populations expected to express normal Bax protein. The proximal tubule cells expressing Sglt2 represent only a portion of the total renal mass. As such, the reduction of Bax expression following Sglt2 promoted Cre-recombinase deletion may be difficult to qualify using western blotting, and can only give an overall indication of protein expression. The insertion of the floxed tags of the Cre-Lox system are located in the non-coding region of the Bax gene. Thus, DNA bands from Bax $^{fl/fl}$ mice will be slightly heavier than those with Bax $^{+/+}$. An analysis of gene length will allow confirmation of the presence of the floxed cassettes, as well as determining if successful excision of the Bax gene has occurred. To confirm that this PCR amplification was performed using primers flanking exon 1 (forward) and within exon 5 (reverse) of the bax gene. As the deletion of exons 2-4 occurs, a smaller gene product in successful generated KO mice was expected. Electrophoresis of renal cortex DNA revealed that the KO mice did indeed have a smaller sized product at ~1.8kB, whilst the WT mice had a single band of ~3.5kB (***Figure 4.2***). The presence of this smaller band was only detected in the Bax $^{fl/fl}$ Cre $^{+}$ mice, and not in the Bax $^{fl/fl}$ Cre $^{-}$ (negative) mice, providing evidence for the success of the conditional KO model. Further, in the Bax $^{fl/fl}$ KO mice, the presence of the floxed cassette is inferred by the slightly increased band size compared with the WT Bax $^{+/+}$ mice. However, in addition to the expected Bax gene bands, data also revealed a band of aproximately ~1.0kB of unknown origin that was also amplified in this PCR

reaction. Both the unknown ~1.0kB band, and the ~1.8kB Bax KO band, were dissected from the gel and prepared for Sanger sequencing.

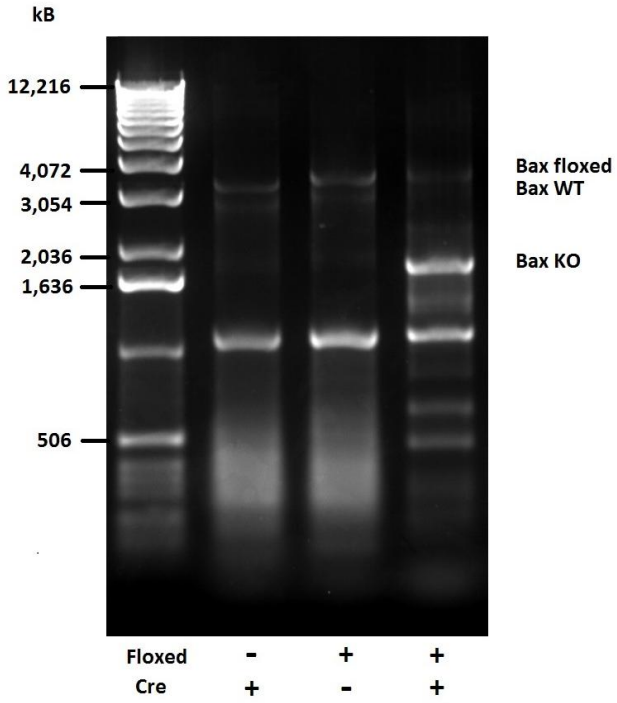

Figure 4.3 Gel was probed for the Bax gene sequence. *Band at ~3.5kB is the Bax gene with the floxed gene migrating slightly higher due to the presence of the floxed cassette. The band around 1.8kB is the Bax KO gene sequence. PCR bands were confirmed by Sanger sequencing. Unknown band at ~1.0kB was identified as Dynein. DNA size ladder is reported in figure as total number of bases.*

SEQUENCING OF BAX KO GENE

PCR bands obtained in the electrophoresis experiment were dissected and sequenced to confirm the genetic deletion of the Bax gene in Sglt2-Cre expressing mice. Sanger sequencing of amplified DNA was performed by Micromon platform facility at Monash University (Clayton, AU). Sequence reads were performed on the PCR product of ~1.8kB (expected Bax KO band) to confirm the deletion of exons 2-4.

Forward and Reverse primer sequences of the band at ~1.8kB were aligned with the reference mouse genome and plotted against the full mouse Bax gene to determine if the conditional KO was successful. (Full sequence and alignment provided in Appendix 4.1) Alignment results revealed that exons 2, 3 and 4 were successfully excised.

Additionally, the unknown PCR product band at ~1.0kB was also analysed to determine its identity. The unknown band produced during the PCR amplification step in Figure 4.3 was aligned with sections of the Dynein gene, downstream of the forward primer. The upstream sequence from the reverse primer was of low confidence, and did not align with any sequence. This sequence was also high in repeating TTT and AAA base repeats, which may indicate that this was an artefact, rather than a complete alignment with the Dynein gene.

4.4.3 CHARACTERISATION OF DIABETES DEVELOPMENT IN THE BAX/BAX KO MICE

The previous chapter explored the progression of DKD and mitochondrial dysfunction in the early progression of STZ induced DKD. In the time-course model presented there, the development of overt nephropathy was minimal by 16 weeks of age. Thus, this study aimed to explores the progression of DKD in a more advanced model of injury. In this study the time period was extended to 24 weeks of STZ induced diabetes. This is also the first study examining the extent of DKD in the Bax/Bak proximal tubular KO mouse model, so the extent of renal injury was unknown.

After 24 weeks of STZ induced diabetes, mice were culled and assessed for phenotypic changes associated with diabetic complications. Statistical differences between CIT control and STZ diabetic mice were analysed by Two-way ANOVA. To compare genotype associated changes, all genotypes were analysed with Bonferroni post hoc test (simple effects) following a significant ($P<0.05$) F-test for genotype and diabetes status. Statistical testing results for all data are included in ***Appendix 4.1***.

EXCLUSION OF NON-DIABETIC MICE

Treatment with the pancreatic β-cell toxin, streptozotocin (STZ) induces diabetes in >90% of male mice; however, this can be dependent on the mouse strain (322). All mice allocated to this study were assessed for body weight and blood glucose weekly, to ensure that each mouse had sufficiently developed diabetes. This was confirmed by the development of persistent hyperglycaemia (>20mmol/L) measured by random spot glucose measurements performed weekly. HbA_{1C} was also measured as an estimate of long term hyperglycaemia. Any mouse which did not meet the glucose criteria (<20mmol/L for 3+ weeks) and had a low HbA_{1C} (<25mmol/mol) were excluded from the final analysis. Through the duration of the study this resulted in the exclusion of eight mice (***Table 4.2***). Of

these eight mice, 7 out of 39 mice (17.9%) were from Bak1 negative mice, compared with 1/41 (2.4%) for Bak1 WT expressing mice, or 8/81 (9.9%) overall. However, most Bak1 deficient mice did develop fulminant and persistent hyperglycaemia.

An additional 10 mice were excluded due to illness, and either culled before endpoint in accordance with ethical guidelines, or excluded due to significant pathology (i.e hydronephrosis, tumour growth) likely not related to diabetes. All remaining mice were included where data was available.

Table 4.2 Total number of mice excluded from study of DKD at 24 weeks of diabetes

		WT	Cre $^{+}$	Bak $^{-/-}$	Bax $^{fl/fl}$ Cre $^{+}$	Bak $^{-/-}$ Bax $^{fl/fl}$ Cre $^{+}$
Total allocated	**CIT**	6	23	15	8	22
	STZ	10	21	15	11	24
Excluded due to illness	**CIT**	0	2	0	0	0
	STZ	1	4	0	3	2
Excluded for poor diabetes development	**CIT**	0	0	0	0	0
	STZ	1	0	4	0	3
Total used for analysis	**CIT**	6	21	15	8	22
	STZ	8	17	11	8	19

Note: CIT = control; STZ = diabetic. WT = wildtype; Cre $^{+}$ = Sglt2 Cre-recombinase control; Bak $^{-/-}$ = Bak SKO; Bax $^{fl/fl}$ Cre $^{+}$= Bax SKO; Bak $^{-/-}$ Bax $^{fl/fl}$ Cre $^{+}$ = Bax/Bak DKO

BLOOD GLUCOSE

Blood glucose levels were measured weekly using random (non-fasted) spot testing. These data show that STZ treated mice developed hyperglycaemia consistent with the development of diabetes, and that deletion of Bax and/or Bak did not alter this metabolic consequence of STZ injections (***Figure 4.4***).

To estimate long term glucose control, $HbA1_C$ levels were measured in whole blood from samples collected at endpoint. As CIT vehicle control mice remain euglycaemic, only a subset of these non-diabetic control mice were tested to confirm relative $HbA1_C$ levels. All STZ diabetic mice were tested where adequate samples were available. STZ diabetic mice had elevated $HbA1_C$, consistent with prolonged hyperglycaemia, compared with the non-diabetic CIT control mice which had low levels of HbA_{1C}, as expected (***Figure 4.5***). These results were also unchanged among the various genetic groups.

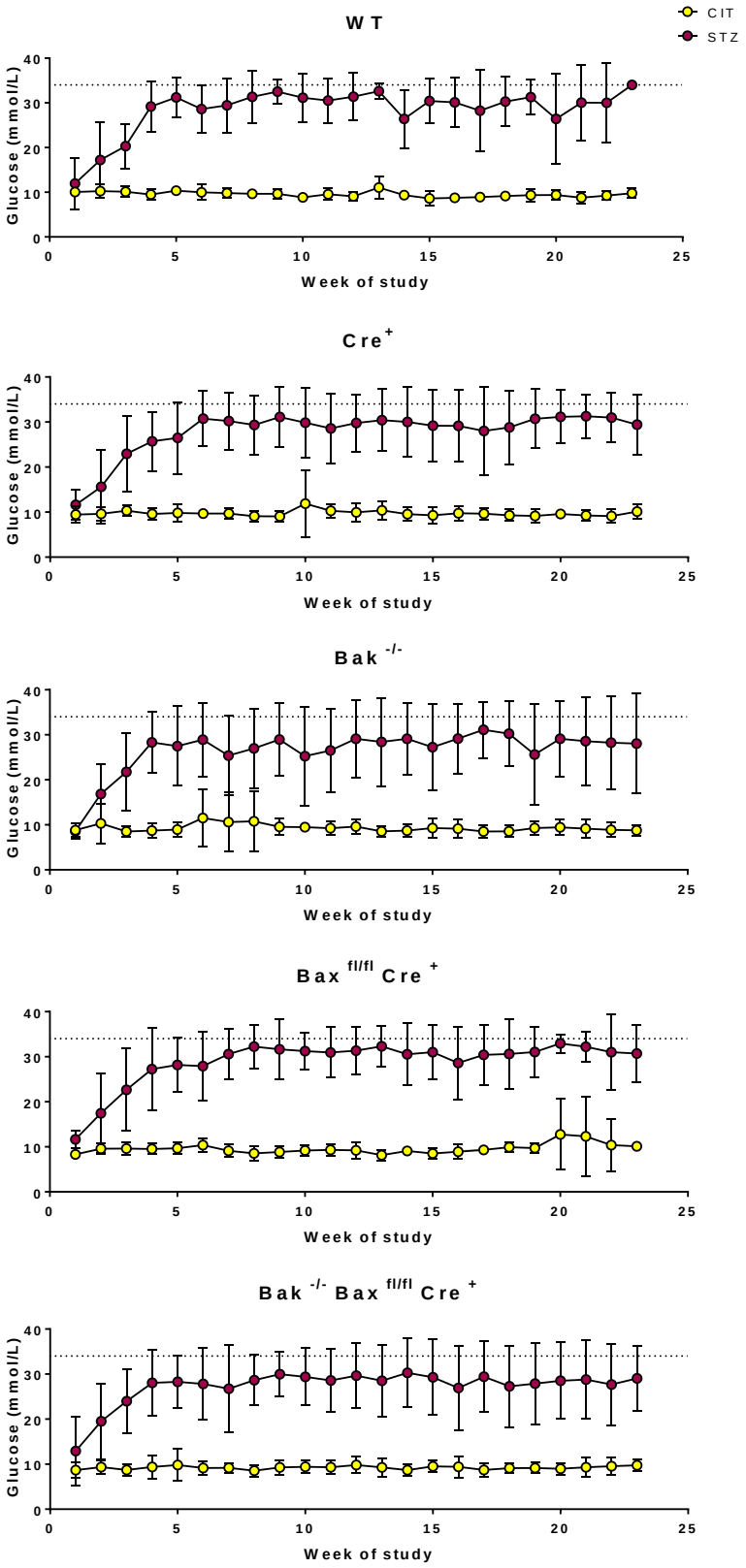

Figure 4.4 Weekly blood glucose monitoring. *All mice were assessed weekly to monitor blood glucose levels. Random spot testing was performed using an Accu-check meter with a maximum limit of detection of 34mmol/L (dotted line). Graphs show mean ±SD for n=6-22 per group.*

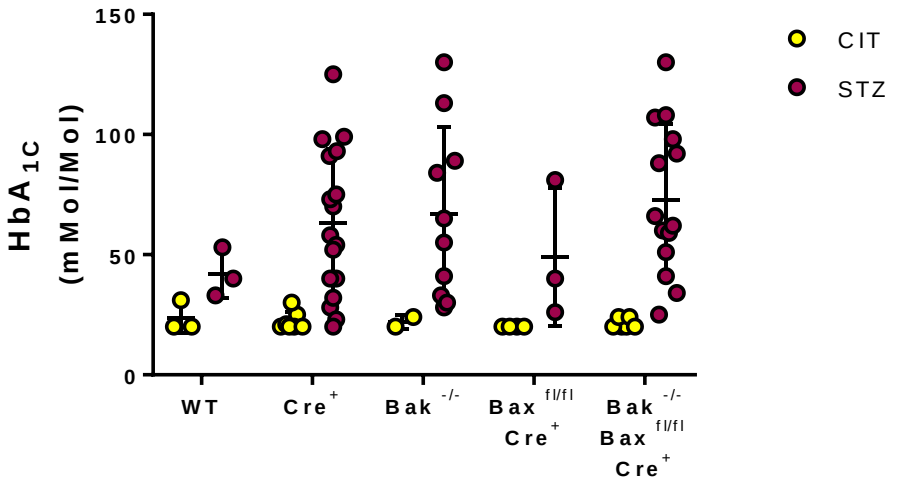

Figure 4.5 HbA_{1C} was elevated in STZ diabetic mice. *Blood samples at endpoint were used to determine glycated haemoglobin (HbA_{1C}). Graph shows mean ±SD for STZ diabetic mice (n=3-18 per group), and a subset of CIT control mice (n=3-6 per group).*

METABOLIC CAGING

Following confirmation that the deletion of the Bax gene in Sglt2 expressing cells was occurring in the $Bax^{fl/fl}$ Sglt2 Cre mouse model, metabolic caging was performed in order to determine 24 hr food and water intake, as well as urine output. This was to ensure that the renal function of these mice is unaltered by the presence of the Cre-cassette in the Sglt2 gene. To achieve this, measurements were taken at both midpoint (12 weeks) and within one week of the endpoint (23 weeks) of STZ diabetes (***Table 4.3***). No difference was found between all non-diabetic CIT control groups at either 12 or 23 weeks. As expected, STZ diabetes was associated with the development of polydipsia, polyphagia and polyuria, with total volumes of water and food intake, and urine volume, significantly increased when compared with the CIT controls. Deletion of Bax and Bak in the renal PTCs did not result in any statistically significant change in these diabetes associated markers.

Table 4.3 24 hour Metabolic caging data

		WT	Cre $^{+}$	Bak $^{-/-}$	Bax $^{fl/fl}$ Cre $^{+}$	Bak $^{-/-}$ Bax $^{fl/fl}$ Cre $^{+}$
Midpoint - 12 weeks						
n	**CIT**	6	22	15	8	22
	STZ	10	17	11	8	19
Water intake (mL)	**CIT**	6.1 ±3.9	6.2 ±4.2	5.1 ±3.0	3.4 ±1.4	4.9 ±2.3
	STZ	19.2 ±9.0 ****	19.9 ±7.2 ****	20.3 ±5.1 ****	20.2 ±7.1 ****	16.8 ±7.8 ****
Food intake (g)	**CIT**	2.1 ±1.1	2.1 ±0.8	3.0 ±0.6	2.0 ±0.3	2.8 ±1.1
	STZ	4.2 ±1.4 ****	4.7 ±0.7 ****	4.4 ±0.7 ***	5.2 ±1.0 ****	4.2 ±0.9 ****
Urine volume (mL)	**CIT**	1.6 ±0.5	0.9 ±0.6	1.2 ±0.9	1.5 ±0.9	1.2 ±0.8
	STZ	14.9 ±8.8 ****	16.6 ±9.1 ****	12.8 ±7.2 ****	15.7 ±7.8 ****	11.6 ±7.7 ****
Endpoint - 23 weeks						
n	**CIT**	6	20	15	7	22
	STZ	6	17	11	7	22
Water intake (mL)	**CIT**	2.7 ±1.2	4.0 ±2.2	5.8 ±3.3	5.0 ±3.7	5.0 ±2.6
	STZ	28.1 ±7.0 ****	25.2 ±9.3 ****	23.8 ±5.4 ****	25.1 ±8.6 ****	20.1 ±9.6 ****
Food intake (g)	**CIT**	2.2 ±0.8	2.2 ±0.9	2.8 ±1.3	2.5 ±0.6	2.9 ±1.3
	STZ	5.9 ±1.0 ****	5.1 ±1.2 ****	4.7 ±1.3 ***	5.9 ±0.9 ****	4.7 ±1.5 ****
Urine volume (mL)	**CIT**	0.9 ±0.3	1.2 ±0.7	1.9 ±1.1	1.6 ±0.9	1.8 ±1.7
	STZ	23.5 ±6.2 ****	21.5 ±11.2 ****	17.5 ±8.0 ****	18.4 ±8.6 ****	15.3 ±9.1 ****

Note: Two-way ANOVA with Bonferroni post hoc test comparing CIT vs STZ was performed. **P*<0.05, ***P*<0.01, ****P*<0.001, *****P*<0.0001.

CULL PARAMETERS

Body weight, blood glucose, and selected organ weights were recorded at endpoint (***Table 4.4***). Body weight was significantly decreased in STZ diabetic mice compared with non-diabetic CIT controls. Genetic group did not influence body weight with no difference between the DKO group and genetic controls. Hyperglycaemia assessed at endpoint also revealed no difference between genetic groups. Increased kidney weight can indicate the development of diabetes associated renal hypertrophy, however no diabetes associated increase in individual gross kidney weights was observed comparing CIT vs STZ mice for any group except the WT genetic group. In this group WT STZ mice had a significant increase in right kidney mass compared with WT CIT controls. Heart mass, and liver mass were also compared. Diabetes was associated with a decrease in total heart mass in all groups except the WT controls. Comparatively, an increase in cardiac left ventricular mass was only observed in the Bak and Bax SKO groups, and the DKO group. Some interaction between genotype and diabetes was found by Two-way ANOVA. Liver mass was unchanged with diabetes status, and differences between genetic groups were not statistically significant.

Overall, few significant differences in diabetes associated phenotype were present between genetic groups, with no obvious effect occurring with deletion of Bax and Bak in this mouse model of DKD.

Table 4.4 Endpoint phenotypic measurements

		WT	Cre $^{+}$	Bak $^{-/-}$	Bax $^{fl/fl}$ Cre $^{+}$	Bak $^{-/-}$ Bax $^{fl/fl}$ Cre $^{+}$
n	**CIT**	6	21	15	8	22
	STZ	8	17	11	8	22
Body weight (g)	**CIT**	33.0 ±2.9	35.0 ±4.7	31.8 ±3.0	33.3 ±4.2	34.1 ±3.7
	STZ	26.6 ±5.1 *	27.4 ±3.2 ****	26.8 ±3.0 **	23.6 ±2.9 ****	26.8 ±3.8 ****
Endpoint blood glucose (mmol/L)	**CIT**	11.8 ±4.2	11.6 ±6.2	8.9 ±2.4	10.1 ±1.4	9.1 ±2.4
	STZ	27.5 ±6.0 **	27.1 ±9.7 ****	27.1 ±11.0 ****	26.6 ±10.2 ***	26.2 ±11.6 ****
Left kidney ‡ (mg)	**CIT**	191 ±29	213 ±32	202 ±29	209 ±15	228 ±47
	STZ	239 ±28	219 ±28	214 ±46	211 ±28	218 ±31
Right kidney (mg)	**CIT**	193 ±37	215 ±29	227 ±41	222 ±27	231 ±39
	STZ	247 ±29 *	236 ±31 ns	233 ±44 ns	232 ± 25 ns	235 ±34 ns
Heart (mg)	**CIT**	147 ±23	165 ±27	171 ±28	166 ±27	180 ±26
	STZ	139 ±18 ns	140 ±29 *	139 ±27 *	130 ±24 *	143 ±27 ****
Left ventricle (mg)	**CIT**	98 ±11	113 ±15	128 ±20	116 ±18	130 ±22
	STZ	100 ±8 ns	102 ±21 ns	100 ±17 **	87 ±14 *	105 ±22 ***
Liver (g)	**CIT**	1.40 ±0.12	1.44 ±0.21	1.26 ±0.20	1.28 ±0.22	1.25 ±0.17
	STZ	1.35 ±0.29 ns	1.44 ±0.32 ns	1.16 ±0.19 ns	1.21 ±0.18 ns	1.27 ±0.23 ns

Note: Two-way ANOVA with Bonferroni post hoc test comparing CIT vs STZ was performed where *P<0.05, **P<0.01, ***P<0.001, ****P<0.0001.
‡ Left kidney F-test was not significant (F>0.05)

KIDNEY TO BODY WEIGHT RATIO

Kidney to body weight ratio (KW:BW) was calculated from total kidney weight for individual mice. Mean results demonstrate that STZ treatment was associated with a significant increase in KW:BW for diabetic mice of all genotypes, relative to their CIT controls (***Figure 4.6)***, consistent with changes in body weight. No difference in KW:BW ratio between genotypes was found.

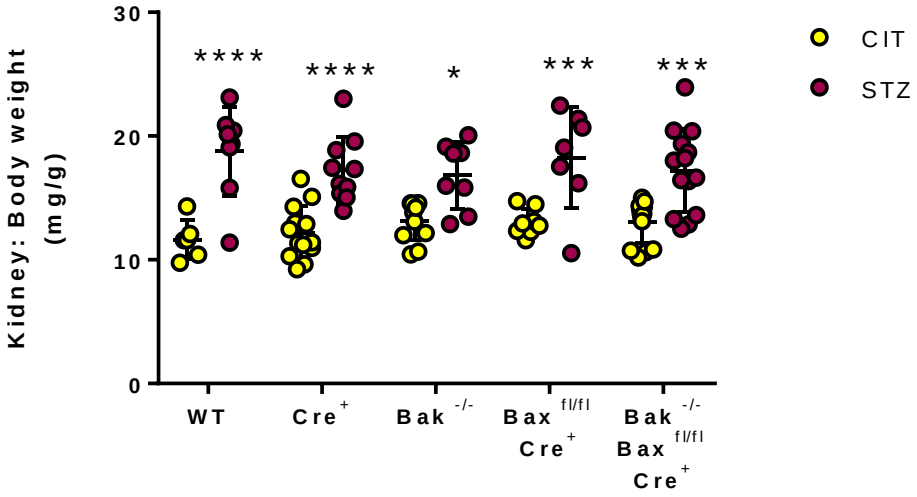

Figure 4.6 Kidney Hypertrophy as assessed by kidney to bodyweight ratio. *Kidney weight was significantly increased in diabetic animals indicative of diabetes associated renal hypertrophy. There was no difference found between genetic groups. Graph shows Mean ±SD. Two-way ANOVA with Bonferroni post hoc test comparing CIT vs STZ was performed where *P<0.05, ***P<0.001, ****P<0.0001. n=6-14 per group.*

ALBUMINURIA

Albuminuria is an indicator of renal damage that occurs in mouse models of diabetes. Urinary albumin excretion, as assessed from 24hr metabolic caging urine at 23 weeks of diabetes, was increased for all diabetic groups, except for the WT group. In the WT mice, the trend was apparent, however this difference was not significant (***Figure 4.7***). No differences between genotypes was found (***Appendix 4.1***). Statistical testing by Two-way ANOVA suggests that an interaction between genotype and diabetes status was present. (Data for this assay were collected by A. Laskowski, and analysed by R. Lindblom)

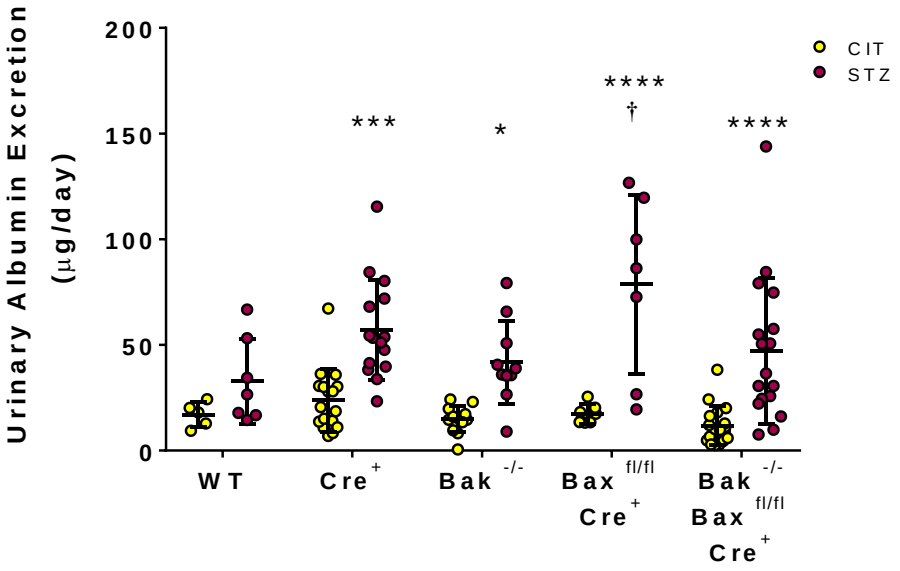

Figure 4.7 Increased 24hr urinary albumin excretion (Albuminuria) developed with STZ diabetes. *Albumin levels were assessed by ELISA on 24hr urine samples collected at 23 weeks of diabetes. Two-way ANOVA with Bonferroni post-hoc test comparing CIT vs STZ *P<0.05; ***P<0.001; ****P<0.0001. Multiple comparison testing between genotypes found Bax$^{fl/fl}$ Cre^{+} were significantly different between all other STZ groups (†P<0.05) except Cre^{+}. No differences between CIT groups was found.*

CYSTATIN C

Cystatin C, as a surrogate marker for glomerular filtration rate, was assessed from plasma samples collected during metabolic cage performed at endpoint (23wks) (***Figure 4.8***). STZ diabetes was associated with a decrease in plasma cystatin C levels, in the Bak$^{-/-}$ and the Bax$^{fl/fl}$ Cre^{+} SKO groups only. No further differences were found.

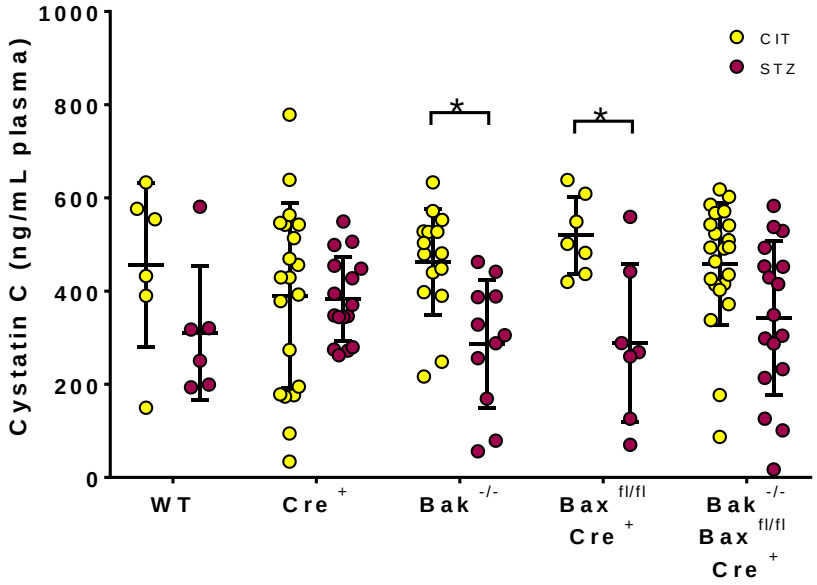

Figure 4.8 Plasma cystatin c. *Cystatin c was measured in plasma samples collected one week before endpoint. Cystatin c was significantly reduced in Bak$^{-/-}$ and Bax$^{fl/fl}$ Cre^{+} STZ mice only. Graphs show mean ±SD. Two-way ANOVA with Bonferroni post hoc test was performed comparing CIT vs STZ where *P<0.05.*

KIM-1

Kidney injury molecule 1 (Kim-1) is a urinary marker that indicates the presence of renal tubular cell related injury. Urine from endpoint metabolic caging revealed that very low levels of the Kim-1 protein were present in both the CIT control and STZ diabetic mice, with no differences amongst genetic control groups (***Figure 4.9***). No statistically significant differences were present between any group.

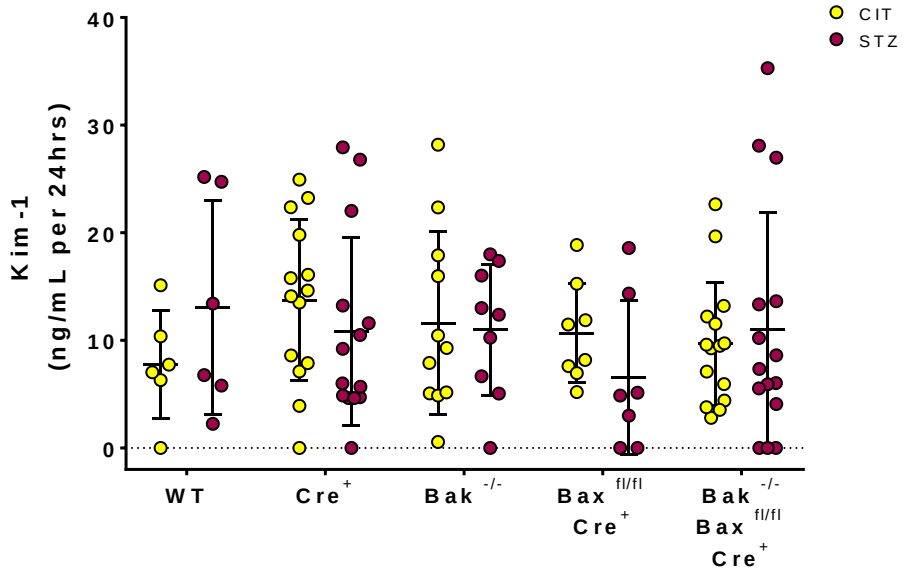

Figure 4.9 Kidney injury molecule-1 was not increased with STZ diabetes. *Kidney injury molecule 1(Kim-1) was detected in low levels only for both CIT control and STZ mice in 24hr urine samples collected after 23 weeks of STZ diabetes. No differences between groups was observed using Two-way ANOVA.*

GLOMERULOSCLEROSIS

Glomerular injury was assessed by examining the increase in mesangial expansion and sclerosis present in Periodic Acid Schiff stained renal cortex. Twenty glomeruli were scored per mouse, and mean scores calculated for each treatment group (***Figure 4.10***). Whilst STZ treated mice did trend toward an increase in GSI, analysis by Two-way ANOVA revealed no statistically significant difference between CIT controls and STZ diabetic mice, nor between genotypes, indicating minimal evidence of glomerulosclerosis after 23 weeks of diabetes. This result was confirmed by an independent assessment by an experienced technician (M. Arnstein).

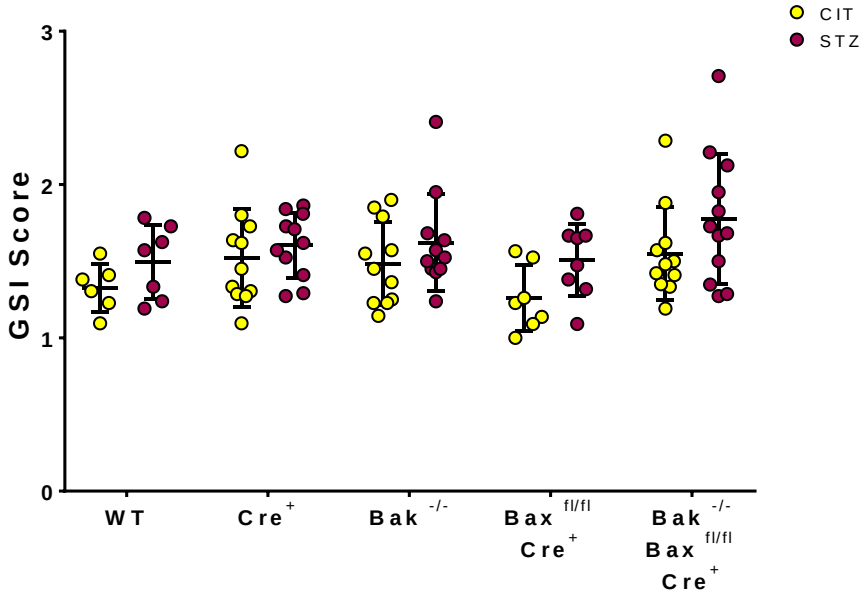

Figure 4.10: Glomerulosclerosis was not significantly increased after 23 weeks of STZ diabetes. *Glomerulosclerosis index (GSI) was assessed in 3µm sections of PAS stained, paraffin embedded kidney, for 20 glomeruli per mouse. Graph shows Mean ±SD for n=6-12 per group. Two-way ANOVA with Bonferroni post hoc test found no significant difference between genotypes, nor between control (CIT) vs diabetic (STZ).*

TUBULAR INJURY

As Sglt2 is expressed in the proximal tubules, an assessment of tubular damage was performed on PAS stained sections. Tubular dilation was variable between groups, however no clear trend was evident and no statistically significant differences between CIT and STZ, or between genotypes was observed (***Figure 4.11A***). Few renal casts were present in STZ mice, with the exception of the Bax $^{fl/fl}$ Cre $^{+}$ group, where there was a significant increase in this parameter compared to the Bax $^{fl/fl}$ Cre $^{+}$ CIT controls (***Figure 4.11B***). Further, in this group this parameter was also significantly increased relative to all other genetic groups of STZ diabetic mice (***Appendix 4.1***). Glycogen accumulation in the proximal tubules was scored, both as intracellular inclusions, and by the presence of glycogenated nuclei. Whole tubules, with glycogen accumulation in all cells, were averaged per field across all images per mouse. Whilst a trend towards an increase in glycogen accumulation was evident in STZ diabetic mice compared with CIT controls, this was not significant for any groups except the DKO Bak $^{-/-}$ Bax $^{fl/fl}$ Cre $^{+}$ mice (***Figure 4.11C***). The number of glycogenated nuclei was significantly increased in both WT and Cre + STZ diabetic mice, when compared to their CIT controls. STZ mice of the KO groups also trended toward an increase in this parameter (***Figure 4.11D***). Further, the Cre $^{+}$ group had significantly more glycogenated nuclei relative to all other genetic groups of STZ diabetic mice (***Appendix 4.1***). These results suggests that Bax and Bak may affect the link between diabetes and glycogenated nuclei.

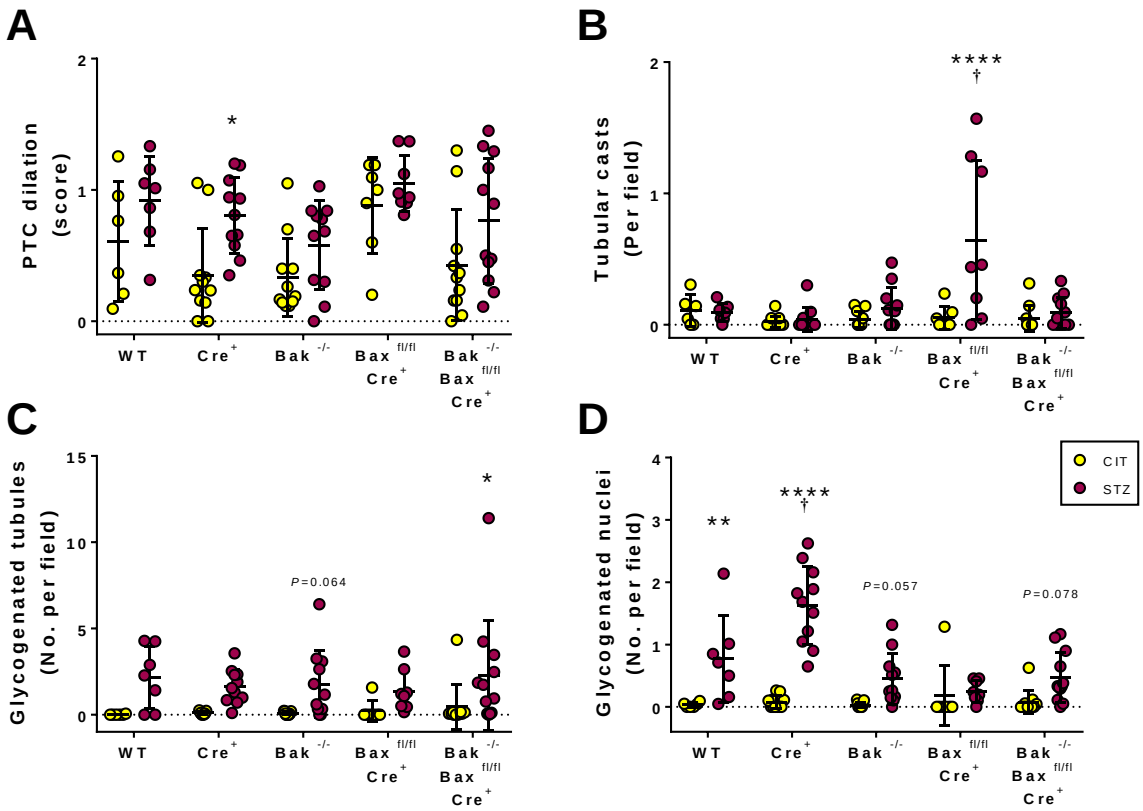

Figure 4.11: Tubular damage in STZ diabetic mice. *Tubular injury was assessed in sections of PAS stained renal cortex, and scored across 15-17 images per mouse at x200 magnification. Tubular damage was scored by: (**A**) proximal tubular dilation; and (**B**) the presence of tubular casts. Data were averaged per image field at x20 magnification Additionally glycogen deposition was assessed by: (**C**) Number of whole tubules where all visible cells had deposited glycogen; (**D**) Number of Glycognenated nuclei per field. Graphs show mean ±SD for n=6-12 per group. Two-way ANOVA with Bonferroni post hoc test comparing CIT vs STZ was performed where *P<0.05, **P<0.01, ****P<0.0001. † represents a significant (P<0.05) difference between one genetic group relative to all other genetic groups within its family.*

4.4.4 MITOCHONDRIAL FUNCTION

CITRATE SYNTHASE

Citrate synthase, as a measure of mitochondrial quality in isolated mitochondrial preparations, was assessed to determine if diabetes was associated with any change. These data indicate similar levels of citrate synthase were present across all groups for both CIT and STZ mice, demonstrating that diabetes was not associated with a change in total enzyme level per gram of isolated mitochondria (***Figure 4.12***). Genotype did not affect the levels of citrate synthase.

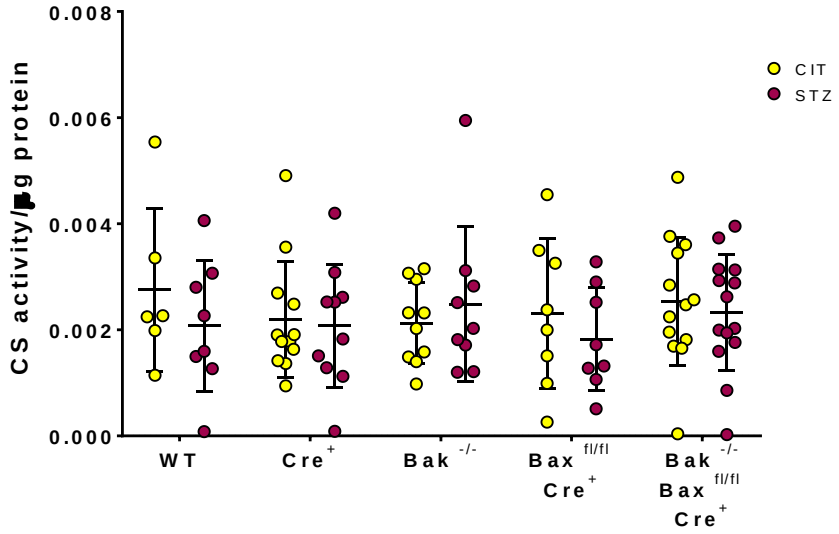

Figure 4.12 Citrate synthase activity of isolated renal mitochondria. *Citrate synthase activity was measured using a colorimetric assay linked to the metabolism of oxaloacetate through the citrate synthase enzyme. Graphs show the background corrected enzymatic rate using linear regression, with mean and ±SD shown. n=6-14 per group.*

COMPLEX I MEDIATED OXYGEN CONSUMPTION RATE

Oxygen consumption rate (OCR) of isolated renal cortex mitochondria was assessed using the Seahorse 96-well Bioanalyzer. Complex I activity was stimulated using glutamate and malate substrates (basal respiration) followed by the addition of ADP. As OCR was very high in some samples, and ADP reserves were depleted over the course of the three-minute measurement, the maximal value for OCR was used to calculate ADP linked, State 3 respiration (ADP Max). State 4 respiration was induced by the addition of oligomycin (Oligo) followed by State 3u by the presence of the uncoupling agent FCCP. Finally, Antimycin-A (Anti-A) was used to inhibit complex IV. Overall, OCR for diabetic animals trended towards an increase in respiration rate in all groups relative to the CIT controls, for all substrates, except the Bax$^{fl/fl}$ Cre^{+} SKO group (***Figure 4.13A***). When data were normalised to baseline (Basal) respiration, this effect mostly disappeared with OCR closely matching that of genetic CIT controls. Whilst no statistically significant difference was found between CIT and STZ mice, the STZ Bak$^{-/-}$ SKO group was the only genotype where this trend persisted for ADP stimulated OCR (***Figure 4.13B***).

Values for State 3 (ADP stimulated) and State 4 (oligomycin stimulated) OCR were then used to calculate the rate of ATP production (= State 3 - 4), proton leak (state 4 - Antimycin A), and the respiratory control ratio (RCR - State 3/4) for each individual mouse. Mean ATP production for WT and Cre^{+} genetic groups trended toward an increase in ATP production for STZ diabetic mice in the raw values (***Figure 4.14A***). This result for the WT group should be interpreted with caution due to the low *n* number, as data from only 2 mice were available for this group. When values were normalised to basal respiration, however, this trend disappeared, indicating that genotype had no overall effect on the relative percentage of OCR with each compound (***Figure 4.14B***). A similar pattern was observed for proton leak, where the trend towards an increase in CIT vs STZ was observed for WT (P=0.067) and Cre^{+} (P=0.082) groups (***Figure 4.14C***). When values were normalised to baseline respiration, this effect size reduced. Spare respiratory capacity is calculated as the difference between ADP stimulated and FCCP stimulated respiration rate. For the renal mitochondria in this study OCR was lower in the FCCP response following oligomycin than the ADP stimulated response (***Figure 4.14E***). The percentage decrease was equal to a decline of between 30 and 60% depending on genotype, although these data were variable between groups. Respiratory control ratio was also calculated and was found to be unchanged between CIT and STZ (***Figure 4.14G***). Few differences between

genotypes were found for any of these parameter of mitochondrial respiration (***Appendix 4.1***). Although there were some statistical changes between genotypes (see ***Appendix 4.1***), no discernible change due to deletion of Bax and Bak were observed.

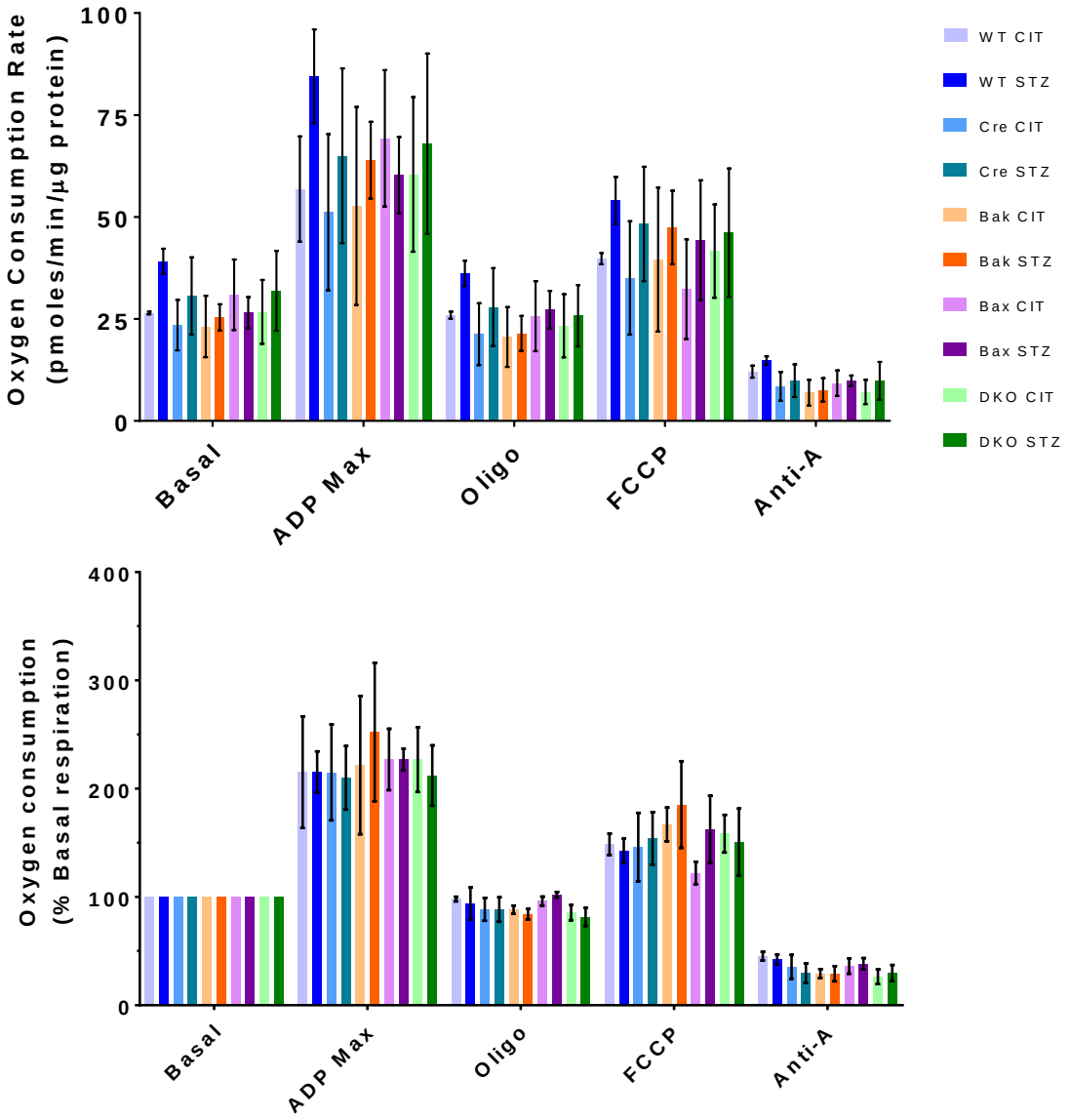

Figure 4.13 Mitochondrial stress test. *Mitochondria isolated from the renal cortex of Bax/Bak DKO mice. OCR was measured in mitochondrial preparations at 37°C (Basal), and then assessed in response to sequential injections of ADP (ADP Max), Oligomycin (Oligo), Carbonyl cyanide-4 (trifluoromethoxy) phenylhydrazone (FCCP) and Antimycin A (Anti-A). Graphs show mean ±SD for n=3-9 per group*

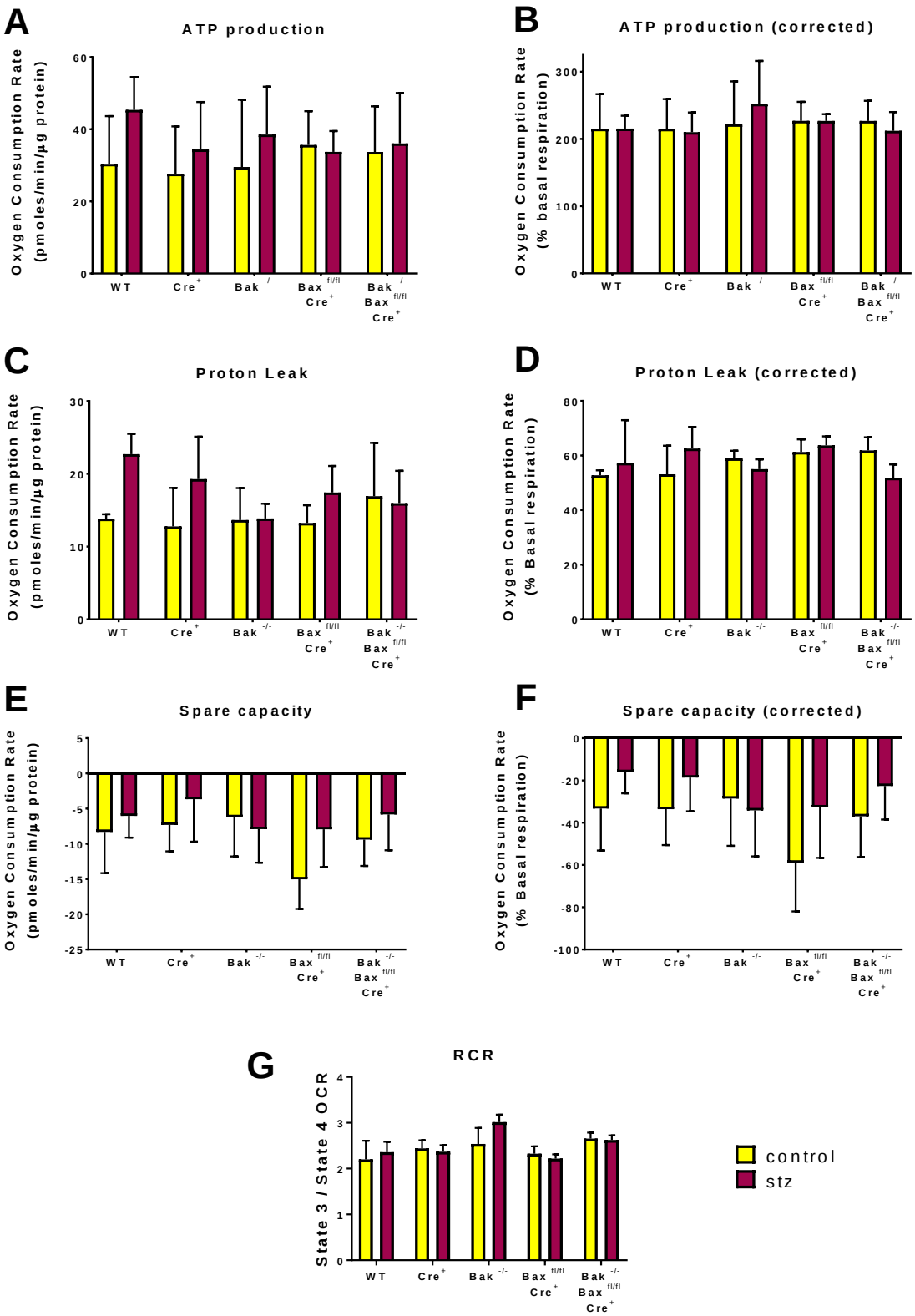

Figure 4.14 ATP production, proton leak and respiratory control ratio. *(**A**) ATP production; (**B**) baseline normalised ATP production; (**C**) Proton leak; (**D**) baseline normalised proton leak; (**E**) Spare capacity; (**F**) baseline normalised spare capacity (**G**) Respiratory control ratio. Graphs show mean ±SD for n=4-11 per group, (except WT CIT: n=2). Analysis by Two-way ANOVA with Bonferroni post hoc test comparing CIT vs STZ.*

MITOCHONDRIAL SWELLING

To assess the propensity for mitochondria to undergo swelling in response to injury, a calcium challenge was performed. This process involves measuring the change in absorbance at 540nm of isolated mitochondria in suspension. A calcium challenge was induced by the addition of free calcium ions (200μM) to the suspensions, and following the response for 30 minutes. Data was also collected for mitochondria with no Ca^{2+} added (untreated), and in the presence of the mPTP inhibitor, Cyclosporine A (CsA). Mean relative absorbance rates were calculated from the individual trace results of *n*=3-10 mice per group over seven independent experiments (***Figure 4.15***). Results revealed that all renal mitochondria underwent rapid swelling following the addition of Ca^{2+}. No difference in the mean rate of swelling was found between isolated mitochondria from the renal cortex of vehicle control (CIT) and diabetic (STZ) mice (***Figure 4.16A***). Additionally, no difference was evident between genetic groups. Interestingly, the addition of CsA only minimally inhibited the induction of calcium induced swelling in this study (***Figure 4.16B***). Individual swelling responses are presented in full in Appendix 4.1.

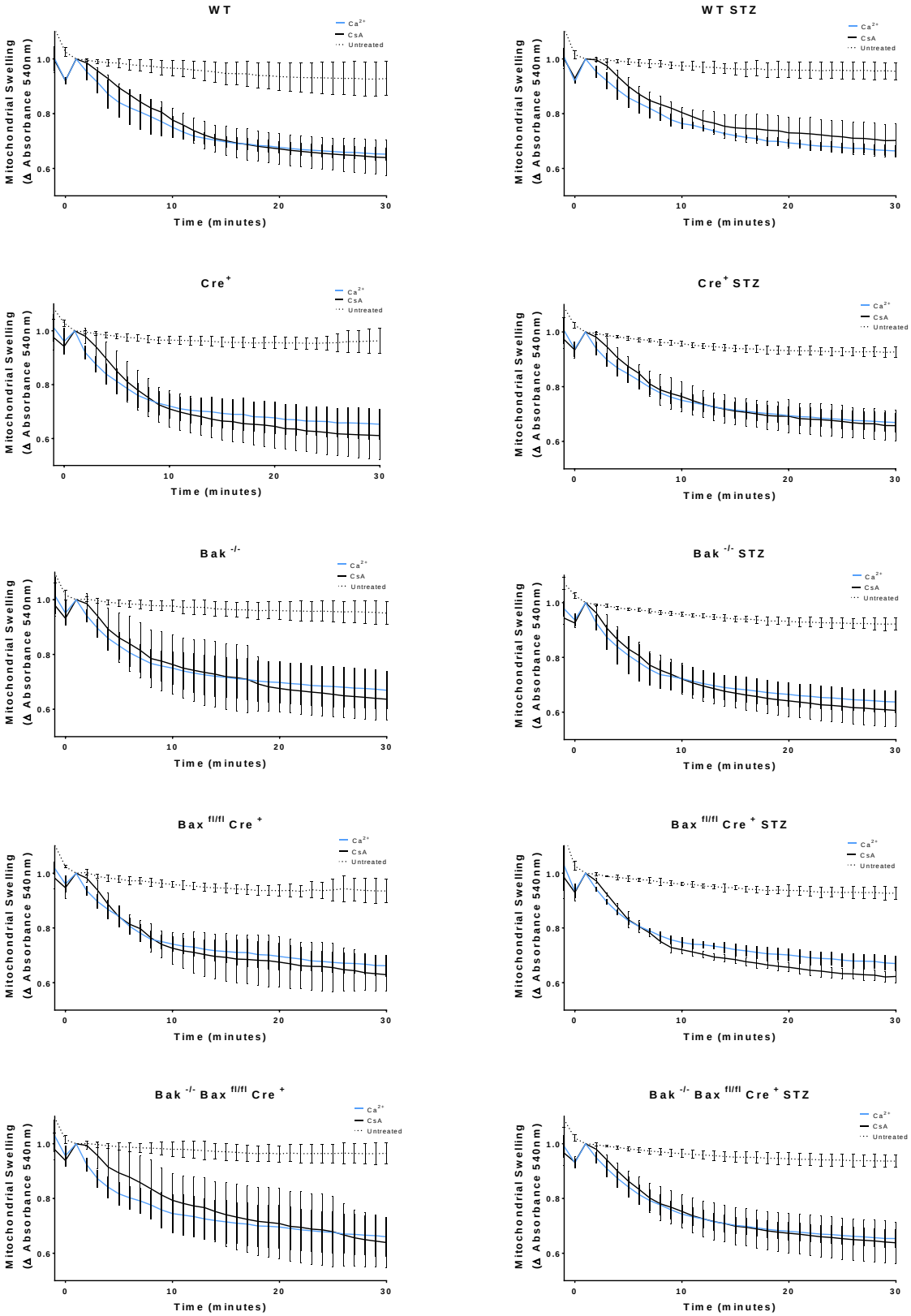

Figure 4.15 Mitochondrial swelling rate was not changed with diabetes. *Swelling response of isolated renal cortex mitochondria was measured via change in absorbance at 540nm, relative to initial optical density, over 30 minutes. Calcium challenge was induced 200μM Calcium (Ca2+) or 200μM Calcium plus Cyclosporine A (CsA), and compared to untreated mitochondria with no calcium (Untreated). Graph shows mean ±SD for n=3-10 mice per group.*

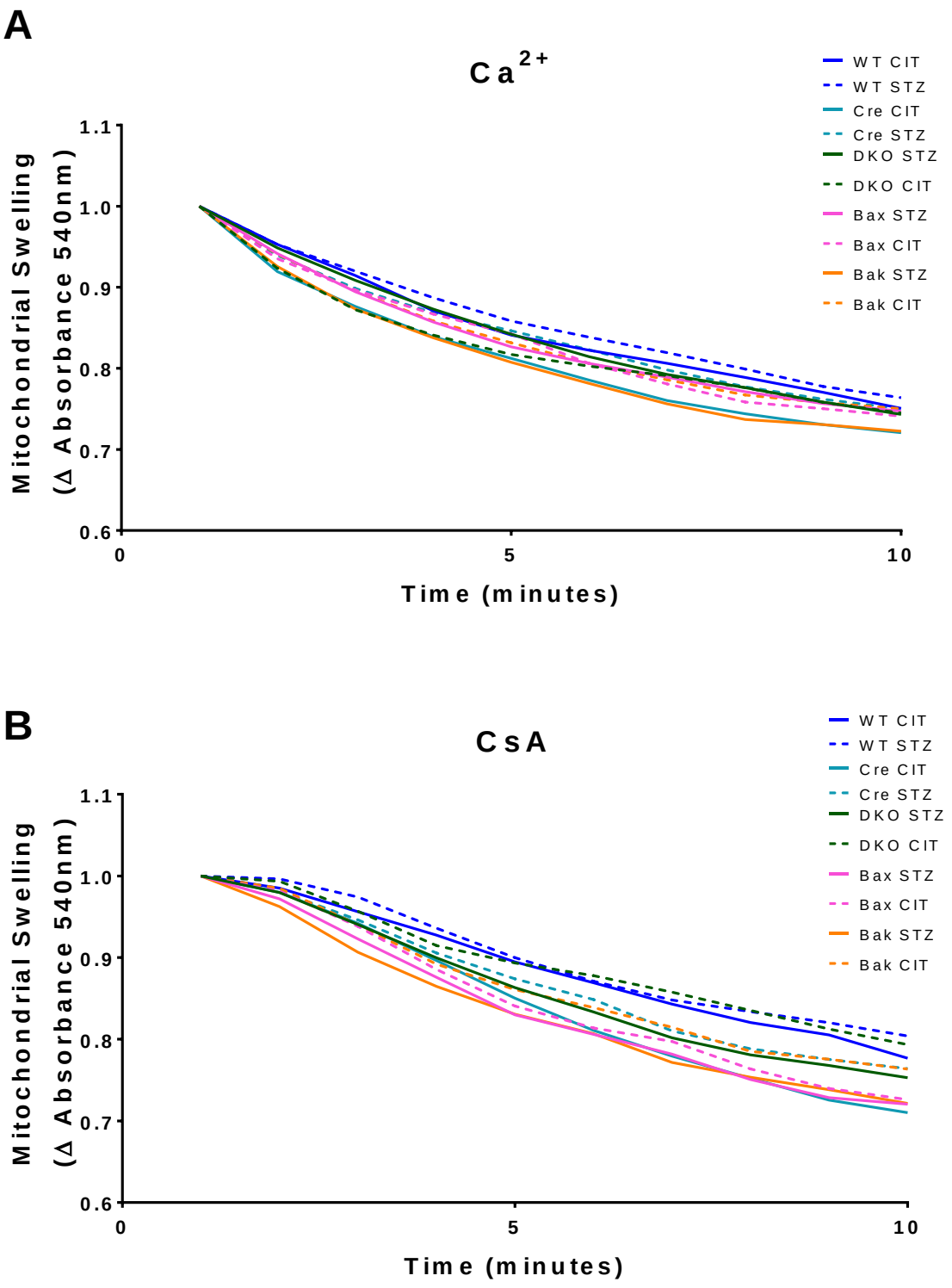

Figure 4.16 Mitochondrial swelling response to calcium challenge. *Swelling response of isolated renal cortex mitochondria was measured via change in absorbance at 540nm. Calcium challenge was induced with (A) 200μM Calcium or (B) 200μM Calcium plus Cyclosporine A (CsA). Graph shows mean ΔAbsorbance, relative to initial optical density, for the first 10 minutes, for n=3-10 mice per group. (SD not shown)*

4.4.5 HYDROGEN PEROXIDE PRODUCTION

Hydrogen peroxide production was estimated in isolated mitochondria via Amplex red H_2O_2-linked assay. No statistically significant difference was found between CIT control and STZ diabetic mice, however a trend towards a decrease may be present when comparing the Bax $^{fl/fl}$ Cre $^{+}$ group and the Bak $^{-/-}$ Bax $^{fl/fl}$ Cre $^{+}$ groups (***Figure 4.17***). Complex II (succinate and rotenone) stimulated H_2O_2 production trended towards a decrease when compared to complex I (glutamate and malate) stimulated production for all genotypes except the WT group. Results for Two-way ANOVA with Bonferroni post hoc test are presented in Appendix 4.1

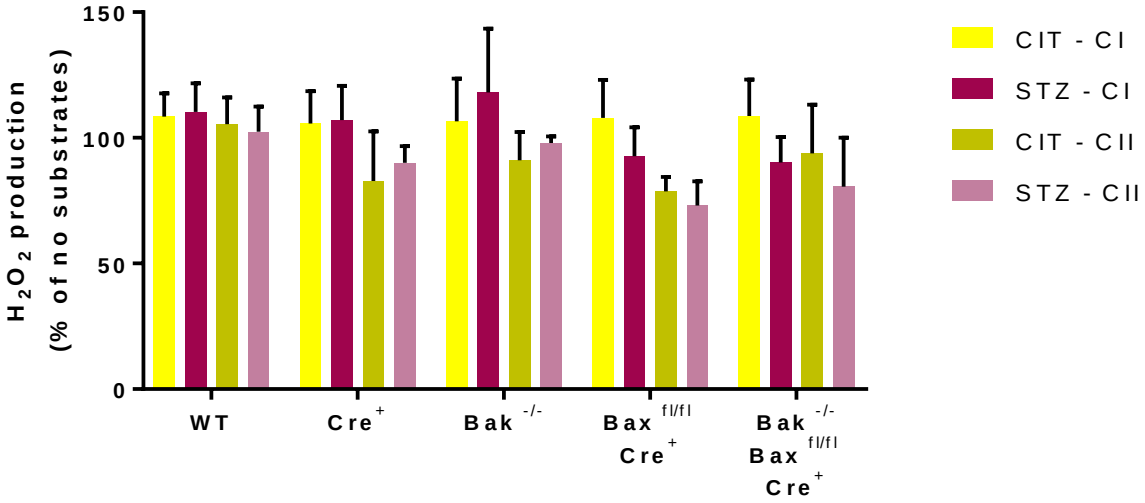

Figure 4.17 Hydrogen peroxide production was unchanged with STZ diabetes. *Rate of hydrogen peroxide (H_2O_2) production, measured via Amplex-red-linked catabolism, comparing CIT control and STZ diabetic mice at 24 weeks of diabetes. Isolated mitochondria were incubated for 30 minutes along with either: complex I (CI); or complex II (CII). Data are expressed relative to the rate of H_2O_2 production with no substrates. Graph shows mean ±SD for n=3-6 per group, except WT with n=2 per group. Analysis by Two-way ANOVA found no difference between CIT and STZ mice.*

4.5 DISCUSSION

In this study, a novel mouse model with a proximal tubule specific double knock out of the mitochondrial pore-forming cell death proteins, Bax and Bak, was successfully generated. Global deletion of Bak1 was confirmed, and the use of an Sglt2 promoted Cre-lox system to delete the Bax gene in renal PTCs was demonstrated. Analysis of protein expression in heart, liver and whole renal cortex found that Bax expression was maintained in the non-target tissue of Bak$^{-/-}$ Bax$^{fl/fl}$ Cre^{+} model. Whilst isolation of individual proximal tubules was not possible, and represents a limitation of this analysis, the presence of both the floxed Bax gene, and the KO gene within the renal homogenate, is consistent with the mixed population of cells within the kidney. This confirmed that allele expression was consistent with genotyping results.

The presence of the Dynein gene band in the PCR gel was unexpected, however the results for the reverse primer sequence suggest that this artefact may be the result of off-target secondary structure self-homology. Given the size and intensity of the band, it is quite possible that competitive binding with the Dynein gene will have obscured amplification of the Bax gene. Whilst the deletion of the Bax gene was clearly evident, quantitation was not possible.

Phenotypic characterisation of the novel proximal tubule specific Bax/Bak DKO mouse model revealed few differences between WT, DKO and the other genetic controls in non-diabetic mice. Indeed, deletion of both Bak and Bax from the renal proximal tubules using the Cre-Lox model was not associated with any overt pathology, nor changes in body weight and organ weights. A trend towards an increase in total kidney weight with deletion of Bak and Bax may have been identified. This trend would be consistent with a reduction in apoptosis of the proximal tubules, however, any difference was not large enough to be confirmed as a real effect. The comparison of kidney to body weight ratio did not find any differences between genotypes.

Loss of functional Sglt2 has previously been demonstrated to lead to polyuria, in the absence of diabetes mellitus, due to osmolytic changes in urine concentration associated with the reduction in glucose reuptake at the apical brush-border of PTCs (90). Further, Sglt2 blockade, induced by pharmacological inhibition is a new strategic therapy used to lower systemic glucose concentrations in patients with diabetes (323). Thus, the use of a transgene embedded within the Sglt2 gene required confirmation that Sglt2 activity was not compromised, and did not confound the results by directly improving various renal parameters. Indeed, renal functional analysis of the Cre positive, Bax SKO

and Bax/Bak DKO mice, revealed no significant increase in 24hr urine volume compared with WT Sglt2 expressing litter mates. Likewise, no change in the severity of polydipsia was found among the various genetic groups. These data provide important evidence that the Sglt2 protein was still able to function as required and that this model is appropriate for the studies of diabetic kidney disease.

One concern with the generation of a mouse model with global deletion of the *Bak1* gene was the possibility that deletion of Bak in the pancreas may interrupt the development of diabetes in response to STZ. In the pancreas, STZ is easily taken up by GLUT 2 expressed on β-cells, as STZ is a glucose analogue. Toxicity is mediated through its alkylating properties causing DNA adduct formation, DNA fragmentation, and activation of oxidative stress responses (291,324). At lower doses, STZ treatment is associated with the engagement of apoptotic pathways, whilst higher doses are more generally associated with necrotic type β-cell death (325). Whilst the exact mechanisms of both autoimmune mediated T1DM, and STZ induced β-cell death, is still being elucidated, a role for Bcl-2 family proteins and the intrinsic apoptotic pathway in their demise, is evident (326). Other studies however suggest that β-cell death is primarily mediated through plasma membrane death-receptor pathways (327). Whilst a detailed analysis of the immunological processes active in this model of STZ diabetes was beyond the scope of this investigation, it is also possible that deletion of Bak may interfere with the activity of immune cells. Bax and Bak are both important regulators of immune cell maturity and differentiation, as well as in the peripheral tissue response to death receptor activation (328,329). Generally, double deletion of both Bak and Bax is associated with an increased susceptibility to the development of autoimmune disease, highlighting the complexity of intrinsic cell death pathways in the development of T1DM (330). Additionally, deficiency of Bak may reduce the effectiveness of Bax activation in forming the MOMP (222). Thus, mice with global deletion of Bak1 may have interrupted MOMP activation in the pancreas. Indeed, results from the novel Bax/Bak DKO mouse model, studied here in this chapter, found that the majority of mice excluded due to poor diabetes development were from the *Bak1* deficient genetic groups (SKO Bak $^{-/-}$; and DKO *Bak* $^{-/-}$ *Bax* $^{fl/fl}$ Cre$^{+)}$. This may suggest a role for Bak in the development of STZ diabetes. However, the parental strain of the *Bak1* $^{-/-}$ *Bax* $^{fl/fl}$ mouse was predominately on a *129* background, which has been demonstrated to be a lower responder to the diabetogenic effect of STZ compared with other common strains, which could also account for this effect (250). Regardless, most of the mice treated with STZ did develop persistent hyperglycaemia. It is also possible that stochastic variation alone accounts for

this discrepancy. Future studies are thus warranted to examine the evidence for such an effect, along with an investigation of the contribution of Bak, and/or Bax in the development of STZ diabetes.

All animals included for final analysis adhered to the strict criteria for the development of diabetes. Any mouse that did not develop persistent hyperglycaemia was excluded, as described. Nevertheless, the Bax/Bak Sglt2-Cre mouse model failed to develop overt renal pathology. Pathological changes were restricted to the development of only mild renal injury after 24 weeks of STZ induced diabetes. Renal hypertrophy was minimal across all groups, with only the WT STZ diabetic mice developing a significant increase in renal mass. This result is interesting, however, as the difference between CIT control WT and DKO animals was +20% for mean kidney mass. Between the DKO CIT vs WT groups, mean kidney mass was identical, with no interaction between genotype and diabetes status reported by two-way ANOVA. Further, values were unchanged between groups when kidney weights were corrected to body weight, indicating a potential variation due to animal size only, particularly as diabetes was also associated with a significant decrease in total body weight. Whilst an increase in total kidney weight could be attributable to absence of Bax and Bak in tissue mass homeostasis, any effect of genotype is unlikely.

STZ treated mice developed polyuria and polydipsia as expected, however, they did not develop significant histological changes in renal morphometry, as determined by evaluation of glomerulosclerotic lesions. Further, the development of diabetes associated urinary albumin excretion was relatively mild. In humans, the excretion of between 30-300µg of protein is classified as microalbuminuria. Indeed, mouse models with higher albumin excretion levels have been reported for STZ diabetes, including in *FVB/N* mice (122). This difference can also be observed by comparing the results in this chapter with those in Chapter 3, section 3.5.3 of this thesis, where urinary albumin levels were much higher than seen here in the Bax/Bak mouse strain. Cystatin C was also mostly unchanged in the Bax/Bak mouse model, although it is unclear whether the decrease observed between Bak and Bax SKO STZ groups is reflective of a general trend, or is specific to these groups. Unfortunately, creatinine clearance data were unavailable, representing a limitation in this study for assessing the role of glomerular hyper filtration in this model.

Tubular injury was also mild in the Bax/Bak Sglt2-cre strain with no increase in the presence of the tubular damage associated marker Kim-1, and minimal variation in the tubular dilation score, between CIT and STZ for all genetic groups. The accumulation of glycogen, as assessed by measuring both glycogenated nuclei and glycogen inclusion bodies, were noted, a phenomenon which has previously been described in the diabetic kidney (331–333). However, a pathological consequence of this phenomenon has not been confirmed. As this study followed mice to 24 weeks of STZ diabetes, the mild renal injury observed in this mouse model (with a mixed genetic background) represents a limitation. It is likely that these mice of mixed genetic background predominantly develop only haemodynamic changes in renal function. Whilst the parent strains, *129*, *DBA* and *C57BL/6* mice have previously been shown to develop good models of renal injury, the lack of injury observed in this mixed background model is a concern (122,251).

As this novel mouse model did not develop overt renal disease, an analysis of mitochondrial function in a more advanced model of STZ induced diabetes was not possible. As such, mitochondrial functional changes with the progression of diabetes is still unclear. Although some trends may be present with mitochondrial oxygen consumption rate (as measured with the Seahorse Bioanalyzer) for WT and Cre groups, no significant difference in the calcium induced mitochondrial swelling assay was found. Hydrogen peroxide production may be reduced with STZ diabetes, as data trended towards a decrease in most genetic groups. However, low *n* number, as a result of experimental limitations and breeding issues, may mean that analyses are underpowered. Overall, limited evidence for changes in mitochondrial function were found in this mouse model. Without demonstrated renal injury these findings are limited in their application to human DKD. These data suggest there are that minimal mitochondrial changes present in the early stages of diabetes associated renal injury.

The genetic backgrounds of inbred mouse strains are known to influence the severity of DKD. Overall, the Bak $^{-/-}$ Bax $^{fl/fl}$ Cre $^{+}$ mouse colony was subject to high intra-assay variation between groups, with few clear results able to be determined. Whilst some trends were evident, many of the results were obscured by the presence of high variation within each genetic group. The mixed background likely accounts for a proportion of the variation observed between groups. The use of multiple genetic control groups allowed a comparison between the multiple alleles within this novel

strain. Indeed, results indicate that the Cre $^{+}$ control group was not entirely consistent with WT mice. This may either be reflective of the different relative percentage of the parent mouse strain between these groups, or indicate that the insertion of Cre-recombinase was not entirely inert. Indeed, the potential for Cre driven off-target effects and toxicity have been reported in other models using Cre-LoxP, emphasizing the importance of Cre only control groups as used here (334). The difficulties in generating the 'WT' and the Bax $^{fl/fl}$ Cre $^{+}$ control groups may also be partially responsible for the degree of inherent variability between groups. Indeed, fewer mice of these genotypes were available for use in the study, leading to a lower *n* number in these two groups. This is most evident within the Bax $^{fl/fl}$ Cre $^{+}$ group, where three of the total number were generated six months after the main cohort of mice. As these mice also had no other groups run in parallel, it is possible that any stochastic variation encountered by these mice affected the overall results. Indeed, it was often observed that these three mice were found to be the outliers during data analysis. For example, the three highest values in the tubular casts graph of the Bax $^{fl/fl}$ Cre $^{+}$ group in figure 4.11B, are these three mice, and may account for this result.

Overall, minimal differences between genotypes demonstrated that under normal conditions the loss of both Bax and Bak in the kidney has minimal impact. However, the significance of the role of Bax and Bak under diabetic conditions remains unclear. As Bax and Bak are particularly important in cell death outcomes, if disease phenotype is insufficient to induce severe cellular stress, any benefit or worsening would not be readily identified. Without overwhelming the cell death response, it is unlikely that markers of apoptosis and other consequences of cellular stress will be noticeably detected. This is because the innate immune system rapidly clears dying cells, even before apoptosis is completed; a process mediated through a range of cell surface markers and chemokines that are released in the initiation and progression of cell death (For recent reviews see (335,336). Additionally, the absence of tubular injury, in this model, along with no diabetes-associated changes in hydrogen peroxide production may mean that the renal tubules are not experiencing significant stress. Importantly, however, no exacerbation of renal injury was observed, which suggests that Bax and Bak are not essential for the normal functioning of the kidney in diabetes. However, previous studies have indicated that under severe acute injury, the absence of Bax and Bak is able to prevent the development of fibrosis (307,337). Indeed, double Bax/Bak knock out in the proximal tubules of mice

demonstrated a reduction in renal fibrosis following unilateral ureteric obstruction (307). This may suggest that loss of Bax and Bak is more apparent where injury is severe. Unlike our own model, Jang et. al. utilised the kidney specific, modified variant of Pepck as the target gene for Cre-recombinase, as developed previously (338). The promising results of this study corroborates the importance of Bax and Bak in the progression of acute kidney disease. The exact role in chronic kidney injury, however, is still being determined. It is possible that under mild, chronic stress, such as that observed in this model of diabetes, the absence of the intrinsic mitochondrial cell death pathway, mediated through Bax and Bak, is neither detrimental, nor beneficial. Successful removal of damaged and stressed cells may be compensated for by the induction of one or another of the failsafe pathways available to ensure that cell death proceeds, such as autophagic cell death (339,340). This may also include the activation of caspase independent cell death, and ER stress mediated pathways (341). Importantly, Bax and Bak are have also been demonstrated to play a crucial role in interfacing the ER with intrinsic apoptosis (342). Something which may be explored with this model in future. Whilst the absence of Bax and Bak may theoretically confer a level of protection from cellular stress in a mild chronic disease setting, this appears to be of insignificant magnitude.

Although the present study did not reveal any novel insights into the mechanisms of mitochondrial dysfunction and the pathological outcomes of cell death in DKD, there may yet be a role for them in chronic disease. To this effect, future studies examining the role of Bax and Bak in the renal proximal tubules should be performed using models of DKD with more progressive renal pathology. This could be achieved, for example, by backcrossing the knockout genes into a mouse strain with increased susceptibility to diabetes related chronic kidney injury.

LIMITATIONS

The novel mouse model generated in this study is limited by the minimal development of diabetes associated renal injury. One additional minor limitation of this study is that the role of Bok was not explored. In addition to Bax and Bak a third functionally homologous protein, Bok, is also expressed in tissue and performs similar roles in death and survival (343,344). It is mostly expressed in reproductive tissues and is localised in the golgi body and ER membranes, as opposed to the outer mitochondria membrane like Bax and Bak (343–345). Although over expression enhances susceptibility to certain stressors it has been demonstrated that Bok's activities rely on the co-

expression of Bax and/or Bak to take effect (343,345). Although Bok may perform mitochondrial outer membrane permeabilisation in the absence of Bax and Bak, the action of Bok is considered to be functionally diminished with very low expression in renal cells. Thus, any compensatory effect should be minimal. Given the mild level of renal damage in the Bax/Bak Sglt2-Cre model, this is of minor concern here, but should be explored in future.

4.6 CONCLUSION

Beyond a potential influence on the development of STZ induced diabetes, deletion of Bax and/or Bak was not associated with any clear phenotypic variations. However, mice from this novel Bax/Bak Sglt2-Cre strain developed only mild renal injury after 24 weeks of STZ induced diabetes, compared with other strains of STZ treated mice. Subsequently, this model is unsuitable for exploring therapeutic interventions in human relevant DKD. The hypothesis that Bax and Bak mediate cellular responses to mitochondrial dysfunction in DKD, remains unclear with additional studies required to elucidate any role for these two proteins in the progression of DKD.

4.7 SUMMARY

A novel mouse model with proximal tubule specific deletion of the mitochondrial outer membrane pore forming proteins, Bax and Bak, was created from mice with global Bak1 deletion and global flox tagged Bax, crossed with an Sglt2-Cre mouse. Deletion of the Bax gene by the use of Sglt2 promoted Cre-recombinase demonstrated successful deletion of the Bax gene. Deletion of Bax and Bak resulted in minimal changes in renal structure and function between genetic control groups.

These data may suggest that Bak is required for the development of STZ associated pancreatic damage and induction of persistent hyperglycaemia and type 1 diabetes mellitus phenotype. However, the role for Bax and Bak in the development of diabetes associated renal injury was not possible as this novel mouse strain did not develop sufficient DKD.

4.8 FUTURE DIRECTIONS

This study has raised a number of ideas for future experimental work. Importantly, the model tested did not develop significant renal injury. Thus, future models will need to explore other mouse strains or gene techniques to ensure an effective model of DKD is available to explore the role of Bax and Bak in DKD.

Additionally, a role for Bak in the development of STZ induced pancreatic destruction of β-cells should be explored to resolve if this is a specific result of the genetic deletion of Bak1 and related to the gene expression of Bak protein, or is simply an artifact related to variation in background strain observed in this heterogeneous model.

In the next chapter, the role of the alternative mitochondrial pore forming process, the mitochondrial permeability transition pore, will be explored. Additionally, it will be interesting to investigate mitochondrial function in an obesity-linked models of diabetes to assist in understanding the contribution of diabetes to mitochondrial function.

CHAPTER 5

Chapter 5. The role of Cyclophilin D on mitochondrial function in diabetic kidney disease

5.1 INTRODUCTION

In the previous chapter, deletion of the mitochondrial outer membrane pore (MOMP) forming proteins: Bax and Bak, was examined in the renal proximal tubules in the context of diabetes. This study provided minimal evidence for the importance of the MOMP in diabetic kidney disease, with additional experimental approaches required to investigate the effect of mitochondrial intrinsic cell death on pathological outcomes. Although classically regarded as mediators of apoptotic cascades initiated at the mitochondrion, recent studies have also placed Bax and Bak at the centre of non-apoptotic cell death pathways including primary necrosis and necroptosis (226,237). In these instances the formation of a pore traversing both the inner and outer membrane, called the mitochondrial permeability transition pore (mPTP), occurs. The exact nature of this double membrane pore remains under debate with research continuing to explore the mechanisms regulating its induction. The dual participation of Bax and Bak in both the MOMP and the mPTP represent an area of therapeutic interest with the potential to selectively alter cell death pathway choice. This may be achieved by targeting upstream events of pore induction initiated as a result of cellular stress events. Indeed, inhibition of the mPTP to prevent necrotic type cell death is being investigated for many acute and chronic pathologies. This chapter will focus on the contribution of the mPTP to the progression of DKD by examining a key regulator of upstream mPTP induction, Cyclophilin D.

Cyclophilin D (CypD) is a key protein involved in non-apoptotic cell death pathways initiated at the mitochondrion (346). Specifically, CypD allows the opening of a non-selective channel in the inner mitochondrial membrane which allows solutes and small proteins (up to 1500 Da) to diffuse through, as part of the mitochondrial permeability transition pore (mPTP). The exact mechanism by which this occurs is still under debate with studies revealing that multiple proteins are likely to be redundantly involved (234,347). Indeed, even CypD negative cells are still able to undergo permeability transition, with the absence of CypD pushing the threshold to swelling to an increased calcium load (348). However, transient opening of the mPTP is an important physiological process which allows for maintenance of calcium and other ion homeostasis, and is not associated with mitochondrial swelling

changes (349,350). Under pathological conditions prolonged opening of the pore can result in calcium influx into the mitochondrial matrix, leading to the development of mitochondrial swelling and alterations to ATP production (227). Swollen mitochondria are unable to maintain normal respiration through the electron transport system and as a consequence ATP production is reduced. Where multiple mitochondria are affected, the inability to maintain ATP production can lead to an energetic imbalance whereby normal cellular functions cannot proceed. If a stressed cell attempts to undergo energy intensive repair processes, a critical reduction in ATP production may stall the appropriate cascades and tip the balance towards necrotic type cell death outcomes (216,351). Multiple studies have also indicated that mPTP activity can trigger the downstream insertion of Bax and Bak into the mitochondrial outer membrane, and research suggests that Bax and Bak interface with both the MOMP and the mPTP (225,237,352). The result of such an interaction is an area of active investigation; with strategies targeting the induction of the mPTP pathway to enable the promotion of cell survival (353). Indeed, inhibiting the mechanisms of mPTP opening has been shown to successfully improve cell survival following acute injury (354,355). In vivo this has been primarily achieved through the use of compounds such as Cyclosporine A (CsA), which binds to, and thus inhibits the action of, Cyclophilin D to prevent mPTP opening. As such, inhibition of CypD represents an area of potential therapeutic interest in multiple human diseases. Indeed, the ability to rescue mitochondrial function and prevent necrotic cell death has been successfully utilised in ischemic injury in cardiac tissue in both clinical and pre-clinical studies (238,356). CypD inhibition has also demonstrated pronounced effects on reducing injury in acute renal ischemia (357–359). These studies provide a promising directive to explore the implications of mPTP inhibition in chronic kidney injury, such as that which is associated with prolonged hyperglycaemia in diabetes. The use of CypD inhibitors in chronic diseases is just beginning to be explored, most notably with the successful prevention of muscle fibre degeneration in muscular dystrophy (360,361).

It is hypothesised that targeting the mPTP, by inhibiting CypD, will rescue dysfunctional mitochondria in diabetic kidney disease in order to improve renal outcomes. This chapter will explore the role of CypD and the mPTP pathway in the development of diabetic renal injury using pre-clinical models. This will develop the ideas initiated in Chapter 4 on the role of mitochondrial pore formation in the development of DKD.

5.1.1 AIMS

- To further investigate diabetes associated mitochondrial dysfunction in additional mouse models of DKD

- To investigate the contribution of CypD to the development of renal injury in DKD

- To determine if CypD inhibitors previously tested in human clinical trials are able to prevent, or improve, the development of DKD

NOTE ON PRESENTATION OF RESULTS

Results for this chapter are presented in three sections. The first section presents the manuscript of publication 2, which includes data describing the CypD (*Ppif*) KO model, as well as the results for a 5mg/kg dose of Alisporivir in *db/db* mice. Following this, the results of a pilot study examining the effects of a dose of 10mg/kg of the drug Alisporivir in *db/db* mice is explored. The final section presents the additional data collected for the studies not presented in publication 2.

5.2 METHODS

5.2.1 ANIMAL STUDIES

Animals used in this study were approved by the Alfred Medical and Research Education Precinct Animal Ethics Committee. *Ppif* KO mice were approved under animal ethics number E/0941/2010/B. *Db/db* mouse experiments were approved for use under ethics number E/1502/2016/B. All procedures were completed according to the guidelines of the National Health and Medical Research Council, and the Australian code for the care and use of animals for scientific purposes (2013) (362). Detailed descriptions of these studies are available in the methods section of Publication 2. Study 1 refers to the *Ppif* KO mouse study, whilst Study 2 refers to the Alisporivir trial in *db/db* mice.

5.2.2 COMPREHENSIVE LABORATORY ANIMAL MONITORING SYSTEM

The comprehensive laboratory animal monitoring system (CLAMS) (Columbus Instruments, Columbus, Ohio, USA) allows indirect calorimetric analysis of individual mice for the purpose of determining changes in metabolism. Individual mice were placed into CLAMS cages one week before endpoint in Study 2 only. Oxygen consumption and Carbon dioxide production are monitored in an enclosed system for 24hrs and used to determine the characteristics of respiration for individual mice. The respiratory exchange ratio can be calculated from this data to infer metabolic status (363,364). Additionally, measurements of movement in X, Y and Z planes allows for an assessment of physical activity.

5.2.3 ECHOMRI

Body composition was assessed in *db/m* and *db/db* mice one week before endpoint at 15 weeks of study by EchoMRI (EchoMRI^{TM}, Houston, TX, USA). The EchoMRI machine was pre-calibrated with Canola oil and used to determine Lean mass and Fat mass. Results were then used to calculate percentage body fat and percentage lean mass for each mouse.

5.2.4 PHENOTYPIC ASSESSMENT OF LIVER AND HEART

Liver and heart mass were measured on freshly excised organs. Heart mass was recorded as total heart, and left ventricular mass after dissection of right ventricle and auricles.

5.2.5 TEM Analysis

Analysis of mitochondrial shape descriptors was performed following the protocol provided in Piccard et al 2013 (365). Briefly, individual mitochondria from *n*=3 mice per group were manually circled for between 5-7 images per mouse using the Fiji (is just) Image J software. Data for a minimum of 1000 mitochondria were obtained with the following parameters measured: area (2D volume); perimeter; Feret's diameter; aspect ratio; and roundness. Circularity was also measured and its inverse derivative used to calculate form factor. Data for each measurement were pooled across all images for each mouse and used to calculate the relative frequency distribution. Frequency distributions were allocated to 20 bins of equal size for the entire data set. To visualise distribution curves easily values for Aspect Ratio, Perimeter and Feret's diameter were truncated at 10, 12µm and 6µm respectively. This was due to the extended range of a small subset of mitochondria in some groups. All data points falling above these bins were placed into the final bin to ensure all data were included for analysis. Data points above final bin represented less than 0.5% of data for any individual mouse. Average of *n*=3 per group for each bin was then calculated.

5.2.6 Review of clinical trial data

A data base search for all clinical trials involving Alisporivir was performed using the U.S. National Library of Medicine database at Clinicaltrials.gov. Search terms to discover drug trials included all of the nomenclature variations for Alisporivir:

- Alisporivir

- Deb025

- Debio-025

- UNIL-02

Within each discovered clinical trial, all with publically available results were then queried for data on blood glucose with the following search terms:

- Glucose

- Glycaemia

- Glycemia

- A1c

- Glycated

All positive results were then analysed for blood glucose information.

5.2.7 CARDIAC MITOCHONDRIAL ISOLATION

Mitochondria were isolated from cardiac tissue to provide a secondary population of mitochondria to compare with renal mitochondria. All procedures were performed on ice or at 4°C. Right ventricles were removed and the middle third of the left ventricle was used to isolate mitochondria. Tissue was placed into 1mL of cold MIB (see page xx) and finely chopped into <1mm pieces. Tissue was then homogenised briefly using a Polytron PT 2100 homogeniser (Kinematica, Luzern, Switzerland) set to low speed. Homogenate was centrifuged at 800*g* for 5 minutes and supernatant collected and centrifuged at 8000*g* for 10 minutes. The mitochondrial pellet was washed in 1mL MIB and centrifuged a second time at 8000*g* for 10 minutes. The pellet was finally resuspended in 50µL of MIB and protein content assessed using the bicinchoninic acid method as described on page xx. This preparation method extracts the subsarcolemma mitochondrial population only.

5.2.8 SEAHORSE BIOANALYSIS

Isolated cardiac mitochondria were assayed using the Seahorse 96-well XFe Bionalyzer as described in Chapter 2, section 2.7.1.

5.3 PUBLICATION 2

Data presented below include additional data to that presented in publication 2. This analysis includes the results of a pilot study evaluating the effects of Alisporivir at a dose of 10mg/kg/day. Additionally, the effects of Alisporivir in *db/db* mice were unclear from the 5mg/kg study as little change in renal function or injury was observed. To determine if this effect was renal specific additional phenotypic data were assessed.

Delineating a role for the Mitochondrial Permeability Transition Pore in Diabetic Kidney Disease by targeting Cyclophilin D

Runa S.J. Lindblom[1], Gavin C. Higgins[1,2], Tuong-Vi Nguyen[2], Maryann Arnstein[1], Darren C. Henstridge[2], Cesare Granata[1], Matthew Snelson[1], Vicki Thallas-Bonke[2], Mark E. Cooper[1], Josephine M. Forbes [3], Melinda T. Coughlan[1,2]

[1]Department of Diabetes, Central Clinical School, Alfred Medical Research and Education Precinct, Monash University, Melbourne, Victoria, Australia.

[2]Baker Heart & Diabetes Institute, Melbourne, Victoria, Australia

[3]Glycation and Diabetes Group, Mater Research Institute-The University of Queensland, Translational Research Institute, Woolloongabba, Queensland, Australia.

Corresponding author: Ms Runa Lindblom

Glycation, Nutrition and Metabolism Laboratory

Department of Diabetes, Central Clinical School

Alfred Medical Research and Education Precinct

Monash University, Melbourne, Victoria, Australia.

Telephone: +613 99030475

Fax: +613 99053288

Email: runa.lindblom@monash.edu

Summary statement:

We identified that blockade of the mitochondrial permeability transition pore via genetic deletion or pharmacological inhibition of the functional unit of the pore, Cyclophilin D, is not renoprotective in diabetic kidney disease. Our data indicates that Cyclophilin D deletion is detrimental, and that targeting the mitochondrial permeability transition pore is not a valid pharmacological strategy for diabetic kidney disease.

Short title: Targeting the mitochondrial transition pore in diabetic kidney disease

Keywords: diabetic kidney disease, mitochondrial permeability transition pore, mitochondria, cyclophilin D, cell death.

Abstract

Mitochondrial stress has been widely observed in Diabetic Kidney Disease (DKD). Cyclophilin D (CypD) is a functional component of the mitochondrial permeability transition pore (mPTP) which allows the exchange of ions and solutes between the mitochondrial matrix to induce mitochondrial swelling and activation of cell death pathways. CypD has been successfully targeted in other disease contexts to improve mitochondrial function and reduced pathology. Two approaches were used to elucidate the role of CypD and the mPTP in DKD. Firstly, mice with a deletion of the gene encoding CypD (*Ppif* $^{-/-}$) were rendered diabetic with streptozotocin (STZ) and followed for 24 weeks. Secondly, Alisporivir, a CypD inhibitor was administered to the db/db mouse model (5mg/kg/day oral gavage for 16 weeks). *Ppif* $^{-/-}$ mice were not protected against diabetes-induced albuminuria and had greater glomerulosclerosis than their WT diabetic littermates. Renal hyperfiltration was lower in diabetic *Ppif* $^{-/-}$ as compared with WT mice. Similarly, Alisporivir did not improve renal function nor pathology in db/db mice as assessed by no change in albuminuria, KIM-1 excretion and glomerulosclerosis. Db/db mice exhibited changes in mitochondrial function, including elevated Respiratory Control Ratio, reduced mitochondrial H_2O_2 generation and increased proximal tubular mitochondrial volume, but these were unaffected by Alisporivir treatment. Taken together, these studies indicate that cyclophilin D has a complex role in DKD and direct targeting of this component of the mPTP will likely not improve renal outcomes.

Clinical perspectives

- Mitochondrial dysfunction, including enhanced susceptibility to mPTP, is an early event in the pathogenesis of DKD, however, the role of the mPTP and its activator, CypD, in DKD has not been fully explored.
- Genetic loss of CypD exacerbated diabetic renal injury, and treatment with a pharmacological inhibitor did not rescue mitochondrial function.
- CypD has a complex physiological and pathological role in the diabetic kidney which should be considered when treating DKD patients with CypD inhibitors

Abbreviations list:

A.	Alisporivir treated mice
ATP	adenosine triphosphate
CKD	chronic kidney disease
CIT	Citrate (vehicle control)
Col IV	Collagen type IV
CsA	Cyclosporine A
CypD	Cyclophilin D
db/db	Diabetic, homozygous Leptin receptor deficient ($Lepr^{db}$ / $Lepr^{db}$)
db/m	Lean, heterozygous Leptin receptor deficient ($Lepr^{db}$ / $Lepr^{+}$)
DKD	diabetic kidney disease
ETS	Electron Transport System
FAO	Fatty Acid Oxidation
FCCP	carbonyl cyanide trifluoromethoxyphenylhydrazone
GSI	glomerulosclerotic index
H_2O_2	hydrogen peroxide
KIM-1	kidney injury molecule -1
KO	Knock Out (genetic deletion)
mPT	mitochondrial permeability transition
mPTP	mitochondrial permeability transition pore
OCR	oxygen consumption rate
OXPHOS	oxidative phosphorylation
Ppif	peptidylprolyl isomerase F
PTEC	proximal tubular epithelial cell
ROS	reactive oxygen species
RCR	Respiratory Control Ratio
RER	Respiratory Exchange Ratio
WT	wild type
STZ	Streptozotocin
UAE	Urine Albumin Excretion
V.	Vehicle control treated (10% Cremophor EL)

Introduction

Chronic kidney disease is recognised as a leading cause of morbidity and mortality amongst the 425 million people estimated to have diabetes globally (1). This represents a significant burden to healthcare systems as the number of people with all types of diabetes is projected to rise over the next few decades (1). Currently, best practice clinical management involves strict glucose control and blood pressure reduction to alleviate risk for progression to end stage renal disease. Although these approaches can successfully stabilise the rate of progression in many patients, they do not entirely eliminate disease or risk for renal replacement therapy (2,3). There remains an urgent need for new therapeutic approaches in targeting diabetic kidney disease (DKD) and a requirement to deepen our understanding of the aetiology and pathogenesis to improve patient outcomes.

The therapeutic potential of maintaining and/or restoring mitochondrial "health" is currently being investigated in DKD, since a decline in mitochondrial function is associated with renal functional decline and injury (4). Mitochondria are considered vital for the function of nephrons which consume high levels of oxygen and ATP to support the metabolic demands of selective reabsorption in the proximal and distal tubules (5,6). Furthermore, mitochondria play an important role in adaptation to the metabolic changes and hypoxia associated with diabetic renal pathophysiology (6,7). Thus, a suite of mitochondria-targeted compounds are currently being developed and tested in pre-clinical models to determine their efficacy in the treatment of DKD. One potential target for therapy is the mitochondrial permeability transition pore (mPTP), which is a stress-sensitive pore that traverses both the inner and outer mitochondrial membranes. Transient mPTP opening is

thought to dissipate chemical and electrical ion build up from the mitochondrial matrix to the cytosol to restore ionic balance (8,9). However, persistent opening of the mPTP results in mitochondrial swelling and subsequent outer membrane rupture, along with a concomitant decline in capacity for oxidative phosphorylation (OXPHOS) (10). Inappropriate mPTP opening is associated with necrotic cell death as the maintenance of ATP production is necessary for the energy demanding process of apoptosis (11,12). Previous preclinical studies of DKD have shown increased mPTP opening events occur in kidney mitochondria, which coincided with the development of renal morphological injury and a decline in renal cortical mitochondrial respiratory chain function in a rat model of streptozotocin-induced diabetes (4).

Although the exact mechanism that enables trafficking through the mPTP is still under debate, newer models suggest several key membrane proteins are involved in pore opening. This includes the outer membrane pore-forming proteins Bax and Bak, the F1alpha unit of ATP synthase, and cyclophilin D (13,14). Cyclophilin D (CypD) is considered to regulate pore opening and it therefore remains as a unique target which can be directly inhibited by broad spectrum immunosuppressants such as Cyclosporine A and its newer non-immunosuppressive analogue Alisporivir (Debio025) (15,16). In the kidney, CypD deletion in mice is protective against the development of renal fibrosis and proximal tubular epithelial cell damage following unilateral ureteral obstruction, and ischemia reperfusion injury (17–19). However, the effects of targeting CypD on DKD progression have not been investigated. This study aims to investigate the role of CypD in DKD by utilising two disparate yet complementary approaches. Firstly, mice with a global genetic knock out of the peptidylprolyl isomerase F gene, *Ppif*, (which is

the gene encoding for CypD), and secondly using pharmacological inhibition by Alisporivir in a murine model of experimental diabetes.

Experimental

Mouse studies

All animal studies were approved by the Alfred Medical Research and Education Precinct Animal Ethics Committee and the National Health and Medical Research Council of Australia. All procedures were performed in accordance with the Australian code of conduct for ethical research involving animals. All animals were housed at the Alfred Medical Research and Education Precinct Animal Centre, Melbourne, Australia, and were maintained following established ethical procedures, in a temperature controlled environment at 22°C with a 12hr light/dark cycle with ad libitum access to rodent chow (standard mouse chow, Specialty Feeds, Perth, WA, Australia) and water.

Ppif $^{-/-}$ mouse studies

Six week old Male C57BL/6 mice with a global deletion of Cyp D (*Ppif* $^{-/-}$) were purchased from the Jackson Laboratory (Bar Harbor, ME, USA). Diabetes was induced at six weeks of age (n=15 mice per group, *Ppif* $^{WT/WT}$ STZ or *Ppif* $^{-/-}$ STZ) by five daily intraperitoneal injections of low dose streptozotocin (55 mg/kg, Sigma-Aldrich, St Louis, MO), with control mice receiving the vehicle, sodium citrate buffer (CIT) alone (n=15 mice per group, *Ppif* $^{WT/WT}$ or *Ppif* $^{-/-}$). After ten days, plasma glucose concentrations were determined to confirm diabetes development and mice with blood glucose not exceeding >15mmol/l glucose (observed in >98% of mice)

were excluded from the study. None of the animals with diabetes required exogenous insulin supplementation to maintain body weight or to prevent ketosis.

At 20 weeks after induction of diabetes, mice were placed individually into metabolic cages (Iffa Credo, L'Arbresele, France) for 24 hours. Urine and plasma from submandibular collections were stored at -80°C for subsequent analysis. Blood glucose was monitored using a glucometer (Accutrend; Boehringer Manheim Biochemica, Manheim, Germany). Glycated haemoglobin (GHb) was determined by turbidimetric inhibition immunoassay using a Cobas Integra 400 autoanalyzer (Roche Diagnostics Corporation, USA) in lysates of erythrocytes separated from whole blood. After 22 weeks, animals were euthanised by sodium pentobarbitone intraperitoneally (100 mg/kg body weight) (Euthatal; Sigma-Aldrich, Castle Hill, NSW, Australia) followed by cardiac exsanguination. The kidneys were rapidly dissected, weighed, and snap-frozen or placed in 10% ($^{v}/_{v}$) neutral buffered formalin for fixation before paraffin embedding. In a subset of mice (*n*=5 per group), mitochondria were isolated from renal cortices as later described.

Pharmacological inhibition of Cyclophilin D

Male *db/db* mice (C57*BKS.Cg-Dock7*$^{m+/+}$*Lepr*^{db}*/J)* and their *db/m* littermate controls, were obtained from colonies maintained at the Alfred Medical Research and Education Precinct Animal Services (Melbourne, Australia). Mice were randomly assigned at 7 weeks of age to either Vehicle (10% Cremophor EL in water) or Alisporivir (Novartis, Basel, Switzerland) at 5mg/kg/day by oral gavage. Animals were treated for 16 weeks with blood glucose and body weight assessed weekly. Any animal which lost 20% of body weight or developed severe ketoacidosis during the study was excluded before endpoint in accordance with ethical guidelines. HbA_{1c}

was determined using the Cobas b 101 system (Roche diagnostics, IN, USA). At week 15, body composition was determined using an EchoMRI (EchoMRI^{TM}, Houston, TX, USA) and mice were placed into individual Comprehensive Laboratory Animal Monitoring System (CLAMS), (Columbus Instruments, Columbus, Ohio, USA) chambers to determine physical activity and respiration by indirect calorimetry as previously described in full (20). Metabolic caging to collect 24 hour urine samples was performed at 8 weeks (midpoint) and 15 weeks (endpoint). Mice were killed and kidneys were harvested and processed as described above. Additionally, mitochondria were isolated from the whole cortex of the left kidney for all animals (described below). A small section of renal cortex was also reserved for transmission electron micrography (described below).

Renal Function and Morphometry

The 24-hour urinary albumin excretion rates were determined using a mouse-specific sandwich ELISA in timed urine collections (Bethyl Laboratories, Montgomery, TX, USA) according to the manufacturer's instructions. Creatinine was assessed in both plasma and urine samples using commercially available kits for the Cobas Integra 400 autoanalyzer (Roche Diagnostics, IN, USA). Plasma cystatin C was measured using ELISA (R&D Systems Inc., Minneapolis MN, USA). Urinary content of Kidney Injury Molecule (KIM)-1 was measured using a commercially available sandwich ELISA (USCN Life Sciences, Wuhan, China) according to the kit protocol. Glomerulosclerotic index (GSI) was assessed in 3-μm paraffin embedded periodic acid Schiff (PAS) stained sections by a semi-quantitative method as previously described (21). Paraffin sections of kidneys were used to stain for collagen type IV

using a goat polyclonal collagen IV antibody (Southern Biotech, Birmingham, AL, USA) (22).

Mitochondrial isolation

Freshly collected kidney cortex was minced on ice and placed into 1mL of ice-cold Isolation Buffer (IsoB) (70mM Sucrose; 210mM D-Mannitol; 5mM HEPES; 1mM EGTA; 0.5% (w/v) fatty acid free Bovine Serum Albumin [Sigma-Aldrich, NSW, Australia]) followed by 6-8 careful strokes in a Potter-Elvehjem homogenizer set in an ice-bath. Lysate was then collected and any remaining tissue homogenised with an additional 1mL IsoB for 2-3 more strokes. The lysate underwent differential centrifugation at 4°C as previously described (23). Briefly, ~2mL total volume was centrifuged for 5 minutes at 800*g*. Supernatant was collected and centrifuged at 8000*g* x10 minutes. Mitochondrial pellet was washed in 500µL IsoB and centrifuged again at 8000*g* x 10 minutes. Final pellet was resuspended in 115µL IsoB and stored on ice for use in functional assays (below). Total protein was determined by the Bicinchoninic acid method and corrected for background protein in IsoB (Pierce-Thermo Fisher Scientific, Melbourne, Australia).

Mitochondrial Oxygen Consumption

Mitochondria were resuspended in Mitochondrial Assay Buffer (MAS) (70mM Sucrose; 220mM D-Mannitol; 10mM KH_2PO4; 5mM $MgCl_2.6H_2O$; 2mM HEPES; 1mM EGTA; 0.2% (w/v) fatty acid free Bovine Serum Albumin, *pH 7.2*) and loaded into a XFe96well Seahorse Bioanalyzer plate (Seahorse Bioscience, Agilent, Santa Clara CA, USA) with a minimum of 5 replicate wells per mouse. For complex I respiration 10µg of mitochondria was loaded per well with 0.5mM glutamate and

0.5mM malate. Plates were centrifuged at 2000*g* for 20 minutes at 4°C before adding substrates and then immediately loaded into the XFe96 Seahorse machine. Basal respiration with substrates was measured twice for 3 minutes each, followed by subsequent injections of: A) 0.5mM ADP (State 3o), B) 2.5µg/uL Oligomycin (State 4), C) 1µM FCCP (State 3u), and D) 4µM Antimycin-A. Data were analysed per individual mouse with each injection point assessed for successful response via pre-defined criteria. Injection measurements were excluded where oxygen consumption was reduced to 0 pmoles/min, or where the compounds did not perform as expected for that individual replicate (e.g., no response to oligomycin). The average value of remaining replicates was used. Individual animals were excluded where ADP injection did not increase oxygen consumption rate (OCR).

Hydrogen Peroxide production

Hydrogen peroxide production in renal cortical mitochondrial preparations was measured by fluorescence using the Amplex Red reagent (Molecular Probes, Invitrogen). In addition, hydrogen peroxide production was assessed in the presence of 10mM glutamate and 10mM malate for complex I, or, 10mM succinate for complex II, plus 5µM rotenone (a complex I inhibitor). Results were then normalised to no substrates group to determine effects of complex I and II stimulation.

Mitochondrial Swelling assay

The induction of mitochondrial permeability transition (mPT) in mouse kidney mitochondria was monitored by absorbance changes at 540 nm based on a microtiter plate procedure developed by Waldmeier et al (15), with the following modifications. Mitochondria, isolated by differential centrifugation as described above

were washed twice and resuspended in energised respiratory buffer (ERB) (210 mM mannitol, 70 mM sucrose, 5mM HEPES, 5 mM glutamate, 5 mM malate, 0.05 M Tris, pH 7.4). Mitochondrial protein, 100μg, was added to each well in 110 μl ERB, then incubated with 10 μM Cyclosporine A (CsA) or ERB control where appropriate for five min before the addition of 5uL of Calcium solution (2.5 mM $CaCl_2.2H_2O$, 1mM K_2HPO_4) or ERB. Total volume = 125μL per well. Δabsorbance was determined over 10 minutes with a microtiter plate reader (*Ppif* study) or 15 min (*db/db* study) using an EnSpire multimode plate reader (Perkin Elmer, Waltham, MA USA).

Quantitative Reverse Transcription-Polymerase Chain Reaction (RT-qPCR)

RNA was isolated from kidney cortex (20-30mg) using TRIzol Reagent (Life Technologies). Contaminating DNA was removed after treatment with DNA-free DNAse according to the manufacturer's specifications (Ambion Inc, Austin, USA). DNA-free RNA was reverse transcribed into cDNA using the Superscript First Strand Synthesis System according to the manufacturer's specifications (Life Technologies BRL, Grand Island, NY). Real-time PCR was performed using SYBR green PCR mix (Applied Biosystems, primer concentration of 500 nM) or Taqman PCR kit (18S rRNA TaqMan Control Reagent kit, ABI Prism 7500; Perkin-Elmer) using a 7500 Fast Real-time PCR System (Applied Biosystem, VIC, Australia), and normalized relative to 18S ribosomal RNA. All values are presented as fold change relative to *Ppif* $^{WT/WT}$ CIT Control or *db/m* Vehicle Control. The nucleotide sequences for primers examined are shown in *Supplementary Table 1*.

Citrate Synthase activity

Citrate synthase activity was assayed as previously described via colorimetric release of Acetyl Coenzyme A the presence of DTNB 5,5-dithiobis-2-nitrobenzoate (24). Calculated activity levels were then normalised to total mitochondrial isolation protein concentrations.

Transmission electron microscopy and analysis of mitochondrial morphology

Mitochondrial morphology (length and width) was determined in electron micrographs of proximal tubule epithelial cells. Immediately following exsanguination, renal cortices were fixed in 2.5% glutaraldehyde in 0.1M sodium cacodylate buffer and tissue was processed for standard transmission electron microscopy using post-fixation in 1% OsO_4 and embedded in Epon resin. Ultrathin sections were cut and stained with lead citrate and uranyl acetate and imaged on a Hitachi H-7500 transmission electron microscope equipped with a Gatan Multiscan 791 CCD camera. Up to ten images of proximal tubule epithelial cells per kidney section were randomly collected for each mouse at x8,000 magnification. Image field size was 17.44x17.44 microns each. Individual complete mitochondria were circled by hand for a subset of n=3 mice per group. Mitochondria in each image per mouse were hand circled and measured with (Fiji Is Just) Image J software and values used to calculate Form Factor (length/width) as previously described (25). In addition, the 2D volume of mitochondria within each field per section were measured and expressed as mitochondrial percentage area per mm^2 cytosol. For purpose of cytosolic area determination nuclei, brush borders, and non-proximal tubular structures were excluded. Cumulative results for each mouse were used to express mean volume and aspect ratio per group.

Western Immunoblotting

Immunoblotting was performed as previously described with minor modifications (26). Briefly, 8 μg of isolated mitochondria were lysed by 3 freeze-thaw cycles and separated by electrophoresis on 4-20% Mini-Protean TGX Stain-Free Gel (Bio-Rad laboratories, Gladesville, NSW, Australia), transferred to polyvinylidene fluoride (PVDF) membranes, before being blocked for 1 h in 5% skim milk in Tris buffered saline with 0.1% Tween-20 (TBS-T). Membranes were incubated overnight with gentle agitation at 4°C with 6.2μg/μl total OXPHOS rodent antibody (ab110413, Abcam, Melbourne, Australia), before being incubated at room temperature in an IRDye® 800CW goat anti-mouse IgG secondary antibody (LI-COR Biosciences, Lincoln, NE, USA) for 90mins. Membranes were visualised using an Odyssey Infra-REd imaginf platform (LI-COR Biosciences, Lincoln, NE, USA) and were quantified using Image Studio Lite v5.2. An internal standard was loaded on each gel to account for gel-to-gel variability. Whole lane stain-free quantification (Bio-Rad Chemi-Doc imaging system, and Bio-Rad Image Lab 5.2.1 imaging software; Bio-Rad laboratories, Gladesville, NSW, Australia) was used to normalise total protein per well, and, qualitatively verify correct loading and equal transfer between lanes. Additionally, an internal control sample was applied across all gels and used to normalise data between gels.

Statistics

All statistical computations were performed using GraphPad Prism version 7.0 (GraphPad Software, San Diego, California, USA). Values of experimental groups are given as mean, with error bars showing SD, unless otherwise stated. Outliers

were only excluded where a valid biological or technical issue indicated exclusion. Two-way ANOVA was performed with unweighted means. Bonferroni post-hoc test was used to determine statistical significance and correct for multiple comparisons between each factor. $P < 0.05$ was considered to be statistically significant. Additionally significance in graphs is indicated as: *P<0.05, **P<0.01,***P<0.001, ****P<0.0001; Where required a Two-way ANOVA with repeated measures was performed on data representing different time points with § P<0.05

Results

CypD deletion does not protect against diabetes-induced renal injury.

As expected, hyperglycemia and decreased body weight occurred with diabetes (***Table 1***). Additionally, diabetes-associated renal hypertrophy developed, shown as an increase in total kidney weight and kidney to body weight ratio. Diabetic mice had increased daily water and food consumption and developed polyuria. Genetic deletion of CypD did not alter fasting blood glucose concentrations in non-diabetic mice nor in the setting of diabetes (***Table 1***). There was a significant decrease in body weight in non-diabetic *Ppif* $^{-/-}$ mice. CypD (*Ppif*) deletion also decreased polyuria at both 12 and 20 weeks of diabetes. Water consumption and food intake remained similar between diabetic *Ppif* $^{WT/WT}$ and *Ppif* $^{-/-}$ groups during the 24hr period.

Albuminuria (Urinary Albumin Excretion) (***Figure 1A***) and Urinary Albumin to Creatinine ratio were significantly increased in all STZ treated mice (***Figure 1B***). In addition, urinary excretion of the tubular damage-associated marker Kidney Injury Molecule 1 (KIM-1) was increased in diabetic animals but was not different *Ppif* $^{-/-}$

mice (***Figure 1C***). Plasma cystatin C, a surrogate marker of glomerular filtration rate, was reduced in the STZ model indicative of hyperfiltration (***Figure 1D***). Genetic deletion of CypD in the setting of diabetes led to a prevention of hyperfiltration, as shown by no decrease in plasma cystatin c in the *Ppif* $^{-/-}$ STZ group. Conversely, deletion of CypD decreased GFR, measured as elevated cystatin C in both control and diabetic Ppif-/- mice.

Glomerular Sclerosis Index was assessed in PAS-stained glomeruli (***Figure 1E***) and mean histology scores were significantly increased in all STZ treated animals compared with controls. *Ppif* $^{-/-}$ STZ mice exhibited higher GSI histology scores compared with wild-type STZ indicating that the absence of CypD exacerbated glomerular injury in a diabetic setting. This was reiterated by an increase in diabetes-associated Glomerular Collagen IV deposition (***Figure 1F***) in the *Ppif* $^{-/-}$ STZ mice. Thus, loss of CypD via deletion of the Ppif gene exacerbated glomerular structural injury in our model of diabetic kidney disease.

Deletion of Cyclophilin D modulates mitochondrial ATP synthase F1-alpha.

To confirm that the renal phenotype was indeed related to a loss of CypD, deletion of the gene encoding for CypD, *Ppif* was confirmed by RT-qPCR. No expression of the *Ppif* gene was detected in the *Ppif* $^{-/-}$ mice (***Figure 2A***). No change in *Ppif* expression was observed between WT control and STZ diabetic animals. To ascertain that deletion of *Ppif* did functionally reduce mitochondrial swelling, a calcium overload assay was performed in isolated mitochondria from *Ppif* $^{WT/WT}$ and *Ppif* $^{-/-}$ animals to induce mPTP opening (***Figure 2B***). Diabetic *Ppif* $^{-/-}$ mice had decreased calcium-induced swelling as compared with WT diabetic mice. Since CypD binds to F_1/F_0 of the ATP synthase complex, we tested the gene expression of

the *F1-α* component. *Ppif* $^{-/-}$ mice had a marked downregulation of this gene, in addition to a 50% reduction seen in the *Ppif* $^{WT/WT}$ STZ treated mice (***Figure 2C***). Another mitochondrial gene, cytochrome *c*, was also downregulated by both STZ treatment and in *Ppif* $^{-/-}$ mice (***Figure 2D***). Gene expression of the fibrosis associated fibronectin protein (***Figure 2E***) was increased 5-fold in *Ppif* $^{WT/WT}$ STZ mice. Genetic deletion of *Ppif* $^{-/-}$ in diabetic mice decreased the fibronectin gene expression similar to control levels. Collagen IV gene expression however was not increased with diabetes, and was downregulated in *Ppif* $^{-/-}$ mice *(**Figure 2F**)*.

Pharmacological inhibition of Cyclophilin D with 5mg/kg Alisporivir did not alter blood glucose control or body composition of db/db mice

Db/db mice had increased body weight compared with *db/m* mice consistently over the course of the study (***Figure 3A***). A decline in body weight towards end point of the study was noted in some diabetic animals, which is considered to reflect the development of pancreatic beta-cell failure. Alisporivir did not reduce diabetes-associated hyperglycaemia nor glycated haemoglobin levels in *db/db* diabetic mice (***Table 2***). Assessment of body composition by EchoMRI (***Table 2***) showed that the increase in body mass was attributable to a two-fold increase in fat mass in all *db/db* mice irrespective of therapy (***Figure 3B***). Endpoint body mass of *db/db* mice also did not differ between Vehicle and Drug treated animals at week 16 of treatment (***Figure 3C*)**. As expected, diabetic *db/db* animals developed renal hypertrophy with increased total kidney weight (***Table 2***). confirmed by an increase in the kidney to body weight ratio (***Figure 3D***) which was not affected by Alisporivir.

Alisporivir does not attenuate renal pathology in db/db mice.

Plasma cystatin C as a marker of glomerular filtration rate, was unchanged for all *db/db* and *db/m* mice in this study (Midpoint - ***Figure 3E***, Endpoint - ***Figure 3F***). Both urinary albumin excretion rate (Midpoint - ***Figure 4A***, Endpoint - ***Figure 4B***) and Albumin to Creatinine ratios (***Figure 4C***) were increased in all *db/db* animals consistent with DKD progression and was not attenuated by Alisporivir. Urinary KIM-1 was also increased in both *db/db* groups and unaffected by Alisporivir (***Figure 4D***). *Db/db* mice had increased Glomerular Sclerosis Index compared to *db/m* controls, however, Alisporivir had no impact on glomerular injury in *db/db* mice (***Figure 4E***). No increase in glomerular *Col IV* deposition between Vehicle *db/m* and *db/db was seen in this study* (***Figure 4F***), however, *Db/m* animals receiving Alisporivir had decreased *Col IV* deposition compared with Vehicle controls. A comparison of these results and those of the *Ppif* study for the effects of diabetes and targetting *Ppif* (CypD) is provided in Table 3.

Alisporivir does not improve sedentary behaviour or whole-body energy calorimetry in dbdb mice .

Daily physical activity was assessed by 'beam breaks' in X+Y+Z directions in the CLAMS system over 24hrs. This data is shown as discrete measurements across the light (inactive/sleep) and dark (active) cycles (***Figure 5A***) and also as cumulative totals (***Figure 5B***). *Db/m* mice performed double the physical activity during the dark cycle (active period) compared to the light cycle. *Db/db* animals remained sedentary during dark cycle, with a significant reduction in physical activity compared to *db/m* controls.

Respiration was analysed via changes in oxygen consumption and carbon dioxide production. All individual mice had increased (§$P<0.05$) respiration during the

dark period compared to the light for both O_2 (***Figure 5C***) and CO_2 data (***Figure 5D***). No significant differences were evident between *db/db* versus *db/m* mice for either oxygen (***Figure 5Ci***) nor carbon dioxide respiration (***Figure 6Ci***) measured in mL per hour. There were, however, slight trends toward an increase in O_2 (***Figure 5Ci***) and a decrease in CO_2 (***Figure 5Di***) for *db/db* mice on Vehicle but not Alisporivir. When normalised to body weight (mL/kg/hr) this trend disappeared and both *db/db* groups were significantly decreased compared with their *db/m* controls (***Figures 5Cii***, and ***6Cii***). Energy expenditure (heat production) was unchanged between all groups (***Figure 5E***) Respiratory exchange ratio (RER), which is reflective of metabolic substrate preference, was calculated from the ratio of Volume of CO_2 to Volume O_2. Once again, values were higher in *db/m* mice during the dark cycle compared to the light, indicating increased carbohydrate metabolism during active hours. Interestingly, however, no such difference was observed in *db/db mice*. Additionally, the slight trends in O_2 and CO_2 respiration observed in figures 5C and 5D synergistically resulted in a statistically significant decrease in RER in *db/db* animals with no change with Alisporivir (***Figure 5F***). This decrease in RER is reflective of a preference for fat metabolism in *db/db* mice. Overall, pharmacological inhibition of CypD had little effect on any parameter observed with the CLAMS system.

Renal cortical mitochondrial oxygen consumption rate was increased in db/db mice

Next, markers of mitochondrial respiratory function and mPTP were assessed. Citrate synthase activity, an overall marker of mitochondrial quality, was determined and revealed no significant difference in enzyme activity between groups per µg of isolated mitochondria (***Figure 6A***) indicating that any differences observed in

mitochondrial activity are attributable to functional measures rather than changes to overall mitochondria quality. The mitochondrial swelling response induced by calcium challenge showed no statistically significant differences for the rate of Δabsorbance at 540nm (***Figure 6B***). The isolated mitochondrial preparations were also pretreated with the mPT inhibitor Cyclosporine A, prior to receiving the calcium challenge. Interestingly, this pretreatment differentially affected the total duration of swelling inhibition between *db/m* and *db/db* mice, whereby mitochondria from the *db/db* mice underwent a rapid drop in absorbance (i.e no swelling inhibition). Treatment with Alisporivir partially restored CsA inhibition of the mPTP in *db/db* mice, however, the mean group average was not significantly different to the Vehicle *db/db* mice.

To assess mitochondrial respiration in the kidney, a mitochondrial stress test was performed in the Seahorse Bioanalyser using glutamate/malate to test complex I-linked respiration in isolated mitochondria (***Figure 6C***). A significant increase in oxygen consumption rate (OCR) following ATP and FCCP injections was observed for Vehicle treated *db/db* mice, but this was lessened in Alisporivir treated *db/db* mice. RCR (State 3/State 4o) and ATP-linked respiration of isolated kidney mitochondria were increased in Vehicle *db/db* mice compared with *db/m* controls (***Figure 6D***). Although there was a trend towards a reduction in complex I-stimulated respiration in Alisporivir treated *db/db* mice this was not statistically significant. No differences in proton leak nor FCCP stimulated respiration were observed.

Hydrogen peroxide species generation was decreased in db/db mice

Hydrogen peroxide (H_2O_2) generated by isolated mitochondria, and measured by Amplex red fluorescence intensity was halved in the *db/db* mice compared to

db/m controls with no difference between vehicle and Alisporivir treated *db/db* mice (***Figure 6E***). Percentage H_2O_2 generation with substrates was normalised to no substrates, and was found to be unchanged between groups (***Figure 6F***), therefore indicating that the decrease in total H_2O_2 was not substrate-dependent.

Db/db mice had altered gene expression profiles for several mitochondrial and cell death genes.

Renal cortical gene expression of several cell death and mitochondrial associated proteins were assessed by RT-qPCR in the *db/db* model to determine the effect of diabetes and treatment with Alisporivir on these mitochondrial centred pathways (***Figure 7A***). Treatment with the *CypD* inhibitor Alisporivir did not alter the gene expression of its associated gene (*Ppif*) in *db/m* mice, however, in the context of diabetes *Ppif* expression was significantly increased. Interestingly there was an upregulation of *Cytc* observed in the *db/m* mice treated with Alisporivir, however no change was present with diabetes in the *db/db* mice in contrast with the STZ model described above. Multiple other genes in both cell death and mitochondrial function were also assessed. Firstly, inflammation associated *TGF-β* and macrophage associated *F4/80* gene expressions were unchanged. Secondly, expression of several cell death activator caspases were also unchanged, although there was a significant increase in the inflammation-associated caspase 12 (Human equivalent of CASP 4) in Vehicle treated *db/db* diabetic mice only. Additionally, some fibrosis related genes, including collagen I and fibronectin, were upregulated in Vehicle *db/db* mice and partially attenuated in those treated with Alisporivir. Smooth muscle actin - alpha (*α-SMA*) and Connective Tissue Growth Factor (*CTGF)* did not change with diabetes.

Changes in genes associated with mitochondrial dynamics were minimal with the exception of a modest increase in *Mief1* expression in *db/db* mice treated with Vehicle which was not seen with Alisporivir. Finally, a fold change increase in the mitochondrial uncoupling protein-2 (*Ucp-2)* gene expression was statistically significant for *db/db* mice treated with and without Alisporivir.

Mitochondrial content was increased in db/db mice with no relative change in Electron Transport System Complexes

Mitochondrial ETS complex protein expression was not different between *db/m* and *db/db* mice with no change in complex I to V protein expression detected by western blot (***Figure 7B***).

Transmission electron microscopy of dissected renal cortices of *db/m* and *db/db* mice at endpoint showed that mitochondrial dynamics were not altered in *db/db* mice compared with *db/m* mice as assessed by the mitochondrial shape descriptors for Form Factor (***Suppl. Figure 1A***). However, *db/db* mice exhibited an increase in 2D volume of mitochondria from approximately 30% to 35% per μm^2 of cytosolic area in the proximal tubule cells (***Figure 7C***). This may be reflected in the shift in the frequency distribution of mitochondrial area (***Suppl. Figure 1B***).

Discussion

The mitochondrial permeability transition pore (mPTP) has long been considered to play an important role in mediating the demise of mitochondria in response to overwhelming stress. Although the exact mechanism of pore activation remains under investigation, the protein cyclophilin D (CypD) continues to be regarded as an important regulator of mitochondrial swelling and function (10,14,27–

29). In this study we demonstrated that global deletion of the CypD gene, *Ppif,* in C57BL6 mice was not associated with the development of any overt systemic pathology. This is consistent with other reports using *Ppif* $^{-/-}$ mice where phenotypes were limited to minor metabolic alterations, for example calcium handling and body fat metabolism (30–32). Indeed, our study showed some significant differences between *Ppif* $^{-/-}$ and *Ppif* $^{WT/WT}$ in non-diabetic mice with changes limited to slightly reduced body weight and lower collagen IV deposition. The increase in cystatin C in *Ppif* $^{-/-}$ mice indicated that deletion of CypD was protective against the development of diabetes-associated hyperfiltration. However, this elevated cystatin C could also be interpreted as a decline kidney function, even in non-diabetic mice, considering that the Albumin creatinine ratio was unchanged between *Ppif* $^{WT/WT}$ and *Ppif* $^{-/-}$. Additionally, lack of CypD was associated with an increase in the structural damage in the kidney in our model of STZ induced DKD. This increase in renal damage, following deletion of a key mPTP sensitising protein, provides supporting evidence for the complex biological role of cyclophilin D beyond providing a failsafe to initiating mitochondrial cell death (33).

Data from our study also revealed that CypD (*Ppif*) deletion was associated with a decrease in the relative fold change expression of multiple genes tested by qPCR (plus additional genes not presented) compared to the WT controls. This reduction in gene expression may be explained by the ability of Cyclophilins to regulate gene expression processes (34). Although the qPCR data for fibrosis genes appear to suggest an improvement in *Ppif* $^{-/-}$ STZ diabetic mice, the histology data may suggest that remodelling has already occurred.

It is generally well established that mPTP activity affects multiple organ systems, including liver function and skeletal muscle (30,35–37). This is in part due

to its role in regulating crucial mitochondrial functions and temporary mPTP depolarisation for physiological purposes (9,33,35). Further, CypD has been shown to negatively regulate F_1/F_0 ATP synthase activity, by binding to the Oligomycin-Sensitivity Conferring Protein (*OSCP*) (which links the F1 portion with the lateral stalk) thereby limiting ATP coupling and energy production (38–40). ATP synthase remains a reasonable candidate for the main component of the mPTP channel, making this interaction with CypD imperative (41,42). The requirement of these processes in the diabetic kidney is highlighted by the apparent increase in Glomerular structural damage observed in the *Ppif* $^{-/-}$ mice in our study. Interestingly, the mechanism for why CypD deletion attenuates other diabetes-related complications, such as pancreatic function and cognitive decline, has been demonstrated previously to be modulated by inhibiting β-oxidation and increasing substrate metabolism through glycolysis (36,43). However, metabolic alterations of CypD deletion have demonstrated variability in different organs for different genetic models, e.g. liver, skeletal muscle (34–36). In the kidney, CypD has also been previously demonstrated to be a key regulator of cellular metabolism with deletion of the *Ppif* gene (CypD) leading to an increase in glycolysis at the expense of fatty acid oxidation (44). These changes in glycolytic metabolism are pertinent in the renal cortex where β-oxidation provides a crucial fuel source to proximal tubular epithelial cells (PTECs) and this switch in fuel generation is likely to be detrimental, as reduced capacity of fatty acid oxidation (FAO) has been associated with increased renal fibrosis as a consequence of acute stress (45). Further, disruption to FAO pathways, as observed in patients with chronic kidney disease, is associated with renal fibrosis (46). Diabetes is also independently associated with changes in renal cellular metabolism including reduced FAO alongside a total increase in lipid

accumulation (47). The combined effect of both loss of CypD and the chronic metabolic stress induced by diabetes could be expected to lead to an increase in renal fibrosis. Indeed, loss of CypD has been previously hypothesised to prime PTECs to stress (44). Thus, a switch to glycolysis in the diabetic kidney, at the expense of β-oxidation, could explain why renal injury is recapitulated in our model.

Although complete loss of CypD, via *Ppif* deletion, was associated with negative consequences with respect to our STZ model of DKD, pharmacological blockade of CypD was still a pertinent option to explore as partial inhibition may allow maintenance of some physiological functions. The drug Alisporivir is a Cyclosporine analogue which has demonstrated ability to bind CypD and prevent its participation in mPT pore formation, without conferring the immunosuppressive effects of earlier Cyclosporines (48-50). Although Alisporivir was initially developed by Debiopharm as an antiviral drug to target HIV and hepatitis C infection, it has demonstrated efficacy in improving mitochondrial function and associated pathological outcomes in a range of acute disease settings by preventing cell death and rescuing mitochondrial function (51–54). The drug profile includes a demonstrated ability to reduce lesion size following cardiac infarction, and potentially as a prophylactic measure to protect kidney cells from renotoxic substances used during cardiac surgery (55,54). This is a promising result since a wide range of commonly used drugs induce renal toxicity and require monitoring of kidney function. Some prominent clinical studies, however, question the efficacy of acute CypD targeted therapy (Cyclosporines) in preventing cardiac pathologies (57,58). Nonetheless, research into Alisporivir's efficacy in treating chronic diseases is now being considered, with promising studies in mouse models of muscular dystrophy

revealing the potential for a long term therapeutic strategy to rescue mitochondrial function in certain chronic diseases (59,60).

Here, we reveal that Alisporivir at a dose of 5mg/kg/day did not protect the kidney from the development of clinical nephropathy markers in DKD. Indeed, we may consider that higher therapeutic doses could have increased efficacy, however in our study, a dose of 10mg/kg was associated with an attenuation of hyperglycaemia in *db/db* mice to *db/m* control levels (Data not shown). This effect is a confounding variable as high blood glucose is a well-established risk factor for diabetic complications. Strict blood glucose control is the gold standard for clinical diabetes care; thus, any renal protection mechanism of the drug alone at such glucose lowering doses cannot be independently assessed. This result may be worth exploring in future studies to further elucidate alterations in glucose metabolism and glycaemic control with such an agent. Our data revealed that treatment with 5mg/kg/day Alisporivir was not associated with an exacerbation of renal damage, in either control or diabetic animals. This is important as Cyclosporines can induce significant nephrotoxicity in a dose dependent manner; mediated through autophagy, oxidative stress and ER stress (61–63). Indeed, dose management concerns are often raised in patients prescribed analogues for immunosuppressant purposes (64–65). Currently there are limited data available on the pharmacodynamics of Alisporivir in renal tissues. Our data indicates that 5mg/kg/day Alisporivir was well tolerated in male *db/db* mice, providing evidence that this modified analogue may have reduced renal toxicity over traditional Cyclosporine analogues.

Interestingly, although Alisporivir had minimal effect on renal injury, there were a number of changes observed in the renal cortical mitochondria of *db/db* mice

compared with *db/m* controls. Some results were unexpected, but may align with previous models of mitochondrial protection. These include changes to fuel substrates, reactive oxygen species generation and oxygen availability per milligram of mitochondria. It is already hypothesised that metabolic changes in diabetes affect fuel preferences in renal proximal tubule cells (66). Indeed, studies of PTEC metabolism indicate a switch to a reliance on fatty acid synthesis is a protective measure against the high glucose present in the proximal tubule cells under normal conditions (67). With insulin resistance a decreased availability of intracellular glucose occurs in peripheral tissue, however, as renal proximal tubules are responsible for both gluconeogenesis and glucose recycling from the urinary ultrafiltrate, glucose uptake and release is increased in these cells under diabetic conditions (68-70). Although CypD deletion induced changes in renal function in our first study, we did not find any statistically significant change in any renal functional parameter with Alisporivir treatment in our *db/db* model, although some trends were evident. However, the trend in body weight data for example is likely to be an artefact of randomisation and stochastic variation in *db/db* body size given the body composition and percentage fat mass remained consistent between treatment groups indicating mice were just smaller, not less obese. This is also demonstrated with the results of the Comprehensive Laboratory Animal Monitoring System. Indeed, body size has been shown to be directly correlated with respiration, thus no real difference can be attributed to Alisporivir (20).

Some diabetes-associated mitochondrial changes, however, were altered with Alisporivir, indicating that some pharmacological activity was occurring in the renal cortex. Our data reveal that both mitochondrial function, and mitochondrial content, were altered in the diabetic kidney. All functional data were assessed per microgram

of mitochondrial protein to confirm that these changes were a constitutive adaptation and did not simply reflect the increased mitochondrial content observed in renal tissue. Mitochondrial ETS components (Citrate synthase activity, Protein expression of ETS complexes) were also unchanged per microgram of protein between all groups. Calcium challenge induced rapid mitochondrial swelling in both *db/m* and *db/db* renal cortical mitochondria. This illustrates that some level of mitochondrial impairment was present in the renal mitochondria as a slower rate of swelling is generally observed in liver and cardiac mitochondria in other models (4,71,72). However, CsA was able to effectively inhibit swelling in mitochondria isolated from *db/m* but not *db/db* mice. This abnormality in *db/db* mice was able to be rescued, with Alisporivir treatment able to partially restore mPTP inhibition. These data indicate that the drug was present in the renal cortical mitochondria, even though it did not alter OCR nor hydrogen peroxide production. CsA has been shown to reduce maximum respiration rates in a dose-dependent manner mediated through calcium sequestration, yet we did not see any respiration changes with Alisporivir at our dose (73).

It is possible that our data reveal that renal mitochondria are still able to adapt to chronic diabetes stressors via endogenous protective mechanisms. For example, previously elucidated adaptations in *db/db* mice include increased ROS generation mediated by ETS uncoupling (74). One adaptation to this involves the upregulation of Ucp-2 which is directly activated by the presence of ROS, and, has been previously shown to act as a *positive* feedback brake on damaging ROS by uncoupling ETS activity (75). In our study we observed an increase in oxygen consumption rate, paired with a concomitant decrease in radical sequestration in the production of H_2O_2. This indicates that mitochondrial uncoupling was occurring in the

db/db mice. As we also observed an upregulation of Ucp-2 gene expression, our data is consistent with this model and other studies demonstrating the protective nature of Ucp-2 from oxidative stress (76,77).

Finally, hypoxia is known to be a stressor of PTECs with decreased intrarenal oxygen levels previously demonstrated under diabetic conditions (78,79). Although this was beyond the scope of our study, it is possible that adaptations to hypoxia may also be responsible for changes in ETS efficiency and ATP generation in addition to those shown here. Many factors influence the behaviour of CypD and the formation of the mPTP in a complex interactive network, however, targeting CypD with Alisporivir was unable to prevent the development of DKD in our *db/db* mice.

This study has demonstrated that neither genetic deletion, nor partial blockade of CypD with Alisporivir, was able to rescue the common pathologies associated with progression of diabetic kidney disease. We conclude that CypD is an unsuitable target for rescuing mitochondrial heath in DKD. Although targeting mitochondrial function via inhibition of the mPTP has been demonstrated as an effective intervention in the pathophysiology of diseases in other organs, renal proximal tubular cells have a unique requirement for CypD under diabetic conditions and are unable to circumvent its physiological function to prevent mPTP associated pathology.

Acknowledgements

The authors would like to thank Sih Min Tan, Sally Penfold, Brooke Harcourt, Amy Morley and Karly Sourris for their technical assistance and also thank the Cellular and Molecular Metabolism Laboratory of the Baker Heart and Diabetes Institute, Melbourne, AU, for use of the CLAMs and EchoMRI equipment. We thank Carlos Rosado for assistance with generating PCR primers specifically for this project. We also acknowledge Georg Ramm, Joan Clark and Adam Costin of the Ramacciotti Centre for Cryo-electron Microscopy, at Monash University for technical assistance; and Monash Micro Imaging, for use of their equipment. We thank Novartis for providing the Alisporivir.

Declarations of interest

The authors have nothing to disclose.

Funding information

This work was completed with support from the Australian Diabetes Society. RSJL was supported by a scholarship from the Australian government Research Training Program. MTC was supported by a postdoctoral fellowship from the Australian Diabetes Society (Skip Martin Early Career Fellowship) and is currently the recipient of a Career Development Award from JDRF Australia, Australian Research Council Special Research Initiative in Type 1 Juvenile Diabetes. GCH was supported by a postdoctoral fellowship from JDRF. JMF and MEC are National Health and Medical Research Council Research Fellows. The authors have no conflicting financial interests.

Author contribution statement

RSJL ran the animal studies, performed experiments, researched the data and co-wrote the paper. MTC conceived the studies, ran the animal studies, researched the data and co-wrote the paper. GCH ran the animal studies, performed experiments and provided intellectual input on the data. TVN, MA, CG, VTB, MS, and JMF performed experiments and assisted in researching and interpreting the data. DH and MEC provided intellectual input on the data. All authors reviewed and edited the paper.

References

1. Ogurtsova K, da Rocha Fernandes JD, Huang Y, Linnenkamp U, Guariguata L, Cho NH, et al. IDF Diabetes Atlas: Global estimates for the prevalence of diabetes for 2015 and 2040. Diabetes Res Clin Pract. 2017 Jun;128:40–50.

2. Brenner BM, Cooper ME, de Zeeuw D, Keane WF, Mitch WE, Parving HH, et al. Effects of losartan on renal and cardiovascular outcomes in patients with type 2 diabetes and nephropathy. N Engl J Med. 2001 Sep 20;345(12):861–869.

3. Estacio RO, Jeffers BW, Gifford N, Schrier RW. Effect of blood pressure control on diabetic microvascular complications in patients with hypertension and type 2 diabetes. Diabetes Care. 2000 Apr;23 Suppl 2:B54–64.

4. Coughlan MT, Nguyen TV, Penfold SA, Higgins GC, Thallas-Bonke V, Tan SM, et al. Mapping Time-course Mitochondrial Adaptations in the Kidney in Experimental Diabetes. Clin Sci. 2016 Feb 1;130(9):711–720.

5. Duann P, Lin PH. Mitochondria damage and kidney disease. Adv Exp Med Biol. 2017;982:529–551.

6. Blantz RC, Deng A, Miracle CM, Thomson SC. Regulation of kidney function and metabolism: a question of supply and demand. Trans Am Clin Climatol Assoc. 2007;118:23–43.

7. Sharma K, Karl B, Mathew AV, Gangoiti JA, Wassel CL, Saito R, et al. Metabolomics reveals signature of mitochondrial dysfunction in diabetic kidney disease. J Am Soc Nephrol. 2013 Nov;24(11):1901–1912.

8. Wang X, Zhang X, Huang Z, Wu D, Liu B, Zhang R, et al. Protons trigger mitochondrial flashes. Biophys J. 2016 Jul 26;111(2):386–394.

9. Shang W, Gao H, Lu F, Ma Q, Fang H, Sun T, et al. Cyclophilin D regulates mitochondrial flashes and metabolism in cardiac myocytes. J Mol Cell Cardiol. 2016 Feb;91:63–71.

10. Baines CP, Kaiser RA, Purcell NH, Blair NS, Osinska H, Hambleton MA, et al. Loss of cyclophilin D reveals a critical role for mitochondrial permeability transition in cell death. Nature. 2005 Mar 31;434(7033):658–662.

11. Nakagawa T, Shimizu S, Watanabe T, Yamaguchi O, Otsu K, Yamagata H, et al. Cyclophilin D-dependent mitochondrial permeability transition regulates some necrotic but not apoptotic cell death. Nature. 2005 Mar 31;434(7033):652–658.

12. Kim JS, Qian T, Lemasters JJ. Mitochondrial permeability transition in the switch from necrotic to apoptotic cell death in ischemic rat hepatocytes. Gastroenterology. 2003 Feb;124(2):494–503.

13. Karch J, Kwong JQ, Burr AR, Sargent MA, Elrod JW, Peixoto PM, et al. Bax and Bak function as the outer membrane component of the mitochondrial

permeability pore in regulating necrotic cell death in mice. elife. 2013 Aug 27;2:e00772.

14. Karch J, Molkentin JD. Identifying the components of the elusive mitochondrial permeability transition pore. Proc Natl Acad Sci U S A. 2014 Jul 22;111(29):10396–10397.

15. Waldmeier PC, Feldtrauer JJ, Qian T, Lemasters JJ. Inhibition of the mitochondrial permeability transition by the nonimmunosuppressive cyclosporin derivative NIM811. Mol Pharmacol. 2002 Jul;62(1):22–29.

16. Lin DT, Lechleiter JD. Mitochondrial targeted cyclophilin D protects cells from cell death by peptidyl prolyl isomerization. J Biol Chem. 2002 Aug 23;277(34):31134–31141.

17. Devalaraja-Narashimha K, Diener AM, Padanilam BJ. Cyclophilin D gene ablation protects mice from ischemic renal injury. Am J Physiol Renal Physiol. 2009 Sep;297(3):F749–59.

18. Park JS, Pasupulati R, Feldkamp T, Roeser NF, Weinberg JM. Cyclophilin D and the mitochondrial permeability transition in kidney proximal tubules after hypoxic and ischemic injury. Am J Physiol Renal Physiol. 2011 Jul;301(1):F134–50.

19. Hou W, Leong KG, Ozols E, Tesch GH, Nikolic-Paterson DJ, Ma FY. Cyclophilin D promotes tubular cell damage and the development of interstitial fibrosis in the obstructed kidney. Clin Exp Pharmacol Physiol. 2018;45(3):250–260.

20. Lancaster GI, Henstridge DC. Body composition and metabolic caging analysis in high fat fed mice. J Vis Exp. 2018 May 24;(135).

21. Saito T, Sumithran E, Glasgow EF, Atkins RC. The enhancement of aminonucleoside nephrosis by the co-administration of protamine. Kidney Int. 1987 Nov;32(5):691–699.

22. Thallas-Bonke V, Thorpe SR, Coughlan MT, Fukami K, Yap FY, Sourris KC, et al. Inhibition of NADPH oxidase prevents advanced glycation end product-mediated damage in diabetic nephropathy through a protein kinase C-alpha-dependent pathway. Diabetes. 2008 Feb;57(2):460–469.

23. Frezza C, Cipolat S, Scorrano L. Organelle isolation: functional mitochondria from mouse liver, muscle and cultured fibroblasts. Nat Protoc. 2007;2(2):287–295.

24. Forbes JM, Ke BX, Nguyen TV, Henstridge DC, Penfold SA, Laskowski A, et al. Deficiency in mitochondrial complex I activity due to Ndufs6 gene trap insertion induces renal disease. Antioxid Redox Signal. 2013 Aug 1;19(4):331–343.

25. Picard M, White K, Turnbull DM. Mitochondrial morphology, topology, and membrane interactions in skeletal muscle: a quantitative three-dimensional electron microscopy study. J Appl Physiol. 2013 Jan 15;114(2):161–171.

26. Granata C, Oliveira RS, Little JP, Renner K, Bishop DJ. Mitochondrial adaptations to high-volume exercise training are rapidly reversed after a reduction in training volume in human skeletal muscle. FASEB J. 2016 Oct;30(10):3413–3423.

27. Baines CP, Gutiérrez-Aguilar M. The still uncertain identity of the channel-forming unit(s) of the mitochondrial permeability transition pore. Cell Calcium. 2018 May 16;73:121–130.

28. Karch J, Molkentin JD. Identity of the elusive mitochondrial permeability transition pore: what it might be, what it was, and what it still could be. Current Opinion in Physiology. 2018 Jun;3:57–62.

29. Dhingra R, Lieberman B, Kirshenbaum LA. Cyclophilin D phosphorylation is critical for mitochondrial calcium uniporter regulated permeability transition pore sensitivity. Cardiovasc Res. 2019 Feb 1;115(2):261–263.

30. Wang X, Du H, Shao S, Bo T, Yu C, Chen W, et al. Cyclophilin D deficiency attenuates mitochondrial perturbation and ameliorates hepatic steatosis. Hepatology. 2018 May 9;68(1):62–77.

31. Porter GA, Beutner G. Cyclophilin D, somehow a master regulator of mitochondrial function. Biomolecules. 2018 Dec 14;8(4).

32. Luvisetto S, Basso E, Petronilli V, Bernardi P, Forte M. Enhancement of anxiety, facilitation of avoidance behavior, and occurrence of adult-onset obesity in mice lacking mitochondrial cyclophilin D. Neuroscience. 2008 Aug 26;155(3):585–596.

33. Elrod JW, Molkentin JD. Physiologic functions of cyclophilin D and the mitochondrial permeability transition pore. Circ J. 2013 Mar 29;77(5):1111–1122.

34. Radhakrishnan J, Bazarek S, Chandran B, Gazmuri RJ. Cyclophilin-D: a resident regulator of mitochondrial gene expression. FASEB J. 2015 Jul;29(7):2734–2748.

35. Laker RC, Taddeo EP, Akhtar YN, Zhang M, Hoehn KL, Yan Z. The Mitochondrial Permeability Transition Pore Regulator Cyclophilin D Exhibits Tissue-Specific Control of Metabolic Homeostasis. PLoS ONE. 2016 Dec 22;11(12):e0167910.

36. Tavecchio M, Lisanti S, Bennett MJ, Languino LR, Altieri DC. Deletion of Cyclophilin D Impairs β-Oxidation and Promotes Glucose Metabolism. Sci Rep. 2015 Oct 30;5:15981.

37. Taddeo EP, Laker RC, Breen DS, Akhtar YN, Kenwood BM, Liao JA, et al. Opening of the mitochondrial permeability transition pore links mitochondrial dysfunction to insulin resistance in skeletal muscle. Molecular metabolism. 2014 Apr;3(2):124–134.

38. Antoniel M, Giorgio V, Fogolari F, Glick GD, Bernardi P, Lippe G. The oligomycin-sensitivity conferring protein of mitochondrial ATP synthase: emerging new roles in mitochondrial pathophysiology. Int J Mol Sci. 2014 Apr 30;15(5):7513–7536.

39. Giorgio V, Bisetto E, Soriano ME, Dabbeni-Sala F, Basso E, Petronilli V, et al. Cyclophilin D modulates mitochondrial F0F1-ATP synthase by interacting with the lateral stalk of the complex. J Biol Chem. 2009 Dec 4;284(49):33982–33988.

40. Chinopoulos C, Konràd C, Kiss G, Metelkin E, Töröcsik B, Zhang SF, et al. Modulation of F0F1-ATP synthase activity by cyclophilin D regulates matrix adenine nucleotide levels. FEBS J. 2011 Apr;278(7):1112–1125.

41. Bernardi P. Why F-ATP Synthase Remains a Strong Candidate as the Mitochondrial Permeability Transition Pore. Front Physiol. 2018 Nov 1;9:1543.

42. Giorgio V, Soriano ME, Basso E, Bisetto E, Lippe G, Forte MA, et al. Cyclophilin D in mitochondrial pathophysiology. Biochim Biophys Acta. 2010 Jul;1797(6-7):1113–1118.

43. Yan S, Du F, Wu L, Zhang Z, Zhong C, Yu Q, et al. F1F0 ATP Synthase-Cyclophilin D Interaction Contributes to Diabetes-Induced Synaptic Dysfunction and Cognitive Decline. Diabetes. 2016 Nov;65(11):3482–3494.

44. Klawitter J, Pennington A, Klawitter J, Thurman JM, Christians U. Mitochondrial cyclophilin D ablation is associated with the activation of Akt/p70S6K pathway in the mouse kidney. Sci Rep. 2017 Sep 5;7(1):10540.

45. Simon N, Hertig A. Alteration of fatty acid oxidation in tubular epithelial cells: from acute kidney injury to renal fibrogenesis. Frontiers in medicine. 2015 Aug 5;2:52.

46. Kang HM, Ahn SH, Choi P, Ko YA, Han SH, Chinga F, et al. Defective fatty acid oxidation in renal tubular epithelial cells has a key role in kidney fibrosis development. Nat Med. 2015 Jan;21(1):37–46.

47. Proctor G, Jiang T, Iwahashi M, Wang Z, Li J, Levi M. Regulation of renal fatty acid and cholesterol metabolism, inflammation, and fibrosis in Akita and OVE26 mice with type 1 diabetes. Diabetes. 2006 Sep;55(9):2502–2509.

48. Halestrap AP, Connern CP, Griffiths EJ, Kerr PM. Cyclosporin A binding to mitochondrial cyclophilin inhibits the permeability transition pore and protects hearts from ischaemia/reperfusion injury. Mol Cell Biochem. 1997 Sep;174(1-2):167–172.

49. Gomez L, Thibault H, Gharib A, Dumont JM, Vuagniaux G, Scalfaro P, et al. Inhibition of mitochondrial permeability transition improves functional recovery and reduces mortality following acute myocardial infarction in mice. Am J Physiol Heart Circ Physiol. 2007 Sep;293(3):H1654–61.

50. Hansson MJ, Mattiasson G, Månsson R, Karlsson J, Keep MF, Waldmeier P, et al. The nonimmunosuppressive cyclosporin analogs NIM811 and UNIL025 display nanomolar potencies on permeability transition in brain-derived mitochondria. J Bioenerg Biomembr. 2004 Aug;36(4):407–413.

51. Flisiak R, Horban A, Gallay P, Bobardt M, Selvarajah S, Wiercinska-Drapalo A, et al. The cyclophilin inhibitor Debio-025 shows potent anti-hepatitis C effect in patients coinfected with hepatitis C and human immunodeficiency virus. Hepatology. 2008 Mar;47(3):817–826.

52. Gallay PA, Lin K. Profile of alisporivir and its potential in the treatment of hepatitis C. Drug Des Devel Ther. 2013 Feb 15;7:105–115.

53. Quarato G, D'Aprile A, Gavillet B, Vuagniaux G, Moradpour D, Capitanio N, et al. The cyclophilin inhibitor alisporivir prevents hepatitis C virus-mediated mitochondrial dysfunction. Hepatology. 2012 May;55(5):1333–1343.

54. Paeshuyse J, Kaul A, De Clercq E, Rosenwirth B, Dumont JM, Scalfaro P, et al. The non-immunosuppressive cyclosporin DEBIO-025 is a potent inhibitor of hepatitis C virus replication in vitro. Hepatology. 2006 Apr;43(4):761–770.

55. Ederoth P, Grins E, Dardashti A, Brondén B, Metzsch C, Erdling A, et al. Ciclosporin to Protect Renal function In Cardiac Surgery (CiPRICS): a study protocol for a double-blind, randomised, placebo-controlled, proof-of-concept study. BMJ Open. 2016 Dec 15;6(12):e012299.

56. Piot C, Croisille P, Staat P, Thibault H, Rioufol G, Mewton N, et al. Effect of cyclosporine on reperfusion injury in acute myocardial infarction. N Engl J Med. 2008 Jul 31;359(5):473–481.

57. Cung TT, Morel O, Cayla G, Rioufol G, Garcia-Dorado D, Angoulvant D, et al. Cyclosporine before PCI in Patients with Acute Myocardial Infarction. N Engl J Med. 2015 Sep 10;373(11):1021–1031.

58. Rahman FA, Abdullah SS, Manan WZWA, Tan LT, Neoh CF, Ming LC, et al. Efficacy and Safety of Cyclosporine in Acute Myocardial Infarction: A Systematic Review and Meta-Analysis. Frontiers in pharmacology. 2018 Jun 19;9:238.

59. Schiavone M, Zulian A, Menazza S, Petronilli V, Argenton F, Merlini L, et al. Alisporivir rescues defective mitochondrial respiration in Duchenne muscular dystrophy. Pharmacol Res. 2017 Nov;125(Pt B):122–131.

60. Palma E, Tiepolo T, Angelin A, Sabatelli P, Maraldi NM, Basso E, et al. Genetic ablation of cyclophilin D rescues mitochondrial defects and prevents muscle

apoptosis in collagen VI myopathic mice. Hum Mol Genet. 2009 Jun 1;18(11):2024–2031.

61. Wu Q, Wang X, Nepovimova E, Wang Y, Yang H, Kuca K. Mechanism of cyclosporine A nephrotoxicity: Oxidative stress, autophagy, and signalings. Food Chem Toxicol. 2018 Aug;118:889–907.

62. Strzelecki T, Kumar S, Khauli R, Menon M. Impairment by cyclosporine of membrane-mediated functions in kidney mitochondria. Kidney Int. 1988 Aug;34(2):234–240.

63. Lee SH, Yoon YC, Jang YY, Song JH, Han ES, Lee CS. Effect of iron and ascorbate on cyclosporine-induced oxidative damage of kidney mitochondria and microsomes. Pharmacol Res. 2001 Feb;43(2):161–171.

64. Kuroyanagi Y, Gotoh Y, Kasahara K, Nagano C, Fujita N, Yamakawa S, et al. Effectiveness and nephrotoxicity of a 2-year medium dose of cyclosporine in pediatric patients with steroid-dependent nephrotic syndrome: determination of the need for follow-up kidney biopsy. Clin Exp Nephrol. 2018 Apr;22(2):413–419.

65. Burdmann EA, Andoh TF, Yu L, Bennett WM. Cyclosporine nephrotoxicity. Semin Nephrol. 2003 Sep;23(5):465–476.

66. Rosca MG, Vazquez EJ, Chen Q, Kerner J, Kern TS, Hoppel CL. Oxidation of fatty acids is the source of increased mitochondrial reactive oxygen species production in kidney cortical tubules in early diabetes. Diabetes. 2012 Aug;61(8):2074–2083.

67. Uchida S, Endou H. Substrate specificity to maintain cellular ATP along the mouse nephron. Am J Physiol. 1988 Nov;255(5 Pt 2):F977–83.

68. Meyer C, Stumvoll M, Dostou J, Welle S, Haymond M, Gerich J. Renal substrate exchange and gluconeogenesis in normal postabsorptive humans. Am J Physiol Endocrinol Metab. 2002 Feb;282(2):E428–34.

69. Stumvoll M, Meyer C, Mitrakou A, Nadkarni V, Gerich JE. Renal glucose production and utilization: new aspects in humans. Diabetologia. 1997 Jul;40(7):749–757.

70. Alsahli M, Gerich JE. Renal glucose metabolism in normal physiological conditions and in diabetes. Diabetes Res Clin Pract. 2017 Nov;133:1–9.

71. Sourris KC, Harcourt BE, Tang PH, Morley AL, Huynh K, Penfold SA, et al. Ubiquinone (coenzyme Q10) prevents renal mitochondrial dysfunction in an experimental model of type 2 diabetes. Free Radic Biol Med. 2012 Feb 1;52(3):716–723.

72. Borillo GA, Mason M, Quijada P, Völkers M, Cottage C, McGregor M, et al. Pim-1 kinase protects mitochondrial integrity in cardiomyocytes. Circ Res. 2010 Apr 16;106(7):1265–1274.

73. Fournier N, Ducet G, Crevat A. Action of cyclosporine on mitochondrial calcium fluxes. J Bioenerg Biomembr. 1987 Jun;19(3):297–303.

74. Persson MF, Franzén S, Catrina SB, Dallner G, Hansell P, Brismar K, et al. Coenzyme Q10 prevents GDP-sensitive mitochondrial uncoupling, glomerular hyperfiltration and proteinuria in kidneys from db/db mice as a model of type 2 diabetes. Diabetologia. 2012 May;55(5):1535–1543.

75. Brand MD, Affourtit C, Esteves TC, Green K, Lambert AJ, Miwa S, et al. Mitochondrial superoxide: production, biological effects, and activation of uncoupling proteins. Free Radic Biol Med. 2004 Sep 15;37(6):755–767.

76. Friederich M, Fasching A, Hansell P, Nordquist L, Palm F. Diabetes-induced up-regulation of uncoupling protein-2 results in increased mitochondrial uncoupling in kidney proximal tubular cells. Biochim Biophys Acta. 2008 Aug;1777(7-8):935–940.

77. Chen XL, Tang WX, Tang XH, Qin W, Gong M. Downregulation of uncoupling protein-2 by genipin exacerbates diabetes-induced kidney proximal tubular cells apoptosis. Ren Fail. 2014 Sep;36(8):1298–1303.

78. Palm F, Cederberg J, Hansell P, Liss P, Carlsson PO. Reactive oxygen species cause diabetes-induced decrease in renal oxygen tension. Diabetologia. 2003 Aug;46(8):1153–1160.

79. Friederich-Persson M, Thörn E, Hansell P, Nangaku M, Levin M, Palm F. Kidney hypoxia, attributable to increased oxygen consumption, induces nephropathy independently of hyperglycemia and oxidative stress. Hypertension. 2013 Nov;62(5):914–919.

	CIT		STZ		Two Way ANOVA			
	WT	KO	WT	KO	WT v KO		CIT v STZ	
	Mean ±SD	Mean ±SD	Mean ±SD	Mean ±SD	CIT	STZ	WT	KO
Body weight (g)	34.9 ±3.3	31.9 ±3.7	24.3 ±3.0	24.6 ±3.3	*	ns	****	****
Fasting blood glucose at cull (mmol/l)	14.2 ±3.5	13.0 ±2.8	29.5 ±4.2	27.9 ±6.4	ns	ns	****	****
Total kidney weight (g)	0.39 ±0.04	0.38 ±0.05	0.47 ±0.07	0.434 ±0.06	ns	ns	****	*
Kidney:Body Weight ratio (mg/kg)	11.1 ±1.2	11.9 ±1.4	19.6 ±3.2	17.9 ±3.4	ns	ns	****	****
24hr metcaging								
- 12 weeks								
Urine (ml)	0.6 ±0.4	0.6 ±0.4	14.9 ±6.8	10.9 ±7.3	ns	*	****	****
H_2O (ml)	4.7 ±2.1	4.7 ±1.5	18.8 ±7.6	16.5 ±7.5	ns	ns	****	****
Food (g)	2.3 ±0.7	2.1 ±0.7	4.6 ±1.1	4.3 ±0.5	ns	ns	****	****
- 20 weeks								
Urine (ml)	0.7 ±0.4	0.8 ±0.5	22.7 ±4.6	18.2 ±8.0	ns	*	****	****
H_2O (ml)	4.1 ± 1.0	4.4 ±1.8	25.7 ±5.0	21.8 ±8.0	ns	ns	****	****
Food (g)	2.3 ±0.6	2.1 ±0.6	5.2 ±0.5	4.7 ±0.8	ns	ns	****	****

Table 1. Phenotypic and metabolic characteristics of wild type (WT) and Ppif $^{-/-}$ (KO) mice

Data are mean±SD, *n*=9-10 per group. Two-way ANOVA was performed comparing factor variables, with Bonferroni Post Hoc test. CIT = Citrate control (non-diabetic); STZ = Streptozotocin induced diabetes

	db/m Vehicle	db/m Alisporivir	db/db Vehicle	db/db Alisporivir	Two Way ANOVA comparison	
	Mean ±SD	Mean ±SD	Mean ±SD	Mean ±SD	Vehicle db/m v. db/db	db/db Vehicle v. Alisporivir
Cull weight (g)	29.1 ±2.3	29.7 ±3.4	38.2 ±8.3	34.4 ±7.3	***	ns
Glucose† (mmol)	10.3 ±1.4	10.1 ±1.8	28.6 ±12.1	25.0 ±13.4	****	ns
HbA_{1C}‡ (%)	4.7 ±0.1	4.6 ±0.6	12.4 ±1.6	11.7 ±2.6	****	ns
EchoMRI						
Fat (g)	5.1 ±1.7	4.4 ±1.3	18.3 ±6.00	14.3 ±6.5	****	ns
Lean (g)	23.5 ±1.9	24.0 ±3.2	21.7 ±2.1	21.1 ±2.1	ns	ns
Total (g)	28.7 ±2.3	28.3 ±3.1	40.0 ±6.6	35.5 ±6.2	****	ns
Total Kidney weight (g)	0.36 ±0.1	0.40 ±0.1	0.46 ±0.1	0.48 ±0.1	*	ns

Table 2. Phenotypic and metabolic characteristics of db/m and db/db mice

Note: †Fasting Spot glucose test at endpoint; ‡HbA_{1C}, for glycated haemoglobin.
Two Way ANOVA performed, with Bonferroni post hoc Test comparing each factor variable.
*P<0.5 ** P <0.01 *** P <0.001 **** P <0.0001; ns is P >0.05); n=11-15

	STZ model of T1DM	Genetic *Ppif* deletion	Interaction†		*db/db* model of T2DM	Alisporivir (5mg/kg/day)	Interaction‡
Renal hypertrophy	Present	No change	No change		Present	No change	No change
Structural glomerular injury	Moderate	Mild	Worsened		Moderate	No change, or mild reduction	No change
Glomerular filtration estimate	Lowered	Increased	Intermediate		No change	No change	No change
Urinary damage markers	Increased	No change	No change		Increased	No change	No change

Table 3: Summary of key results

Comparison of key pathological changes observed in both mouse models. The impact of diabetes and targeting CypD (*Ppif*) are summarised in comparison to control mice. The interactive effects between diabetes and reduction in CypD represent the changes observed in: † the *Ppif* $^{-/-}$ STZ treated group; and ‡ the db/db mice treated with Alisporivir. T1DM = Type 1 diabetes; T2DM = Type 2 diabetes.

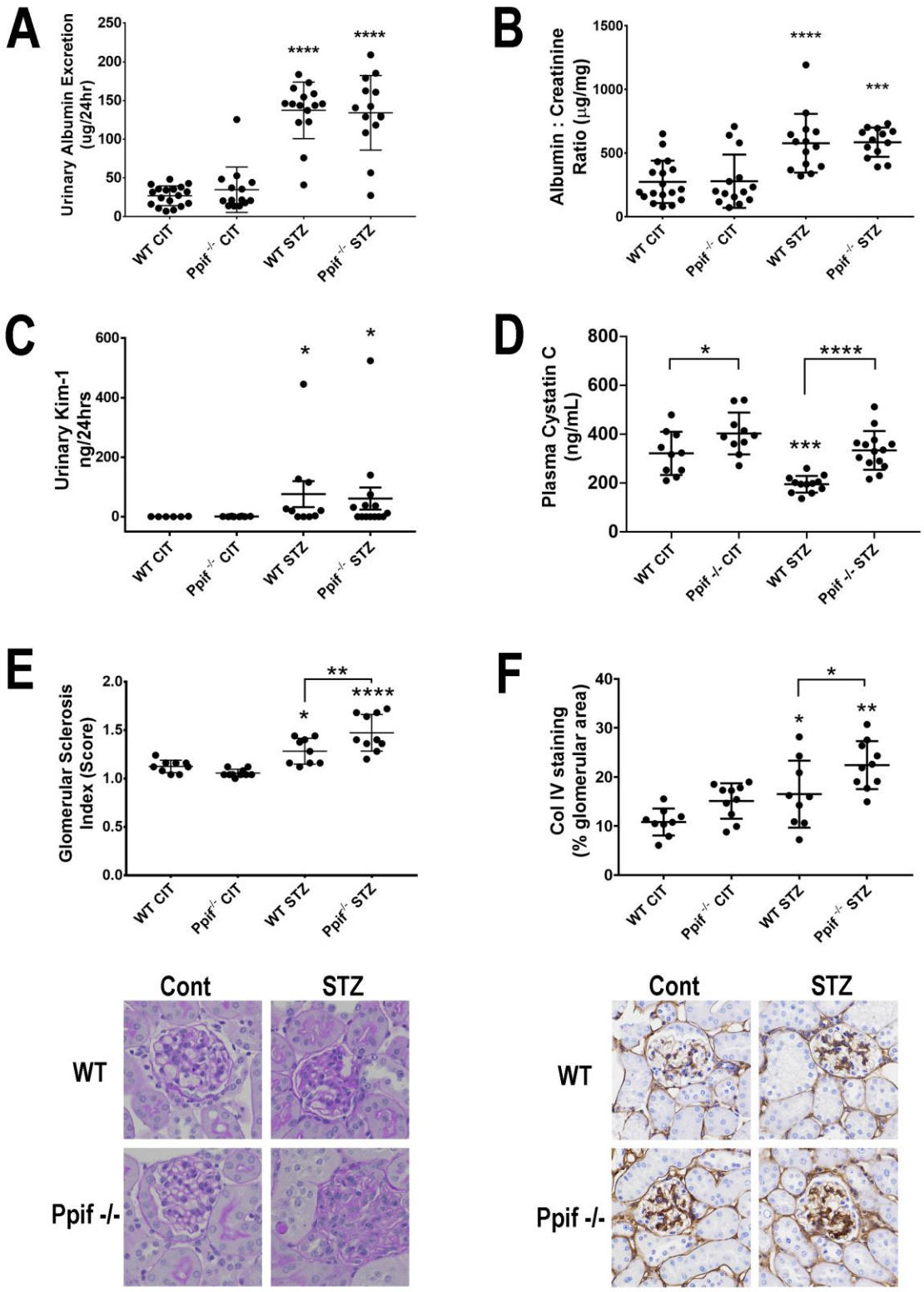
A
Urinary Albumin Excretion (ug/24hr)
250
200
150
100
50
0
****
****
WT CIT
Ppif -/- CIT
WT STZ
Ppif -/- STZ
B
Albumin : Creatinine Ratio (µg/mg)
1500
1000
500
0
****
***
WT CIT
Ppif -/- CIT
WT STZ
Ppif -/- STZ
C
Urinary Kim-1 ng/24hrs
600
400
200
0
*
*
WT CIT
Ppif -/- CIT
WT STZ
Ppif -/- STZ
D
Plasma Cystatin C (ng/mL)
800
600
400
200
0
*
****
***
WT CIT
Ppif -/- CIT
WT STZ
Ppif -/- STZ
E
Glomerular Sclerosis Index (Score)
2.0
1.5
1.0
0.5
0.0
**
*
****
WT CIT
Ppif -/- CIT
WT STZ
Ppif -/- STZ
F
Col IV staining (% glomerular area)
40
30
20
10
0
*
*
**
WT CIT
Ppif -/- CIT
WT STZ
Ppif -/- STZ
Cont
STZ
WT
Ppif -/-
Cont
STZ
WT
Ppif -/-

Figure 1

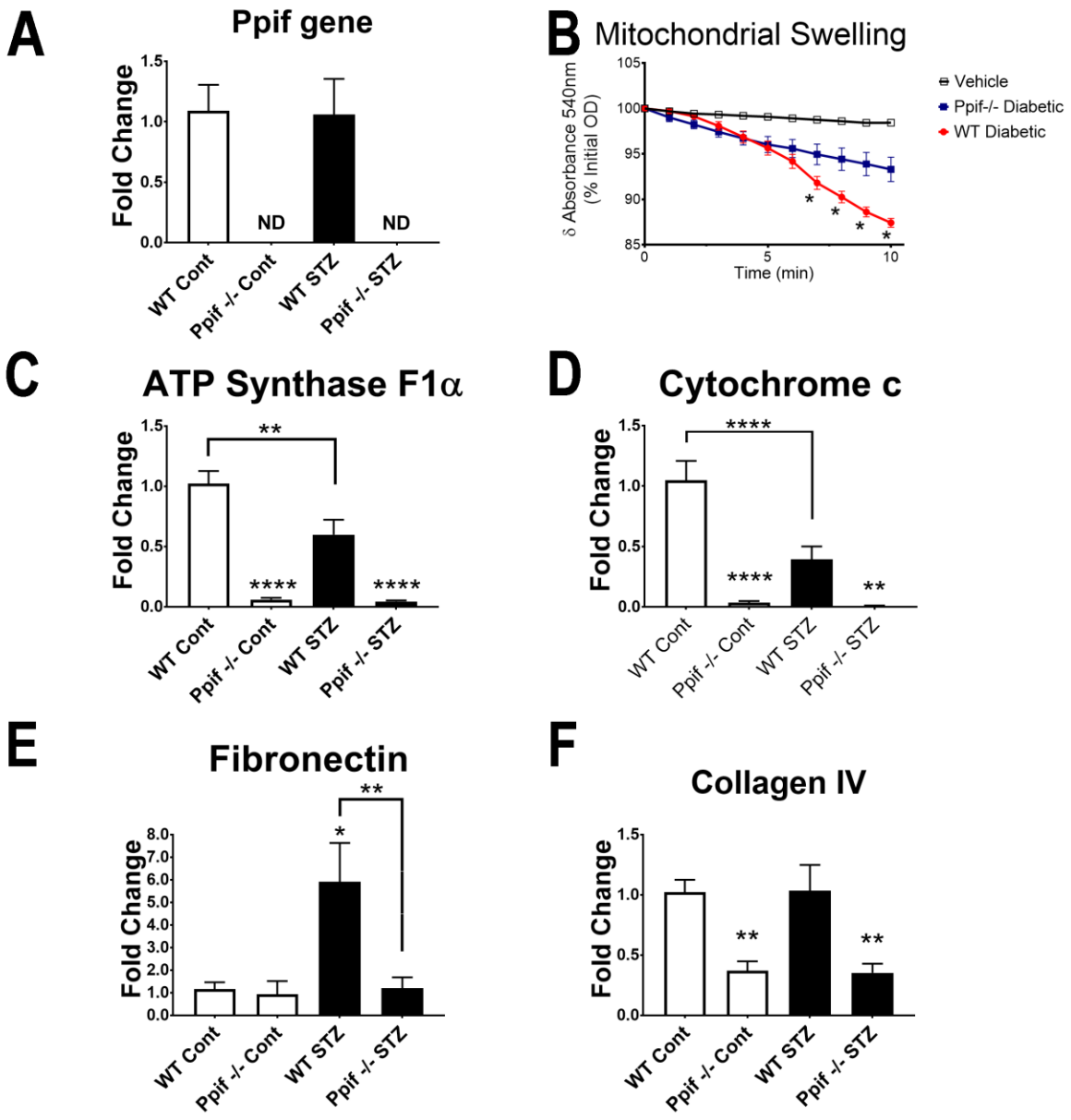
A
Ppif gene
Fold Change
1.5
1.0
0.5
0.0
ND
ND
WT Cont
Ppif -/- Cont
WT STZ
Ppif -/- STZ
B
Mitochondrial Swelling
δ Absorbance 540nm
(% Initial OD)
105
100
95
90
85
0
5
10
Time (min)
Vehicle
Ppif-/- Diabetic
WT Diabetic
C
ATP Synthase F1α
**
****
****
D
Cytochrome c
****
****
**
E
Fibronectin
**
*
8.0
7.0
6.0
5.0
4.0
3.0
2.0
1.0
0.0
F
Collagen IV
**
**

Figure 2

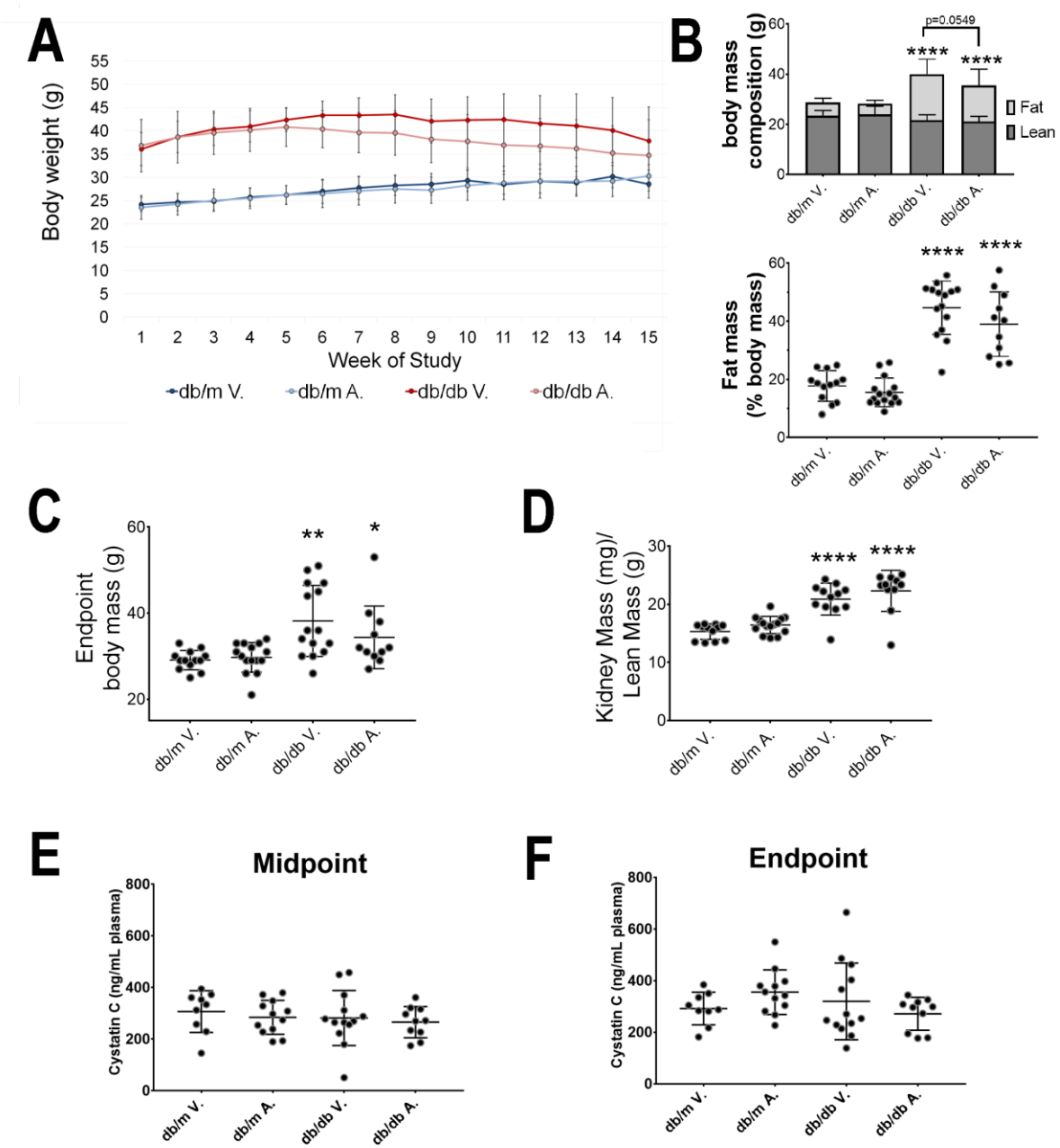
A
Body weight (g)
Week of Study
db/m V.
db/m A.
db/db V.
db/db A.
B
body mass composition (g)
p=0.0549
****
Fat
Lean
Fat mass (% body mass)
C
Endpoint body mass (g)
**
*
D
Kidney Mass (mg)/ Lean Mass (g)
E
Midpoint
Cystatin C (ng/mL plasma)
F
Endpoint

Figure 3

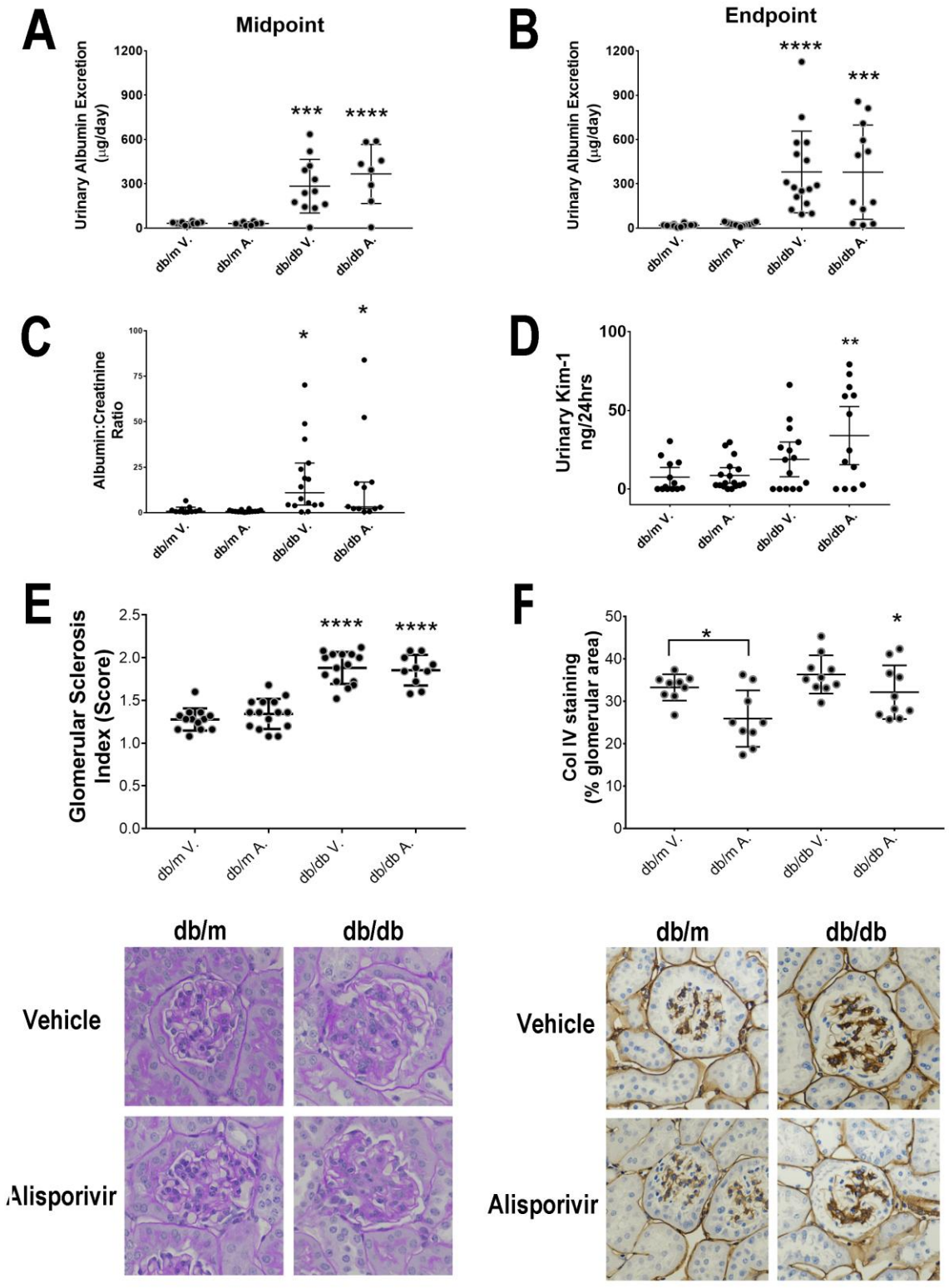
A
Midpoint
Urinary Albumin Excretion (µg/day)
1200
900
600
300
0
***
****
db/m V.
db/m A.
db/db V.
db/db A.
B
Endpoint
Urinary Albumin Excretion (µg/day)
****
***
C
Albumin:Creatinine Ratio
100
75
50
25
0
*
*
D
Urinary Kim-1 ng/24hrs
100
50
0
**
E
Glomerular Sclerosis Index (Score)
2.5
2.0
1.5
1.0
0.5
0.0
****
****
F
Col IV staining (% glomerular area)
50
40
30
20
10
0
*
*
db/m
db/db
Vehicle
Alisporivir

Figure 4

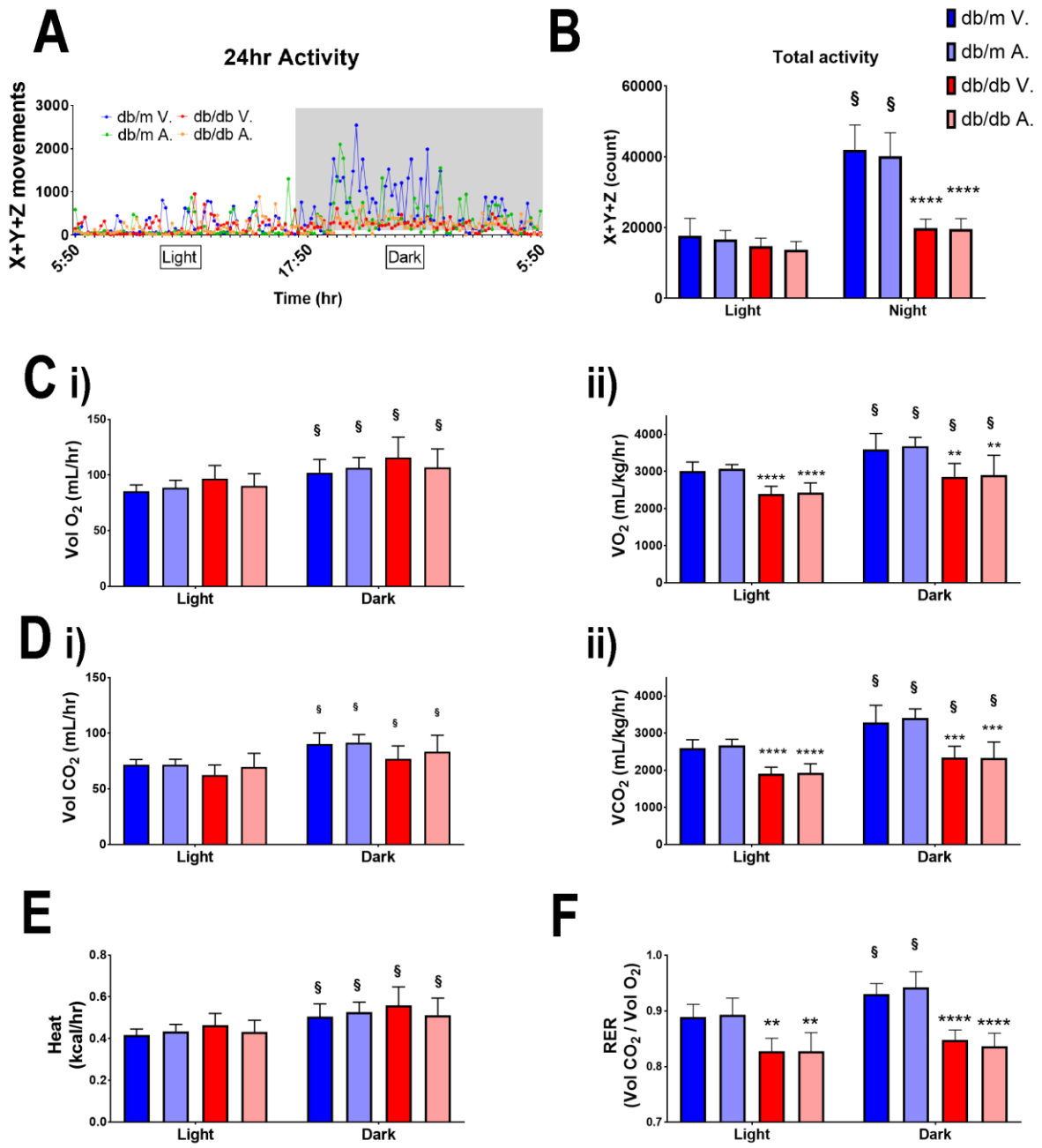
A
24hr Activity
X+Y+Z movements
db/m V.
db/m A.
db/db V.
db/db A.
Light
Dark
5:50
17:50
5:50
Time (hr)
B
Total activity
X+Y+Z (count)
db/m V.
db/m A.
db/db V.
db/db A.
Light
Night
C i)
Vol O2 (mL/hr)
Light
Dark
ii)
VO2 (mL/kg/hr)
Light
Dark
D i)
Vol CO2 (mL/hr)
Light
Dark
ii)
VCO2 (mL/kg/hr)
Light
Dark
E
Heat (kcal/hr)
Light
Dark
F
RER (Vol CO2 / Vol O2)
Light
Dark

Figure 5

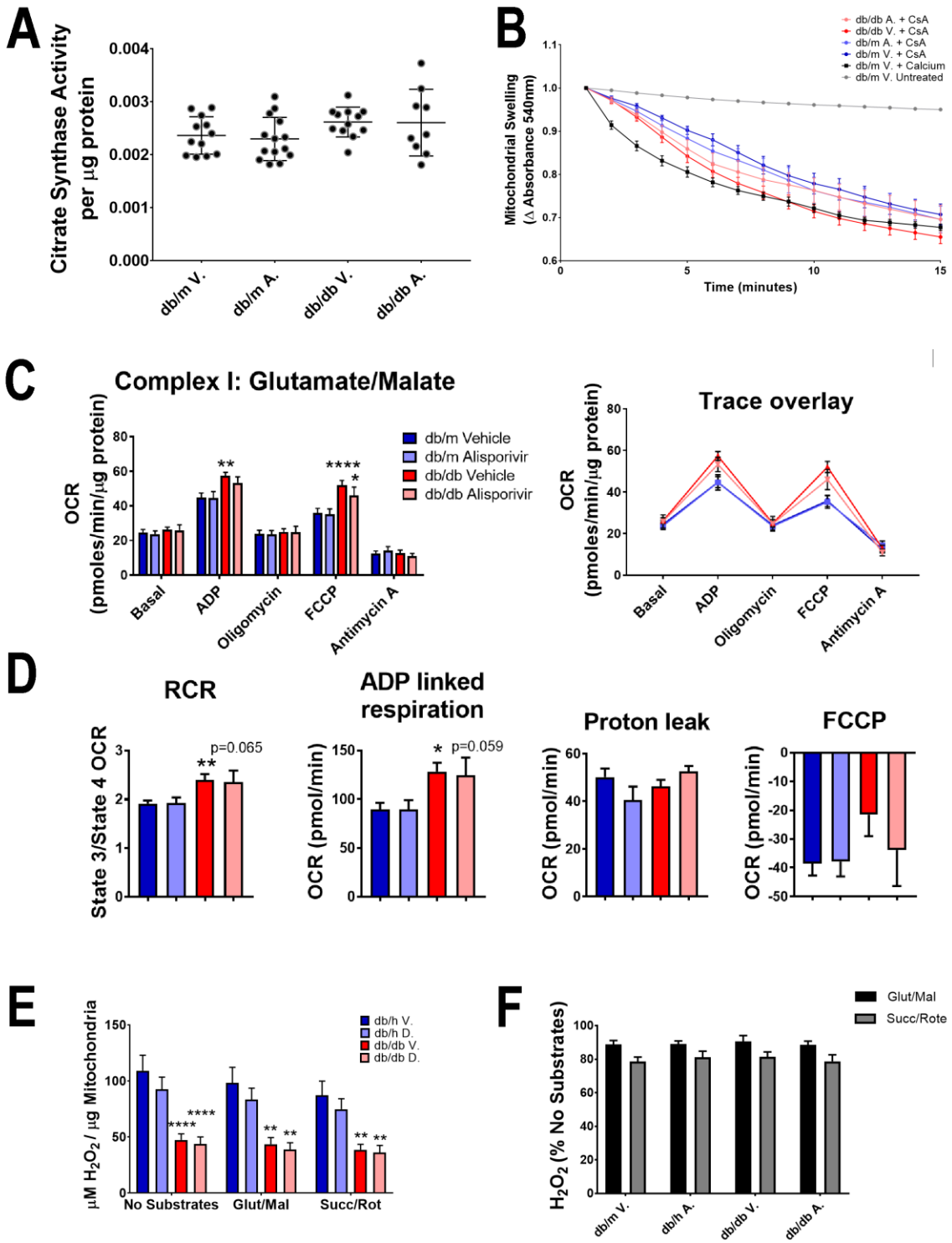
A
Citrate Synthase Activity per µg protein
0.004
0.003
0.002
0.001
0.000
db/m V.
db/m A.
db/db V.
db/db A.
B
Mitochondrial Swelling (Δ Absorbance 540nm)
Time (minutes)
db/db A. + CsA
db/db V. + CsA
db/m A. + CsA
db/m V. + CsA
db/m V. + Calcium
db/m V. Untreated
C
Complex I: Glutamate/Malate
OCR (pmoles/min/µg protein)
db/m Vehicle
db/m Alisporivir
db/db Vehicle
db/db Alisporivir
Basal
ADP
Oligomycin
FCCP
Antimycin A
Trace overlay
D
RCR
State 3/State 4 OCR
p=0.065
ADP linked respiration
OCR (pmol/min)
p=0.059
Proton leak
FCCP
E
µM H2O2 / µg Mitochondria
db/h V.
db/h D.
db/db V.
db/db D.
No Substrates
Glut/Mal
Succ/Rot
F
H2O2 (% No Substrates)
Glut/Mal
Succ/Rote
db/m V.
db/h A.
db/db V.
db/db A.

Figure 6

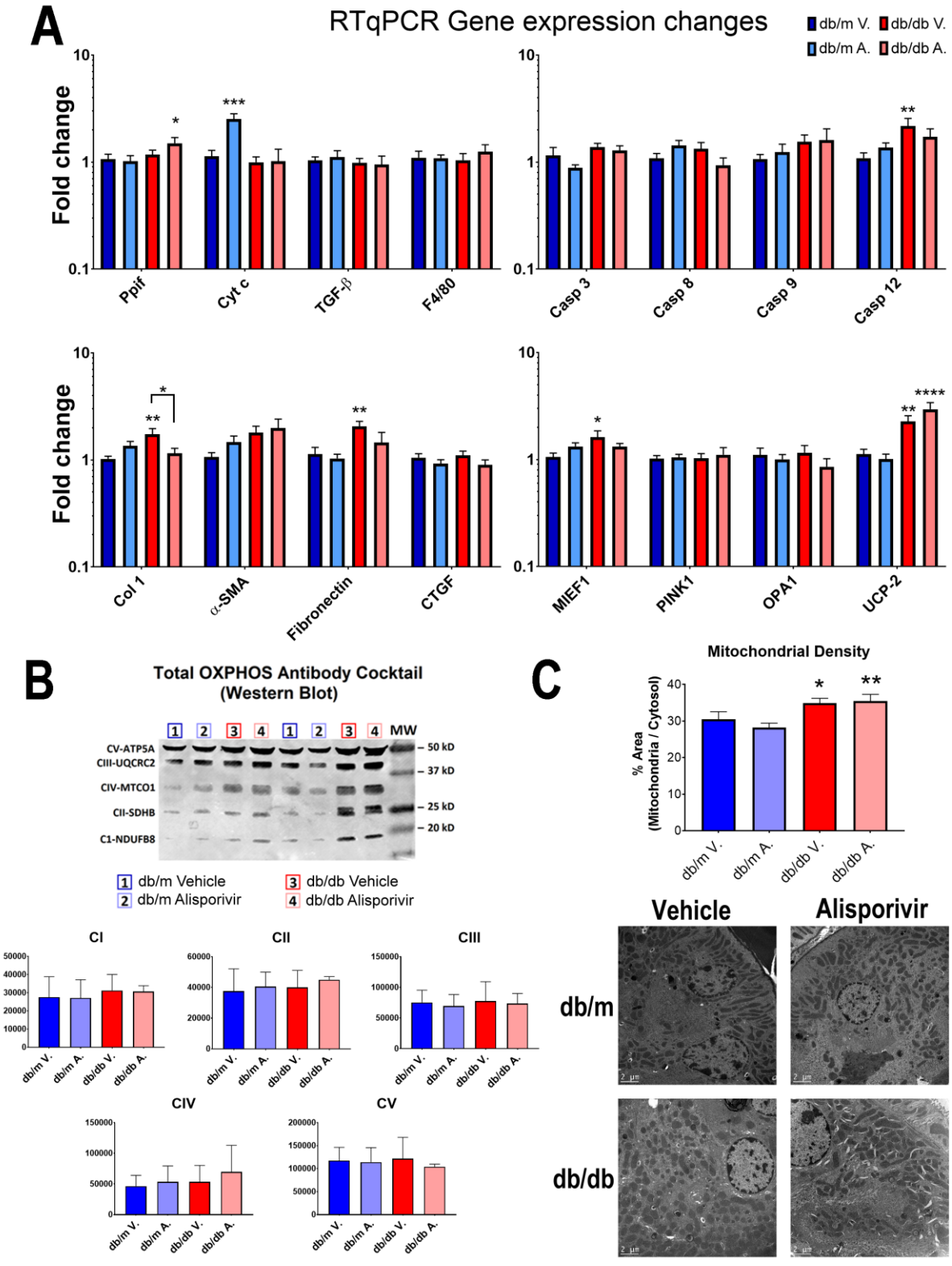
A
RTqPCR Gene expression changes
db/m V.
db/db V.
db/m A.
db/db A.
Fold change
Ppif
Cyt c
TGF-β
F4/80
Casp 3
Casp 8
Casp 9
Casp 12
Col 1
α-SMA
Fibronectin
CTGF
MIEF1
PINK1
OPA1
UCP-2
B
Total OXPHOS Antibody Cocktail
(Western Blot)
MW
CV-ATP5A
CIII-UQCRC2
CIV-MTCO1
CII-SDHB
C1-NDUFB8
50 kD
37 kD
25 kD
20 kD
1 db/m Vehicle
2 db/m Alisporivir
3 db/db Vehicle
4 db/db Alisporivir
CI
CII
CIII
CIV
CV
C
Mitochondrial Density
% Area
(Mitochondria / Cytosol)
Vehicle
Alisporivir
db/m
db/db

Figure 7

Figure Legends

Figure 1: **Cyclophilin D deletion does not protect against diabetes-induced renal injury**. (A) Urinary albumin excretion; (B) Urinary albumin-to-creatinine ratio, mean ±SD shown; (C) Urinary excretion of kidney injury molecule-1 (KIM-1); (D) Plasma cystatin C; (E) Glomerulosclerotic index (GSI), with representative photomicrographs of PAS-stained renal cortex, x400 magnification; (F) Collagen IV deposition, with representative photomicrographs of Collagen IV immunohistochemistry in renal cortex, x400 magnification. Data are mean ±SEM unless otherwise stated, *n*=9-14 mice per group. Two-way ANOVA with Bonferroni post hoc test was performed where *P<0.05, **P<0.01, ***P<0.001, ****P<0.0001.

Figure 2: Deletion of Cyclophilin D (*Ppif*) inhibits mitochondrial swelling and alters gene expression profiles. (A) Deletion of Ppif gene confirmed by RTqPCR; (B) Mitochondrial swelling by Calcium challenge; (C) qPCR for ATP Synthase F1α gene; (D) RTqPCR for Cytochrome c gene; (E) RTqPCR for Fibronectin gene; (F) RTqPCR for Collagen IV gene. Data are mean ±SEM, *n*=9-14 mice per group. Two-way ANOVA with Bonferroni post hoc test was performed with *P<0.05, **P<0.01, ***P<0.001, ****P<0.0001.

Figure 3: *Db/db* mice develop obesity and hyperglycaemia with associated renal hypertrophy and Albuminuria, which was unchanged with Alisporivir. (A) Average body weights during study; (B) Body mass index as assessed by EchoMRI showing average lean and fat mass (top) and individual % body fat (bottom). (C) Final body mass at 16 weeks of study; (D) Kidney weight to lean body mass; Plasma Cystatin C measured at midpoint (E) and endpoint (F). Data are mean ±SD, Two-way ANOVA with Bonferroni post hoc test was performed with *P<0.05, **P<0.01, ***P<0.001, ****P<0.0001. *n*=9-15 mice per group.

Figure 4: Treatment with Alisporivir does not alleviate markers of diabetes associated renal injury. Albuminuria measured as Urinary Albumin excretion per day for midpoint (A)

and endpoint (B); (C) Albumin to Creatinine Ratio at endpoint; (D) Detection of Kidney Injury Molecule 1 (Kim-1) in 24hr Urine by ELISA, Mean with 95% CI shown; (E) Glomerular Sclerosis Index (GSI) assessed in 3mm Periodic Acid Shift stained sections of renal cortex, with representative photomicrographs at x400 magnification; (F) Glomerular Collagen IV deposition assessed by immunohistochemistry in 4 micron renal cortical sections, with representative photomicrographs, x400 magnification. Data are mean ±SD. Two-way ANOVA with Bonferroni post hoc test was performed with *P<0.05, **P<0.01, ***P<0.001, ****P<0.0001. n=9-15 mice per group.

Figure 5: Comprehensive Laboratory Animal Monitoring (CLAMs) revealed Alisporivir has no effect on activity or respiration in db/db mice. (**A**) Representative graphs (n=1 per group) for total movements assessed by beam breaks in X+Y+Z planes over 24hrs, (**B**) Mean and 95% CI for Sum of all movements during light (sleep) and dark (active) periods; (**C**) Oxygen consumption: i) mL/hr ii) mL/kg/hr; (**D**) Carbon dioxide production: i) mL/hr, ii) mL/kg/hr; (**E**) Heat production (**F**) Respiratory Exchange Ratio (RER) Vol CO_2 / Vol O_2. Data are mean ±95% CI. n=8-10 mice per group. Two-way ANOVA with Bonferroni post hoc test comparing *db/m* vs *db/db* *P<0.05, **P<0.01, ***P<0.001, ****P<0.0001. No difference between Vehicle (V.) and Alisporivir (A.) was found for any parameter. Two-way ANOVA with repeated measures was performed comparing Light and Dark time points with Bonferroni post hoc test where § shows P<0.05.

Figure 6: *Db/db* mice exhibit changes in mitochondrial function with minor modulation by Alisporivir. (A) Citrate synthase activity in isolated renal cortex mitochondria mean ±SD; (B) Calcium induced mitochondrial swelling; (C) Mitochondrial stress test with Glutamate + Malate-stimulated Complex I respiration, (right) respiration trace overlay; (D) Calculated Respiratory Control Ratio (RCR), ADP linked respiration, proton leak and FCCP-stimulated OCR; (E) Hydrogen peroxide production in isolated mitochondria; (F) Hydrogen peroxide production normalised to 'no substrate' control. Data are mean ±SEM unless otherwise

stated. Two-way ANOVA with Bonferroni post hoc test was performed with *P<0.05, **P<0.01, ***P<0.001, ****P<0.0001. n=9-15 mice per group.

Figure 7: Alisporivir treatment induced minor changes in Diabetes-induced mitochondrial gene expression but did not alter ETS protein expression, nor increased 2D volume. (A) RTqPCR gene expression changes in whole renal cortex, relative fold change compared with db/m Vehicle (V.). Mean ±SEM, n=9-14 per group (B) ETS Complexes, protein expression assessed by Western blot. Representative image with n=2 per gel, per experimental group. Graphs show mean ± SD of n=6 total; (C) Transmission Electron Microscopy assessment of 2D mitochondrial volume in renal Proximal Tubule Epithelia Cells (PTECs). Graph shows mean ±SEM for n=3 per group with representative Electron micrographs (17.44 x 17.44µm). Two-way ANOVA with Bonferroni post hoc test was performed with *P<0.05, **P<0.01, ***P<0.001, ****P<0.0001.

Gene (*Mus muscularis*)	Forward 5' – 3'	Reverse 5' – 3'	Genebank accession
Ppif ‡ (Cyclophilin F, Cyclophilin D)	TGGCTCTCAGTTCTTTATCTGC	ACATCCATGCCCTCTTTGAC	NM_134084.1
Cyt c	CATCTTGGTTTCAAGCCCAGA	CTGCCCAGGCCAAAATTGC	JF919281.1
ATP synthase, F1-α	TGTCCGCTTACATTCCAACAAA	CAGGGCGGATGCCTTTATAG	BC020417
Fibronectin	ACATGGCTTTAGGCGGACAA	ACATTCGGCAGGTATGGTCTTG	M10905
TGF-β	GCAGTGGCTGAACCAAGGA	GCAGTGAGCGCTGAATCGA	NM_011577
F4/80	GGTACAGTCATCTCCCTGGTATGTCT	GGTTCTGAACAGCACGACACA	X93328
Casp 3	GACGGTCCTCCTGGTCTTTG	GTGGCTGGCTGCATTGC	NM_009810
Casp 8	CAACTTCCTAGACTGCAACCG	TCCAACTCGCTCACTTCTTCT	NM_009812.2
Casp 9	TCCTGGTACATCGAGACCTTG	AAGTCCCTTTCGCAGAAACAG	NM_015733.5
Casp 12	AGACAGAGTTAATGCAGTTTGCT	TTCACCCCACAGATTCCTTCC	NM_009808.4
Col I	GACTGGAAGAGCGGAGAGTACTG	CCTTGATGGCGTCCAGGTT	NM_007742
α-SMA	GACGCTGAAGTATCCGATAGAACA	GGCCACACGAAGCTCGTTAT	NM_007392
CTGF	GCTGCCTACCGACTGGAAGA	CTTAGAACAGGCGCTCCACTCT	BC006783
Mief1	GCTTCGCTACACTGATCGAGACT	CTCAAGCTTCTGATTTTTCCTGAAT	NM_178719
Pink1	AGAAAACCAAGCGCGTGTCT	GGAAGCCCTGCCAGCAT	NM_026880
Opa1 ǂ	ATACTGGGATCTGCTGTTGG	AAGTCAGGCACAATCCACTT	NM_001199177.1
Ucp-2	CCGTAATGCCATTGTCAACTGT	GGCTTTCAGGAGAGTATCTTTGATG	BC012697

Notes: All genes were generated against sequences for *Mus muscularis*
‡Ppif primer sequence from Lam, CK et al *PNAS* 2015

Supplementary Table 1. List of Primers sequences used

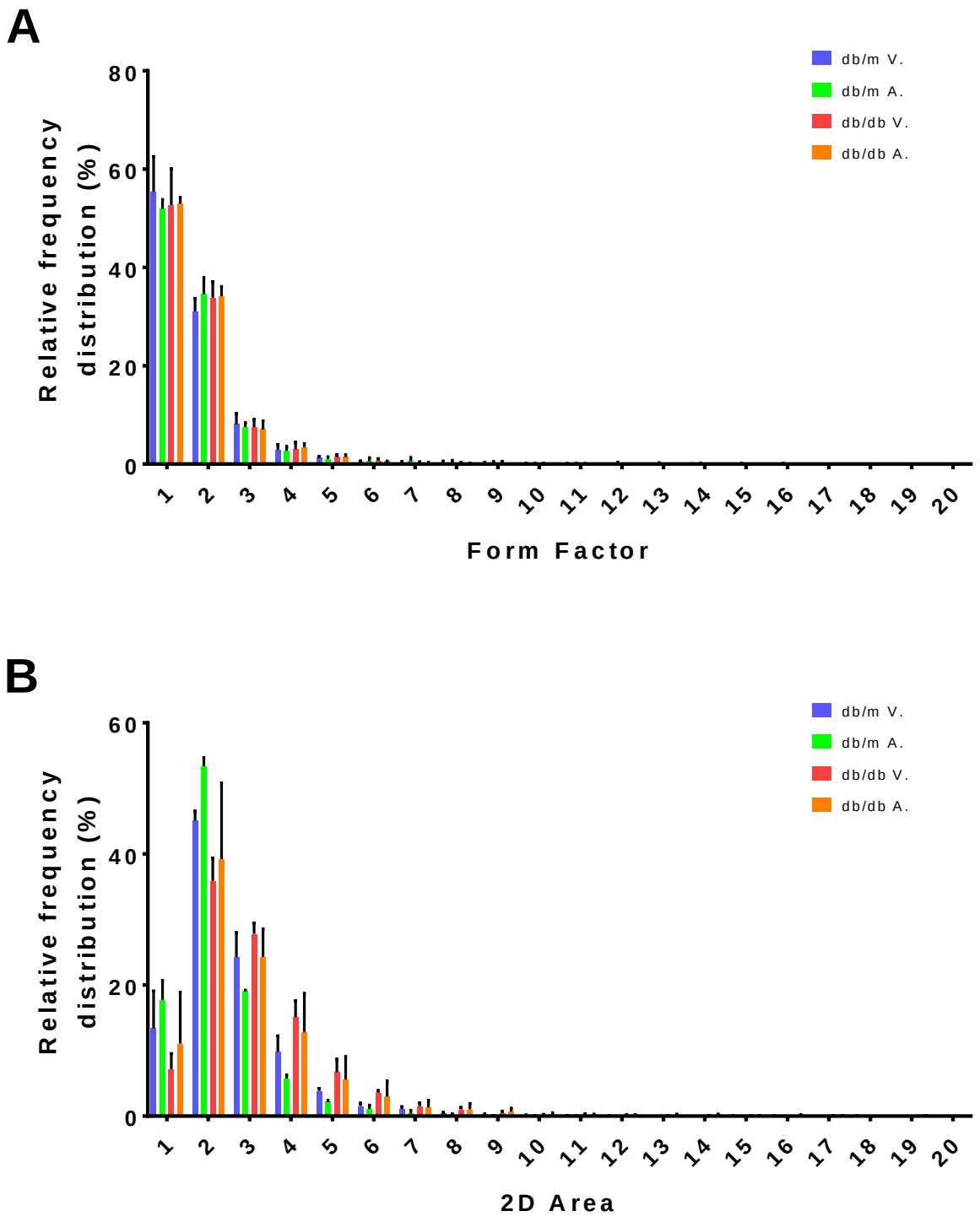

Supplementary Figure 1. Frequency Distribution Data for analysis of Electron Microscopy 2D sections of PTEC mitochondria. (A) Shape descriptors of 'Form Factor'. (B) Frequency Distribution of % Area mitochondria in 2D cytosol volume. Frequency data was divided into 20 bins of equal size. Graphs show mean and SD of n=3 per group.

5.4 ADDITIONAL DATA

5.4.1 OVERVIEW

This section presents the results for the 10mg/kg/day pilot study in *db/db* mice. Additionally, data and details for the 5mg/kg/day study and the Ppif KO study not presented in publication 2 are also included below.

5.4.2 ALLOCATION OF MICE TO *DB/DB* STUDY

Db/db mice, and their *db/m* litter mate controls, were allocated to the study (under ethics number E/1502/2016/B) from pups born within the in house *db/db* mouse colony housed at the AMREP animal facility. Mouse pups were randomly assigned into Vehicle or Alisporivir treatment groups for each litter, thus maintaining equal numbers across groups where possible. This was performed to ensure that at least one mouse from each group was represented in experiments performed on isolated mitochondria at endpoint. Mice were culled in batches of 4-9 mice as this was the maximum that could be assessed at one time in a single 96-well plate for the Seahorse Bioanalyzer. Total number of mice allocated to each group are presented in Table 5.1 below.

Table 5.1: Total number of mice allocated to this study

	db/m		db/db	
	Vehicle	Alisporivir	Vehicle	Alisporivir
Total	16	19	20	16
Excluded	0	0	3	2
5mg/kg total	13	15	16	12
Excluded	0	0	2	1
10mg/kg	3	4	4	4
Excluded	0	0	1	1

EXCLUSION OF ANIMALS

Animals were excluded where illness necessitated culling prior to endpoint, according to ethical guidelines, or, upon cull an individual mouse was found to have significant pathology not related to the development of diabetic kidney disease.

5.4.3 PILOT STUDY OF 10MG/KG/DAY DOSE OF ALISPORIVIR

A small group of mice (*n*=3) received a dose of 10mg/kg Alisporivir per day by oral gavage to assess the effects of this dose in vivo. Results for this pilot study are presented in ***Table 5.2***. Both groups of *db/db* mice had higher body weight at endpoint; however *db/db* mice treated with Alisporivir weighed slightly less. This apparent difference is likely due to variation in total body size; as when assessed by EchoMRI no difference in fat mass or percentage body fat was evident. No difference in lean body mass was present between Vehicle treated *db/m* or *db/db* mice, however the slight decrease in *db/db* mice on Alisporivir was also likely to be a result of the variable body size. Random spot blood glucose at endpoint indicated that the *db/db* mice on Alisporivir may not have been as hyperglycaemic as expected. These values were confirmed by HbA_{1C} measurement, performed to assess long-term blood glucose levels. Indeed, the *db/db* mice did not have sustained hyperglycaemia as evident by a decreased HbA_{1c} level similar to the *db/m* controls (***Figure 5.2***). To determine if this result affected the development of kidney hypertrophy, renal mass was assessed. Total kidney weight was slightly lower in *db/db* mice treated with Alisporivir compared to *db/db* mice on Vehicle, when corrected to lean body mass. This result suggests that the dose of 10mg/kg per day is unsuitable for distinguishing the effects of the drug from the effects of lowered blood glucose, which is thus a confounding factor. Data from the 5mg/kg/day dose suggest that Alisporivir affected body fat percentage; however the confidence of any effect is low with no statistically significant difference found with the 10mg/kg/day dose.

Table 5.2 Phenotypic results for 10mg/kg Alisporivir pilot study in *db/db* mice

	db/m		db/db		Vehicle	Alisporivir	db/db
	Vehicle	Alisporivir (10mg/kg)	Vehicle	Alisporivir (10mg/kg)	db/m vs db/db	db/m vs db/db	Vehicle Vs Alisporivir
Cull weight	26.7 ±3.1	26.8 ±1.7	45.0 ±12.1	32.3 ±13.7	*P*= 0.062	ns	ns
EchoMRI							
Fat	4.3 ±2.1	3.9 ±1.1	21.3 ±10.6	18.9 ±7.4	*	*	ns
Lean	21.8 ±0.7	22.6 ±1.3	21.0 ±2.2	15.9 ±3.9	ns	**	*
%Body fat	16.0 ±6.6	14.4 ±2.9	47.8 ±13.0	53.5 ±4.9	**	***	**
Glucose							
Spot test at endpoint	6.5 ±1.1	9.6 ±1.6	29.7 ±4.7	9.6 ±6.0	****	ns	***
HbA_{1C}							
%	4.4 ±0.3	4.6 ±0.7	9.6 ±1.7	4.3 ±0.1	***	ns	***
mmol/mol	25.0 ±3.6	27.0 ±7.0	81.3 ±18.6	23.0 ±1.0	***	ns	****
Metabolic caging							
End point							
Food intake (g)	2.5 ±1.2	3.1 ±0.3	4.6 ±1.9	3.6 ±1.2	ns	ns	ns
Water intake (mL)	3.2 ±1.5	5.6 ±1.2	12.9 ±3.9	3.3 ±2.9	**	ns	**
Urine output (mL)	0.8 ±0.5	0.7 ±0.6	9.6 ±4.9	0.2 ±0.3	**	ns	**
Organ mass							
Total kidney mass (mg)	327 ± 10	352 ± 49	453 ±71	265 ±58	*	ns	**
Kidney to lean body mass ratio (mg/g)	15.0 ±0.9	15.6 ±1.8	20.3 ±0.4	16.7 ±0.4	**	ns	*
Heart mass (mg)	127 ±20	123 ±13	144 ±27	100 ±27	ns	ns	ns
Heart to lean body mass ratio (mg/g)	5.8 ±0.8	5.4 ±0.3	6.8 ±0.8	6.2 ±0.2	ns	ns	ns
Liver mass (g)	1.34 ±0.05	1.43 ±0.07	2.78 ±0.24	1.15 ±0.60	***	ns	***
Liver to lean body mass ratio (mg/g)	61.5 ± 1.2	62.0 ±5.1	132.4 ±5.7	68.5 ±19.3	****	ns	****

Notes: Data are shown as mean ±SD. Statistical analysis performed using Two-way ANOVA with Bonferroni post hoc test. ns = not significant; *p<0.05; **p<0.01; ***p<0.001; ****p<0.0001.

LIVER AND HEART MASS

Liver mass was assessed in this study as *db/db* mice are prone to developing non-alcoholic fatty liver disease, even with consumption of a standard mouse chow diet (366). Indeed, liver mass was increased in *db/db* mice compared with *db/m* controls (***Table 5.2***). This increase was reversed by treatment with 10mg/kg Alisporivir. Detailed analysis of diabetes associated liver injury, however, is beyond the scope of this study. *Db/db* mice are also known to develop diabetes associated cardiac dysfunction. Heart weight and left ventricular mass were measured (***Table 5.2***) however no statistically significant change in heart weight was evident in this study.

ALISPORIVIR AND BLOOD GLUCOSE

Alisporivir reduced blood glucose levels in diabetic *db/db* mice at a dose of 10mg/kg (***Table 5.2***), but not at 5mg/kg (see ***Publication 2, Table 2***). Following on from these results, a literature review of publically available clinical trial results was performed to determine if there are any existing data for blood glucose levels in patients treated with Alisporivir. To date, no diabetes specific trials have been performed. Thus available data were extracted from Alisporivir trials in patients with Chronic Hepatitis C receiving antiviral therapy. ***Table 5.3*** reports the results for the database search. In total, 14 clinical trials of Alisporivir, were discovered using the predetermined search terms. Of these 14 studies, nine studies had published results available. Interestingly, one of the studies yet to report results, aims to examine the effects of Alisporivir in Chronic Kidney Disease. The remaining four studies without results were also investigating HCV or hepatic disorders.

Out of the nine studies with results available, only two yielded query results for defined terms. Clinical trial no. 8 had a positive result for the term "Glycaemia". In the results table the value reported was 'Hypoglycaemia'. This was listed as an adverse reaction, of which one patient scored across the whole study. Clinical trial no. 9 had two positive query terms, both of which were listed under adverse events. "Glucose" was located as the value 'Blood Glucose Increase', of which one patient was scored positively across the whole cohort. "Glycaemia" was located as the value 'Hyperglycemia' of which one patient was scored positive. Both events were scored from cohorts receiving 800mg/day Alisporivir.

Table 5.3 Results of database search for clinical trials of Alisporivir

Search term	No. of studies found	No. of studies with results available	No. of studies not found with previous search terms	List of studies with results (Clinical Trials identification number)	Study number
Alisporivir	14	9	**-**	***NCT02753699***	***1***
			-	***NCT02094443***	***2***
			-	***NCT01500772***	***3***
			-	***NCT01446250***	***4***
			-	***NCT01318694***	***5***
			-	***NCT01215643***	***6***
			-	***NCT02465203***	***7***
			-	***NCT01183169***	***8***
			-	***NCT00537407***	***9***
DEB025	13	9	0		
Debio-025	3	2	0		
UNIL-025	0	0	0		

Table 5.4 Results for search terms used to query clinical study data

Study no.	1	2	3	4	5	6	7	8	9
Trial phase	3	2	3	3	3	2	3	2	2
Trial Status†	C	C	Tm.	Tm.	C	C	Tm.	C	C
Total no. participants	723	52	6	8	1077	340	105	459	50
Search Terms									
Glucose	-	-	-	-	-	-	-	-	+
Glycemia	-	-	-	-	-	-	-	-	-
Glycaemia	-	-	-	-	-	-	-	+	+
A1c	-	-	-	-	-	-	-	-	-
Glycated	-	-	-	-	-	-	-	-	-

Notes: † C = completed; Tm. = Terminated; negative query "-"; positive query "+"

5.4.4 Additional data for the 5mg/kg/day Alisporivir group

Alisporivir was given prophylactically to *db/db* mice by daily oral gavage. This systemic route of therapy thus allows the possibility that other organs may also be affected by treatment with Alisporivir. Diabetes is associated with a number of microvascular complications; however, their investigation requires specialist knowledge and extended methodology, which is beyond the scope of this study. Thus, a brief investigation is presented here to briefly consider if Alisporivir was able to modulate phenotypes in other organs, given the absence of an effect in diabetic kidney disease.

Additional phenotypic data

Liver mass was assessed to determine the effect of both diabetes status and treatment with Alisporivir. Gross liver weight was found to be increased in *db/db* mice compared with *db/m* controls (***Table 5.5***). This significant increase in liver mass was also apparent when values were corrected to whole body weight and also lean body mass, as determined previously by EchoMRI. This indicates that a diabetes increase in liver mass was present in this model. A comparison with the 10mg/kg/day dose indicated that Alisporivir had no effect on liver mass at the dose of 5mg/kg. No differences in heart weight were found between control and diabetic mice in this study (***Table 5.5***).

Table 5.5 Additional phenotypic data for db/db mouse study

	db/m		db/db			
	Vehicle	Alisporivir (5mg/kg)	Vehicle	Alisporivir (5mg/kg)	Db/m vs db/db	Vehicle vs Alisporivir
Organ weights						
Liver (g)	1.33 ±0.18	1.44 ±0.28	2.18 ±0.44	2.09 ±0.47	****	ns
Liver to body weight ratio (mg/g)	45.6 ±5.4	48.2 ± 6.6	58.0 ±11.1	62.5 ±17.9	**	ns
Liver to Lean mass ratio (mg/g)	56.2 ±4.6	59.7 ±5.8	100.1 ±17.1	97.8 ±18.8	****	ns
Heart weight (mg)	133 ±16	140 ±19	126 ±13	127 ±21	ns	ns
Left ventricle (mg)	92 ±10	101 ±12	86 ±14	89 ±19	ns	ns
LV % (total heart)	69.4 ±4.4	71.1 ±3.4	67.3 ±8.1	69.2 ±5.0	ns	ns
Metabolic Caging: Mid point						
Food intake (g)	2.4 ±0.4	2.8 ±0.6	2.3 ±0.7	2.9 ±0.9	ns	ns
Water intake (mL)	3.7 ±1.5	3.1 ±1.9	9.7 ±5.00	10.1 ±7.2	**	ns
Urine output (mL)	0.8 ±0.4	1.2 ±1.3	7.0 ±4.4	7.7 ±6.2	****	ns
End point						
Food intake† (g)	2.5 ±0.5	2.6 ±0.8	3.1 ±1.0	3.7 ±1.2	*bb*	ns
Water intake (mL)	3.5 ±2.2	3.2 ±1.4	13.6 ±6.2	17.2 ±11.4	***	ns
Urine output (mL)	0.8 ±0.3	0.9 ±0.5	14.1 ±7.8	14.7 ±9.0	****	ns

Notes: Two-way ANOVA with Bonferroni post hoc test run for all. **P*<0.05; ***P*<0.01; ****P*<0.001; *****P*<0.001. † *db/m* vs *db/db* only significant for Alisporivir groups ^{bb}P<0.01. *n*=11-16 per group

ACR AND CREATININE CLEARANCE

Urine creatinine was measured and used to calculate the urinary Albumin to Creatinine ratio (ACR) (***Figure 5.1***). To normalise data for analysis by Two-way ANOVA two rounds of log transformation were required. Bonferroni post hoc test on transformed data revealed that ACR was significantly increased in both *db/db* groups. Creatinine clearance however was unchanged between all groups.

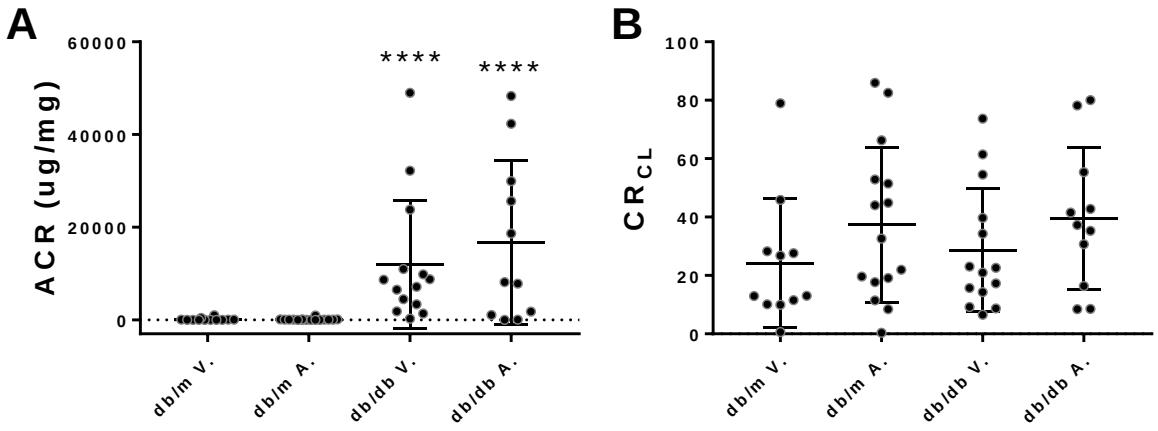

*Figure 5.1: The urinary Albumin to creatinine ratio was increased in db/db mice with no change in creatinine clearance. Creatinine was measured from urine and plasma samples collected from endpoint metabolic caging. (A) Urinary creatinine (mg) was used to correct urinary Albumin (µg) excretion data in order for the Albumin to Creatinine ratio (ACR) to be determined. (B) Creatinine clearance was calculated from both urine and plasma creatinine values. Graphs show individual data points with mean ±SD. Two-way ANOVA with Bonferroni post hoc test was performed. ****p<0.0001, n=9-15 per group.*

TRANSMISSION ELECTRON MICROSCOPY

In addition to assessing Form Factor and 2D Area, as presented in Publication 2, data for transmission electron micrograph (TEM) images were also assessed for mitochondrial perimeter length, aspect ratio, roundness and Feret's diameter. Data are presented as frequency distributions of all data (***Figure 5.2***). No change in frequency distribution was observed for aspect ratio between *db/m* and *db/db* mice (***Figure 5.2A***). The frequency distribution curve for perimeter length was slightly shifted toward an increase in *db/db* mice; although data were variable with no statistical significance found using Two-way ANOVA comparisons of each bin (***Figure 5.2B***). Feret's diameter, which measures the longest distance between two points in each manually circled mitochondria, also appeared to be shifted slightly higher (***Figure 5.2C***). Assessment of roundness showed no change between all groups (F***igure 5.2D***).

Autophagosomes and Mitophagosomes were also counted per mm^2 for each mouse to investigate if changes in turnover were detectable using this method (***figure 5.3***). Results for *n*=3 suggest that there is no significant difference in the presence of autophagosomes at this static moment; however, data were quite variable among mice in the same group. The relative number of mitophagosomes was reflective of total autophagosomes (***figure 5.3B***).

-> ***Figure 5.2: Distribution of variables assessing mitochondrial Perimeter length and Aspect ratio.*** *Transmission electron micrograph images of proximal tubule cells were assessed for changes in mitochondria. Mitochondria were circled by hand for a minimum of 7 images per mouse and data for each animal were pooled. Frequency distribution of (A) Aspect ratio; (B) Perimeter; (C) Feret's diameter; and (D) Roundness, were compiled using 20 bins of equal size. Graphs show mean ±SD of n=3 mice per group.*

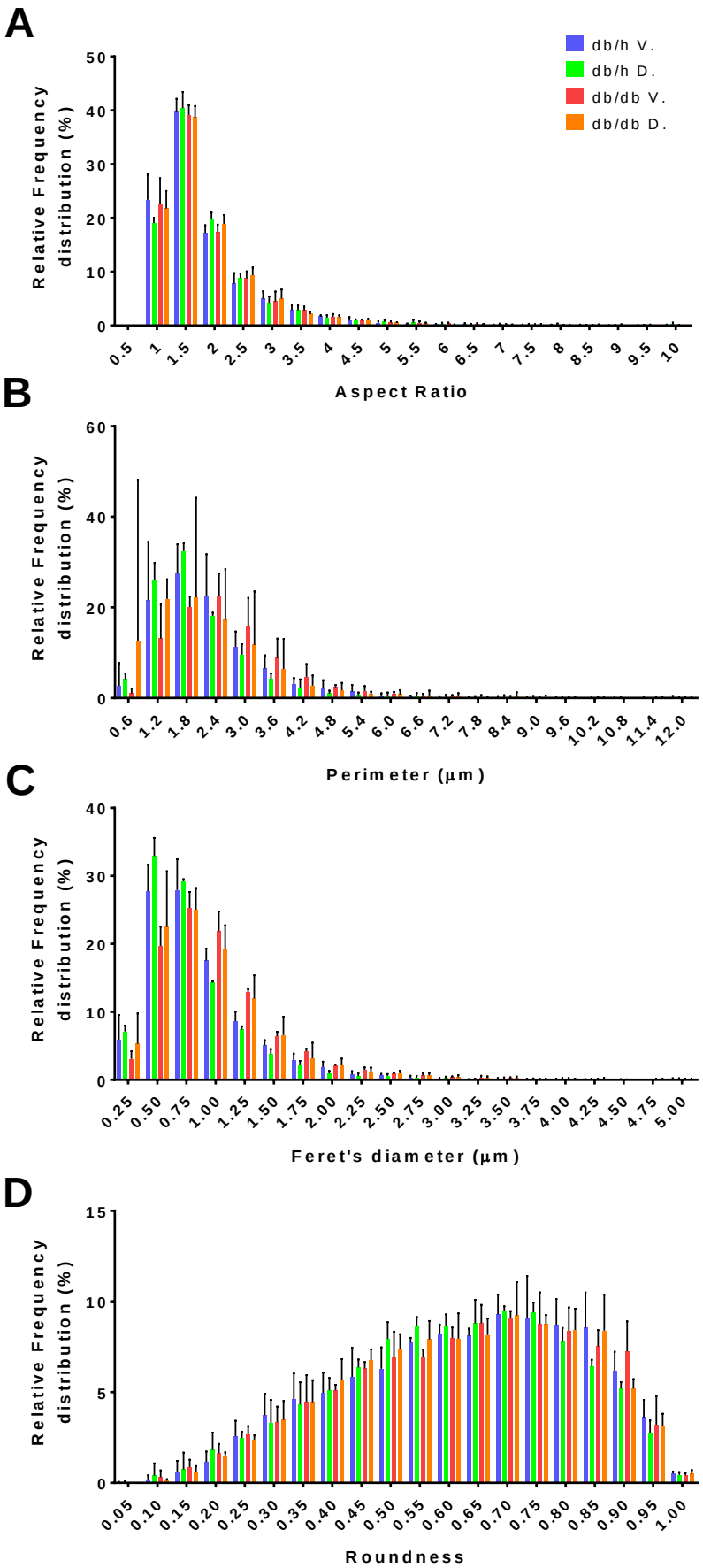
A
db/h V.
db/h D.
db/db V.
db/db D.
Relative Frequency distribution (%)
Aspect Ratio
B
Relative Frequency distribution (%)
Perimeter (µm)
C
Relative Frequency distribution (%)
Feret's diameter (µm)
D
Relative Frequency distribution (%)
Roundness

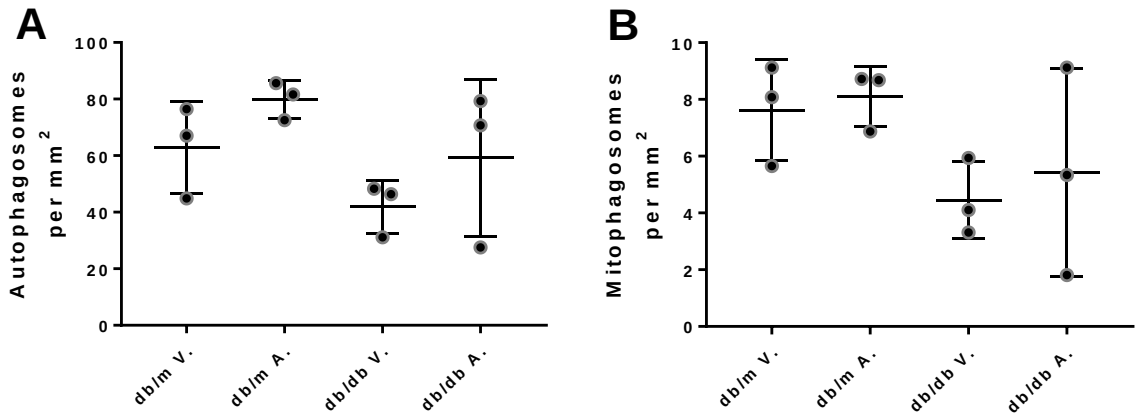

Figure 5.3: Autophagosome and Mitophagosome score for renal proximal tubule cells. *Total number of autophagosomes and mitophagosomes were scored from 5-7 transmission electron micrograph images of renal proximal tubule cells per mouse. Total cytosolic area of tissue scored was used to calculate the number of phagosomes per mm^2. n=3 mice per group.*

BRIEF ASSESSMENT OF CARDIAC MITOCHONDRIAL FUNCTION IN DB/DB MICE

Cardiac mitochondria were assessed for their respiratory capacity using the same conditions as for the renal mitochondria in **Publication 2**. This was performed to allow for a direct comparison of the effects of Alisporivir in another population of mitochondria and explore the biological availability at a lower dose. Data were available for *n*=4-6 mice per group and means were calculated across four seahorse experimental repeats. Values for basal OCR for *db/db* mice were slightly higher than in *db/m* mice (***Figure 5.4A***). When all values were corrected to basal respiration a non-significant trend towards a decrease in respiration in *db/db* mice was observed for complex I stimulated ADP driven respiration (***Figure 5.4B***). *Db/m* mice treated with Alisporivir also trended towards a decrease in respiration. Complex II data were similar per µg of protein (***Figure 5.4C***); however when corrected to basal respiration only the *db/db* Vehicle group showed a trend towards a decrease in ADP driven OCR (***Figure 5.4D***). Inter-assay variability was high, so no real difference among groups is assumed.

Respiratory control ratio (RCR) complex I-driven respiration was higher in cardiac mitochondria compared to renal mitochondria, as shown in publication 2 (***Figure 5.5A***). RCR for complex II values were lower in vehicle treated mice; although Alisporivir appeared to raise RCR in both *db/m* and *db/db* mice (***Figure 5.5B***) this did not reach statistical significance. These values are divergent from those seen in the renal mitochondria in Publication 2, Figure 4 where complex I RCR trended towards an increase in *db/db* mice only. Complex II RCR were not able to be calculated for renal tissue, so unfortunately any difference here is unknown. ATP production can be inferred from the increase in OCR observed following the addition of ADP (State 3 respiration) (***Figure 5.5C,D***). The percentage increase in respiration was calculated by normalising to baseline respiration in order to determine the magnitude of change in state 3 respiration compared with state 4 (following addition of oligomycin). Complex I stimulated respiration trended towards a decrease from *db/m* Vehicle controls with both Alisporivir treatment and diabetes (***Figure 5.5C***), with no changes in complex II respiration (***Figure 5.5D***). Finally, Alisporivir reduced proton leak through cardiac mitochondria with a trend towards a decrease in complex I respiration (F***igure 5.6E***), and a statistically significant decrease in complex II respiration (***Figure 5.6F***) for both *db/m* and *db/db* mice compared with vehicle controls.

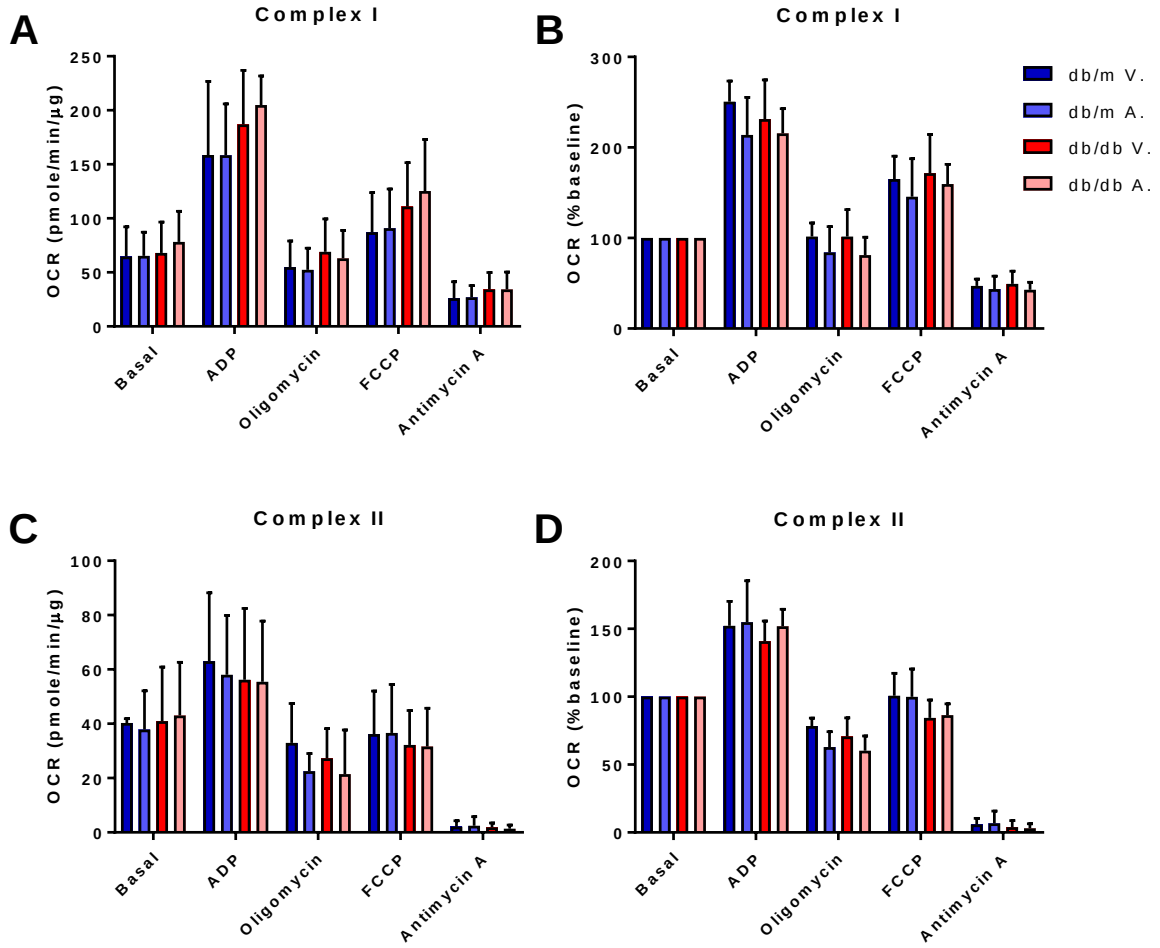

Figure 5.4 Oxygen consumption rate (OCR) for subsarcolemma mitochondria of cardiac tissue. *(A) Complex I respiration stimulated with glutamate and Malate; (B) Complex I data normalise to basal respiration; (C) Complex II respiration stimulated with succinate and rotenone; (D) Complex II data normalised to basal respiration. Graphs show mean ±SD for n=3-6 per group.*

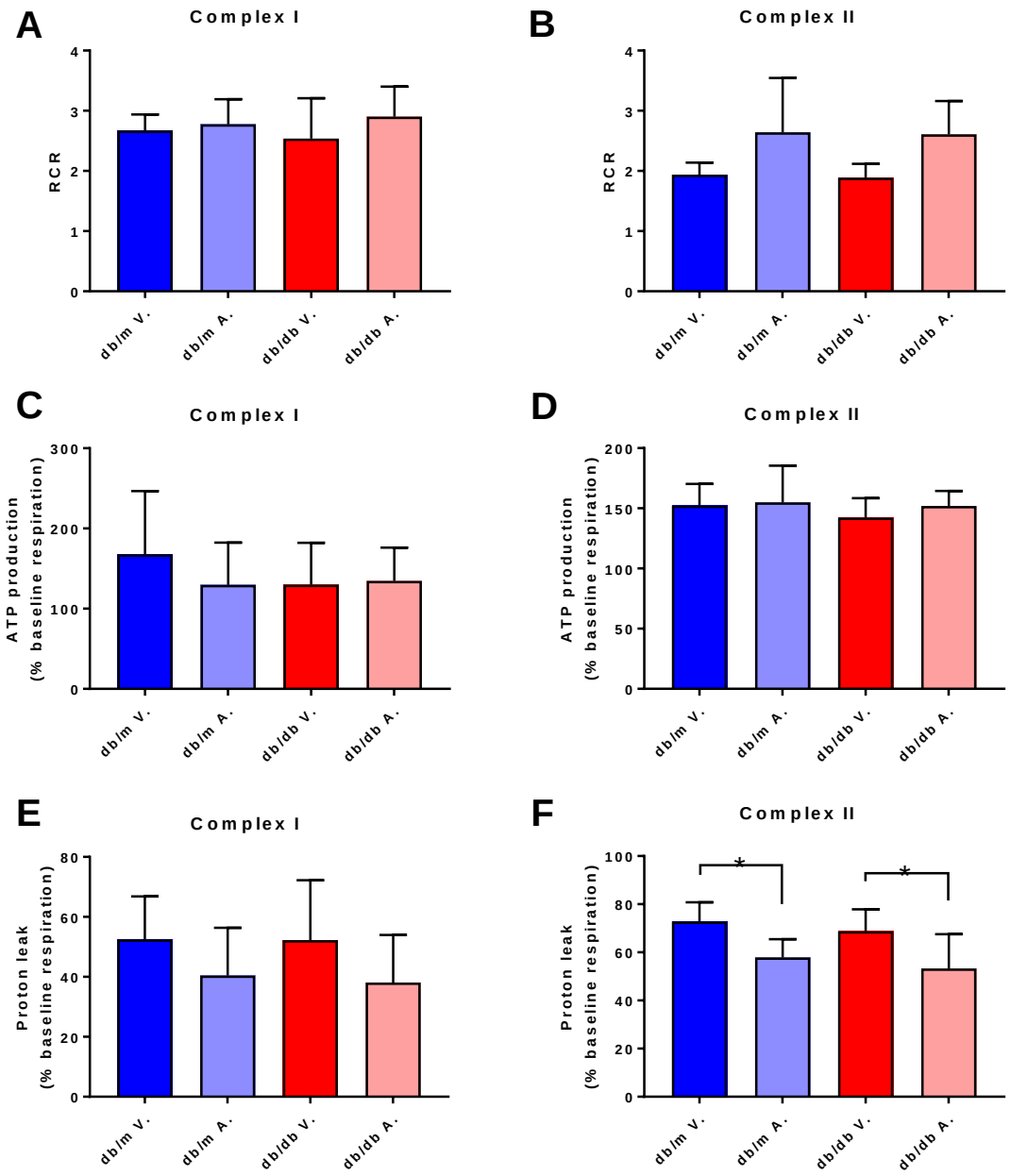

Figure 5.5: Respiratory Control Ratio (RCR) and proton leak in a population of subsarcolemma mitochondria isolated from the left ventricle. *Respiratory Control Ratio was calculated from the results for ADP stimulated respiration (State III) and Oligomycin (State IV) using the ratio of State III to State IV. (A) RCR for complex I stimulated respiration using Glutamate and Malate; (B) complex II respiration using Succinate and rotenone. ATP production is reported as percentage increase in state 3 (ADP driven) OCR relative to State 4 (Oligomycin) relative to baseline OCR for (C) complex I; and (D) complex II. Proton leak was calculated using percentage for the difference between Oligomycin and Antimycin A stimulated respiration for (E) Complex I, with Glutamate and Malate; and (E) Complex II, with succinate and rotenone. Graphs show mean ±SD for n=3-6 per group. Two-way ANOVA with Bonferroni post hoc tests were performed. *p<0.05.*

5.4.5 ADDITIONAL DATA FOR *PPIF* KO STUDY

In addition to the data presented in Publication 2 the following results are presented from the *Ppif* $^{-/-}$ STZ mouse study.

ASSESSMENT OF BLOOD GLUCOSE

Blood glucose was routinely monitored throughout the study using random spot checks (***figure 5.6***). These data enable an estimation of long-term changes in blood glucose levels; however, data are limited to a maximum detection measurement of 34mmol/. Results potentially indicate that a minor decrease in blood glucose occurred in the *Ppif* $^{-/-}$ STZ mice compared with *Ppif* $^{WT/WT}$ STZ mice (***Figure 5.6***). Values were significantly decreased at several time points; however, the extent of any real difference remains inconclusive. Thus, to resolve the limitations in blood glucose measurement, plasma glucose was assessed by enzyme-linked colorimetric analysis of samples from whole blood extracted at endpoint (***Figure 5.7***). Blood glucose was significantly increased for STZ mice in the *Ppif* $^{-/-}$ group as expected. However, the difference between CIT and STZ *Ppif* $^{WT/WT}$ mice trended toward an increase but was not significant (p=0.0625). It is important to note that values were obtained from non-fasted mice and thus variability may be reflective of this. No statistically significant difference between *Ppif* $^{-/-}$ and *Ppif* $^{WT/WT}$ mice were found.

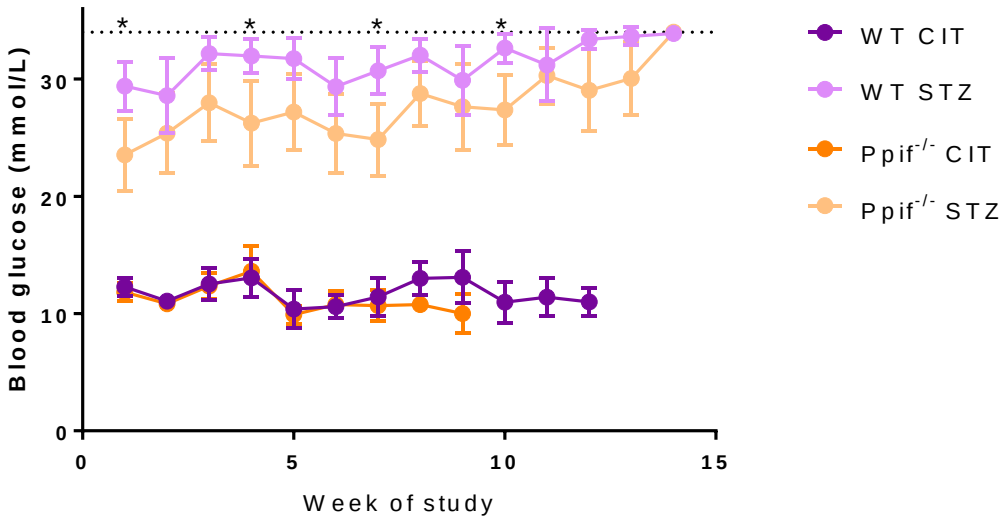

Figure 5.6: Spot blood glucose monitoring during the study period. Diabetic mice developed hyperglycaemia immediately following treatment with Streptozotocin, which was sustained throughout the study. Glucose data were measured using an Accucheck glucometer with a maximum reading of 34mmol/L (indicated by the dotted line)- and is a limit of this approach. Data are presented as mean and 95% CI for n=17-20 mice per group. Two-way ANOVA revealed a slight decrease in blood glucose at several time points for Ppif $^{-/-}$ versus Ppif $^{WT/WT}$ diabetic mice.

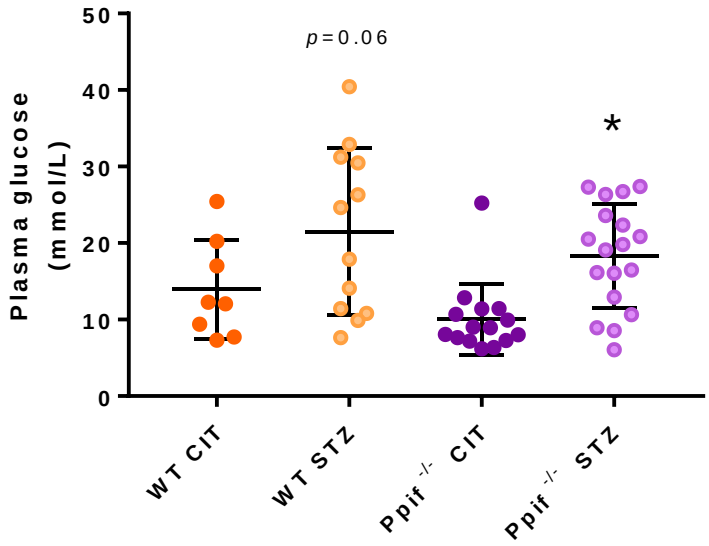

*Figure 5.7: Plasma glucose assessed at endpoint. Glucose levels within plasma, separated from whole blood collected at endpoint, was assessed with a colorimetric enzyme assay. Graph shows all values with bars showing mean ±SD, n=8-18 per group. Two-way ANOVA with Bonferroni post hoc test was performed where *p<0.05 comparing CIT vs STZ.*

5.5 DISCUSSION

The initial results for the 10mg/kg pilot study data revealed the potential for Alisporivir to be investigated as a therapeutic to target diabetes associated renal disease. Although the pilot study of the 10mg/kg/day dose was limited to *n*=3 per group, these data revealed significant improvements in a range of diabetes associated markers, including: reduced blood glucose and HbA_{1c} values, as well as significant reductions in polydipsia and polyuria in *db/db* mice. The higher dose was also associated with a reduction in both kidney and liver hypertrophy. This is in contrast to the 5mg/kg dose, which was not associated with any change in these markers. Critically, the blood glucose lowering effects of the drug are potentially confounding in any diabetes study, as it is not possible to differentiate any effect of the drug from the known benefit of reduced hyperglycaemia (as discussed further in Publication 2). This pharmacological effect of Alisporivir has not been previously reported in the literature. The present study is perhaps the first to test Alisporivir in the context of diabetes. Furthermore, any effect of Alisporivir on glucose metabolism is likely to have been previously overlooked as glucose is not a routinely measured parameter in non-diabetic mice.

In humans, Alisporivir has been prepared in oral formulations for use in clinical trials at doses of between 400mg and 1200mg Alisporivir per day. For an adult of 80kg this would be an equivalent dose of between 5 and 15mg/kg per day. Whilst these doses demonstrate some variability, they are comparable to the dosage used in the present study in *db/db* mice. The extent to which these data are applicable to the general activity of the drug in humans, however, requires further investigation. The available human data for Alisporivir predominantly arises from clinical trials with Hepatitis C Virus (HCV) infected patients being concomitantly administered Interferon therapies or Ribavirin antivirals. Thus, a detailed examination of the pharmacokinetics of Alisporivir in the context of diabetes in human patients remains to be explored.

Very few data are available tracking changes in blood glucose homeostasis in patients enrolled in clinical studies of Alisporivir. This is primarily due to the history of the development of this drug for treating HCV infected patients. Indeed, the literature review performed here, on publically available clinical trial data in the U.S National Library of Medicine database, found only one report of a hypoglycaemic event, and two reported hyperglycaemic events. These data do not provide any detailed insight into the mechanism of the observed changes in glucose seen in the Alisporivir treated

mice. Interestingly, the incidence of blood glucose anomalies has been examined in a population of HCV patients enrolled across three of these clinical trials with authors reporting that ~20% of these patients had impaired fasting glucose associated with the disease (367). Unfortunately, these data were extracted from the screening blood glucose samples collected prior to commencement of each treatment intervention arm and no data are presented on follow up data. Therefore, the effect of Alisporivir on blood glucose is unknown It is also pertinent that Chronic HCV associated hepatic dysfunction can lead to diabetes-like phenotypes; as the liver provides a key role in modulating systemic glucose homeostasis. Thus, any improvement seen with Alisporivir treatment may be difficult to distinguish from its demonstrated ability to reduce HCV associated liver pathology. An indirect benefit on glucose control by Alisporivir could be mediated through improving hepatic function., although this is unlikely.

Alisporivir is a derivative of the broad immunosuppressive agent, Cyclosporine A, and evidence for the blood glucose lowering effect of CsA itself has been established in relation to its use in a range of settings (368). Clinical data have indicated that CsA has some capacity to reduce the incidence of post-transplant associated diabetes, which is a frequent complication observed in patients followed after long-term CsA therapy (369,370). Opposing this, clinical data have also revealed that CsA treatment may also be diabetogenic (371–373). The exact mechanisms by which Cyclosporines alter glucose homeostasis is yet to be elucidated, but may involve variable effects on glucose and insulin signalling in different organ systems, including the pancreas (370,374). It is uncertain from the literature if these pharmacokinetic effects result from the immunosuppressant action of CsA or other mechanisms; however, higher CsA dosage remains one of the clear risk factors associated with its nephrotoxicity (375). A confounding factor has been that low dose steroid use, concomitantly administered in transplant patients, is also known to raise blood glucose levels (376). Nonetheless, it is reasonable to assume that CsA and its derivative Alisporivir exert complex interactions with systemic glucose homeostasis in addition to any direct negative regulation of cellular metabolism in renal tissue. Data presented in this study thus support the hypothesis that the action of CsA is inherent to its interaction with CypD, as the non-immunosuppressant derivative, Alisporivir was also shown to alter glucose metabolism.

To date, little is known about the effects of Alisporivir itself on blood glucose levels from human studies. It may be worth evaluating blood glucose levels and HbA_{1C} in future studies to enable an investigation into its effect on glucose homeostasis. The dose-dependent metabolic effect of Alisporivir observed here, in the context of diabetes, should be investigated further, particularly as the 5mg/kg data revealed no blood glucose lowering effect. Pragmatically, higher doses may also exhibit nephrotoxicity as has been seen with other CsA compounds. While it is possible that Alisporivir has a narrow therapeutic window, we cannot rule out the possibility that the efficacy of Alisporivir is directly related to its blood glucose lowering effect. These data underscore the importance of screening new targeted therapies for off-target blood-glucose lowering mechanisms, which must be considered when examining the benefits of Alisporivir treatment reported in diabetes related studies.

Genetic studies of CypD negative (*Ppif* $^{-/-}$) mice also allow an insight into the potential mechanisms of Alisporivir's action. However, the complexity of this phenomenon is complicated by the variable impact of genetic deletion of CypD (*Ppif*) on glucose homeostasis in animal studies. These findings are consistent with the observations in human patients treated with Cyclosporines as detailed above. Generally, genetic deletion of CypD has been associated with dysregulation of glucose homeostasis; however, the magnitude of this effect remains unclear. Metabolic effects previously reported include changes in glucose and fat metabolism, as well as the accumulation of excess adipose tissue (377,378). For diabetes specifically, effects range from no observed difference in blood glucose in STZ treated diabetic mice to others reporting improved glucose handling, as assessed by glucose tolerance testing, in CypD (*Ppif*) KO mice (378,379). Blood glucose data from the *Ppif* $^{-/-}$ mouse study presented in this chapter were shown to be slight lower in *Ppif* $^{-/-}$ STZ mice; however the potential effect size was small. Curiously, any potential reduction in blood glucose in the *Ppif* $^{-/-}$ STZ mice, although minor, did not confer protection from diabetes associated renal complications, as may be predicted from any glucose lowering intervention. The increase in renal damage observed with deletion of CypD lends weight to the hypothesis that CypD modulates mitochondrial function in the diabetic kidney. Data indicates that inhibition of CypD, with agents such as CsA and Alisporivir, is specifically detrimental in renal tissue, and is supported by historic studies demonstrating that CsA treatment exacerbates the risk of both glomerular and tubulo-intersitial injury in diabetes (380,381). This has also been demonstrated to occur in a rat model of STZ diabetes similar to the study presented here (382). Indeed, CypD mediated regulation of ATP synthase and ATP production rate,

links CypD with the fundamental metabolic processes performed within the mitochondrion (383–385). Unfortunately, a more detailed assessment of underlying metabolism in the renal cortex was unavailable for the *Ppif* $^{-/-}$ mouse study presented in this chapter, but may be worth exploring in more detail in the future. The conclusion that loss of *Ppif* in the diabetic kidney is detrimental to the development of DKD is in direct contrast to the benefits observed in other organs and disease systems and even in the normal kidney (359).

Additional data presented in this chapter expand on the characteristics of renal health and mitochondrial function in the context of diabetic kidney disease (DKD) explored in Publication 2. Creatinine clearance can provide further evidence of the renal changes associated with diabetes in the *db/db* mice. Although urinary albumin to creatinine ratios were increased in *db/db* mice, creatinine clearance was unchanged when compared with *db/m* mice at 22 weeks of age. Previous studies have demonstrated that creatinine clearance shows an initial increase in db/db mice by 8 weeks of age, followed by a slow decline. It is possible that at this time point that these results are unable to distinguish this decline from comparative control levels (386,387).

Mitochondrial dynamics were explored in more detail using additional data presented in section 5.6. Although limited to *n*=3 per group, data were adequate for assessing mitochondrial density; however, more data would enable a deeper assessment of any changes. For autophagosome analysis, data were quite variable and suggest that larger data sets are required in order to perform a robust analysis of this extremely dynamic process. Assessment of renal proximal tubule cells by TEM initiated in Publication 2 revealed that mitochondrial density was increased in *db/db* mice compared to *db/m* mice. Interestingly, additional results for shape descriptors together suggest that this increase represents the presence of enlarged mitochondria as there was no difference in shape descriptors (aspect ratio or roundness) alongside the increase in size descriptors (2D area, perimeter length and Feret's diameter). The measurement of these values in real volume (μm^2) demonstrates that this change in density did not result from any decrease in cytosolic volume but rather represents an actual increase in mitochondrial size. Further, this increase appears to be unrelated to the presence of swollen mitochondria, as there was no difference in the distributions for roundness or form factor in *db/db* mice. Indeed, swollen mitochondria were infrequently found in TEM images in renal PTECs assessed by this method. This is in contrast to previous research reporting the

presence of swollen mitochondria in animal models of DKD (388,389). We may consider that mitochondrial depolarisation can occur without overt mitochondrial swelling in vivo (349). Indeed, data obtained in the mitochondrial swelling assay suggest that this is the case as isolated kidney mitochondria were prone to calcium induced challenge. Therefore, minor activation of mPTP mediated dysfunction is not detectable using TEM analysis and it may be present prior to overt swelling.

One potential limitation inherent to the Alisporivir study which must be addressed, is the use of Cremophor EL oil. Although direct evidence for Cremophor EL (or other castor oil preparation) induced mitochondrial change is scarce, the divergence of the *db/db* mitochondrial function from other published studies may indicate a vehicle specific effect (390,391). Studies have shown that both positive and negative effects for Cremophor EL vehicle carried pharmaceuticals can occur (391–393). At lower concentrations Cremophor EL is not expected to induce toxic effects, however, it is possible that the unique mitochondrial characteristics observed in renal mitochondria in this study may result from its use and could be investigated in future. Mitochondrial function is likely to be vulnerable to myriad changes which occur in the context of diabetes.

Finally, a comparison of cardiac mitochondria was performed specifically to determine if the 5mg/kg/day dose of Alisporivir was able to pharmacologically alter function in extra-renal mitochondria. *Db/db* mice have previously demonstrated overt mitochondrial dysfunction, alongside diabetes associated pathological changes, in cardiac tissue (394,395). Further, cardiac mitochondria have been successfully targeted with other mitochondrial targeted compounds in *db/db* mice (396). As populations of mitochondria in different organs have previously been demonstrated to have variable responses to the diabetic environment, the response of kidney mitochondria to Alisporivir was uncertain (397). Results from the 5mg/kg per day study seemed to suggest that Alisporivir was not biologically active at this dose. Functional analysis of heart pathology was beyond the scope of this study and the primary aim of this analysis was to establish if the 5mg/kg/day dose of Alisporivir had any physiological impact on mitochondrial function in these mice. Indeed, results demonstrated that cardiac mitochondrial responded to the lower dose of Alisporivir. Albeit only assessed in a limited manner, this demonstrates that the drug maintained bioactive potential. This result provides a key

example of the differences between different populations of mitochondria which may occur within an organism. Particularly notable was the apparent trend towards a decrease in ADP production with Alisporivir in cardiac mitochondria in contrast to no such trend in renal mitochondria. Differences between cardiac and renal mitochondria were also suggested with ADP production potentially decreased in cardiac mitochondria but increased in the renal mitochondria of *db/db* mice. These results support the hypothesis that tissue-specific mitochondrial variation exists and that renal mitochondria have a unique metabolic profile; with fewer studies of renal mitochondrial function available in the literature (397,398). The response of cardiac mitochondria to Alisporivir at a lower dose allows us to consider the challenges of targeting renal mitochondria specifically in diabetes. Paired with the unexpected finding that deletion of CypD in *Ppif* $^{-/-}$ mice exacerbated DKD instead of restoring renal function, this comparison provides the impetus for a deeper exploration of the unique metabolic environment in the diabetic kidney.

5.6 CONCLUSIONS

It is possible that the unique metabolic profile of renal mitochondria render them susceptible to insult where adaptations to hyperglycaemia have already occurred. Results from both the *Ppif* $^{-/-}$ STZ and the *db/db* Alisporivir studies reveal that Cyclophilin D has a highly complex role in the diabetic kidney. Whilst CypD is known for its role in mediating mPTP opening, its physiological role in renal mitochondria may be independently more important. Thus, inhibition of Cyclophilin D to prevent mPTP opening will likely not improve renal outcomes for patients with diabetes.

5.7 SUMMARY

The mitochondrial permeability transition pore (mPTP) is a key part of non-apoptotic cell death, whereby the formation of a pore traversing both the inner and outer mitochondrial membranes, results in mitochondrial depolarisation and loss of ATP production. Cyclophilin D is a key protein involved in the opening of the mPTP, which may be pharmacologically inhibited in order to prevent necrotic cell death by prolonging mitochondrial function. However, diabetic mice lacking CypD (*Ppif*) developed increased renal damage compared to WT mice as reflected by an increase in the glomerulosclerosis index and increased collagen IV deposition.

Initial studies of Alisporivir treatment suggested that a dose of 10mg/kg per day lowered blood glucose in *db/db* mice but a dose of 5mg/kg per day did not. However, detailed preclinical evaluation of a 5mg/kg dose demonstrated no change in the progression of diabetes associated renal injury when compared with *db/db* mice treated with Vehicle only. Results from these studies suggest that the role of CypD is complex in the diabetic kidney.

5.8 FUTURE DIRECTIONS

Given these data, and the review of the literature, it would be interesting to directly explore the potential effect of diabetes on the development of nephrotoxic complications associated with CsA compounds. It would also be pertinent to examine the details of metabolic alterations in the kidney associated with both diabetes and with CypD inhibition. Such investigations may assist in determining the potential of mitochondria-targeted interventions for improving renal outcomes in diabetic patients.

Chapter 6

Chapter 6. Discussion of overall study results

6.1 BRIEF SUMMARY OF RESULTS

Diabetic kidney disease remains a significant health burden to individuals living with diabetes. Currently, between 25 to 40% of people with diabetes will develop renal complications, however, the risk factors associated with renal decline are not always clear (29,54,399). Whilst aggressive management of blood glucose and blood pressure are known to slow the rate of progression, many patients continue to experience renal decline. As such, new therapeutic strategies are required to not only halt the progression, but also to alleviate the increased morbidity and mortality risk associated with declining renal function. Mitochondrial dysfunction has been demonstrated to occur in the kidneys of patients living with diabetic kidney disease (134,266). As mitochondria are crucial mediators of cellular metabolism it has been hypothesised that targeting this dysfunction may lead to an improvement in renal cell health and prevent, or at least retard, the progression of DKD. However, mitochondria are also crucial to the progression of intrinsic cell death processes, and as such dysfunctional mitochondria may influence these processes. As a result, it was hypothesised that mitochondrial pore-forming cell death proteins would play a role in the progression of DKD pathology. Thus, this study aimed to evaluate the role of the mitochondrial pore-forming cell death associated proteins; with a focus on Bax, Bak and CypD. To do so, four different mouse models of DKD were employed to examine the changes in mitochondrial function in association with the progression of DKD and to determine if targeting these proteins revealed a role for them in the pathogenesis of the disease.

CHAPTER 3: MODEL 1

In Chapter 3, a time-course model of STZ induced diabetes was performed in the albuminuria prone *FVB/N* mouse strain to evaluate mitochondrial function in the early development of DKD. Renal structure and function were evaluated at 4, 8, 12 and 16 weeks of diabetes following treatment with STZ and results revealed that this model developed predominantly haemodynamic changes associated with persistent hyperglycaemia, including very high albuminuria but low glomerular structural change, as has been demonstrated previously (250). However, tubular structural changes were detected in the 16 week STZ group as

demonstrated by the development of glycogen associated accumulation and tubular dilation. Whilst RTqPCR determined that several cell death associated proteins were upregulated in the 4wk group, these increases had resolved by 16 weeks, and thus did not correlate with this tubular change. Further, assessment of apoptotic cells by TUNEL analysis revealed no correlation with these results. An assessment of mitochondrial function using the Seahorse Bioanalyzer was performed. Data indicated that STZ diabetes was not associated with any change in complex I mediated oxygen consumption rate (OCR). Further, mitochondrial swelling, as induced by calcium challenge revealed that there was minimal change in the sensitivity of isolated renal mitochondria to undergo the swelling response. Whilst there was no change across all four time-points, the 16 week group data suggested that a trend towards an increase in swelling rate was developing. Overall this study highlighted that mitochondrial dysfunction was not associated with the early progression of DKD in an STZ mouse model of T1DM.

CHAPTER 4: MODEL 2

Following the results of Chapter 3, the role of Bax and Bak in the progression of DKD were investigated to determine if these two mitochondrial pore-forming cell death proteins affect mitochondrial function and/or the progression of DKD. This was explored by generating a novel mouse model with proximal tubule specific deletion of the mitochondrial cell death proteins, Bax and Bak, using an Sglt2 promoted Cre-loxP genetic deletion of the Bax gene. Further, renal injury and mitochondrial function were examined after 24 weeks of STZ-induced diabetes to determine their progression after a longer duration of diabetes compared with Model 1. Whilst this Bax/Bak/Sglt2-Cre model developed only very mild renal injury in association with persistent hyperglycaemia, the deletion of both Bax and Bak in the proximal tubular cells neither lead to an improvement nor a worsening of renal outcomes. These data indicate that deletion of Bax and Bak in the PTCs does not impact the progression of DKD or mitochondrial function in early T1DM.

CHAPTER 5: MODELS 3 AND 4

Cyclophilin D (CypD) is regarded as a key regulator for the opening of the mitochondrial permeability transition pore (mPTP) and subsequent initiation of mitochondrial induced necroptosis and necrosis. Blockade of CypD represents a promising clinical target in

multiple acute and chronic diseases but its role in DKD was unknown. Two distinct mouse models were used to evaluate the role of CypD from different perspectives.

The first study (Model 3) investigated renal function and injury after 16 weeks of STZ induced diabetes in mice with a global deletion of the CypD gene: *Ppif*. This was a proof-of-principle study that revealed that deletion of CypD resulted in an exacerbation of diabetes associated renal injury. The second study (Model 4) was performed in the *db/db* mouse (a model of type 2 diabetes) where the data indicated that mitochondrial dysfunction developed along with renal injury in association with T2DM at 22 weeks of age. Treatment with the CypD inhibitor, Alisporivir, from 8 weeks of age revealed that a dose of 5µg/kg did not have any effect on renal function or mitochondrial functional parameters. The 10µg/kg dose however, was found to impart anti-diabetogenic effects. Together, these data indicate that CypD has a unique physiological role in both the pathogenesis of diabetes per se, and particularly in the diabetic kidney. Inhibition of CypD did not improve renal outcomes in DKD, rather, it may be that the expression of CypD will provide an important mechanism for renal protection in the context of diabetes.

6.2 EVALUATION OF MOUSE MODELS OF DKD

In this thesis, all animals were assessed by strict criteria for the development of hyperglycaemia to ensure that the results were relevant to the pathology specifically with diabetes. In each experimental mouse model, the development of renal injury can thus be directly correlated with persistent hyperglycaemia. The use of several different mouse models provided an array of perspectives from which to assess the early progression of DKD. Each model developed a unique profile of renal injury with varying alterations in glomerular function and morphometry observed. This ranged from the mild structural damage but excessive albuminuria seen in the *FVB/N* time-course study of STZ induced T1DM in Chapter 3, to the very mild injury observed in the characterisation of the novel Bax/Bak/Sglt2-Cre mice generated in Chapter 4. Comparatively, more advanced morphometric changes were observed in Chapter 5, where diabetes-associated renal injury, including glomerulosclerosis and collagen deposition, was exacerbated in the STZ *Ppif* mice after 16 weeks; and in the significant renal pathology that developed in the *db/db* mice by 22 weeks of age.

All mice used were male mice as they tend to survive STZ toxin better than females and are generally considered to develop more pronounced diabetes associated renal injury (400–402). Indeed, oestrogen is likely to have a protective effect on the development of renal pathology (401,403). Human studies have indentified that male characteristics may be an independent risk factor in the development of renal decline (404). However, women may be disproportionately affected by DKD (405). Further, sexual dimorphism of risk factors for the progression of renal decline have been previously observed in both human and rodent models of DKD (399,401,406). Whilst this study did not explore the pathology in female mice, the consistent use of male mice allows an inference of the pathophysiology in males only.

In the study of mouse models of diabetes, the development of renal injury reflecting human disease is an important area for consideration in preclinical research. Experimental models must be able to reflect the pathogenesis and progression of the human disease they aim to simulate (407). Indeed, DKD is a chronic disease with a prolonged duration. However, for patients with T2DM the development of microalbuminuria (>30mg/24h4 to <300mg/24hr) may be present even before a diagnosis of diabetes is confirmed (46). In the initial stages of human kidney disease, renal injury clinically manifests with microalbuminuria and changes in glomerular filtration rate. The progression to more advanced disease is categorised based on a decline in glomerular filtration rate of <90ml/min/1.73m^2 which is usually accompanied by the development of macroalbuminuria (>300mg/24hr). Prognostic markers currently used to evaluate the risk of progression, and of potential adverse outcomes such as acute renal injury, rely on the indirect markers of renal function that are easily identifiable by routine pathological examination. These include urinary albumin excretion, and estimates of glomerular filtration rate by either creatinine clearance or serum cystatin C. However, risk for progression to ESRD is highly variable among patients. The use of multiple mouse models of DKD allows an exploration of the progression of DKD that is not restricted to one specific genetic background. This has allowed a general evaluation of DKD features representative of the varying degrees of diabetes-associated pathology found among mice of different background strains.

All STZ and *db/db* diabetic mice had increased urine output, along with a compensatory increase in water intake, reflective of hyperglycaemia. Indeed, an increase in urine volume

commonly occurs with diabetes and is associated with changes in osmotic balance and the expression of transport proteins (408). Renal hypertrophy is another commonly observed consequence of diabetes that is observed in mouse models. An increase in renal mass was observed for all diabetic mice in Chapters 3 and 5. Results from Chapter 4, however, found that renal mass was only increased in the WT STZ mice relative to WT CIT controls. All remaining groups and genetic control were not different. However, it was unclear whether this was reflective of the unique genetic profile of this novel strain with proximal tubule specific KO of Bax and Bak, or specifically to an absence of this pathological feature.

Mean 24hr urine albumin levels were similar across all strains with between 10 and 50µg of albumin excreted per day in non-diabetic mice. Results from the *FVB/N* mice in Chapter 3 demonstrated very high levels of albuminuria which developed as early as 4 wks, and was sustained at 16 wks. Mean albumin excretion values were as high as ~600µg/24hrs, representing an increase of 20-30 times higher than their non-diabetic controls. Comparatively, the urinary albumin excretion of STZ diabetic mice were much lower in the Bax/Bak Sglt2 Cre colony studied in Chapter 4, where albumin excretion was only 2-4 times higher than the appropriate CIT controls. This was despite the increased duration of diabetes to 24 weeks post STZ treatment. In Chapter 5, the *Ppif* STZ mice had urinary albumin values five times higher than those of the CIT controls., where as the *db/db* mice had 10 times higher urinary albumin excretion levels compared to the *db/h* controls. Given the various time points assessed, the differences in albuminuria observed most likely reflect the phenotypic variation among strains and was unrelated to the duration of diabetes. Indeed, albumin excretion varies significantly between strains, with previous studies having demonstrated that the *FVB/N* strain is the most susceptible (250,322). Nonetheless, the minimal level of albuminuria seen in the novel Bax/Bak/Sglt2-Cre model was unexpected as previous studies have also demonstrated that mice from various *DBA*, *129* and *C57* strains all develop diabetes-associated increase in albuminuria (122,250).

Other common pathological features may also vary between the different mouse models, including other urinary and plasma markers, as well as renal structural pathology. Other markers of renal disease such as glomerular filtration rate and ACR (where available) were mostly

elevated with STZ diabetes. Plasma cystatin C levels were reduced in a few of the STZ mice in Chapter 3 and 4. These data indicate hyperfiltration, which is frequently observed in mouse models of diabetes. Together, these studies represent different degrees of early renal injury, and are relevant to the initial stages of DKD defined by increase in urinary albumin excretion.

Kim-1 protein expression can be observed as a consequence of renal injury. Indeed, urinary excretion of Kim-1 is generally absent in non-diabetic mice. Results from the animal studies in Chapters 3 and 5 reflected this phenotype, where only STZ treated mice had detectable levels of Kim-1 in their urine. Although not all diabetic mice had increased Kim-1, group means were significantly increased compared to the controls. The mice in the Bax/Bak/Sglt2-Cre study, however, were observed to have very minimal urinary Kim-1 excretion after 24 wks of STZ induced diabetes.

Glomerulosclerosis is an important marker of mesangial expansion and morphological renal injury. Whilst GSI score was increased in both the STZ diabetic *Ppif* and *db/db* studies, comparatively, the *FVB/N* time-course and the novel Bax/Bak/Sglt2-Cre mice displayed minimal glomerular injury. The mice in the Bax/Bak study developed the mildest DKD associated pathology, even though they were followed for the longest duration of time. These mice were also the most genetically diverse in terms of background. Indeed, these mice had *DBA*, *129* and *C57BL/6*. It is possible that the mix of background strains influenced the degree of renal injury among control groups. Indeed, pathological features of human relevant DKD are not always mimicked with mouse models and are highly dependent on the background strain and specific genetic models. Several studies have evaluated the specific differences between commonly used strains in the research of DKD. These include, *C57BLK/6*, *C57BL/6J*, *129*, *DBA* and *FVB/NJ*, as used in Chapters 3-5. Results from all of these studies highlight the differences in renal pathology that occurred between the various models and illustrate the disparity of phenotypes which may develop in response to hyperglycaemia. More advanced models of DKD are available, for example the *CD1* mouse model (409). However, of the various mouse models available, no individual strain is able to capture all the structural and functional features associated with human DKD.

While biopsies are not routinely performed in patients due to their invasive nature, data from available human studies predict that glomerulosclerosis coincides with the decline in renal function in diabetes (410,411). Further, urinary and blood analysis of Kim-1 can also predict the degree of renal damage sustained by a patient (412). Most of these features can be replicated to some degree in rodent models of diabetes. Indeed, rat and mouse models of DKD are able to capture the development of albuminuria, polyuria, and glomerulosclerosis that occurs in the early stages of DKD. However, no rodent model as yet develops hyalinosis of glomeruli, or develops phenotypes consistent with ESRD. However, targeting the early stages of DKD is potentially important, as mortality and morbidity risks are still significant, or possibly equal to those with moderate DKD (258,261,413). For example, data from human clinical studies have suggested that the cardiovascular and renal outcomes are similar between stage 1, 2 and 3 chronic kidney disease, indicating that adverse events can develop early in the disease (413). The importance of albuminuria levels in stratifying ESRD risk is re-evaluated frequently. In general, the development of macroalbuminuria is associated with a higher risk of ESRD in various populations, yet the risks from microalbuminuria may be underestimated (257,414,415). Additional studies have demonstrated that the methods used to examine the relationship between albumin excretion and risk of progression are essential. An investigation into the use of total estimated albumin excretion rate (eAER) compared with albumin to creatinine ratio (ACR) revealed that neither value provided additional prognostic value (416). Kim-1 on the other hand, is now recognised as a potentially valuable prognostic marker (412,417,418).

Overall, the different genetic background strains provide a reflection of the pathological variation that may be found when modelling human DKD in mice. The differences between models also highlight the importance of investigating multiple pre-clinical models of DKD to examine the natural variation in DKD severity and co-morbidity. Indeed, there are many unknown genetic factors that may underlie an individual's relative risk for the progression to ESRD. Whilst therapies targeting the early stages of DKD can provide an important intervention to the insidious decline in glomerular filtration rate, strategies for reversal of advanced nephropathy are still urgently required.

6.3 EVALUATION OF MITOCHONDRIAL FINDINGS

Mitochondria may demonstrate adaptations to prolonged hyperglycaemia in the very early stages of DKD, enacted via compensatory shifts designed to maintain energy generation. In this study, mitochondrial function was mostly unchanged in the early and moderate progression of STZ induced DKD, as determined by analysis of isolated mitochondria from experimental mice. Regardless of the duration of diabetes no statistically significant changes in renal mitochondrial function were observed with STZ induced diabetes. Both the *FVB/N* time-course model at up to 16 weeks of diabetes, and the Bax/Bak/Sglt2-Cre model at 24 weeks of diabetes, demonstrated that mild renal injury was not associated with an alteration in complex I stimulated oxygen consumption rate, nor the swelling response to calcium challenge. Urinary albumin excretion varied considerably between the two models, however both had a mild trends towards a decrease in plasma cystatin C. Thus, the development of albuminuria and early glomerular filtration changes (i.e hyperfiltration) were not associated with the development of mitochondrial dysfunction. Previous studies have demonstrated that albumin itself induces renal tubular injury (419,420). As such, the *FVB/N* mice used in this study may begin to develop more advanced injury beyond 16 weeks as a consequence of the very high albuminuria. Indeed, results from the mitochondrial swelling assay suggested that a trend towards an increase in swelling rate for STZ mice was occurring. Similar results have been reported in an STZ rat model where an increased propensity for swelling developed in the later course of the disease (267). Additionally, both the *FVB/N* and the Bax/Bak/Sglt2-Cre STZ mouse models developed minimal glomerular pathology; suggesting that mitochondrial dysfunction did not precede renal structural changes. Whilst rat models of STZ induced diabetes have demonstrated significant mitochondrial functional changes in the earlier stages of DKD, all of these models report structural changes (GSI, fibrosis) not seen in the mouse studies here (421–423). The absence of both structural injury and albuminuria in the *Bax/Bak/Sglt2 Cre* model at 24 weeks of diabetes suggests that hyperglycaemia alone was not sufficient to induce a measureable defect in mitochondrial function as per the methods used above. These data do not support the hypothesis that mitochondrial function is altered in the early progression of T1DM associated DKD as mitochondrial functional decline did not occur in these models with mild renal injury. Rather, results suggest that mitochondrial functional decline may develop later in the course of DKD. This is inferred from the

minimal functional changes seen in the STZ mouse models in Chapter 3 and 4. Indeed, mitochondrial alterations may be more closely associated with structural injury, or the cumulative effects of persistent metabolic dysregulation.

In contrast, the T2DM *db/db* model in Chapter 5 developed a clear change in mitochondrial phenotype at 22 weeks of age. Data revealed that renal mitochondria were able to develop compensatory mechanisms, including increased mitochondrial density, elevated respiratory control ratio and reduced sequestration of hydrogen peroxide. ADP stimulated respiration was also increased in the *db/db* mice compared with the *db/h* controls in contrast to no change in the STZ models. However, the T2DM model also developed more severe structural pathology; including greater GSI score and renal fibrosis. These data lend support to the hypothesis that mitochondrial dysfunction develops in association with the structural pathological changes, rather than preceding it. Additional experiments in future will allow this finding to be explored in specific detail. Data from both human studies and rodent models have demonstrated that insulin deficiency (T1DM) and insulin resistance (T2DM) are associated with general underlying changes in mitochondrial function (265,397,424). However, as the *db/db* model is an obesity-associated model of T2DM it is also possible that other factors play an important role in modulating mitochondrial function, including insulin resistance and dyslipidemia (425). Indeed, mitochondrial dysfunction and metabolic alterations have been observed to occur in pre-diabetes and the metabolic syndrome (426,427). Although this suggests that mitochondrial dysfunction may occur prior to diabetes itself, it possible that multiple mechanisms contribute to the defects in mitochondrial activity that occur (289,421,428). Some studies have even reported that mitochondrial dysfunction may precede the metabolic syndrome while others hypothesise that a feedback mechanism exists that leads to exacerbation of metabolic dysfunction at the level of the mitochondrion (426,429–431).

Compared with the T2DM mouse model, the T1DM STZ models may impart only mild metabolic disruption beyond hyperglycaemia in the early stages. However, the lack of defects observed with complex 1 stimulated respiration have been observed by others. For example, an early study of STZ induced diabetes in rats also reported no change in glutamate stimulated

respiration (432). They did however demonstrate that functional defects in the metabolism of other substrates were occurring. Complex I defects and over-activation have previously been observed to occur in early DKD in other rodent models and are associated with dysregulation of mitochondrial ROS production (421,422). This is also thought to drive the over-production of ROS: mediated through reverse electron transport chain events (433). Even without diabetes, specific genetic defects within complex I result in chronic renal injury (434). Interestingly, inhibition of complex I activity by low dose rotenone treatment has been demonstrated to prevent structural injury and fibrosis in DKD (421). Other electron transport (ETS) respiratory complexes also develop defects associated with diabetes, including complexes II and III (435). Further, functional defects at coenzyme Q result in impaired fatty acid oxidation pathways, and demonstrate that non-ETS complex defects occur in early DKD (180). An exploration of the changes in fatty acid and beta oxidation may lead to elucidation of specific mechanisms for therapeutic intervention in early DKD.

Similar to the data presented in the current investigation, a study in Akita diabetic mice revealed that mitochondrial function was maintained in the kidney at 12 weeks of age (398). It is possible that the initial response to hyperglycaemia includes adaptive biochemical processes that enable proximal tubule cells to maintain ATP production in response to these stress-associated demands. It is also likely that the renal PTCs have a flexible functional capacity as result of the high abundance of mitochondria within their cytoplasm. Thus, a decline in a small portion of total mitochondria could hypothetically lead to a compensatory change in the remaining mitochondria. As such, a diabetes-driven decline in mitochondrial function may take time to reveal a defect. Indeed, studies examining the effect of high glucose in renal tubular cells have demonstrated that shifts in metabolic flexibility occur at the mitochondrial level with changes in substrate flux (421,436). Interestingly, the demonstration that glycogen accumulation was occurring in the tubules of STZ mice do indicate that some intracellular metabolic pathways are altered in the renal proximal tubule as a result of type 1 diabetes (332). Further, changes associated with obesity and a high fat diet have also been demonstrated as risk factors for mitochondrial dysfunction in the kidney, and some studies demonstrate that an initial bioenergetic adaptation can occur in T2DM (271,437,438).

One interesting result, observed across all the experimental mouse models used in this investigation, was that the FCCP mediated complex I OCR was decreased relative to ADP stimulated respiration. Interestingly, it was noted that the age of experimental mice appeared to affect the magnitude of this response. In routine mitochondrial stress tests, FCCP stimulated respiration provides an estimate of spare respiratory capacity relative to basal respiration. This phenomenon is regarded to indicate the flexibility of a specific mitochondrial population to respond to an increase in energy demand. However, in isolated mitochondria, FCCP stimulated respiration (state 3u) is frequently lower than ADP stimulated OCR (state 3_{ADP}). This effect relates to the oxygen utilisation and hypoxia sensing of different tissues and substrate availability (186,439,440). However, it may also be possible that the negative values are produced as an artefact of oligomycin treatment, given that oligomycin may induce a state that mimics hypoxia via inhibition of oxygen sensing mechanisms (441,442). Thus a reduction in oxygen sensing capacity could result in a decline in OCR.

Regardless, isolated renal mitochondria presented with lowered state 3u OCR; thus a negative value for spare capacity, relative to state $3_{ADP,}$ is observed even with carefully titrated FCCP concentrations. This effect was also observed in the *db/db* heart mitochondria explored in Chapter 5, and has been demonstrated in previous studies of cardiac mitochondria in mice from 3 months of age (443). In the renal mitochondria studied in this investigation, the reduction relative to ADP stimulated OCR was highest in those models with the longest duration of diabetes. The results for the *FVB/N* time-course study suggest that this reduction is temporally associated with the age of the mice, as both the 4 and 8 week time points were only very slightly increased. An age associated decline in maximal respiratory capacity is well established in the literature (444,445). It has also been demonstrated that in response to such an age related decline in mitochondrial quality, a compensatory increase in mitochondrial content occurs in order to maintain similar oxidative capacity, similar to that observed in Model 4 in Chapter 5 (446). This protective mechanism, as demonstrated by Larsen et, al., was however limited to mitochondria with functional complex IV suggesting that mitochondrial ETS defects may overcome this compensation. While analysis of mitochondrial density by EM was not available in the STZ models, the possibility of a compensatory change in total mitochondria remains. Curiously, a decline in state 3u OCR relative to state 3_{ADP} has also been specifically associated with the

duration of hyperglycaemia, but not normoglycaemia, in a cell culture model of renal tubular cells (HK-2) (447). The effect was demonstrated to be cell specific as this effect was not observed in the same conditions for mesangial cells (HMCs). Although age is associated with a decline in this phenomenon of reduced state 3u respiration, few studies have linked this independently with the early progression of DKD.

One limitation of mitochondrial function in the experimental procedures used above, is the possibility of loss of mitochondrial populations during the isolation protocol. For this reason all data were normalised per milligram of mitochondrial protein to account for changes in intracellular mitochondrial content. Further, previous studies have demonstrated that mitochondrial isolation procedures can induce changes in mitochondrial populations (448). Additionally, isolated mitochondria may be sensitised to mPTP opening and mimic in vivo changes observed with stress (448). Results from all of the experimental models in this investigation demonstrated that isolated renal mitochondria underwent rapid swelling in response to the calcium challenge. Indeed, renal mitochondria had very limited capacity to resist swelling, even with CsA treatment in the studies used here. However, a comparison with liver mitochondria was performed in Chapter 3 and this revealed that the renal mitochondria were more sensitive to mPTP induction. Whilst this represents a limitation, mitochondrial isolation does allow a rapid analysis of mitochondrial electron transfer independent of glycolytic processes as performed with the Seahorse Bioanalyzer. In future, an exploration of additional complex mediated activities may assist in determining if mitochondrial dysfunction relates to other important cellular functions of mitochondria in DKD.

6.4 IMPLICATIONS FOR MITOCHONDRIAL FUNCTION IN DKD

The mechanisms of adaptive mild mitochondrial uncoupling, as discussed in Chapter 5, Publication 2, is an interesting area in mitochondrial functional analysis. Whilst the theory of ROS driven mitochondrial damage prevails, evidence exists to suggest that under some conditions the development of mild uncoupling is a protective mechanism designed to reduce the damage produced by ROS at the level of the mitochondrion (286,449). The exact mechanism by which this is possible has been explored in the literature, with some insight available. For example, the role of the UCP family of proteins in uncoupling the ETS from ATP production has been

demonstrated to be part of this protective system (449,450). Another example of mild uncoupling being protective has also been described from a study with very low doses of the uncoupling compound, FCCP (451). At higher doses FCCP is associated with the collapse of the inner mitochondrial membrane potential by interacting with the lipid membranes, leading to maximal ETS shuttling without ATP production (452).

As explored in Chapter 5, treatment with a drug that inhibits CypD to reduce FAO may be detrimental in the kidney. The importance of FAO in kidney is an area of current interest. Studies have demonstrated that FAO is altered in the diabetic kidney compared with the non-diabetic kidney. However, therapies which induce impairment in this process are detrimental. In non-diabetic chronic kidney disease restoration of FAO allows the reversal of fibrotic phenotypes (283). By restricting metabolism to FAO this adaptation allows the renal cells to by-pass the damaging ROS produced under a high glucose environment. It is also possible that the mechanisms available to mitochondria to control membrane potential in the development of DKD may be robust enough to prevent the over-production of damaging ROS, as demonstrated in Chapter 5, Publication 2. Collectively, these data indicate that energy production and the mitochondrial membrane potential are sensitive to changes at the mitochondrial outer membrane. Further, modification of ATP production and ROS can be achieved by the strategic targeting of mitochondrial channel forming proteins.

6.5 The role of Mitochondrial pore-forming cell death proteins in DKD

Cell death is a natural consequence of stress when an adequate pathological stimulus is received. Targeting the mitochondrial pore-forming cell death proteins, as performed in this investigation, did not affect the outcomes of DKD. Indeed, no specific effect for the role of the MOMP forming proteins, Bax and Bak, was found for the development of mitochondrial dysfunction in DKD. This investigation determined that in the early progression of STZ models of DKD, Bax and Bak do not affect pathological outcomes. As Bax and Bak are also important for the induction of the mPTP as well as the MOMP, the findings from the Ppif study suggested that it may be the physiological role of CypD that is important in the development of increased renal

injury (225,226,237,453). However, the differentiation between the mPTP inhibitory activity and its physiological functions is difficult given the protective role of CypD in the diabetic kidney.

Indeed, previous studies have shown that it may be the physiological role of CypD that is important in mediating tubular cell health in the context of chronic kidney disease. This includes the key regulation process whereby CypD allows specific promotion of FAO pathways (359). CypD has also been demonstrated to be a key regulator of mitochondrial metabolism and function by regulating mitochondrial gene expression, as well as metabolic processes (385,454,455). Whilst in most tissues, inhibition of CypD is protective against acute injury and some chronic insults, the unique characteristics of the kidney mean that inhibition of CypD is instead detrimental. Thus, mitochondrial cell death mediated through the mitochondrial pore-forming cell death proteins at the double membrane do not affect the progression of DKD. Rather, other processes may play a more significant role in deciding cell fate. Whilst a detailed investigation into the immunological consequences of cell death in the diabetic kidney was beyond the scope of this study, the interplay between innate immunity and the induction of cell death pathways is important to consider. Further, local tissue surveillance and circulating immune cells may clear damaged and dying cells prior to the execution of these pathways. Thus, extrinsic cell death induction may exceed the capacity of intrinsic apoptosis to effect pathway choice (456). Influx of a variety of immune cells has been confirmed to occur in DKD (457–459). The interactions between mitochondrial dysfunction and the induction of immune cell mediated efferocytosis could thus be explored in future.

Finally, the necroptotic cell death mechanism, ferroptosis, has been demonstrated to contribute significantly to the loss of renal tubular cells in many acute pathology settings (246,460). The potential for cell death mechanisms to involve intrinsic cell death pathways that do not involve the MOMP or mPTP must be explored in future in order to establish if mitochondrial dysfunction affects the induction of alternative pathways instead.

6.6 CONCLUSION

Mitochondrial pore-forming cell death proteins do not play a significant role in the initiation of DKD pathology. However, it would appear that renal mitochondria undergo unique adaptation processes which may allow them to overcome the altered energy demand under diabetic conditions. Therefore, targeting the renal mitochondria is likely to requires a different approach than that being conducted for other major organs.

References

References

1. Coppieters KT, Dotta F, Amirian N, Campbell PD, Kay TW, Atkinson MA, et al. Demonstration of islet-autoreactive CD8 T cells in insulitic lesions from recent onset and long-term type 1 diabetes patients. J Exp Med. 2012 Jan 16;209(1):51–60.
2. Yoon JW, Jun HS. Autoimmune destruction of pancreatic beta cells. Am J Ther. 2005 Dec;12(6):580–591.
3. Mbongue JC, Nieves HA, Torrez TW, Langridge WH. The Role of Dendritic Cell Maturation in the Induction of Insulin-Dependent Diabetes Mellitus. Front Immunol. 2017 Mar 27;8:327.
4. Newsholme EA, Dimitriadis G. Integration of biochemical and physiologic effects of insulin on glucose metabolism. Exp Clin Endocrinol Diabetes. 2001;109 Suppl 2:S122–34.
5. Moore MC, Coate KC, Winnick JJ, An Z, Cherrington AD. Regulation of hepatic glucose uptake and storage in vivo. Adv Nutr. 2012 May 1;3(3):286–294.
6. Himsworth HP. Diabetes mellitus. Its differentiation into insulin-sensitive and insulin-insensitive types. Lancet [Internet]. 1936; Available from: https://www.cabdirect.org/cabdirect/abstract/19361401054
7. Brown SD, Ehrlich SF, Kubo A, Tsai AL, Hedderson MM, Quesenberry CP, et al. Lifestyle behaviors and ethnic identity among diverse women at high risk for type 2 diabetes. Soc Sci Med. 2016 May 14;160:87–93.
8. Temelkova-Kurktschiev T, Stefanov T. Lifestyle and genetics in obesity and type 2 diabetes. Exp Clin Endocrinol Diabetes. 2012 Jan;120(1):1–6.
9. Djoussé L, Driver JA, Gaziano JM, Buring JE, Lee IM. Association between modifiable lifestyle factors and residual lifetime risk of diabetes. Nutr Metab Cardiovasc Dis. 2013 Jan;23(1):17–22.
10. Joseph JJ, Echouffo-Tcheugui JB, Talegawkar SA, Effoe VS, Okhomina V, Carnethon MR, et al. Modifiable lifestyle risk factors and incident diabetes in african americans. Am J Prev Med. 2017 Nov;53(5):e165–e174.
11. Gu HF, Brismar K. Genetic association studies in diabetic nephropathy. Curr Diabetes Rev. 2012 Sep;8(5):336–344.

12. Sikhayeva N, Talzhanov Y, Iskakova A, Dzharmukhanov J, Nugmanova R, Zholdybaeva E, et al. Type 2 diabetes mellitus: distribution of genetic markers in Kazakh population. Clin Interv Aging. 2018 Mar 5;13:377–388.

13. Sánchez-Pozos K, Menjívar M. Genetic component of type 2 diabetes in a mexican population. Arch Med Res. 2016;47(7):496–505.

14. Garg DK, Dutta MK. Body Mass composition among Underweight Type 2 Diabetes Mellitus Patients-A Cross-sectional Comparative Study. Indian J Endocrinol Metab. 2019 Apr;23(2):222–226.

15. Gaffney CJ, Mansell P, Stephens FB, Macdonald IA, Tsintzas K. Exercise Metabolism in Nonobese Patients with Type 2 Diabetes Following the Acute Restoration of Normoglycaemia. J Diabetes Res. 2017 May 29;2017:8248725.

16. Chandra GB, Kumar B, Singh S. A comparative study of lean, obese and non-obese type 2 diabetes mellitus with special reference to renal status and lipid profile in Jharkhand. International Journal of Scientific Research [Internet]. 2019 Jul 20; Available from: http://worldwidejournals.co.in/index.php/ijsr/article/view/2402

17. Benhalima K, Devlieger R, Van Assche A. Screening and management of gestational diabetes. Best Pract Res Clin Obstet Gynaecol. 2015 Apr;29(3):339–349.

18. Shen Y, Wang P, Wang L, Zhang S, Liu H, Li W, et al. Gestational diabetes with diabetes and prediabetes risks: a large observational study. Eur J Endocrinol. 2018 Jul;179(1):51–58.

19. Eades CE, Styles M, Leese GP, Cheyne H, Evans JM. Progression from gestational diabetes to type 2 diabetes in one region of Scotland: an observational follow-up study. BMC Pregnancy Childbirth. 2015 Feb 3;15:11.

20. De la Monte SM, Wands JR. Alzheimer's disease is type 3 diabetes-evidence reviewed. J Diabetes Sci Technol. 2008 Nov;2(6):1101–1113.

21. Barton JC, Acton RT. Diabetes in HFE hemochromatosis. J Diabetes Res. 2017 Feb 26;2017:9826930.

22. Behrendt CE, Ruiz RB. Hyperglycemia among persons with hepatitis C: not the classical diabetic phenotype. Diabetes Res Clin Pract. 2006 Jan;71(1):68–74.

23. Tuomi T. Type 1 and type 2 diabetes: what do they have in common? Diabetes. 2005 Dec;54 Suppl 2:S40–5.

24. Ogurtsova K, da Rocha Fernandes JD, Huang Y, Linnenkamp U, Guariguata L, Cho NH, et al. IDF Diabetes Atlas: Global estimates for the prevalence of diabetes for 2015 and 2040. Diabetes Res Clin Pract. 2017 Jun;128:40–50.

25. Shaw JE, Sicree RA, Zimmet PZ. Global estimates of the prevalence of diabetes for 2010 and 2030. Diabetes Res Clin Pract. 2010 Jan;87(1):4–14.

26. Chen L, Magliano DJ, Zimmet PZ. The worldwide epidemiology of type 2 diabetes mellitus--present and future perspectives. Nat Rev Endocrinol. 2011 Nov 8;8(4):228–236.

27. Molitch ME, Steffes M, Sun W, Rutledge B, Cleary P, de Boer IH, et al. Development and progression of renal insufficiency with and without albuminuria in adults with type 1 diabetes in the diabetes control and complications trial and the epidemiology of diabetes interventions and complications study. Diabetes Care. 2010 Jul 1;33(7):1536–1543.

28. Forbes JM, Cooper ME. Mechanisms of diabetic complications. Physiol Rev. 2013 Jan;93(1):137–188.

29. Diabetes Control and Complications Trial (DCCT)/Epidemiology of Diabetes Interventions and Complications (EDIC) Study Research Group. Intensive Diabetes Treatment and Cardiovascular Outcomes in Type 1 Diabetes: The DCCT/EDIC Study 30-Year Follow-up. Diabetes Care. 2016 May;39(5):686–693.

30. Gaede P, Vedel P, Larsen N, Jensen GV, Parving HH, Pedersen O. Multifactorial intervention and cardiovascular disease in patients with type 2 diabetes. N Engl J Med. 2003 Jan 30;348(5):383–393.

31. Roussel R, Steg PG, Mohammedi K, Marre M, Potier L. Prevention of cardiovascular disease through reduction of glycaemic exposure in type 2 diabetes: A perspective on glucose-lowering interventions. Diabetes Obes Metab. 2018;20(2):238–244.

32. Miller RG, Secrest AM, Sharma RK, Songer TJ, Orchard TJ. Improvements in the life expectancy of type 1 diabetes: the Pittsburgh Epidemiology of Diabetes Complications study cohort. Diabetes. 2012 Nov;61(11):2987–2992.

33. Huo L, Shaw JE, Wong E, Harding JL, Peeters A, Magliano DJ. Burden of diabetes in Australia: life expectancy and disability-free life expectancy in adults with diabetes. Diabetologia. 2016 Apr 14;59(7):1437–1445.

34. Canadian Diabetes Association Clinical Practice Guidelines Expert Committee, Goldenberg R, Punthakee Z. Definition, classification and diagnosis of diabetes, prediabetes and metabolic syndrome. Can J Diabetes. 2013 Apr;37 Suppl 1:S8–11.

35. Twigg SM, Kamp MC, Davis TM, Neylon EK, Flack JR, Australian Diabetes Society, et al. Prediabetes: a position statement from the Australian Diabetes Society and Australian Diabetes Educators Association. Med J Aust. 2007 May 7;186(9):461–465.

36. Dall TM, Yang W, Halder P, Pang B, Massoudi M, Wintfeld N, et al. The economic burden of elevated blood glucose levels in 2012: diagnosed and undiagnosed diabetes, gestational diabetes mellitus, and prediabetes. Diabetes Care. 2014 Dec;37(12):3172–3179.

37. Ligthart S, van Herpt TT, Leening MJ, Kavousi M, Hofman A, Stricker BH, et al. Lifetime risk of developing impaired glucose metabolism and eventual progression from prediabetes to type 2 diabetes: a prospective cohort study. The lancet Diabetes & endocrinology. 2016 Jan;4(1):44–51.

38. Sénéchal M, Slaght J, Bharti N, Bouchard DR. Independent and combined effect of diet and exercise in adults with prediabetes. Diabetes Metab Syndr Obes. 2014 Oct 31;7:521–529.

39. Hrubeniuk TJ, Bouchard DR, Goulet EDB, Gurd B, Sénéchal M. The ability of exercise to meaningfully improve glucose tolerance in people living with prediabetes: A meta-analysis. Scand J Med Sci Sports. 2020 Feb;30(2):209–216.

40. Dorcely B, Katz K, Jagannathan R, Chiang SS, Oluwadare B, Goldberg IJ, et al. Novel biomarkers for prediabetes, diabetes, and associated complications. Diabetes Metab Syndr Obes. 2017 Aug 14;10:345–361.

41. Malmström H, Walldius G, Grill V, Jungner I, Gudbjörnsdottir S, Hammar N. Fructosamine is a useful indicator of hyperglycaemia and glucose control in clinical and epidemiological studies--cross-sectional and longitudinal experience from the AMORIS cohort. PLoS ONE. 2014 Oct 29;9(10):e111463.

42. Stefan N, Fritsche A, Schick F, Häring HU. Phenotypes of prediabetes and stratification of cardiometabolic risk. The lancet Diabetes & endocrinology. 2016 May 13;4(9):789–798.

43. Milman S, Crandall JP. Mechanisms of vascular complications in prediabetes. Med Clin North Am. 2011 Mar;95(2):309–25, vii.

44. Brannick B, Wynn A, Dagogo-Jack S. Prediabetes as a toxic environment for the initiation of microvascular and macrovascular complications. Exp Biol Med (Maywood). 2016;241(12):1323–1331.

45. Huang D, Refaat M, Mohammedi K, Jayyousi A, Al Suwaidi J, Abi Khalil C. Macrovascular Complications in Patients with Diabetes and Prediabetes. BioMed research international. 2017 Nov 7;2017:7839101.

46. Venkatesh P, K. J, K. S, Green SR. Cross sectional study of microalbuminuria, C-peptide and fundal changes in pre-diabetics. International Journal of Advances in Medicine. 2018 Mar 21;5(2):271.

47. Lorenzo C, Okoloise M, Williams K, Stern MP, Haffner SM, San Antonio Heart Study. The metabolic syndrome as predictor of type 2 diabetes: the San Antonio heart study. Diabetes Care. 2003 Nov;26(11):3153–3159.

48. Wannamethee SG, Shaper AG, Lennon L, Morris RW. Metabolic syndrome vs Framingham Risk Score for prediction of coronary heart disease, stroke, and type 2 diabetes mellitus. Arch Intern Med. 2005 Dec 26;165(22):2644–2650.

49. Eckel RH, Alberti KG, Grundy SM, Zimmet PZ. The metabolic syndrome. The Lancet. 2010 Jan 16;375(9710):181–183.

50. Cameron AJ, Magliano DJ, Zimmet PZ, Welborn TA, Colagiuri S, Tonkin AM, et al. The metabolic syndrome as a tool for predicting future diabetes: the AusDiab study. J Intern Med. 2008 Aug;264(2):177–186.

51. Rao Kondapally Seshasai S, Kaptoge S, Thompson A, Di Angelantonio E, Gao P, Sarwar N, et al. Diabetes mellitus, fasting glucose, and risk of cause-specific death. N Engl J Med. 2011 Mar 3;364(9):829–841.

52. Anjana RM, Unnikrishnan R, Mugilan P, Jagdish PS, Parthasarathy B, Deepa M, et al. Causes and predictors of mortality in Asian Indians with and without diabetes-10 year follow-up of the Chennai Urban Rural Epidemiology Study (CURES - 150). PLoS ONE. 2018 Jul 9;13(7):e0197376.

53. Yu OH, Suissa S. Identifying causes for excess mortality in patients with diabetes: closer but not there yet. Diabetes Care. 2016;39(11):1851–1853.

54. Nathan DM, Cleary PA, Backlund JY, Genuth SM, Lachin JM, Orchard TJ, et al. Intensive diabetes treatment and cardiovascular disease in patients with type 1 diabetes. N Engl J Med. 2005 Dec 22;353(25):2643–2653.

55. ACCORD Study Group, Gerstein HC, Miller ME, Genuth S, Ismail-Beigi F, Buse JB, et al. Long-term effects of intensive glucose lowering on cardiovascular outcomes. N Engl J Med. 2011 Mar 3;364(9):818–828.

56. Reaven PD, Emanuele NV, Wiitala WL, Bahn GD, Reda DJ, McCarren M, et al. Intensive Glucose Control in Patients with Type 2 Diabetes - 15-Year Follow-up. N Engl J Med. 2019 Jun 6;380(23):2215–2224.

57. Mostafa SA, Coleman RL, Agbaje OF, Gray AM, Holman RR, Bethel MA. Modelling incremental benefits on complications rates when targeting lower HbA1c levels in people with Type 2 diabetes and cardiovascular disease. Diabet Med. 2018;35(1):72–77.

58. Brownlee M. Glycosylation products as toxic mediators of diabetic complications. Annu Rev Med. 1991;42:159–166.

59. Lorenzi M. Glucose toxicity in the vascular complications of diabetes: the cellular perspective. Diabetes Metab Rev. 1992 Jul;8(2):85–103.

60. Emdin CA, Rahimi K, Neal B, Callender T, Perkovic V, Patel A. Blood pressure lowering in type 2 diabetes: a systematic review and meta-analysis. JAMA. 2015 Feb 10;313(6):603–615.

61. Jia G, DeMarco VG, Sowers JR. Insulin resistance and hyperinsulinaemia in diabetic cardiomyopathy. Nat Rev Endocrinol. 2016 Mar;12(3):144–153.

62. White S, Chadban S. Diabetic kidney disease in Australia: current burden and future projections. Nephrology (Carlton). 2014 Aug;19(8):450–458.

63. Grace BS, Clayton P, McDonald SP. Increases in renal replacement therapy in Australia and New Zealand: understanding trends in diabetic nephropathy. Nephrology (Carlton). 2012 Jan;17(1):76–84.

64. Conway J, Lawn S, Crail S, McDonald S. Indigenous patient experiences of returning to country: a qualitative evaluation on the Country Health SA Dialysis bus. BMC Health Serv Res. 2018 Dec 29;18(1):1010.

65. Liyanage T, Ninomiya T, Jha V, Neal B, Patrice HM, Okpechi I, et al. Worldwide access to treatment for end-stage kidney disease: a systematic review. The Lancet. 2015 May 16;385(9981):1975–1982.

66. Ruggenenti P, Cravedi P, Remuzzi G. Mechanisms and treatment of CKD. J Am Soc Nephrol. 2012 Dec;23(12):1917–1928.

67. Wanner C, Inzucchi SE, Lachin JM, Fitchett D, von Eynatten M, Mattheus M, et al. Empagliflozin and Progression of Kidney Disease in Type 2 Diabetes. N Engl J Med. 2016 Jul 28;375(4):323–334.

68. Gerstein HC, Colhoun HM, Dagenais GR, Diaz R, Lakshmanan M, Pais P, et al. Dulaglutide and cardiovascular outcomes in type 2 diabetes (REWIND): a double-blind, randomised placebo-controlled trial. The Lancet. 2019 Jul 13;394(10193):121–130.

69. Ficociello LH, Perkins BA, Silva KH, Finkelstein DM, Ignatowska-Switalska H, Gaciong Z, et al. Determinants of progression from microalbuminuria to proteinuria in patients who have type 1 diabetes and are treated with angiotensin-converting enzyme inhibitors. Clin J Am Soc Nephrol. 2007 May;2(3):461–469.

70. Dunkler D, Gao P, Lee SF, Heinze G, Clase CM, Tobe S, et al. Risk Prediction for Early CKD in Type 2 Diabetes. Clin J Am Soc Nephrol. 2015 Aug 7;10(8):1371–1379.

71. Walker AM, Bott PA, Oliver J, MacDowell MC. THE COLLECTION AND ANALYSIS OF FLUID FROM SINGLE NEPHRONS OF THE MAMMALIAN KIDNEY. American Journal of Physiology -- Legacy Content [Internet]. 1941 Sep 30; Available from: http://ajplegacy.physiology.org/content/134/3/580.full

72. Leung WK, Gao L, Siu PM, Lai CW. Diabetic nephropathy and endothelial dysfunction: Current and future therapies, and emerging of vascular imaging for preclinical renal-kinetic study. Life Sci. 2016 Dec 1;166:121–130.

73. Markus MRP, Ittermann T, Baumeister SE, Huth C, Thorand B, Herder C, et al. Prediabetes is associated with microalbuminuria, reduced kidney function and chronic kidney disease in the general population: The KORA (Cooperative Health Research in the Augsburg Region) F4-Study. Nutr Metab Cardiovasc Dis. 2018;28(3):234–242.

74. Macisaac RJ, Jerums G. Diabetic kidney disease with and without albuminuria. Curr Opin Nephrol Hypertens. 2011 May;20(3):246–257.

75. Vallon V. The proximal tubule in the pathophysiology of the diabetic kidney. Am J Physiol Regul Integr Comp Physiol. 2011 May;300(5):R1009–22.

76. Phillips AO, Steadman R. Diabetic nephropathy: the central role of renal proximal tubular cells in tubulointerstitial injury. Histol Histopathol. 2002 Jan;17(1):247–252.

77. Gilbert RE, Cooper ME. The tubulointerstitium in progressive diabetic kidney disease: more than an aftermath of glomerular injury? Kidney Int. 1999 Nov;56(5):1627–1637.

78. Vallon V, Platt KA, Cunard R, Schroth J, Whaley J, Thomson SC, et al. SGLT2 mediates glucose reabsorption in the early proximal tubule. J Am Soc Nephrol. 2011 Jan;22(1):104–112.

79. Sun L, Xiao L, Nie J, Liu FY, Ling GH, Zhu XJ, et al. p66Shc mediates high-glucose and angiotensin II-induced oxidative stress renal tubular injury via mitochondrial-dependent apoptotic pathway. Am J Physiol Renal Physiol. 2010 Nov;299(5):F1014–25.

80. Habib SL. Diabetes and renal tubular cell apoptosis. World J Diabetes. 2013 Apr 15;4(2):27–30.

81. Rector FC. Sodium, bicarbonate, and chloride absorption by the proximal tubule. Am J Physiol. 1983 May;244(5):F461–71.

82. Kobori H, Harrison-Bernard LM, Navar LG. Expression of angiotensinogen mRNA and protein in angiotensin II-dependent hypertension. J Am Soc Nephrol. 2001 Mar;12(3):431–439.

83. Ingelfinger JR, Zuo WM, Fon EA, Ellison KE, Dzau VJ. In situ hybridization evidence for angiotensinogen messenger RNA in the rat proximal tubule. An hypothesis for the intrarenal renin angiotensin system. J Clin Invest. 1990 Feb;85(2):417–423.

84. Ramkumar N, Kohan DE. Proximal tubule angiotensinogen modulation of arterial pressure. Curr Opin Nephrol Hypertens. 2013 Jan;22(1):32–36.

85. Romano G, Giagu P, Favret G, Bartoli E. Effect of endothelin 1 on proximal reabsorption and tubuloglomerular feedback. Kidney Blood Press Res. 2000;23(6):360–365.

86. Forbes JM, Thorburn DR. Mitochondrial dysfunction in diabetic kidney disease. Nat Rev Nephrol. 2018 Feb 19;14(5):291–312.

87. Hallow KM, Gebremichael Y, Helmlinger G, Vallon V. Primary proximal tubule hyperreabsorption and impaired tubular transport counterregulation determine glomerular hyperfiltration in diabetes: a modeling analysis. Am J Physiol Renal Physiol. 2017 May 1;312(5):F819–F835.

88. Carmines PK. The renal vascular response to diabetes. Curr Opin Nephrol Hypertens. 2010 Jan;19(1):85–90.

89. Lee YJ, Lee YJ, Han HJ. Regulatory mechanisms of Na(+)/glucose cotransporters in renal proximal tubule cells. Kidney Int Suppl. 2007 Aug;(106):S27–35.

90. Ly JP, Onay T, Sison K, Sivaskandarajah G, Sabbisetti V, Li L, et al. The Sweet Pee model for Sglt2 mutation. J Am Soc Nephrol. 2011 Jan;22(1):113–123.

91. Abdul-Ghani MA, Norton L, DeFronzo RA. Renal sodium-glucose cotransporter inhibition in the management of type 2 diabetes mellitus. Am J Physiol Renal Physiol. 2015 Dec 1;309(11):F889–900.

92. Gallo LA, Wright EM, Vallon V. Probing SGLT2 as a therapeutic target for diabetes: basic physiology and consequences. Diab Vasc Dis Res. 2015 Mar;12(2):78–89.

93. DeFronzo RA, Lewin A, Patel S, Liu D, Kaste R, Woerle HJ, et al. Combination of empagliflozin and linagliptin as second-line therapy in subjects with type 2 diabetes inadequately controlled on metformin. Diabetes Care. 2015 Mar;38(3):384–393.

94. Devineni D, Curtin CR, Polidori D, Gutierrez MJ, Murphy J, Rusch S, et al. Pharmacokinetics and pharmacodynamics of canagliflozin, a sodium glucose co-transporter 2 inhibitor, in subjects with type 2 diabetes mellitus. J Clin Pharmacol. 2013 Jun;53(6):601–610.

95. Scheen AJ. Pharmacodynamics, efficacy and safety of sodium-glucose co-transporter type 2 (SGLT2) inhibitors for the treatment of type 2 diabetes mellitus. Drugs. 2015 Jan;75(1):33–59.

96. Kurosaki E, Ogasawara H. Ipragliflozin and other sodium-glucose cotransporter-2 (SGLT2) inhibitors in the treatment of type 2 diabetes: preclinical and clinical data. Pharmacol Ther. 2013 Jul;139(1):51–59.

97. Cherney DZ, Perkins BA, Soleymanlou N, Maione M, Lai V, Lee A, et al. Renal hemodynamic effect of sodium-glucose cotransporter 2 inhibition in patients with type 1 diabetes mellitus. Circulation. 2014 Feb 4;129(5):587–597.

98. Malatiali S, Francis I, Barac-Nieto M. Phlorizin prevents glomerular hyperfiltration but not hypertrophy in diabetic rats. Exp Diabetes Res. 2008;2008:305403.

99. Alicic RZ, Johnson EJ, Tuttle KR. SGLT2 inhibition for the prevention and treatment of diabetic kidney disease: A review. Am J Kidney Dis. 2018 Jun 14;72(2):267–277.

100. Kramer CK, Zinman B. Sodium-Glucose Cotransporter-2 (SGLT-2) Inhibitors and the Treatment of Type 2 Diabetes. Annu Rev Med. 2019 Jan 27;70:323–334.

101. Scheen AJ. Evaluating SGLT2 inhibitors for type 2 diabetes: pharmacokinetic and toxicological considerations. Expert Opin Drug Metab Toxicol. 2014 May;10(5):647–663.

102. Perkovic V, Jardine MJ, Neal B, Bompoint S, Heerspink HJL, Charytan DM, et al. Canagliflozin and renal outcomes in type 2 diabetes and nephropathy. N Engl J Med. 2019 Jun 13;380(24):2295–2306.

103. Zinman B, Wanner C, Lachin JM, Fitchett D, Bluhmki E, Hantel S, et al. Empagliflozin, cardiovascular outcomes, and mortality in type 2 diabetes. N Engl J Med. 2015 Nov 26;373(22):2117–2128.

104. Kohan DE, Fioretto P, Johnsson K, Parikh S, Ptaszynska A, Ying L. The effect of dapagliflozin on renal function in patients with type 2 diabetes. J Nephrol. 2016 Jun;29(3):391–400.

105. Kato ET, Silverman MG, Mosenzon O, Zelniker TA, Cahn A, Furtado RHM, et al. Effect of dapagliflozin on heart failure and mortality in type 2 diabetes mellitus. Circulation. 2019 May 28;139(22):2528–2536.

106. Mudaliar S, Alloju S, Henry RR. Can a Shift in Fuel Energetics Explain the Beneficial Cardiorenal Outcomes in the EMPA-REG OUTCOME Study? A Unifying Hypothesis. Diabetes Care. 2016 Jul;39(7):1115–1122.

107. Layton AT, Vallon V, Edwards A. Predicted consequences of diabetes and SGLT inhibition on transport and oxygen consumption along a rat nephron. Am J Physiol Renal Physiol. 2016 Jun 1;310(11):F1269–83.

108. Layton AT, Vallon V, Edwards A. Modeling oxygen consumption in the proximal tubule: effects of NHE and SGLT2 inhibition. Am J Physiol Renal Physiol. 2015 Jun 15;308(12):F1343–57.

109. Hawley SA, Ford RJ, Smith BK, Gowans GJ, Mancini SJ, Pitt RD, et al. The na+/glucose cotransporter inhibitor canagliflozin activates AMPK by inhibiting mitochondrial function and increasing cellular AMP levels. Diabetes. 2016 Jul 5;65(9):2784–2794.

110. Noël J, Tejedor A, Vinay P, Laprade R. Substrate-induced modulation of ATP turnover in dog and rabbit proximal tubules. J Membr Biol. 1992 Jun;128(3):205–218.

111. Prince A, Zhang Y, Croniger C, Puchowicz M. Oxidative metabolism: glucose versus ketones. Adv Exp Med Biol. 2013;789:323–328.

112. Sato K, Kashiwaya Y, Keon CA, Tsuchiya N, King MT, Radda GK, et al. Insulin, ketone bodies, and mitochondrial energy transduction. FASEB J. 1995 May;9(8):651–658.

113. Lopaschuk GD, Ussher JR. Evolving concepts of myocardial energy metabolism: more than just fats and carbohydrates. Circ Res. 2016 Nov 11;119(11):1173–1176.

114. Friedrichs D, Schoner W. Stimulation of renal gluconeogenesis by inhibition of the sodium pump. Biochimica et Biophysica Acta (BBA) - General Subjects. 1973 Mar;304(1):142–160.

115. Nagami GT, Lee P. Effect of luminal perfusion on glucose production by isolated proximal tubules. Am J Physiol. 1989 Jan;256(1 Pt 2):F120–7.

116. Perlman A, Heyman SN, Matok I, Stokar J, Muszkat M, Szalat A. Acute renal failure with sodium-glucose-cotransporter-2 inhibitors: Analysis of the FDA adverse event report system database. Nutr Metab Cardiovasc Dis. 2017 Dec;27(12):1108–1113.

117. Chu C, Lu YP, Yin L, Hocher B. The SGLT2 inhibitor empagliflozin might be a new approach for the prevention of acute kidney injury. Kidney Blood Press Res. 2019 Apr 2;44(2):149–157.

118. Nadkarni GN, Ferrandino R, Chang A, Surapaneni A, Chauhan K, Poojary P, et al. Acute Kidney Injury in Patients on SGLT2 Inhibitors: A Propensity-Matched Analysis. Diabetes Care. 2017 Aug 21;40(11):1479–1485.

119. Amsellem S, Gburek J, Hamard G, Nielsen R, Willnow TE, Devuyst O, et al. Cubilin is essential for albumin reabsorption in the renal proximal tubule. J Am Soc Nephrol. 2010 Nov;21(11):1859–1867.

120. Cui S, Verroust PJ, Moestrup SK, Christensen EI. Megalin/gp330 mediates uptake of albumin in renal proximal tubule. Am J Physiol. 1996 Oct;271(4 Pt 2):F900–7.

121. Birn H, Fyfe JC, Jacobsen C, Mounier F, Verroust PJ, Orskov H, et al. Cubilin is an albumin binding protein important for renal tubular albumin reabsorption. J Clin Invest. 2000 May;105(10):1353–1361.

122. Qi Z, Fujita H, Jin J, Davis LS, Wang Y, Fogo AB, et al. Characterization of susceptibility of inbred mouse strains to diabetic nephropathy. Diabetes. 2005 Sep;54(9):2628–2637.

123. Bonventre JV. Can we target tubular damage to prevent renal function decline in diabetes? Semin Nephrol. 2012 Sep;32(5):452–462.

124. Dickson LE, Wagner MC, Sandoval RM, Molitoris BA. The proximal tubule and albuminuria: really! J Am Soc Nephrol. 2014 Mar;25(3):443–453.

125. Chesney RW. Interactions of vitamin D and the proximal tubule. Pediatr Nephrol. 2016 Jan;31(1):7–14.

126. Nykjaer A, Fyfe JC, Kozyraki R, Leheste JR, Jacobsen C, Nielsen MS, et al. Cubilin dysfunction causes abnormal metabolism of the steroid hormone 25(OH) vitamin D(3). Proc Natl Acad Sci U S A. 2001 Nov 20;98(24):13895–13900.

127. Ibeh CL, Yiu AJ, Kanaras YL, Paal E, Birnbaumer L, Jose PA, et al. Evidence for a regulated Ca2+ entry in proximal tubular cells and its implication in calcium stone formation. J Cell Sci. 2019 Apr 30;132(9).

128. Fink BD, Bai F, Yu L, Sivitz WI. Regulation of ATP production: dependence on calcium concentration and respiratory state. Am J Physiol, Cell Physiol. 2017 Aug 1;313(2):C146–C153.

129. Sánchez-Hernández RM, García-Cantón C, Lorenzo DL, Quevedo V, Bosch E, López-Ríos L, et al. The specific relationship between vitamin D deficiency and diabetic nephropathy among patients with advanced chronic kidney disease: a cross-sectional study in Gran Canaria, Spain. Clin Nephrol. 2015 Apr;83(4):218–224.

130. Tourigny A, Charbonneau F, Xing P, Boukrab R, Rousseau G, St-Arnaud R, et al. CYP24A1 exacerbated activity during diabetes contributes to kidney tubular apoptosis via caspase-3 increased expression and activation. PLoS ONE. 2012 Oct 31;7(10):e48652.

131. Moe S, Drüeke T, Cunningham J, Goodman W, Martin K, Olgaard K, et al. Definition, evaluation, and classification of renal osteodystrophy: a position statement from Kidney Disease: Improving Global Outcomes (KDIGO). Kidney Int. 2006 Jun;69(11):1945–1953.

132. Khoshjou F, Dadras F. Mitochondrion and its role in diabetic nephropathy. Iran J Kidney Dis. 2014 Sep;8(5):355–358.

133. Coughlan MT, Thallas-Bonke V, Pete J, Long DM, Gasser A, Tong DC, et al. Combination therapy with the advanced glycation end product cross-link breaker, alagebrium, and angiotensin converting enzyme inhibitors in diabetes: synergy or redundancy? Endocrinology. 2007 Feb;148(2):886–895.

134. Sharma K, Karl B, Mathew AV, Gangoiti JA, Wassel CL, Saito R, et al. Metabolomics reveals signature of mitochondrial dysfunction in diabetic kidney disease. J Am Soc Nephrol. 2013 Nov;24(11):1901–1912.

135. Tao M, You CP, Zhao RR, Liu SJ, Zhang ZH, Zhang C, et al. Animal mitochondria: evolution, function, and disease. Curr Mol Med. 2014 Jan;14(1):115–124.

136. Shellman ER, Chen Y, Lin X, Burant CF, Schnell S. Metabolic network motifs can provide novel insights into evolution: The evolutionary origin of Eukaryotic organelles as a case study. Comput Biol Chem. 2014 Sep 21;53PB:242–250.

137. Lane N. Energetics and genetics across the prokaryote-eukaryote divide. Biol Direct. 2011 Jun 30;6:35.

138. Zaremba-Niedzwiedzka K, Caceres EF, Saw JH, Bäckström D, Juzokaite L, Vancaester E, et al. Asgard archaea illuminate the origin of eukaryotic cellular complexity. Nature. 2017 Jan 19;541(7637):353–358.

139. Spang A, Saw JH, Jørgensen SL, Zaremba-Niedzwiedzka K, Martijn J, Lind AE, et al. Complex archaea that bridge the gap between prokaryotes and eukaryotes. Nature. 2015 May 14;521(7551):173–179.

140. Lane N, Martin W. The energetics of genome complexity. Nature. 2010 Oct 21;467(7318):929–934.

141. Stefano GB, Kream RM. Glycolytic coupling to mitochondrial energy production ensures survival in an oxygen rich environment. Med Sci Monit. 2016 Jul 20;22:2571–2575.

142. Pfeiffer T, Schuster S, Bonhoeffer S. Cooperation and competition in the evolution of ATP-producing pathways. Science. 2001 Apr 20;292(5516):504–507.

143. Friedman JR, Nunnari J. Mitochondrial form and function. Nature. 2014 Jan 16;505(7483):335–343.

144. Chernorudskiy AL, Zito E. Regulation of Calcium Homeostasis by ER Redox: A Close-Up of the ER/Mitochondria Connection. J Mol Biol. 2017 Mar 10;429(5):620–632.

145. Xu W, Barrientos T, Andrews NC. Iron and copper in mitochondrial diseases. Cell Metab. 2013 Mar 5;17(3):319–328.

146. Pan X, Liu J, Nguyen T, Liu C, Sun J, Teng Y, et al. The physiological role of mitochondrial calcium revealed by mice lacking the mitochondrial calcium uniporter. Nat Cell Biol. 2013 Dec;15(12):1464–1472.

147. Koonin EV, Aravind L. Origin and evolution of eukaryotic apoptosis: the bacterial connection. Cell Death Differ. 2002 Mar 28;9(4):394–404.

148. Mather M, Rottenberg H. Polycations induce the release of soluble intermembrane mitochondrial proteins. Biochim Biophys Acta. 2001 Jan 19;1503(3):357–368.

149. Stefanelli C, Stanic I, Zini M, Bonavita F, Flamigni F, Zambonin L, et al. Polyamines directly induce release of cytochrome c from heart mitochondria. Biochem J. 2000 May 1;347 Pt 3:875–880.

150. Morales AI, Detaille D, Prieto M, Puente A, Briones E, Arévalo M, et al. Metformin prevents experimental gentamicin-induced nephropathy by a mitochondria-dependent pathway. Kidney Int. 2010 May;77(10):861–869.

151. Castro MA, Dalmolin RJ, Moreira JC, Mombach JC, de Almeida RM. Evolutionary origins of human apoptosis and genome-stability gene networks. Nucleic Acids Res. 2008 Nov;36(19):6269–6283.

152. Oberst A, Bender C, Green DR. Living with death: the evolution of the mitochondrial pathway of apoptosis in animals. Cell Death Differ. 2008 Jul;15(7):1139–1146.

153. Lee H, Yoon Y. Mitochondrial fission: regulation and ER connection. Mol Cells. 2014 Feb 19;37(2):89–94.

154. Purkanti R, Thattai M. Ancient dynamin segments capture early stages of host-mitochondrial integration. Proc Natl Acad Sci U S A. 2015 Mar 3;112(9):2800–2805.

155. Leger MM, Petrů M, Žárský V, Eme L, Vlček Č, Harding T, et al. An ancestral bacterial division system is widespread in eukaryotic mitochondria. Proc Natl Acad Sci U S A. 2015 Aug 18;112(33):10239–10246.

156. Ishihara N, Nomura M, Jofuku A, Kato H, Suzuki SO, Masuda K, et al. Mitochondrial fission factor Drp1 is essential for embryonic development and synapse formation in mice. Nat Cell Biol. 2009 Aug;11(8):958–966.

157. Gomes LC, Di Benedetto G, Scorrano L. During autophagy mitochondria elongate, are spared from degradation and sustain cell viability. Nat Cell Biol. 2011 May;13(5):589–598.

158. Brooks C, Cho SG, Wang CY, Yang T, Dong Z. Fragmented mitochondria are sensitized to Bax insertion and activation during apoptosis. Am J Physiol, Cell Physiol. 2011 Mar;300(3):C447–55.

159. Montessuit S, Somasekharan SP, Terrones O, Lucken-Ardjomande S, Herzig S, Schwarzenbacher R, et al. Membrane remodeling induced by the dynamin-related protein Drp1 stimulates Bax oligomerization. Cell. 2010 Sep 17;142(6):889–901.

160. Wang P, Wang P, Liu B, Zhao J, Pang Q, Agrawal SG, et al. Dynamin-related protein Drp1 is required for Bax translocation to mitochondria in response to irradiation-induced apoptosis. Oncotarget. 2015 Sep 8;6(26):22598–22612.

161. Karbowski M, Lee YJ, Gaume B, Jeong SY, Frank S, Nechushtan A, et al. Spatial and temporal association of Bax with mitochondrial fission sites, Drp1, and Mfn2 during apoptosis. J Cell Biol. 2002 Dec 23;159(6):931–938.

162. Zhan M, Usman IM, Sun L, Kanwar YS. Disruption of renal tubular mitochondrial quality control by Myo-inositol oxygenase in diabetic kidney disease. J Am Soc Nephrol. 2015 Jun;26(6):1304–1321.

163. Zhan M, Usman I, Yu J, Ruan L, Bian X, Yang J, et al. Perturbations in mitochondrial dynamics by p66Shc lead to renal tubular oxidative injury in human diabetic nephropathy. Clin Sci. 2018 Jun 29;132(12):1297–1314.

164. Jeong HY, Kang JM, Jun HH, Kim DJ, Park SH, Sung MJ, et al. Chloroquine and amodiaquine enhance AMPK phosphorylation and improve mitochondrial fragmentation in diabetic tubulopathy. Sci Rep. 2018 Jun 8;8(1):8774.

165. Lee SY, Kang JM, Kim DJ, Park SH, Jeong HY, Lee YH, et al. Pgc1α activators mitigate diabetic tubulopathy by improving mitochondrial dynamics and quality control. J Diabetes Res. 2017 Mar 20;2017:6483572.

166. Fernández-Vizarra E, Enríquez JA, Pérez-Martos A, Montoya J, Fernández-Silva P. Tissue-specific differences in mitochondrial activity and biogenesis. Mitochondrion. 2011 Jan;11(1):207–213.

167. Pagliarini DJ, Calvo SE, Chang B, Sheth SA, Vafai SB, Ong SE, et al. A mitochondrial protein compendium elucidates complex I disease biology. Cell. 2008 Jul 11;134(1):112–123.

168. Bereiter-Hahn J, Vöth M. Dynamics of mitochondria in living cells: shape changes, dislocations, fusion, and fission of mitochondria. Microsc Res Tech. 1994 Feb 15;27(3):198–219.

169. Youle RJ, van der Bliek AM. Mitochondrial fission, fusion, and stress. Science. 2012 Aug 31;337(6098):1062–1065.

170. Chan DC. Fusion and fission: interlinked processes critical for mitochondrial health. Annu Rev Genet. 2012 Aug 29;46:265–287.

171. Wang S, Xiao W, Shan S, Jiang C, Chen M, Zhang Y, et al. Multi-patterned dynamics of mitochondrial fission and fusion in a living cell. PLoS ONE. 2012 May 23;7(5):e19879.

172. Twig G, Elorza A, Molina AJ, Mohamed H, Wikstrom JD, Walzer G, et al. Fission and selective fusion govern mitochondrial segregation and elimination by autophagy. EMBO J. 2008 Jan 23;27(2):433–446.

173. Ashrafi G, Schwarz TL. The pathways of mitophagy for quality control and clearance of mitochondria. Cell Death Differ. 2013 Jan;20(1):31–42.

174. Schmitt S, Schulz S, Schropp EM, Eberhagen C, Simmons A, Beisker W, et al. Why to compare absolute numbers of mitochondria. Mitochondrion. 2014 Nov;19 Pt A:113–123.

175. Epstein FH. Oxygen and renal metabolism. Kidney Int. 1997 Feb;51(2):381–385.

176. Friederich-Persson M, Thörn E, Hansell P, Nangaku M, Levin M, Palm F. Kidney hypoxia, attributable to increased oxygen consumption, induces nephropathy independently of hyperglycemia and oxidative stress. Hypertension. 2013 Nov;62(5):914–919.

177. Kwong LK, Sohal RS. Substrate and site specificity of hydrogen peroxide generation in mouse mitochondria. Arch Biochem Biophys. 1998 Feb 1;350(1):118–126.

178. Balaban RS, Mandel LJ. Metabolic substrate utilization by rabbit proximal tubule. An NADH fluorescence study. Am J Physiol. 1988 Mar;254(3 Pt 2):F407–16.

179. Mootha VK, Arai AE, Balaban RS. Maximum oxidative phosphorylation capacity of the mammalian heart. Am J Physiol. 1997 Feb;272(2 Pt 2):H769–75.

180. Rosca MG, Vazquez EJ, Chen Q, Kerner J, Kern TS, Hoppel CL. Oxidation of fatty acids is the source of increased mitochondrial reactive oxygen species production in kidney cortical tubules in early diabetes. Diabetes. 2012 Aug;61(8):2074–2083.

181. Makrecka-Kuka M, Krumschnabel G, Gnaiger E. High-Resolution Respirometry for Simultaneous Measurement of Oxygen and Hydrogen Peroxide Fluxes in Permeabilized Cells, Tissue Homogenate and Isolated Mitochondria. Biomolecules. 2015 Jun 29;5(3):1319–1338.

182. Krebs HA, Yoshida T. Renal gluconeogenesis. 2. the gluconeogenic capacity of the kidney cortex of various species. Biochem J. 1963 Nov;89:398–400.

183. Gerich JE, Meyer C, Woerle HJ, Stumvoll M. Renal gluconeogenesis: its importance in human glucose homeostasis. Diabetes Care. 2001 Feb;24(2):382–391.

184. Cersosimo E, Garlick P, Ferretti J. Renal substrate metabolism and gluconeogenesis during hypoglycemia in humans. Diabetes. 2000 Jul;49(7):1186–1193.

185. Uchida S, Endou H. Substrate specificity to maintain cellular ATP along the mouse nephron. Am J Physiol. 1988 Nov;255(5 Pt 2):F977–83.

186. Cohen JJ, Kook YJ, Little JR. Substrate-limited function and metabolism of the isolated perfused rat kidney: effects of lactate and glucose. J Physiol (Lond). 1977 Mar;266(1):103–121.

187. Newsholme P, Procopio J, Lima MM, Pithon-Curi TC, Curi R. Glutamine and glutamate--their central role in cell metabolism and function. Cell Biochem Funct. 2003 Mar;21(1):1–9.

188. Dominguez JH, Camp K, Maianu L, Feister H, Garvey WT. Molecular adaptations of GLUT1 and GLUT2 in renal proximal tubules of diabetic rats. Am J Physiol. 1994 Feb;266(2 Pt 2):F283–90.

189. Tabatabai NM, Sharma M, Blumenthal SS, Petering DH. Enhanced expressions of sodium-glucose cotransporters in the kidneys of diabetic Zucker rats. Diabetes Res Clin Pract. 2009 Jan;83(1):e27–30.

190. Gerich JE. Role of the kidney in normal glucose homeostasis and in the hyperglycaemia of diabetes mellitus: therapeutic implications. Diabet Med. 2010 Feb;27(2):136–142.

191. Giralt M, Villarroya F. Mitochondrial uncoupling and the regulation of glucose homeostasis. Curr Diabetes Rev. 2016 Feb 17;

192. Rolfe DF, Brown GC. Cellular energy utilization and molecular origin of standard metabolic rate in mammals. Physiol Rev. 1997 Jul;77(3):731–758.

193. Fedorenko A, Lishko PV, Kirichok Y. Mechanism of fatty-acid-dependent UCP1 uncoupling in brown fat mitochondria. Cell. 2012 Oct 12;151(2):400–413.

194. Shabalina IG, Petrovic N, de Jong JM, Kalinovich AV, Cannon B, Nedergaard J. UCP1 in brite/beige adipose tissue mitochondria is functionally thermogenic. Cell Rep. 2013 Dec 12;5(5):1196–1203.

195. Pecqueur C, Bui T, Gelly C, Hauchard J, Barbot C, Bouillaud F, et al. Uncoupling protein-2 controls proliferation by promoting fatty acid oxidation and limiting glycolysis-derived pyruvate utilization. FASEB J. 2008 Jan;22(1):9–18.

196. Liberti MV, Locasale JW. The warburg effect: how does it benefit cancer cells? Trends Biochem Sci. 2016 Mar;41(3):211–218.

197. Persson MF, Welch WJ, Wilcox CS, Palm F. Kidney function after in vivo gene silencing of uncoupling protein-2 in streptozotocin-induced diabetic rats. Adv Exp Med Biol. 2013;765:217–223.

198. Brand MD. The efficiency and plasticity of mitochondrial energy transduction. Biochem Soc Trans. 2005 Nov;33(Pt 5):897–904.

199. Brand MD, Esteves TC. Physiological functions of the mitochondrial uncoupling proteins UCP2 and UCP3. Cell Metab. 2005 Aug;2(2):85–93.

200. Simonyan RA, Skulachev VP. Thermoregulatory uncoupling in heart muscle mitochondria: involvement of the ATP/ADP antiporter and uncoupling protein. FEBS Lett. 1998 Sep 25;436(1):81–84.

201. Schlagowski AI, Isner-Horobeti ME, Dufour SP, Rasseneur L, Enache I, Lonsdorfer-Wolf E, et al. Mitochondrial function following downhill and/or uphill exercise training in rats. Muscle Nerve. 2016 Nov;54(5):925–935.

202. Granata C, Oliveira RS, Little JP, Renner K, Bishop DJ. Mitochondrial adaptations to high-volume exercise training are rapidly reversed after a reduction in training volume in human skeletal muscle. FASEB J. 2016 Oct;30(10):3413–3423.

203. Morselli E, Maiuri MC, Markaki M, Megalou E, Pasparaki A, Palikaras K, et al. Caloric restriction and resveratrol promote longevity through the Sirtuin-1-dependent induction of autophagy. Cell Death Dis. 2010;1:e10.

204. Wu H, Chen Q. Hypoxia activation of mitophagy and its role in disease pathogenesis. Antioxid Redox Signal. 2015 Apr 20;22(12):1032–1046.

205. Barlow AD, Thomas DC. Autophagy in diabetes: β-cell dysfunction, insulin resistance, and complications. DNA Cell Biol. 2015 Apr;34(4):252–260.

206. Fang L, Zhou Y, Cao H, Wen P, Jiang L, He W, et al. Autophagy attenuates diabetic glomerular damage through protection of hyperglycemia-induced podocyte injury. PLoS ONE. 2013 Apr 11;8(4):e60546.

207. D'Aquila P, Bellizzi D, Passarino G. Mitochondria in health, aging and diseases: the epigenetic perspective. Biogerontology. 2015 Oct;16(5):569–585.

208. Chistiakov DA, Sobenin IA, Revin VV, Orekhov AN, Bobryshev YV. Mitochondrial aging and age-related dysfunction of mitochondria. BioMed research international. 2014 Apr 10;2014:238463.

209. Lindblom R, Higgins G, Coughlan M, de Haan JB. Targeting Mitochondria and Reactive Oxygen Species-Driven Pathogenesis in Diabetic Nephropathy. Rev Diabet Stud. 2015 Aug 10;12(1-2):134–156.

210. Elliott HR, Samuels DC, Eden JA, Relton CL, Chinnery PF. Pathogenic mitochondrial DNA mutations are common in the general population. Am J Hum Genet. 2008 Aug;83(2):254–260.

211. Flatters SJ. The contribution of mitochondria to sensory processing and pain. Prog Mol Biol Transl Sci. 2015 Feb 7;131:119–146.

212. Correia SC, Santos RX, Cardoso S, Carvalho C, Candeias E, Duarte AI, et al. Alzheimer disease as a vascular disorder: where do mitochondria fit? Exp Gerontol. 2012 Nov;47(11):878–886.

213. Nadanaciva S, Dykens JA, Bernal A, Capaldi RA, Will Y. Mitochondrial impairment by PPAR agonists and statins identified via immunocaptured OXPHOS complex activities and respiration. Toxicol Appl Pharmacol. 2007 Sep 15;223(3):277–287.

214. Zheng H, Xiao WH, Bennett GJ. Functional deficits in peripheral nerve mitochondria in rats with paclitaxel- and oxaliplatin-evoked painful peripheral neuropathy. Exp Neurol. 2011 Dec;232(2):154–161.

215. Kerr JF, Wyllie AH, Currie AR. Apoptosis: a basic biological phenomenon with wide-ranging implications in tissue kinetics. Br J Cancer. 1972 Aug;26(4):239–257.

216. Lieberthal W, Menza SA, Levine JS. Graded ATP depletion can cause necrosis or apoptosis of cultured mouse proximal tubular cells. Am J Physiol. 1998;274(2):F315–27.

217. Kalai M, Van Loo G, Vanden Berghe T, Meeus A, Burm W, Saelens X, et al. Tipping the balance between necrosis and apoptosis in human and murine cells treated with interferon and dsRNA. Cell Death Differ. 2002 Sep;9(9):981–994.

218. Jürgensmeier JM, Xie Z, Deveraux Q, Ellerby L, Bredesen D, Reed JC. Bax directly induces release of cytochrome c from isolated mitochondria. Proc Natl Acad Sci U S A. 1998 Apr 28;95(9):4997–5002.

219. Salvador-Gallego R, Mund M, Cosentino K, Schneider J, Unsay J, Schraermeyer U, et al. Bax assembly into rings and arcs in apoptotic mitochondria is linked to membrane pores. EMBO J. 2016 Feb 15;35(4):389–401.

220. Du C, Fang M, Li Y, Li L, Wang X. Smac, a mitochondrial protein that promotes cytochrome c-dependent caspase activation by eliminating IAP inhibition. Cell. 2000 Jul 7;102(1):33–42.

221. Li P, Nijhawan D, Budihardjo I, Srinivasula SM, Ahmad M, Alnemri ES, et al. Cytochrome c and dATP-dependent formation of Apaf-1/caspase-9 complex initiates an apoptotic protease cascade. Cell. 1997 Nov 14;91(4):479–489.

222. Ma SB, Nguyen TN, Tan I, Ninnis R, Iyer S, Stroud DA, et al. Bax targets mitochondria by distinct mechanisms before or during apoptotic cell death: a requirement for VDAC2 or Bak for efficient Bax apoptotic function. Cell Death Differ. 2014 Dec;21(12):1925–1935.

223. Yamagata H, Shimizu S, Nishida Y, Watanabe Y, Craigen WJ, Tsujimoto Y. Requirement of voltage-dependent anion channel 2 for pro-apoptotic activity of Bax. Oncogene. 2009 Oct 8;28(40):3563–3572.

224. Zhang Y, Iqbal S, O'Leary MF, Menzies KJ, Saleem A, Ding S, et al. Altered mitochondrial morphology and defective protein import reveal novel roles for Bax and/or Bak in skeletal muscle. Am J Physiol, Cell Physiol. 2013 Sep;305(5):C502–11.

225. Karch J, Kwong JQ, Burr AR, Sargent MA, Elrod JW, Peixoto PM, et al. Bax and Bak function as the outer membrane component of the mitochondrial permeability pore in regulating necrotic cell death in mice. elife. 2013 Aug 27;2:e00772.

226. Karch J, Kanisicak O, Brody MJ, Sargent MA, Michael DM, Molkentin JD. Necroptosis Interfaces with MOMP and the MPTP in Mediating Cell Death. PLoS ONE. 2015 Jun 10;10(6):e0130520.

227. Ferrari R, Pedersini P, Bongrazio M, Gaia G, Bernocchi P, Di Lisa F, et al. Mitochondrial energy production and cation control in myocardial ischaemia and reperfusion. Basic Res Cardiol. 1993 Oct;88(5):495–512.

228. Neginskaya MA, Solesio ME, Berezhnaya EV, Amodeo GF, Mnatsakanyan N, Jonas EA, et al. ATP Synthase C-Subunit-Deficient Mitochondria Have a Small Cyclosporine A-Sensitive Channel, but Lack the Permeability Transition Pore. Cell Rep. 2019 Jan 2;26(1):11–17.e2.

229. Baines CP, Kaiser RA, Purcell NH, Blair NS, Osinska H, Hambleton MA, et al. Loss of cyclophilin D reveals a critical role for mitochondrial permeability transition in cell death. Nature. 2005 Mar 31;434(7033):658–662.

230. Gutiérrez-Aguilar M, Pérez-Vázquez V, Bunoust O, Manon S, Rigoulet M, Uribe S. In yeast, Ca2+ and octylguanidine interact with porin (VDAC) preventing the mitochondrial permeability transition. Biochim Biophys Acta. 2007 Oct;1767(10):1245–1251.

231. Baines CP, Kaiser RA, Sheiko T, Craigen WJ, Molkentin JD. Voltage-dependent anion channels are dispensable for mitochondrial-dependent cell death. Nat Cell Biol. 2007 May;9(5):550–555.

232. Karch J, Molkentin JD. Identifying the components of the elusive mitochondrial permeability transition pore. Proc Natl Acad Sci U S A. 2014 Jul 22;111(29):10396–10397.

233. Crichton PG, Parker N, Vidal-Puig AJ, Brand MD. Not all mitochondrial carrier proteins support permeability transition pore formation: no involvement of uncoupling protein 1. Biosci Rep. 2010 Jun;30(3):187–192.

234. Baines CP, Gutiérrez-Aguilar M. The still uncertain identity of the channel-forming unit(s) of the mitochondrial permeability transition pore. Cell Calcium. 2018 May 16;73:121–130.

235. Javadov S, Kuznetsov A. Mitochondrial permeability transition and cell death: the role of cyclophilin d. Front Physiol. 2013 Apr 11;4:76.

236. Waldmeier PC, Zimmermann K, Qian T, Tintelnot-Blomley M, Lemasters JJ. Cyclophilin D as a drug target. Curr Med Chem. 2003 Aug;10(16):1485–1506.

237. Whelan RS, Konstantinidis K, Wei AC, Chen Y, Reyna DE, Jha S, et al. Bax regulates primary necrosis through mitochondrial dynamics. Proc Natl Acad Sci U S A. 2012 Apr 24;109(17):6566–6571.

238. Javadov S, Karmazyn M, Escobales N. Mitochondrial permeability transition pore opening as a promising therapeutic target in cardiac diseases. J Pharmacol Exp Ther. 2009 Sep;330(3):670–678.

239. Shanmuganathan S, Hausenloy DJ, Duchen MR, Yellon DM. Mitochondrial permeability transition pore as a target for cardioprotection in the human heart. Am J Physiol Heart Circ Physiol. 2005 Jul;289(1):H237–42.

240. Kumar D, Robertson S, Burns KD. Evidence of apoptosis in human diabetic kidney. Mol Cell Biochem. 2004 Apr;259(1-2):67–70.

241. Ortiz A, Ziyadeh FN, Neilson EG. Expression of apoptosis-regulatory genes in renal proximal tubular epithelial cells exposed to high ambient glucose and in diabetic kidneys. J Investig Med. 1997 Feb;45(2):50–56.

242. Lorz C, Benito-Martín A, Boucherot A, Ucero AC, Rastaldi MP, Henger A, et al. The death ligand TRAIL in diabetic nephropathy. J Am Soc Nephrol. 2008 May;19(5):904–914.

243. Sanchez-Niño MD, Benito-Martin A, Ortiz A. New paradigms in cell death in human diabetic nephropathy. Kidney Int. 2010 Oct;78(8):737–744.

244. Baba K, Minatoguchi S, Sano H, Kagawa T, Murata I, Takemura G, et al. Involvement of apoptosis in patients with diabetic nephropathy: A study on plasma soluble Fas levels and pathological findings. Nephrology (Carlton). 2004 Apr;9(2):94–99.

245. Kikuchi Y, Nonoguchi H, Machida K, Wakamatsu S, Koga H, Tomita K. Regulation of the apoptosis-related genes, Bax and Bcl-2, in the early stage of diabetes mellitus. 2002 Dec;7(6):294–302.

246. Linkermann A, Skouta R, Himmerkus N, Mulay SR, Dewitz C, De Zen F, et al. Synchronized renal tubular cell death involves ferroptosis. Proc Natl Acad Sci U S A. 2014 Nov 25;111(47):16836–16841.

247. Kers J, Leemans JC, Linkermann A. An overview of pathways of regulated necrosis in acute kidney injury. Semin Nephrol. 2016;36(3):139–152.

248. Rossini AA, Like AA, Chick WL, Appel MC, Cahill GF. Studies of streptozotocin-induced insulitis and diabetes. Proc Natl Acad Sci U S A. 1977 Jun;74(6):2485–2489.

249. Rossini AA, Appel MC, Williams RM, Like AA. Genetic influence of the streptozotocin-induced insulitis and hyperglycemia. Diabetes. 1977 Oct;26(10):916–920.

250. Gurley SB, Clare SE, Snow KP, Hu A, Meyer TW, Coffman TM. Impact of genetic background on nephropathy in diabetic mice. Am J Physiol Renal Physiol. 2006 Jan;290(1):F214–22.

251. Brosius FC, Alpers CE, Bottinger EP, Breyer MD, Coffman TM, Gurley SB, et al. Mouse models of diabetic nephropathy. J Am Soc Nephrol. 2009 Dec;20(12):2503–2512.

252. Saito T, Sumithran E, Glasgow EF, Atkins RC. The enhancement of aminonucleoside nephrosis by the co-administration of protamine. Kidney Int. 1987 Nov;32(5):691–699.

253. Thallas-Bonke V, Thorpe SR, Coughlan MT, Fukami K, Yap FY, Sourris KC, et al. Inhibition of NADPH oxidase prevents advanced glycation end product-mediated damage in diabetic nephropathy through a protein kinase C-alpha-dependent pathway. Diabetes. 2008 Feb;57(2):460–469.

254. Srere PA. [1] Citrate synthase. Citric Acid Cycle. Elsevier; 1969. p. 3–11.

255. Bjornstad P, Snell-Bergeon JK, Rewers M, Jalal D, Chonchol MB, Johnson RJ, et al. Early diabetic nephropathy: a complication of reduced insulin sensitivity in type 1 diabetes. Diabetes Care. 2013 Nov;36(11):3678–3683.

256. Wiseman M, Viberti G, Mackintosh D, Jarrett RJ, Keen H. Glycaemia, arterial pressure and micro-albuminuria in type 1 (insulin-dependent) diabetes mellitus. Diabetologia. 1984 Jun;26(6):401–405.

257. Wada J, Makino H. Innate immunity in diabetes and diabetic nephropathy. Nat Rev Nephrol. 2016 Jan;12(1):13–26.

258. Schievink B, Kröpelin T, Mulder S, Parving HH, Remuzzi G, Dwyer J, et al. Early renin-angiotensin system intervention is more beneficial than late intervention in delaying end-stage renal disease in patients with type 2 diabetes. Diabetes Obes Metab. 2016 Jan;18(1):64–71.

259. Testa R, Bonfigli AR, Prattichizzo F, La Sala L, De Nigris V, Ceriello A. The “metabolic memory” theory and the early treatment of hyperglycemia in prevention of diabetic complications. Nutrients. 2017 Apr 28;9(5).

260. Batu Demir D, Cooper ME. New strategies to tackle diabetic kidney disease. Curr Opin Nephrol Hypertens. 2016 Jul;25(4):348–354.

261. Rossing P, Persson F, Frimodt-Møller M. Prognosis and treatment of diabetic nephropathy: Recent advances and perspectives. Nephrol Ther. 2018 Apr;14 Suppl 1:S31–S37.

262. Fraser SDS, Roderick PJ. Kidney disease in the Global Burden of Disease Study 2017. Nat Rev Nephrol. 2019 Apr;15(4):193–194.

263. Hallan S, Sharma K. The role of mitochondria in diabetic kidney disease. Curr Diab Rep. 2016;16(7):61.

264. Sivitz WI, Yorek MA. Mitochondrial dysfunction in diabetes: from molecular mechanisms to functional significance and therapeutic opportunities. Antioxid Redox Signal. 2010 Apr;12(4):537–577.

265. Swan EJ, Maxwell AP, McKnight AJ. Distinct methylation patterns in genes that affect mitochondrial function are associated with kidney disease in blood-derived DNA from individuals with Type 1 diabetes. Diabet Med. 2015 Aug;32(8):1110–1115.

266. Swan EJ, Salem RM, Sandholm N, Tarnow L, Rossing P, Lajer M, et al. Genetic risk factors affecting mitochondrial function are associated with kidney disease in people with Type 1 diabetes. Diabet Med. 2015 Aug;32(8):1104–1109.

267. Coughlan MT, Nguyen TV, Penfold SA, Higgins GC, Thallas-Bonke V, Tan SM, et al. Mapping Time-course Mitochondrial Adaptations in the Kidney in Experimental Diabetes. Clin Sci. 2016 Feb 1;130(9):711–720.

268. Chacko BK, Reily C, Srivastava A, Johnson MS, Ye Y, Ulasova E, et al. Prevention of diabetic nephropathy in Ins2(+/)$^{-}$(AkitaJ) mice by the mitochondria-targeted therapy MitoQ. Biochem J. 2010 Nov 15;432(1):9–19.

269. Persson MF, Franzén S, Catrina SB, Dallner G, Hansell P, Brismar K, et al. Coenzyme Q10 prevents GDP-sensitive mitochondrial uncoupling, glomerular hyperfiltration and proteinuria in kidneys from db/db mice as a model of type 2 diabetes. Diabetologia. 2012 May;55(5):1535–1543.

270. Sas KM, Kayampilly P, Byun J, Nair V, Hinder LM, Hur J, et al. Tissue-specific metabolic reprogramming drives nutrient flux in diabetic complications. Journal of Clinical Investigation Insight. 2016 Sep 22;1(15):e86976.

271. Ruggiero C, Ehrenshaft M, Cleland E, Stadler K. High-fat diet induces an initial adaptation of mitochondrial bioenergetics in the kidney despite evident oxidative stress and mitochondrial ROS production. Am J Physiol Endocrinol Metab. 2011 Jun;300(6):E1047–58.

272. Proctor G, Jiang T, Iwahashi M, Wang Z, Li J, Levi M. Regulation of renal fatty acid and cholesterol metabolism, inflammation, and fibrosis in Akita and OVE26 mice with type 1 diabetes. Diabetes. 2006 Sep;55(9):2502–2509.

273. Zorova LD, Popkov VA, Plotnikov EY, Silachev DN, Pevzner IB, Jankauskas SS, et al. Mitochondrial membrane potential. Anal Biochem. 2018 Jul 1;552:50–59.

274. Izyumov DS, Avetisyan AV, Pletjushkina OY, Sakharov DV, Wirtz KW, Chernyak BV, et al. Wages of fear": transient threefold decrease in intracellular ATP level imposes apoptosis. Biochim Biophys Acta. 2004 Jul 23;1658(1-2):141–147.

275. Gärtner K. Glomerular hyperfiltration during the onset of diabetes mellitus in two strains of diabetic mice (c57bl/6j db/db and c57bl/ksj db/db). Diabetologia. 1978 Jul;15(1):59–63.

276. Mahato HS, Ahlstrom C, Jansson-Löfmark R, Johansson U, Helmlinger G, Hallow KM. Mathematical model of hemodynamic mechanisms and consequences of glomerular hypertension in diabetic mice. npj Systems Biology and Applications. 2019;5:2.

277. Eid AA, Gorin Y, Fagg BM, Maalouf R, Barnes JL, Block K, et al. Mechanisms of podocyte injury in diabetes: role of cytochrome P450 and NADPH oxidases. Diabetes. 2009 May;58(5):1201–1211.

278. Munusamy S, Saba H, Mitchell T, Megyesi JK, Brock RW, Macmillan-Crow LA. Alteration of renal respiratory Complex-III during experimental type-1 diabetes. BMC Endocr Disord. 2009 Jan 23;9:2.

279. Evstafieva AG, Garaeva AA, Khutornenko AA, Klepikova AV, Logacheva MD, Penin AA, et al. A sustained deficiency of mitochondrial respiratory complex III induces an apoptotic cell death through the p53-mediated inhibition of pro-survival activities of the activating transcription factor 4. Cell Death Dis. 2014 Nov 6;5(11):e1511.

280. Kim J, Villarroel JP, Zhang W, Yin T, Shinozaki K, Hong A, et al. The Responses of Tissues from the Brain, Heart, Kidney, and Liver to Resuscitation following Prolonged Cardiac Arrest by Examining Mitochondrial Respiration in Rats. Oxid Med Cell Longev. 2016;2016:7463407.

281. Van Erp AC, Rebolledo RA, Hoeksma D, Jespersen NR, Ottens PJ, Nørregaard R, et al. Organ-specific responses during brain death: increased aerobic metabolism in the liver and anaerobic metabolism with decreased perfusion in the kidneys. Sci Rep. 2018 Mar 13;8(1):4405.

282. Bagnasco S, Good D, Balaban R, Burg M. Lactate production in isolated segments of the rat nephron. Am J Physiol. 1985 Apr;248(4 Pt 2):F522–6.

283. Kang HM, Ahn SH, Choi P, Ko YA, Han SH, Chinga F, et al. Defective fatty acid oxidation in renal tubular epithelial cells has a key role in kidney fibrosis development. Nat Med. 2015 Jan;21(1):37–46.

284. Chen Y, Fry BC, Layton AT. Modeling glucose metabolism and lactate production in the kidney. Math Biosci. 2017 May 8;289:116–129.

285. Schiffer TA, Friederich-Persson M. Mitochondrial reactive oxygen species and kidney hypoxia in the development of diabetic nephropathy. Front Physiol. 2017 Apr 11;8:211.

286. Friederich M, Fasching A, Hansell P, Nordquist L, Palm F. Diabetes-induced up-regulation of uncoupling protein-2 results in increased mitochondrial uncoupling in kidney proximal tubular cells. Biochim Biophys Acta. 2008 Aug;1777(7-8):935–940.

287. Fan Y, Yi Z, D'Agati VD, Sun Z, Zhong F, Zhang W, et al. Comparison of kidney transcriptomic profiles of early and advanced diabetic nephropathy reveals potential new mechanisms for disease progression. Diabetes. 2019 Dec;68(12):2301–2314.

288. Rubin A, Salzberg AC, Imamura Y, Grivitishvilli A, Tombran-Tink J. Identification of novel targets of diabetic nephropathy and PEDF peptide treatment using RNA-seq. BMC Genomics. 2016 Nov 17;17(1):936.

289. Qi H, Casalena G, Shi S, Yu L, Ebefors K, Sun Y, et al. Glomerular endothelial mitochondrial dysfunction is essential and characteristic of diabetic kidney disease susceptibility. Diabetes. 2017;66(3):763–778.

290. Kahraman S, Aydin C, Elpek GO, Dirice E, Sanlioglu AD. Diabetes-resistant NOR mice are more severely affected by streptozotocin compared to the diabetes-prone NOD mice: correlations with liver and kidney GLUT2 expressions. J Diabetes Res. 2015 Jan 28;2015:450128.

291. Hosokawa M, Dolci W, Thorens B. Differential sensitivity of GLUT1- and GLUT2-expressing beta cells to streptozotocin. Biochem Biophys Res Commun. 2001 Dec 21;289(5):1114–1117.

292. Romano AD, Greco E, Vendemiale G, Serviddio G. Bioenergetics and mitochondrial dysfunction in aging: recent insights for a therapeutical approach. Curr Pharm Des. 2014;20(18):2978–2992.

293. Erikstein BS, Hagland HR, Nikolaisen J, Kulawiec M, Singh KK, Gjertsen BT, et al. Cellular stress induced by resazurin leads to autophagy and cell death via production of reactive oxygen species and mitochondrial impairment. J Cell Biochem. 2010 Oct 15;111(3):574–584.

294. Akbar M, Essa MM, Daradkeh G, Abdelmegeed MA, Choi Y, Mahmood L, et al. Mitochondrial dysfunction and cell death in neurodegenerative diseases through nitroxidative stress. Brain Res. 2016 Apr 15;1637:34–55.

295. Kumar V, Santhosh Kumar TR, Kartha CC. Mitochondrial membrane transporters and metabolic switch in heart failure. Heart Fail Rev. 2019 Mar;24(2):255–267.

296. Robertson CL. Mitochondrial dysfunction contributes to cell death following traumatic brain injury in adult and immature animals. J Bioenerg Biomembr. 2004 Aug;36(4):363–368.

297. Yonutas HM, Vekaria HJ, Sullivan PG. Mitochondrial specific therapeutic targets following brain injury. Brain Res. 2016 Jun 1;1640(Pt A):77–93.

298. Szeto HH, Liu S, Soong Y, Wu D, Darrah SF, Cheng FY, et al. Mitochondria-targeted peptide accelerates ATP recovery and reduces ischemic kidney injury. J Am Soc Nephrol. 2011 Jun;22(6):1041–1052.

299. Garcia I, Martinou I, Tsujimoto Y, Martinou JC. Prevention of programmed cell death of sympathetic neurons by the bcl-2 proto-oncogene. Science. 1992 Oct 9;258(5080):302–304.

300. Adams JM, Cory S. The Bcl-2 protein family: arbiters of cell survival. Science. 1998 Aug 28;281(5381):1322–1326.

301. Fletcher JI, Meusburger S, Hawkins CJ, Riglar DT, Lee EF, Fairlie WD, et al. Apoptosis is triggered when prosurvival Bcl-2 proteins cannot restrain Bax. Proc Natl Acad Sci U S A. 2008 Nov 25;105(47):18081–18087.

302. Cheng EH, Sheiko TV, Fisher JK, Craigen WJ, Korsmeyer SJ. VDAC2 inhibits BAK activation and mitochondrial apoptosis. Science. 2003 Jul 25;301(5632):513–517.

303. Priault M, Chaudhuri B, Clow A, Camougrand N, Manon S. Investigation of bax-induced release of cytochrome c from yeast mitochondria permeability of mitochondrial membranes, role of VDAC and ATP requirement. Eur J Biochem. 1999 Mar;260(3):684–691.

304. Zhang M, Zheng J, Nussinov R, Ma B. Release of Cytochrome C from Bax Pores at the Mitochondrial Membrane. Sci Rep. 2017 Jun 1;7(1):2635.

305. O'Neill KL, Huang K, Zhang J, Chen Y, Luo X. Inactivation of prosurvival Bcl-2 proteins activates Bax/Bak through the outer mitochondrial membrane. Genes Dev. 2016 Apr 15;30(8):973–988.

306. Zhang J, Huang K, O'Neill KL, Pang X, Luo X. Bax/Bak activation in the absence of Bid, Bim, Puma, and p53. Cell Death Dis. 2016 Jun 16;7:e2266.

307. Jang HS, Padanilam BJ. Simultaneous deletion of Bax and Bak is required to prevent apoptosis and interstitial fibrosis in obstructive nephropathy. Am J Physiol Renal Physiol. 2015 Sep 15;309(6):F540–50.

308. Lindsten T, Ross AJ, King A, Zong WX, Rathmell JC, Shiels HA, et al. The combined functions of proapoptotic Bcl-2 family members bak and bax are essential for normal development of multiple tissues. Mol Cell. 2000 Dec;6(6):1389–1399.

309. Wei MC, Zong WX, Cheng EH, Lindsten T, Panoutsakopoulou V, Ross AJ, et al. Proapoptotic BAX and BAK: a requisite gateway to mitochondrial dysfunction and death. Science. 2001 Apr 27;292(5517):727–730.

310. Li R, Zhang L, Shi W, Zhang B, Liang X, Liu S, et al. NFAT2 mediates high glucose-induced glomerular podocyte apoptosis through increased Bax expression. Exp Cell Res. 2013 Apr 15;319(7):992–1000.

311. Xi X, Gao L, Hatala DA, Smith DG, Codispoti MC, Gong B, et al. Chronically elevated glucose-induced apoptosis is mediated by inactivation of Akt in cultured Müller cells. Biochem Biophys Res Commun. 2005 Jan 21;326(3):548–553.

312. Tien T, Zhang J, Muto T, Kim D, Sarthy VP, Roy S. High glucose induces mitochondrial dysfunction in retinal müller cells: implications for diabetic retinopathy. Invest Ophthalmol Vis Sci. 2017 Jun 1;58(7):2915–2921.

313. Bojunga J, Nowak D, Mitrou PS, Hoelzer D, Zeuzem S, Chow KU. Antioxidative treatment prevents activation of death-receptor- and mitochondrion-dependent apoptosis in the hearts of diabetic rats. Diabetologia. 2004 Dec 10;47(12):2072–2080.

314. Kepp O, Rajalingam K, Kimmig S, Rudel T. Bak and Bax are non-redundant during infection- and DNA damage-induced apoptosis. EMBO J. 2007 Feb 7;26(3):825–834.

315. Knudson CM, Tung KS, Tourtellotte WG, Brown GA, Korsmeyer SJ. Bax-deficient mice with lymphoid hyperplasia and male germ cell death. Science. 1995 Oct 6;270(5233):96–99.

316. Hoess RH, Abremski K. The Cre-lox Recombination System. In: Eckstein F, Lilley DMJ, editors. Nucleic acids and molecular biology 4. Berlin, Heidelberg: Springer Berlin Heidelberg; 1990. p. 99–109.

317. Kanai Y, Lee WS, You G, Brown D, Hediger MA. The human kidney low affinity Na+/glucose cotransporter SGLT2. Delineation of the major renal reabsorptive mechanism for D-glucose. J Clin Invest. 1994 Jan;93(1):397–404.

318. Chen J, Williams S, Ho S, Loraine H, Hagan D, Whaley JM, et al. Quantitative PCR tissue expression profiling of the human SGLT2 gene and related family members. Diabetes therapy : research, treatment and education of diabetes and related disorders. 2010 Dec 17;1(2):57–92.

319. Rubera I, Poujeol C, Bertin G, Hasseine L, Counillon L, Poujeol P, et al. Specific Cre/Lox recombination in the mouse proximal tubule. J Am Soc Nephrol. 2004 Aug;15(8):2050–2056.

320. Li XC, Zhu D, Chen X, Zheng X, Zhao C, Zhang J, et al. Proximal Tubule-Specific Deletion of the NHE3 (Na+/H+ Exchanger 3) in the Kidney Attenuates Ang II (Angiotensin II)-Induced Hypertension in Mice. Hypertension. 2019 Sep;74(3):526–535.

321. Udi S, Hinden L, Earley B, Drori A, Reuveni N, Hadar R, et al. Proximal Tubular Cannabinoid-1 Receptor Regulates Obesity-Induced CKD. J Am Soc Nephrol. 2017 Dec;28(12):3518–3532.

322. Tesch GH, Allen TJ. Rodent models of streptozotocin-induced diabetic nephropathy. Nephrology (Carlton). 2007 Jun;12(3):261–266.

323. Chen LH, Leung PS. Inhibition of the sodium glucose co-transporter-2: its beneficial action and potential combination therapy for type 2 diabetes mellitus. Diabetes Obes Metab. 2013 May;15(5):392–402.

324. Nagaki Y, Ito K, Kuwahara M. WTC rat has unique characteristics such as resistant to streptozotocin. Biochemistry and Biophysics Reports. 2016 Dec;8:157–161.

325. Saini KS, Thompson C, Winterford CM, Walker NI, Cameron DP. Streptozotocin at low doses induces apoptosis and at high doses causes necrosis in a murine pancreatic beta cell line, INS-1. Biochem Mol Biol Int. 1996 Aug;39(6):1229–1236.

326. Grunnet LG, Aikin R, Tonnesen MF, Paraskevas S, Blaabjerg L, Størling J, et al. Proinflammatory cytokines activate the intrinsic apoptotic pathway in beta-cells. Diabetes. 2009 Aug;58(8):1807–1815.

327. Pisarev VB, Snigur GL, Spasov AA, Samokhina MP, Bulanov AE. Mechanisms of toxic effect of streptozotocin on β-cells in the islets of langerhans. Bull Exp Biol Med. 2009 Dec;148(6):937–939.

328. Biswas S, Shi Q, Matise L, Cleveland S, Dave U, Zinkel S. A role for proapoptotic Bax and Bak in T-cell differentiation and transformation. Blood. 2010 Dec 9;116(24):5237–5246.

329. Galluzzi L, Vanpouille-Box C. BAX and BAK at the gates of innate immunity. Trends Cell Biol. 2018 Mar 16;28(5):343–345.

330. Takeuchi O, Fisher J, Suh H, Harada H, Malynn BA, Korsmeyer SJ. Essential role of BAX,BAK in B cell homeostasis and prevention of autoimmune disease. Proc Natl Acad Sci U S A. 2005 Aug 9;102(32):11272–11277.

331. Abraham S, Furth EE. Receiver operating characteristic analysis of glycogenated nuclei in liver biopsy specimens: quantitative evaluation of their relationship with diabetes and obesity. Hum Pathol. 1994 Oct;25(10):1063–1068.

332. Kang J, Dai XS, Yu TB, Wen B, Yang ZW. Glycogen accumulation in renal tubules, a key morphological change in the diabetic rat kidney. Acta Diabetol. 2005 Jun;42(2):110–116.

333. Glastras SJ, Chen H, Teh R, McGrath RT, Chen J, Pollock CA, et al. Mouse models of diabetes, obesity and related kidney disease. PLoS ONE. 2016 Aug 31;11(8):e0162131.

334. Lam PT, Padula SL, Hoang TV, Poth JE, Liu L, Liang C, et al. Considerations for the use of Cre recombinase for conditional gene deletion in the mouse lens. Hum Genomics. 2019 Feb 15;13(1):10.

335. Green DR, Oguin TH, Martinez J. The clearance of dying cells: table for two. Cell Death Differ. 2016 Mar 18;23(6):915–926.

336. Arandjelovic S, Ravichandran KS. Phagocytosis of apoptotic cells in homeostasis. Nat Immunol. 2015 Sep;16(9):907–917.

337. Mei S, Li L, Wei Q, Hao J, Su Y, Mei C, et al. Double knockout of Bax and Bak from kidney proximal tubules reduces unilateral urethral obstruction associated apoptosis and renal interstitial fibrosis. Sci Rep. 2017 Mar 20;7:44892.

338. Rankin EB, Tomaszewski JE, Haase VH. Renal cyst development in mice with conditional inactivation of the von Hippel-Lindau tumor suppressor. Cancer Res. 2006 Mar 1;66(5):2576–2583.

339. Tait SW, Ichim G, Green DR. Die another way--non-apoptotic mechanisms of cell death. J Cell Sci. 2014 May 15;127(Pt 10):2135–2144.

340. Arakawa S, Tsujioka M, Yoshida T, Tajima-Sakurai H, Nishida Y, Matsuoka Y, et al. Role of Atg5-dependent cell death in the embryonic development of Bax/Bak double-knockout mice. Cell Death Differ. 2017 Jun 2;24(9):1598–1608.

341. Zamorano S, Rojas-Rivera D, Lisbona F, Parra V, Court FA, Villegas R, et al. A BAX/BAK and cyclophilin D-independent intrinsic apoptosis pathway. PLoS ONE. 2012 Jun 12;7(6):e37782.

342. Zong WX, Li C, Hatzivassiliou G, Lindsten T, Yu QC, Yuan J, et al. Bax and Bak can localize to the endoplasmic reticulum to initiate apoptosis. J Cell Biol. 2003 Jul 7;162(1):59–69.

343. Carpio MA, Michaud M, Zhou W, Fisher JK, Walensky LD, Katz SG. BCL-2 family member BOK promotes apoptosis in response to endoplasmic reticulum stress. Proc Natl Acad Sci U S A. 2015 Jun 9;112(23):7201–7206.

344. Hsu SY, Kaipia A, McGee E, Lomeli M, Hsueh AJ. Bok is a pro-apoptotic Bcl-2 protein with restricted expression in reproductive tissues and heterodimerizes with selective anti-apoptotic Bcl-2 family members. Proc Natl Acad Sci U S A. 1997 Nov 11;94(23):12401–12406.

345. Echeverry N, Bachmann D, Ke F, Strasser A, Simon HU, Kaufmann T. Intracellular localization of the BCL-2 family member BOK and functional implications. Cell Death Differ. 2013 Jun;20(6):785–799.

346. Nakagawa T, Shimizu S, Watanabe T, Yamaguchi O, Otsu K, Yamagata H, et al. Cyclophilin D-dependent mitochondrial permeability transition regulates some necrotic but not apoptotic cell death. Nature. 2005 Mar 31;434(7033):652–658.

347. Karch J, Molkentin JD. Identity of the elusive mitochondrial permeability transition pore: what it might be, what it was, and what it still could be. Current Opinion in Physiology. 2018 Jun;3:57–62.

348. Basso E, Fante L, Fowlkes J, Petronilli V, Forte MA, Bernardi P. Properties of the permeability transition pore in mitochondria devoid of Cyclophilin D. J Biol Chem. 2005 May 13;280(19):18558–18561.

349. Dumas JF, Argaud L, Cottet-Rousselle C, Vial G, Gonzalez C, Detaille D, et al. Effect of transient and permanent permeability transition pore opening on NAD(P)H localization in intact cells. J Biol Chem. 2009 May 29;284(22):15117–15125.

350. Arrázola MS, Inestrosa NC. Monitoring mitochondrial membranes permeability in live neurons and mitochondrial swelling through electron microscopy analysis. Methods Mol Biol. 2015;1254:87–97.

351. Skulachev VP. Bioenergetic aspects of apoptosis, necrosis and mitoptosis. Apoptosis. 2006 Apr;11(4):473–485.

352. Correa F, Soto V, Zazueta C. Mitochondrial permeability transition relevance for apoptotic triggering in the post-ischemic heart. Int J Biochem Cell Biol. 2007 Jan 21;39(4):787–798.

353. Miura T, Tanno M. The mPTP and its regulatory proteins: final common targets of signalling pathways for protection against necrosis. Cardiovasc Res. 2012 May 1;94(2):181–189.

354. Halestrap AP, Connern CP, Griffiths EJ, Kerr PM. Cyclosporin A binding to mitochondrial cyclophilin inhibits the permeability transition pore and protects hearts from ischaemia/reperfusion injury. Mol Cell Biochem. 1997 Sep;174(1-2):167–172.

355. Sachewsky N, Hunt J, Cooke MJ, Azimi A, Zarin T, Miu C, et al. Cyclosporin A enhances neural precursor cell survival in mice through a calcineurin-independent pathway. Dis Model Mech. 2014 Aug;7(8):953–961.

356. Halestrap AP, Clarke SJ, Javadov SA. Mitochondrial permeability transition pore opening during myocardial reperfusion--a target for cardioprotection. Cardiovasc Res. 2004 Feb 15;61(3):372–385.

357. Devalaraja-Narashimha K, Diener AM, Padanilam BJ. Cyclophilin D gene ablation protects mice from ischemic renal injury. Am J Physiol Renal Physiol. 2009 Sep;297(3):F749–59.

358. Park JS, Pasupulati R, Feldkamp T, Roeser NF, Weinberg JM. Cyclophilin D and the mitochondrial permeability transition in kidney proximal tubules after hypoxic and ischemic injury. Am J Physiol Renal Physiol. 2011 Jul;301(1):F134–50.

359. Hou W, Leong KG, Ozols E, Tesch GH, Nikolic-Paterson DJ, Ma FY. Cyclophilin D promotes tubular cell damage and the development of interstitial fibrosis in the obstructed kidney. Clin Exp Pharmacol Physiol. 2018;45(3):250–260.

360. Palma E, Tiepolo T, Angelin A, Sabatelli P, Maraldi NM, Basso E, et al. Genetic ablation of cyclophilin D rescues mitochondrial defects and prevents muscle apoptosis in collagen VI myopathic mice. Hum Mol Genet. 2009 Jun 1;18(11):2024–2031.

361. Schiavone M, Zulian A, Menazza S, Petronilli V, Argenton F, Merlini L, et al. Alisporivir rescues defective mitochondrial respiration in Duchenne muscular dystrophy. Pharmacol Res. 2017 Nov;125(Pt B):122–131.

362. Australian code for the care and use of animals for scientific purposes | NHMRC [Internet]. [cited 2019 Oct 17]. Available from: https://www.nhmrc.gov.au/about-us/publications/australian-code-care-and-use-animals-scientific-purposes

363. Lusk, Graham. ANIMAL CALORIMETRY. Twenty-Fourth Paper ANALYSIS OF THE OXIDATION OF MIXTURES OF CARBOHYDRATE AND FAT. Journal of Biological Chemistry [Internet]. 1924 Jan 2; Available from: http://www.jbc.org/cgi/framedreprint/59/1/41

364. Bois EFD. CLINICAL CALORIMETRY Thirty-Fifth Paper. A GRAPHIC REPRESENTATION OF THE RESPIRATORY QUOTIENT AND THE PERCENTAGE OF CALORIES FROM PROTEIN, FAT, AND CARBOHYDRATE. Journal of Biological Chemistry [Internet]. 1924 Jan 2; Available from: http://www.jbc.org/content/59/1/43.citation

365. Picard M, White K, Turnbull DM. Mitochondrial morphology, topology, and membrane interactions in skeletal muscle: a quantitative three-dimensional electron microscopy study. J Appl Physiol. 2013 Jan 15;114(2):161–171.

366. Trak-Smayra V, Paradis V, Massart J, Nasser S, Jebara V, Fromenty B. Pathology of the liver in obese and diabetic ob/ob and db/db mice fed a standard or high-calorie diet. Int J Exp Pathol. 2011 Dec;92(6):413–421.

367. Bo Q, Orsenigo R, Wang J, Griffel L, Brass C. Glucose abnormalities in Asian patients with chronic hepatitis C. Drug Des Devel Ther. 2015 Nov 9;9:6009–6017.

368. Ghisdal L, Bouchta NB, Broeders N, Crenier L, Hoang AD, Abramowicz D, et al. Conversion from tacrolimus to cyclosporine A for new-onset diabetes after transplantation: a single-centre experience in renal transplanted patients and review of the literature. Transpl Int. 2008 Feb;21(2):146–151.

369. Vincenti F, Friman S, Scheuermann E, Rostaing L, Jenssen T, Campistol JM, et al. Results of an international, randomized trial comparing glucose metabolism disorders and outcome with cyclosporine versus tacrolimus. Am J Transplant. 2007 Jun;7(6):1506–1514.

370. Sato T, Inagaki A, Uchida K, Ueki T, Goto N, Matsuoka S, et al. Diabetes mellitus after transplant: relationship to pretransplant glucose metabolism and tacrolimus or cyclosporine A-based therapy. Transplantation. 2003 Nov 15;76(9):1320–1326.

371. Düfer M, Krippeit-Drews P, Lembert N, Idahl LA, Drews G. Diabetogenic effect of cyclosporin A is mediated by interference with mitochondrial function of pancreatic B-cells. Mol Pharmacol. 2001 Oct;60(4):873–879.

372. Peláez-Jaramillo MJ, Cárdenas-Mojica AA, Gaete PV, Mendivil CO. Post-Liver Transplantation Diabetes Mellitus: A Review of Relevance and Approach to Treatment. Diabetes therapy : research, treatment and education of diabetes and related disorders. 2018 Apr;9(2):521–543.

373. Montori VM, Basu A, Erwin PJ, Velosa JA, Gabriel SE, Kudva YC. Posttransplantation diabetes: a systematic review of the literature. Diabetes Care. 2002 Mar;25(3):583–592.

374. Rodríguez-Rodríguez AE, Triñanes J, Porrini E, Velázquez-García S, Fumero C, Vega-Prieto MJ, et al. Glucose homeostasis changes and pancreatic β-cell proliferation after switching to cyclosporin in tacrolimus-induced diabetes mellitus. Nefrología (English Edition). 2015 May;35(3):264–272.

375. Kuroyanagi Y, Gotoh Y, Kasahara K, Nagano C, Fujita N, Yamakawa S, et al. Effectiveness and nephrotoxicity of a 2-year medium dose of cyclosporine in pediatric patients with steroid-dependent nephrotic syndrome: determination of the need for follow-up kidney biopsy. Clin Exp Nephrol. 2018 Apr;22(2):413–419.

376. Tillmann FP, Schmitz M, Rump LC, Quack I. Impact of low-dose steroids on HbA1c levels and development of pre-diabetes and NODAT in non-diabetic renal transplant recipients on long-term follow-up. Int Urol Nephrol. 2018 Apr;50(4):771–777.

377. Luvisetto S, Basso E, Petronilli V, Bernardi P, Forte M. Enhancement of anxiety, facilitation of avoidance behavior, and occurrence of adult-onset obesity in mice lacking mitochondrial cyclophilin D. Neuroscience. 2008 Aug 26;155(3):585–596.

378. Tavecchio M, Lisanti S, Bennett MJ, Languino LR, Altieri DC. Deletion of Cyclophilin D Impairs β-Oxidation and Promotes Glucose Metabolism. Sci Rep. 2015 Oct 30;5:15981.

379. Yan S, Du F, Wu L, Zhang Z, Zhong C, Yu Q, et al. F1F0 ATP Synthase-Cyclophilin D Interaction Contributes to Diabetes-Induced Synaptic Dysfunction and Cognitive Decline. Diabetes. 2016 Nov;65(11):3482–3494.

380. Feutren G, Mihatsch MJ. Risk factors for cyclosporine-induced nephropathy in patients with autoimmune diseases. International Kidney Biopsy Registry of Cyclosporine in Autoimmune Diseases. N Engl J Med. 1992 Jun 18;326(25):1654–1660.

381. Fioretto P, Steffes MW, Mihatsch MJ, Strøm EH, Sutherland DE, Mauer M. Cyclosporine associated lesions in native kidneys of diabetic pancreas transplant recipients. Kidney Int. 1995 Aug;48(2):489–495.

382. Wittmann S, Daniel C, Stief A, Vogelbacher R, Amann K, Hugo C. Long-term treatment of sirolimus but not cyclosporine ameliorates diabetic nephropathy in the rat. Transplantation. 2009 May 15;87(9):1290–1299.

383. Fayaz SM, Raj YV, Krishnamurthy RG. Cypd: the key to the death door. CNS Neurol Disord Drug Targets. 2015;14(5):654–663.

384. Giorgio V, Bisetto E, Soriano ME, Dabbeni-Sala F, Basso E, Petronilli V, et al. Cyclophilin D modulates mitochondrial F0F1-ATP synthase by interacting with the lateral stalk of the complex. J Biol Chem. 2009 Dec 4;284(49):33982–33988.

385. Laker RC, Taddeo EP, Akhtar YN, Zhang M, Hoehn KL, Yan Z. The Mitochondrial Permeability Transition Pore Regulator Cyclophilin D Exhibits Tissue-Specific Control of Metabolic Homeostasis. PLoS ONE. 2016 Dec 22;11(12):e0167910.

386. Cohen MP, Clements RS, Hud E, Cohen JA, Ziyadeh FN. Evolution of renal function abnormalities in the db/db mouse that parallels the development of human diabetic nephropathy. Exp Nephrol. 1996 Jun;4(3):166–171.

387. Sun H, Wang W, Han P, Shao M, Song G, Du H, et al. Astragaloside IV ameliorates renal injury in db/db mice. Sci Rep. 2016 Sep 2;6:32545.

388. Sun L, Xie P, Wada J, Kashihara N, Liu FY, Zhao Y, et al. Rap1b GTPase ameliorates glucose-induced mitochondrial dysfunction. J Am Soc Nephrol. 2008 Dec;19(12):2293–2301.

389. Coughlan MT, Higgins GC, Nguyen TV, Penfold SA, Thallas-Bonke V, Tan SM, et al. Deficiency in Apoptosis-Inducing Factor Recapitulates Chronic Kidney Disease via Aberrant Mitochondrial Homeostasis. Diabetes. 2016 Jan 28;65(4):1085–1098.

390. Said T, Dutot M, Christon R, Beaudeux JL, Martin C, Warnet JM, et al. Benefits and side effects of different vegetable oil vectors on apoptosis, oxidative stress, and P2X7 cell death receptor activation. Invest Ophthalmol Vis Sci. 2007 Nov;48(11):5000–5006.

391. Gelderblom H, Verweij J, Nooter K, Sparreboom A. Cremophor EL: the drawbacks and advantages of vehicle selection for drug formulation. Eur J Cancer. 2001 Sep;37(13):1590–1598.

392. Desai N, Trieu V, Yao Z, Louie L, Ci S, Yang A, et al. Increased antitumor activity, intratumor paclitaxel concentrations, and endothelial cell transport of cremophor-free, albumin-bound paclitaxel, ABI-007, compared with cremophor-based paclitaxel. Clin Cancer Res. 2006 Feb 15;12(4):1317–1324.

393. Ramadan LA, El-Habit OH, Arafa H. Effect of cremophor-el on cisplatin-induced organ toxicity in normal rat. J Egyptian Nat … [Internet]. 2001; Available from: https://www.researchgate.net/profile/Ola_El-Habit/publication/242537312_Effect_of_Cremophor-EL_on_Cisplatin-Induced_Organ_Toxicity_in_Normal_Rat/links/53da6a150cf2e38c63368afc.pdf

394. Belke DD, Swanson EA, Dillmann WH. Decreased sarcoplasmic reticulum activity and contractility in diabetic db/db mouse heart. Diabetes. 2004 Dec;53(12):3201–3208.

395. Marciniak C, Marechal X, Montaigne D, Neviere R, Lancel S. Cardiac contractile function and mitochondrial respiration in diabetes-related mouse models. Cardiovasc Diabetol. 2014 Aug 21;13(1):118.

396. Ni R, Cao T, Xiong S, Ma J, Fan GC, Lacefield JC, et al. Therapeutic inhibition of mitochondrial reactive oxygen species with mito-TEMPO reduces diabetic cardiomyopathy. Free Radic Biol Med. 2016 Jan;90:12–23.

397. Holmström MH, Iglesias-Gutierrez E, Zierath JR, Garcia-Roves PM. Tissue-specific control of mitochondrial respiration in obesity-related insulin resistance and diabetes. Am J Physiol Endocrinol Metab. 2012 Mar 15;302(6):E731–9.

398. Bugger H, Chen D, Riehle C, Soto J, Theobald HA, Hu XX, et al. Tissue-specific remodeling of the mitochondrial proteome in type 1 diabetic akita mice. Diabetes. 2009 Sep;58(9):1986–1997.

399. Afghahi H, Cederholm J, Eliasson B, Zethelius B, Gudbjörnsdottir S, Hadimeri H, et al. Risk factors for the development of albuminuria and renal impairment in type 2 diabetes--the Swedish National Diabetes Register (NDR). Nephrol Dial Transplant. 2011 Apr;26(4):1236–1243.

400. Maclaren NK, Neufeld M, McLaughlin JV, Taylor G. Androgen sensitization of streptozotocin-induced diabetes in mice. Diabetes. 1980 Sep;29(9):710–716.

401. Kang DH, Yu ES, Yoon KI, Johnson R. The impact of gender on progression of renal disease: potential role of estrogen-mediated vascular endothelial growth factor regulation and vascular protection. Am J Pathol. 2004 Feb;164(2):679–688.

402. Neugarten J, Golestaneh L. Gender and the prevalence and progression of renal disease. Adv Chronic Kidney Dis. 2013 Sep;20(5):390–395.

403. Velasquez MT, Bhathena SJ. Dietary phytoestrogens: a possible role in renal disease protection. Am J Kidney Dis. 2001 May;37(5):1056–1068.

404. De Hauteclocque A, Ragot S, Slaoui Y, Gand E, Miot A, Sosner P, et al. The influence of sex on renal function decline in people with Type 2 diabetes. Diabet Med. 2014 Sep;31(9):1121–1128.

405. Yu MK, Lyles CR, Bent-Shaw LA, Young BA, Pathways Authors. Risk factor, age and sex differences in chronic kidney disease prevalence in a diabetic cohort: the pathways study. Am J Nephrol. 2012 Sep 4;36(3):245–251.

406. Halbesma N, Brantsma AH, Bakker SJ, Jansen DF, Stolk RP, De Zeeuw D, et al. Gender differences in predictors of the decline of renal function in the general population. Kidney Int. 2008 Aug;74(4):505–512.

407. Azushima K, Gurley SB, Coffman TM. Modelling diabetic nephropathy in mice. Nat Rev Nephrol. 2018 Jan;14(1):48–56.

408. Kim D, Sands JM, Klein JD. Changes in renal medullary transport proteins during uncontrolled diabetes mellitus in rats. Am J Physiol Renal Physiol. 2003 Aug;285(2):F303–9.

409. Sugimoto H, Grahovac G, Zeisberg M, Kalluri R. Renal fibrosis and glomerulosclerosis in a new mouse model of diabetic nephropathy and its regression by bone morphogenic protein-7 and advanced glycation end product inhibitors. Diabetes. 2007 Jul;56(7):1825–1833.

410. Mauer SM, Steffes MW, Ellis EN, Sutherland DE, Brown DM, Goetz FC. Structural-functional relationships in diabetic nephropathy. J Clin Invest. 1984 Oct;74(4):1143–1155.

411. Bader R, Bader H, Grund KE, Mackensen-Haen S, Christ H, Bohle A. Structure and function of the kidney in diabetic glomerulosclerosis. Pathology - Research and Practice. 1980 Jun;167(2-4):204–216.

412. Khan FA, Fatima SS, Khan GM, Shahid S. Evaluation of kidney injury molecule-1 as a disease progression biomarker in diabetic nephropathy. Pak J Med Sci Q. 2019 Aug;35(4):992–996.

413. Brantsma AH, Bakker SJ, Hillege HL, de Zeeuw D, de Jong PE, Gansevoort RT, et al. Cardiovascular and renal outcome in subjects with K/DOQI stage 1-3 chronic kidney disease: the importance of urinary albumin excretion. Nephrol Dial Transplant. 2008 Dec;23(12):3851–3858.

414. Fung CS, Wan EY, Chan AK, Lam CL. Association of estimated glomerular filtration rate and urine albumin-to-creatinine ratio with incidence of cardiovascular diseases and mortality in chinese patients with type 2 diabetes mellitus - a population-based retrospective cohort study. BMC Nephrol. 2017 Feb 2;18(1):47.

415. Berhane AM, Weil EJ, Knowler WC, Nelson RG, Hanson RL. Albuminuria and estimated glomerular filtration rate as predictors of diabetic end-stage renal disease and death. Clin J Am Soc Nephrol. 2011 Oct;6(10):2444–2451.

416. Mafham MM, Staplin N, Emberson J, Haynes R, Herrington W, Reith C, et al. Prognostic utility of estimated albumin excretion rate in chronic kidney disease: results from the Study of Heart and Renal Protection. Nephrol Dial Transplant. 2018 Feb 1;33(2):257–264.

417. Huo W, Zhang K, Nie Z, Li Q, Jin F. Kidney injury molecule-1 (KIM-1): a novel kidney-specific injury molecule playing potential double-edged functions in kidney injury. Transplant Rev (Orlando). 2010 Jul;24(3):143–146.

418. Vaidya VS, Ozer JS, Dieterle F, Collings FB, Ramirez V, Troth S, et al. Kidney injury molecule-1 outperforms traditional biomarkers of kidney injury in preclinical biomarker qualification studies. Nat Biotechnol. 2010 May;28(5):478–485.

419. Jheng HF, Tsai PJ, Chuang YL, Shen YT, Tai TA, Chen WC, et al. Albumin stimulates renal tubular inflammation through an HSP70-TLR4 axis in mice with early diabetic nephropathy. Dis Model Mech. 2015 Oct 1;8(10):1311–1321.

420. Xu D, Chen P, Wang B, Wang Y, Miao N, Yin F, et al. NIX-mediated mitophagy protects against proteinuria-induced tubular cell apoptosis and renal injury. Am J Physiol Renal Physiol. 2019 Feb 1;316(2):F382–F395.

421. Wu M, Li S, Yu X, Chen W, Ma H, Shao C, et al. Mitochondrial activity contributes to impaired renal metabolic homeostasis and renal pathology in STZ-induced diabetic mice. Am J Physiol Renal Physiol. 2019 Sep 1;317(3):F593–F605.

422. Raza H, Prabu SK, John A, Avadhani NG. Impaired mitochondrial respiratory functions and oxidative stress in streptozotocin-induced diabetic rats. Int J Mol Sci. 2011 May 13;12(5):3133–3147.

423. Nordquist L, Friederich-Persson M, Fasching A, Liss P, Shoji K, Nangaku M, et al. Activation of hypoxia-inducible factors prevents diabetic nephropathy. J Am Soc Nephrol. 2015 Feb;26(2):328–338.

424. Ruegsegger GN, Creo AL, Cortes TM, Dasari S, Nair KS. Altered mitochondrial function in insulin-deficient and insulin-resistant states. J Clin Invest. 2018 Aug 31;128(9):3671–3681.

425. Kim JA, Wei Y, Sowers JR. Role of mitochondrial dysfunction in insulin resistance. Circ Res. 2008 Feb 29;102(4):401–414.

426. Gonzalez-Franquesa A, Patti ME. Insulin resistance and mitochondrial dysfunction. Adv Exp Med Biol. 2017;982:465–520.

427. Eirin A, Woollard JR, Ferguson CM, Jordan KL, Tang H, Textor SC, et al. The metabolic syndrome induces early changes in the swine renal medullary mitochondria. Transl Res. 2017 Mar 11;184:45–56.e9.

428. Rolo AP, Palmeira CM. Diabetes and mitochondrial function: role of hyperglycemia and oxidative stress. Toxicol Appl Pharmacol. 2006 Apr 15;212(2):167–178.

429. Lim S, Cho YM, Park KS, Lee HK. Persistent organic pollutants, mitochondrial dysfunction, and metabolic syndrome. Ann N Y Acad Sci. 2010 Jul;1201:166–176.

430. Gastaldi G, Giacobino JP, Ruiz J. [Metabolic syndrome, a mitochondrial disease?]. Rev Med Suisse. 2008 Jun 4;4(160):, 1390.

431. Sorriento D, Pascale AV, Finelli R, Carillo AL, Annunziata R, Trimarco B, et al. Targeting mitochondria as therapeutic strategy for metabolic disorders. ScientificWorldJournal. 2014 Mar 13;2014:604685.

432. Katyare SS, Satav JG. Effect of streptozotocin-induced diabetes on oxidative energy metabolism in rat kidney mitochondria. A comparative study of early and late effects. Diabetes Obes Metab. 2005 Sep;7(5):555–562.

433. Austin S, Klimcakova E, St-Pierre J. Impact of PGC-1α on the topology and rate of superoxide production by the mitochondrial electron transport chain. Free Radic Biol Med. 2011 Dec 15;51(12):2243–2248.

434. Forbes JM, Ke BX, Nguyen TV, Henstridge DC, Penfold SA, Laskowski A, et al. Deficiency in mitochondrial complex I activity due to Ndufs6 gene trap insertion induces renal disease. Antioxid Redox Signal. 2013 Aug 1;19(4):331–343.

435. Ortiz-Avila O, Sámano-García CA, Calderón-Cortés E, Pérez-Hernández IH, Mejía-Zepeda R, Rodríguez-Orozco AR, et al. Dietary avocado oil supplementation attenuates the alterations induced by type I diabetes and oxidative stress in electron transfer at the complex II-complex III segment of the electron transport chain in rat kidney mitochondria. J Bioenerg Biomembr. 2013 Jun;45(3):271–287.

436. Czajka A, Ajaz S, Gnudi L, Parsade CK, Jones P, Reid F, et al. Altered mitochondrial function, mitochondrial DNA and reduced metabolic flexibility in patients with diabetic nephropathy. EBioMedicine. 2015 Jun;2(6):499–512.

437. Stacchiotti A, Favero G, Giugno L, Lavazza A, Reiter RJ, Rodella LF, et al. Mitochondrial and metabolic dysfunction in renal convoluted tubules of obese mice: protective role of melatonin. PLoS ONE. 2014 Oct 27;9(10):e111141.

438. Szeto HH, Liu S, Soong Y, Alam N, Prusky GT, Seshan SV. Protection of mitochondria prevents high-fat diet-induced glomerulopathy and proximal tubular injury. Kidney Int. 2016 Aug 9;90(5):997–1011.

439. Chowdhury SR, Djordjevic J, Albensi BC, Fernyhough P. Simultaneous evaluation of substrate-dependent oxygen consumption rates and mitochondrial membrane potential by TMRM and safranin in cortical mitochondria. Biosci Rep. 2015 Dec 8;36(1):e00286.

440. Nakazawa H, Ikeda K, Shinozaki S, Kobayashi M, Ikegami Y, Fu M, et al. Burn-induced muscle metabolic derangements and mitochondrial dysfunction are associated with activation of HIF-1α and mTORC1: Role of protein farnesylation. Sci Rep. 2017 Jul 26;7(1):6618.

441. Wyatt CN, Buckler KJ. The effect of mitochondrial inhibitors on membrane currents in isolated neonatal rat carotid body type I cells. J Physiol (Lond). 2004 Apr 1;556(Pt 1):175–191.

442. Ward JP. Oxygen sensors in context. Biochim Biophys Acta. 2008 Jan;1777(1):1–14.

443. Das KC, Muniyappa H. Age-dependent mitochondrial energy dynamics in the mice heart: role of superoxide dismutase-2. Exp Gerontol. 2013 Sep;48(9):947–959.

444. Porter C, Hurren NM, Cotter MV, Bhattarai N, Reidy PT, Dillon EL, et al. Mitochondrial respiratory capacity and coupling control decline with age in human skeletal muscle. Am J Physiol Endocrinol Metab. 2015 Aug 1;309(3):E224–32.

445. Horton AA, Spencer JA. Decline in respiratory control ratio of rat liver mitochondria in old age. Mech Ageing Dev. 1981 Nov;17(3):253–259.

446. Larsen S, Hey-Mogensen M, Rabøl R, Stride N, Helge JW, Dela F. The influence of age and aerobic fitness: effects on mitochondrial respiration in skeletal muscle. Acta Physiol (Oxf). 2012 Jul;205(3):423–432.

447. Czajka A, Malik AN. Hyperglycemia induced damage to mitochondrial respiration in renal mesangial and tubular cells: Implications for diabetic nephropathy. Redox Biol. 2016 Sep 17;10:100–107.

448. Picard M, Taivassalo T, Ritchie D, Wright KJ, Thomas MM, Romestaing C, et al. Mitochondrial structure and function are disrupted by standard isolation methods. PLoS ONE. 2011 Mar 28;6(3):e18317.

449. Brand MD, Affourtit C, Esteves TC, Green K, Lambert AJ, Miwa S, et al. Mitochondrial superoxide: production, biological effects, and activation of uncoupling proteins. Free Radic Biol Med. 2004 Sep 15;37(6):755–767.

450. Rousset S, Alves-Guerra MC, Mozo J, Miroux B, Cassard-Doulcier AM, Bouillaud F, et al. The biology of mitochondrial uncoupling proteins. Diabetes. 2004 Feb;53 Suppl 1:S130–5.

451. Brennan JP, Berry RG, Baghai M, Duchen MR, Shattock MJ. FCCP is cardioprotective at concentrations that cause mitochondrial oxidation without detectable depolarisation. Cardiovasc Res. 2006 Nov 1;72(2):322–330.

452. Andreyev AYu, Bondareva TO, Dedukhova VI, Mokhova EN, Skulachev VP, Tsofina LM, et al. The ATP/ADP-antiporter is involved in the uncoupling effect of fatty acids on mitochondria. Eur J Biochem. 1989 Jul 1;182(3):585–592.

453. Renault TT, Chipuk JE. Death upon a kiss: mitochondrial outer membrane composition and organelle communication govern sensitivity to BAK/BAX-dependent apoptosis. Chem Biol. 2014 Jan 16;21(1):114–123.

454. Radhakrishnan J, Bazarek S, Chandran B, Gazmuri RJ. Cyclophilin-D: a resident regulator of mitochondrial gene expression. FASEB J. 2015 Jul;29(7):2734–2748.

455. Porter GA, Beutner G. Cyclophilin D, somehow a master regulator of mitochondrial function. Biomolecules. 2018 Dec 14;8(4).

456. Gordon S, Plüddemann A. Macrophage clearance of apoptotic cells: A critical assessment. Front Immunol. 2018 Jan 30;9:127.

457. Zheng Z, Zheng F. Immune cells and inflammation in diabetic nephropathy. J Diabetes Res. 2016;2016:1841690.

458. Hickey FB, Martin F. Role of the immune system in diabetic kidney disease. Curr Diab Rep. 2018 Mar 12;18(4):20.

459. Navarro-González JF, Mora-Fernández C. The role of inflammatory cytokines in diabetic nephropathy. J Am Soc Nephrol. 2008 Mar;19(3):433–442.

460. Martin-Sanchez D, Poveda J, Fontecha-Barriuso M, Ruiz-Andres O, Sanchez-Niño MD, Ruiz-Ortega M, et al. Targeting of regulated necrosis in kidney disease. Nefrologia. 2018;38(2):125–135.

Appendices

SOCIETY FOR BIOMEDICAL DIABETES RESEARCH

SBDR – Gneisenaustr. 86 – 47057 Duisburg – Germany

RDS Publication Office
SBDR – Society for Biomedical
Diabetes Research
Gneisenaustr. 86
D-47057 Duisburg
Germany
Tel: +49 203 9413 722
Fax: +49 203 9413 724
E-mail: info@soc-bdr.org

October 17, 2019

To whom it may concern:

Permission for Reuse of the article Lindblom et al. "Targeting mitochondria- and reactive oxygen species-driven pathogenesis in diabetic nephropathy", Rev Diabet Stud 2015, 12(1-2):134-156

We grant permission for the use and republication of the abovementioned article from our journal, The Review of Diabetic Studies, in the thesis by Runa Lindblom, Monash University, Australia.

Sincerely,

Your RDS Publication Office

Appendix Chapter 1.1: Types of cell death

Type of cell death			Reference	Description
1.		Apoptosis	(Kerr et al., 1972)	Type I cell death. Programmed cell death, with membrane blebbing, activation of caspase 3, 7, 9. Also, developmental programmed cell death. **Extrinsic** - FAS-L, TRAIL-L mediated **Intrinsic** - mediated by formation of mitochondrial outer membrane pore
2.		Immunogenic cell death	(Peter et al., 2008)	"phagocytic", release of DAMPs or PAMPs to attract immunogenic response eg monocytes. ATP is a DAMP, also underlies some cancer vaccination responses
	3	Caspase independent apoptosis	(Xiang et al., 1996)	Programmed cell death that does not activate caspases
4.		Anoikis	(Frisch and Francis, 1994)	Subtype of apoptosis, programmed cell death. Follows separation from neighbouring cells/withdrawal of anchoring ligands. Isolation induced.
	5.	Ferroptosis	(Dixon, 2017)	Iron dependent programmed cell death
	6.	Ferroxitosis	(Lakhter et al., 2014)	Iron and oxygen dependent cell death
	7.	Oxeiptosis	(Holze et al., 2018)	ROS induced, caspase independent, apoptotic-like cell death. Non-inflammatory.
	8.	Alkaliptosi	(Song et al., 2018)	pH-dependent cell death, induced by a specific g-protein coupled receptor binding ligand, to treat pancreatic cancer cells
	9.	Parthanatos	(David et al., 2009)	PARP-1 overactivation mediated cell death
	10.	Necrosis		Non-physiological. Accidental, destructive cell death
	11.	Necroptosis	(Degterev et al., 2008)	Programmed, destructive cell death, requires RIPK1
	12.	Pyronecrosis	(Willingham et al., 2007)	Uncertain, but is casp-1 independent. May just be necrosis
	13.	Pyroptosis	(Bergsbaken et al., 2009)	inflammatory cell death

	14	Mitotic catastrophe	(Castedo et al., 2004)	Replicative stress induced cell death, related to errors in DNA and structural instability. Observed in cancer.
	15.	Autophagy*		Type II cell death. "Eaten from within death", characterised by autophagic vacuolisation of cytoplasmic contents without chromatin degradation.
	16.	Paraptosis	(Sperandio et al., 2004)	Excessive vacuolisation of cytosol, caspase independent
	17.	Autoschizis	(Jamison et al., 2002)	Oxidative stress induced with unusual morphological changes
	18.	Entosis	(Overholtzer et al., 2007)	One cell eats another cell. Engulfed cell may or may not die. May replicate or escape instead of being degraded.)
	18.	Cornification	*(Candi et al., 2005)*	*Specialised* - skin epithelial cell transformative cell death
	19.	NETosis	(Brinkmann et al., 2004)	*Specialised* - neutrophil specific, sacrificial death to assist in clearing bacterial infection
	20.	Activation induced cell death		Triggered by over activation of effector T-cells, FAS, TNF-alpha and TRAIL mediated cell death. Helps remove autoreactive T-cells. (Several models have been developed.)
	21.	Excitotoxicity	(Olney, 1969)	Glutamate mediated, "excitation" induced cell death in neurons
	X.	Wallerian Degeneration	(Waller, 1850)	→ selective death of neural axons without killing the cell body. Caspase 3 independent, probably mediated by calpains etc. Death of a *part* of a cell only.
* The Nomenclature Committee on Cell Death recommends the term “cell death with Autophagy” or "Autophagic cell death" as "Autophagy" is in fact a pro-survival response, and its status as a unique form of cell death is debated. (Kroemer et al., 2009).				

Bibliography

Bergsbaken, T., Fink, S.L., and Cookson, B.T. (2009). Pyroptosis: host cell death and inflammation. Nat Rev Microbiol *7*, 99–109.

Brinkmann, V., Reichard, U., Goosmann, C., Fauler, B., Uhlemann, Y., Weiss, D.S., Weinrauch, Y., and Zychlinsky, A. (2004). Neutrophil extracellular traps kill bacteria. Science *303*, 1532–1535.

Candi, E., Schmidt, R., and Melino, G. (2005). The cornified envelope: a model of cell death in the skin. Nat Rev Mol Cell Biol *6*, 328–340.

Castedo, M., Perfettini, J.L., Roumier, T., Andreau, K., Medema, R., and Kroemer, G. (2004). Cell death by mitotic catastrophe: a molecular definition. Oncogene *23*, 2825–2837.

David, K.K., Andrabi, S.A., Dawson, T.M., and Dawson, V.L. (2009). Parthanatos, a messenger of death. Front Biosci (Landmark Ed) *14*, 1116–1128.

Degterev, A., Hitomi, J., Germscheid, M., Ch'en, I.L., Korkina, O., Teng, X., Abbott, D., Cuny, G.D., Yuan, C., Wagner, G., et al. (2008). Identification of RIP1 kinase as a specific cellular target of necrostatins. Nat Chem Biol *4*, 313–321.

Dixon, S.J. (2017). Ferroptosis: bug or feature? Immunol Rev *277*, 150–157.

Frisch, S.M., and Francis, H. (1994). Disruption of epithelial cell-matrix interactions induces apoptosis. J Cell Biol *124*, 619–626.

Holze, C., Michaudel, C., Mackowiak, C., Haas, D.A., Benda, C., Hubel, P., Pennemann, F.L., Schnepf, D., Wettmarshausen, J., Braun, M., et al. (2018). Oxeiptosis, a ROS-induced caspase-independent apoptosis-like cell-death pathway. Nat Immunol *19*, 130–140.

Jamison, J.M., Gilloteaux, J., Taper, H.S., Calderon, P.B., and Summers, J.L. (2002). Autoschizis: a novel cell death. Biochem Pharmacol *63*, 1773–1783.

Kerr, J.F., Wyllie, A.H., and Currie, A.R. (1972). Apoptosis: a basic biological phenomenon with wide-ranging implications in tissue kinetics. Br J Cancer *26*, 239–257.

Kroemer, G., Galluzzi, L., Vandenabeele, P., Abrams, J., Alnemri, E.S., Baehrecke, E.H., Blagosklonny, M.V., El-Deiry, W.S., Golstein, P., Green, D.R., et al. (2009). Classification of cell death: recommendations of the Nomenclature Committee on Cell Death 2009. Cell Death Differ *16*, 3–11.

Lakhter, A.J., Hamilton, J., Dagher, P.C., Mukkamala, S., Hato, T., Dong, X.C., Mayo, L.D., Harris, R.A., Shekhar, A., Ivan, M., et al. (2014). Ferroxitosis: a cell death from modulation of oxidative phosphorylation and PKM2-dependent glycolysis in melanoma. Oncotarget *5*, 12694–12703.

Olney, J.W. (1969). Brain lesions, obesity, and other disturbances in mice treated with monosodium glutamate. Science *164*, 719–721.

Overholtzer, M., Mailleux, A.A., Mouneimne, G., Normand, G., Schnitt, S.J., King, R.W., Cibas, E.S., and Brugge, J.S. (2007). A nonapoptotic cell death process, entosis, that occurs by cell-in-cell invasion. Cell *131*, 966–979.

Peter, C., Waibel, M., Radu, C.G., Yang, L.V., Witte, O.N., Schulze-Osthoff, K., Wesselborg, S., and Lauber, K. (2008). Migration to apoptotic “find-me” signals is mediated via the phagocyte receptor G2A. J Biol Chem *283*, 5296–5305.

Song, X., Zhu, S., Xie, Y., Liu, J., Sun, L., Zeng, D., Wang, P., Ma, X., Kroemer, G., Bartlett, D.L., et al. (2018). JTC801 Induces pH-dependent Death Specifically in Cancer Cells and Slows Growth of Tumors in Mice. Gastroenterology *154*, 1480–1493.

Sperandio, S., Poksay, K., de Belle, I., Lafuente, M.J., Liu, B., Nasir, J., and Bredesen, D.E. (2004). Paraptosis: mediation by MAP kinases and inhibition by AIP-1/Alix. Cell Death Differ *11*, 1066–1075.

Waller, A. (1850). Experiments on the section of the glossopharyngeal and hypoglossal nerves of the frog, and observations of the alterations produced thereby in the structure of their primitive fibres. Philosophical Transactions of the Royal Society of London *140*, 423–429.

Willingham, S.B., Bergstralh, D.T., O’Connor, W., Morrison, A.C., Taxman, D.J., Duncan, J.A., Barnoy, S., Venkatesan, M.M., Flavell, R.A., Deshmukh, M., et al. (2007). Microbial pathogen-induced necrotic cell death mediated by the inflammasome components CIAS1/cryopyrin/NLRP3 and ASC. Cell Host Microbe *2*, 147–159.

Xiang, J., Chao, D.T., and Korsmeyer, S.J. (1996). BAX-induced cell death may not require interleukin 1 beta-converting enzyme-like proteases. Proc Natl Acad Sci U S A *93*, 14559–14563.

Table A2.1: List of primer sequences used for RTqPCR experiments

Gene (*Mus musculus*)	Forward 5' – 3'	Reverse 5' – 3'	Genebank accession
Syber reagents			
Acox1	CCTGGCCACGCCCTATG	TTAATCCGCATGTAGGTCTCCTTT	NM_015729
Bax	GGCCTTTTTGCTACAGGGTTT	GTGTCTCCCCAGCCATCCT	NM_007527
Bak1	TGATACCAGTTCCTGCCAGTCA	GGGCTTGCTGGCTGCTT	NM_007523
Bcl-2	AAGGGCTTCACACCCAAATCT	TTCTACGTCTGCTTGGCTTTGA	NM_009741
Casp 3	GACGGTCCTCCTGGTCTTTG	GTGGCTGGCTGCATTGC	NM_009810
Casp 8 ǂ	CAACTTCCTAGACTGCAACCG	TCCAACTCGCTCACTTCTTCT	NM_009812.2
Casp 9 ǂ	TCCTGGTACATCGAGACCTTG	AAGTCCCTTTCGCAGAAACAG	NM_015733.5
Casp 12 ǂ	AGACAGAGTTAATGCAGTTTGCT	TTCACCCCACAGATTCCTTCC	NM_009808.4
CTGF	GCTGCCTACCGACTGGAAGA	CTTAGAACAGGCGCTCCACTCT	BC006783
Cyt c ǂ	CATCTTGGTTTCAAGCCCAGA	CTGCCCAGGCCAAAATTGC	JF919281.1
F4/80	GGTACAGTCATCTCCCTGGTATGTCT	GGTTCTGAACAGCACGACACA	X93328
Mief1	GCTTCGCTACACTGATCGAGACT	CTCAAGCTTCTGATTTTTCCTGAAT	NM_178719
Mief2	AGGGCTCCCTGCCTTATACC	TCGTGGCCCATAGAGAAAACC	NM_001009927
Nqo1	CCAGCTGCTCAGCCAATCA	GCCATGGCTCCAGATGTTG	CT010284.1
Opa1 ǂ	ATACTGGGATCTGCTGTTGG	AAGTCAGGCACAATCCACTT	NM_001199177.1
Pink1	AGAAAACCAAGCGCGTGTCT	GGAAGCCCTGCCAGCAT	NM_026880
Ppif ‡ (Cyclophilin F, Cyclophilin D)	TGGCTCTCAGTTCTTTATCTGC	ACATCCATGCCCTCTTTGAC	NM_134084.1
Usp30	TTAGGGCCATGCTCTAAGAGTGT	GAGAGGCCCAGTGTACCGTTT	NM_001033202
TaqMan reagents			
AIF	CCTCAGATCAGGGCACCAA	GCAGTCCCTCCACCAATCA	AF100927
AIF probe: 6-FAM CACGTCCCTTTCCTG			
α-SMA	GACGCTGAAGTATCCGATAGAACA	GGCCACACGAAGCTCGTTAT	NM_007392
α-SMA probe: 6- FAM TGCCAGATCTTTTCC			
Collagen I	GACTGGAAGAGCGGAGAGTACTG	CCTTGATGGCGTCCAGGTT	NM_007742
Collagen I probe: 6- FAM ATCGACCCTAACCAAG			

Collagen 4	GGCGGTACACAGTCAGACCAT	GGAATAGCCGATCCACAGTGA	J04694
Collagen 4 probe: 6- FAM CAGTGCCCTAACGGT			
ATP synthase, F1-α	TGTCCGCTTACATTCCAACAAA	CAGGGCGGATGCCTTTATAG	BC020417
F1-α probe: 6-FAM TCTTGGAAACAGAATTGT			
Fibronectin	ACATGGCTTTAGGCGGACAA	ACATTCGGCAGGTATGGTCTTG	M10905
Fibronectin probe: 6- FAM CCCCGTCAGGCTTA			
TGF-β	GCAGTGGCTGAACCAAGGA	GCAGTGAGCGCTGAATCGA	NM_011577
TGF-β probe: 6- FAM AAAGCCCTGTATTCCGT			
Sod2	GGGACATATTAATCACACCATTTTCT	CCCAAAGTCACGCTTGATAGC	XM_128337
Sod2 Probe: 6- FAM CCTGAGCCCTAAGGG			
Ucp2	CCGTAATGCCATTGTCAACTGT	GGCTTTCAGGAGAGTATCTTTGATG	BC012697
Ucp2 probe: 6- FAM ATAGGTCACCAGCTCAG			

Notes: All genes were generated against sequences for *Mus musculus*
[‡]Ppif primer sequence from Lam, CK et al *PNAS* 2015

Appendix 2.2

Table A2.2 HbA_{1C} reference ranges for in-house colonies of the following mouse strains collected within the Department of Diabetes (unpublished data)

	Control		Diabetic†	
Mouse strain	**NGSP (%)**	**mmol/mol**	**NGSP (%)**	**mmol/mol**
C57BL/6	4.4 ± 0.48	25 ± 5.2	11.0 ± 2.1	84.6 ± 22.9
db/h, db/db	4.1 ± 0.2	21.1 ± 1.9	11.7 ± 0.7	104 ± 7.7
FVB/N	4.1 ± 0.2	21.8 ± 1.9	10.0 ± 0.6	86.0 ± 6.4

Note: Values are mean ± standard deviation, showing results for HbA_{1C} obtained from cohorts of mice previously tested in our laboratory, for *n* = 8-12 per group. Detection range limited to between 4.0% (20mmol/mol) and 14.4% (134mmol/mol).

† *C57BL/6* and *FVB/N* diabetic mice are STZ treated, *FVB/N* represents values at 10 weeks of diabetes

Appendix 3.1: black and white TUNEL stain image

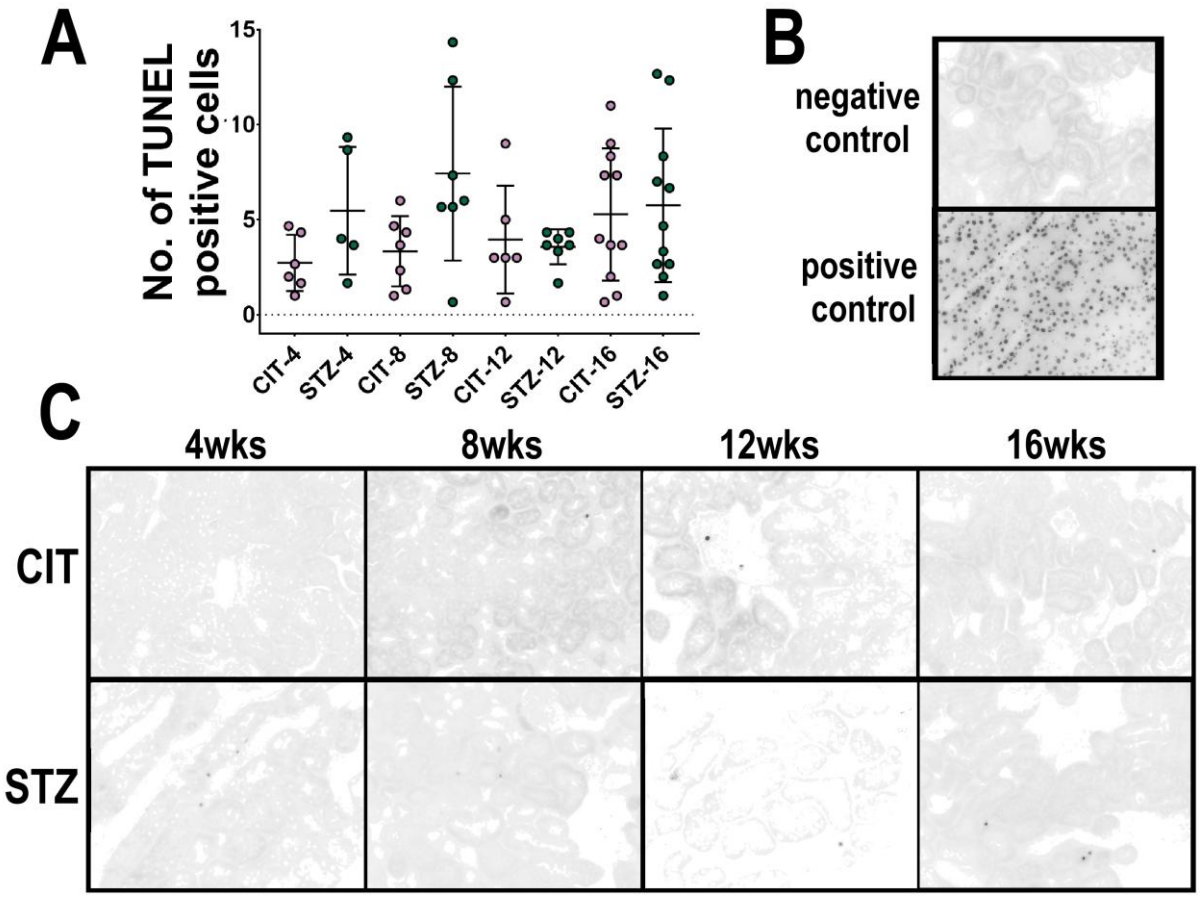

3.1: Negative, black and white image of Figure 3.10. Black dots represent TUNEL positive nuclei.

Appendix 4.1: Sequencing data

Primers

Forward: 5'- ATGTTGCGGGGCACCCACGTGAGGG -3'

Reverse: 3' - TCTGATCAGCTCGGGCACTTTAGTG - 5'

complementary: 5'- CACTAAAGTGCCCGAGCTGATCAGA -3'

Bax KO forward sequence result

5'-

CCCCGATCAGTCCGTGACCGTGGTGCGCCGCAGCCGCCGGGGCGCACCCGGCGAGAGGCAGCGGC

AGTG

ATGGACGGGTCCGGGGAGCAGCTTGGGAGCGGCGGTGAGGCGGGAGGCGGAGGACTAGGCCCGG

TCCAAGAACCCTAGGACCCCTCCGGCTTTGGGCTCGGGCGGGAGCAGGCTGGGGCGCGCGGATCCG

AATTCCGATCATATTCAATAACCCTTAATATAACTTCGTATAATGTATGCTATACGAAGTTATCAGTACA

AGCCGAATTCTGCAGATATCGGCGCTCTGATTGATGGTGGATACATGTAAGGTAGACTATTGAGATG

GGCCAGAGAAACCTAGAAAGATTTCTCAGTGTAGGTGGTCTTAAACTGATCTGGTGGCACATGCCTG

TAATTCCAGGACTTGCGGTAGGAGTTGAAGGTTAGCTGCAGTTAAATACTGAGTTTCAGGCTATCCTG

AGCTACCTAAACCTAAGACCTATTTTTTTGGGGGGGGTTTTGTTTGTTTATTTGTTTTTTGTTGCTGTTG

TTCCAACCGGAAGCTATCGGTCCCCC -3'

Bak KO reverse sequence result

3'-

GTGAGGGAGATTACACTTGGGGACTGAATCTTGTCCCCACTGCCCAGAGGTGATC

TCAAGCTCTTGCTTTTA

ACCCTCTGCCTCTGCTAAGCGGTCTCTCCTCTACTAATTATAAACTAAAGCTTCCC

TTACCTGCTCAGGAGCCCTGACTCCTCAGCACCCTCTAGGTAAAAACCAAAAGGC

TGAGGTAAGGCTCAAGACCAGGCTGACCTCAAACTCAGAAATCCGCCTGCCTCT

GCCTCCCGAGTGCTGGGATTAAAGGCGTGCGCCACCACTGCCCGGCCTGCCTAA

GTCACTTCCTAGAGTGGTTTTCTAGACCAGAGAAGACCACCTCCTGGCCAACTGA

GGCTCTGCTCTCCTGACTGGAACAATGCTCTCTTCCTGGCCTACATTCCTTTCACC

TCCAATACTGAAGACCCGTCAGCTCAGGCATGAAACCTCATCAAGGAGGTGGGG

GATGGCATGGAGGACAATCAAGAGTGTCCCAAATGTGACAGTAGCACTACAAAT

AACAAGTAAAATATGCCACAGTGGCTCTGCAGCAACTTCCTGCTCCAACACACCC

CACCACAGCCTAGTCTTGAACTTGTGATCCTCCTACCTCCAACTTCCCAAGTGCT

AGCACTGCAGGCATGTTCCAACCACCCCTAGTTCATGTGGCACTGACCCAGGGCC

AGGACACATGCCAGCCAAGCACCACCAGCTGATCTGCAGTCCCAGCGCCTCTTTT

GGTATTTGTGTGTATGCTGATAGGAGACAGAACCTAAGGCTTTCATCCATGTTAT

GCTCAGGCCCCCAAAACTCAACTACACTACCACACCTACTGTCACGTCCATTTCC

TGTCTTTTGCTTTTGTTTGCTCTTAATTAAAAAAATAAATAAAATAAAAACTACG

GTCAGGGCCTAGAGAACT -**5'**

5'-

TCTCTAGCCCTGACCTAGTTTATTTATTTATTTATTTTTTAATAAAAGCAAACAAAAACAAAGACAGAAATGGACGTGAC

AGTAGGTGTGGTAGTGTAGCTGAGTTTTGGGGGCCTGAGCATAACATGGATGAAGCCTTAGGTTCTGTCTCCTATCAGCAT

ACACACAAATACCAAAGAGGCGCTGGGACTGCAGATCAGCTGGTGGTGCTTGGCTGGCATGTGTCCTGGCCCTGGGTCAG

TGCCACATGAACTAGGGGTGGTTGGAACATGCCTCCAGTGCTAGCACTTGGAAGTTGGAGGTAGGAGGATCACAAGTTCA

AGACTAGGCTGTGGTGGGGTGTGTTGGAGCAGGAAGTTGCTGCAGAGCCACTGTGGCATATTTTACTTGTTATTTGTAGTG

CTACTGTCACATTTGGGACACTCTTGATTGTCCTCCATGCCATCCCCCACCTCCTTGATGAGGTTTCATGCCTGAGCTGACGG

GTCTTCAGTATTGGAGGTGAAAGGAATGTAGGTCAGGAAGAGAGCATTGTTCCAGTCAGGAGAGCAGAGCCTCAGTTGGC

CAGGAGGTGGTCTTCTCTGGTCTAGAAAACCACTCTAGGAAGTGACTTAGGCAGGCCGGGCAGTGGTGGCGCACGCCTTT

AATCCCAGCACTCGGGAGGCAGAGGCAGGCGGATTTCTGAGTTTGAGGTCAGCCTGGTCTTGAGCCTTACCTCAGCCTTTT

GGTTTTTACCTAGAGGGTGCTGAGGAGTCAGGGCTCCTGAGCAGGTAAGGGAAGCTTTAGTTTATAATTAGTAGAGGAGA

GACCGCTTAGCAGAGGCAGAGGGTTAAAAGCAAGGGCTTGAGATCACCTCTGGGCAGTGGGGACAAGATTCAGTCCCCA

AGTGTAATCTTCCCAC -3'

Bax mRNA transcript exons 5' - 3'

Exon 1

ATGGACGGGTCCGGGGAGCAGCTTGGGAGCGGCG

Exon 2

GGCCCACCAGCTCTGAACAGATCATGAAGACAGG

Exon 3

TTTCATCCAGGATCGAGCAGGGAGGATGGCTGGGGAGACACCTGAGCTGACCTTGGAGCAGCCGCCCCAGGAT
GCGTCCACCAAGAAGCTGAGCGAGTGTCTCCGGCGAATTGGAGATGAACTGGACAGCAATATGGAGCTGCAGAG

Exon 4

GATGATTGCTGACGTGGACACGGACTCCCCCCGAGAGGTCTTCTTCCGGGTGGCAGCTGACATGTTTGCTGATG
GCAACTTCAACTGGGGCCGCGTGGTTGCCCTCTTCTACTTTGCTAGCAAACTGGTGCTCAAG

Exon 5

GCCCTGTGCACTAAAGTGCCCGAGCTGATCAGAACCATCATGGGCTGGACACTGGACTTCCTCCGTGAGCGGCT
GCTTGTCTGGATCCAAGACCAGGGTGGCTGG

Exon 6

CCTCGCTCACCATCTGGAAGAAGATGGGCTGAGGCCTCCC

Transcript of Bax gene: *Mus musculus*_Chromosome 7, GRCm38.p6 C57BL/6J

5'-

AATGCCCAGCTATGTTGATTGATTGATTTTCATGTGAAACACCTCTCAAGGCCCAGGGACATATCTGACTTCTGAGAAGA
CTTGAGTTTCAAAGGCAGCCACTGTCTCTAGTACATCAGCCAGGCATTAAAGGATACATTTGGAGATCACCATGTGTCAAG
CAGTGTGCTAGTTTCTAGGGAATTGAGAACAAATGAATACAGTCTTCTTGGGAAACCAAGGTAGGTGAGAGCCACCAGCA
ATGAACGAAAACACTGCACACAAAATTAATTACAGTGCTGTGAAGCATAATAAAACCCAGTGGTTAAAAAAAGAGAAAAGA
AAAGAAAAGAAAAGAAGAGAAAAGAAAGCCGGGTGTGGTGGCACACGCCTTTAATCCCAGCACTGGGGAGGCAGAGGC
AGGCGGATTTCGGAGTTCGAGGCCAGCCTGGTCTACAAAGTGAGTTCCAGGATAGCCAGGGCTATACAGAGAAACCCTGT
CTCAAAAAACCCACCAAAACAGAAAAGAAAAGAAAAGAAAAGAAAAGAAAAGAAAAGAAGGGAAAAGAAAAGAAAAAG
GAGAGCTGCCCGTGGTGGTGCACACCTTCAATCCCCACACAGAAGAAGAGGCAGGCAGTTCTCTATGTTCGAGGCCAGTTT
GGTCTACAGACTGAGTTTCAGGACAGCCAGGGCTACACAGAAGCTGTTTCAAATAACAAACAAAAACTCTGGGTGCTTTCA
GAGCTTTTTCAACAGAGGACTCAAGCCAAGAGACTTTCTGACACCCAGATAACTCTACCCTTCCCCTGCTCAAAACTTCCCCT
GGGTCTCAGGTCTCAGACACCCTCAGAAGACTGATAAATTCCTGCTAGAAAACTCCAGAGTGTCTGTCCTGGCCTGCTGCT
ACTTCACATTATTCCTCCTCTTCCTCCTTCTTCTCTTTTTTTTCTTTCTCTTCTTTTTTTTTTTTTTTCCAAACCAGGGTTTCTCTAA
GTAGCCATGGCTGTCCTGGAACTGGCTTTGTAGTCCAGGCTGACCTCGAACTCAGAGATCTACCTTCCTGCGTTCTGAGGG
CTGGGATTAAAAGCATACACAACCACCATCTGACTCTTTTTTCTTCTTCCTCCTCTTCTCCTTCCTCCTCCTCCTCTTCCTTTTG
CTTGGCATCCTAGGCTGGCTTCAGATTCACAGCAATTCTTCATAGGTTTCCATGTTCTGGGGTTACAGGTATGGGCCACCAT
ACCAGGGTCTCTTTGCAACTCCCATCTTCCTCCCGGTTTCTTGTTTTGATTAAGGATCTCAGTATCTAACTTAATTGACCTGTC
ACTTGCTATGTAGACTTGTGTTTTGTAAGGTATGAGTGAGGTATGGTGAGGTGAGAAGGGTACCTCAGAGGGCCCATCAC
TGAGAAATCCCTTCCTCCTGAAGTACCGGCCATGTAGTATGTAGCACCAGATGATGTAGTATGGAATAGAGTTTATTTAGG
ACATGGGAAGTAGAGTTGGGAAAGGAGGAGAGAGAGAGAAAGGAGGGGAGGAGAAGTAGTGGAGAGAGAAGAGGCC
CTCCAGGAACACCTGGAAGGCGGGGAAGAGGAGAGAAGGAGAAACAGGGCAGGGAGAGAAGGGGCAGGAAGTAAGAG
AATAAGACAAGTAAGTAAGTGAGCAGGAGAGCGAGGAGGGGGCAAACAGTCCTTATATAGTAGGCTAGGCATACCTGAC
TGTTGCCAGGTAACTATGGGGCGGAGCCTAGAAGGACTGCTTCTAGGATGTCTCAATTTCACAGGCATCTGCTTGCTTGTA
GTTCCCAAGGCTGAAATTAAAGATGTTGTAGCCACCACGTACAGCCTGTTTTTGTGTTTTGAGATAGATTCTTACTTAATGGT
GCAGCTTGGACTCAAACTATTTTATCCAGGTTTGCCTCGAACTCTTTAGCAATCTTCTTGCTTCACTCTATCAGAGGTATGGA
CCATCACTCTGGTCAACTGGTTTTTTTTTTTTCTCCCCAGATTGGAGCAATCTCTTATAGTGCAGGTTGGTTTTGAGCTCGA
GGCAATACTCCCGTCCTGCCTCAGCCTCTCAATGCTGGGATGACAAGCATATCCCAGGCAAGCTTTGAACTTGCGGCAATTC
TGCTTTAACCTCCTTAGTGCTCTCTACCATGAATCTATGGGAAGAAGAAATAATGGGGGCGGGGGGGGAAACAACCAACTC
TGGGCATCAGTTCGGATTAAGGTCGATCCGCGCATGCGTTCATTTAGTACCCGCGGCCCCGCCCCTGCAGCGAGCGATGAT
GATCACGTGACTAGTCCTGCGGGGCGGAGGCCATGTTGCGGGGCACCCACGTGAGGGCCGCACGTCCACGATCAGTCAC
GTGACCGTGGTGCGCCGCAGCCGCCGGGGCGCACCCGGCGAGAGGCAGCGGCAGTGATGGACGGGTCCGGGGAGCAG
CTTGGGAGCGGCGGTGAGGCGGGAGGCGGAGGACTAGGCCCGGTCCAAGAACCCTAGGACCCCTCCGGCTTTGGGCTCG
GGCGGGAGCAGGCTGGGGCGCGCGGATCCATTCCCACCGGCTCATCCGCACCCCGAGAGCGGACATCCGCGTGCGCGCC
CCCGGGCAGGCCCGGGCTTGTCGCTGGCGCCACTTCCTGCTGGTGGCCTGGGATGGGACAGAAGGCCAGCGCCACCTCCT
CCCACCCCCAGCTGGGGGTCTGTTTGCTTTTGGCATTCTGCTCTCTGGGTTTGCTGTGGAGCTGGGATGCAGGCCGGGTCC
CGCCCCCTGTCCATCAGAAGCAGTAGCCAGGCCTTCCATGCTACTTGTCACTACTAGGGTCCCCAGCTCTGTCTCCCCTCAG
GGTTATGAGCCTACCTATCCATCCCCCTGACTCTCCCTGGGACCCAGGAGTCCAGGCACCCCTTTCCTCCTCTCTCCCCCAG
GGCCCACCAGCTCTGAACAGATCATGAAGACAGGGGCCTTTTTGCTACAGGGGTGAGTGCGATGCTACTAGTGTGGCGGG
ATGGGCTTTCAGAACACCGCTTGGTTCTCAACATTCTGCTCCTCTCCCCCCTTTCCATTCACATGTAGTTTCATCCAGGATCG
AGCAGGGAGGATGGCTGGGGAGACACCTGAGCTGACCTTGGAGCAGCCGCCCCAGGATGCGTCCACCAAGAAGCTGAGC
GAGTGTCTCCGGCGAATTGGAGATGAACTGGACAGCAATATGGAGCTGCAGAGGTGTGCTTCCTGGGACCTGGGGTCCGT
CAAGGGGTCTCCTGCCGAACTGGGCACTGTTGTTCTTCTCCCAAGAGACTAGGTATCCTCCACTCAACTCAGATAGAATCCA
GAGCTTGTTTACGTGGTGGGCCAGCCCCTTACCCTTGAGCCGCATCCCTTGCTTGGTGGGTGTCAGTCTCTTGCTCGTGGAT
GCTTGGCAGGTGCCATACCTCCAGCTGGTTATGGCGGGTTCTAGTAGGCGGTGCTCTGCTACCAGGCTGTGCTCACAGCCC
CTCACTGGTGACTGCTAGGTGGAGCTCTCTACCTTTGAGCTTCTCACTTGTGGATGCTGTGCAAATGCTGGACCATGAAGCC
GTGGGTCCAGCCCCTCACGGCTGAGCCATGACCCAGCTCTCCACGTGTAGATATTTAGGAAAACATGCTTTTGCTCAGTCA
AGCCCCAGTCCACATTCCCCAGGACCCTGAATTTACAATTCAAGGTCCCACTTTCTTTGCTTTCTTAGGTGTACGTCTTGTCT
CCTTCCCAGTCTGCTAGCCATAGTTTCAGCCTGGGCTGGTCCTTGTGTCCTTCTCTGTAGTCTGGGGGAAAATGTGGGAACT
CCCATACTGGGCCCGACATCTCACCCAGCGTCTGTTTGCCCCTGTCCTGTAGGATGATTGCTGACGTGGACACGGACTCCCC
CCGAGAGGTCTTCTTCCGGGTGGCAGCTGACATGTTTGCTGATGGCAACTTCAACTGGGGCCGCGTGGTTGCCCTCTTCTA
CTTTGCTAGCAAACTGGTGCTCAAGGTAGGCAGCCGGACGAGCCCAGAGGTGCACCCCGCTCAGGTCTGTGAGGACCAGG
GAACAGAGAGAGATGGCTGTGTAATAAATGCCTGTACCTTCATTTAGTCATTCCACAAATGTATCGGCCCTAATGTGTGGT
GGGCTATCTCCAGCACCTGAACTCTGCTCCAAACAGCGCAAGCTAGCCCTTCCTTGATGGCGCTCTGATTGATGGTGGATA
CATGTAAGGTAGACTATTGAGATGGGCCAGAGAAACCTAGAAAGATTTCTCAGTGTAGGTGGTCTTAAACTGATCTGGTGG
CACATGCCTGTAATTCCAGGACTTGCGGTAGGAGTTGAAGGTTAGCTGCAGTTAAATACTGAGTTTCAGGCTATCCTGAGC

TACCTAAACCTAAGACCTATTTTTTTTGGGGGGGTTTTGTTTGTTTATTTGTTTTTTGTTGTTGTTGTTTTTTTTTTGAGACAG
GGTTTCTCTGTGTAGCCCTGGCTTGTCCTGGAACTCACTCTGTACACCAGGCTGGCCTTGAACTCATAAATCTACTTGCCTCT
GCCTCCTGAGTGCTGGGATAAAAGGCGTGCGCCACCACGCCCGGCTTCATTACATTTTTTAAAAAAGATTTATTTACTTATTT
TATTTATGTGAGTACATTGTAGCTGTCTTCAGACACTCCAGAAGAGGGGGGCAGATCTCATTACTGATGGTTGTGAGTCAC
CATGTGGTTGTGGGATTTGAACTCTGGACCTTCGGGAGAGCAGTCAGGGCTCTTAACTGCTGAGCTCTCTAGCCCTGACCT
AGTTTATTTATTTATTTATTTTTTAATAAAAGCAAACAAAAACAAAGACAGAAATGGACGTGACAGTAGGTGTGGTAGTGTA
GCTGAGTTTTGGGGGCCTGAGCATAACATGGATGAAGCCTTAGGTTCTGTCTCCTATCAGCATACACACAAATACCAAAGA
GGCGCTGGGACTGCAGATCAGCTGGTGGTGCTTGGCTGGCATGTGTCCTGGCCCTGGGTCAGTGCCACATGAACTAGGG
GTGGTTGGAACATGCCTCCAGTGCTAGCACTTGGAAGTTGGAGGTAGGAGGATCACAAGTTCAAGACTAGGCTGTGGTGG
GGTGTGTTGGAGCAGGAAGTTGCTGCAGAGCCACTGTGGCATATTTTACTTGTTATTTGTAGTGCTACTGTCACATTTGGG
ACACTCTTGATTGTCCTCCATGCCATCCCCCACCTCCTTGATGAGGTTTCATGCCTGAGCTGACGGGTCTTCAGTATTGGAG
GTGAAAGGAATGTAGGTCAGGAAGAGAGCATTGTTCCAGTCAGGAGAGCAGAGCCTCAGTTGGCCAGGAGGTGGTCTTC
TCTGGTCTAGAAAACCACTCTAGGAAGTGACTTAGGCAGGCCGGGCAGTGGTGGCGCACGCCTTTAATCCCAGCACTCGG
GAGGCAGAGGCAGGCGGATTTCTGAGTTTGAGGTCAGCCTGGTCTTGAGCCTTACCTCAGCCTTTTGGTTTTTACCTAGAG
GGTGCTGAGGAGTCAGGGCTCCTGAGCAGGTAAGGGAAGCTTTAGTTTATAATTAGTAGAGGAGAGACCGCTTAGCAGA
GGCAGAGGGTTAAAAGCAAGGGCTTGAGATCACCTCTGGGCAGTGGGGACAAGATTCAGTCCCCAAGTGTAATCTTCCCA
CTCCTGCAGGCCCTGTGCACTAAAGTGCCCGAGCTGATCAGAACCATCATGGGCTGGACACTGGACTTCCTCCGTGAGCGG
CTGCTTGTCTGGATCCAAGACCAGGGTGGCTGGGTGAGACCCCTCAGGCCTAGCTATACTTGAGACCTTCCTGGTGCTGTG
ATCCTTTAATACACTCCTCATATTATGACCCCCAGCCATTAAGTTATTTCTTTTTTTTTTCTTTAAAGATGTATTTATTTATTTTA
TGTATGTGAGTCCACTGTAACTGTGCAGATGGTTGTGAGCCTTCATGTGGTTGTTGGGAATTGAATTTAGGACTCCTACGCA
CTCTGGTCAACCCAGCTTGCTTAGTCCCTGCTTGCTCTGGCCTAAAGATTTATTATTATCTTTATTTAATATAATCTTTATTATA
TTAAAGGTTATTTTAAGTAAACCGTTGCTGTCTTCAGACACACCAGAAGAGGGCGCCAGATCTCATTATGGGTGGTTGTGA
GCCACTATGTGGTTGCTGGGATTTGAACTCAGGACTTTTGGAAGAGTAATCAATGAGCCATCTTGCCAGCCCTATAAAGTTA
TTTCATTGCTACTTCATAACTGTAATTTTGCTGCTGTTATGAATCATAATGTAAATATTTGATACGTGACCCCTCTGGGATCAT
GAACTAAAAGGTTGAGAGCCACTTTTTCAGATCTAAGGGTCAGCACAGAGGTGCCCCCGGGCATTCAGACAATGATCTAAG
CTAGGTATCCTTAGATCTACTATCTTAGTGCCTCTGGTACCCACTGACTTCCATGGCCTGACTTGATTGCTCCCTTCCTTTCTG
GAATCTCTCACATGCACTGGGTGATCCTTTGACGACCATCTTGTTGTGTTTCTCGTTTATTTATTTACATCGTGAGATGGCCT
CCTGTATCTCAGGCTGTCTTCAGACTCACTCTGTAGCTGAAGATGCCCTTGACCATTTGAGCTCCTGCTTCCACATGTCAGTG
TAGGAGCTAATGGGATAGACAGACCCCAGGCCTTGTGCGCTCTAGGCAAGCACCCTACAGGCTGAGCCTTTGTCCTCCCTG
TCATGCATACAAGCCTGGTCTGGAAGTTACTATGTAGCCCATACTAGTCCAAACATGTGGTCTTCAGTCTTACCTTCTCAAGT
GCTGAGATTACTGCTATGGGCTACCACTTCCAGATGTTAATCACGGGTTTTTGGTTTTTTATTTTGTTTTGTTTTGTTTTGTTT
TCATTTTGTTTTGTTTTCCCATTTTGGGATCGTGGGTTGAGTGGGATACTTTTTACATTTGCGCGCACGCGCGCGCGCGTGT
GTGTCCTTTTGTGCATGAGCTATCTTGCTGGCCCTAAGTTTTGTTTTCTGAGTGAGGATCTCAATAAACTTCACAGGTTGGCA
TTAGGCTTACAGCCCTCCTTCCTAGGGTTCCTGAGTGCTGGGGTTATAAGCCCAGGAGCGCCTTAGCATCCCTTCATGGGA
AATCTCTTTCTTCCCCCTGCAATTTGGTATTGAAGTCACACCCATCTCTCTGTTCTCAGGAAGGCCTCCTCTCCTACTTCGGGA
CCCCCACATGGCAGACAGTGACCATCTTTGTGGCTGGAGTCCTCACCGCCTCGCTCACCATCTGGAAGAAGATGGGCTGAG
GCCTCCCACTGCCTTGGACTGTGTCTTTTCTTCATAAATTATGACATTTTCCTGGGATGAATGGGGGAAGGGGAAAGGCATT
TTTCTTACTTTTGTAATTATTGGGAGGGGTGGGAATGGTGGCCTGGGGAGGCGCCAATAAACCTCAGGTCCACTTTGGATT
GTATGGTCCCTTGTCCGCCCAGCTGCCATCCCAAGCACAGGCGCCAGGCCCACCTGGTATCCCTGAGGCTCCAATCAGGGA
CCCGCTCCATAAAGAGTACACACCGCAGCTGCAGAGCTGTCTTCAGCCCTGGGGACAGGAGCCTGGAATTCCAGAGATCCT
GCAGATTCTGAAAGGACAAGATGGAGGGAGGGAGGGAGGGAGGGAGGGAGGGAGGGAGGGAGGGAGGGAGGGAGGGAGG
GAGGGAGGGAGGAGGCCACCGGAACTGGAGCAGACTCCTAGATGCTGGATTACCAGAGGTGCCAGAAGGGAAGAGGAA
GCCATTTTAAGGGGACTTGGTCTTTTGTTCCACCCTCAATCCCCCAGTCTGAGATTCTGCCACTCAAATTTGTGTACCTCTCT
CCTTTCCTTGTCCCCTGTGGCTTCCGGGTTTTATCTTTTTCCACCTTTACAGCCTTGTCCAGGCCTGTCGGGTTGAAGGCCAG
AGGTCAGGTTCTGGAGCACTGTGGTTAATGAGTAACTCTGACCCCCAAATCAACAGACCACCGCAGACGTCAAGTCAGGA
GAAAGATACGTGTAGGCTAGCCACTCCAGAGCCGTACAGCTGCCTGACCACACAGGGAAAACAGACCACAAGCCCCTTAG
CCGGGGGACTTCTGGCTGTCAGCCCGGGTGTGGCCTGCCGCCCGCCCCACTGCCTAGCTGAGCTCAGCGTGACTCAGCAG
AACTGGCCTTGCTACCCCTTCCACTAAGGGCCTCAGCAGCACATTCTTCCTGCTCCGCGTGGCTCCCTTGACCCATCTTACTG
TTTCTTCCTTTAGCCCCTTTTCATGATTGGGCTCGTTTCCCTTTGCTCTCTTCCCAGGCTTCTGAGATTAGACCCTGGTATGAG
CCCGTCCTGTCCTCAAAAGTCCAGTTGGGCCTTGCATGCCCCAACTGTTCTGCGTAAGACTGACTGTCTGTTTCTGGGTCCT
GAGTTCTTGCT **-3'**

Unknown Band (Dynein)

Unknown forward

5'-

AAGCTCGGGCACCGTGGCATTCGCTAGTTACCCTCTTAAAAGCCTCCCTGGGGTC

GCCGGCTTACCTTCTTT

CCGGGGGTTCCCCGGGTTGGCCACATTGACCATGTATGACTGTCTCAGCCTGAAT

CCTGTCTGTGGACGGAACCTGGCTACTGCAGGAGGCAGACCCCCTGACCCCTCTT

GCTGATGACCTCTGCCTTCATATCCTCCTCATCCGCTCTGACTTTCTCTTTGCCGA

CCTTCTCCGCTTCCCCCCCCCCCACCTGGATCAGCTTGACTTTATTCTCATTCTTCT

GCTTCAACTCATCTCCTCTCTCAACTTATTGCTTTTTATATCGTCCACCTATTTTTG

TAGGAGCCCTGTCGGTGCTGAAACTCGCTGTATAGAGTGCTGCTTGCTTTTACTTT

CGTCATACTGCCCCTGCCGCCCCCATGTCCGAAGCACTCCCTTAAGCCCTTTTGTC

CCCCAAACCGAAATTATATTGACATTTTTGAATCTGGTCACATTGACTCCTATCTT

ACACGGACTATGTCTTACTATATGTAATTCCCTGTAAACACTTTCCTCGATATAA

AATTTCCTTCGATATATTGAAAAGACTCCAGAGAGTCCCTGGGAGTTGGGGGCAC

CACGGCTGCTCTCCTGAATCTAAAGGCAAGCATCACACAGACCACCATCTCTAGG

CCGCCTCCTGGCTCCTCCCTCCCTAGGTGGACTACCTAAAGGCCAATCTGGCCAT

GCAGGATACTGATCTGAATCAGAAAATGAGAATGCAGACAAGCCTGATCCAGGT

GGTGGGTGTGGAGACGGAAAGGTCACCACGGA -3'

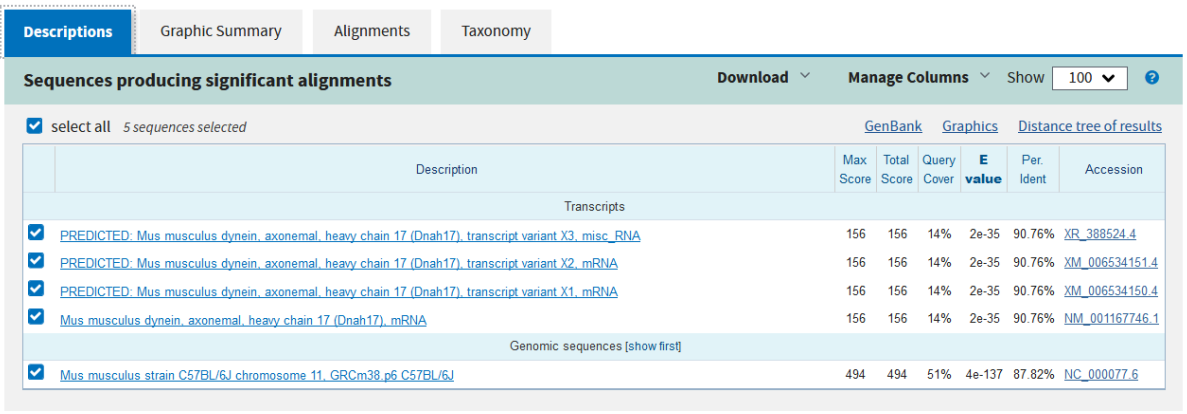

Descriptions | Graphic Summary | Alignments | Taxonomy

Sequences producing significant alignments — Download — Manage Columns — Show 100

select all 5 sequences selected — GenBank | Graphics | Distance tree of results

Description	Max Score	Total Score	Query Cover	E value	Per. Ident	Accession
Transcripts						
PREDICTED: Mus musculus dynein, axonemal, heavy chain 17 (Dnah17), transcript variant X3, misc_RNA	156	156	14%	2e-35	90.76%	XR_388524.4
PREDICTED: Mus musculus dynein, axonemal, heavy chain 17 (Dnah17), transcript variant X2, mRNA	156	156	14%	2e-35	90.76%	XM_006534151.4
PREDICTED: Mus musculus dynein, axonemal, heavy chain 17 (Dnah17), transcript variant X1, mRNA	156	156	14%	2e-35	90.76%	XM_006534150.4
Mus musculus dynein, axonemal, heavy chain 17 (Dnah17), mRNA	156	156	14%	2e-35	90.76%	NM_001167746.1
Genomic sequences [show first]						
Mus musculus strain C57BL/6J chromosome 11, GRCm38.p6 C57BL/6J	494	494	51%	4e-137	87.82%	NC_000077.6

Unknown reverse (lower confidence)

3'-

CGGGGCGGTGGTGCCGATCCCATGGTATCTACTTCTTCCTAGTGCTCTCCTATAA

GATTTCAAAAAAAAAGG

AAGGCTCAGGAAACGCTTTTTTTAATCGGGTTTTTTCCTTGAACAAAGATTAATT

GGGTTTCTCACAACTTCCTCCCTGGGTGCGCTGGGCCGTAGGATTAAATAGTGAG

CCCTCGTTTTGGGTTTTTTTCCCGGGGGGGTTTTTTTTTTGGGGGGTGCTCCAAAA

ACAAAAAACACCCGCCCGGAGAAAAATAATTCCTTTTTCCTTTTTTTCTTTTTTTT

TTTCCTCCTCCCAAACAAAACAACCAAAAAAAAACAAAAAAAAACCAATTTTTT

TTTTTTTTTT -5'

Note: No significant similarity found

Full western blot from gene characterisation as displayed in Chapter 4, Figure 4.3

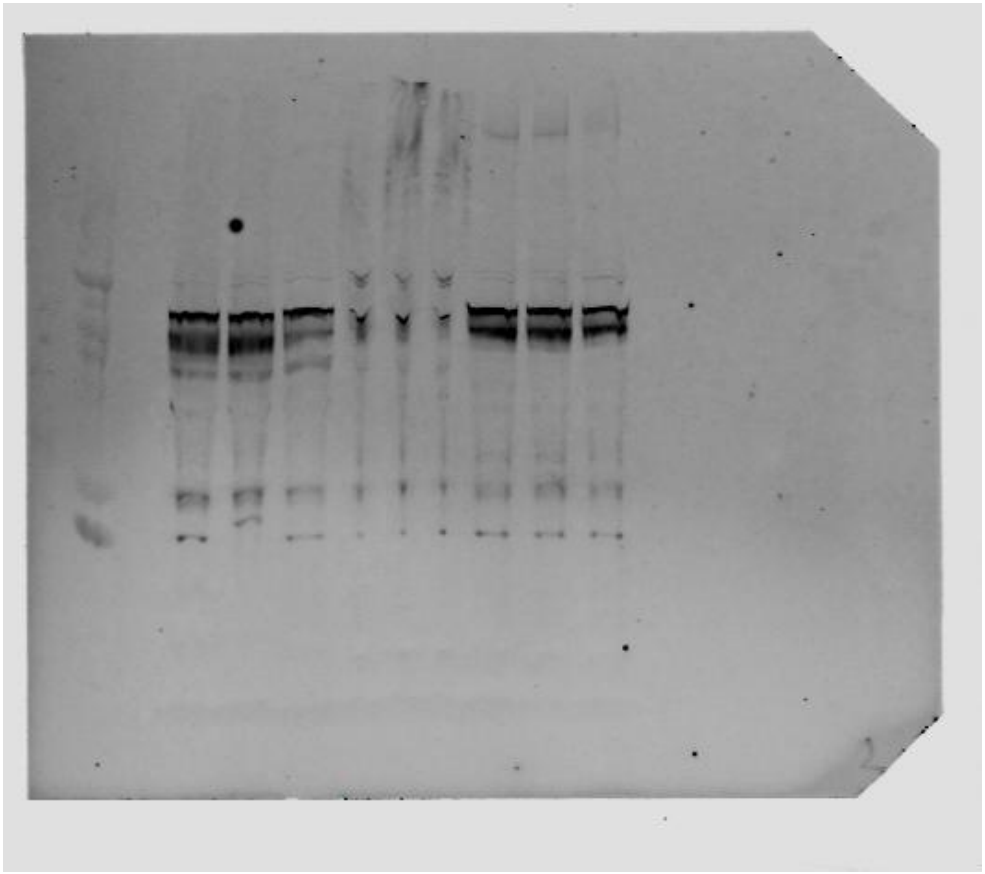

Full mitochondrial swelling traces from Chapter 4, Figure 4.15

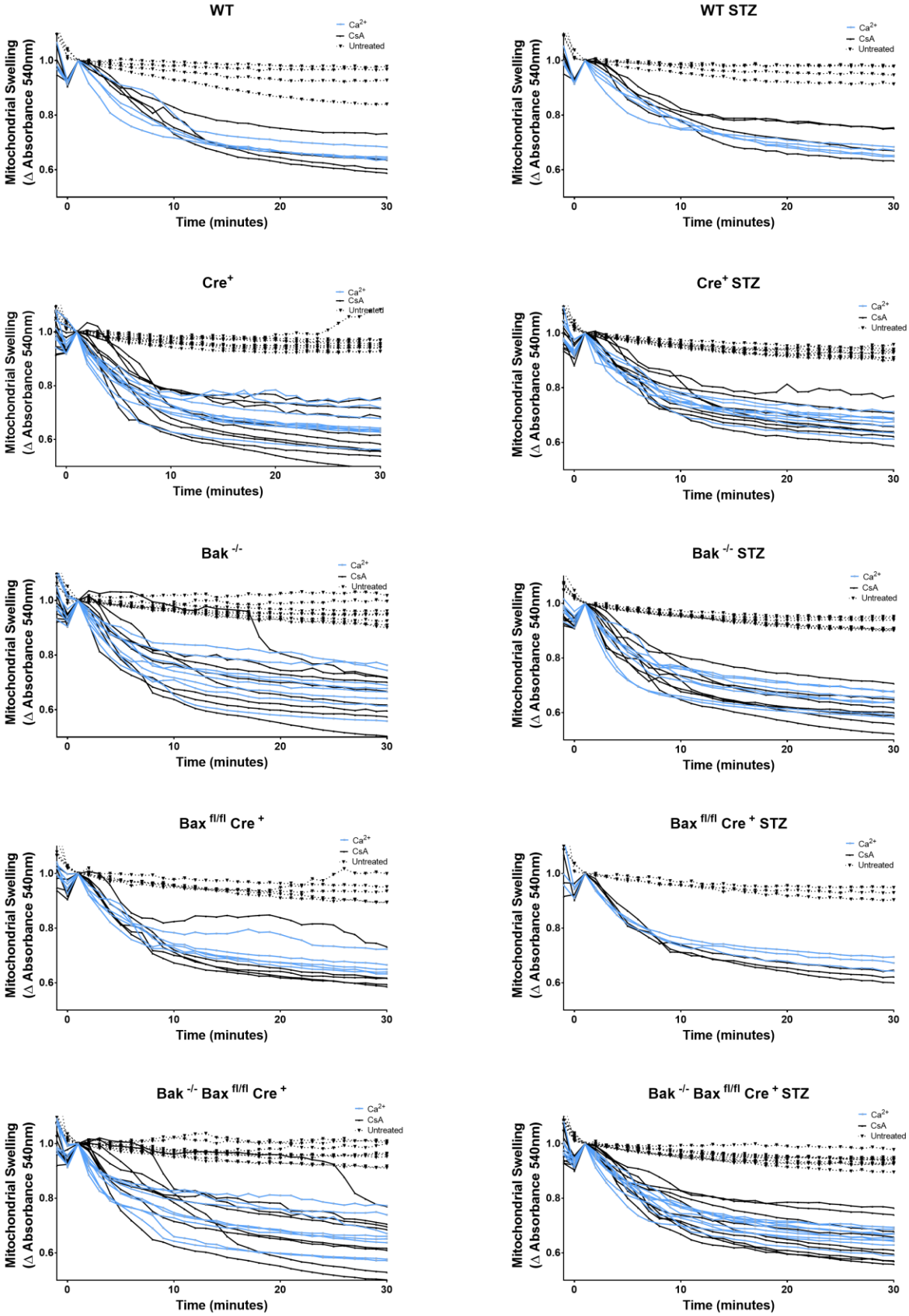

Statistical analyses of data presented in Chapter 4

Two-way ANOVA with Bonferroni post hoc test performed where F was >0.05.

Genotype: number of Families: 2

number of comparisons: 10

Table 4.1

12 weeks – water intake

Source of Variation	% of total variation	P value	P value summary	Significant?
Interaction	0.8411	0.6139	ns	No
genotype	0.7198	0.6824	ns	No
diabetes	58.27	<0.0001	****	Yes

Bonferroni's multiple comparisons test	Mean Diff.	95.00% CI of diff.	Significant?	Summary	Adjusted P Value
CIT - STZ					
WT	-13.16	-20.65 to -5.667	Yes	**	<0.01
Cre+	-13.72	-18.4 to -9.033	Yes	**	<0.01
Bak -/-	-15.24	-21 to -9.485	Yes	**	<0.01
Bax fl/fl Cre+	-16.79	-24.04 to -9.533	Yes	**	<0.01
Bak -/- Bax fl/fl Cre+	-11.88	-16.43 to -7.337	Yes	**	<0.01

12 weeks – food intake

Source of Variation	% of total variation	P value	P value summary	Significant?
Interaction	5.621	0.0022	**	Yes
genotype	1.536	0.3089	ns	No
diabetes	52.29	<0.0001	****	Yes

Bonferroni's multiple comparisons test	Mean Diff.	95.00% CI of diff.	Significant?	Summary	Adjusted P Value
CIT - STZ					
WT	-2.053	-3.262 to -0.843	Yes	**	<0.01
Cre+	-2.63	-3.386 to -1.873	Yes	**	<0.01
Bak -/-	-1.404	-2.334 to -0.4739	Yes	**	0.0006
Bax fl/fl Cre+	-3.246	-4.417 to -2.074	Yes	*	<0.01
Bak -/- Bax fl/fl Cre+	-1.443	-2.177 to -0.7097	Yes	**	<0.01

Within each column, compare rows (simple effects within columns)						
Number of families	2					
	1					
Number of comparisons per family	0					
	0					
Alpha	.05					
Bonferroni's multiple comparisons test	Mean Diff.	95.00% CI of diff.	Significant?	Summary	Adjusted P Value	
CIT						
WT vs. Cre+	0.05197	-1.127 to 1.231	No	ns	>0.9999	
WT vs. Bak -/-	-0.872	-2.108 to 0.3641	No	ns	0.4599	
WT vs. Bax fl/fl	0.1733	-1.209 to 1.555	No	ns	>0.9999	
WT vs. Bak -/- Bax fl/fl Cre+	0.6176	-1.796 to 0.561	No	ns	>0.9999	
Cre+ vs. Bak -/-	0.924	-1.781 to -0.06709	Yes	*	0.0253	
Cre+ vs. Bax fl/fl	0.1214	-0.9352 to 1.178	No	ns	>0.9999	
Cre+ vs. Bak -/- Bax fl/fl Cre+	0.6695	-1.441 to 0.102	No	ns	0.1449	
Bak -/- vs. Bax fl/fl	1	-	No	ns		
Bak -/- vs. Bak -/- Bax fl/fl Cre+	0.045	0.07501 to 2.166	No	ns	0.0868	
Bax fl/fl vs. Bak -/- Bax fl/fl Cre+	0	-0.6025 to 1.111	No	ns	>0.9999	
STZ						
WT vs. Cre+	-0.2544	-1.847 to 0.7909	No	ns	0.3439	
WT vs. Bak -/-	0.5252	-1.545 to 0.4947	No	ns	>0.9999	
WT vs. Bax fl/fl	0.2231	-1.341 to 0.895	No	ns	>0.9999	
WT vs. Bak -/- Bax fl/fl Cre+	-1.02	-2.234 to 0.1941	No	ns	0.1785	
Cre+ vs. Bak -/-	0.008211	-1.008 to 0.9916	No	ns	>0.9999	
Cre+ vs. Bax fl/fl	0	-0.6881 to 0.6881	No	ns	>0.9999	
Cre+ vs. Bak -/- Bax fl/fl Cre+	0.3021	-1.292 to 1.592	No	ns	>0.9999	
Bak -/- vs. Bax fl/fl	-0.4945	-1.592 to 0.6026	No	ns	0.9999	
Bak -/- vs. Bak -/- Bax fl/fl Cre+	0	-0.3374 to 0.3374	No	ns		
Bax fl/fl vs. Bak -/- Bax fl/fl Cre+	0.517	-1.371 to 0.986	No	ns	0.8631	

12 weeks – urine output

Source of Variation	% of total variation	P value	P value summary	Significant?
Interaction	1.099	0.5361	ns	No
genotype	1.054	0.5571	ns	No
diabetes	53.14	<0.0001	****	Yes

Bonferroni's multiple comparisons test	Mean Diff.	95.00% CI of diff.	Significant?	Summary	Adjusted P Value
CIT - STZ					
WT	-13.27	-20.87 to -5.656	Yes	**	<0.0001
Cre+	-15.66	-20.42 to -10.9	Yes	**	<0.0001
Bak -/-	-11.56	-17.41 to -5.709	Yes	**	<0.0001
Bax fl/fl Cre+	-14.2	-21.57 to -6.835	Yes	**	<0.0001

Bak -/- Bax fl/fl Cre+	-10.39	-15 to -5.772	Yes	**	<0.0001

23 weeks - Water intake

Source of Variation	% of total variation	P value	P value summary	Significant?		
Interaction	1.912	0.1173	ns	No		
Row Factor	0.6611	0.6267	ns	No		
Column Factor	66.24	<0.0001	****	Yes		

Bonferroni's multiple comparisons test	Mean Diff.	95.00% CI of diff.	Significant?	Summary	Adjusted P Value
CIT - STZ					
WT	-25.31	-34.74 to -15.89	Yes	* ***	<0.0001
Cre+	-21.17	-26.56 to -15.78	Yes	* ***	<0.0001
Bak -/-	-17.98	-24.46 to -11.5	Yes	* ***	<0.0001
Bax fl/fl Cre+	-20.06	-28.78 to -11.33	Yes	* ***	<0.0001
Bak -/- Bax fl/fl Cre+	-15.14	-20.06 to -10.21	Yes	* ***	<0.0001

Within each column, compare rows (simple effects within columns)

Number of families	21
Number of comparisons per family	10
Alpha	0.05

Bonferroni's multiple comparisons test	Mean Diff.	95.00% CI of diff.	Significant?	Summary	Adjusted P Value
CIT					
WT vs. Cre+	-1.269	-9.573 to 7.035	No	ns	>0.9999
WT vs. Bak -/-	-3.064	-11.68 to 5.553	No	ns	>0.9999
WT vs. Bax fl/fl	-2.307	-12.23 to 7.618	No	ns	>0.9999
WT vs. Bak -/-	-2.262	-10.48 to 5.954	No	ns	>0.9999
Cre+ vs. Bak -/-	-1.795	-7.888 to 4.298	No	ns	>0.9999
Cre+ vs. Bax fl/fl	-1.038	-8.872 to 6.796	No	ns	>0.9999
Cre+ vs. Bak -/-	-0.9932	-6.505 to 4.518	No	ns	>0.9999
Bak -/- vs. Bax fl/fl	.7571	-7.409 to 8.923	No	ns	>0.9999
Bak -/- vs. Bak -/-	.8018	-5.172 to 6.775	No	ns	>0.9999
Bax fl/fl vs. Bak -/-	.04468	-7.697 to 7.786	No	ns	>0.9999
STZ					
WT vs. Cre+	2.875	-5.596 to 11.35	No	ns	>0.9999
WT vs. Bak -/-	.2684	-4.786 to 13.32	No	ns	>0.9999
WT vs. Bax fl/fl	.952	-6.975 to 12.87	No	ns	>0.9999
WT vs. Bak -/-	.9177	-0.2995 to 16.13	No	ns	0.0677
Cre+ vs. Bak -/-	.3931	-5.51 to 8.296	No	ns	>0.9999
Cre+ vs. Bax fl/fl	.0750	-7.936 to 8.086	No	ns	>0.9999
Cre+ vs. Bak -/-	.0425	-0.719 to 10.8	No	ns	0.1367
Bak -/- vs. Bax fl/fl	-9.943	-9.943	No	ns	>0.9999

		1.318	to 7.307	o	s	9
		3	-2.939	N	n	>0.999
	Bak -/- vs. Bak -/-	.648	to 10.24	o	s	9
		4	-2.775	N	n	
	Bax fl/fl vs. Bak -/-	.967	to 12.71	o	s	0.6907

23 weeks – food intake

Source of Variation	% of total variation	P value	P value summary	Significant?		
Interaction	3.715	0.0466	*	Yes		
genotype	1.184	0.5316	ns	No		
diabetes	49.23	<0.0001	****	Yes		

Bonferroni's multiple comparisons test	Mean Diff.	95.00% CI of diff.	Significant?	Summary	Adjusted P Value
CIT - STZ					
WT	-3.64	-5.452 to -1.828	Yes	* ***	<0.0001
Cre+	-2.919	-3.954 to -1.883	Yes	* ***	<0.0001
Bak -/-	-1.93	-3.177 to -0.6842	Yes	* **	0.0004
Bax fl/fl Cre+	-3.355	-5.033 to -1.677	Yes	* ***	<0.0001
Bak -/- Bax fl/fl Cre+	-1.777	-2.724 to -0.831	Yes	* ***	<0.0001

Within each column, compare rows (simple effects within columns)

Number of families	21
Number of comparisons per family	10
Alpha	.05

Bonferroni's multiple comparisons test	Mean Diff.	95.00% CI of diff.	Significant?	Summary	Adjusted P Value
CIT					
WT vs. Cre+	0.02667	-1.57 to 1.623	No	ns	>0.9999
WT vs. Bak -/-	-0.5466	-2.203 to 1.11	No	ns	>0.9999
WT vs. Bax fl/fl	0.3205	-2.229 to 1.588	No	ns	>0.9999
WT vs. Bak -/-	-0.672	-2.252 to 0.9077	No	ns	>0.9999
Cre+ vs. Bak -/-	-0.5733	-1.745 to 0.5982	No	ns	>0.9999
Cre+ vs. Bax fl/fl	0.3471	-1.853 to 1.159	No	ns	>0.9999
Cre+ vs. Bak -/-	-0.6986	-1.758 to 0.361	No	ns	0.6184
Bak -/- vs. Bax fl/fl	0.2261	-1.344 to 1.796	No	ns	>0.9999
Bak -/- vs. Bak -/-	0.1254	-1.274 to 1.023	No	ns	>0.9999
Bax fl/fl vs. Bak -/-	0.3515	-1.84 to 1.137	No	ns	>0.9999
STZ					
WT vs. Cre+	0.7478	0.8808 to 2.377	No	ns	>0.9999
WT vs. Bak -/-	0.163	0.5777 to 2.904	No	ns	0.5847
WT vs. Bax fl/fl	0.035	-1.943 to 1.873	No	ns	>0.9999
WT vs. Bak -/-	0.191	0.3891 to 2.77	No	ns	0.3315
Cre+ vs. Bak -/-	0.4152	-0.912 to 1.742	No	ns	>0.9999
Cre+ vs. Bax fl/fl	-0.323	-2.323 to 1.677	No	ns	>0.9999

		0.7828	to 0.7574	o	s	9
		0	-	N	n	>0.999
	Cre+ vs. Bak -/-	.4427	0.6648 to 1.55	o	s	9
		-	-2.856	N	n	
	Bak -/- vs. Bax fl/fl	1.198	to 0.4603	o	s	0.4101
		0	-1.239	N	n	>0.999
	Bak -/- vs. Bak -/-	.02753	to 1.294	o	s	9
		1	-	N	n	
	Bax fl/fl vs. Bak -/-	.226	0.2628 to 2.714	o	s	0.2017

23 weeks –urine output

Source of Variation	% of total variation	P value	P value summary	Significant?		
Interaction	2.041	0.1596	ns	No		
Row Factor	1.237	0.4019	ns	No		
Column Factor	59.29	<0.0001	****	Yes		
Bonferroni's multiple comparisons test		Mean Diff.	95.00% CI of diff.	Significant?	Summary	Adjusted P Value
CIT - STZ						
WT		-22.65	-32.38 to -12.93	Yes	**	<0.001
Cre+		-20.29	-25.84 to -14.73	Yes	**	<0.001
Bak -/-		-15.62	-22.31 to -8.934	Yes	**	<0.001
Bax fl/fl Cre+		-16.78	-25.79 to -7.779	Yes	**	<0.001
Bak -/- Bax fl/fl Cre+		-13.46	-18.54 to -8.385	Yes	**	<0.001

Table 4.3 Endpoint phenotypic measurements

Body weight

Source of Variation	% of total variation	P value	P value summary	Significant?		
Interaction	1.902	0.3385	ns	No		
genotype	2.982	0.1339	ns	No		
diabetes	41.94	<0.0001	****	Yes		
Bonferroni's multiple comparisons test		Mean Diff.	95.00% CI of diff.	Significant?	Summary	Adjusted P Value
CIT - STZ						
WT		6.375	1.051 to 11.7	Yes	*	0.0108
Cre+		7.636	4.42 to 10.85	Yes	****	<0.0001
Bak -/-		4.982	1.069 to 8.895	Yes	**	0.0057
Bax fl/fl Cre+		9.625	4.696 to 14.55	Yes	****	<0.0001
Bak -/- Bax fl/fl Cre+		7.249	4.277 to 10.22	Yes	****	<0.0001

Blood glucose

Source of Variation	% of total variation	P value	P value summary	Significant?		
Interaction	0.1801	0.9764	ns	No		
genotype	0.436	0.8887	ns	No		
diabetes	50.05	<0.0001	****	Yes		
Bonferroni's multiple comparisons test		Mean Diff.	95.00% CI of diff.	Significant?	Summary	Adjusted P Value
CIT - STZ						
WT		-15.65	-26.51 to -4.779	Yes	**	0.0013
Cre+		-15.57	-22.14 to -9.008	Yes	****	<0.0001

		-	-26.25	Y	**	<0.00
	Bak -/-	18.26	to -10.27	es	**	01
		-	-26.54	Y	**	0.000
	Bax fl/fl Cre+	16.48	to -6.418	es	*	2
		-	-23.15	Y	**	<0.00
	Bak -/- Bax fl/fl Cre+	17.08	to -11.02	es	**	01

Left kidney

	Source of Variation	% of total variation	P value	P value summary	Significant?
	Interaction	7.692	0.1013	ns	No
	genotype	2.043	0.7132	ns	No
	diabetes	2.735	0.0952	ns	No

Right kidney

	Source of Variation	% of total variation	P value	P value summary	Significant?
	Interaction	5.259	0.1190	ns	No
	genotype	1.262	0.7722	ns	No
	diabetes	5.816	0.0047	**	Yes

	Bonferroni's multiple comparisons test	Mean Diff.	95.00% CI of diff.	Significant?	Summary	Adjusted P Value
	CIT - STZ					
	WT	-0.05388	-0.1029 to -0.004898	Yes	*	0.0236
	Cre+	-0.02075	-0.05085 to 0.009346	No	ns	0.3686
	Bak -/-	-0.005866	-0.04241 to 0.03068	No	ns	>0.9999
	Bax fl/fl Cre+	-0.01066	-0.0576 to 0.03629	No	ns	>0.9999
	Bak -/- Bax fl/fl Cre+	-0.004775	-0.03212 to 0.02257	No	ns	>0.9999

Heart

	Source of Variation	% of total variation	P value	P value summary	Significant?
	Interaction	2.704	0.3394	ns	No
	genotype	3.761	0.1811	ns	No
	diabetes	18.42	<0.0001	****	Yes

	Bonferroni's multiple comparisons test	Mean Diff.	95.00% CI of diff.	Significant?	Summary	Adjusted P Value
	CIT - STZ					
	WT	-0.008417	-0.02895 to 0.04578	No	ns	>0.9999
	Cre+	-0.02501	0.002049 to 0.04797	Yes	*	0.0256
	Bak -/-	-0.03264	0.005179 to 0.06011	Yes	*	0.0116
	Bax fl/fl Cre+	-0.03669	0.002091 to 0.07128	Yes	*	0.0319
	Bak -/- Bax fl/fl Cre+	-0.03732	0.01646 to 0.05818	Yes	***	<0.0001

Left ventricle

	Source of Variation	% of total variation	P value	P value summary	Significant?
	Interaction	6.096	0.0360	*	Yes
	genotype	8.289	0.0080	**	Yes
	diabetes	13.84	<0.0001	****	Yes

	Bonferroni's multiple comparisons test	Mean Diff.	95.00% CI of diff.	Significant?	Summary	Adjusted P Value

CIT - STZ					
	-	-0.03036	N	n	>0.99
WT	0.002375	to 0.02561	o	s	99
	0	-0.005035	N	n	0.365
Cre+	.01125	to 0.02754	o	s	7
	0	0.008108	Y	*	0.001
Bak -/-	.02759	to 0.04708	es	*	6
	0	0.003236	Y		0.019
Bax fl/fl	.02864	to 0.05405	es	*	0
	0	0.009948	Y	*	0.000
Bak -/-	.02475	to 0.03955	es	**	1

Within each column, compare rows (simple effects within columns)

Number of families	2
	1
Number of comparisons per family	0
	0
Alpha	.05

Bonferroni's multiple comparisons test	Mean Diff.	95.00% CI of diff.	Significant?	Summary	Adjusted P Value
CIT					
	-	-0.04212 to	N	n	>0.999
WT vs. Cre+	0.01544	0.01125	o	s	9
	-	-0.05733 to	Y		
WT vs. Bak -/-	0.02964	-0.001945	es	*	0.0272
	-	-0.04913 to	N	n	>0.999
WT vs. Bax fl/fl	0.01773	0.01367	o	s	9
	-	-0.05825 to	Y	*	
WT vs. Bak -/- Bax fl/fl Cre+	0.03168	-0.005111	es	*	0.0088
	-	-0.03233 to	N	n	
Cre+ vs. Bak -/-	0.0142	0.003926	o	s	0.2694
	-	-0.0257 to	N	n	>0.999
Cre+ vs. Bax fl/fl	0.002294	0.02111	o	s	9
	-	-0.03261 to	N	n	
Cre+ vs. Bak -/- Bax fl/fl Cre+	0.01625	0.0001151	o	s	0.0531
	0	-0.01264 to	N	n	>0.999
Bak -/- vs. Bax fl/fl	.01191	0.03646	o	s	9
	-	-0.02 to	N	n	>0.999
Bak -/- vs. Bak -/- Bax fl/fl Cre+	0.002043	0.01591	o	s	9
	-	-0.03722 to	N	n	
Bax fl/fl vs. Bak -/- Bax fl/fl Cre+	0.01395	0.00932	o	s	0.8915
STZ					
	-	-0.02503 to	N	n	>0.999
WT vs. Cre+	0.001806	0.02142	o	s	9
	0	-0.02459 to	N	n	>0.999
WT vs. Bak -/-	.00033	0.02525	o	s	9
	0	-0.01353 to	N	n	>0.999
WT vs. Bax fl/fl	.01329	0.0401	o	s	9
	-	-0.0267 to	N	n	>0.999
WT vs. Bak -/- Bax fl/fl Cre+	0.004557	0.01758	o	s	9
	0	-0.01887 to	N	n	>0.999
Cre+ vs. Bak -/-	.002136	0.02314	o	s	9
	0	-0.008129	N	n	
Cre+ vs. Bax fl/fl	.01509	to 0.03832	o	s	0.6561
	-	-0.02037 to	N	n	>0.999
Cre+ vs. Bak -/- Bax fl/fl Cre+	0.002751	0.01487	o	s	9
	0	-0.01196 to	N	n	>0.999
Bak -/- vs. Bax fl/fl	.01296	0.03788	o	s	9
	-	-0.02469 to	N	n	>0.999
Bak -/- vs. Bak -/- Bax fl/fl Cre+	0.004887	0.01492	o	s	9
	-	-0.03999 to	N	n	
Bax fl/fl vs. Bak -/- Bax fl/fl Cre+	0.01784	0.004297	o	s	0.2293

Liver

Source of Variation	% of total variation	P value	P value summary	Significant?
Interaction	0.7772	0.8908	ns	No
genotype	11.61	0.0033	**	Yes
diabetes	0.6925	0.3	ns	No

Within each column, compare rows (simple effects within columns)

Number of families	2
Number of comparisons per family	1 0
Alpha	0 .05

Bonferroni's multiple comparisons test	Mean Diff.	95.00% CI of diff.	Significant?	Summary	Adjusted P Value
CIT					
WT vs. Cre+	-0.04311	-0.3415 to 0.2553	No	ns	>0.999
WT vs. Bak -/-	-0.1391	-0.1706 to 0.4488	No	ns	>0.999
WT vs. Bax fl/fl	-0.1199	-0.2263 to 0.4661	No	ns	>0.999
WT vs. Bak -/- Bax fl/fl Cre+	-0.1506	-0.1462 to 0.4473	No	ns	>0.999
Cre+ vs. Bak -/-	-0.1822	-0.4012 to 0.03679	No	ns	0.1894
Cre+ vs. Bax fl/fl	-0.163	-0.1052 to 0.4312	No	ns	0.8486
Cre+ vs. Bak -/- Bax fl/fl Cre+	-0.1937	-0.394 to 0.006634	No	ns	0.0659
Bak -/- vs. Bax fl/fl	0.01917	-0.2998 to 0.2615	No	ns	>0.999
Bak -/- vs. Bak -/- Bax fl/fl Cre+	-0.01149	-0.2052 to 0.2282	No	ns	>0.999
Bax fl/fl vs. Bak -/- Bax fl/fl Cre+	-0.03066	-0.2357 to 0.297	No	ns	>0.999
STZ					
WT vs. Cre+	-0.08785	-0.3627 to 0.187	No	ns	>0.999
WT vs. Bak -/-	-0.1917	-0.1062 to 0.4896	No	ns	0.6830
WT vs. Bax fl/fl	-0.1412	-0.1793 to 0.4618	No	ns	>0.999
WT vs. Bak -/- Bax fl/fl Cre+	-0.07763	-0.1887 to 0.344	No	ns	>0.999
Cre+ vs. Bak -/-	-0.2795	0.03147 to 0.5276	Yes	*	0.0163
Cre+ vs. Bax fl/fl	-0.2291	-0.4579 to 0.0039	No	ns	0.1875
Cre+ vs. Bak -/- Bax fl/fl Cre+	-0.1655	-0.3746 to 0.04368	No	ns	0.2549
Bak -/- vs. Bax fl/fl	-0.05047	-0.3484 to 0.2474	No	ns	>0.999
Bak -/- vs. Bak -/- Bax fl/fl Cre+	-0.1141	-0.3527 to 0.1245	No	ns	>0.999
Bax fl/fl vs. Bak -/- Bax fl/fl Cre+	-0.0636	-0.33 to 0.2028	No	ns	>0.999

Figure 4.6 Kidney to body weight ratio

Source of Variation	% of total variation	P value	P value summary	Significant?
Interaction	2.355	0.3694	ns	No
genotype	0.6662	0.8728	ns	No
diabetes	48.06	<0.0001	****	Yes

Bonferroni's multiple comparisons test	Mean Diff.	95.00% CI of diff.	Significant?	Summary	Adjusted P Value
CIT - STZ					
WT	-7.152	-10.81 to -3.497	Yes	**	<0.0001
Cre+	-5.083	-7.93 to -2.236	Yes	**	<0.0001

		-	-6.828	Y		0.013
	Bak -/-	3.683	to -0.5375	es	*	7
		-	-8.74 to	Y	**	0.000
	Bax fl/fl Cre+	5.237	-1.734	es	*	8
		-	-6.719	Y	**	0.000
	Bak -/- Bax fl/fl Cre+	4.161	to -1.602	es	*	2

Figure 4.7 Urinary albumin excretion

Source of Variation	% of total variation	P value	P value summary	Significant?
Interaction	5.986	0.0246	*	Yes
genotype	7.984	0.0054	**	Yes
diabetes	31.71	<0.0001	****	Yes

Bonferroni's multiple comparisons test	Mean Diff.	95.00% CI of diff.	Significant?	Summary	Adjusted P Value
CIT - STZ					
WT	-15.9	-48.91 to 17.11	No	ns	>0.9999
Cre +	-33.28	-53.25 to -13.31	Yes	***	0.0001
Bak -/-	-27.02	-50.73 to -3.308	Yes	*	0.0174
Bax fl/fl Cre+	-61.41	-91.54 to -31.28	Yes	****	<0.0001
Bak -/- Bax fl/fl Cre+	-35.26	-54.33 to -16.19	Yes	****	<0.0001

Within each column, compare rows (simple effects within columns)

Number of families	2
Number of comparisons per family	10
Alpha	.05

Bonferroni's multiple comparisons test	Mean Diff.	95.00% CI of diff.	Significant?	Summary	Adjusted P Value
CIT					
WT vs. Cre+	-6.91	-38.26 to 24.44	No	ns	>0.9999
WT vs. Bak -/-	2.16	-30.26 to 34.58	No	ns	>0.9999
WT vs. Bax fl/fl	-0.425	-36.5 to 35.66	No	ns	>0.9999
WT vs. Bak -/- Bax fl/fl Cre+	5.149	-26.01 to 36.29	No	ns	>0.9999
Cre+ vs. Bak -/-	9.076	-13.63 to 31.77	No	ns	>0.9999
Cre+ vs. Bax fl/fl	6.485	-21.18 to 34.16	No	ns	>0.9999
Cre+ vs. Bak -/- Bax fl/fl Cre+	12.05	-8.789 to 32.89	No	ns	>0.9999
Bak -/- vs. Bax fl/fl	-2.581	-31.47 to 26.31	No	ns	>0.9999
Bak -/- vs. Bak -/- Bax fl/fl Cre+	2.981	-19.45 to 25.41	No	ns	>0.9999
Bax fl/fl vs. Bak -/- Bax fl/fl Cre+	5.562	-21.89 to 33.01	No	ns	>0.9999
STZ					
WT vs. Cre+	-24.29	-52.49 to 3.914	No	ns	0.1514
WT vs. Bak -/-	-8.963	-39.32 to 21.4	No	ns	>0.9999
WT vs. Bax fl/fl	-45.93	-78.87 to -12.99	Yes	*	0.0012
WT vs. Bak -/- Bax fl/fl Cre+	-14.22	-41.89 to 13.45	No	ns	>0.9999
Cre+ vs. Bak -/-	15.33	-9.825 to 40.48	No	ns	0.8349

		5.33	to 40.48	o	s	
		-	-49.84	N		
	Cre+ vs. Bax fl/fl	21.64	to 6.564	o	s	0.3000
		:	-11.76	N		>0.999
	Cre+ vs. Bak -/- Bax fl/fl Cre+	0.07	to 31.9	o	s	9
		-	-67.33	Y		
	Bak -/- vs. Bax fl/fl	36.97	to -6.605	es	*	0.0070
		-	-29.82	N		>0.999
	Bak -/- vs. Bak -/- Bax fl/fl Cre+	5.26	to 19.3	o	s	9
		:	4.039	Y		
	Bax fl/fl vs. Bak -/- Bax fl/fl Cre+	1.71	to 59.38	es		0.0138

Figure 4.8 Cystatin C

	Source of Variation	% of total variation	P value	P value summary	Significant?
	Interaction	5.681	0.0917	ns	No
	genotype	0.4231	0.9614	ns	No
	diabetes	14.88	<0.0001	****	Yes

	Bonferroni's multiple comparisons test	Mean Diff.	95.00% CI of diff.	Significant?	Summary	Adjusted P Value
	CIT - STZ					
	WT	14	-75.54 to 366.8	No	ns	0.4366
	Cre +	7.8	-120.6 to 136.3	No	ns	>0.9999
	Bak -/-	17	23.49 to 327.6	Yes	*	0.0154
	Bax fl/fl Cre+	23	26.88 to 436.4	Yes	*	0.0185
	Bak -/- Bax fl/fl Cre+	11	-8.478 to 238.9	No	ns	0.0811

Figure 4.9 Kim-1

	Source of Variation	% of total variation	P value	P value summary	Significant?
	Interaction	3.827	0.4861	ns	No
	genotype	1.461	0.8560	ns	No
	diabetes	0.004061	0.9517	ns	No

Figure 4.10 Glomerular sclerosis

	Source of Variation	% of total variation	P value	P value summary	Significant?
	Interaction	0.918	0.9142	ns	No
	genotype	10.76	0.0297	*	Yes
	diabetes	7.455	0.0063	**	Yes

	Bonferroni's multiple comparisons test	Mean Diff.	95.00% CI of diff.	Significant?	Summary	Adjusted P Value
	CIT - STZ					
	WT	-0.1676	-0.5951 to 0.2599	No	ns	>0.9999
	Cre+	-0.08137	-0.409 to 0.2463	No	ns	>0.9999
	Bak-/-	-0.1377	-0.4654 to 0.1899	No	ns	>0.9999
	Bax fl/fl Cre+	-0.2493	-0.647 to 0.1484	No	ns	0.5114
	Bak -/- Bax fl/fl Cre+	-0.2261	-0.5468 to 0.09469	No	ns	0.3338

Within each column, compare rows (simple effects within columns)

Number of families 2

Number of comparisons per family	10				
Alpha	0.05				
Bonferroni's multiple comparisons test	Mean Diff.	95.00% CI of diff.	Significant?	Summary	Adjusted P Value
CIT					
WT vs. Cre+	-0.1941	-0.6207 to 0.2324	No	ns	>0.9999
WT vs. Bak -/-	-0.1562	-0.5828 to 0.2704	No	ns	>0.9999
WT vs. Bax fl/fl	0.07004	-0.3976 to 0.5377	No	ns	>0.9999
WT vs. Bak -/- Bax fl/fl Cre+	-0.2213	-0.6479 to 0.2053	No	ns	>0.9999
Cre+ vs. Bak -/-	0.03794	-0.3205 to 0.3963	No	ns	>0.9999
Cre+ vs. Bax fl/fl	0.2642	-0.1422 to 0.6705	No	ns	0.6442
Cre+ vs. Bak -/- Bax fl/fl Cre+	-0.02716	-0.3855 to 0.3312	No	ns	>0.9999
Bak -/- vs. Bax fl/fl	0.2262	-0.1801 to 0.6326	No	ns	>0.9999
Bak -/- vs. Bak -/- Bax fl/fl Cre+	-0.06509	-0.4235 to 0.2933	No	ns	>0.9999
Bax fl/fl vs. Bak -/- Bax fl/fl Cre+	-0.2913	-0.6977 to 0.115	No	ns	0.4186
STZ					
WT vs. Cre+	-0.1079	-0.5142 to 0.2985	No	ns	>0.9999
WT vs. Bak -/-	-0.1263	-0.5327 to 0.2801	No	ns	>0.9999
WT vs. Bax fl/fl	-0.01161	-0.4466 to 0.4234	No	ns	>0.9999
WT vs. Bak -/- Bax fl/fl Cre+	-0.2797	-0.6794 to 0.12	No	ns	0.4688
Cre+ vs. Bak -/-	-0.01842	-0.3768 to 0.34	No	ns	>0.9999
Cre+ vs. Bax fl/fl	0.09625	-0.2943 to 0.4868	No	ns	>0.9999
Cre+ vs. Bak -/- Bax fl/fl Cre+	-0.1718	-0.5227 to 0.179	No	ns	>0.9999
Bak -/- vs. Bax fl/fl	0.1147	-0.2759 to 0.5052	No	ns	>0.9999
Bak -/- vs. Bak -/- Bax fl/fl Cre+	-0.1534	-0.5043 to 0.1974	No	ns	>0.9999
Bax fl/fl vs. Bak -/- Bax fl/fl Cre+	-0.2681	-0.6517 to 0.1155	No	ns	0.4716

Figure 4.11

4.11A PTC dilation

Source of Variation	% of total variation	P value	P value summary	Significant?
Interaction	1.372	0.7877	ns	No
genotype	16.05	0.0011	**	Yes
diabetes	12.42	0.0002	***	Yes

Bonferroni's multiple comparisons test	Mean Diff.	95.00% CI of diff.	Significant?	Summary	Adjusted P Value
CIT - STZ					
WT	-0.3079	-0.8414 to 0.2256	No	ns	0.6602
Cre+	-0.4582	-0.8671 to -0.04935	Yes	*	0.0203
Bak -/-	-0.2412	-0.65 to 0.1677	No	ns	0.6195
Bax fl/fl Cre+	-0.1678	-0.6641 to 0.3285	No	ns	>0.9999

Bak -/- Bax fl/fl Cre+	-0.3387	-0.739 to 0.06157	No	ns	0.1421

Within each column, compare rows (simple effects within columns)

Number of families	21
Number of comparisons per family	10
Alpha	.05

Bonferroni's multiple comparisons test	Mean Diff.	95.00% CI of diff.	Significant?	Summary	Adjusted P Value
CIT					
WT vs. Cre+	0.2620	-0.2703 to 0.7944	No	ns	>0.9999
WT vs. Bak -/-	0.2722	-0.2602 to 0.8045	No	ns	>0.9999
WT vs. Bax fl/fl	-0.2743	-0.8578 to 0.3093	No	ns	>0.9999
WT vs. Bak -/- Bax fl/fl Cre+	0.1797	-0.3527 to 0.712	No	ns	>0.9999
Cre+ vs. Bak -/-	0.01015	-0.4371 to 0.4574	No	ns	>0.9999
Cre+ vs. Bax fl/fl	-0.5363	-1.043 to -0.02915	Yes	*	0.0307
Cre+ vs. Bak -/- Bax fl/fl Cre+	-0.08237	-0.5296 to 0.3649	No	ns	>0.9999
Bak -/- vs. Bax fl/fl	-0.5465	-1.054 to -0.0393	Yes	*	0.0258
Bak -/- vs. Bak -/- Bax fl/fl Cre+	-0.09252	-0.5398 to 0.3547	No	ns	>0.9999
Bax fl/fl vs. Bak -/- Bax fl/fl Cre+	0.4539	-0.05322 to 0.9611	No	ns	0.1161
STZ					
WT vs. Cre+	0.1117	-0.3955 to 0.6188	No	ns	>0.9999
WT vs. Bak -/-	0.3389	-0.1682 to 0.8461	No	ns	0.5742
WT vs. Bax fl/fl	-0.1341	-0.677 to 0.4087	No	ns	>0.9999
WT vs. Bak -/- Bax fl/fl Cre+	0.1489	-0.35 to 0.6477	No	ns	>0.9999
Cre+ vs. Bak -/-	0.2272	-0.22 to 0.6745	No	ns	>0.9999
Cre+ vs. Bax fl/fl	-0.2458	-0.7332 to 0.2416	No	ns	>0.9999
Cre+ vs. Bak -/- Bax fl/fl Cre+	0.03716	-0.4007 to 0.475	No	ns	>0.9999
Bak -/- vs. Bax fl/fl	-0.4731	-0.9605 to 0.01431	No	ns	0.0637
Bak -/- vs. Bak -/- Bax fl/fl Cre+	-0.1901	-0.6279 to 0.2478	No	ns	>0.9999
Bax fl/fl vs. Bak -/- Bax fl/fl Cre+	0.283	-0.1958 to 0.7618	No	ns	0.9210

4.11B Tubular casts

Source of Variation	% of total variation	P value	P value summary	Significant?
Interaction	16.61	0.0002	***	Yes
genotype	17.75	0.0001	***	Yes
diabetes	7.878	0.0009	***	Yes

Bonferroni's multiple comparisons test	Mean Diff.	95.00% CI of diff.	Significant?	Summary	Adjusted P Value
CIT - STZ					
WT	0.01696	-0.275 to 0.3089	No	ns	>0.9999
Cre+	-0.01879	-0.2426 to 0.205	No	ns	>0.9999

	-	-0.3093	N	n	
Bak -/-	0.0855	to 0.1383	o	s	>0.9999
	-	-0.8628	Y	*	
Bax fl/fl Cre+	0.5912	to -0.3196	es	***	<0.0001
	-	-0.2624	N	n	
Bak -/- Bax fl/fl Cre+	0.04337	to 0.1757	o	s	>0.9999

Within each column, compare rows (simple effects within columns)

Number of families	2
Number of comparisons per family	1 0
Alpha	0 .05

Bonferroni's multiple comparisons test	Mean Diff.	95.00% CI of diff.	Significant?	Summary	Adjusted P Value
CIT					
WT vs. Cre+	0 .08667	-0.2047 to 0.378	N o	n s	>0.999 9
WT vs. Bak -/-	0 .06801	-0.2233 to 0.3594	N o	n s	>0.999 9
WT vs. Bax fl/fl	0 .05433	-0.2651 to 0.3737	N o	n s	>0.999 9
WT vs. Bak -/- Bax fl/fl Cre+	0 .06257	-0.2288 to 0.3539	N o	n s	>0.999 9
Cre+ vs. Bak -/-	- 0.01866	-0.2634 to 0.2261	N o	n s	>0.999 9
Cre+ vs. Bax fl/fl	- 0.03234	-0.3099 to 0.2452	N o	n s	>0.999 9
Cre+ vs. Bak -/- Bax fl/fl Cre+	- 0.0241	-0.2689 to 0.2207	N o	n s	>0.999 9
Bak -/- vs. Bax fl/fl	- 0.01368	-0.2912 to 0.2639	N o	n s	>0.999 9
Bak -/- vs. Bak -/- Bax fl/fl Cre+	- 0.005442	-0.2502 to 0.2393	N o	n s	>0.999 9
Bax fl/fl vs. Bak -/- Bax fl/fl Cre+	0 .008241	-0.2693 to 0.2858	N o	n s	>0.999 9
STZ					
WT vs. Cre+	0 .05093	-0.2266 to 0.3285	N o	n s	>0.999 9
WT vs. Bak -/-	- 0.03444	-0.312 to 0.2431	N o	n s	>0.999 9
WT vs. Bax fl/fl	- 0.5539	-0.851 to -0.2567	Y es	* ***	<0.000 1
WT vs. Bak -/- Bax fl/fl Cre+	0 .002244	-0.2708 to 0.2753	N o	n s	>0.999 9
Cre+ vs. Bak -/-	- 0.08537	-0.3302 to 0.1594	N o	n s	>0.999 9
Cre+ vs. Bax fl/fl	- 0.6048	-0.8715 to -0.338	Y es	* ***	<0.000 1
Cre+ vs. Bak -/- Bax fl/fl Cre+	- 0.04868	-0.2883 to 0.1909	N o	n s	>0.999 9
Bak -/- vs. Bax fl/fl	- 0.5194	-0.7862 to -0.2527	Y es	* ***	<0.000 1
Bak -/- vs. Bak -/- Bax fl/fl Cre+	0 .03669	-0.2029 to 0.2763	N o	n s	>0.999 9
Bax fl/fl vs. Bak -/- Bax fl/fl Cre+	0 .5561	0.2941 to 0.8181	Y es	* ***	<0.000 1

4.11C Glycogenated tubules

Source of Variation	% of total variation	P value	P value summary	Significant?
Interaction	0.6976	0 .9380	ns	No
genotype	1.445	0 .7987	ns	No
diabetes	22.18	< 0.0001	****	Yes

Bonferroni's multiple comparisons test	Mean Diff.	95.00% CI of diff.	Significant?	Summary	Adjusted P Value
CIT - STZ					
WT	-	-4.449	N	n	0.079

		2.149	to 0.1515	o	s	3
		-	-3.31 to	N	n	0.115
	Cre+	1.547	0.2156	o	s	8
		-	-3.463	N	n	0.064
	Bak -/-	1.7	to 0.06259	o	s	3
		-	-3.284	N	n	0.813
	Bax fl/fl Cre+	1.144	to 0.9959	o	s	1
		-	-3.53 to	Y		0.036
	Bak -/- Bax fl/fl Cre+	1.804	-0.07808	es	*	0

4.11D Glycogenated nuclei

	Source of	% of total	F	P value		
Variation		variation	value	summary	Significant?	
	Interactio		<			
n		18.26	0.0001	****	Yes	
			<			
	genotype	16.81	0.0001	****	Yes	
			<			
	diabetes	25.74	0.0001	****	Yes	

	Bonferroni's multiple comparisons	M	95.00%	S	S	Adjusted P
test		ean Diff.	CI of diff.	ignificant?	ummary	Value
	CIT - STZ					
		-	-1.302 to	Y	*	
	WT	0.7419	-0.1822	es	*	0.0038
		-	-1.979 to	Y	*	
	Cre+	1.55	-1.121	es	***	<0.0001
		-	-0.8504	N	r	
	Bak -/-	0.4214	to 0.007589	o	s	0.0567
		-	-0.5882	N	r	
	Bax fl/fl Cre+	0.0675	to 0.4532	o	s	>0.9999
		-	-0.8136	N	r	
	Bak -/- Bax fl/fl Cre+	0.3937	to 0.02624	o	s	0.0775

	Within each column, compare rows					
(simple effects within columns)						
	Number of families	2				
		1				
	Number of comparisons per family	0				
		0				
	Alpha	.05				
		M	95.00%	S	S	Adjust
	Bonferroni's multiple comparisons test	ean Diff.	CI of diff.	ignificant?	ummary	ed P Value
	CIT					
		-	-0.6031	N	r	>0.999
	WT vs. Cre+	0.04458	to 0.5139	o	s	9
		0	-0.5564	N	r	>0.999
	WT vs. Bak -/-	.002096	to 0.5606	o	s	9
		-	-0.7639	N	r	>0.999
	WT vs. Bax fl/fl	0.1517	to 0.4605	o	s	9
		-	-0.6034	N	r	>0.999
	WT vs. Bak -/- Bax fl/fl Cre+	0.04488	to 0.5136	o	s	9
		0	-0.4225	N	r	>0.999
	Cre+ vs. Bak -/-	.04668	to 0.5159	o	s	9
		-	-0.6392	N	r	>0.999
	Cre+ vs. Bax fl/fl	0.1071	to 0.4249	o	s	9
		-	-0.4695	N	r	>0.999
	Cre+ vs. Bak -/- Bax fl/fl Cre+	0.0002953	to 0.4689	o	s	9
		-	-0.6859	N	r	>0.999
	Bak -/- vs. Bax fl/fl	0.1538	to 0.3782	o	s	9
		-	-0.5162	N	r	>0.999
	Bak -/- vs. Bak -/- Bax fl/fl Cre+	0.04697	to 0.4223	o	s	9
		0	-0.4252	N	r	>0.999
	Bax fl/fl vs. Bak -/- Bax fl/fl Cre+	.1068	to 0.6389	o	s	9
	STZ					
		-	-1.385	Y	*	
	WT vs. Cre+	0.853	to -0.321	es	**	0.0001
		0	-0.2094	N	r	
	WT vs. Bak -/-	.3226	to 0.8547	o	s	0.8413
		0	-	N	r	
	WT vs. Bax fl/fl	.5227	0.04683 to 1.092	o	s	0.0972
	WT vs. Bak -/- Bax fl/fl Cre+	0	-0.22 to	N	r	0.9850

	.3033	0.8267	o	s	
	1	0.7064	Y	*	<0.000
Cre+ vs. Bak -/-	.176	to 1.645	es	***	1
	1	0.8644	Y	*	<0.000
Cre+ vs. Bax fl/fl	.376	to 1.887	es	***	1
	1	0.697 to	Y	*	<0.000
Cre+ vs. Bak -/- Bax fl/fl Cre+	.156	1.616	es	***	1
	0	-0.3113	N	r	>0.999
Bak -/- vs. Bax fl/fl	.2001	to 0.7114	o	s	9
	-	-0.4786	N	r	>0.999
Bak -/- vs. Bak -/- Bax fl/fl Cre+	0.01929	to 0.4401	o	s	9
	-	-0.7216	N	r	>0.999
Bax fl/fl vs. Bak -/- Bax fl/fl Cre+	0.2194	to 0.2829	o	s	9

Figure 4.12 Citrate synthase activity

Source of Variation	% of total variation	P value	P value summary	Significant?
Interaction	2.008	0.7643	ns	No
genotype	1.614	0.8292	ns	No
diabetes	0.9095	0.3634	ns	No

Figure 4.13A Seahorse, raw values

Tukey's multiple comparisons test	Mean Diff.	95.00% CI of diff.	Significant?	Summary	Adjusted P Value
CIT					
Basal					
WT vs. Cre+	2.953	-22.16 to 28.07	No	ns	0.9976
WT vs. Bak -/-	3.313	-23.57 to 30.19	No	ns	0.9971
WT vs. Bax fl/fl	-4.46	-31.34 to 22.42	No	ns	0.9908
WT vs. Bak -/- Bax fl/fl Cre+	-0.286	-25.17 to 24.6	No	ns	>0.999 9
Cre+ vs. Bak -/-	0.36	-17.56 to 18.28	No	ns	>0.999 9
Cre+ vs. Bax fl/fl	-7.413	-25.33 to 10.51	No	ns	0.7826
Cre+ vs. Bak -/- Bax fl/fl Cre+	-3.239	-18 to 11.52	No	ns	0.9738
Bak -/- vs. Bax fl/fl	-7.773	-28.09 to 12.55	No	ns	0.8274
Bak -/- vs. Bak -/- Bax fl/fl Cre+	-3.599	-21.2 to 14	No	ns	0.9797
Bax fl/fl vs. Bak -/- Bax fl/fl Cre+	4.174	-13.42 to 21.77	No	ns	0.9652
ADP Max					
WT vs. Cre+	5.681	-19.44 to 30.8	No	ns	0.9707
WT vs. Bak -/-	4.169	-22.71 to 31.05	No	ns	0.9929
WT vs. Bax fl/fl	-12.44	-39.32 to 14.44	No	ns	0.7036
WT vs. Bak -/- Bax fl/fl Cre+	-3.589	-28.48 to 21.3	No	ns	0.9946
Cre+ vs. Bak -/-	1.512	-19.43 to 16.41	No	ns	0.9993
Cre+ vs. Bax fl/fl	-18.12	-36.04 to -0.2036	Yes	*	0.0460
Cre+ vs. Bak -/- Bax fl/fl Cre+	-9.27	-24.03 to 5.492	No	ns	0.4150
Bak -/- vs. Bax fl/fl	-16.61	-36.93 to 3.708	No	ns	0.1642
Bak -/- vs. Bak -/- Bax fl/fl Cre+	-7.758	-25.36 to 9.84	No	ns	0.7400
Bax fl/fl vs. Bak -/- Bax fl/fl Cre+	8.854	-8.744 to 26.45	No	ns	0.6339
Oligo					

	4.6	-20.46 to		n	
WT vs. Cre+	53	29.77	No	s	0.9860
	5.3	-21.55 to		n	
WT vs. Bak -/-	34	32.21	No	s	0.9819
	0.2	-26.66 to		n	>0.999
WT vs. Bax fl/fl	24	27.1	No	s	9
	2.5	-22.3 to		n	
WT vs. Bak -/- Bax fl/fl Cre+	9	27.48	No	s	0.9985
	0.6	-17.24 to		n	>0.999
Cre+ vs. Bak -/-	81	18.6	No	s	9
	-	-22.35 to		n	
Cre+ vs. Bax fl/fl	4.429	13.49	No	s	0.9597
	-	-16.83 to		n	
Cre+ vs. Bak -/- Bax fl/fl Cre+	2.063	12.7	No	s	0.9952
	-	-25.43 to		n	
Bak -/- vs. Bax fl/fl	5.11	15.21	No	s	0.9571
	-	-20.34 to		n	
Bak -/- vs. Bak -/- Bax fl/fl Cre+	2.744	14.85	No	s	0.9927
	2.3	-15.23 to		n	
Bax fl/fl vs. Bak -/- Bax fl/fl Cre+	66	19.96	No	s	0.9959
FCCP					
	4.7	-20.38 to		n	
WT vs. Cre+	34	29.85	No	s	0.9851
	0.2	-26.64 to		n	>0.999
WT vs. Bak -/-	38	27.12	No	s	9
	7.4	-19.39 to		n	
WT vs. Bax fl/fl	94	34.37	No	s	0.9384
	-	-26.73 to		n	
WT vs. Bak -/- Bax fl/fl Cre+	1.845	23.04	No	s	0.9996
	-	-22.42 to		n	
Cre+ vs. Bak -/-	4.496	13.42	No	s	0.9575
	2.7	-15.16 to		n	
Cre+ vs. Bax fl/fl	6	20.68	No	s	0.9930
	-	-21.34 to		n	
Cre+ vs. Bak -/- Bax fl/fl Cre+	6.579	8.183	No	s	0.7322
	7.2	-13.06 to		n	
Bak -/- vs. Bax fl/fl	56	27.58	No	s	0.8604
	-	-19.68 to		n	
Bak -/- vs. Bak -/- Bax fl/fl Cre+	2.083	15.51	No	s	0.9975
	-	-26.94 to		n	
Bax fl/fl vs. Bak -/- Bax fl/fl Cre+	9.339	8.259	No	s	0.5849
Anti-A					
	3.5	-21.53 to		n	
WT vs. Cre+	83	28.7	No	s	0.9948
	5.1	-21.74 to		n	
WT vs. Bak -/-	37	32.02	No	s	0.9843
	2.8	-24.06 to		n	
WT vs. Bax fl/fl	24	29.7	No	s	0.9984
	4.9	-19.92 to		n	
WT vs. Bak -/- Bax fl/fl Cre+	64	29.85	No	s	0.9815
	1.5	-16.37 to		n	
Cre+ vs. Bak -/-	54	19.47	No	s	0.9993
	-	-18.68 to		n	>0.999
Cre+ vs. Bax fl/fl	0.759	17.16	No	s	9
	1.3	-13.38 to		n	
Cre+ vs. Bak -/- Bax fl/fl Cre+	81	16.14	No	s	0.9990
	-	-22.63 to		n	
Bak -/- vs. Bax fl/fl	2.313	18.01	No	s	0.9978
	-	-17.77 to		n	>0.999
Bak -/- vs. Bak -/- Bax fl/fl Cre+	0.173	17.42	No	s	9
	2.1	-15.46 to		n	
Bax fl/fl vs. Bak -/- Bax fl/fl Cre+	4	19.74	No	s	0.9972
	Me	95.00%	Sig	S	Adjust
Tukey's multiple comparisons test	an Diff.	CI of diff.	nificant?	ummary	ed P Value
STZ					
Basal					
	8.4	-10.73 to		n	
WT vs. Cre+	94	27.72	No	s	0.7395
WT vs. Bak -/-	13.	-7.33 to	No	n	0.3770

	73	34.79		s	
	12.	-8.475 to		n	
WT vs. Bax fl/fl	59	33.64	No	s	0.4677
	7.2	-10.9 to		n	
WT vs. Bak -/- Bax fl/fl Cre+	28	25.35	No	s	0.8055
	5.2	-12.66 to		n	
Cre+ vs. Bak -/-	36	23.13	No	s	0.9278
	4.0	-13.81 to		n	
Cre+ vs. Bax fl/fl	91	21.99	No	s	0.9697
	-	-15.6 to		n	
Cre+ vs. Bak -/- Bax fl/fl Cre+	1.266	13.06	No	s	0.9992
	-	-21 to		n	
Bak -/- vs. Bax fl/fl	1.145	18.71	No	s	0.9999
	-	-23.21 to		n	
Bak -/- vs. Bak -/- Bax fl/fl Cre+	6.502	10.21	No	s	0.8192
	-	-22.07 to		n	
Bax fl/fl vs. Bak -/- Bax fl/fl Cre+	5.357	11.35	No	s	0.9018
ADP Max					
	19.	0.2483	Ye		
WT vs. Cre+	47	to 38.7	s	*	0.0455
	20.	-0.5027		n	
WT vs. Bak -/-	56	to 41.62	No	s	0.0593
	24.	3.174 to	Ye		
WT vs. Bax fl/fl	23	45.29	s	*	0.0153
	16.	-1.604 to		n	
WT vs. Bak -/- Bax fl/fl Cre+	52	34.65	No	s	0.0923
	1.0	-16.81 to		n	
Cre+ vs. Bak -/-	84	18.98	No	s	0.9998
	4.7	-13.14 to		n	
Cre+ vs. Bax fl/fl	61	22.66	No	s	0.9480
	-	-17.28 to		n	
Cre+ vs. Bak -/- Bax fl/fl Cre+	2.952	11.38	No	s	0.9793
	3.6	-16.18 to		n	
Bak -/- vs. Bax fl/fl	77	23.53	No	s	0.9861
	-	-20.75 to		n	
Bak -/- vs. Bak -/- Bax fl/fl Cre+	4.036	12.67	No	s	0.9631
	-	-24.42 to		n	
Bax fl/fl vs. Bak -/- Bax fl/fl Cre+	7.713	8.998	No	s	0.7069
Oligo					
	8.2	-10.93 to		n	
WT vs. Cre+	91	27.52	No	s	0.7564
	14.	-6.329 to		n	
WT vs. Bak -/-	73	35.79	No	s	0.3051
	8.9	-12.12 to		n	
WT vs. Bax fl/fl	35	29.99	No	s	0.7673
	10.	-7.709 to		n	
WT vs. Bak -/- Bax fl/fl Cre+	42	28.54	No	s	0.5078
	6.4	-11.46 to		n	
Cre+ vs. Bak -/-	4	24.34	No	s	0.8577
	0.6	-17.25 to		n	>0.999
Cre+ vs. Bax fl/fl	44	18.54	No	s	9
	2.1	-12.2 to		n	
Cre+ vs. Bak -/- Bax fl/fl Cre+	25	16.45	No	s	0.9940
	-	-25.65 to		n	
Bak -/- vs. Bax fl/fl	5.796	14.06	No	s	0.9283
	-	-21.03 to		n	
Bak -/- vs. Bak -/- Bax fl/fl Cre+	4.315	12.4	No	s	0.9532
	1.4	-15.23 to		n	
Bax fl/fl vs. Bak -/- Bax fl/fl Cre+	81	18.19	No	s	0.9992
FCCP					
	5.7	-13.5 to		n	
WT vs. Cre+	27	24.95	No	s	0.9232
	6.5	-14.46 to		n	
WT vs. Bak -/-	99	27.66	No	s	0.9090
	9.6	-11.37 to		n	
WT vs. Bax fl/fl	91	30.75	No	s	0.7093
	7.8	-10.25 to		n	
WT vs. Bak -/- Bax fl/fl Cre+	75	26	No	s	0.7513
	0.8	-17.03 to		n	>0.999
Cre+ vs. Bak -/-	72	18.77	No	s	9
	3.9	-13.93 to		n	
Cre+ vs. Bax fl/fl	64	21.86	No	s	0.9730

Cre+ vs. Bak -/- Bax fl/fl Cre+	2.148	-12.18 to 16.48	No	ns	0.9938
Bak -/- vs. Bax fl/fl	3.092	-16.76 to 22.95	No	ns	0.9928
Bak -/- vs. Bak -/- Bax fl/fl Cre+	1.276	-15.43 to 17.99	No	ns	0.9996
Bax fl/fl vs. Bak -/- Bax fl/fl Cre+	-1.816	-18.53 to 14.89	No	ns	0.9982
Anti-A					
WT vs. Cre+	4.955	-14.27 to 24.18	No	ns	0.9535
WT vs. Bak -/-	7.214	-13.85 to 28.27	No	ns	0.8782
WT vs. Bax fl/fl	4.989	-16.07 to 26.05	No	ns	0.9656
WT vs. Bak -/- Bax fl/fl Cre+	5.004	-13.12 to 23.13	No	ns	0.9408
Cre+ vs. Bak -/-	2.259	-15.64 to 20.16	No	ns	0.9968
Cre+ vs. Bax fl/fl	0.034	-17.86 to 17.93	No	ns	>0.9999
Cre+ vs. Bak -/- Bax fl/fl Cre+	0.049	-14.28 to 14.38	No	ns	>0.9999
Bak -/- vs. Bax fl/fl	-2.225	-22.08 to 17.63	No	ns	0.9980
Bak -/- vs. Bak -/- Bax fl/fl Cre+	-2.21	-18.92 to 14.5	No	ns	0.9962
Bax fl/fl vs. Bak -/- Bax fl/fl Cre+	0.015	-16.7 to 16.73	No	ns	>0.9999

Figure 4.13B Seahorse, Baseline corrected

Tukey's multiple comparisons test	Mean Diff.	95.00% CI of diff.	Significant?	Summary	Adjusted P Value
CIT					
Basal					
WT vs. Cre+	0	-46.92 to 46.92	No	ns	>0.9999
WT vs. Bak -/-	0	-50.21 to 50.21	No	ns	>0.9999
WT vs. Bax fl/fl	0	-50.21 to 50.21	No	ns	>0.9999
WT vs. Bak -/- Bax fl/fl Cre+	0	-46.49 to 46.49	No	ns	>0.9999
Cre+ vs. Bak -/-	0	-33.48 to 33.48	No	ns	>0.9999
Cre+ vs. Bax fl/fl	0	-33.48 to 33.48	No	ns	>0.9999
Cre+ vs. Bak -/- Bax fl/fl Cre+	0	-27.58 to 27.58	No	ns	>0.9999
Bak -/- vs. Bax fl/fl	0	-37.96 to 37.96	No	ns	>0.9999
Bak -/- vs. Bak -/- Bax fl/fl Cre+	0	-32.87 to 32.87	No	ns	>0.9999
Bax fl/fl vs. Bak -/- Bax fl/fl Cre+	0	-32.87 to 32.87	No	ns	>0.9999
ADP Max					
WT vs. Cre+	0.1857	-46.73 to 47.1	No	ns	>0.9999
WT vs. Bak -/-	-6.617	-56.83 to 43.6	No	ns	0.9962
WT vs. Bax fl/fl	-11.75	-61.96 to 38.46	No	ns	0.9669
WT vs. Bak -/- Bax fl/fl Cre+	-11.62	-58.11 to 34.87	No	ns	0.9580
Cre+ vs. Bak -/-	-6.802	-40.28 to 26.67	No	ns	0.9802
Cre+ vs. Bax fl/fl	-11.94	-45.41 to 21.54	No	ns	0.8610
Cre+ vs. Bak -/- Bax fl/fl Cre+	-11.8	-39.38 to 15.77	No	ns	0.7603

Bak -/- vs. Bax fl/fl	-5.134	-43.09 to 32.82	No	ns	0.9958
Bak -/- vs. Bak -/- Bax fl/fl Cre+	-5.002	-37.87 to 27.87	No	ns	0.9934
Bax fl/fl vs. Bak -/- Bax fl/fl Cre+	0	-32.74 to 33	No	ns	>0.9999
Oligo	.1311				
WT vs. Cre+	9.476	-37.44 to 56.39	No	ns	0.9807
WT vs. Bak -/-	9.833	-40.38 to 60.05	No	ns	0.9828
WT vs. Bax fl/fl	1.87	-48.34 to 52.08	No	ns	>0.9999
WT vs. Bak -/- Bax fl/fl Cre+	1 2.490	-34 to 58.97	No	ns	0.9459
Cre+ vs. Bak -/-	0.3569	-33.12 to 33.83	No	ns	>0.9999
Cre+ vs. Bax fl/fl	-7.606	-41.08 to 25.87	No	ns	0.9702
Cre+ vs. Bak -/- Bax fl/fl Cre+	3 .009	-24.57 to 30.58	No	ns	0.9982
Bak -/- vs. Bax fl/fl	-7.963	-45.92 to 29.99	No	ns	0.9778
Bak -/- vs. Bak -/- Bax fl/fl Cre+	2 .652	-30.22 to 35.52	No	ns	0.9994
Bax fl/fl vs. Bak -/- Bax fl/fl Cre+	1 0.62	-22.26 to 43.49	No	ns	0.8989
FCCP					
WT vs. Cre+	2 .514	-44.4 to 49.43	No	ns	0.9999
WT vs. Bak -/-	-18.42	-68.63 to 31.79	No	ns	0.8481
WT vs. Bax fl/fl	2 6.43	-23.78 to 76.65	No	ns	0.5926
WT vs. Bak -/- Bax fl/fl Cre+	-9.84	-56.33 to 36.65	No	ns	0.9770
Cre+ vs. Bak -/-	-20.93	-54.41 to 12.54	No	ns	0.4193
Cre+ vs. Bax fl/fl	2 3.92	-9.556 to 57.39	No	ns	0.2832
Cre+ vs. Bak -/- Bax fl/fl Cre+	-12.35	-39.93 to 15.22	No	ns	0.7283
Bak -/- vs. Bax fl/fl	4 4.858	6.896 to 82.81	Yes	*	0.0119
Bak -/- vs. Bak -/- Bax fl/fl Cre+	.58	-24.29 to 41.45	No	ns	0.9511
Bax fl/fl vs. Bak -/- Bax fl/fl Cre+	-36.27	-69.15 to -3.401	Yes	*	0.0227
Anti-A					
WT vs. Cre+	9 .85	-37.07 to 56.77	No	ns	0.9777
WT vs. Bak -/-	1 6.06	-34.15 to 66.27	No	ns	0.9021
WT vs. Bax fl/fl	9 .14	-41.07 to 59.35	No	ns	0.9869
WT vs. Bak -/- Bax fl/fl Cre+	1 8.976	-27.52 to 65.46	No	ns	0.7910
Cre+ vs. Bak -/-	-.21	-27.27 to 39.69	No	ns	0.9859
Cre+ vs. Bax fl/fl	-0.71	-34.19 to 32.77	No	ns	>0.9999
Cre+ vs. Bak -/- Bax fl/fl Cre+	9 .12	-18.46 to 36.7	No	ns	0.8907
Bak -/- vs. Bax fl/fl	-6.92	-44.88 to 31.04	No	ns	0.9868
Bak -/- vs. Bak -/- Bax fl/fl Cre+	2 .91	-29.96 to 35.78	No	ns	0.9992
Bax fl/fl vs. Bak -/- Bax fl/fl Cre+	9 .83	-23.04 to 42.7	No	ns	0.9217

Tukey's multiple comparisons test	Mean Diff.	95.00% CI of diff.	Significant?	Summary	Adjusted P Value

STZ					
Basal					
WT vs. Cre+	0	-34.86 to 34.86	No	ns	>0.9999
WT vs. Bak -/-	0	-38.19 to 38.19	No	ns	>0.9999
WT vs. Bax fl/fl	0	-38.19 to 38.19	No	ns	>0.9999
WT vs. Bak -/- Bax fl/fl Cre+	0	-32.86 to 32.86	No	ns	>0.9999
Cre+ vs. Bak -/-	0	-32.45 to 32.45	No	ns	>0.9999
Cre+ vs. Bax fl/fl	0	-32.45 to 32.45	No	ns	>0.9999
Cre+ vs. Bak -/- Bax fl/fl Cre+	0	-25.98 to 25.98	No	ns	>0.9999
Bak -/- vs. Bax fl/fl	0	-36 to 36	No	ns	>0.9999
Bak -/- vs. Bak -/- Bax fl/fl Cre+	0	-30.3 to 30.3	No	ns	>0.9999
Bax fl/fl vs. Bak -/- Bax fl/fl Cre+	0	-30.3 to 30.3	No	ns	>0.9999
ADP Max					
WT vs. Cre+	5.422	-29.44 to 40.28	No	ns	0.9928
WT vs. Bak -/-	-36.83	-75.02 to 1.354	No	ns	0.0644
WT vs. Bax fl/fl	-11.35	-49.54 to 26.83	No	ns	0.9237
WT vs. Bak -/- Bax fl/fl Cre+	3.329	-29.54 to 36.19	No	ns	0.9986
Cre+ vs. Bak -/-	-42.25	-74.7 to -9.801	Yes	*	0.0040
Cre+ vs. Bax fl/fl	-16.77	-49.23 to 15.68	No	ns	0.6107
Cre+ vs. Bak -/- Bax fl/fl Cre+	-2.093	-28.07 to 23.89	No	ns	0.9995
Bak -/- vs. Bax fl/fl	25.48	-10.52 to 61.48	No	ns	0.2935
Bak -/- vs. Bak -/- Bax fl/fl Cre+	40.16	9.86 to 70.46	Yes	*	0.0032
Bax fl/fl vs. Bak -/- Bax fl/fl Cre+	14.68	-15.62 to 44.98	No	ns	0.6677
Oligo					
WT vs. Cre+	5.481	-29.38 to 40.34	No	ns	0.9925
WT vs. Bak -/-	9.743	-28.46 to 47.92	No	ns	0.9553
WT vs. Bax fl/fl	-8.138	-46.32 to 30.05	No	ns	0.9766
WT vs. Bak -/- Bax fl/fl Cre+	12.43	-20.56 to 45.16	No	ns	0.8393
Cre+ vs. Bak -/-	4.248	-28.2 to 36.7	No	ns	0.9963
Cre+ vs. Bax fl/fl	-13.62	-46.07 to 18.83	No	ns	0.7744
Cre+ vs. Bak -/- Bax fl/fl Cre+	6.819	-19.16 to 32.8	No	ns	0.9504
Bak -/- vs. Bax fl/fl	-17.87	-53.87 to 18.13	No	ns	0.6472
Bak -/- vs. Bak -/- Bax fl/fl Cre+	2.571	-27.73 to 32.87	No	ns	0.9993
Bax fl/fl vs. Bak -/- Bax fl/fl Cre+	20.44	-9.862 to 50.74	No	ns	0.3419
FCCP					
WT vs. Cre+	-11.58	-46.44 to 23.27	No	ns	0.8896
WT vs. Bak -/-	-42.8	-80.98 to -4.611	Yes	*	0.0196
WT vs. Bax fl/fl	-	-58.12 to	No	n	0.6016

	19.93	18.25		s	
	-	-41.14 to		n	
WT vs. Bak -/- Bax fl/fl Cre+	8.279	24.59	No	s	0.9571
	-	-63.66 to		n	
Cre+ vs. Bak -/-	31.21	1.239	No	s	0.0656
	-	-40.8 to		n	
Cre+ vs. Bax fl/fl	8.35	24.1	No	s	0.9538
	3.3	-22.68 to		n	
Cre+ vs. Bak -/- Bax fl/fl Cre+	05	29.29	No	s	0.9967
	22.	-13.14 to		n	
Bak -/- vs. Bax fl/fl	86	58.86	No	s	0.4044
	34.	4.217 to	Ye		
Bak -/- vs. Bak -/- Bax fl/fl Cre+	52	64.82	s	*	0.0169
	11.	-18.65 to		n	
Bax fl/fl vs. Bak -/- Bax fl/fl Cre+	65	41.95	No	s	0.8253
Anti-A					
	12.	-22.23 to		n	
WT vs. Cre+	63	47.49	No	s	0.8545
	13.	-25.17 to		n	
WT vs. Bak -/-	01	51.2	No	s	0.8803
	3.8	-34.32 to		n	
WT vs. Bax fl/fl	66	42.05	No	s	0.9986
	12.	-20.44 to		n	
WT vs. Bak -/- Bax fl/fl Cre+	42	45.29	No	s	0.8344
	0.3	-32.07 to		n	>0.999
Cre+ vs. Bak -/-	794	32.83	No	s	9
	-	-41.22 to		n	
Cre+ vs. Bax fl/fl	8.766	23.69	No	s	0.9451
	-	-26.19 to		n	>0.999
Cre+ vs. Bak -/- Bax fl/fl Cre+	0.2102	25.77	No	s	9
	-	-45.15 to		n	
Bak -/- vs. Bax fl/fl	9.146	26.86	No	s	0.9558
	-	-30.89 to		n	>0.999
Bak -/- vs. Bak -/- Bax fl/fl Cre+	0.5897	29.71	No	s	9
	8.5	-21.74 to		n	
Bax fl/fl vs. Bak -/- Bax fl/fl Cre+	56	38.86	No	s	0.9360

Figure 4.14

4.14A ATP production

Source of Variation	% of total variation	P value	P value summary	Significant?
Interaction	3.414	0.7278	ns	No
genotype	4.659	0.5971	ns	No
diabetes	0.0716	0.8367	ns	No

4.14B ATP production (corrected)

Source of Variation	% of total variation	P value	P value summary	Significant?
Interaction	10.63	0.1139	ns	No
genotype	14.45	0.0422	*	Yes
diabetes	0.2147	0.6924	ns	No

Within each column, compare rows (simple effects within columns)

Number of families	2
Number of comparisons per family	1
Alpha	0.05

Bonferroni's multiple comparisons test CIT	Mean Diff.	95.00 % CI of diff.	Significant?	Summary	Adjusted P Value
WT vs. Cre+	2.222	-65.08 to 69.52	No	ns	>0.9999
WT vs. Bak -/-	-13.67	-85.7 to 58.36	No	ns	>0.9999
WT vs. Bax fl/fl	9.	-62.6	N	n	>0.999

		434	to 81.46	o	s	9
		-	-80.18	N	n	>0.999
	WT vs. Bak -/- Bax fl/fl Cre+	13.49	to 53.19	o	s	9
		-	-63.92	N	n	>0.999
	Cre+ vs. Bak -/-	15.9	to 32.12	o	s	9
		7.	-40.81	N	n	>0.999
	Cre+ vs. Bax fl/fl	212	to 55.23	o	s	9
		-	-55.27	N	n	>0.999
	Cre+ vs. Bak -/- Bax fl/fl Cre+	15.72	to 23.84	o	s	9
		2	-31.34	N	n	>0.999
	Bak -/- vs. Bax fl/fl	3.11	to 77.56	o	s	9
		0.	-46.97	N	n	>0.999
	Bak -/- vs. Bak -/- Bax fl/fl Cre+	18	to 47.33	o	s	9
		-	-70.08	N	n	>0.999
	Bax fl/fl vs. Bak -/- Bax fl/fl Cre+	22.93	to 24.23	o	s	9
	STZ					
		-	-73.52	N	n	>0.999
	WT vs. Cre+	20.8	to 31.92	o	s	9
		-	-125.3	Y		
	WT vs. Bak -/-	67.56	to -9.808	es	*	0.0118
		-	-101 to	N	n	
	WT vs. Bax fl/fl	43.28	14.47	o	s	0.3265
		-	-66.88	N	n	>0.999
	WT vs. Bak -/- Bax fl/fl Cre+	17.17	to 32.53	o	s	9
		-	-95.85	N	n	
	Cre+ vs. Bak -/-	46.76	to 2.316	o	s	0.0729
		-	-71.56	N	n	>0.999
	Cre+ vs. Bax fl/fl	22.48	to 26.6	o	s	9
		3.	-35.67	N	n	>0.999
	Cre+ vs. Bak -/- Bax fl/fl Cre+	623	to 42.92	o	s	9
		2	-30.17	N	n	>0.999
	Bak -/- vs. Bax fl/fl	4.28	to 78.73	o	s	9
		5	4.561	Y		
	Bak -/- vs. Bak -/- Bax fl/fl Cre+	0.39	to 96.21	es	*	0.0218
		2	-19.72	N	n	>0.999
	Bax fl/fl vs. Bak -/- Bax fl/fl Cre+	6.11	to 71.93	o	s	9

4.14C Proton leak

Variation	Source of	% of total variation	P value	P value summary	Significant?		
			0				
	Interaction	11.81	.1008	ns	No		
			0				
	genotype	8.475	.2236	ns	No		
			0				
	diabetes	10.9	.0082	**	Yes		
			M	95.00%	Si	S	Adjust
	Bonferroni's multiple comparisons test		ean Diff.	CI of diff.	gnificant?	ummary	ed P Value
	CIT - STZ						
			-	-22.97	N	n	0.066
	WT		11.24	to 0.4954	o	s	8
			-	-13.51	N	n	0.082
	Cre+		6.501	to 0.511	o	s	1
			-	-7.939	N	n	>0.99
	Bak -/-		0.215	to 7.509	o	s	99
			-	-15.93	N	n	>0.99
	Bax fl/fl Cre+		4.194	to 7.539	o	s	99
			0	-5.426	N	n	>0.99
	Bak -/- Bax fl/fl Cre+		.961	to 7.348	o	s	99

4.14 D Proton leak (corrected)

Variation	Source of	% of total variation	P value	P value summary	Significant?
			0.0		
	Interaction	19.78	179	*	Yes
			0.4		
	genotype	6.085	086	ns	No
			0.4		
	diabetes	0.7474	833	ns	No

4.14E Spare capacity

Variation	Source of	% of total variation	P value	P value summary	Significant?
	Interaction	5.902	0.4	ns	No

			637		
			0.1		
	genotype	11.69	427	ns	No
			0.0		
	diabetes	6.521	502	ns	No

4.14F Spare capacity (corrected)

Source of Variation	% of total variation	P value	P value summary	Significant?
		0.5		
Interaction	5.124	339	ns	No
		0.1		
genotype	10.73	736	ns	No
		0.0		
diabetes	8.497	261	*	Yes

Bonferroni's multiple comparisons test	Mean Diff.	95.00% CI of diff.	Significant?	Summary	Adjusted P Value
CIT - STZ					
	-	-63.46 to			>0.9
WT	17.25	28.96	No	ns	
	-	-41.17 to			
Cre+	14.97	11.23	No	ns	0.65
	5.6	-23.24 to			>0.9
Bak -/-	22	34.48	No	ns	
	-	-70 to			
Bax fl/fl	26.17	17.67	No	ns	0.57
	-	-38.2 to			
Bak -/-	14.33	9.529	No	ns	0.56

4.14G RCR

Source of Variation	% of total variation	P value	P value summary	Significant?
Interaction	5.777	0.3677	ns	No
genotype	24.44	0.0028	**	Yes
	1.655e-005			
diabetes		0.9972	ns	No

Within each column, compare rows (simple effects within columns)

Number of families	2
	1
Number of comparisons per family	0
	0
Alpha	.05

Bonferroni's multiple comparisons test	Mean Diff.	95.00% CI of diff.	Significant?	Summary	Adjusted P Value
CITI					
	-	-1.106	N	n	>0.999
WT vs. Cre+	0.191	to 0.7235	o	s	9
	-	-1.352	N	n	>0.999
WT vs. Bak -/-	0.373	to 0.6058	o	s	9
	0	-0.8838	N	n	>0.999
WT vs. Bax fl/fl	.09502	to 1.074	o	s	9
	-	-1.338	N	n	>0.999
WT vs. Bak -/- Bax fl/fl Cre+	0.432	to 0.4742	o	s	9
	-	-0.8345	N	n	>0.999
Cre+ vs. Bak -/-	0.182	to 0.4705	o	s	9
	0	-0.3665	N	n	>0.999
Cre+ vs. Bax fl/fl	.286	to 0.9385	o	s	9
	-	-0.7785	N	n	>0.999
Cre+ vs. Bak -/- Bax fl/fl Cre+	0.241	to 0.2965	o	s	9
	0	-0.2719	N	n	
Bak -/- vs. Bax fl/fl	.468	to 1.208	o	s	0.6947
	-	-0.6998	N	n	>0.999
Bak -/- vs. Bak -/- Bax fl/fl Cre+	0.059	to 0.5818	o	s	9
	-	-1.168	N	n	
Bax fl/fl vs. Bak -/- Bax fl/fl Cre+	0.527	to 0.1138	o	s	0.1949
STZ					
	-	-1.026	N	n	>0.999
WT vs. Cre+	0.31	to 0.4064	o	s	9
	-	-1.776	Y		
WT vs. Bak -/-	0.991	to -0.2062	es	**	0.0052

	-	-1.111	N	n	>0.999
WT vs. Bax fl/fl	0.284	to 0.5432	o	s	9
	-	-1.131	N	n	
WT vs. Bak -/- Bax fl/fl Cre+	0.448	to 0.2351	o	s	0.6009
	-	-1.348	Y		
Cre+ vs. Bak -/-	0.681	to -0.01407	es	*	0.0421
	0	-0.6904	N	n	>0.999
Cre+ vs. Bax fl/fl	.026	to 0.7424	o	s	9
	-	-0.6816	N	n	>0.999
Cre+ vs. Bak -/- Bax fl/fl Cre+	0.138	to 0.4056	o	s	9
	0	-	N	n	
Bak -/- vs. Bax fl/fl	.707	0.07778 to 1.492	o	s	0.1089
	0	-	N	n	
Bak -/- vs. Bak -/- Bax fl/fl Cre+	.543	0.08799 to 1.174	o	s	0.1475
	-	-0.8471	N	n	>0.999
Bax fl/fl vs. Bak -/- Bax fl/fl Cre+	0.164	to 0.5191	o	s	9

Figure 4.17 Hydrogen peroxide production

Glutamate and Malate

Variation	Source of	% of total variation	P value	P value summary	Significant?
	Interaction	13.76	.1889	ns	No
	genotype	10.78	.2979	ns	No
	Diabetes	1.56	.3959	ns	No

Succinate and Rotenone

Variation	Source of	% of total variation	P value	P value summary	Significant?
	Interaction	5.676	.5762	ns	No
	genotype	32.17	.0080	**	Yes
	diabetes	0.2178	.7395	ns	No

Bonferroni's multiple comparisons test	Mean Diff.	95.00% CI of diff.	Significant?	Summary	Adjusted P Value
CIT					
WT vs. Cre+	2.612	-11.57 to 56.8	No	ns	0.5468
WT vs. Bak -/-	4.371	-21.88 to 50.63	No	ns	>0.9999
WT vs. Bax fl/fl	6.752	-11.46 to 64.97	No	ns	0.4272
WT vs. Bak -/- Bax fl/fl Cre+	1.591	-26.63 to 49.81	No	ns	>0.9999
Cre+ vs. Bak -/-	-8.238	-35.26 to 18.79	No	ns	>0.9999
Cre+ vs. Bax fl/fl	4.141	-25.46 to 33.75	No	ns	>0.9999
Cre+ vs. Bak -/- Bax fl/fl Cre+	-11.03	-40.63 to 18.58	No	ns	>0.9999
Bak -/- vs. Bax fl/fl	2.381	-19.6 to 44.36	No	ns	>0.9999
Bak -/- vs. Bak -/- Bax fl/fl Cre+	-2.788	-34.76 to 29.19	No	ns	>0.9999
Bax fl/fl vs. Bak -/- Bax fl/fl Cre+	-15.17	-49.35 to 19.02	No	ns	>0.9999
STZ					
WT vs. Cre+	2.3	-15.79 to 40.38	No	ns	>0.9999
WT vs. Bak -/-	.441	-26.13 to 35.02	No	ns	>0.9999
WT vs. Bax fl/fl	9.312	3.953 to 54.66	Yes	*	0.0145
WT vs. Bak -/- Bax fl/fl Cre+	1.832	-3.523 to 47.18	No	ns	0.1413
Cre+ vs. Bak -/-	-7.857	-39.83 to 24.12	No	ns	>0.9999
Cre+ vs. Bax fl/fl	7.012	-10.02 to 44.03	No	ns	0.6685
Cre+ vs. Bak -/- Bax fl/fl Cre+	.5312	-17.5 to 36.56	No	ns	>0.9999
Bak -/- vs. Bax fl/fl	4.869	-4.741 to 54.47	No	ns	0.1644

Bak -/- vs. Bak -/- Bax fl/fl Cre+	1 7.39	-12.22 to 46.99	N o	n s	0.861 3
Bax fl/fl vs. Bak -/- Bax fl/fl Cre+	- 7.477	-31.65 to 16.7	N o	n s	>0.99 99